2024

Geological Survey Paper 14:

Structural Geology of the Eastern Tyennan Subdomain, Tasmania — An Overview and Structural Synthesis

Author: David Grey and Michael Vicary
Date: 16/10/2024
Email: info@mrt.tas.gov.au
Website: www.mrt.tas.gov.au

REPORT No.: GSP14

Mesoscopic isoclinal F1 fold bounded on the photo left by an intensely foliated phyllite (high strain zone) containing relict isoclinal fold hinges and strung out quartz veins. The fold occurs within isoclinally folded quartzite in the bed of the Serpentine River at the newly constructed Serpentine Dam. The photo was taken in 1976 with Clive Boulter for scale.

Tasmanian Government
Mineral Resources Tasmania
mrt

CONTENTS

APPENDICES

Abstract

The Eastern Tyennan subdomain occupies the central and easternmost part of the Tyennan Domain (allochthon). It is a fault-bounded, arcuate, structural domain with curved north and south lateral terminations. The western boundary of the subdomain is defined by the arcuate Olga Fault, an inverted Late Cambrian extensional fault. The eastern boundary is a series of syn- to post obduction thrust faults that form a "lid" of ophiolitic mélange and fault-bounded ultramafics (ophiolite relicts) to the Proterozoic quartzite-pelite sequence.

The Eastern Tyennan subdomain is continuous with, and has structural similarities with, the Central Tyennan subdomain to the north, but shows structural discordance and differences with the Southern Tyennan subdomain to the south. It has an interpreted litho-tectonic sequence of high-grade garnet schists and amphibolite, overlying low-grade quartzite±phyllite, overlying low-grade dolomitic phyllite and dolomite. The schists are only partially preserved as synformal keels or infolds within the low-grade sequence of quartzite and pelite, and as a klippe at Algonkian Mountain. These are considered erosional remnants of an once continuous sheet. However, significant pressure differences between the garnet schist of The Starfish-Knob Basin synformal keel and the amphibolite and banded ironstones of the Atkins Range keel, or pod require a composite nature of the high-grade sheet.

The Eastern Tyennan subdomain has a stacking of sheets with the uppermost sheets on the east (Upper Allochthon and External Zone) and the structurally lowest sheet on the west as a parautochthon (Scotchfire sheet). Wedged between is the Lower Allochthon (the Tyennan sheet or Domain). The parauochthon, made up of dolomitic phyllite and dolomite, is deformed by a regional scale, tight to isoclinal, macro-fold (Maxwell Valley macro-fold) with reclined geometry. Overlying this the Tyennan sheet is dominated by an isoclinal, asymmetric macro-fold pair. The repeated isoclinal fold pair through the various ridgelines is part of a fold "wave train" in the lowest part of the Tyennan allochthon. The central part, or core of the subdomain is a zone of polydeformation dominated by upright, tight to isoclinal regional-scale F3 folds that refold the early-formed F1/F2 macro-folds. The core is north-south trending, elongated and ovoid-shaped mirroring the arcuate form of the Olga Fault. This is further typified by marked curvature within the So/Sm formlines and a horsetail fault splay system at the southern ends of the Olga and Prince of Wales Faults.

Polydeformation was recognised by the earliest workers in the Eastern Tyennan subdomain. There is apparent clockwise rotation of all the developed fabrics So, S1, S2 and S3 at Strathgordon related to an overall west-over-east sense of shear. The polydeformation is now considered part of a progressive shear-related deformation related to continental margin subduction-exhumation. In this scenario, multiple overprinting foliations can form by repeated cycles of foliation development, foliation rotation and then re-crenulation to produce a new crenulation cleavage. This progressive, rotational shear-related deformation dominates in the core of the Eastern Tyennan subdomain. Increased shear strain rate and shear strain magnitude have been localised within the "kernel" of the subdomain. The subdomain core shows a lateral decrease in shear strain both to the north and to the south, evidenced by a drop-off in overprinting cleavages and the lack of F3 macro-refolding.

The northern part of the Eastern Tyennan subdomain has quartzite-capped ridgelines where isolated quartzite klippe contain an asymmetric, isoclinal fold pair. The fold pair is laterally continuous along individual ridgelines in tube-like quartzite bodies, expressed in the Prince of Wales-Hamilton Range-Wilmot-Frankland Range and the Twelvetrees Range, or in spindle-shaped bodies expressed in the Spires and Mt Curly ridgeline. The hinge pairs are repeated in the adjacent ridges as part of a fold couplet "wave train" where hinges in the structural profiles appear to surge like ocean waves. The hinge zones have a periodicity of ~ 8.5 km (n = 2) and ~ 6.7 km (n = 3) in the northern structural profiles. The fold pair has an approximate limb separation distance of ~1 km. The quartzite is underlain by dolomite and dolomitic phyllite ± quartzite in the northeastern part that most likely extends to the northwestern part, but listed as undifferentiated (Pu) due to lack of mapping. The relationships are similar to those at Frenchmans Cap where the basal quartzite sits on dolomitic phyllite of the Scotchfire sheet (parautochthon).

Tasmanian Government

Mineral Resources Tasmania

Department of State Growth
www.mrt.tas.gov.au

Structural geology of the Eastern Tyennan subdomain, Tasmania — an overview and structural synthesis

David R. Gray[1] and Michael J. Vicary[2]
[1] *Consultant Structural Geologist to Mineral Resources Tasmania*
[2] *Geological Survey Branch - Mineral Resources Tasmania*

ARTICLE INFO

Published: 16 October 2024
Publisher: Mineral Resources Tasmania
Report No.: GSP14

KEYWORDS

Structural Geology
Isoclinal folds
Mega-sheath folds
Eastern Tyennan region
High P metamorphism

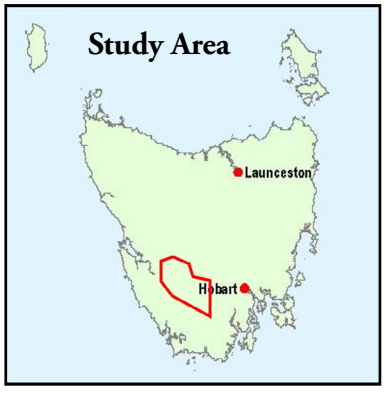

1.0 INTRODUCTION

The Eastern Tyennan subdomain represents the middle and easternmost part of the Tyennan Domain (Figure 1). It is continuous with, and has structural similarities to, the Central Tyennan subdomain to the north. There is, however, a discordance with – as well as differences in structural character to – the Southern Tyennan subdomain to the south. It has an interpreted litho-tectonic sequence of high-grade garnet schists and amphibolite, overlying low-grade quartzite±phyllite, overlying low-grade dolomitic phyllite and dolomite. The schists are only partially preserved as synformal keels or infolds within the low-grade sequence of quartzite and pelite, and as a klippe at Algonkian Mountain. These are considered erosional remnants of an interpreted, once continuous, sheet.

The Proterozoic age units are continental margin deposits that were subducted to depths of ~20 to 60 km beneath an advancing ophiolite sheet during a Cambrian arc-continent collision along the eastern margin of Gondwana (Berry and Crawford, 1988; Berry, 2014, Figure 4.10). Cambrian-Ordovician overlap sequences bound both the eastern and western parts of the Eastern Tyennan domain (Brown et al., 1989). These include the Cambro-Ordovician sandstone-conglomerate sequences flanking the Olga Valley on the west side and the Denison Range on the east.

This Tasmanian Geological Survey Paper is part of a series of papers revisiting the structural geology of the Tyennan Domain of Tasmania (Figure 1). The aim of this study has been to re-examine the structure of the Tyennan Proterozoic rocks in the context of Cambrian continental margin subduction-obduction. Deformation of this former Cambrian continental margin beneath the advancing ophiolite sheet has involved crustal-scale stacking of sheets of different metamorphic grade, isoclinal folding and internal sheet deformation, with sheets welded along their contacts by shear zones and/or brittle faulting. Subsequent erosional removal of the ophiolite sheet has provided an exposed 50-100 km window into these underlying rocks (Gray et al., 2024).

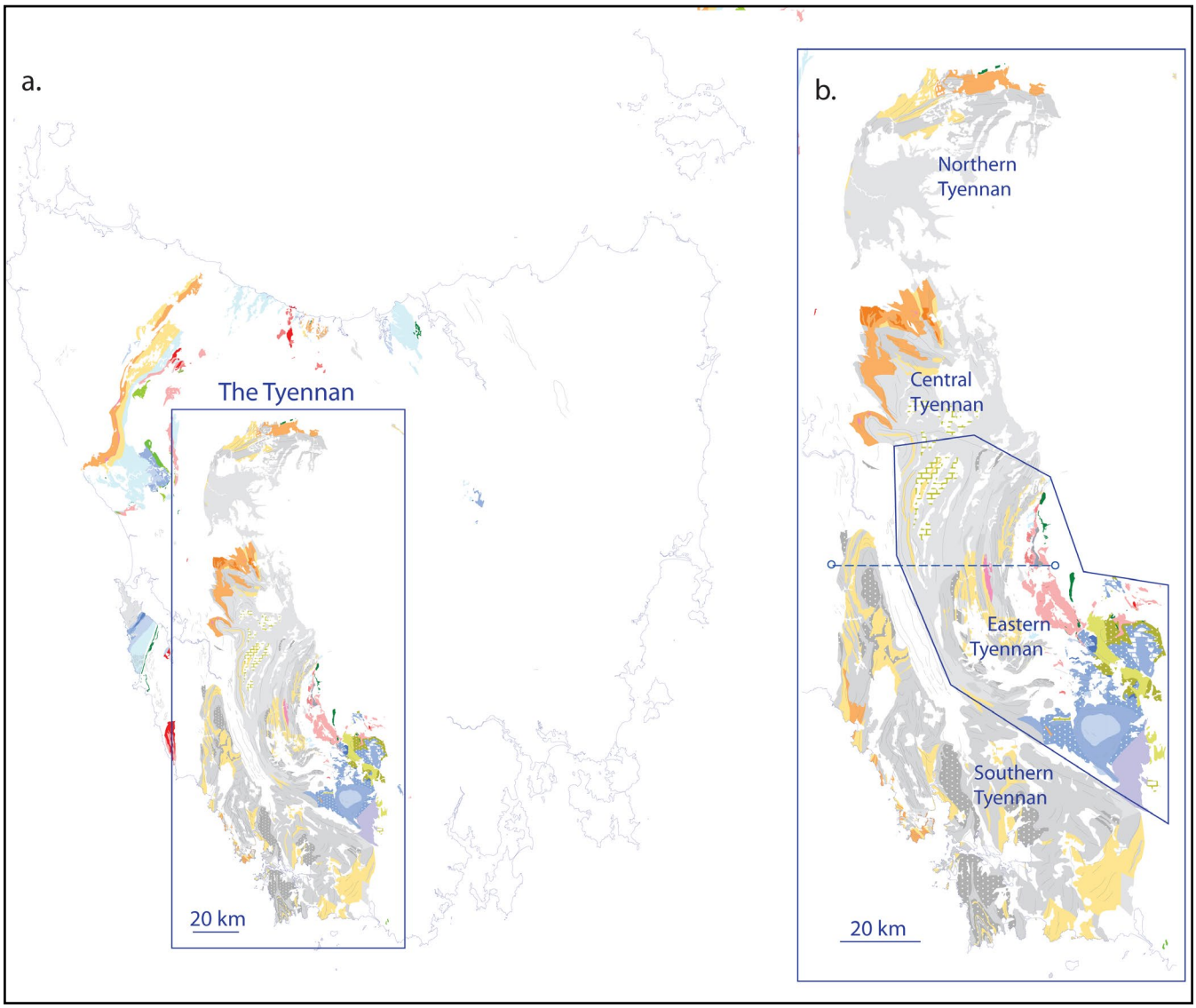

Figure 1. The Proterozoic Tyennan Domain of Tasmania shown in: a) Map base is Mineral Resources Tasmania 1:25,000 and 1:250,000 digital geological atlas; b) Enlarged map with the location of the Eastern Tyennan subdomain. The divisions within the Tyennan are after Berry (2014). The approximate Southern Tyennan map sheet polygon boundaries are 5 345 400 mN (northern boundary), 5 165 000 mN (southern boundary), 467 000 mE (eastern boundary) and 386 000 mE (western boundary). The dashed line is the position of the structural profile shown in Figure 19.

This paper represents a synthesis of the regional structure of the Eastern Tyennan subdomain with companion Geological Survey Papers 7 and 13 defining the structures and structural relationships in the adjoining Central Tyennan subdomain (Gray and Vicary, 2021b) and Southern Tyennan subdomain (Gray and Vicary, 2023) respectively. Appendix 1 provides the bushwalker photographs and interpretation that enabled construction of photo profiles along the individual ranges, as well as a summary of the local geology. Appendix 2 shows construction of a structural profile utilising outcrops along the Gordon River Road between Gordon Dam and Hermit Hill. Appendix 3 outlines strain determinations from the quartzites of the eastern Tyennan subdomain. Newly acquired structural data is tabulated in Appendix 4.

2.0 BACKGROUND

2.1 Geographic Elements

Geographically the Eastern Tyennan subdomain consists of several long, arcuate, ridge-lines made up of successive ranges (Figures 2 and 3). These ranges include from west to east:

1. Norway Range - Princess Range - Nicholls Range - Dohertys Range (~60 km combined length)
2. Gum Ridge - Algonkian Mountain (~18 km combined length)
3. Prince of Wales Range - Hamilton Range - Wilmot Range - Frankland Range (~80 km combined length)
4. The Spires - Twelvetrees Range (~40 km combined length)
5. North Star - The Pleiades - Junction Range (~36 km combined length)

The region is cut by the Jane, Gordon, Denison and Maxwell Rivers and is now dominated by the Hydro impoundments of Lakes Pedder (filled in 1972) and Gordon (filled in 1974) (Figures 2 and 3). Elevations of the ranges are generally around 1000 m (Figures 2 and 3).

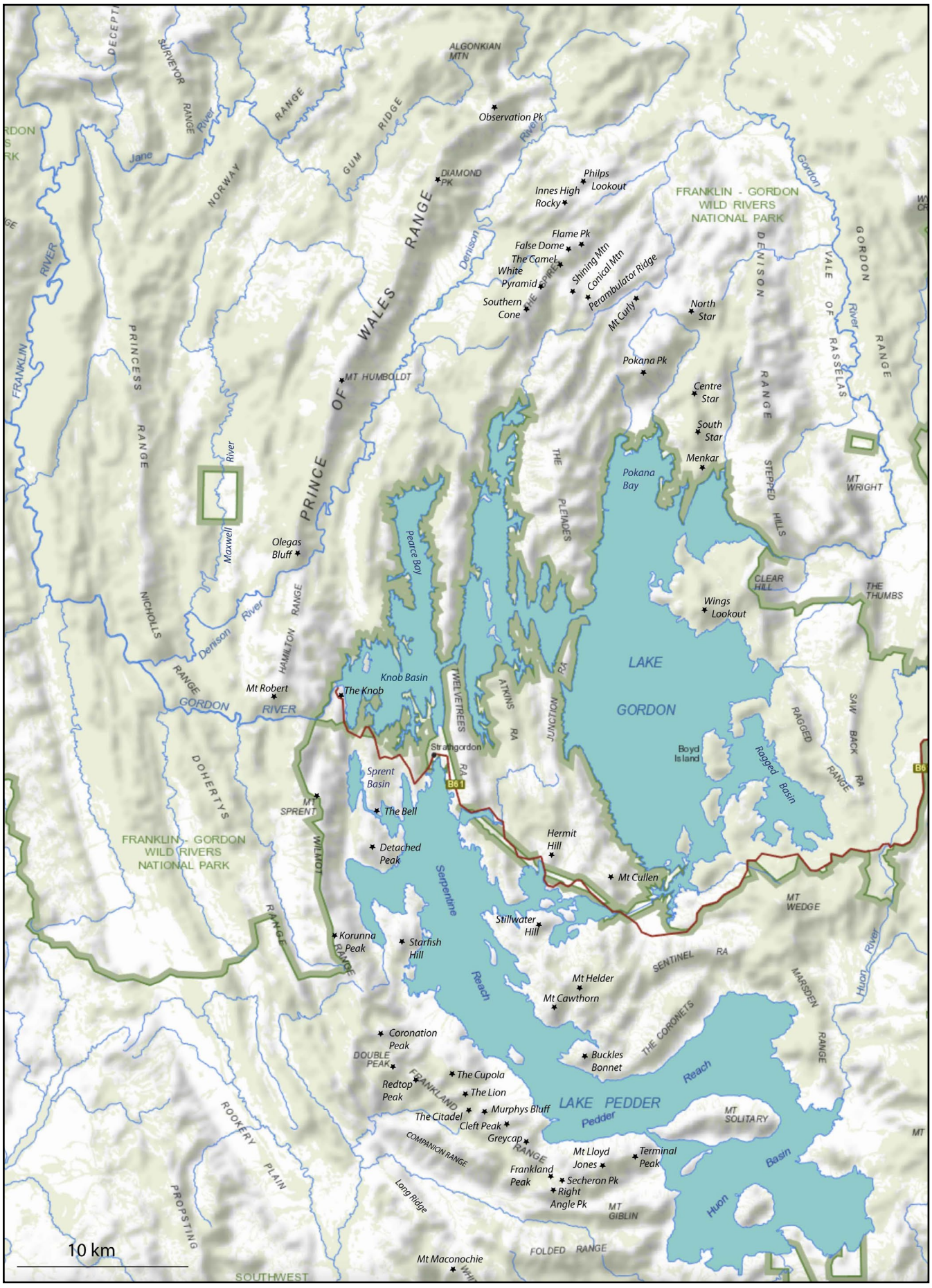

Figure 2. ListMap topographic map of the Eastern Tyennan subdomain showing geographic elements and place names listed in the text.

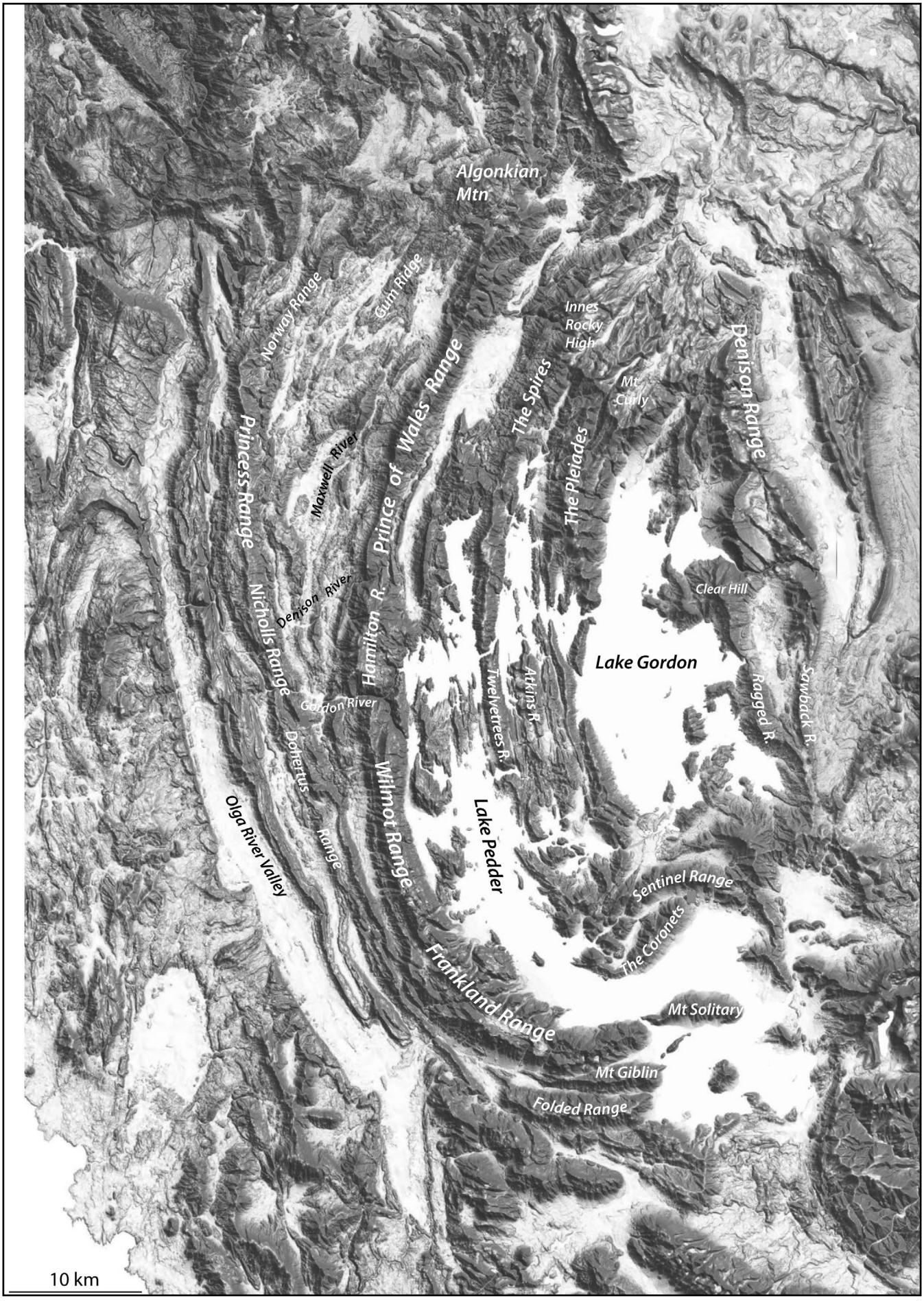

Figure 3. ListMap digital elevation model of the Eastern Tyennan subdomain. The subdomain is defined by long, arcuate ridgelines that show marked curvature towards their southern terminations. Major geographic elements, including Lakes Pedder and Gordon as well as the main ridges, are highlighted.

Peaks along the Prince of Wales Range include Observation Peak (952 m), Diamond Peak (1,066 m), Mount Humboldt (1,069 m) and Olegas Bluff (659 m) at the southern termination. For the Wilmot Range, Mt Sprent (1,059 m) and Koruna Peak (930 m) transitioning into the Frankland Range that includes from north to south Coronation Peak (1,054 m), Double Peak (1,061 m), The Cupola (970 m), The Lion (988 m), The Citadel (929 m), Murphys Bluff (888 m), Cleft Peak (946 m), Greycap (808 m), Frankland Peak (1,083 m), Secheron Peak (1,068 m), Mt Lloyd Jones (982 m) and Terminal Peak (796 m). East of the Prince of Wales Range, The Spires Range from north to south includes Flame Peak (1,122 m), False Dome (1,099 m), The Camel (1,009 m), White Pyramid (1,075 m) and Southern Cone (1,028 m). Between the Spires and North Star - The Pleiades ridges a series of peaks include from west to east: Shining Mountain (1,110 m), Conical Mountain (1,124 m), Mt Curly (1,065 m) and Pokana Peak (1,127 m). To the north of these are Innes Rocky High (1,083 m) and Philps Lookout (854 m).

2.2 Lithology and litho-tectonic units

The Eastern Tyennan region (Figure 4) consists of regionally metamorphosed phyllite, schistose quartzite, massive quartzite, garnet schist and amphibolite (Boulter, 1978; Brown et al., 1989, p. 12-31; Calver et al., 1990, p.13-18). It is dominated by quartzite and quartz-dominant to phengite-dominant phyllite. Quartzite bands range in thickness up several tens of metres. The quartzite normally occupies the north-trending ridges with phyllitic rock occupying the intervening valleys and lower ground.

Areas of interlayered dolomite, calcareous-dolomitic phyllite, quartz-mica and mica-quartz phyllite occur in the upper reaches of the Pokana River, north of Shining Mountain, the lower western and eastern slopes of the Northern Pleiades and north of North Star (Brown et al., 1989). Dolomite and dolomitic phyllite also occurs in the bed of the Dension River between the Nicholls and Hamilton Ranges and throughout the Maxwell River valley between the Princess Range and the Prince of Wales Range (Dixon, 1992). The high-grade schist and amphibolite occur as isolated remnants in fold cores in the Strathgordon - Twelvetrees Range - Atkins Range area, as well as an erosional outlier at Algonkian Mountain (Figure 4). Construction of structural profiles has enabled establishment of a stacking order (Figure 4).

In map projection, the Eastern Tyennan subdomain has a ~75 km length and ~35 km width and is made up of three major map components (Figure 4):

A. On the west, a triangular-shaped wedge of low-grade dolomitic phyllite and dolomite (Scotchfire metamorphic sheet; Spry, 1963; Dixon, 1992) occurs within a south-closing macro-fold with an east plunge and reclined geometry. This sheet is continuous into the Central Tyennan subdomain (Gray and Vicary, 2021b).
B. On the east, an isoclinally folded, thin quartzite sheet with S-vergent asymmetric fold pairs is preserved within long ridgelines that extend for 20-40 km. The quartzite is overlain by an eroded, discontinuous, thin high-grade sheet which crops out at the Bell Basin near Strathgordon, as an outlier at Algonkian Mountain (orange units in Figure 4), and as a large pod of amphibolite east of the Twelvetrees Range (magenta unit on Figure 4). These units combined form this part of the Tyennan allochthon.
C. On the east flank are an overlying External Zone "lid" of fault-emplaced oceanic mélange (Ragged Basin Complex), ultramafics (Adamsfield Ultramafics), and low-grade Proterozoic meta-sedimentary sequences (Clark Group and Harrison Opening Formation) (Crawford et al., 2014; Everard and Calver, 2014). This eastern region shows structural intercalation between the low-grade Proterozoic meta-sedimentary sequences (e.g. Wings Quartzite) of the middle allochthon, and the mélange and ultramafics of the upper allochthon. The relationship between the low-grade, relatively undeformed quartzite units to the more strongly deformed quartzite typical of the Tyennan domain remains unclear and is now largely hidden under Lake Gordon.

2.3 Nature of the Layering, Foliations and Lineations

The schists, quartzites and phyllites of the Eastern Tyennan region show varying degrees of deformation, from relatively undeformed with preserved bedding features (So), to highly deformed rocks with high-strain fabrics typified by strong to intense foliation and transposition layering/foliation (Sm), rodding fabrics within the transposition layering (So/Sm), mesoscopic isoclinal folds, rootless isoclinal fold pairs, and multiple crenulation cleavages (Scc).

Quartzites are white or pink, banded and schistose. The more massive quartzites appear less deformed and commonly preserve cross bedding. Thinner quartzite bands appear as pinch-and-swell structures (boudins) particularly where interlayered with quartz-mica and mica-quartz phyllite (McClenaghan and McClenaghan, p.66-79, in Brown et al., 1989). The phyllites tend to be strongly deformed with a distinct foliation.

There are six types of layering and foliation:

1. Bedding So: relatively undeformed bedding.
2. Bedding-parallel foliation So/Sm: compositional banding sub-parallel to a strong to intense foliation that is folded by recumbent isoclinal folding.
3. Intense foliation (Sm): the dominant foliation that is axial surface to the major recumbent isoclinal macro-folds. Associated with this layering is a marked rodding fabric within the Sm layering. This is the regional foliation that envelopes macro- to meso-fold "pods". The pods occur at all scales.
4. Crenulation cleavages (Scc): associated with development of transposition layering in the basal high-strain zones and to younger folding events.

5. Shear Band foliation (Sb) or S-C' fabrics: as a form of extensional crenulation cleavage that reflects shear-induced, foliation-oblique late-stage flattening. These zones are essentially secondary shear zones that record the overall shear sense and/or emplacement direction.
6. Spaced cleavage (Scl): a younger Devonian cleavage that overprints all three foliations listed above.

2.4 Previous mapping

Reconnaissance investigations carried out in the late 1950s and 1960s by the Lyell Electrolytic Zinc (Sampey, 1957; Scott, 1959, 1960) and BHP (Hall et al., 1969) provided a basic geological framework for the Eastern Tyennan subdomain as part of a broad assessment of the Precambrian rocks of southwest Tasmania (Figure 5).

The earliest structural investigations and mapping were undertaken in the late 1960s and the early 1970s (Figure 5) during the early stages of the Gordon Dam site-investigation and construction with the new access of the Gordon River/Strathgordon Road into the middle stretches of the Gordon River completed in 1967. Powell (1969) undertook structural analyses in July and August 1967 on the southern side of the proposed Gordon Dam site as part of contract work for the Hydro-Electric Commission of Tasmania. Boulter (1974, 1978) undertook structural mapping of the Wilmot and Frankland Ranges from April 1971 over a 2-3 year period culminating in a PhD (Boulter, 1978). Williams (1973, 1976) undertook structural mapping in the McPartlans Pass area as part of a University of Tasmania BSc Hons thesis.

This early structural mapping was accompanied by Tasmanian Geological Survey mapping of the Huntley 1:50,000 Series map sheet (Brown et al., 1982) and the Pedder 1:50,000 Series map sheet (Turner et al., 1985). Mapping in both areas was started in 1973 and completed in the summer of 1975-1976 prior to the flooding of Lakes Gordon and Pedder, with map publications in 1985, and Explanatory Notes published in 1989 and 1990 (Brown et al., 1989; Calver et al., 1990).

Dixon (1992) and Kiernan (1995) described and mapped the distribution of the Proterozoic Jane Dolomite in the Maxwell and Gordon River areas.

More recently, Meffre et al. (2021) undertook a reconnaissance traverse along 1) the south side of Hermit Narrows, and 2) part of the Frankland Range including Cleft Peak, The Citadel and Murphys Bluff. Port (2023) completed a BSc (Hons) project on the Hermit Narrows and Strathgordon area.

2.5 Early structural investigations and significance

The first structural investigation undertaken by Chris Powell (1969) demonstrated poly-deformation with: 1) three major phases (D1, D2 and D3) and a later minor phase of deformation (D4) recognised, and 2) the fold phases were coaxial with general low plunges to the north (Powell, 1969; Boulter 1974, 1978; Williams, 1973, 1976; McClenaghan and McClenaghan, in Brown et al., 1989).

Powell (1969) undertook structural analysis in newly developed exposures at the Gordon Dam site for the Tasmanian Hydro. Boulter (1978) subsequently revised Powell's classification based on more extensive structural mapping of the Wilmot and Frankland Ranges, including the Gordon Dam exposures (Figures 6 and 7).

Boulter (1978) recognised early (D1) east facing, recumbent folds with Z-asymmetry (looking north) suggesting overriding from the west or southwest (Figures 6 and 7). These early recumbent folds were considered fold-nappes with extensive lower limbs and limb inversions in the order of ~5 km. Boulter argued they were comparable to Alpine nappes with bulk translation in slices bounded by discrete thrust surfaces (high strain zones) but that they lacked an Alpine-style root zone.

Boulter (1978) noted a general decrease in strain from the north, in the Wilmot and the northern Frankland Ranges, to the south in the southeast Frankland Range. Observations include:

- Major D1 folds have strain distributions matching concentric shearing strains within layering on fold limbs, accompanied by an overall homogeneous flattening (Z shortening) of 25 % (based on strain analysis of sedimentary fabrics and cross bedding).
- Variation in the stretching direction (X) relationships to macro-isoclinal fold hinges through the pile:
  - ◊ Below the thrust in the eastern Frankland Range the X direction is about 30° away from the major fold axes.
  - ◊ Above the thrust the stretching lineation (X-direction) is at high angle (~ 90°) to major isoclinal fold axes.
  - ◊ North of Cleft peak: S1 is parallel to bedding.
  - ◊ South of Cleft Peak: S1 is at an angle to bedding and sedimentary structures are better preserved.
- D2 folds have consistent sense of asymmetry throughout the region and are coaxial with F1 folds, suggesting a continuous deformation/tectonic regime from D1 to D2.
- D3 folds have amplitudes close to 1 km but locally generally less than 10 m. They largely occur in flaggy and micaceous quartzite, with almost no effects in pure quartzite sequences.
- D3 folds are almost coaxial with D1 and D2 folds but show opposite sense of overriding.
- Apparent conjugate relationship between axial surfaces of D2 and D3 folds, but overprinting is always consistent and the nature of the microfabrics is quite different.
- D4 folds are major upright folds with little or no plunge. The largest D4 fold has an amplitude of ~ 4 km.
- Strain in D4 increases towards D4 fold hinges.

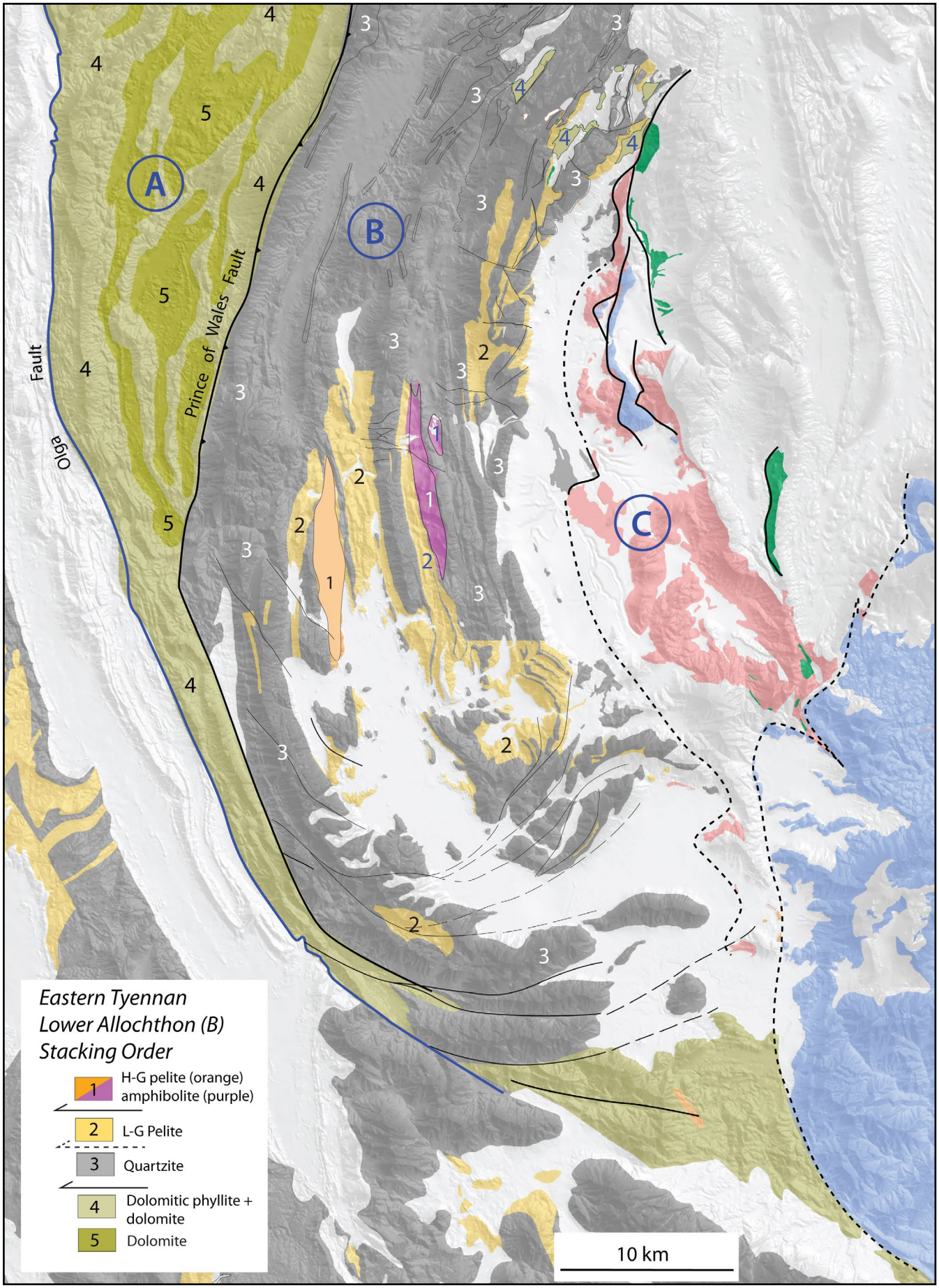

Figure 4. Geological map of the Eastern Tyennan subdomain showing the distribution of the litho-tectonic units and the stacking order from point to point based on the regional folding relationships, namely lowest units in anticline cores versus uppermost in synclinal cores. The stacking order is shown in the inset lower left. H-G: high grade. L-G: low grade. The three major map components are labeled:

A. The Scotchfire Metamorphic sheet (lithotectonic units 4 and 5) or parautochthon;
B. The Tyennan allochthon (units 1, 2 and 3); and
C. A composite of structurally intercalated upper allochthon (External Zone), consisting of Early Cambrian oceanic mélange (pink) and ultramafic rocks (green), and Proterozoic low-grade meta-sedimentary rocks (blue) of the middle allochthon.

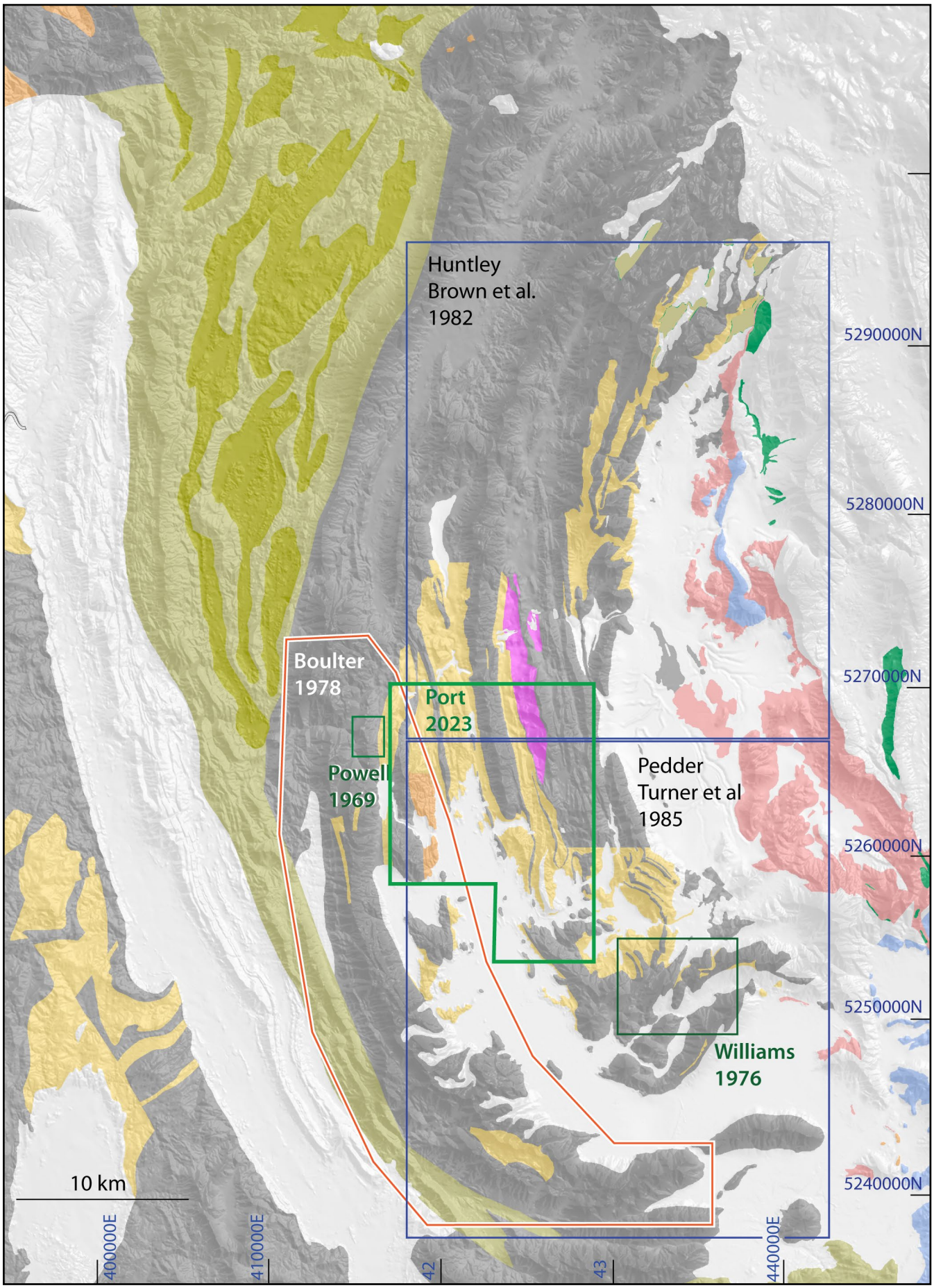

Figure 5. Index map of structural data sources for the Eastern Tyennan domain. Geological mapping was initiated in the late 1960s and 1970s with the Lake Gordon - Lake Pedder Hydro electricity schemes.

University of Tasmania PhD Thesis by Boulter (1978) and an Honours Thesis by Williams (1976) at McPartlans Pass followed an initial structural investigation by Powell (1969) utilising the new Gordon Dam site cuttings and excavations. Map base is the Mineral Resources Tasmania 1:25,000 and 1:250,000 digital atlas series. The Huntley and Pedder 1:50,000 Map Series were completed by the Tasmanian Geological Survey in 1989 (Brown et al., 1982) and 1990 (Turner et al., 1985). Recent mapping by Port (2023) also shown.

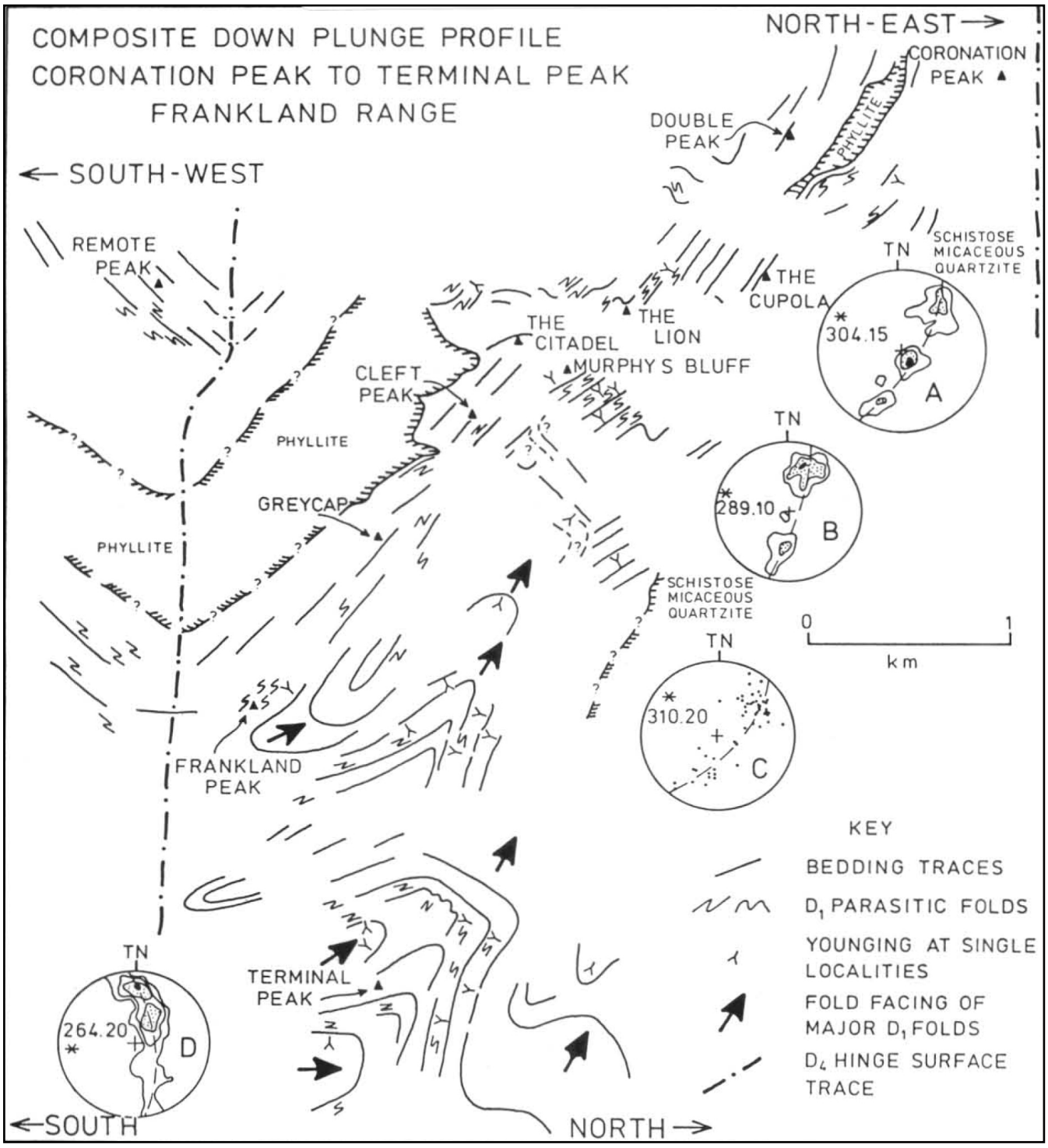

Figure 6. Composite down-plunge profile of the Frankland Range (Figure 2, Boulter, 1990) showing the relationships between the early F1 folds, the positions of phyllite and micaceous quartzite, F1 fold facing and younging. Stereographic projections show poles to bedding (So/Sm) for different segments of the Frankland Range: A) Coronation Peak to Double Peak. B) Redtop to Cleft Peak. C) Cleft Peak to Frankland Saddle. D) Frankland Saddle to eastern end of the Frankland Range.

Episodic or continuous deformation?

- Stepwise process of folding, translation and strain during D1 suggested the transition from D1 to D2 is not continuous.

Alpine-style recumbent folds were argued by Spry (1963) for the Frenchmans Cap and Raglan Range areas and documented by Boulter (1978) for the Wilmot-Frankland Range areas.

2.6 Structural observations from geological survey mapping of the Huntley and Pedder 1:50,000 map sheets.

Work by Marcus and Jean McClennaghan and Nic Turner on: 1) the Huntley sheet (Brown et al., 1989, p.66-79) provided detailed structural interpretations through the Twelvetrees, Atkins, Junction and Pleiades Ranges that extended the structural understanding of the northeastern parts of the Eastern Tyennan subdomain (see Section 5);

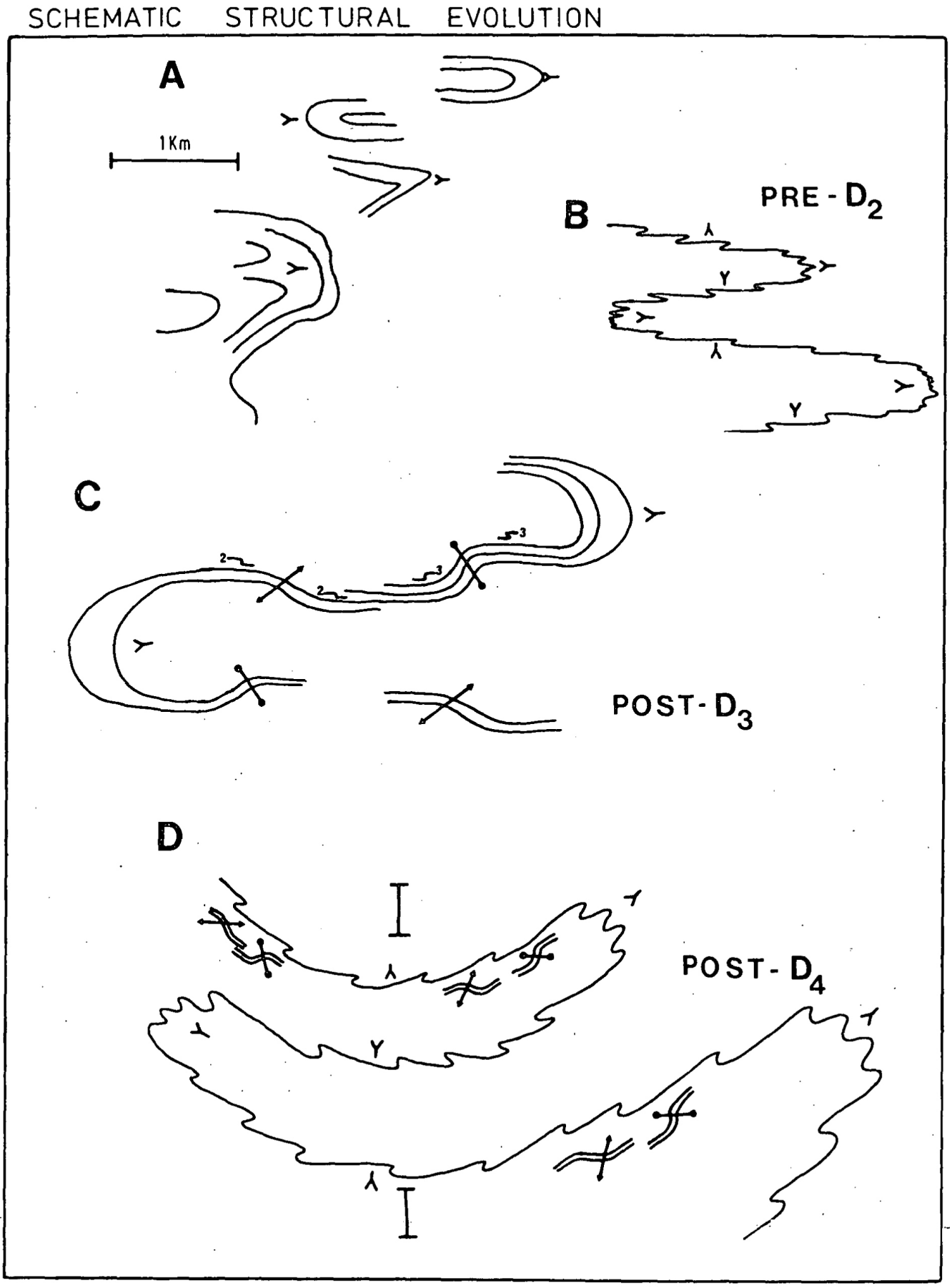

Figure 7. Boulter (1978, Figure 8.3) structural sequence based on field structural studies of the Wilmot-Frankland Ranges. A and B show tight to isoclinal folds that Boulter considered D1 (pre-D2), with conjugate box-like folding in D3 and upright, open folding as the D4 event

and 2) the Pedder map sheet (Calver et al., 1990, p.62-80) provided detailed structural interpretations of White Spur and the Twelvetrees Range, and through the Lake Pedder area including The Hermit, Mt Cullen, Stillwater Hill, Mt Helder, Mt Cawthorn, the Sentinel Range, The Coronets and Mt Solitary.

2.7 Metamorphism and Metamorphic Petrology Investigations and Significance

Most of the Eastern Tyennan domain is low-grade greenschist facies metamorphism with isolated belts or pockets of garnet schist and amphibolite (Boulter, 1978; Boulter and Råheim, 1974; Calver et al., 1990). Named as the Strathgordon Metamorphic Complex (Turner, 1989a; Chmielowski, 2009), the overall lower metamorphic grade and poor preservation have given this complex downgraded significance. It was not treated or discussed in Meffre et al. (2000) and given restricted occurrence to the core of south-plunging synform west of Strathgordon (Calver et al., 1990; Chmielowski, 2009).

The presence of garnet bearing rocks and structurally intercalated amphibolite (Figure 8) has been used to designate areas of high-grade metamorphism in the Tyennan Domain (Meffre et al., 2000). In the Eastern Tyennan subdomain garnet schists have been recorded at:

1. The area east of Detached Peak (Boulter, 1978, Figure 9)
2. The Hamilton Range (Scott, 1959)
3. Algonkian Mountain (Turner, 1990)
4. Huon River Valley headwaters, south of Lake Pedder (Hall et al., 1969)

Amphibolite occurs east of the Twelvetrees Range as a large pod (~15 km length and ~1.5 km maximum width) associated with, and enveloped by, pockets of sodic, blue amphiboles in haematitic banded ironstones from the Atkins Range and the Gordon River north of the Atkins Range (see blue dots and stars, Figure 8). The amphibolite crops out as strongly foliated, dull green schist containing albite, epidote, actinolite and chlorite. Details of the petrography, chemistry and fabric/mineral growth relationships are provided in Brown et al. (1989, p.14-18).

2.6.1 Metamorphic PT Determinations

The earliest studies on the metamorphism of the Eastern Tyennan domain were undertaken on quartz-chlorite assemblages including garnet by Råheim and Boulter in the early 1970s, as part of University of Tasmania PhD theses, with eventual publications by Råheim (1977) and Boulter and Råheim (1974). Data and PT calculations were also included in theses by Williams (1973) and Boulter (1978). Subsequent studies by Brown et al. (1989) on blue amphibole bearing lithologies from the Atkins Range and the Gordon River north of the Atkins Range provided other PT estimates for the Eastern Tyennan domain.

Mulder (2013, Appendix 7) provides an excellent summary of the earlier work and results, and also provides a revision of the original PT estimates using THERMOCALC on the data of Boulter (1978), Råheim (1977) and Brown et al. (1989). PT estimates have included (Figure 8):

1. 0.1-0.9 GPa and 200-350 °C (lower greenschist facies) based on a quartz-albite-muscovite-chlorite assemblage at McPartlan Pass (Williams, 1973)
2. up to 0.6 GPa and 400-500 °C for the highest-grade, garnet-bearing zone surrounding Detached Peak (Boulter, 1978)
3. 0.3± 0.1 GPa and 400-500 °C using the Si-in-phengite curves of Velde (1967) and garnet stability (Råheim, 1977)
4. 0.4 ± 0.1 GPa at ~500 °C based on the average THERMOCALC PT estimates from garnet and phengite bearing phyllite (Mulder, 2013, p.51-52)
5. ~0.5 GPa and 540 °C (Port, 2023, Appendix D)

The PT estimates of Boulter (1978) and Raheim (1977) used the Si-in-phengite curves of Velde (1967). These data have been updated by Mulder (2013, Appendix 7) using the Si-in-phengite curves of Massone and Schreyer (1987). The revised estimates give minimum pressures of 0.5-0.8 GPa within a temperature range of 400-500 °C (Mulder, 2013, Figure 1).

A pressure estimate >0.7 GPa was obtained by Mulder (2013, Figure 2) for the sodic amphibole from the now submerged Gordon River locality using the Na (B) versus AlIV diagram of Brown (1977). Amphibole compositions from the amphibolites structurally intercalated with schist and quartzite within the Strathgordon part of the "complex" indicate pressures <0.5 GPa (Mulder 2013, Figure 2) matching the pressure estimates from the phengites. The marked pressure difference between the Atkins Range body and the Strathgordon rocks suggests either: 1) two discrete metamorphic sheets within the Strathgordon Metamorphic Complex; or 2) that the interpreted sheet is composite and represents an amalgam of metamorphic slices (cf. Mulder, 2013, Appendix 7, p.55).

2.6.2 Metamorphic Textural Relationships

Boulter (1978) made the following textural observations:

1. Garnet mostly occurs with skeletal form
2. Small, inclusion free garnets are wrapped by foliation S2 (either Sm or Scc) and have pressure shadow zones
3. Albite porphyroblasts have straight inclusion trails

This textural evidence suggests the peak of metamorphic crystallisation in the Eastern Tyennan subdomain occurred immediately before and during the second deformation phase D2, with small garnets mainly pre-D2, and large garnets pre- to syn-D2 (Boulter, 1978). Chemical variation in phengite grains from S1 to S2 is gradual, reflecting continuous metamorphic changes, whereas fabrics S3, S4 and S5 suggest fabric development under lower PT conditions (Boulter, 1978; Boulter and Raheim, 1974). Structurally, D1 gives pronounced tectonic fabrics almost everywhere parallel to bedding/compositional layering, and isoclinal D2 folds generally have an axial surface crenulation cleavage fabric.

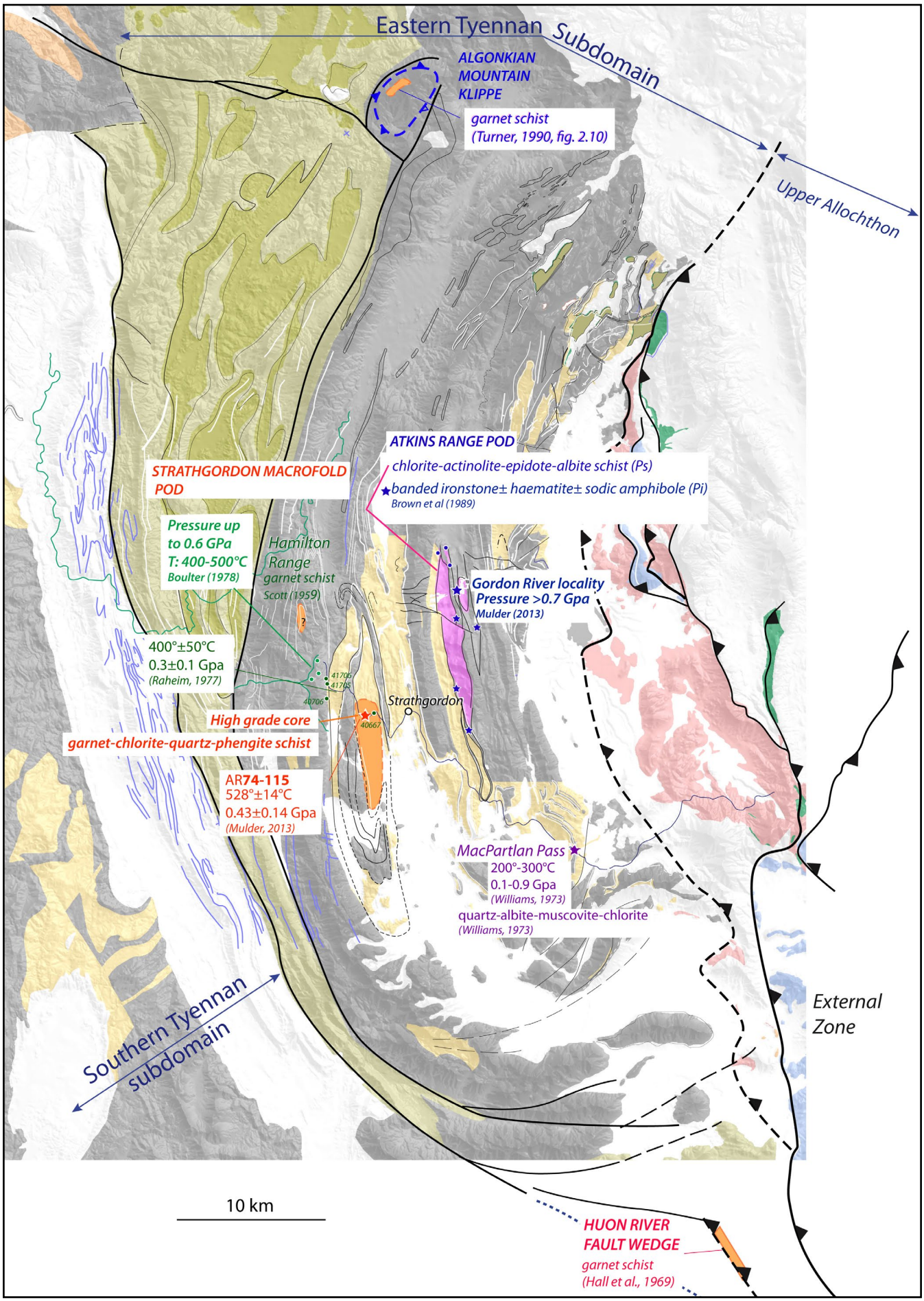

Figure 8. Eastern Tyennan subdomain metamorphic map showing the distribution of garnet-bearing rocks (orange) and location of samples utilised in PT estimates of the Strathgordon area rocks. The base map is a modified Mineral Resources Tasmania 1:250,000 map sheet. The stars indicate the locations of the various assemblages in coloured text matching the star colour.

Stars = PT estimate sample; Dots = Other notable high grade samples.

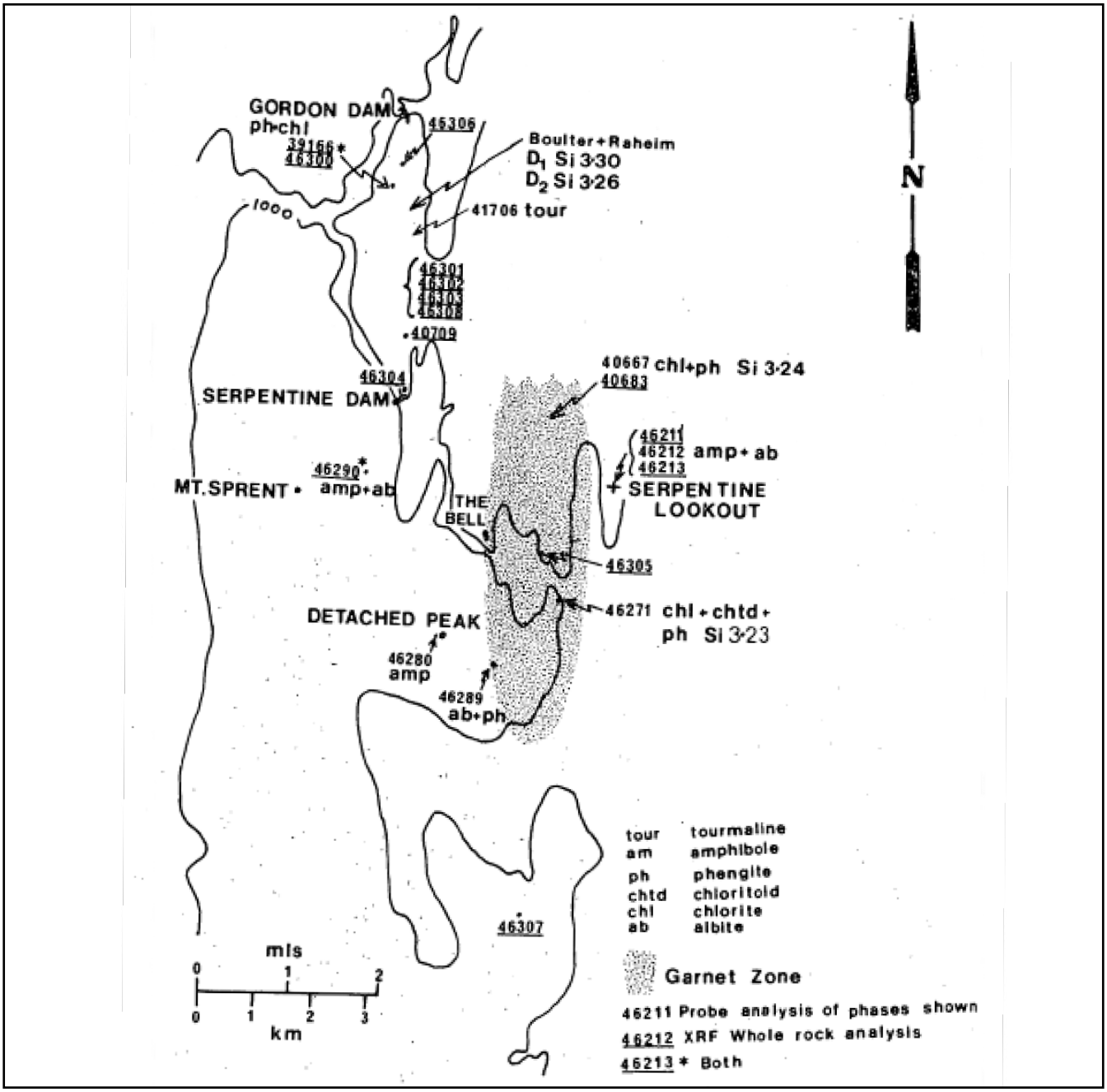

Figure 9. Metamorphic specimen locality map from Boulter (1978, Figure 5.1) with the stippled area east of Detached Peak showing the region of garnet-bearing rocks.

2.8 Current Work

This synopsis and analysis of the structure of the Eastern Tyennan is based on 1) bushwalker photographs, 2) photographs and field measurements by Sebastien Meffre and David Green of Mappes Cove and the Lion-Citadel region of the Frankland Range, 3) photographs from Grant Dixon, 4) traverses by the authors along the Gordon River Road from the Sentinels to the Gordon Dam site, the Twelvetrees Range, shorelines of Lake Pedder along Bell Narrows and Bell Basin, and the shoreline of Wilmot Bay north Starfish Hill, 5) analysis, interpretation and compilation of all existing data primarily from Clive Boulter's University of Tasmania PhD Thesis (Boulter, 1978) and the Explanatory Reports for Huntley (Sheet 73; Brown et al., 1989) and Pedder (Sheet 80: Calver et al., 1990).

Bushwalker photographs were accessed from:

1. david-noble.net

i. A Traverse of the Frankland Range, Tasmania - January 2002
ii. Prince of Wales Range Traverse, Tasmania - January 1981
iii. A Traverse of the Wilmot and Frankland Ranges, Tasmania - Dec-Jan 1980
iv. Traverse of the King William Range, Spires and Prince of Wales Range, Tasmania - Jan-Feb 1977

2. rockmonkeyadventures.worpress.com-Becca Lunnon

i. Hamilton Range: 1-5 March 2023
ii. The Pleiades: 14 February 2021
iii. The Prince of Wales Range: 16-25 February 2020
iv. Terminal Peak, Lloyd Jones and Secheron: 22-24 December 2019
v. The Spires: 16-24 January 2016
vi. The Frankland Range: 26-31 January 2013

3. Wandering Foxbat U-Tube videos of flights through the area, including:

i. Highlights of W and SW Tasmania/Conical Mountain traverse

ii. Side View Highlights: Conical Mountain-Mt Anne-Lake Pedder-Federation Peak-Bathurst Harbour

The bushwalker ridgeline photographs were used to construct structural profiles along individual ranges and then assembled to make regional structural profiles across parts of the Eastern Tyennan subdomain.

All measurements/orientations cited in the text are true unless stated. Structural data collected by the authors is presented in Appendix 4.

All map grids and grid references in the text have a GDA94 datum with MGA coordinates in Zone 55.

3.0 EASTERN TYENNAN SUBDOMAIN GEOLOGY OVERVIEW

The Eastern Tyennan region (Figure 10) consists of regionally metamorphosed phyllite, schistose quartzite, massive quartzite, garnet schist and amphibolite (Boulter, 1978; Brown et al., 1989, p. 12-31; Calver et al., 1990, p.13-18). It is dominated by quartzite and quartz-dominant to phengite dominant phyllite. Quartzite bands range in thickness up several tens of metres. The quartzite normally occupies the north-trending ridges with phyllitic rock occupying the intervening valleys and lower ground.

Areas of interlayered dolomite, calcareous-dolomitic phyllite, quartz-mica and mica-quartz phyllite occur in the upper reaches of the Pokana River, north of Shining Mountain, the lower western and eastern slopes of the Northern Pleiades and north of North Star (Brown et al., 1989). Dolomite and dolomitic phyllite also occurs in the bed of the Dension River between the Nicholls and Hamilton Ranges, and throughout the Maxwell River valley between the Princess Range and the Prince of Wales Range (Dixon, 1992; Gray et al., 2024).

The high-grade schist and amphibolite occur as isolated remnants within interpreted fold cores in the Strathgordon - Twelvetrees Range - Atkins Range area as well as an erosional outlier at Algonkian Mountain (Figure 10). The high-grade (H-G) pelitic rocks ± amphibolite have limited preservation within the Eastern Tyennan subdomain. They occur:

1. as interpreted infolds within the cores of upright, north-south-trending, doubly-plunging synformal F3 folds;
2. and as a klippe at Algonkian Mountain (Figures 10 and 11).

3.1 Map Pattern and Regional Relationships

The Eastern Tyennan subdomain is a fault-bounded, arcuate, structural domain with curved north and south lateral terminations (Figures 10, 11 and 12). The western boundary of the subdomain is defined by the arcuate Olga Fault, an inverted Late Cambrian extensional fault. The eastern boundary is a complex series of syn- to post-obduction thrust faults that form a "lid" of ophiolitic mélange, ophiolite (Upper Allochthon) and associated low-grade Proterozoic meta-sediments to the Proterozoic quartzite-pelite sequence that defines the Lower Allochthon or Internal Zone (Figure 12).

The Eastern Tyennan subdomain has a north-south-trending, elongated, ovoid-shaped "core" mirroring the arcuate form of the Olga Fault (Figures 12 and 13). This is a zone of polydeformation dominated by upright regional F3 folds that refold the early-formed F1/F2 macro-folds (Figure 13). It is typified by marked curvature within the So/Sm formlines and a horsetail fault splay system at the southern end. Accompanying this is a transition to lower strain, shown in: 1) the Wilmot to Frankland Range to Terminal Peak (Boulter, 1978); and 2) the Twelvetrees Range to the Coronets/Sentinel Range with a relatively undeformed character. At the northern end there is an apparent transition to higher strain where the main quartzite bands (layers) appear segmented into isolated, elongated pods within and bounded by intensely foliated pelitic units. The Twelvetrees Range thins and tapers northwards into the pods and augen that make up the Spires (Figure 13), with similar changes of the Atkins Range quartzites into the Mt Curly pod or augen.

The mapped distribution of bedding (So) and foliation (Sm) measurements provides a qualitative indicator of deformation intensity throughout the Eastern Tyennan subdomain (compare the distribution in Figures 10 and 11). Where bedding is still preserved (Figure 10) the rocks are relatively undeformed and/or the deformation intensity is least. These areas include the south end of the Frankland Range and The Sentinels-Coronet Peak area. Where Sm is dominant the deformation is strongest, such as in the Strathgordon - Atkins Range region. Many areas show both So and Sm reflecting heterogeneous deformation through the sequence. These areas include the Pleiades - Junction Range and the Mt Helder - Buckies Bonnet - MacPartlan Pass region (Figures 10, 11 and 13).

Another discriminator of deformation within the Eastern Tyennan subdomain is the location of the post-F2 (designated as F3) fold axial surface traces (Figure 12). These highlight areas of tight to isoclinal refolding of the early F2 macro-folds (Figure 13). Domains of different styles and intensity of deformation are shown by the coloured dashed envelopes in Figure 13. These include:

1. Magenta dashed envelope (Figure 13): approximate domain of polydeformation characterised by refolded macro-folds, multiple overprinting foliations and higher strain recorded by the nature and development of the dominant foliation Sm.
2. Orange dashed envelope (Figure 13): domain dominated by macroscale refolding of the early F2 asymmetric fold pairs.
3. Green dashed envelope (Figure 13): domain of dismembered quartzite layers, now preserved as lenticular, spindle-shaped tubes, that commonly contain remnants of the early-formed asymmetric fold pairs. The Spires area is the best example of this deformation style.

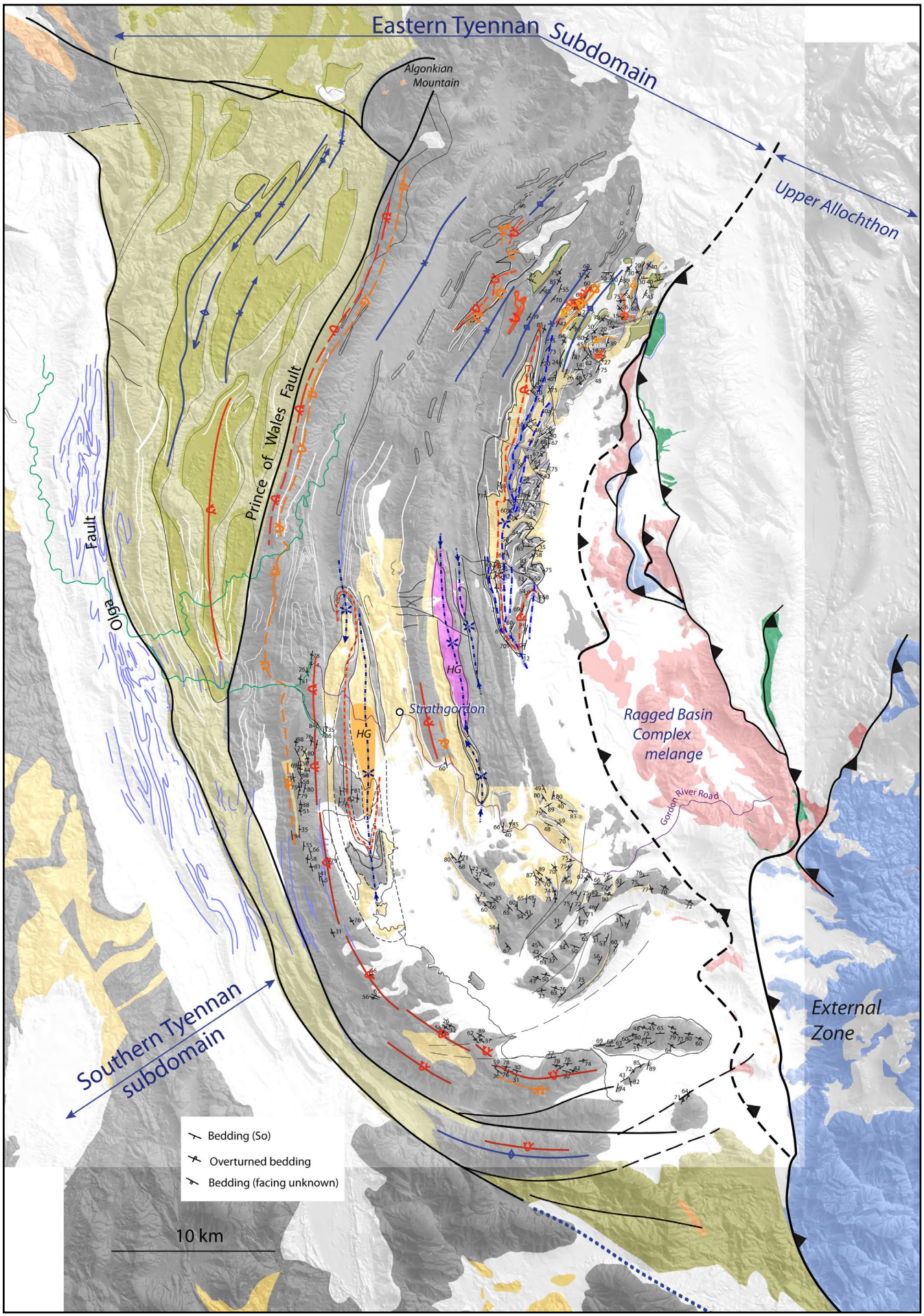

Figure 10. Eastern Tyennan subdomain bedding (So) attitude map showing fault traces, macro-fold axial surface traces (red traces: north and/or west closing; orange traces: south and/or east closing) and bedding strike and dip measurements. The base map is modified from the Mineral Resources Tasmania 1:250,000 and 1:25,000 digital atlas.

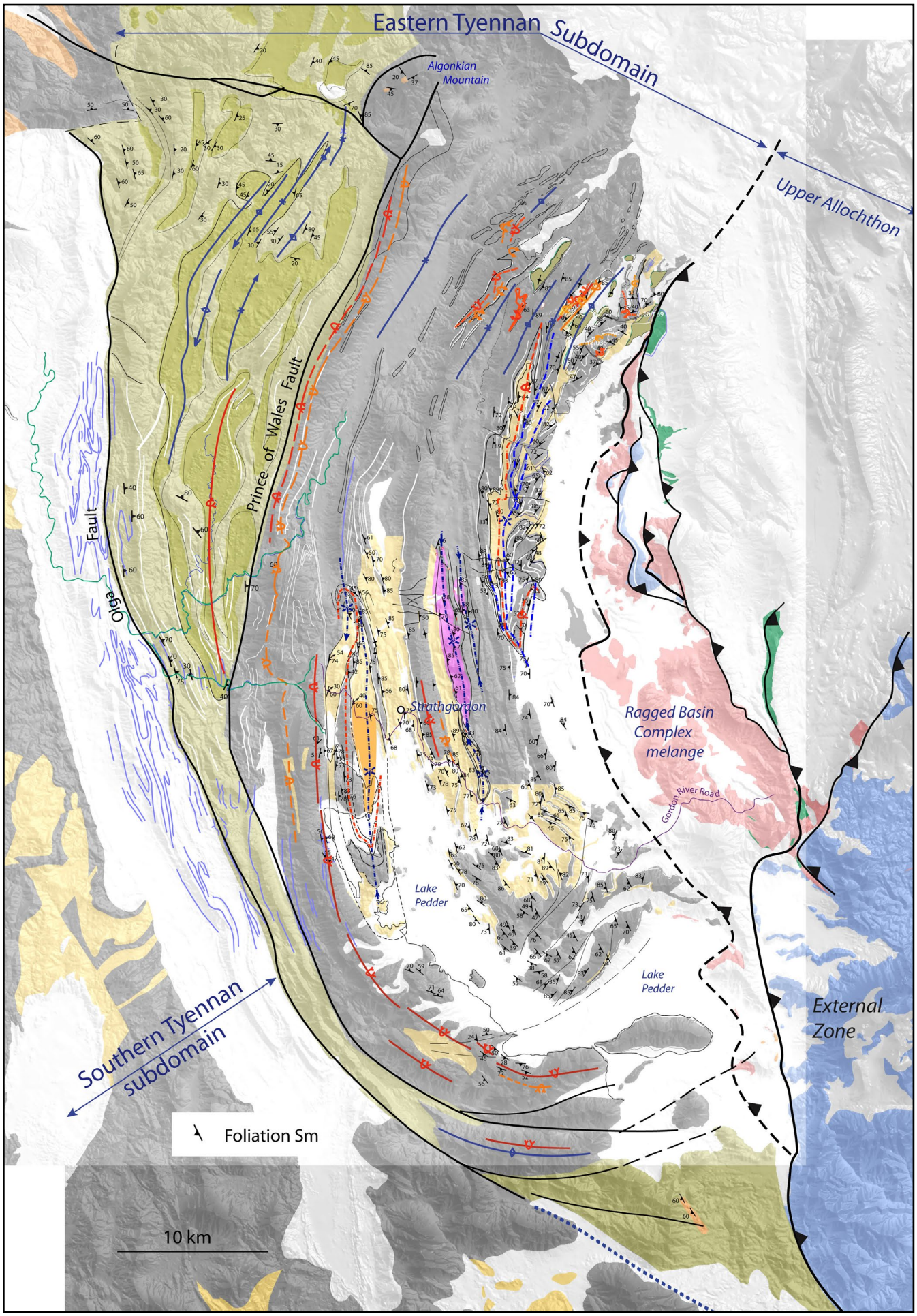

Figure 11. Eastern Tyennan subdomain foliation (Sm) map showing fault traces, macro-fold axial surface traces (red traces: north and/or west closing; orange traces: south and/or east closing) and the foliation strike and dip measurements. The base map is modified from the Mineral Resources Tasmania 1:250,000 and 1:25,000 digital atlas.

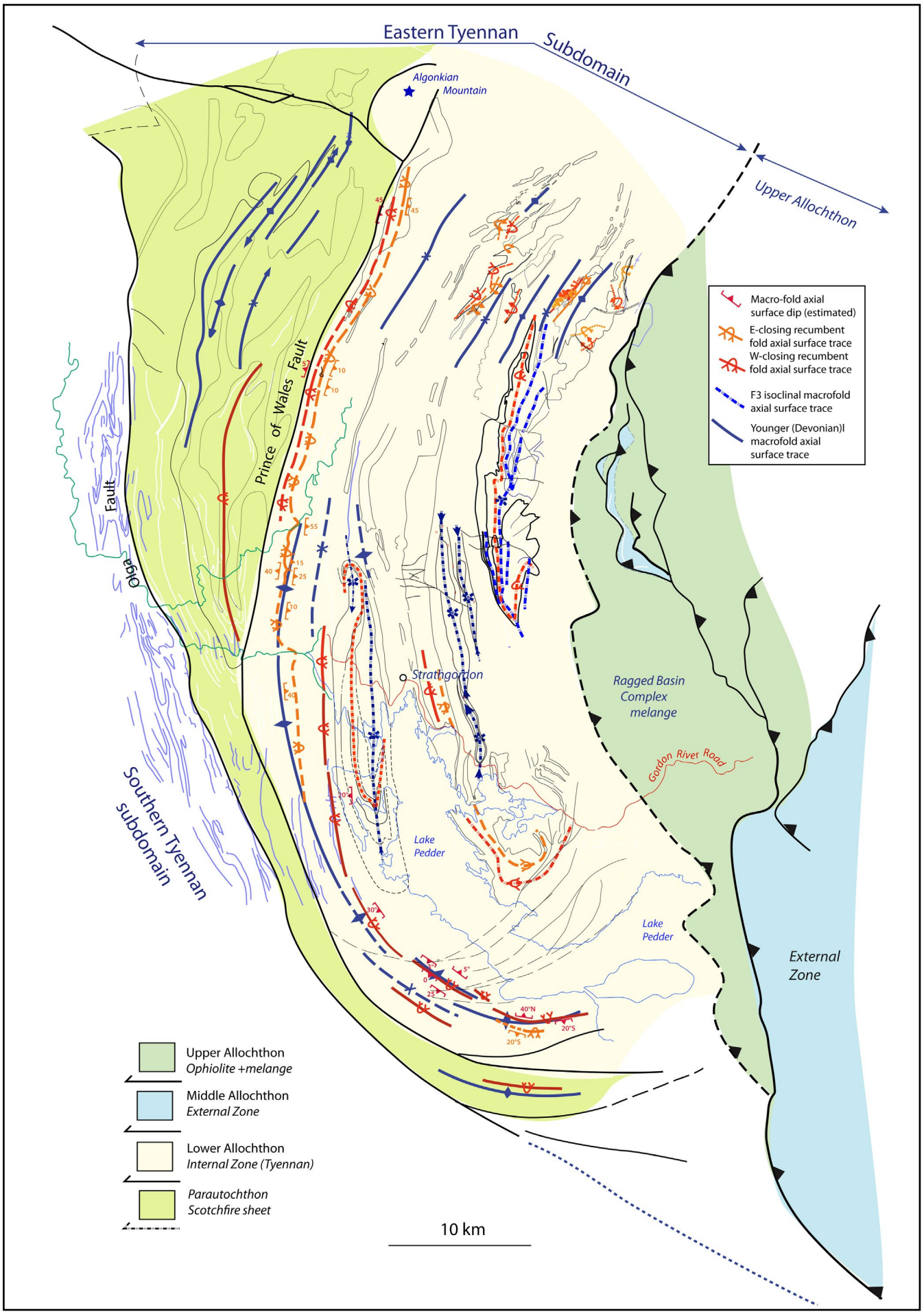

Figure 12. Eastern Tyennan subdomain macro-fold axial surface trace map (red traces: north and/or west closing isoclinal folds; orange traces: south and/or east closing isoclinal folds; blue dashed traces: F3 tight to isoclinal folds; blue traces: younger Devonian fold axial surface traces). The orange and red axial surface traces are coupled, asymmetric isoclinal macro-fold pairs. Macro-fold axial surface strike/dips are also shown. These have been interpreted from the various photo profiles for each of the quartzite dominated mountain ranges.

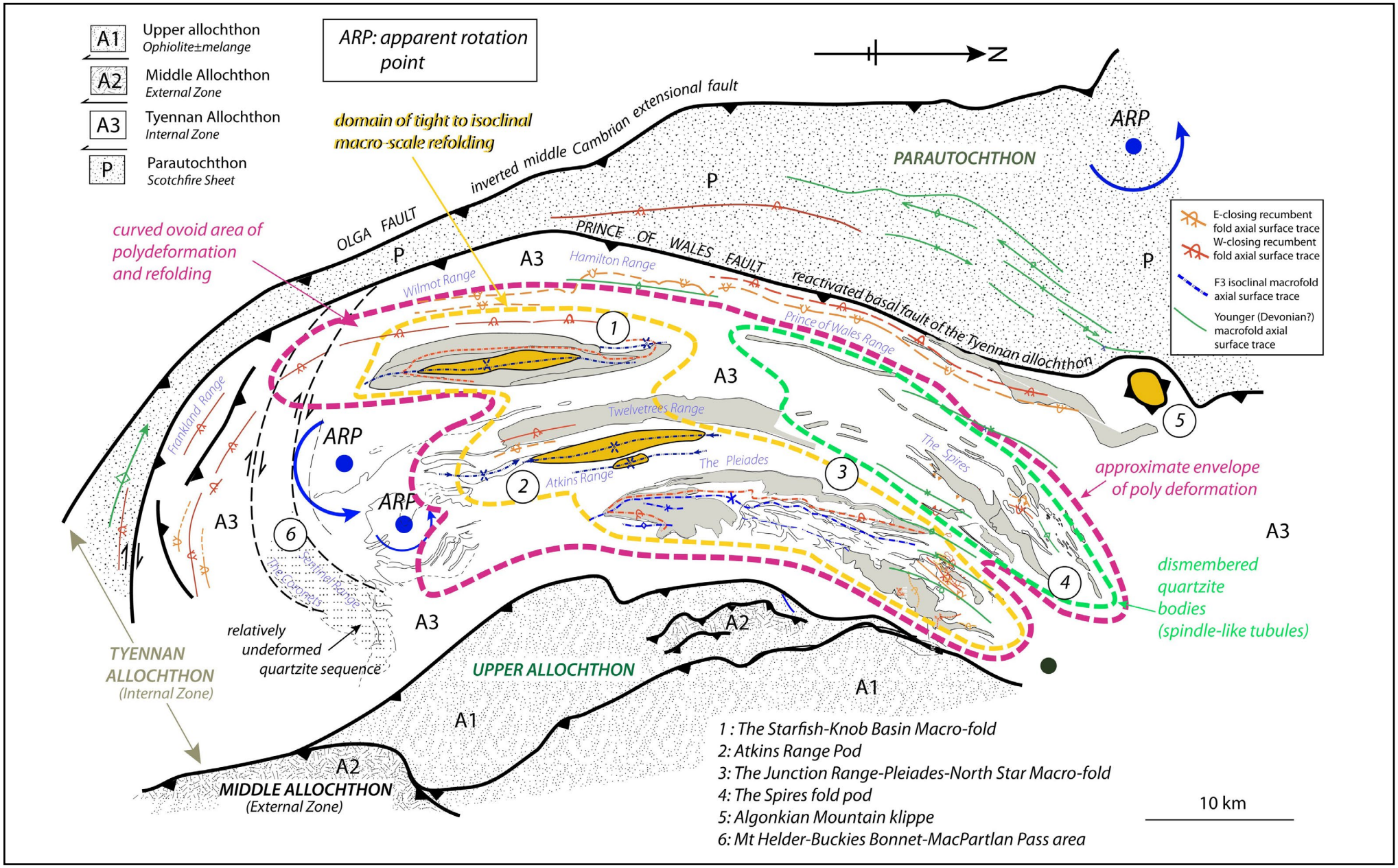

Figure 13. Rotated, longitudinal, simplified structural map of the Eastern Tyennan subdomain showing the subdomain structural character and major structural elements. Tectonic stacking order is shown on Upper left. The magenta dashed envelope outlines the interpreted core of polydeformation. The high-grade (H-G) rocks, including amphibolite, are shown in orange.

In summary, the Eastern Tyennan subdomain shows partitioned deformation that has some similarities to, but also contrasts with, the adjoining Central and Southern Tyennan subdomains.

3.2 Major Structural Elements of the Eastern Tyennan Subdomain

The major structural elements of the Eastern Tyennan subdomain include (Figure 14):

1. A tight to isoclinal, regional macro-fold (Maxwell River Valley macro-fold) with reclined geometry in dolomite and dolomitic phyllite (Scotchfire Metamorphic sheet or equivalent) as part of the lowest sheet or parautochthon (Element 1, Figure 14).
2. Isoclinal macro-fold pair in quartzite exposed as isolated hinge pairs in the successive ranges (Figures 14 and 15), including the:
    - Prince of Wales - Hamilton Range (Element 2, Figure 14) - Wilmot Range - Frankland Range fold pair (Element 3, Figure 14).
    - The Spires (Element 6, Figure 14) - Twelvetrees Range - Trappes Hill - Stillwater Hill - Mt Helder fold pair (Element 5, Figure 14).
    - Sentinel Range - The Coronets fold pair, possibly part of the upper low-grade allochthon (the External Zone of Berry, 2014).
3. H-G pelite ± amphibolite pods/augen as infolds or synformal keels bounded by zones of intense foliation Sm (Figures 14 and 15). These include:
    - Bell Basin - The Starfish keel that closes out in the Denison Valley to the north (Element 4, Figure 14).
    - Atkins Range amphibolite body (Element 7, Figure 14).
4. H-G pelite klippen at Algonkian Mountain (Element 10, Figure 14).
5. The Junction Range - Pleiades fold system an ovoid, doubly terminating and plunging macro-sheath fold in the eastern part of the subdomain (Element 8, Figure 14 and Figure 15).
6. A structural core as a polydeformed internal domain defined by overprinting, multiple cleavages and major north-south-trending, upright regional F3 folds that refold the early formed F1/F2 folds (magenta dashed polygon shown in Figure 13). Structural relationships in the core typify development in rotational shear (Gray et al., 2024).
7. A stacking of sheets that has uppermost sheets on the east (Upper Allochthon and External Zone) and the structurally lowest sheet on the west (parautochthon) (Figure 15). Wedged between is the Lower Allochthon (the Tyennan sheet or Domain). Each of the sheets has a distinct internal structure (Figures 14 and 15).

3.3 Early Fold Axis (FA) Pattern

Fold axis data to define the early isoclinal fold axis pattern (Figure 16) is limited to measurements from the Huntley and Pedder 1:50,000 mapsheets (Brown et al., 1982; Turner et al., 1985), PhD mapping in the Wilmot and Frankland Range (Boulter, 1978) and data collected by the authors along the Gordon River Road. Macro-fold fold axis determinations were determined from π and β plots of So, So/Sm and Sm data in the hinge areas of these folds from the various sources.

The early fold axis trend map (Figure 17) highlights a pattern where the dominant fold axis trends are sub-parallel to the regional structural strike. Fold axes mirror the ridgeline trends dominated by quartzites, noticeably following the curvature of the southern part of the Frankland Range.

A subset of fold axes are at higher angles to the strike trends (Figure 16) and show an approximate east-west pattern across the Maxwell River Valley macro-fold, parts of the synformal H-G keels of F3 macro-folds in the Eastern Tyennan subdomain "core" (The Starfish-Knob Basin macro-fold pod and the Atkins Range pod) and the southern nose of the Junction Range - Pleiades macro-fold. Macro-fold axes along the eastern side of the Pleaides swing to the northeast towards North Star (Figure 17).

3.4 Early Lineation (Lm) Pattern

Mineral/stretching lineation (Lm) measurements collected by the authors are limited to the Strathgordon area along the Gordon River Road and around the shores of Lake Pedder (Figure 18a). Previous workers have not recorded the mineral stretching lineation Lm.

The mineral lineation shows three apparent trends and/or groupings (Figure 18). This includes a northeast trend, a southeast trend and a north-south trend. Overall the northeast trend is predominant in broad correlation with the transport direction (TD) (Figure 18b). The southwest trend relates to folding of the lineation across the tight to open north trending F3 folds. Isoclinal folding of the northeast-trending lineation produces a southeast trending lineation on the opposite limb of the isoclinal folds. The lineation has a more north-south trend in the hinge areas of the tight to isoclinal F3 folds suggesting reworking in these areas of higher strain in the polydeformed, isoclinally refolded "core" zone.

3.5 Transport Direction (TD) Pattern

Determinations of local transport direction (TD) by restoration of shear bands give a west-over-east sense of shear about a vector mean of ~070° (n = 4). The restored shear band vectors are 070°, 088° and 052° from outcrops along the Gordon River Road, and 073° along the Hermit Narrows (Figure 18b). Description and discussion of shear band restoration are presented in Gray et al. (2022, p. 77-84).

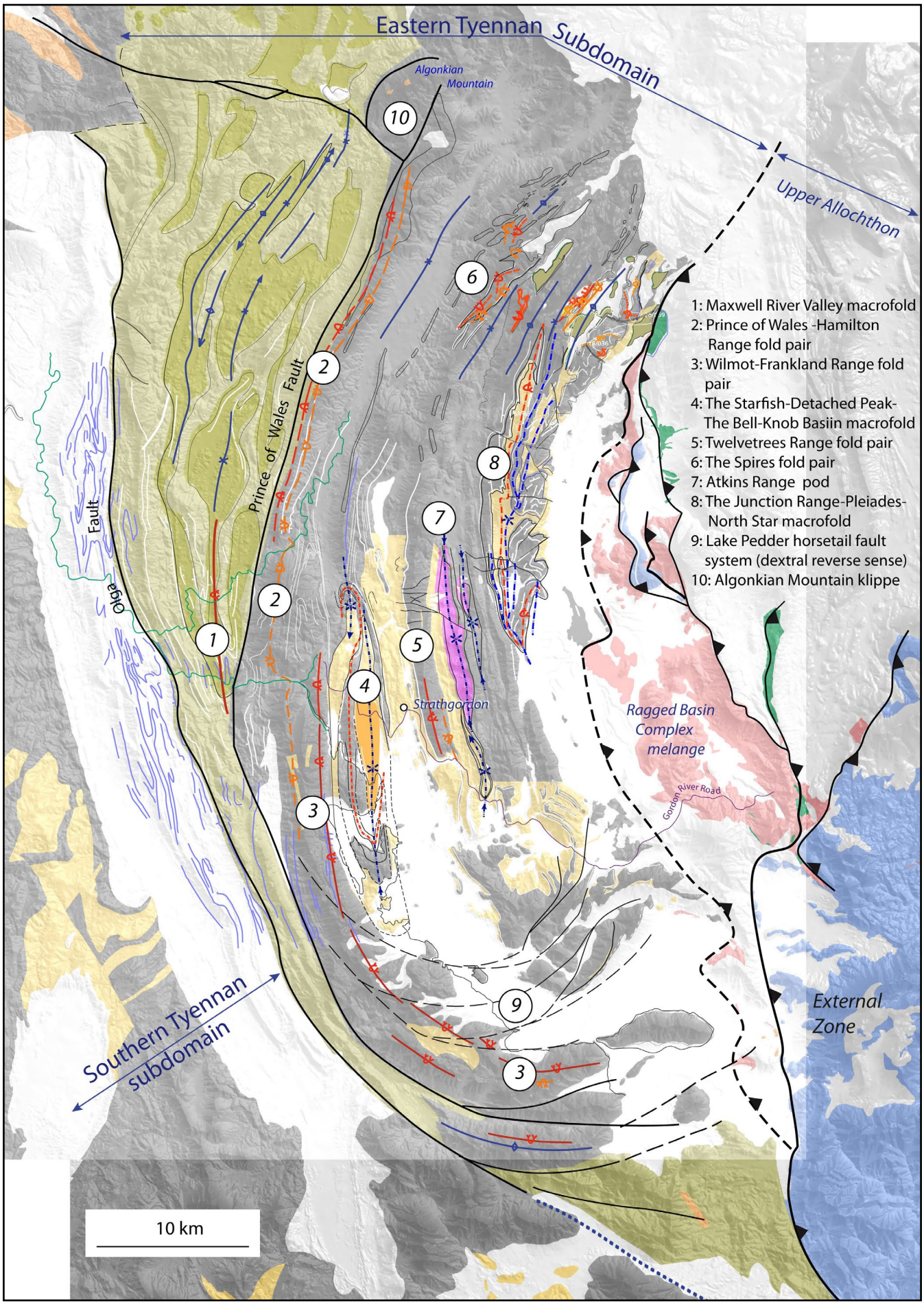

Figure 14. Eastern Tyennan subdomain structural element map. Elements are numbered 1 through 9. The base map is modified from the Mineral Resources Tasmania 1:250,000 and 1:25,000 digital atlas.

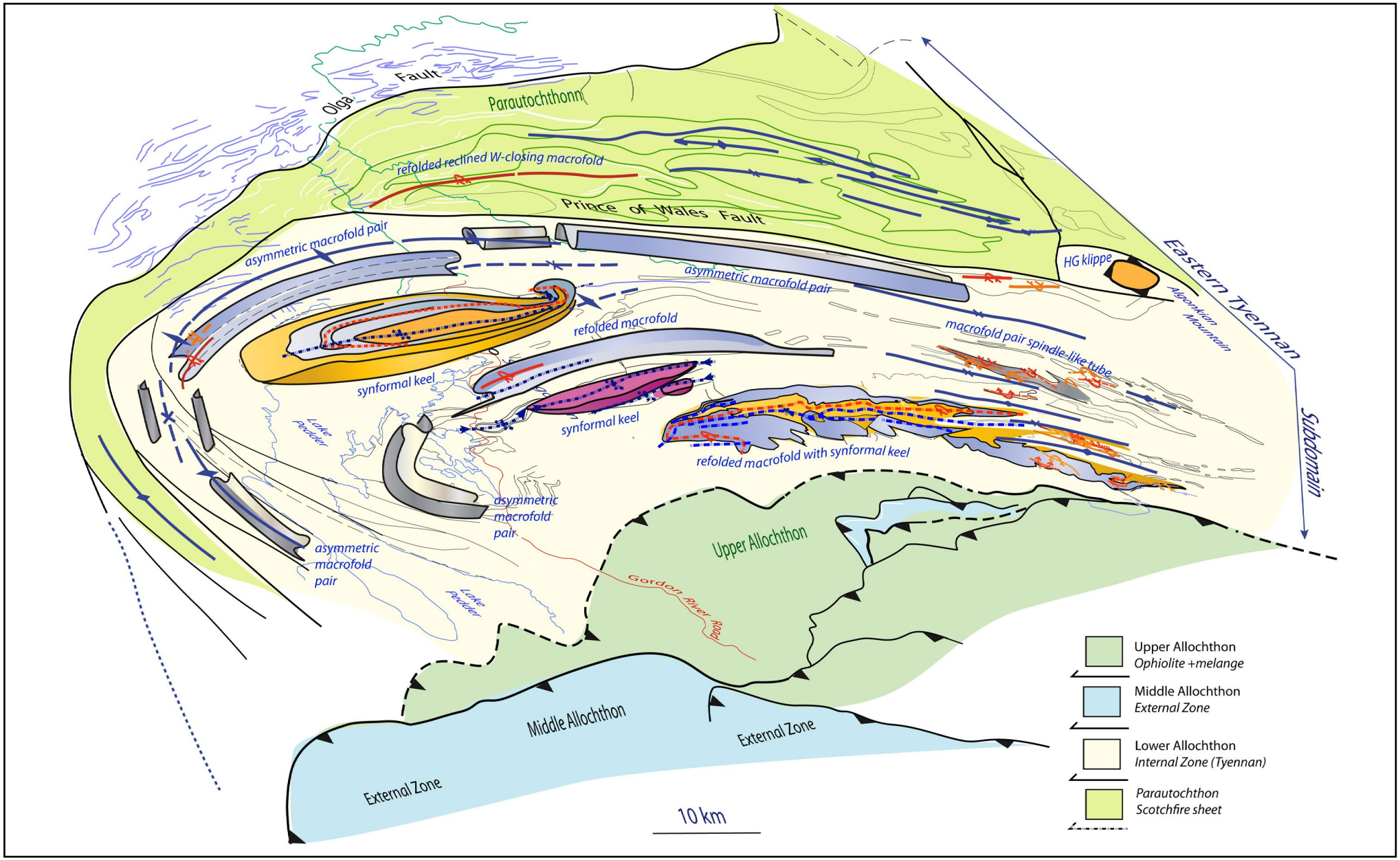

Figure 15. The 3D geometry of the major structural elements of the Eastern Tyennan subdomain shown on an oblique tilted map view looking west-southwest. The view also shows the stacking order of the component sheets in map pattern.

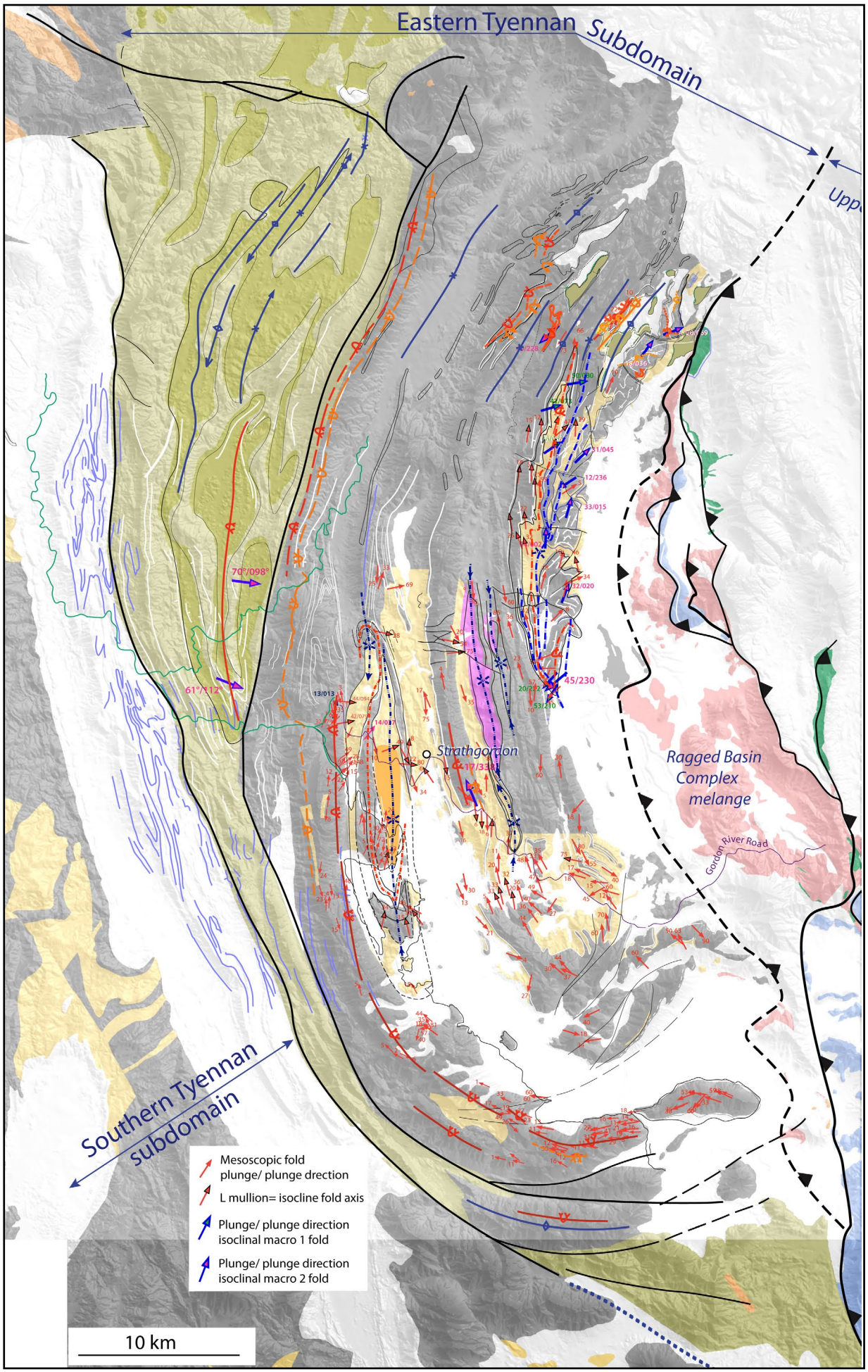

Figure 16. Eastern Tyennan subdomain early isoclinal fold axis map. The base map is modified from the Mineral Resources Tasmania 1:250,000 and 1:25,000 digital atlas.

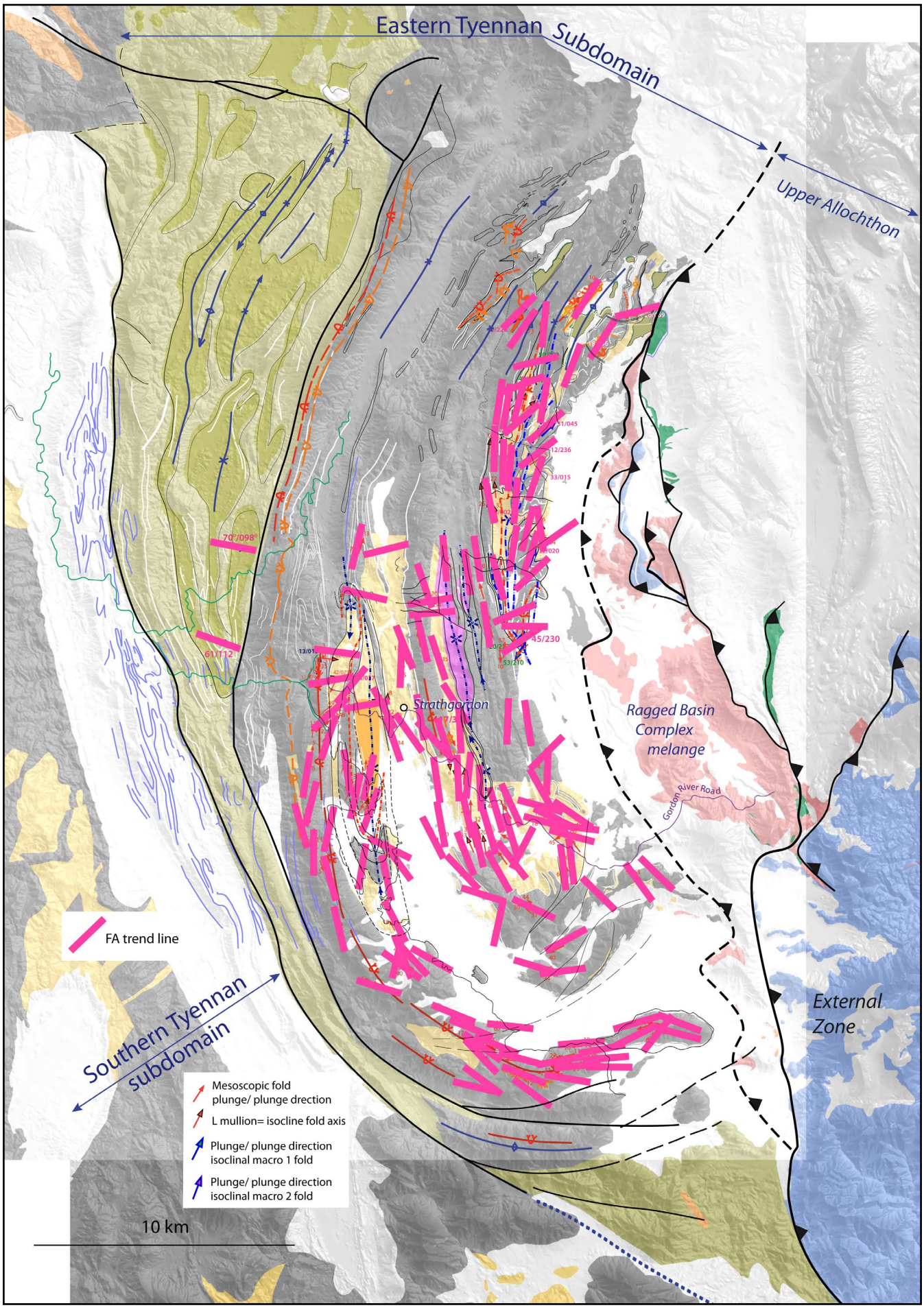

Figure 17. Summary map of the early isoclinal fold axis trends shown by the heavy pink lines defining a regional fold axis pattern. The geological base map is modified from the Mineral Resources Tasmania 1:250,000 and 1:25,000 digital atlas.

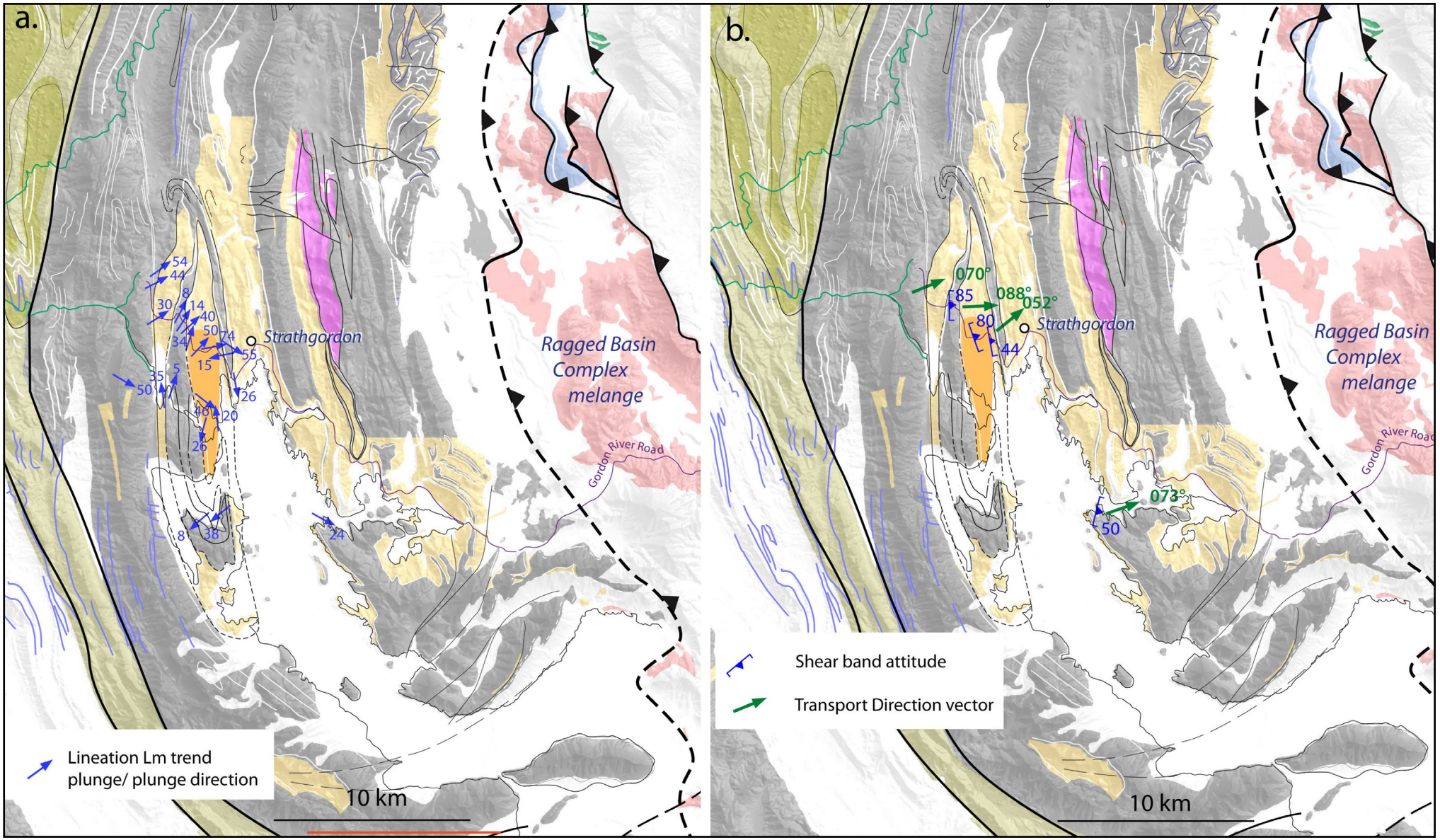

Figure 18. Eastern Tyennan subdomain structural element maps on a modified Mineral Resources Tasmania 1:250,000 and 1:25,000 digital atlas map base. a) Lineation (Lm) map. b) Transport direction (TD) vector map based on measured shear bands. All the data have been collected by the authors.

4.0 STRUCTURAL PROFILES OF THE EASTERN TYENNAN SUBDOMAIN

The regional structural profile (Figure 19) from the northern part of the Southern Tyennan subdomain across the Eastern Tyennan subdomain shows:

1. Younger Devonian open, upright refolding of the early Cambrian tectonic pile and included early macro-fold structures. This includes coplanar, tightening of the interpreted Cambrian F3 folds in the core of the Tyennan subdomain during the Devonian "refolding" event.
2. Devonian folding of the Late Cambrian erosional surface and associated Cambrian-Ordovician sandstones and conglomerate preserved in synclinoria (e.g. Olga Synclinorium).
3. A fault-emplaced "lid" of Cambrian mélange on the eastern side of the subdomain. The mélange includes chert and lithic sandstones. Many of the early Cambrian faults responsible for the stacking within the Tyennan allochthon have been reactivated during the Devonian deformation (Tabberabberan Orogeny). They have also been crosscut and offset by the younger Devonian faults, particularly those involving slices of the ultramafic rocks/serpentinite as interpreted as remnants of the uppermost obducted ophiolite sheet.
4. Extremely pinched, tight to isoclinal synforms with cuspate form that represent "keels" preserving the H-G layer. The major synforms include The Starfish-Knob Basin macro-fold, the Atkins Range macro-fold pod and the Junction Range-Pleiades-North Star macro-fold.
5. A consistent Z-vergence of the asymmetric fold-pairs within quartzite of the "core" of the Eastern Tyennan subdomain (blue full and dashed lines in the light grey regions, Figure 19).
6. A refolded east-verging macro-fold within the Scotchfire sheet of the parautochthon (khaki colour, Figure 19).
7. Emplacement of the "core" of the Eastern Tyennan subdomain over the parautochthon during the younger Devonian thrusting and folding event. This included inversion and reactivation of the mid Cambrian extensional fault (Olga Fault) along the eastern side of the Olga synclinorium (Figure 10).

Five radially arranged, detailed structural profiles were constructed across the Eastern Tyennan subdomain (see Figures 20 and 21 for profile location). The profiles (Figure 22) are approximately orthogonal to the structural trends defined by the strike of the deformed layering. They reflect the internal curvature within the subdomain.

4.1 Northern Profiles

Profiles 1 and 2 at the northern end of the Eastern Tyennan subdomain have limited structural control (Figure 22). The interpretations are based on bushwalker photographs of the ridges as well as data from the northeast corner of the Huntley 1:50,000 map sheet (see Section 5.2). The interpretation has: 1) quartzite preserved as a series of quartzite klippen; 2) truncation of a Z-vergent asymmetric fold pair preserved in each ridge along the basal quartzite contact (Figures 22, 23 and 24); and 3) the sequence folded by a series of younger, broad, open, upright folds (see Figures 22 and 23).

These east or Z-vergent, asymmetric fold pairs have been interpreted as part of a "wave train" (Figure 25) not unlike that observed and interpreted for the eastern part of the Southern Tyennan subdomain (Gray and Vicary, 2022b). This geometry (Figures 25 and 26) shows markedly attenuated, long, connecting limbs leaving the asymmetric fold pair hinges and common limb preserved as knots or augen. These quartzite augen make up the ridgelines.

4.2 Mid Profiles

Profiles 3 and 4 (Figure 22) transect the polydeformed folded "core" of the Eastern Tyennan subdomain (Figures 12 and 13). They are dominated by tight, to almost isoclinal, refolding of the early macro-folds (Figure 14). The H-G garnet schist of The Bell Basin - Gordon River Road and amphibolite of the Atkins Range are interpreted as remnant "keels" within cuspate, attenuated synforms as part of a once continuous but composite H-G layer (Figure 22). The intervening antiforms are preserved within the quartzite sequence and have more open, rounded form. These are best exemplified in the Strathgordon profile (Figure 27) where the early macro-fold hinges have been documented, in particular the west-closing Knob fold at the Gordon Dam, the east-closing synform on the Gordon River Road and the west-closing Twelvetrees fold.

4.3 Southern Profile

Profile 5 (Figure 22) in the southern part of the Eastern Tyennan subdomain (Figures 20 and 21) shows more gently undulating form in the western part and no preservation of the inferred H-G layer. The antiformal geometry across Lake Pedder - Mt Helder and the adjoining synform is affected more by the steeply plunging axes of the apparent rotation points (ARP on Figure 13) to give oblique, non-profile sections through these structures. The apparent synformal closure shows complex refolding and interdigitation along the pelite (Ptp)-quartzite (Ptq) interface of the early isoclinal folds.

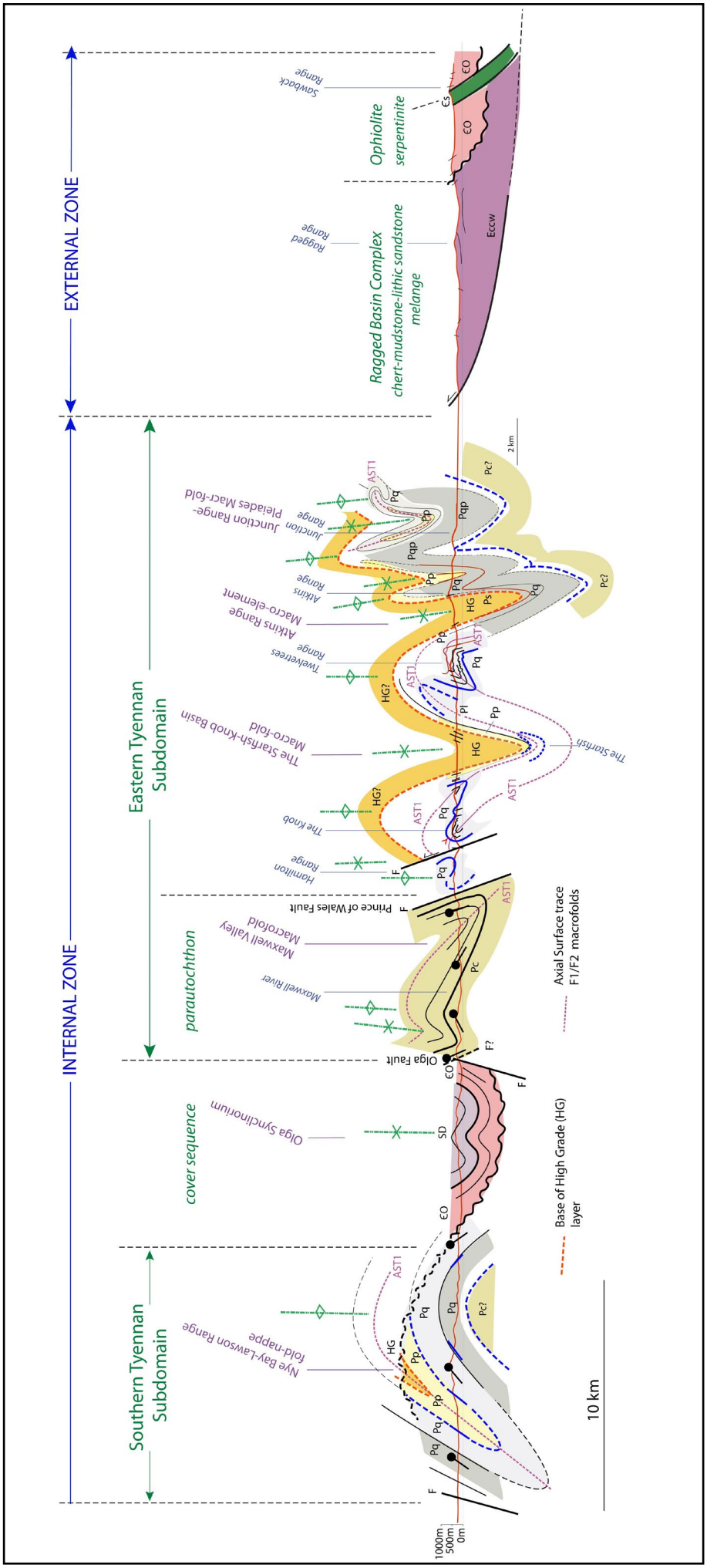

Figure 19. Structural profile across the central part of the Tyennan Domain including the polydeformed, refolded core of the Eastern Tyennan subdomain. The profile extends from the Lawson Range on the west, to the Sawback Range on the east (see Figure 1 for location).

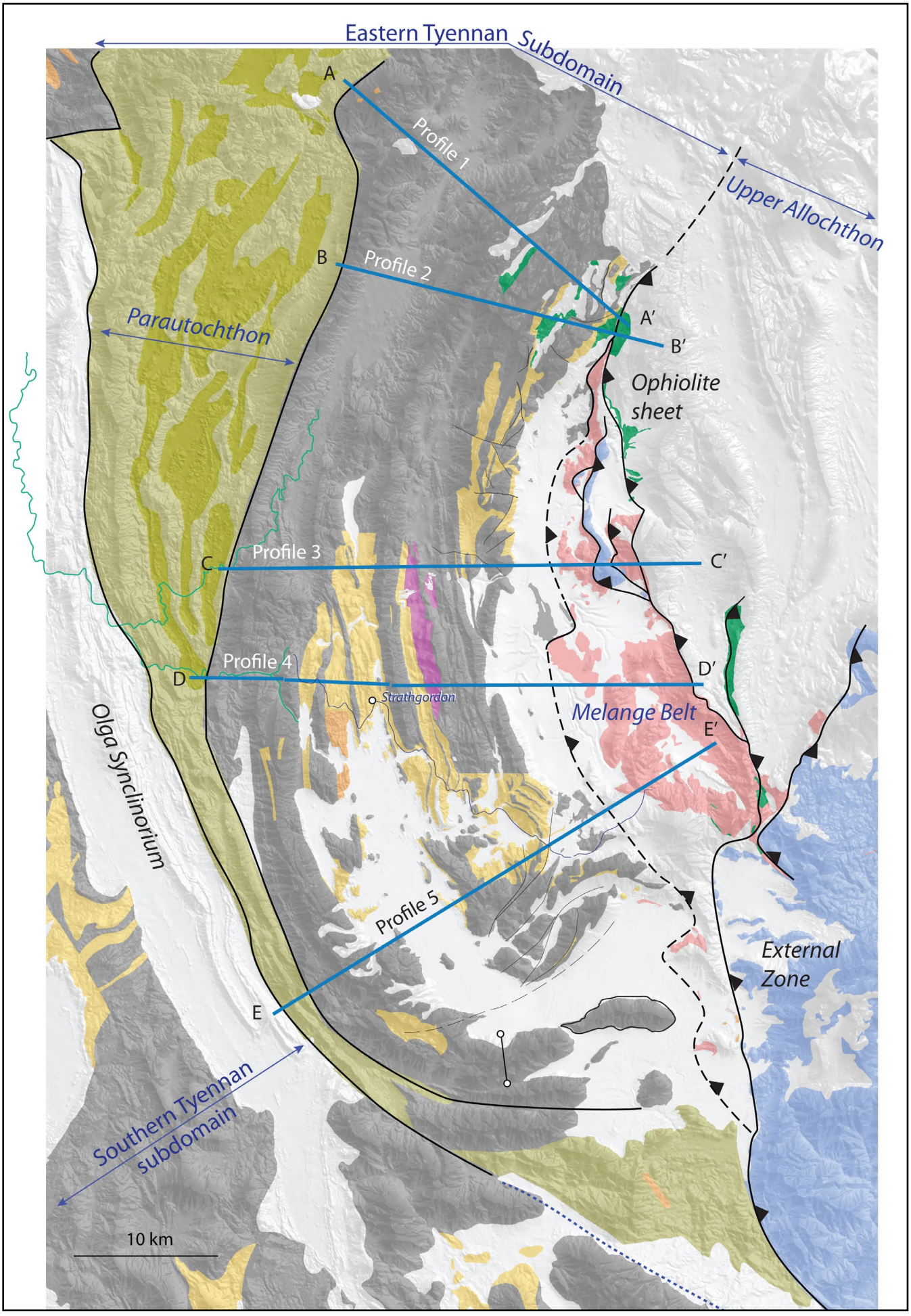

Figure 20. Profile 1 to 5 positions shown on a geological base map modified from the Mineral Resources Tasmania 1:250,000 and 1:25,000 digital atlas.

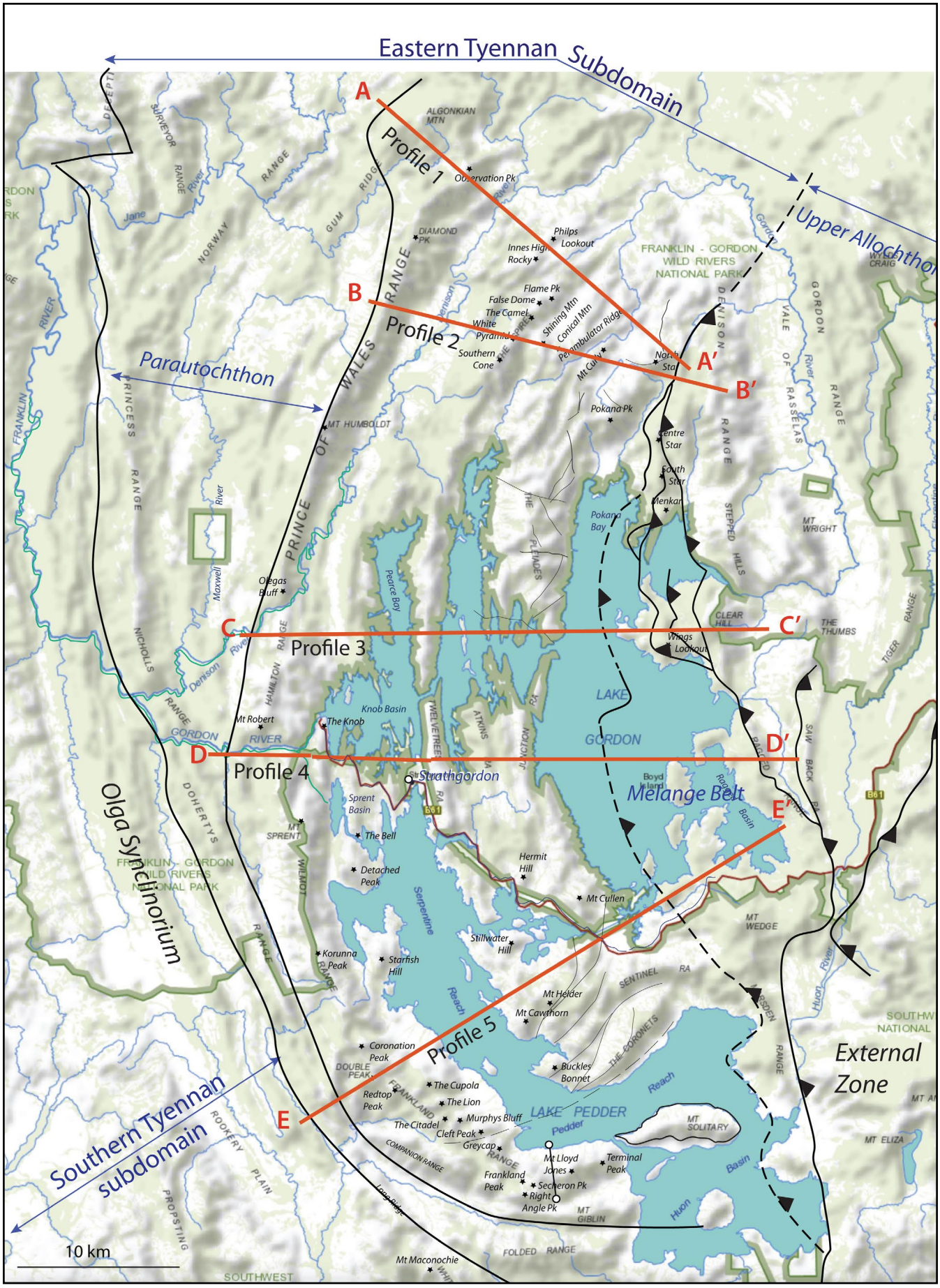

Figure 21. Profile 1 to 5 positions on a ListMap™ topographic map base that shows the profile locations relative to geographic elements.

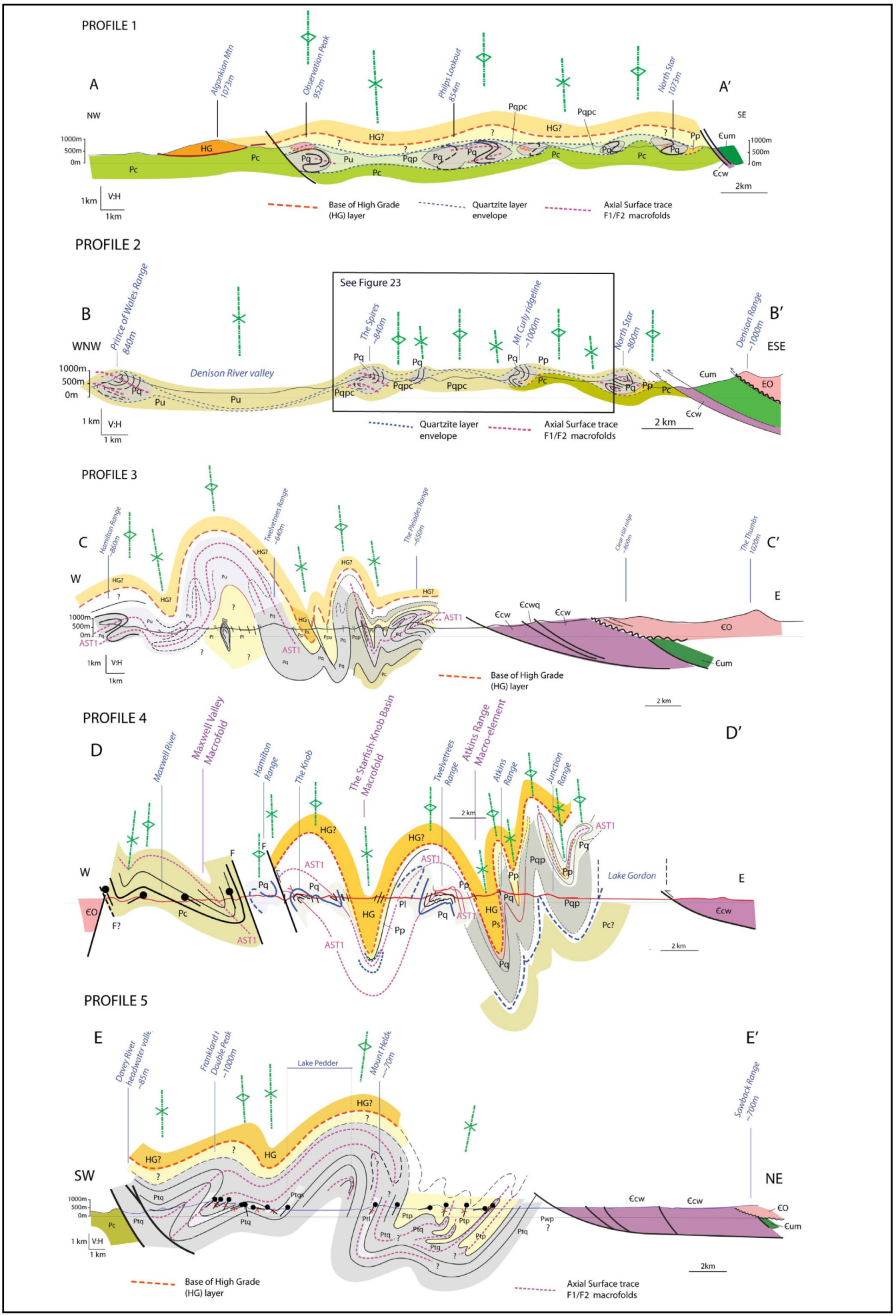

Figure 22. Structural profiles for the Eastern Tyennan subdomain. For profile locations see Figures 20 and 21.

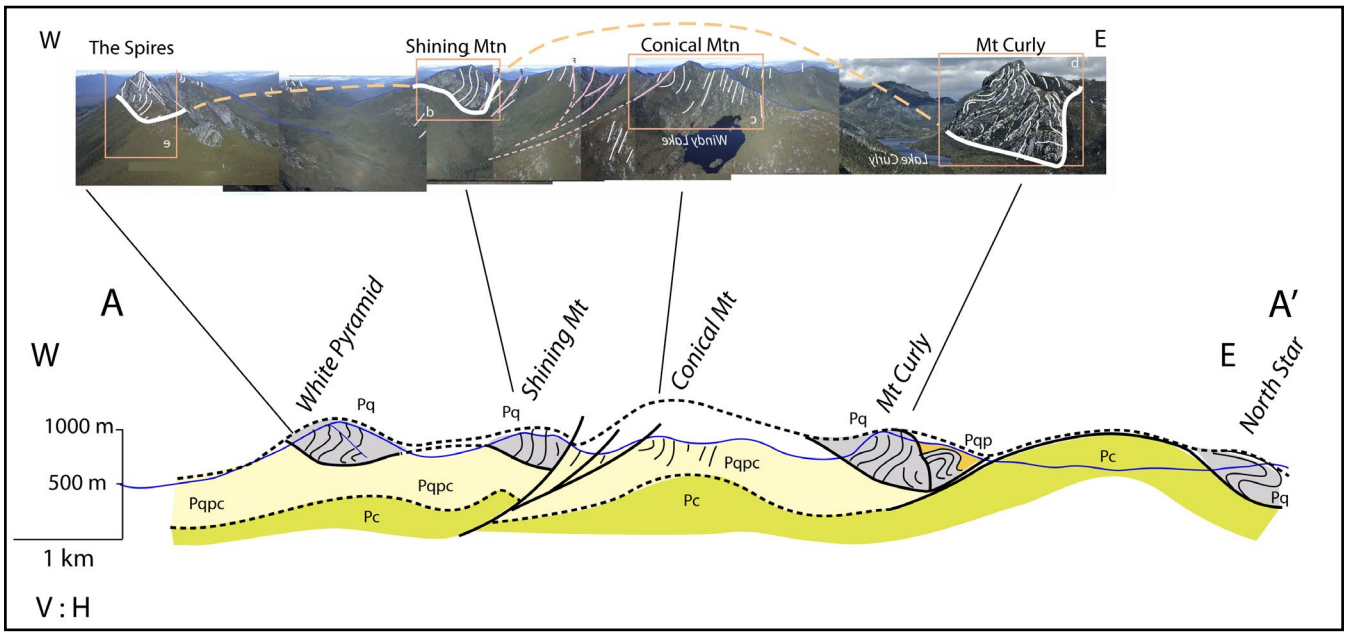

Figure 23. Structural profile for the Spires (White Pyramid)-Shining Mountain-Conical Mountain-Mt Curly-North Star transect. Top: Annotated stitched photo profile showing truncation of the internal structure within the quartzite along the basal quartzite contact. (Photo credit: Wandering Foxbat video) Bottom: Profile interpretation showing the ridgelines capped by quartzite (Pq), the valleys underlain by a layered quartzite-phyllite-carbonate calc schist (Pqpc) sequence and carbonate (Pc). This is section A-A' shown in Figures 48 and 49.

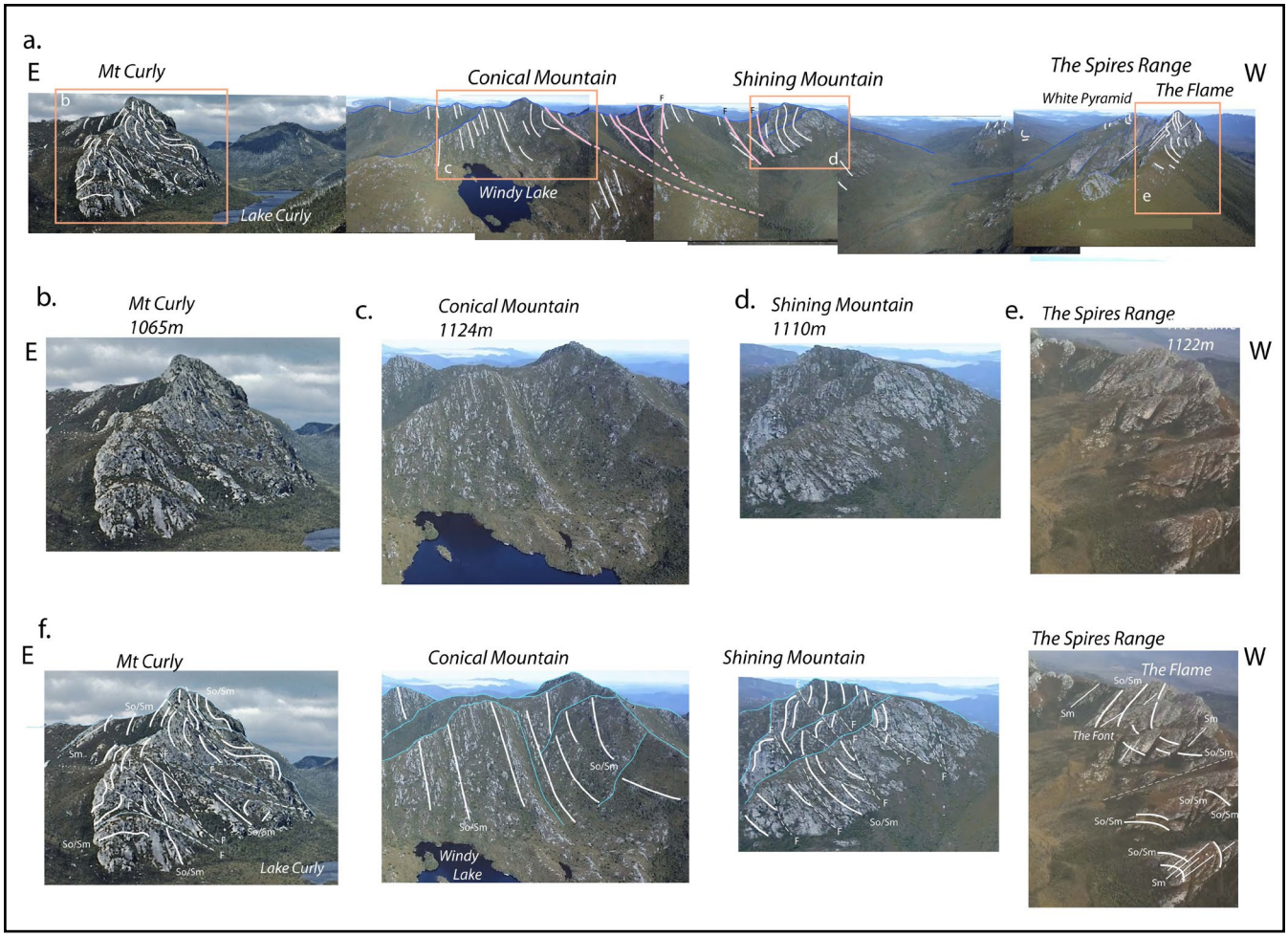

Figure 24. Structural detail of the quartzite ridges in The Spires - Mt Curly photo profile shown in Figure 23 (video grab-shots). The profile is viewed looking south based on the flight path of the Wandering Foxbat video.

a) Composite photo profile of stitched photos extracted from the video clip (see Figure 23). b), c), d) and e) Enlargement photographs of the major geographic elements. f) Structural interpretations with So/Sm formlines shown by the white line traces.

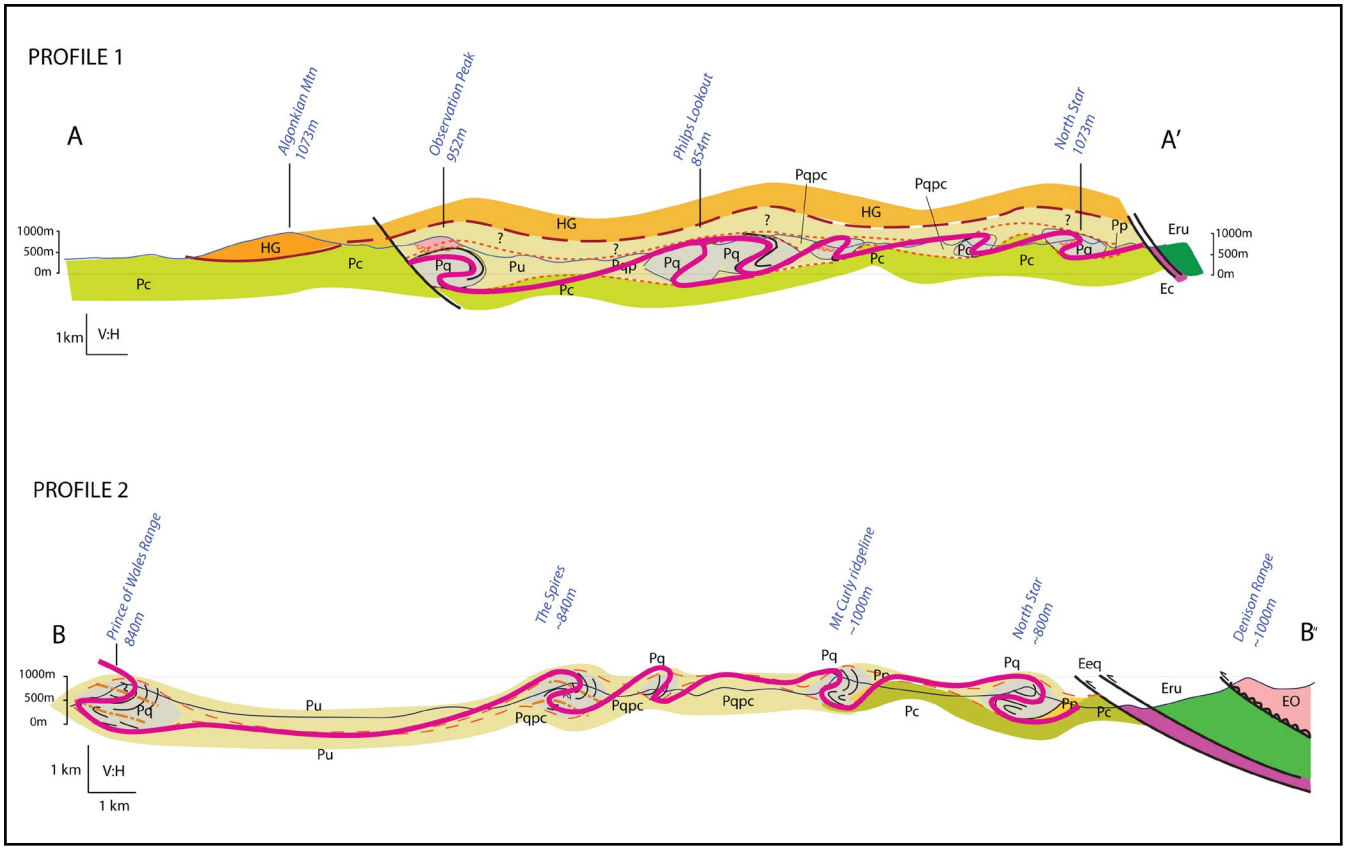

Figure 25. "Wave train" interpretation of the asymmetric z-vergent fold pair that dominates the quartzite ridgelines of the northern part of the Eastern Tyennan subdomain. The pink line is a formline drawn along the top of the quartzite. Compare this geometry with the asymmetrically folded quartzite layer in Figure 26.

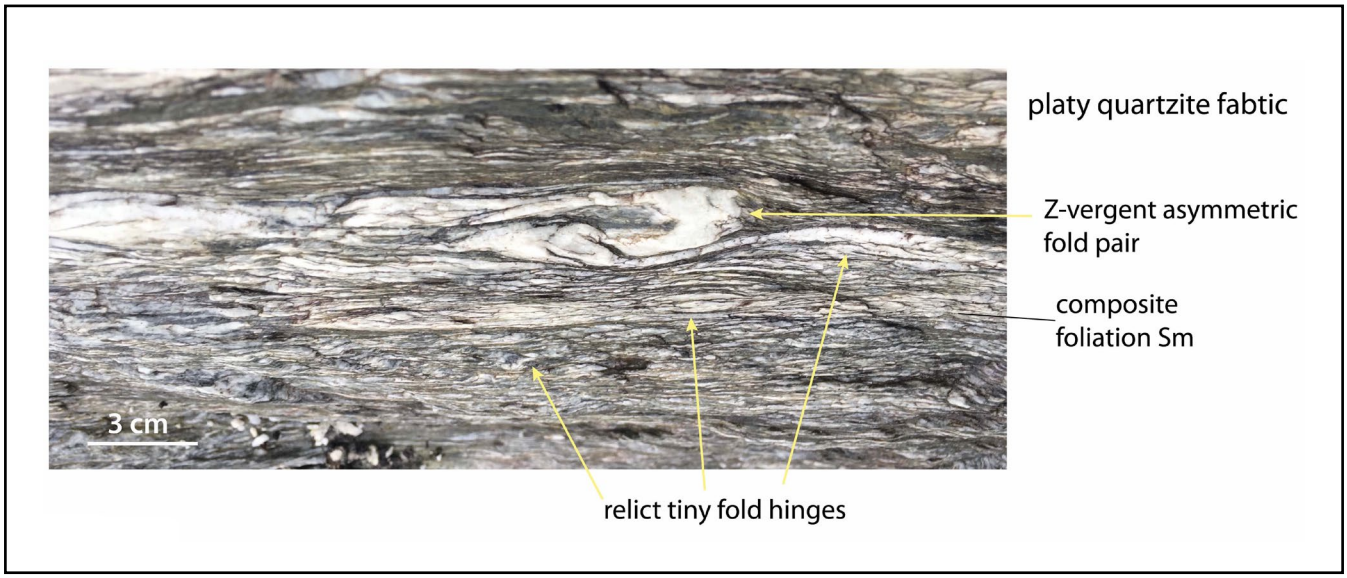

Figure 26. Centimetre-scale example of an asymmetric Z-vergent fold pair in a thin quartzite band within platy quartz mylonite. The fold pair is preserved as an augen with the trailing and forward limbs markedly thinned due to extreme flattening and elongation in a rotational shear-related deformation. Photo taken on the access road for the Lake Gordon boat ramp.

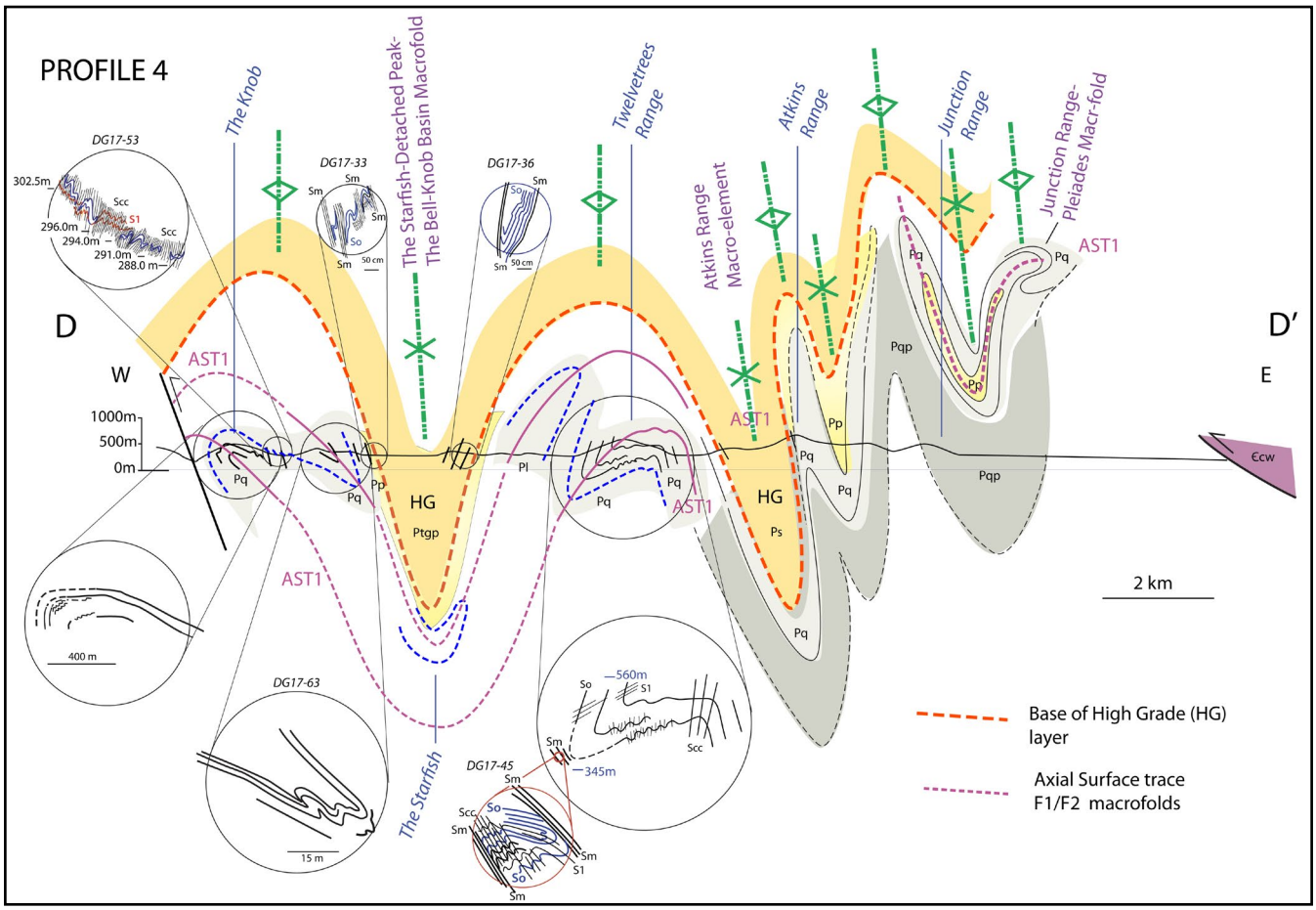

Figure 27. The Strathgordon profile construction (eastern part of Profile 4 shown in Figure 22). The profile is based on outcrop data and structural relationships collected and observed by the authors in a Gordon River Road transect from Gordon Dam to Hermit Hill (see Appendix 2). The insets show sketches of structural relationships at outcrops that were used to construct the macro-structure of the profile.

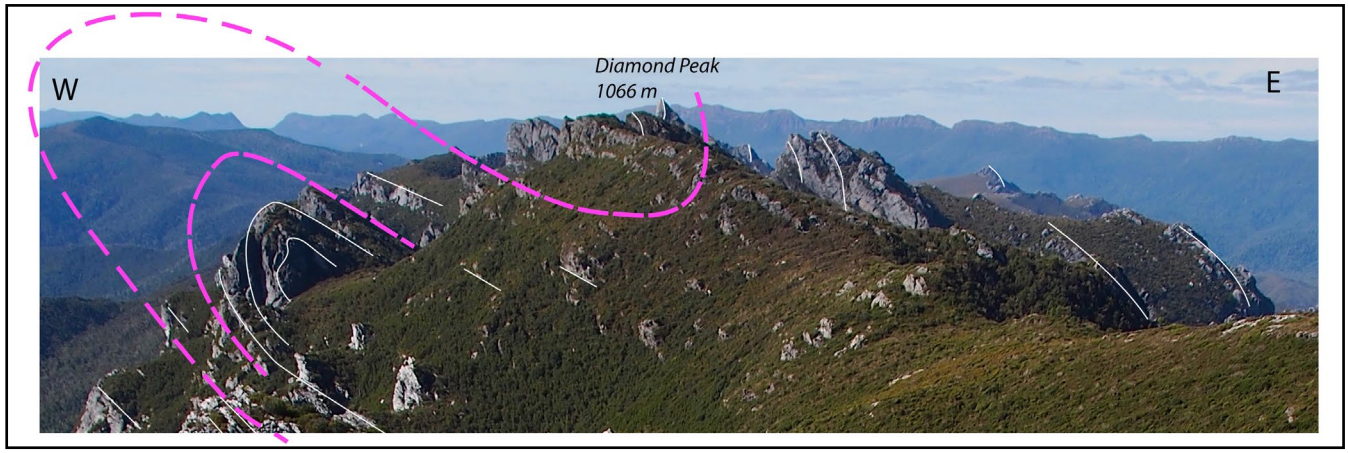

Figure 28. West-closing macro-isoclinal fold along the west side of the Prince of Wales Range sitting below the east-closing macro-fold at Diamond Peak. View is to the north. (POW2 profile, Figures 29 and 30d) (Photo Credit: Becca Lunnon, rockmonkeyadvetures)

5.0 MAJOR STRUCTURES OF THE EASTERN TYENNAN SUBDOMAIN

5.1 Asymmetric Z-Vergence Fold Pairs

The quartzite ridges of the Eastern Tyennan subdomain (Figures 3 and 10) contain relicts of an asymmetric, east-vergent fold pair that are preserved as klippe above a fault-like basal contact (Figure 15). Much of the structural geology of these ridges is based on interpretation of structure from bushwalker photographs presented in Appendix 1. The structural geology of each range is presented below.

5.1.1 The Prince of Wales Range

Quartzite caps the ridgeline of the Prince of Wales Range. It is dominated by an east-closing recumbent macro-fold (Element 2, Figure 14) with sections through the fold hinge seen at Diamond Peak, the ridgeline north of Mt Humboldt, at Mt Humboldt and Olegas Bluff (Figures 28, 29 and 30). This hinge zone is cut by a series of steeply west to east dipping reverse faults (Figures 30e, f). A structurally lower, west-closing recumbent macro-isoclinal fold occurs as erosional relicts along the west side of the range

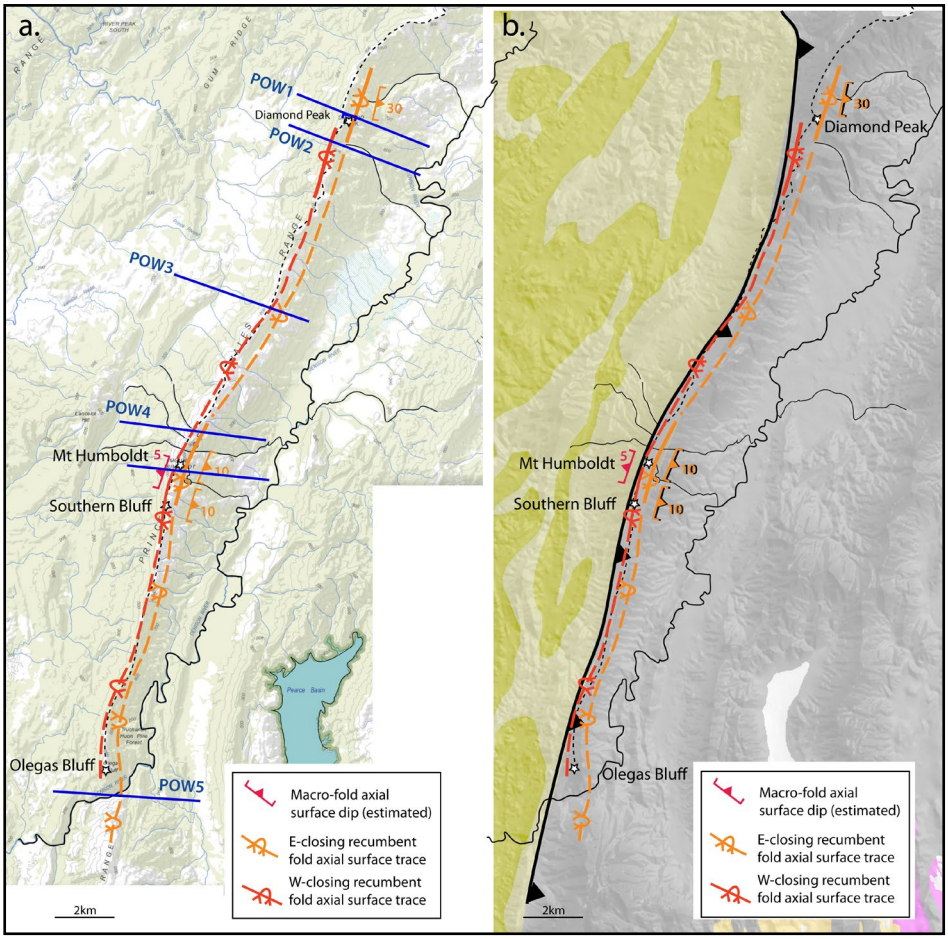

Figure 29 (Left). Structure maps of the Prince of Wales Range compiled from photo profile interpretations (see Appendix 1 Section 1). The maps show axial surface traces of the designated east-closing (orange line traces) and west-closing (red line traces) isoclinal macro-fold folds as part of the regional asymmetric macro-fold pair. Dips of the macro-fold axial surfaces are shown at different position along the range. a) ListMap topographic base. The blue lines are the positions of the photo profiles POW1 to POW5 (see Figure 30). b) Lithological map base modified from the Mineral Resources Tasmania 1:250,000 digital atlas.

Figure 30 (Below). Photo profiles along the Prince of Wales Range with pink line traces showing the macro-fold geometry. Profiles a), b), c) and d) are at the north end of the range near Diamond Peak showing prominent east-dipping dip slopes in the foliation Sm (orange line traces). e) and f) are photo profiles near Mt. Humboldt. g) Photo profile through Olegas Bluff with Mt. Humboldt in the distance. See Figure 29a for profile locations.

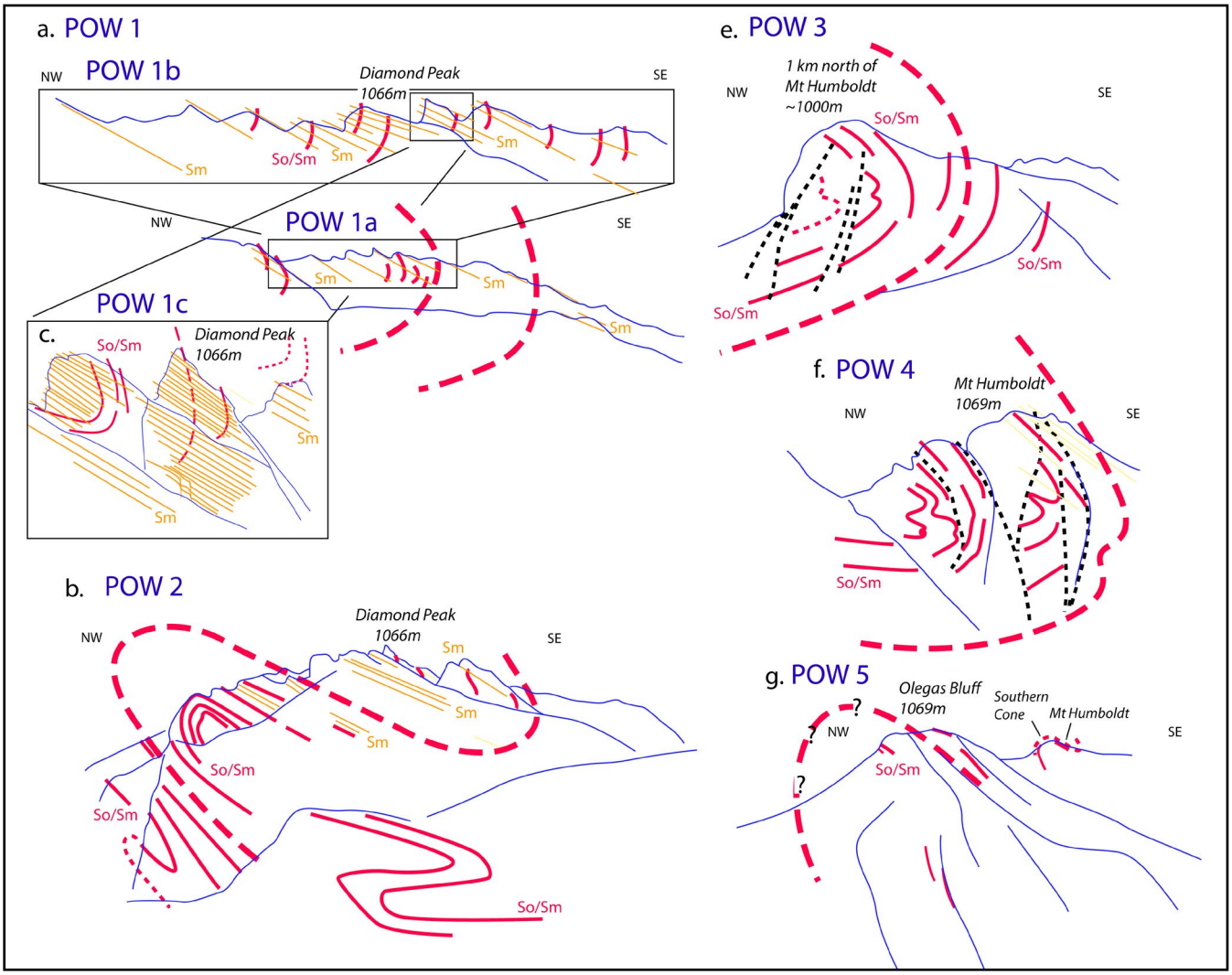

south of Diamond Peak (Figure 28) and south of Southern Bluff. This is due to the east dip of the macro-fold axial surfaces and Sm (Figures 30b and g).

The Prince of Wales ridgeline (Figure 31a) preserves a partially eroded, tube-like form in quartzite containing the asymmetric, east-vergent macro-fold pair (Figure 31b). The tube form is truncated at the base by a basal, strongly foliated, quartzite and/or brittle fault(s).

5.1.2 The Hamilton Range

The Hamilton Range, the southern continuation of the Prince of Wales Range (see Appendix 1 Section 2) beyond the Denison River extending to the Gordon River (Figure 13) also consists of an east-closing macro-fold hinge (Element 2, Figure 14). Made up of foliated quartzite, photo profiles show an east-closing macro-isoclinal fold hinge along the western side of the range (Figures 32 and 33) with a zone of intense foliation/transposition layering along the eastern side (Figure 33). Dip changes in the axial surface of the macro-fold (Figures 33 and 34) suggest the macro-fold is refolded by an open, south-plunging Devonian anticline (Figure 34). The macro-fold sits along the hinge of this anticline such that: 1) the axial surface projections are essentially sub-horizontal; and 2) the axial surface trace of the early, east-closing recumbent macro-fold (blue dashed trace, Figure 32) is coincident with and colinear with the younger anticline axial surface trace (green line trace, Figure 33). The interpreted 3D geometry for the Hamilton Range is shown in Figure 35 with the younger, superimposed anticline shown by the folded axial surfaces AS1 and AS2 of the macro-fold pair.

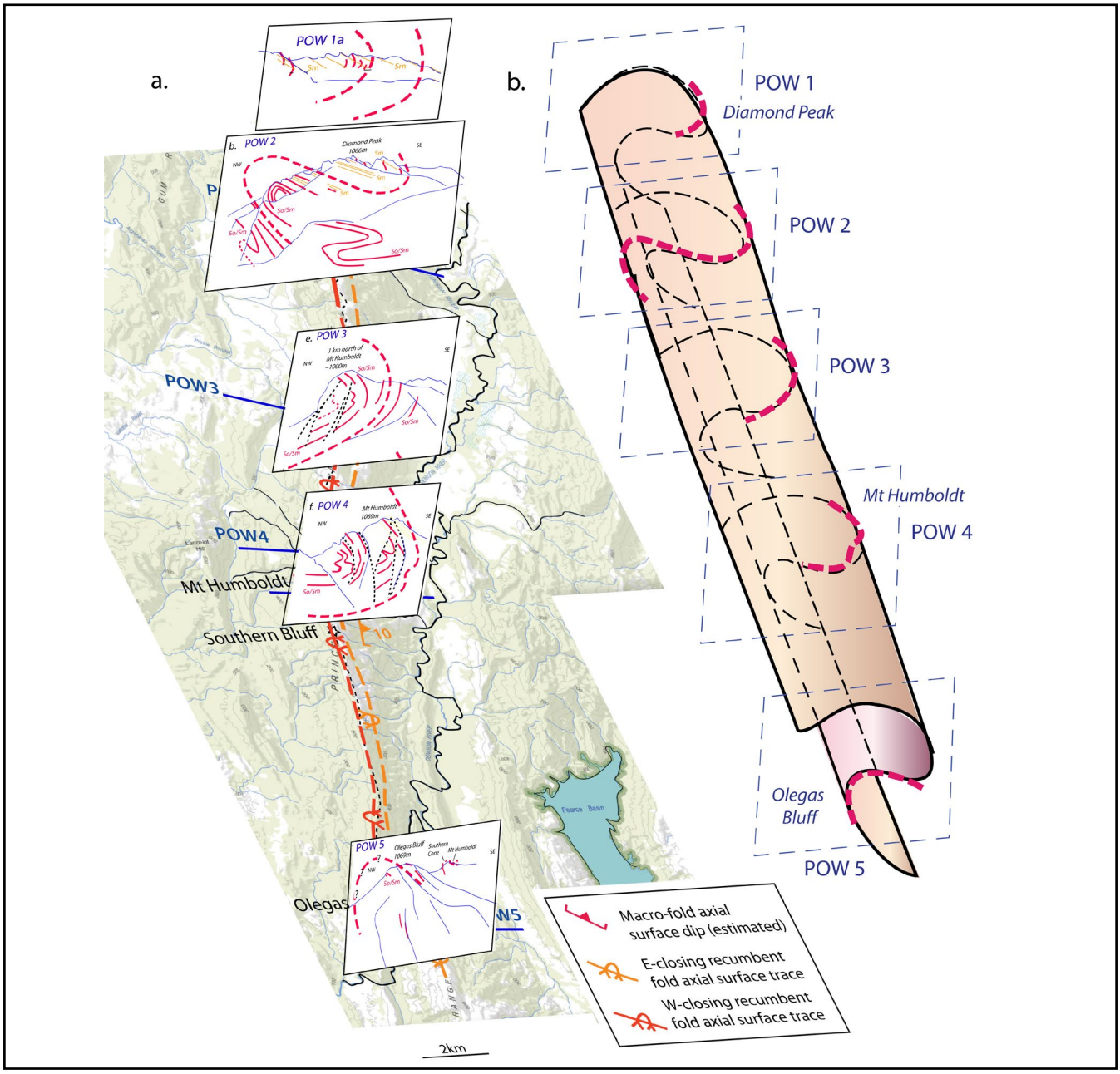

Figure 31. Oblique tilted view looking to the northeast of the structure of the Prince of Wales Range. a) Tilted map view with superimposed photo profiles (compare with Figure 6). b) Reconstructed 3D form of the quartzite macro-fold structure along the Prince of Wales Range. Construction was by fitting a generalised "shell" to the macro-folded layer. The heavy pink dashed lines show the layer exposed in the corresponding photo profiles.

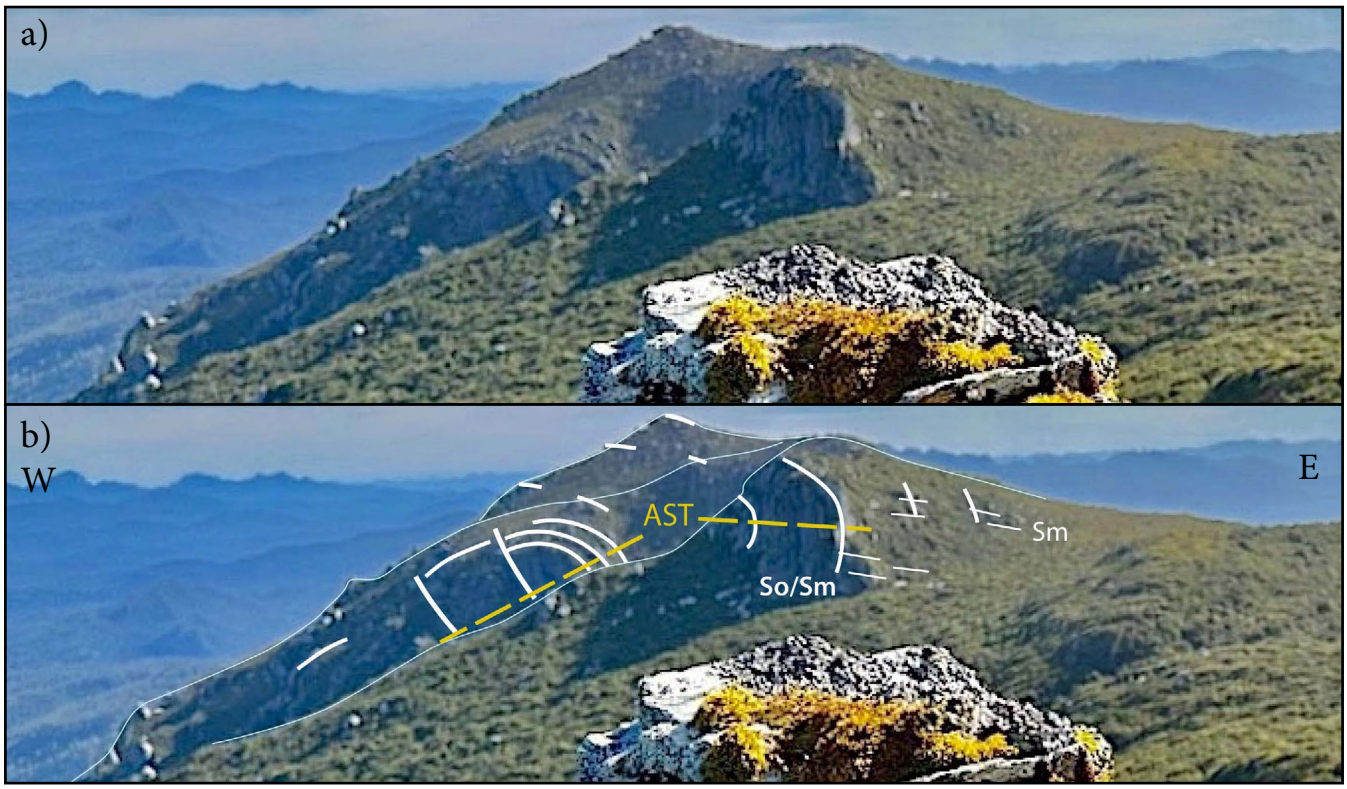

Figure 32 (Above). View to the north from the northern slope of Mt Robert showing an east-closing macro-isoclinal fold cut by steeply east-dipping reverse faults (Profile HR2 in Figure 34). The view is of the west flank of the Hamilton Range. AST: axial surface trace. (Photo Credit: Becca Lunnon, rockmonkeyadvetures)

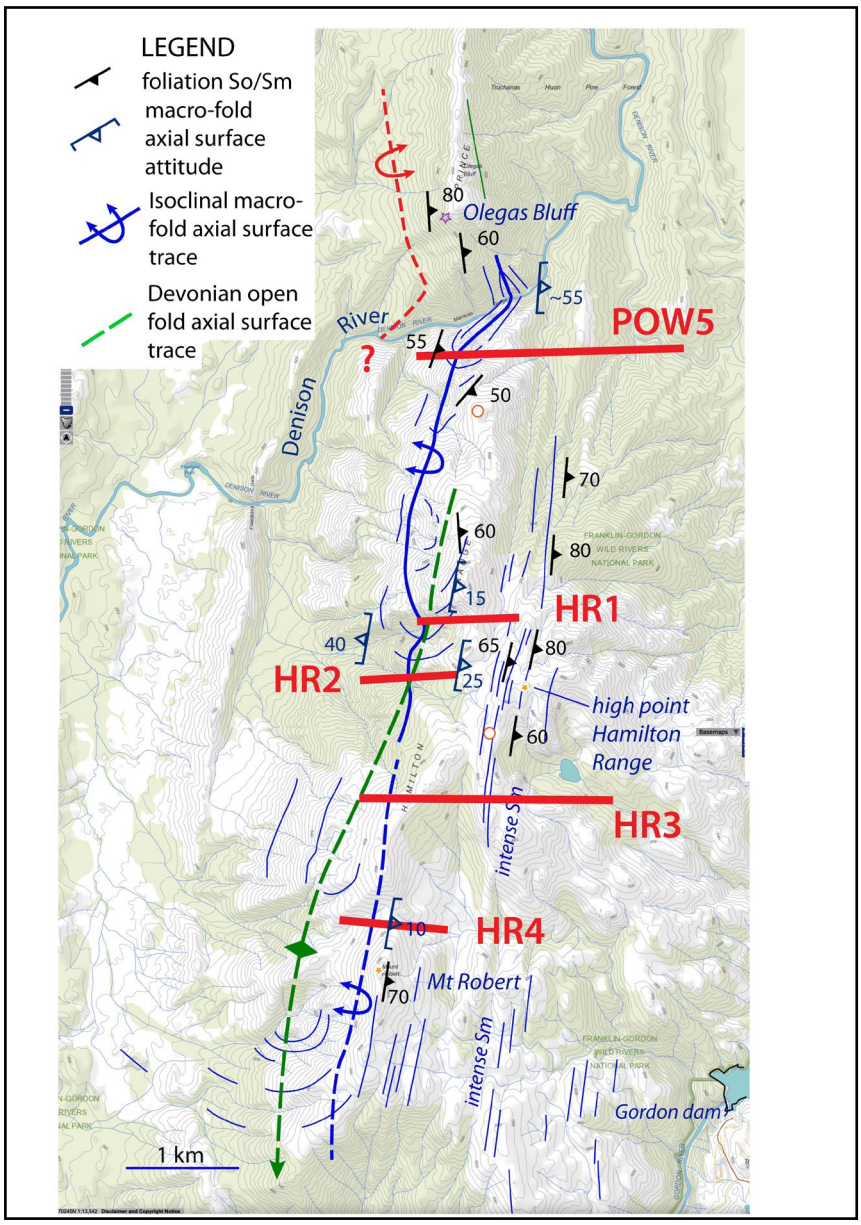

Figure 33 (Left). Hamilton Range structure map on a ListMap topographic base. Thin blue lines are formlines in So/Sm based on the Google Earth satellite image interpretation. The heavy blue line is the axial surface trace of the east-closing, isoclinal macro-fold. The heavy green dashed line is the axial surface trace of the inferred younger Devonian anticline that appears to refold the axial surface of the macro-fold. The red lines with red HR numbers are the locations of the photo profiles shown in Figure 34.

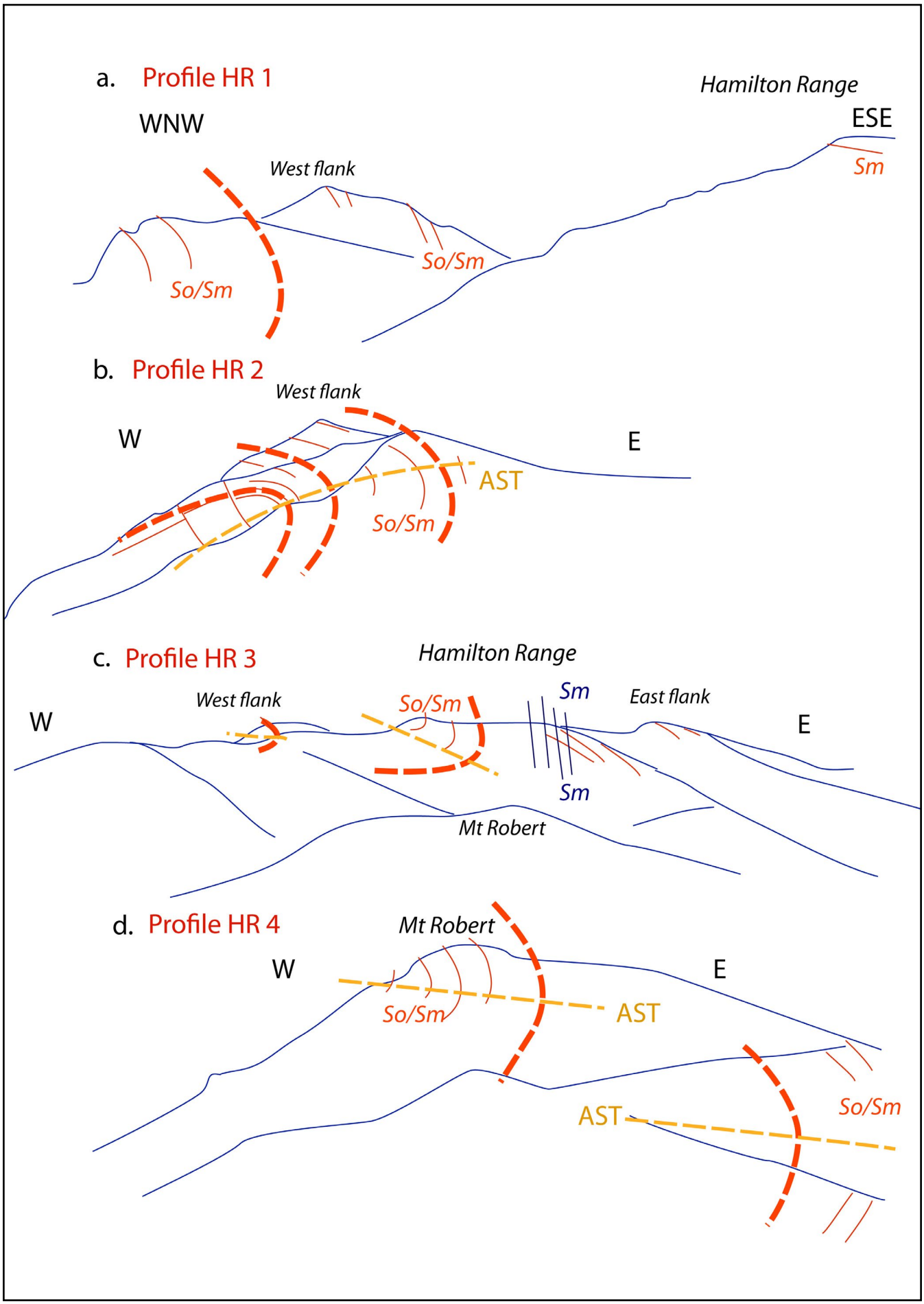

Figure 34. Photo profiles across ridgeline segments of the Hamilton Range. Arranged from north to south, the photo profiles are at different scales with (c) across the entire Hamilton Range with (a), (b) and (c) more local profiles.

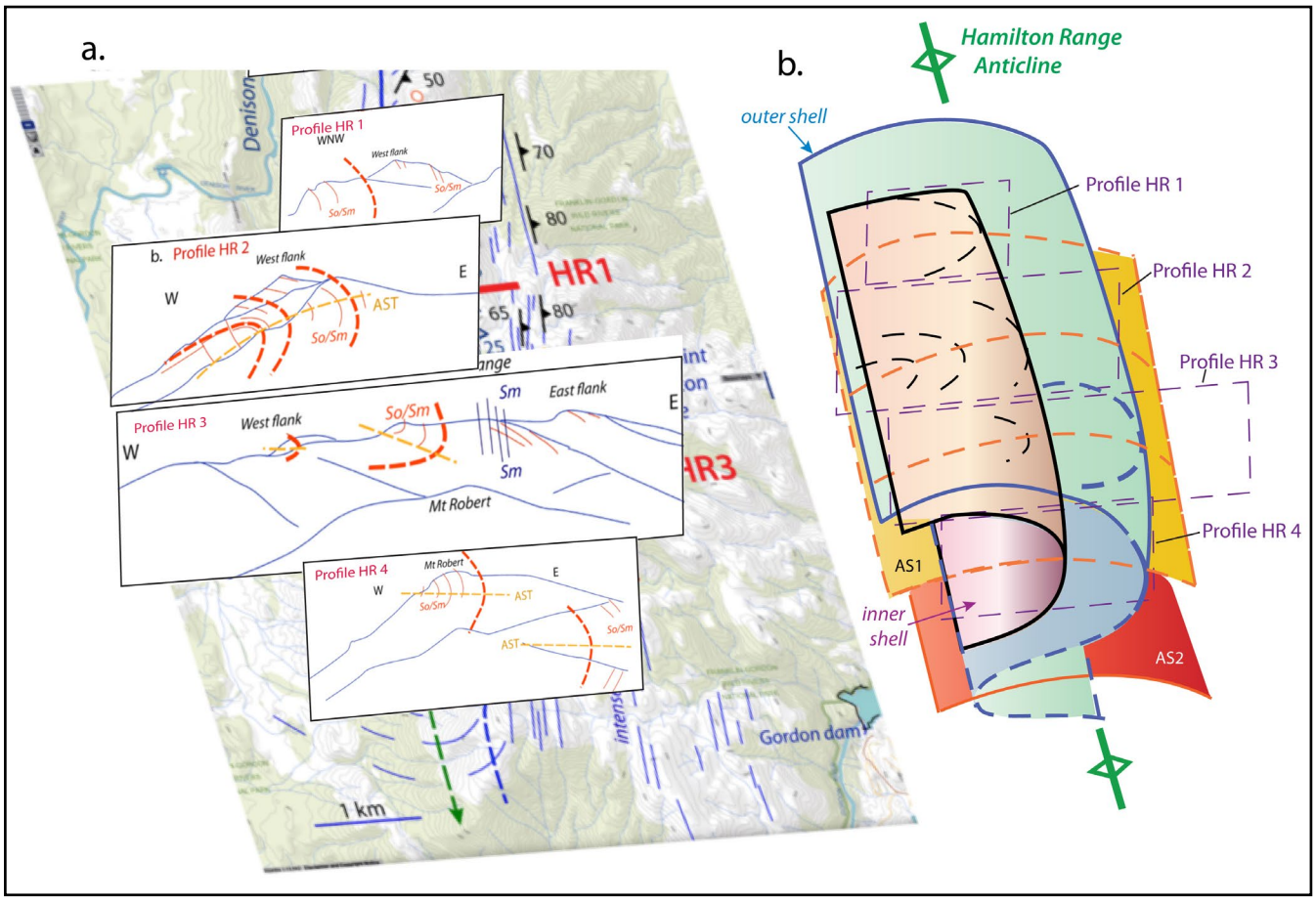

Figure 35. Oblique tilted view looking to the northeast of the structure of the Hamilton Range. a) Tilted map view with superimposed photo profiles HR 1 to HR 4 (compare with Figure 34). b) Reconstructed 3D form of the quartzite macro-fold structure along the Hamilton Range. An inner shell is shown in mauve and an outer shell in blue. AS1 (orange layer) is the axial surface for the east-closing macro-fold hinge. AS2 (red layer) is the axial surface of the structurally lower, west-closing macro-fold hinge. Note the erosion surface is at the level of the east-closing hinge with the upper limb partially removed by erosion. The lower west-closing hinge occurs below the ground surface.

5.1.3 The Wilmot-Frankland Range

The combined Wilmot - Frankland Range (Element 3, Figure 14) shows marked curvature with a strike swing from north-south trending in the Wilmot Range to east-west trending in the southern part of the Frankland Range near Terminal Peak (Figures 2 and 3). The Wilmot - Frankland Range is a continuation of the Prince of Wales and Hamilton Ranges to the north (Figure 2).

Geometrically complex at the outcrop scale (Boulter, 1974, 1978) a relatively simple macrostructure defines the structure of the ranges (Figures 36 and 37). As in other parts of the Eastern Tyennan subdomain, the macrostructure consists of an asymmetric, east-vergent fold pair in quartzite that is variably exposed along the range (Figures 38 and 39). Outcrops in the northern part of the range, from Mt Sprent to Greycap, are dominated by the west-closing macro-fold (Figures 36 and 39) with the upper, east-closing macro-fold eroded and no longer preserved along the western side of the range (Figure 39). The fold pair is only preserved in the southeastern part of the Frankland Range from Frankland Saddle to Terminal Peak (Figures 38 and 39).

Belts or domains of overturned and right-way-up bedding have helped to define the macro-fold limb versus hinge positions. Limitations in exposure however, provide a patchy data distribution that has made macro-fold recognition, as well as macro-fold axial surface trace definition, problematic. The macro-fold recognition, their positions and axial surface trace delineation (Figure 38), have largely been done by formline analysis of outcrops in bushwalker photographs taken at various positions through the range ridgelines (see Appendix 1, Section 3). This was enabled by construction of a series of photo profiles (Figures 40 and 41) where the axial trace position was joined from photo profile to adjacent profiles to create the axial surface trace map (Figures 38 and 40).

Photo profiles (Figures 41 and 42) show the ridgeline is dominated by a west-closing, isoclinal, recumbent, macro-fold hinge (Figures 36 and 37). This hinge is cut by several high angle reverse faults. A younger Devonian? crenulation cleavage overprints the folded layering (green line traces in Figures 36, 41a and c). The macro-fold hinge, as shown by the orange axial surface trace, is folded by a younger anticline (Figure 41e), with the dip of the axial surface changing along the range (Figures 39 and 41).

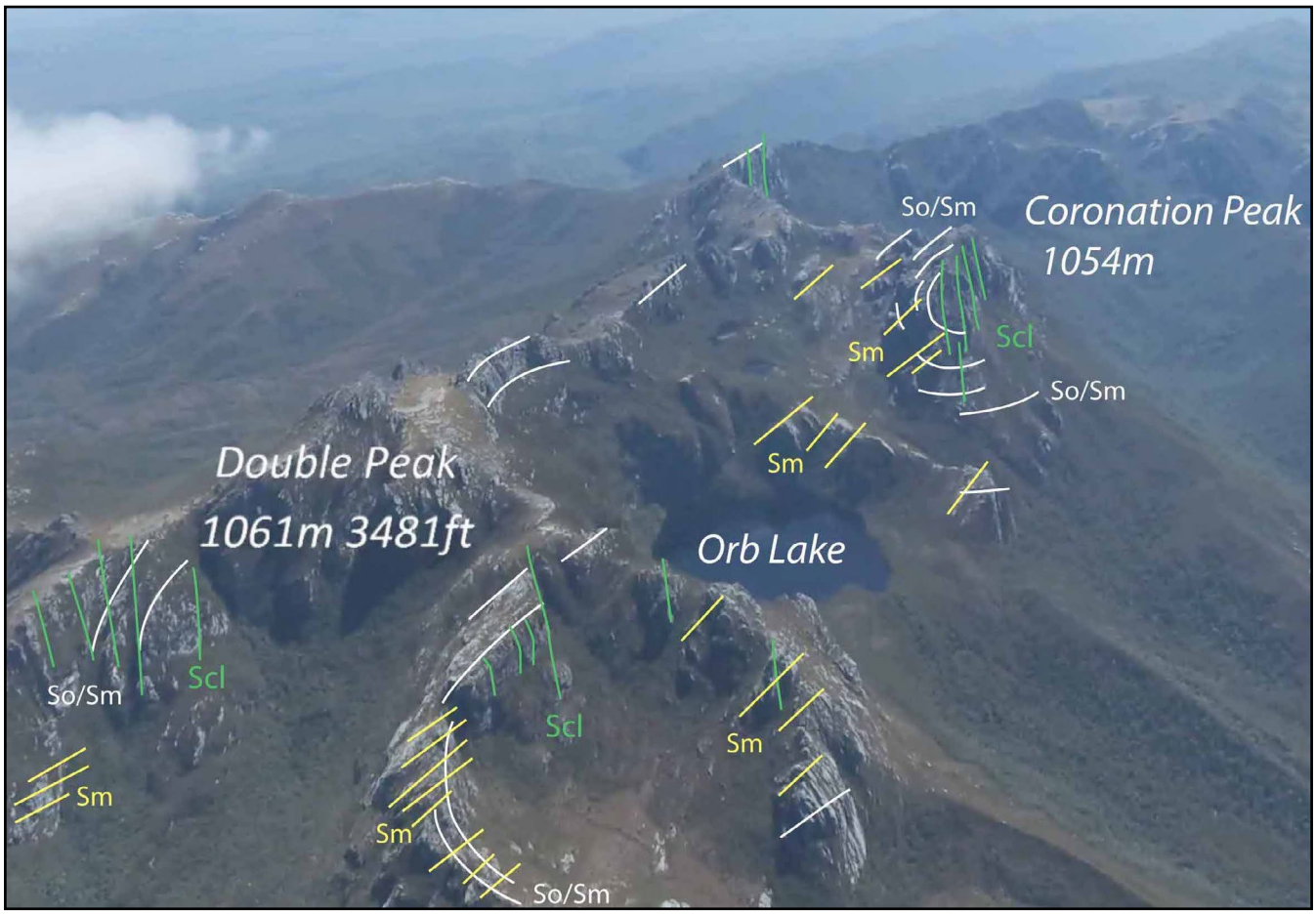

Figure 36. Aerial view looking northwards along the Frankland Range showing structural interpretation in serial ridge sections between Coronation Peak and Double Peak at the junction between the Wilmot Range and the Frankland Range. The ridgeline is clearly dominated by a west-closing and westerly inclined, synformal macro-isoclinal fold. The fold axial surface trace sits on the east side of each peak and passes through Orb Lake.

So/Sm: white line traces. Sm: yellow line traces. Devonian cleavage: green line traces. Photo profile PP3 in Figure 40. (Photo Credit: Wandering Foxbat)

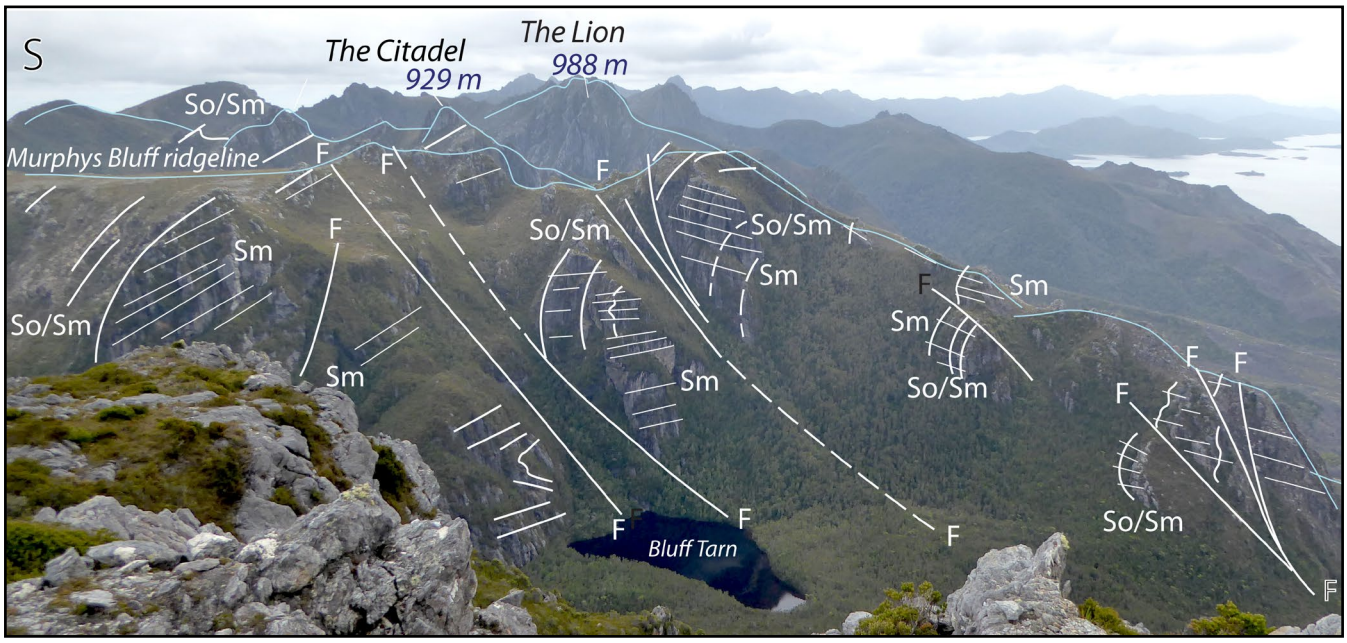

Figure 37. Murphys Bluff view looking northwest from Cleft Peak showing the southwest-closing, recumbent macro-isoclinal fold hinge cut by a series of reverse faults. Photo profile PP5 in Figure 40. (Photo Credit: David Green)

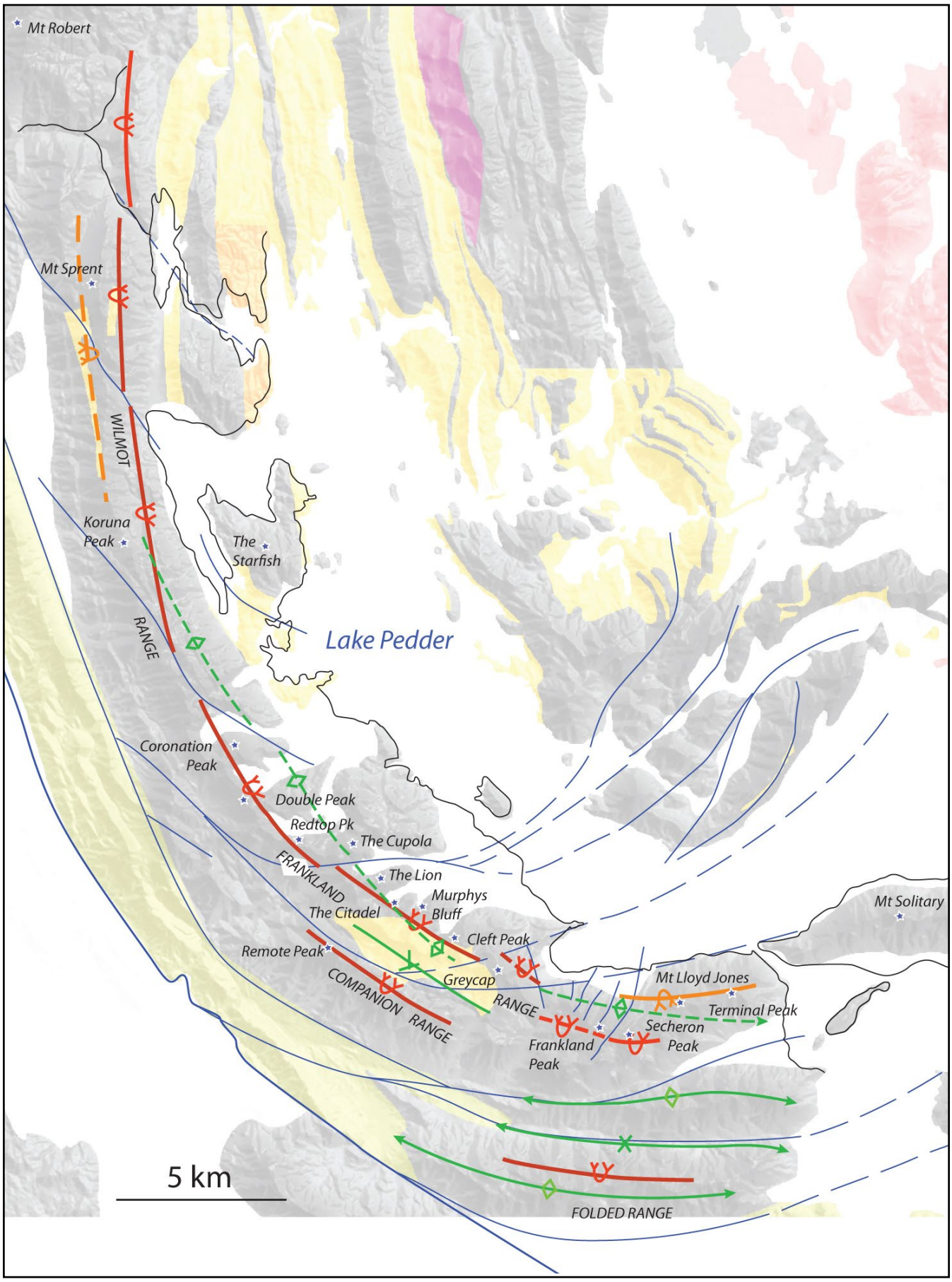

Figure 38. Axial surface trace map of the Wilmot - Frankland Ranges based on photo profiles (Figures 40, 41 and 42). Red line traces: west-closing recumbent isoclinal macro-fold axial surface trace. Orange line traces: west-closing recumbent isoclinal macro-fold axial surface trace. Green line traces: younger syncline and anticline axial surface traces. Blue line traces: fault outcrop traces.

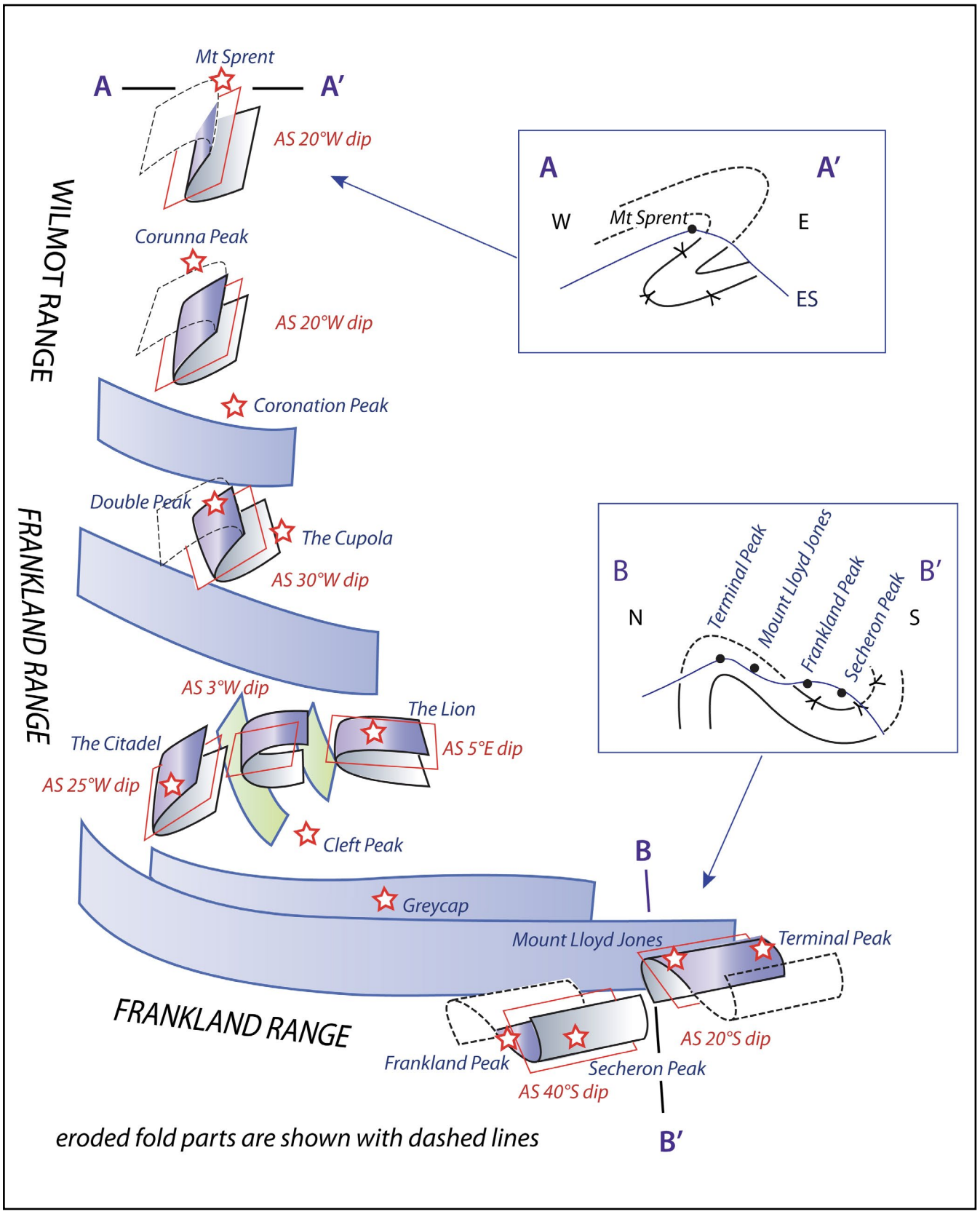

Figure 39. 3D macro-fold geometry diagram of the Wilmot - Frankland Ranges. The diagram shows the varying fold attitude changes of the asymmetric, isoclinal macro fold pair along the length of the range ridgeline. This is highlighted by the changes in axial surface dip and the swing in orientation from north-south trending to east-west trending along the range. The grey surfaces represent the curved sub-vertical faults that offset the macro-fold pair, particularly in the southern part of the range.

Cross Section A-A' across the Wilmot Range near Mt Sprent shows the dominant, west-closing, recumbent macro-fold with an inferred eroded complementary east-closing macro-fold.

Cross Section B-B' is a composite profile with outcrop relations at Mount Lloyd Jones and Terminal Peak projected onto a plane through Frankland Peak and Secheron Peak. The profile shows the asymmetric fold pair with axial surfaces dipping to the south.

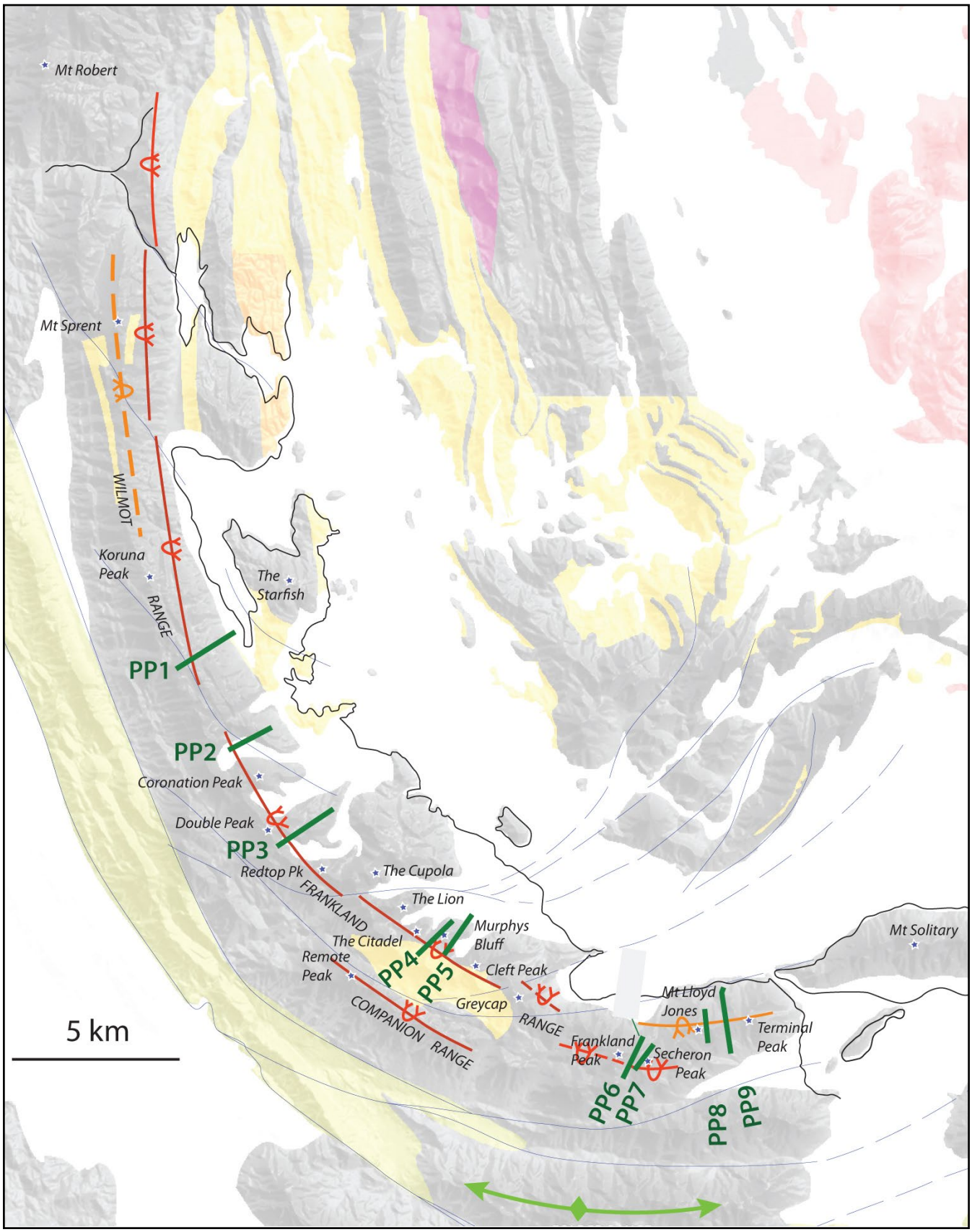

Figure 40. Photo profile positions (green lines and green PP numbers) shown on an axial surface trace map of macro isoclinal folds along the Wilmot and Frankland Ranges. Base map is a revised lithological map based on the Mineral Resources Tasmania 1:250,000 and 1:50,000 digital atlas. The positions of the axial surface traces are based on formline interpretation from the individual photo profiles. The orange line shows the axial surface trace of the structurally higher, east-closing macro-fold. The red line trace is the axial surface trace of the west-closing macro-fold that dominates the range.

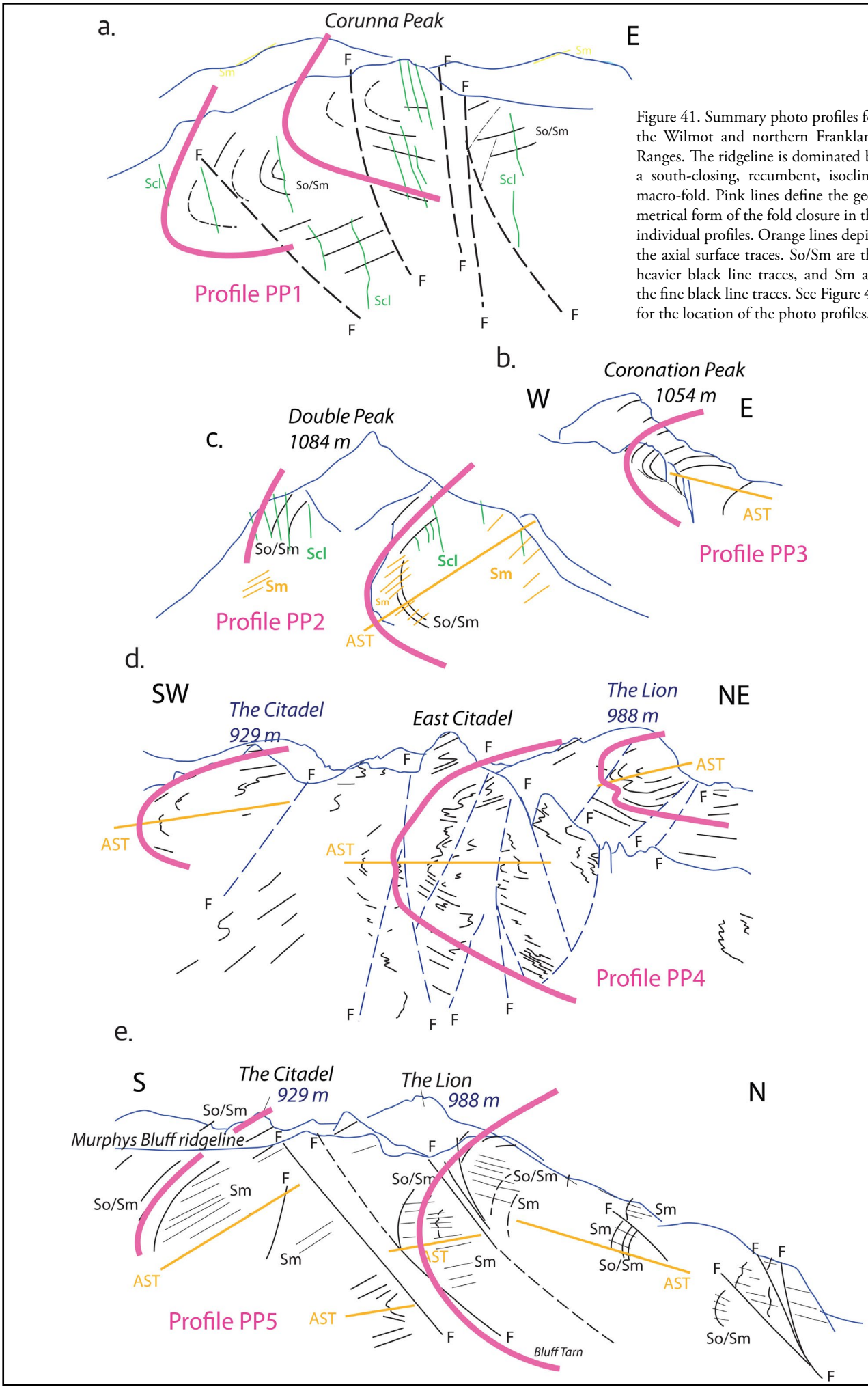

Figure 41. Summary photo profiles for the Wilmot and northern Frankland Ranges. The ridgeline is dominated by a south-closing, recumbent, isoclinal macro-fold. Pink lines define the geometrical form of the fold closure in the individual profiles. Orange lines depict the axial surface traces. So/Sm are the heavier black line traces, and Sm are the fine black line traces. See Figure 40 for the location of the photo profiles.

Detailed structural mapping undertaken by Boulter (1974,1978) enabled construction of down-plunge profiles along the Range (see composite profile Figure 6). This work encapsulates the geometry, structural style and structural sequence of the Wilmot - Frankland Range (Figures 6 and 7) but the low fold plunges (commonly <20°) require creation of spaced, sub-vertical profiles rather than stacking of profiles into a single plane (Figure 43). The current work, using spaced photo profiles, shows differences in the overall geometrical interpretation (see Appendix 1). Fault offsets and displacements clearly impact the positions and levels of the elements in Boulter's summary schematic diagram (Figure 6).

A revised geometry is shown in Figure 39. The important features are: 1) the structurally lower west-closing macro-fold hinge occurs at the level of the current erosion surface and therefore dominates the Wilmot and northern part of the Frankland Range; 2) the west-closing hinge and axial surface is folded in the vicinity of The Citadel, The Lion and Murphys Bluff ridgeline; 3) the southern Frankland Range shows partial erosion through the asymmetric macro-fold pair; and 4) offsets occur in the macro-fold hingeline along the range due to oblique slip along the curved horsetail fault splay system (Figures 38 and 39) and a series of normal faults through Frankland Saddle (Figure 44). Both sets of faults facilitate the counterclockwise rotation of the southern part of the Frankland Range.

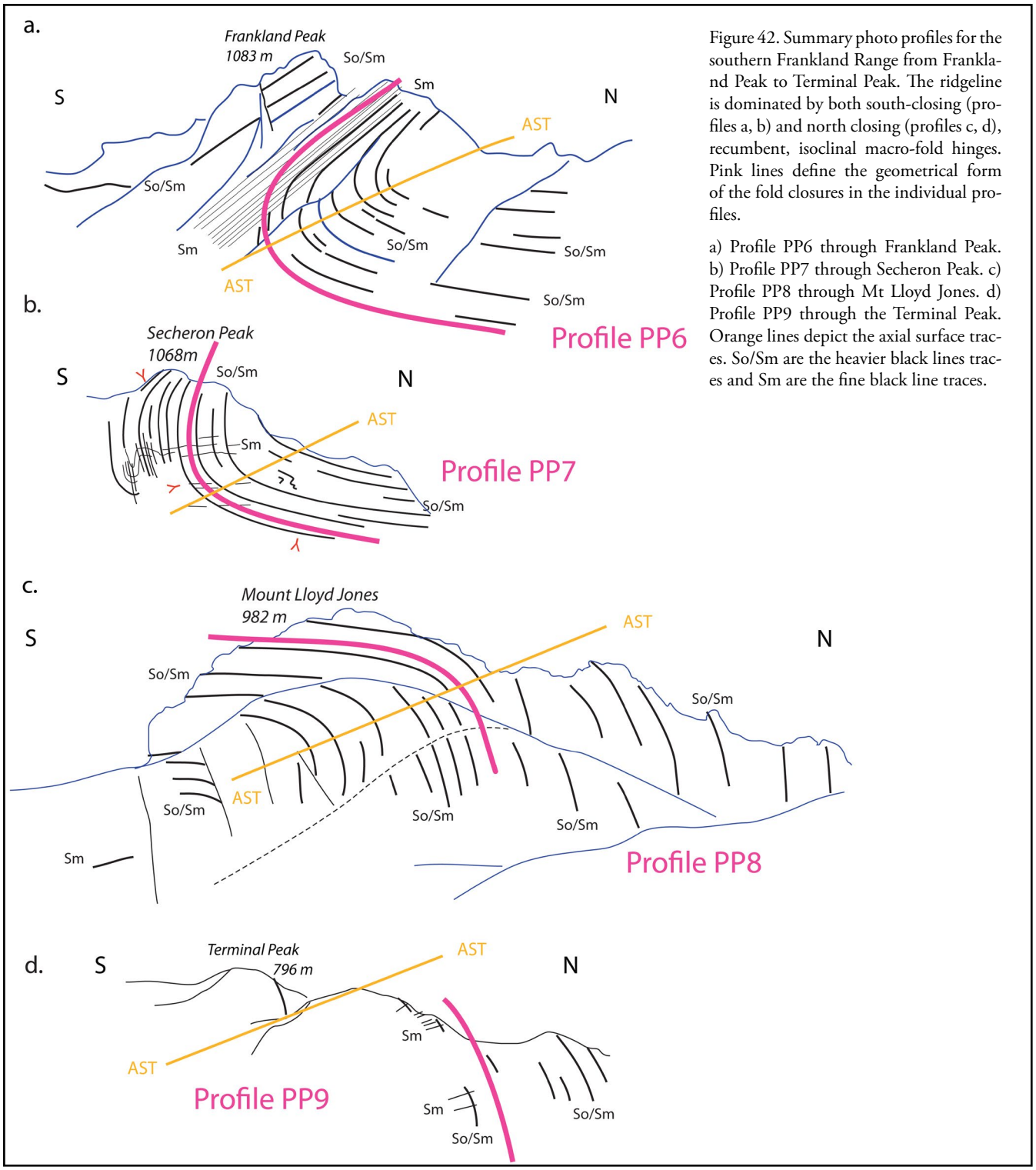

Figure 42. Summary photo profiles for the southern Frankland Range from Frankland Peak to Terminal Peak. The ridgeline is dominated by both south-closing (profiles a, b) and north closing (profiles c, d), recumbent, isoclinal macro-fold hinges. Pink lines define the geometrical form of the fold closures in the individual profiles.

a) Profile PP6 through Frankland Peak. b) Profile PP7 through Secheron Peak. c) Profile PP8 through Mt Lloyd Jones. d) Profile PP9 through the Terminal Peak. Orange lines depict the axial surface traces. So/Sm are the heavier black lines traces and Sm are the fine black line traces.

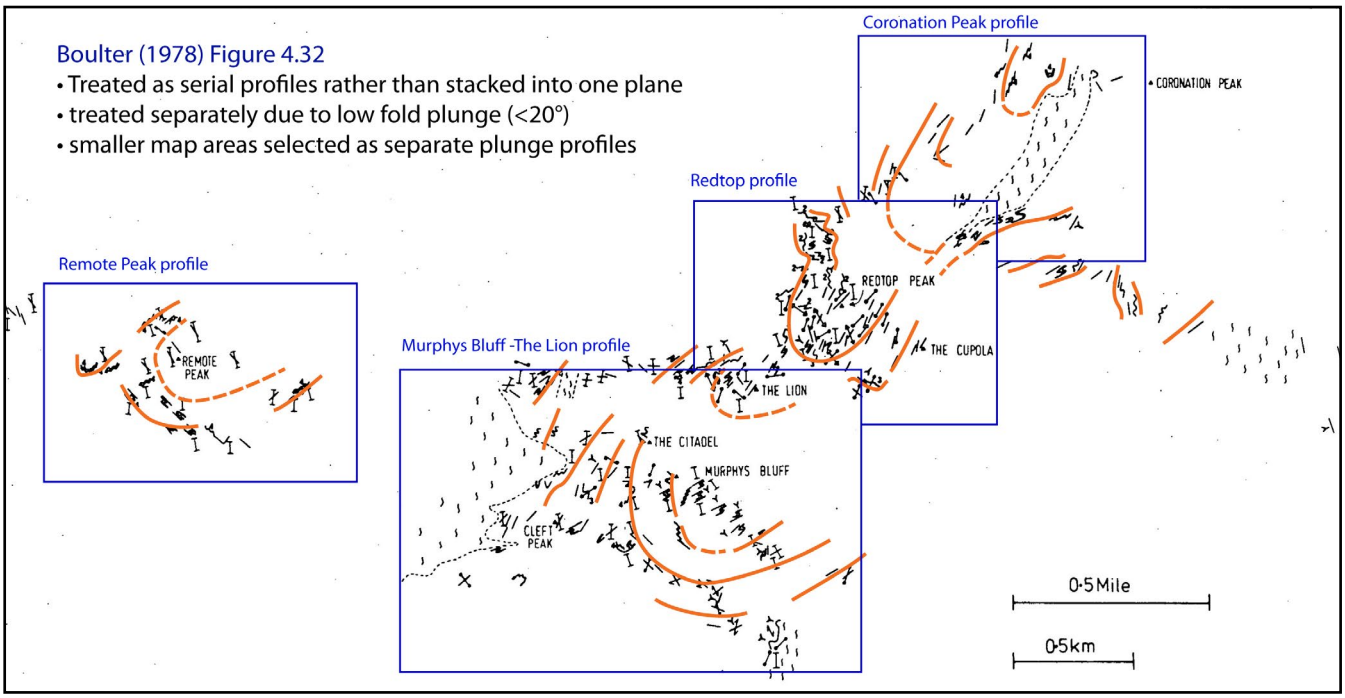

Figure 43. Boulter (1978, Fig.4.32) down plunge profile from map projection from Coronation Peak to Cleft Peak including Remote Peak. The red formlines are an interpretation based on Boulter's figure utilising So traces on the projection plane. The superimposed blue rectangles represent individual profile sections rather than stacking into one plane required by the original thesis Figure 4.32. Compare with photo profiles in Figure 42.

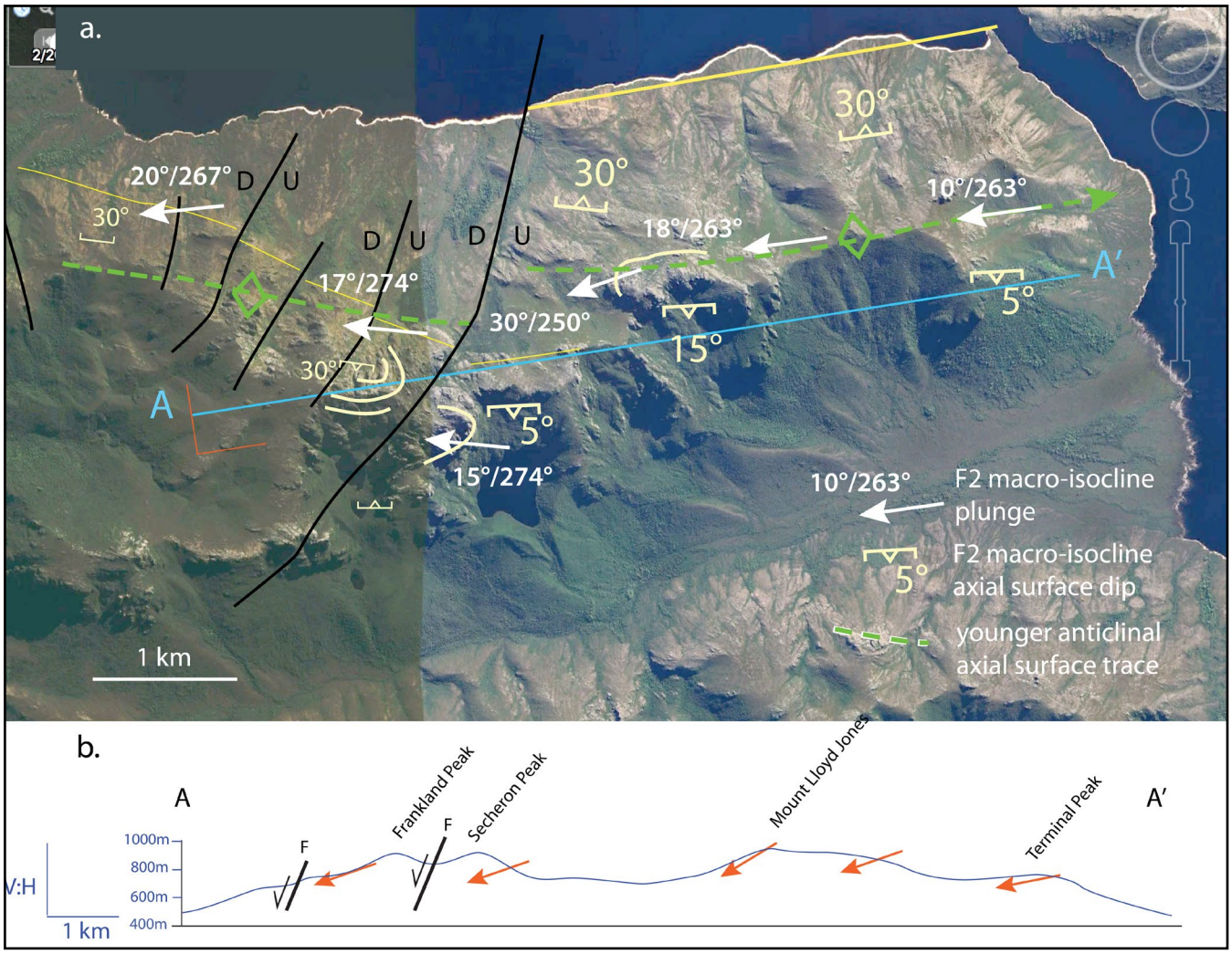

Figure 44. a) Structure map of the southern end of the Frankland Range from Frankland Saddle to Terminal Peak on a ListMapTM Google satellite image. Normal fault traces are shown through Frankland Saddle. Formline traces in So/Sm are shown by the yellow line traces. The white arrows are generalised macro-fold plunges from Boulter (1978). The light green axial surface dips of the macro-isocline folds are shown by the pale yellow dip/strike symbol. Both the south-closing hinges at Secheron and Frankland Peaks and the north-closing hinges at Mount Lloyd Jones and Terminal Peak are folded by a younger anticline shown by the light green dashed axial surface trace (Compare with Figures 38 and 39). b) Topographic profile A-A' showing macro-fold plunges (red arrows) and normal faults through Frankland Saddle. The profile position is shown in (a).

5.1.4 The Twelvetrees Range

The Twelvetrees Range is dominated by a west-closing macro-fold (Element 5, Figure 14), upright folding through the centre of the range and an inclined F2 fold refolding the lower, gently west dipping eastern limb on the eastern side of the range (Figure 45). Three coaxial deformation phases (D1, D2 and D3) with F1 and F2 coplanar and similar folds plunge generally to the south at 20° to 40° (Figure 3, Brown et al., 1989). A zone of intense transposition layering with overprinting crenulation cleavages (Scc) is part of a high strain zone exposed at the southwestern side of the range (Figures 46 and 47). This zone is considered part of a broader high-strain zone with large-scale, dismembered quartzite layers, that passes through the Strathgordon township. The high-strain zone potentially envelopes, and is folded with, the quartzite of the Twelvetrees Range. Road outcrops (DG17-66, DG17-67 and DG17-68, Figure 45) also show intense foliation and multiple overprinting crenulation cleavages (Scc) on the southeastern part of the range as part of an Atkins Range bounding high-strain zone (Figure 47).

5.2 Asymmetric Fold Pair within Lozenge-shaped Augen

Elongated, pod-like quartzite bodies as lozenge-shaped pods (augen) at a regional scale (Element 6, Figure 14) dominate the Spires Range - Shining Mountain - Conical Mountrain - Mt Curly - North Star region (Figures 48 and 49). The region occupies the northeastern-most part of the Eastern Tyennan subdomain. The quartzite body at Shining Mountain has tadpole-like shape and is underlain and infolded with mixed layer quartzite-phyllite-calcareous phyllite (Pqpc) (Figures 48 and 49). The lozenge-shaped structural morphology is distinct from the long continuous, tube-like quartzite ridgelines of other parts of the Eastern Tyennan subdomain, such as the Prince of Wales - Hamilton - Wilmot - Frankland Range ridgeline system and the Twelvetrees Range (see Section 5.1.1 and 5.1.4 above).

The quartzite peaks and ridgeline exposed as The Spires range, Shining Mountain and Mt Curly contain segments, or relicts, of the macro isoclinal fold pair (Figure 23). The structures internal to the quartzite are truncated by a basal fault and/or high strain zone (HSZ) (Figure 23). The level of this basal discontinuity changes due to the younger west-dipping thrust fault system. The structurally lower quartzite + interlayered quartz-mica phyllite and carbonate (Pqpc) is also folded with the quartzite by the regional F3 fold set (Figures 22 and 23).

5.2.1 The Spires

The Spires is an elongated, northeast-trending, tapered, pod-shaped quartzite (Element 6, Figure 14) ridgeline with inferred opposing fold plunges at the northern and southern terminations (Figure 50). The ridgeline exposes varying intersections through the asymmetric, east-vergent recumbent fold pair (Figures 51 and 52). The fold pair consists of a structurally higher east-closing synformal macro-fold connected to a structurally lower, west-vergent macro-fold. The envelope geometry of The Spires range has an overall cigar shape (Figure 53) and/or spindle-like tube shape (Figure 54) with a forked southern termination due to the closeouts of the macro-fold hinges (Figure 50).

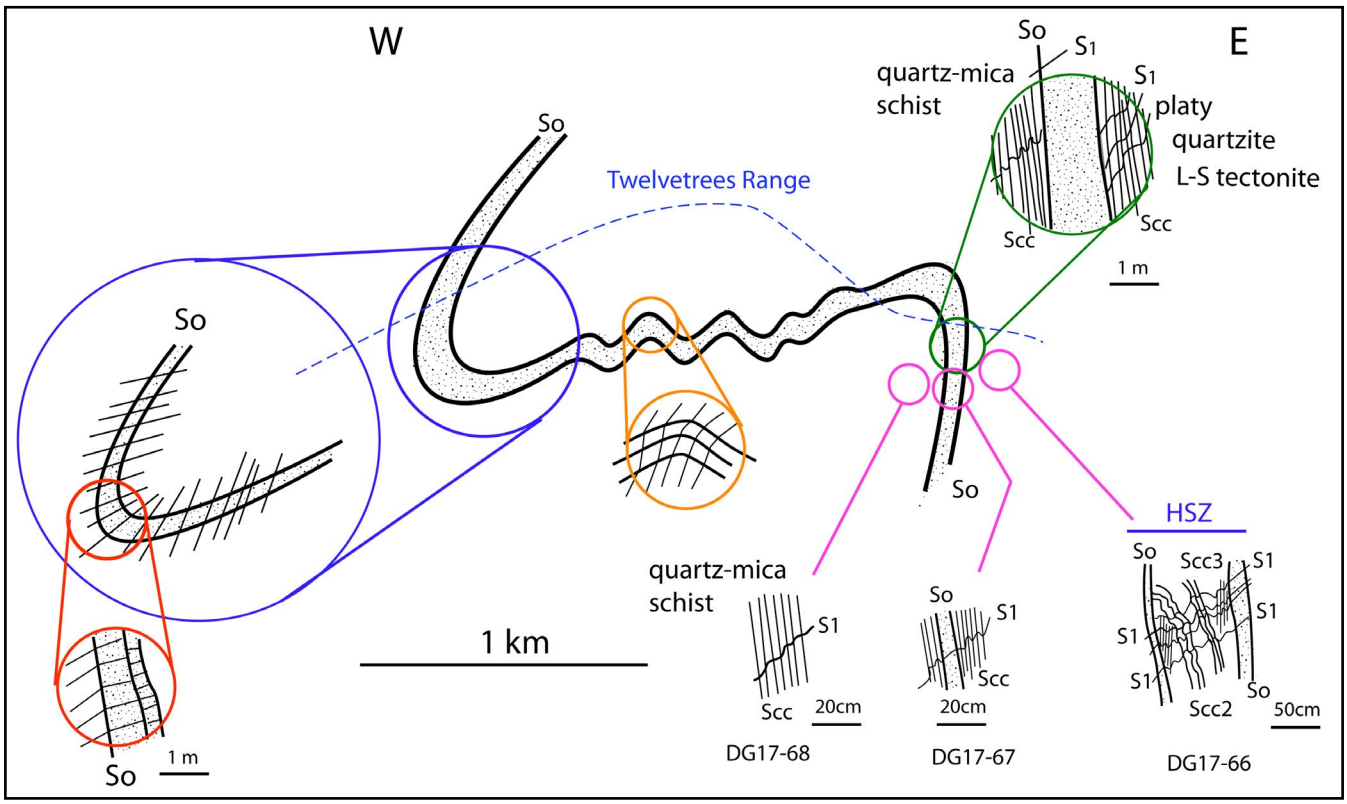

Figure 45. Geometry of the Twelvetrees Range macro-isoclinal fold shown as a structural profile across the south end of the Twelvetrees Range. The profile construction is based on a road traverse up to the Twelvetrees Range communications tower (see Figures 46 and 47) and outcrops on the Gordon River Road and along Trappes Inlet.

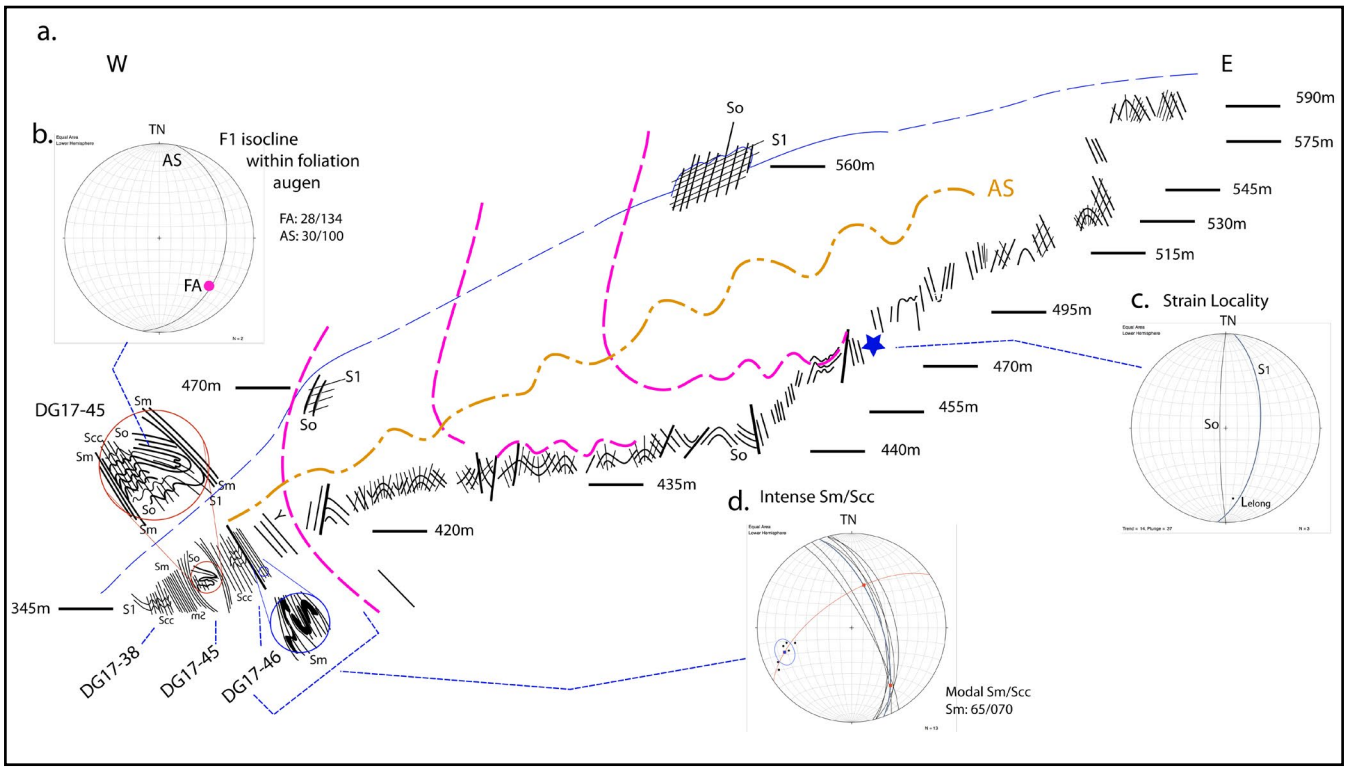

Figure 46. Composite, stacked sketch-profile based on the outcrop sketches along the road to the communications tower at the south end of Twelvetrees Range. The blue line is the approximate topographic range profile. Pink dashed lines are So/Sm trends that define the hinge of a west-closing Twelvetrees macro-isoclinal fold. a) Profile with enlargements of parts of the outcrop, particularly in the high strain zone that envelopes the fold closure. b) Stereonet of F1 isocline fold axis and axial surface. c) Stereonet with bedding and cleavage attitudes and the elongation direction (Lelong) at the strain locality (see Appendix 3). d) Stereonet of intense foliation Sm transitional with crenulation cleavage Scc within the high strain zone (HSZ) exposed in cuttings and outcrops along the lower part of the road.

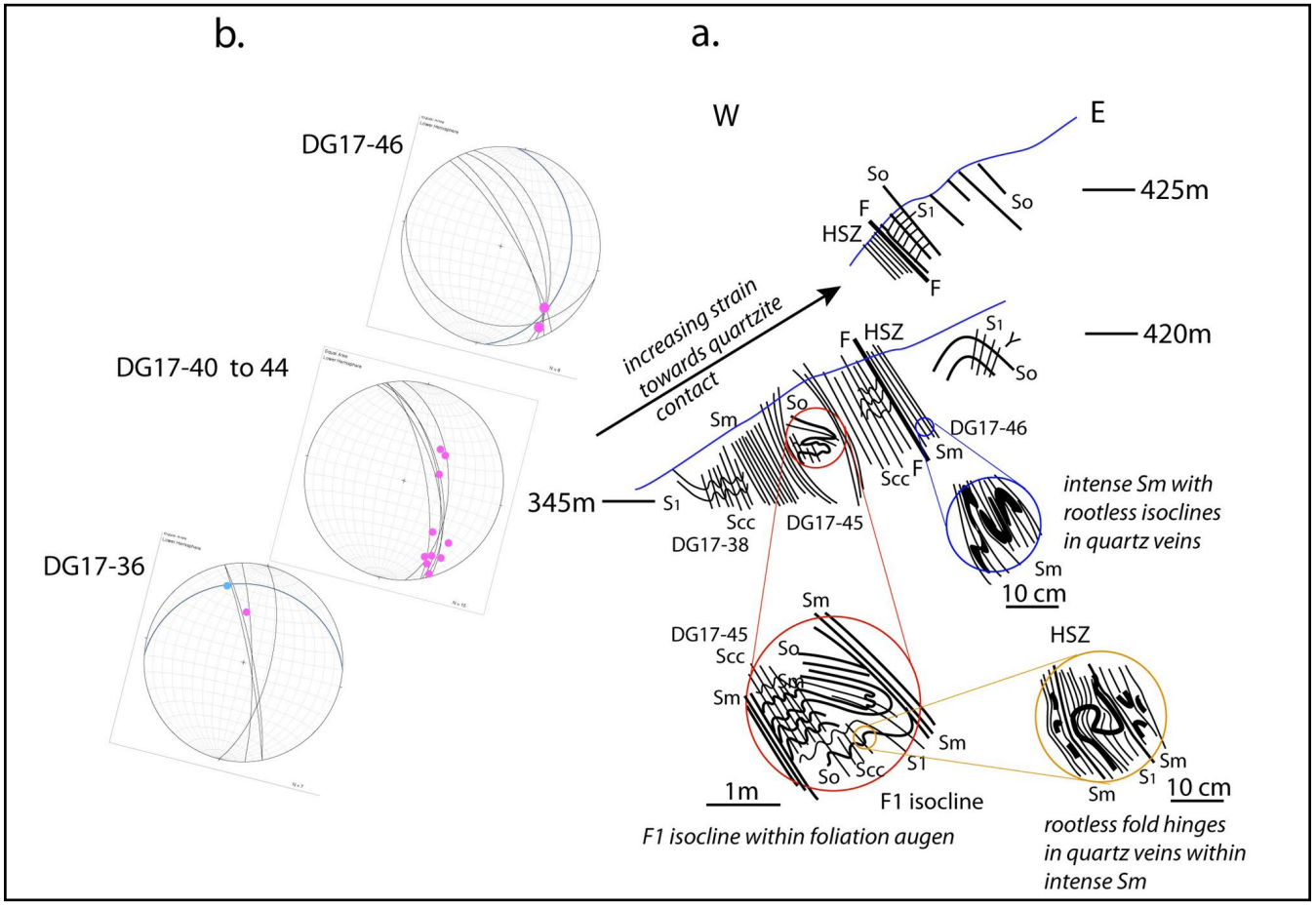

Figure 47. Twelvetrees Range strain gradient into the quartzite contact at the macro-isoclinal fold hinge. a) Superimposed sketch profiles on different road bends with enlargements of the observed fabric relationships. b) Stereonets of foliation Sm, fold axial surface (AS) and fold axis attitudes (pink dots) at different positions in the profile.

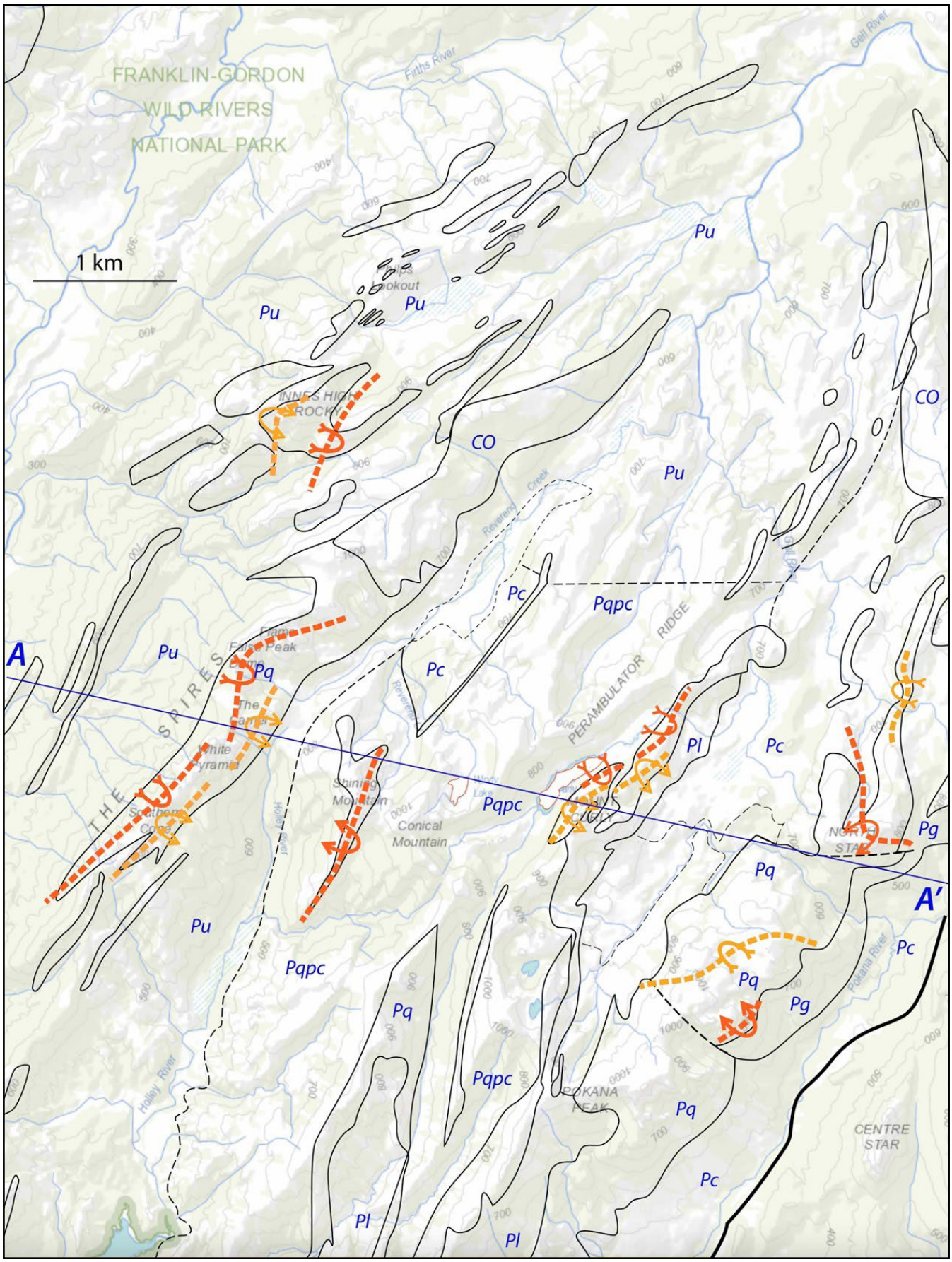

Figure 48. Axial surface trace map of the macro-fold pair that occupy the quartzite ridgelines showing geological contact traces based on the Mineral Resources Tasmania 1:250,000 geological atlas. The fold pair consists of a structurally higher east-closing fold hinge (red dashed line trace) and a structurally lower west closing fold hinge (orange dashed line trace). The position of the cross section line A-A' (Figure 23) is shown. Proterozoic (P) geological units include: Pq: quartzite, Pqpc: interlayered quartzite-pelite and calcareous pelite, Pl: pelite, Pg: black carbonaceous phyllite, Pc: carbonate, Pu: undifferentiated and CO: Late Cambrian to Ordovician sandstone-conglomerate sequences.

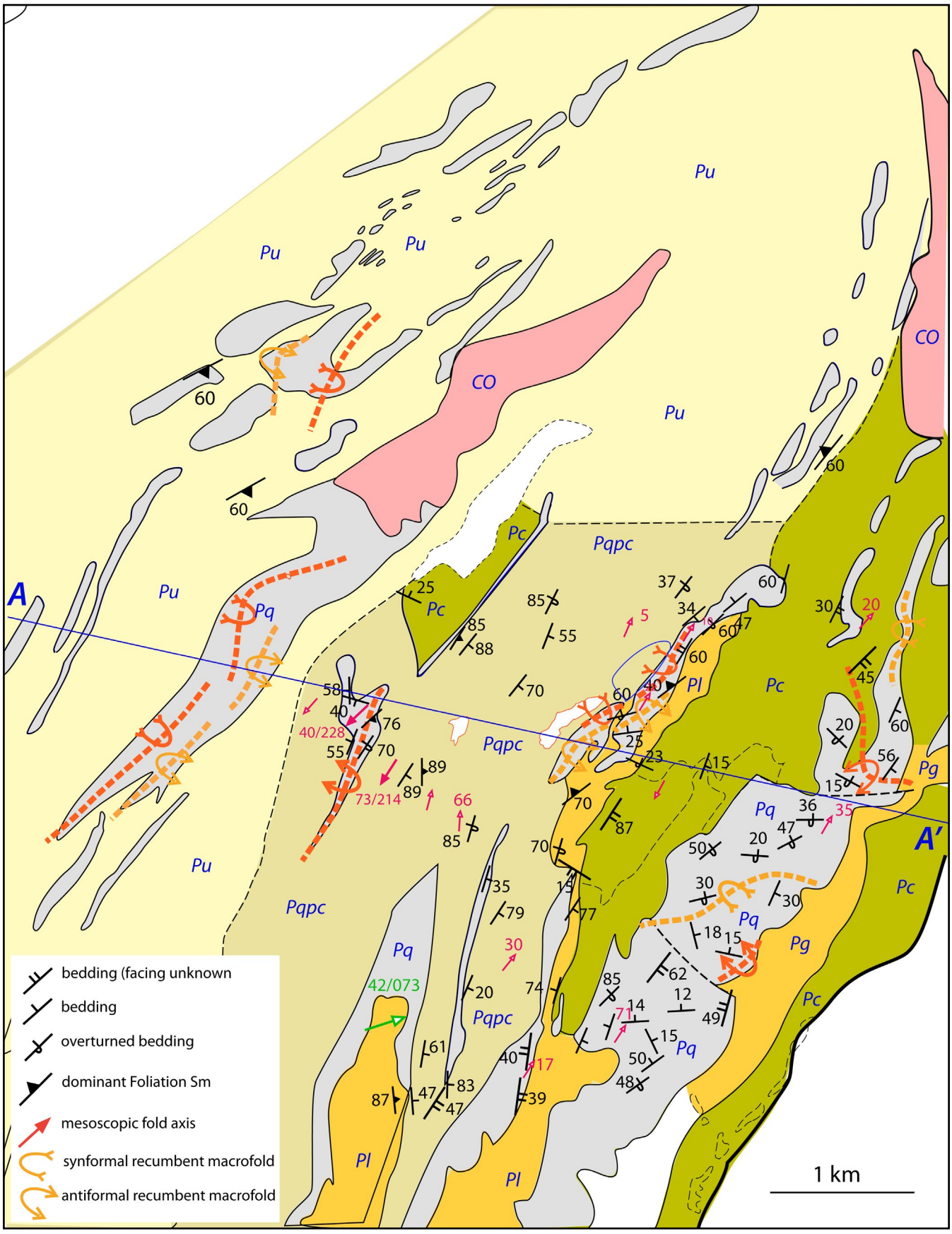

Figure 49. Structural map of The Spires, Shining and Conical Mountains, Mt Curly and North Star area. The map base is modified from the Mineral Resources Tasmania 1:250,000 geological atlas. The position of the cross section line A-A' (Figure 23) is shown. Proterozoic (P) geological units include:

Pq: quartzite
Pqpc: interlayered quartzite-pelite and calcareous pelite
Pl: pelite
Pg: black carbonaceous phyllite
Pc: carbonate
Pu: undifferentiated
CO: Late Cambrian to Ordovician sandstone-conglomerate sequences

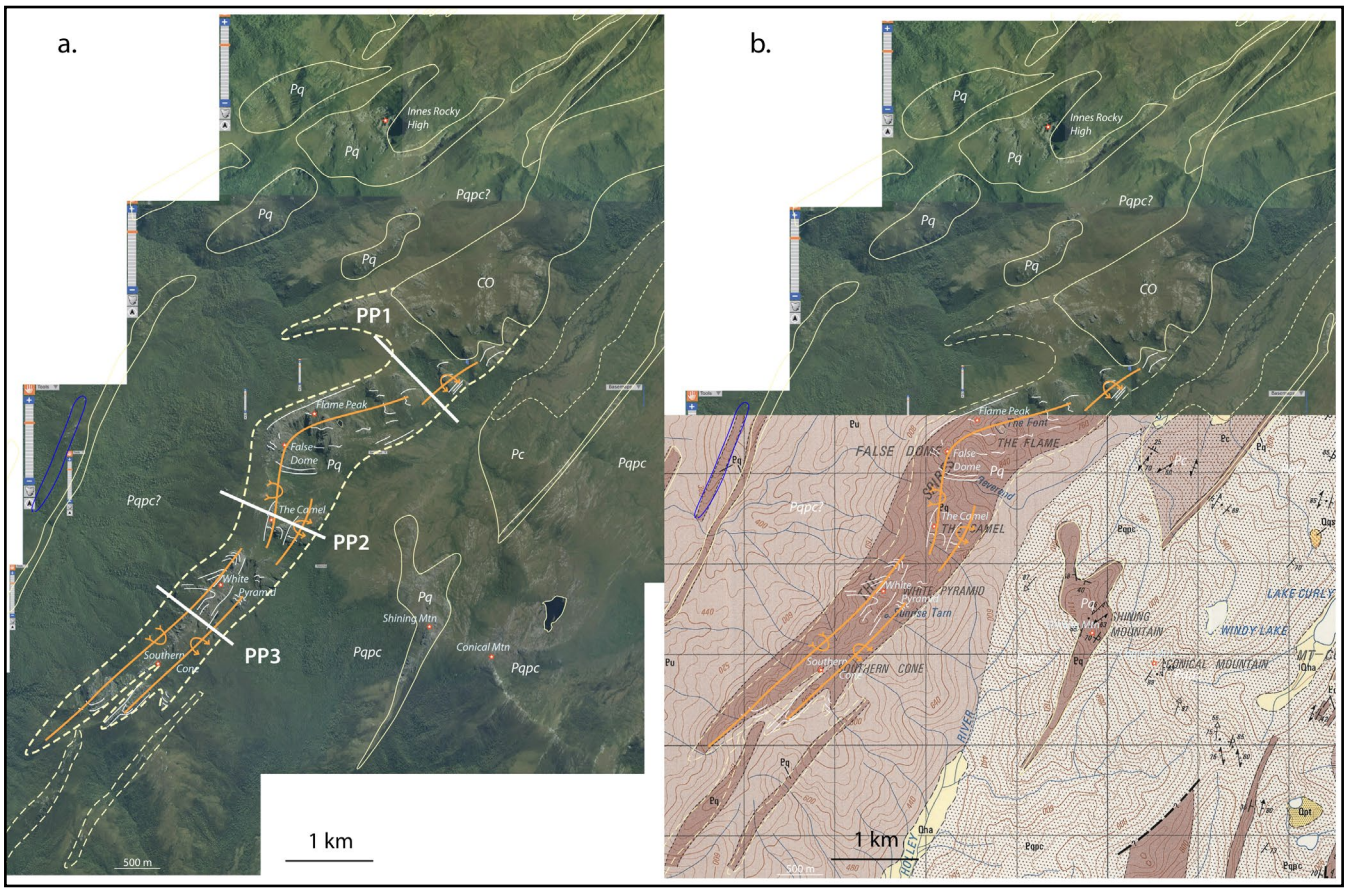

Figure 50. Structural interpretation map of the Spires area. a) ListMap Google satellite image showing formlines in So/Sm (white line traces), interpreted geological contacts (dashed white line traces), mapped geological contacts (pale yellow line traces) and the axial surface traces of the regional, isoclinal macro-fold pair (orange line traces). Listmap airphoto base. The positions of the photo profiles are shown by the heavy white lines labelled PP1 to PP3. b) Huntley sheet 1:50,000 map base superimposed on ListMap Google satellite image shown in (a).

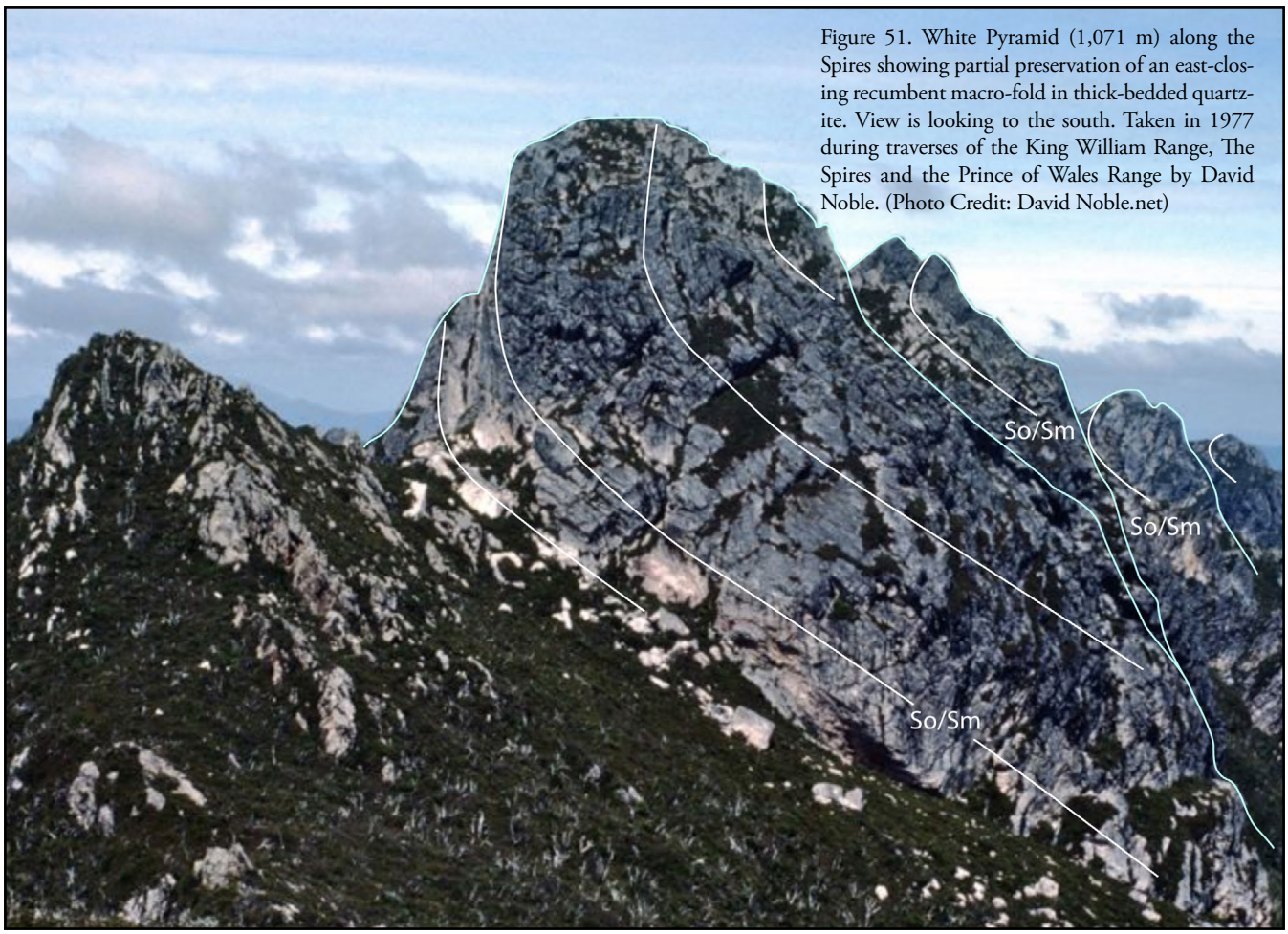

Figure 51. White Pyramid (1,071 m) along the Spires showing partial preservation of an east-closing recumbent macro-fold in thick-bedded quartzite. View is looking to the south. Taken in 1977 during traverses of the King William Range, The Spires and the Prince of Wales Range by David Noble. (Photo Credit: David Noble.net)

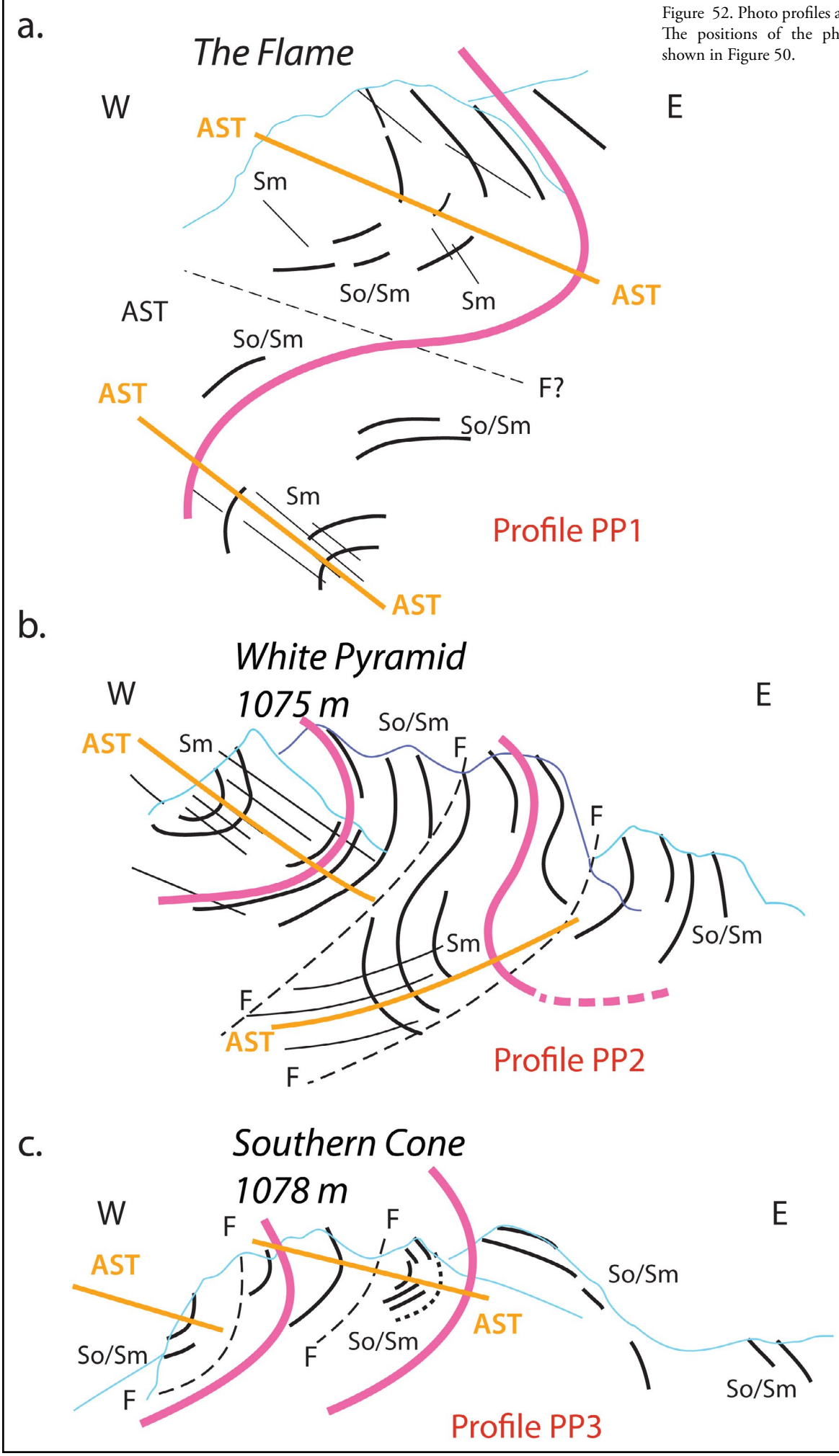

Figure 52. Photo profiles across The Spires. The positions of the photo profiles are shown in Figure 50.

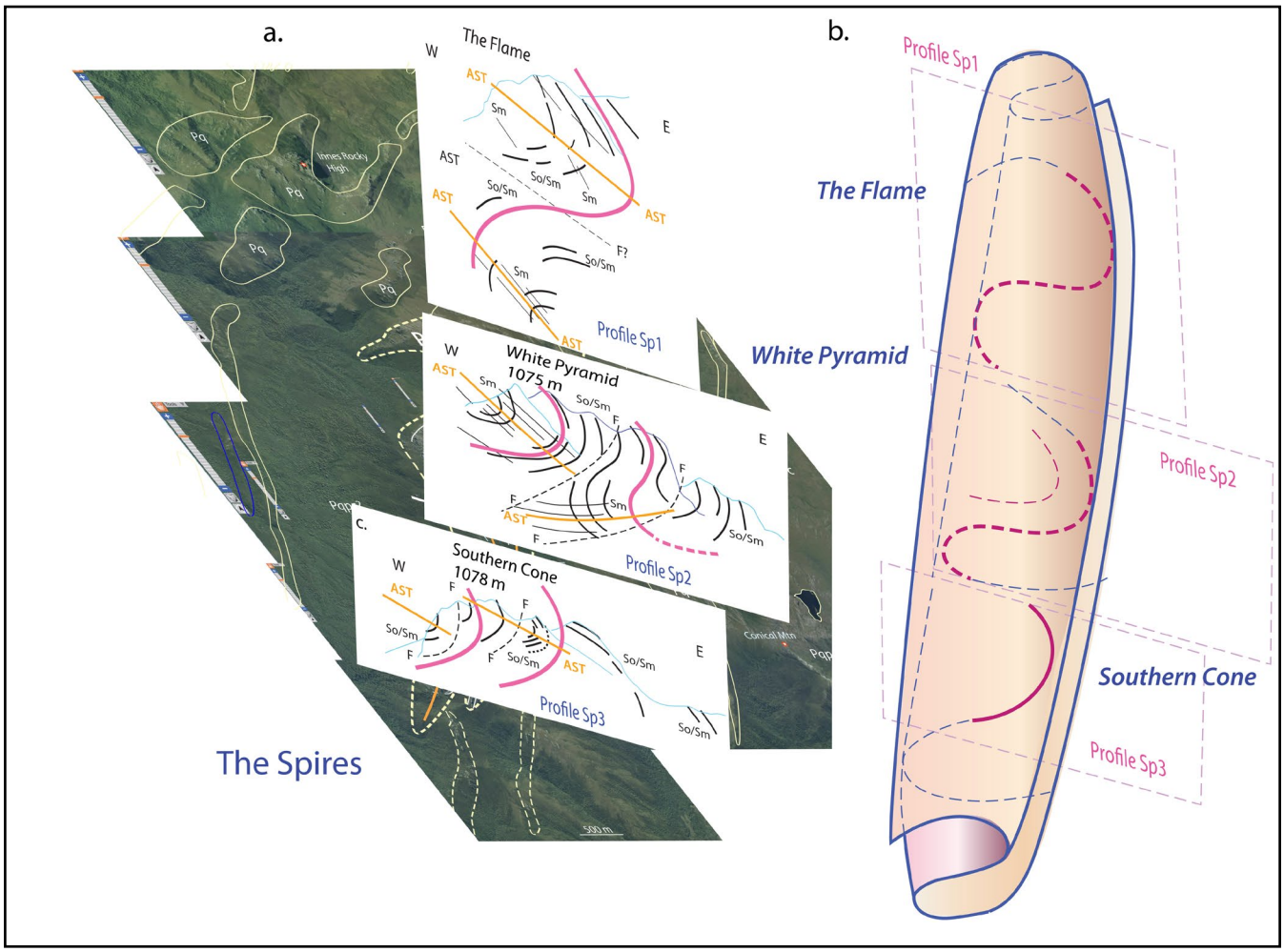

Figure 53. Oblique tilted view looking to the northeast of the structure of The Spires. a) Tilted map view with superimposed photo profiles Sp1 to Sp3 (compare with Figure 52). b) Reconstructed 3D form of the quartzite macro-fold structure along The Spires. Fold plunges are unknown but appear to be sub-horizontal from the photos.

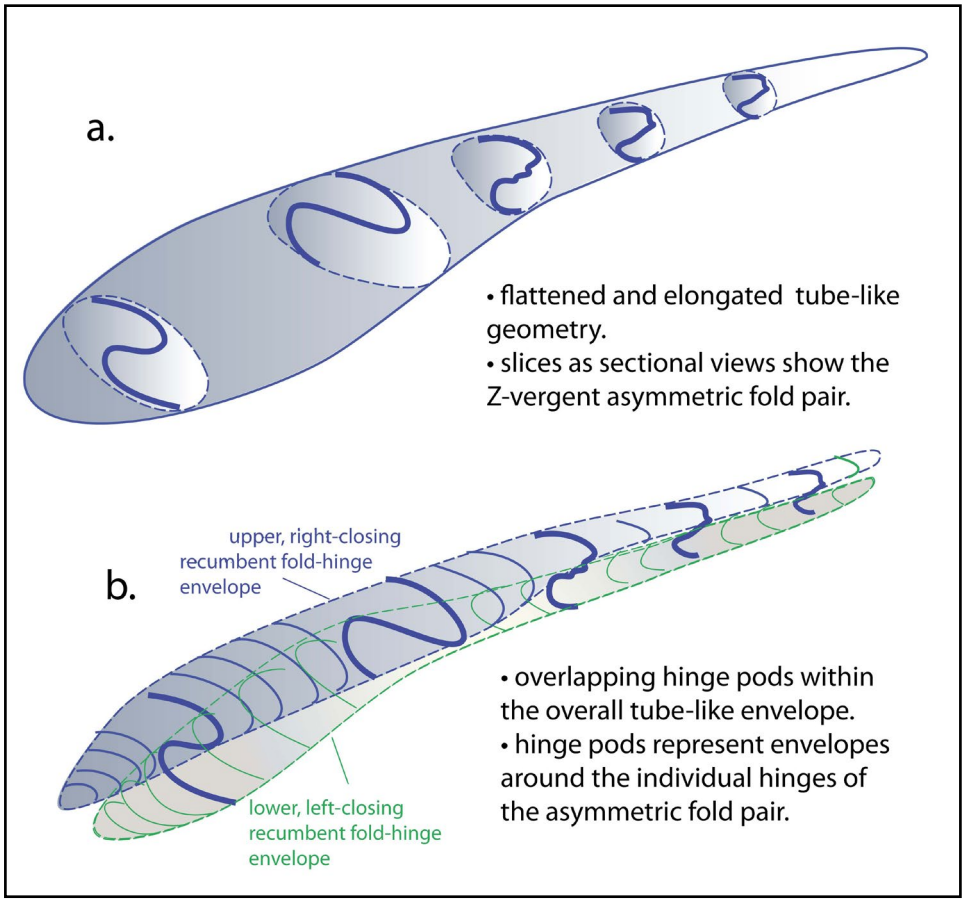

Figure 54 (Left). Schematic diagrams of the interpreted 3D structure of The Spires as a flattened and elongated pod - or tadpole-shaped augen. a) The quartzite envelope (grey) enclosing the Z-vergent, recumbent, asymmetric fold pair of the range. Sectional views are superimposed. b) Envelopes about the upper and lower oppositely-closing hinges of the fold pair. Note the hinge separation at the left closeout matches the forked nature of the southern termination of The Spires (see Figure 50).

5.2.2 Shining Mountain - Conical Mountain

Shining Mountain consists of an elongated, north-east-trending, tadpole-like outcrop of quartzite (Figure 55). Limited structural data from a ridgeline traverse by Nic Turner during the Huntley sheet mapping (Figure 55a), combined with the outcrop pattern (Figure 55b) suggest the quartzite is dominated by a major southwest-plunging recumbent fold that is refolded by north-northeast-trending F3 folds on the northern part of the ridge (FA: 40°/228°, Figure 55a).

The southern tail of the quartzite "tadpole" (Pq) contains a prominent southwest plunging hinge of the early fold that shows the bedding So/Sm formline traces truncated or discontinuous against the enveloping mixed layer quartzite-phyllite (Pqpc) sequence (inset, Figure 55c).

Structures within the quartzite appear truncated at the base of the quartzite by a brittle/fault high strain zone (HSZ) (Figure 56). The quartzite appears in-folded with the underlying, interlayered quartzite-quartz-mica phyllite and carbonate (Pqpc) (Figure 55). This interlayered quartzite-phyllite contains steeply plunging folds that occur along the ridgeline between Shining and Conical Mountains (Figures 57a, b). This area is dominated by a series of tall quartzite pillars (menhir) that have tapered, elongated ellipsoidal, pod-like form (Figure 57a). The steeply plunging pods with ~70° fold plunges (Figures 57b, d) are quartzite shear-lozenges. They contain relict isoclinal fold hinge zones, either as individual folds or asymmetric fold pairs, where the limbs have been completely attenuated. The result is that the quartzites are large augen enveloped by the schistosity of the surrounding interlayed quartzite-phyllite (Pqpc) (Figures 57a, b).

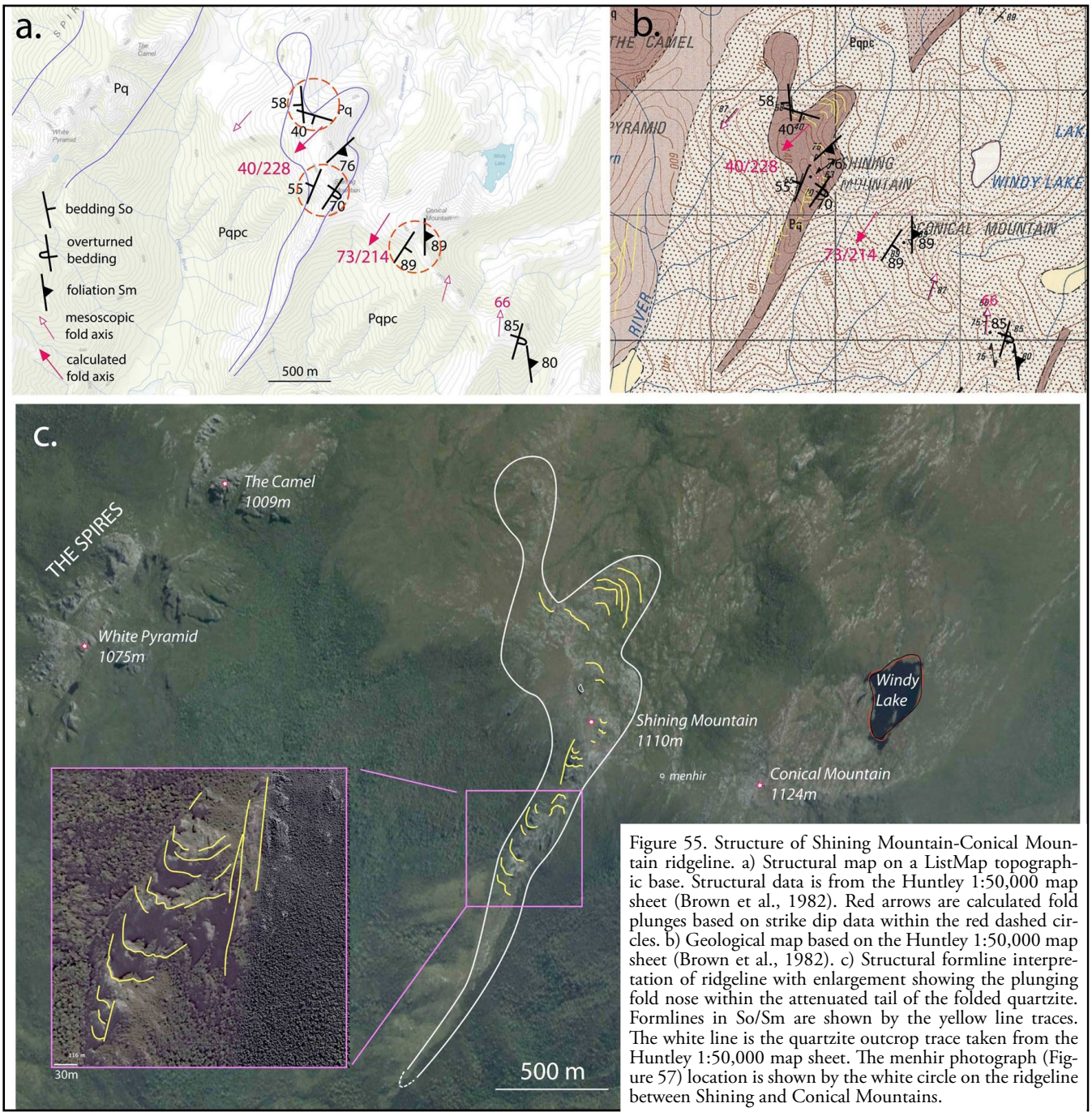

Figure 55. Structure of Shining Mountain-Conical Mountain ridgeline. a) Structural map on a ListMap topographic base. Structural data is from the Huntley 1:50,000 map sheet (Brown et al., 1982). Red arrows are calculated fold plunges based on strike dip data within the red dashed circles. b) Geological map based on the Huntley 1:50,000 map sheet (Brown et al., 1982). c) Structural formline interpretation of ridgeline with enlargement showing the plunging fold nose within the attenuated tail of the folded quartzite. Formlines in So/Sm are shown by the yellow line traces. The white line is the quartzite outcrop trace taken from the Huntley 1:50,000 map sheet. The menhir photograph (Figure 57) location is shown by the white circle on the ridgeline between Shining and Conical Mountains.

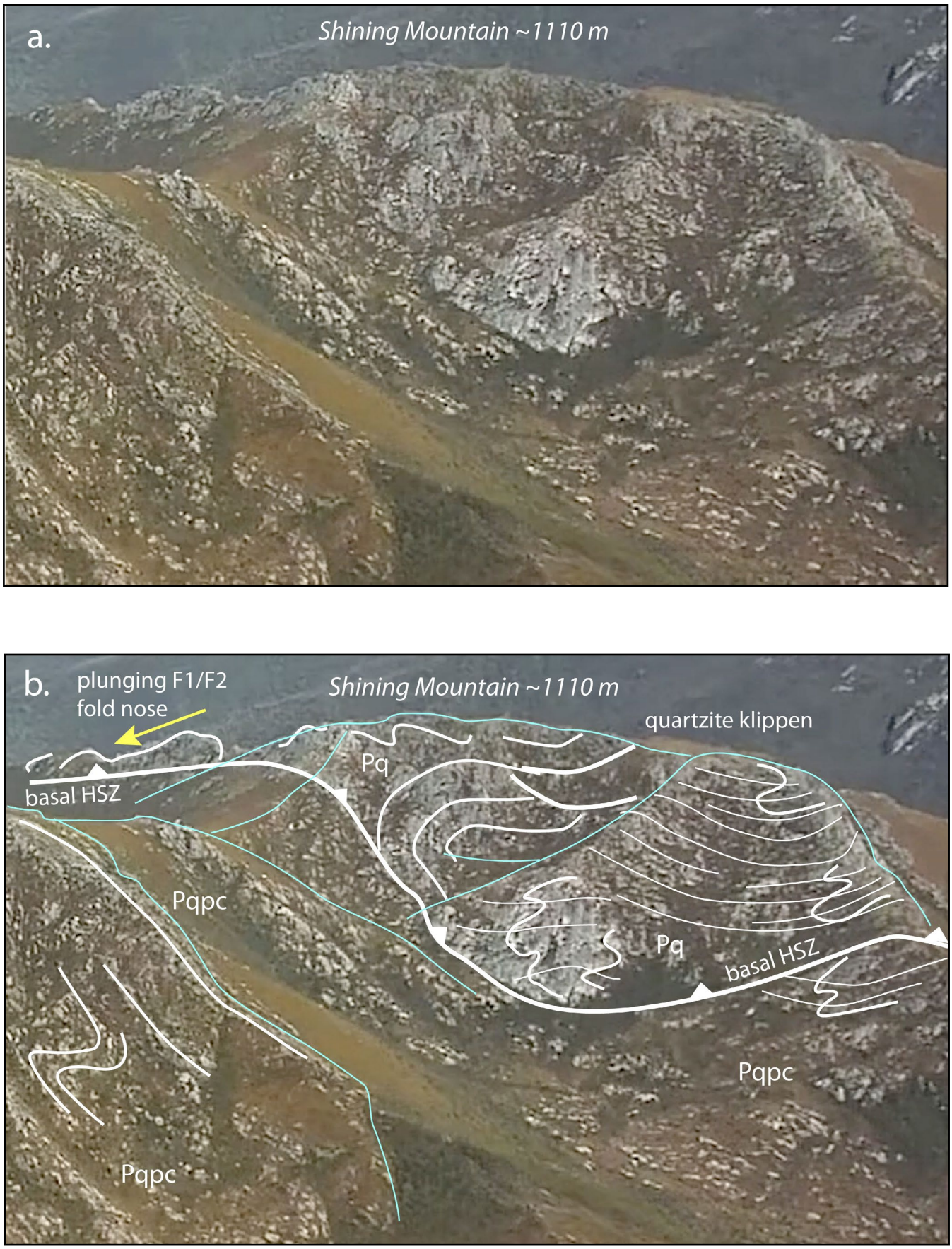

Figure 56. Quartzite (Pq) cap on Shining Mountain showing a marked, irregular basal contact with the underlying interlayered quartzite-phyllite-calcareous pelite (Pqpc). The contact is clearly discordant to foliation and macrostructure in the quartzite, and to the foliation in the underlying brownish interlayered quartzite and calcareous phyllite. The view to the west-northwest also shows an oblique intersection with the east-closing macro-fold. The apparent plunge of the fold in the trailing ridgeline is ~30° as shown by the yellow arrow. Heavy white lines: fault traces. Medium white lines: So/Sm formlines. Thin white lines: Sm traces.

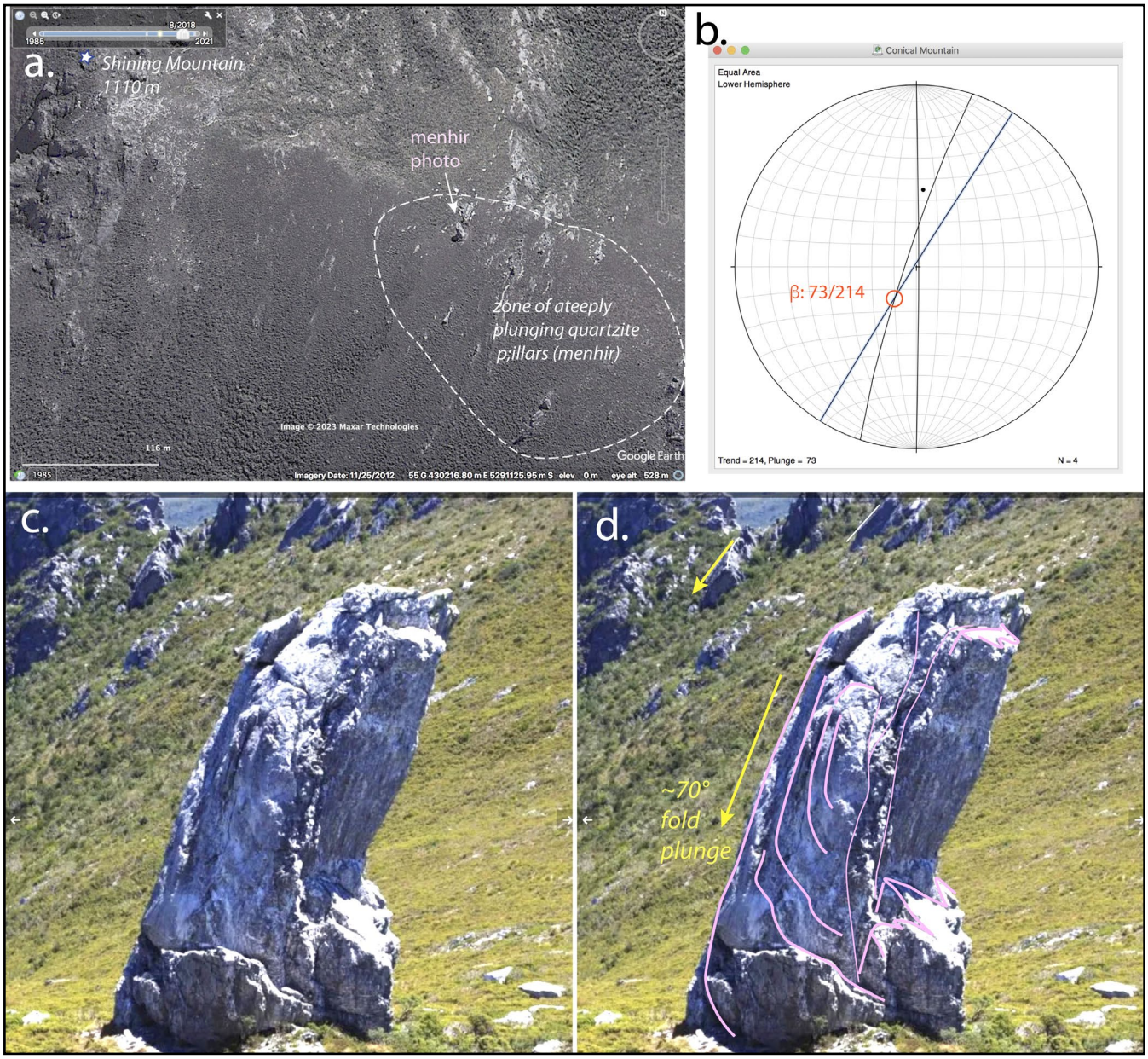

Figure 57. Zone of steeply plunging folds in quartzite pillars (menhirs) on the ridgeline between Shining Mountain and Conical Mountain. a) Google Earth image showing the area of quartzite pillars and the menhir shown in (c) and (d). b) Stereonet of bedding great circle traces and foliation Sm with β intersection (fold plunge) of 73°/214°. Data are from Conical Mountain on the Huntley 1:50,000 map sheet. c) Photograph of ~8 m high quartzite pillar (menhir) (Photo credit: Zane Robnik). The menhir location is shown in (a). d) Formline interpretation in bedding So/Sm (pink line traces) showing a steeply plunging tight to isoclinal fold hinge within the menhir.

5.2.3 Mt Curly

The Mt Curly region shows two elongated, northeast-trending, spaced, en echelon bodies of quartzite that define two ridgelines separated by a valley low in pelite (Pl) (Figure 58). The quartzites contain an asymmetric, recumbent, isoclinal macro-fold pair cut by west-dipping oblique-slip faults with sinistral sense and west-over-east transport (Figure 59).

The overall structural geometry of the Mt Curly region was determined from photo profiles (Figure 58a, Appendix 1 Section 4) with the axial surface traces fitted to the Google imagery (Figure 58a). Mesoscopic fold axis data from the Huntley map sheet (Brown et al., 1989) show the folds plunge gently (10°-25°) to the northeast (Figure 58b).

Erosion has led to partial preservation of the macro-fold pair with parts of the macro-fold pair shown at different levels and positions across the ridgeline (Figures 59 and 60). Most of the southern and highest part of the Mt Curly ridgeline contain the east-closing structurally higher macro-fold hinge (Figures 58a and 59). The structurally lower hinge is exposed along the lower western part of ridgeline adjacent to the northeastern shoreline of Lake Curly (Figure 58a). Below the west-closing macro-fold, the basal part of the quartzite is an intensely foliated zone (see Appendix 1 Section 4). This has fault-like character in places with clear truncation of the internal structure of the quartzite (see Section 5.3 below).

The second, more easterly ridgeline also contains both macro-fold hingelines, but is dominated by the west-closing macro-fold hinge. The structurally higher east-closing hinge has been removed by erosion with only partial preservation in the highest part of the ridge (Figures 60b and 61). The quartzite (Pq) appears interleaved and in-folded with the intervening pelite (Pl). This package overlies interlayered quartzite-phyllite-calcareous phyllite (Pqpc) on the west and carbonate and calcareous pelite (Pc) on the east (Figure 58b).

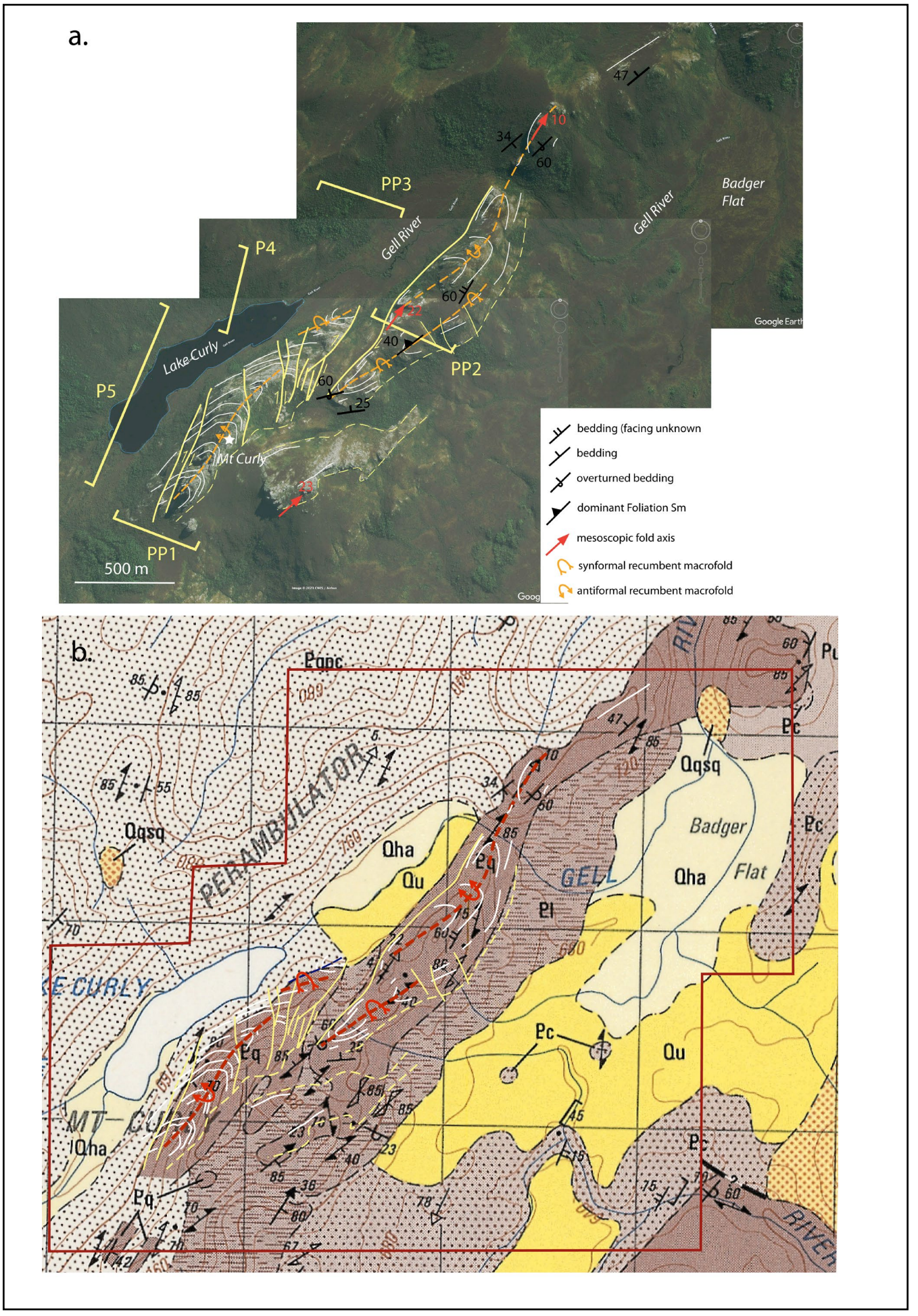

Figure 58. Mt Curly region structural interpretation. a) Google satellite image showing geographic elements, the positions of photo profiles PP1, PP2 and PP3 used in the map scale structural interpretation and a structural formline map. b) Structural formline map of the Mt Curly region on The Huntley 1:50,000 map base. Both a) and b) show recumbent, isoclinal, macro-fold axial surface traces (orange dashed lines), formlines in So/Sm (white line traces) and faults with apparent dextral sense (yellow line traces).

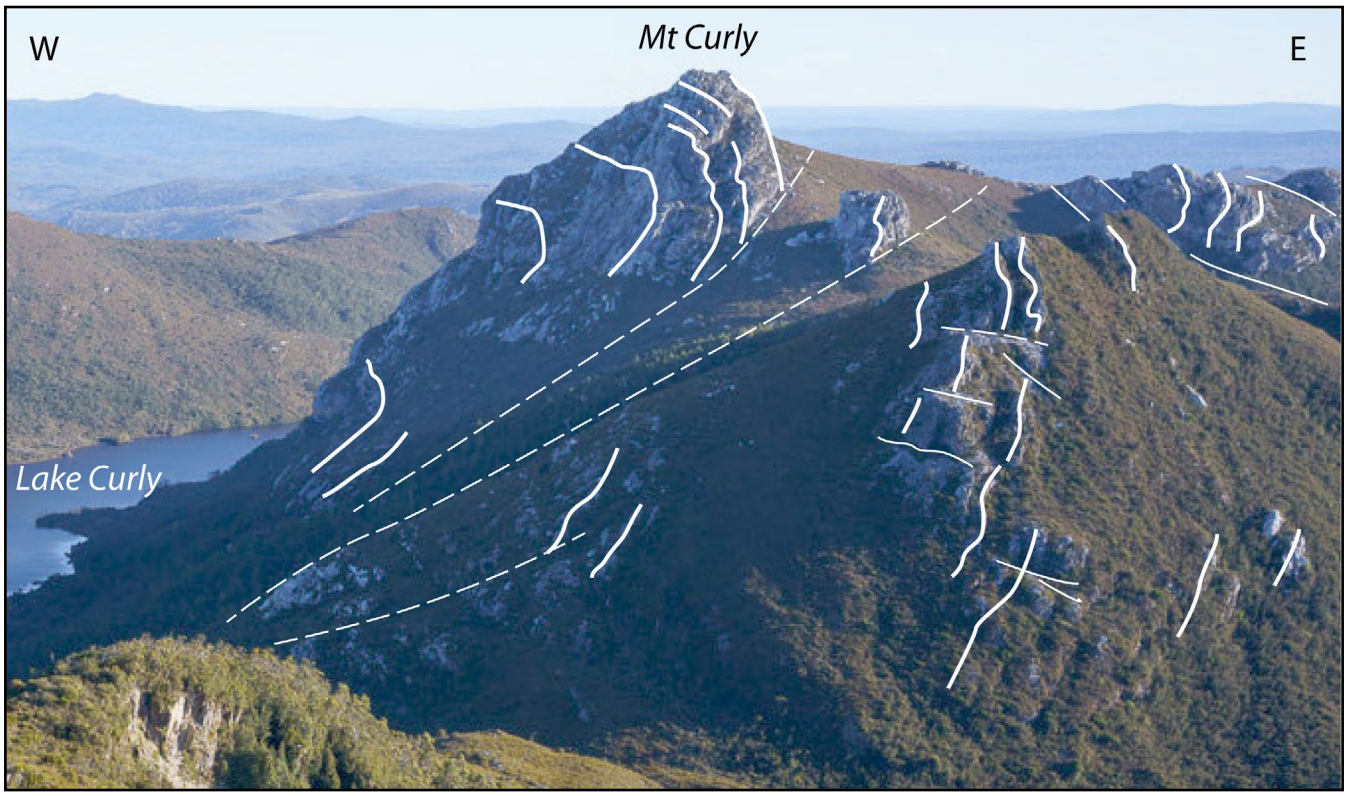

Figure 59 (Above). South end of Mt Curly ridgeline showing an east-closing macro-isoclinal fold cut by west-dipping oblique-slip faults. Photo profile PP1 with location shown in Figure 58. (Photo Credit: Grant Dixon)

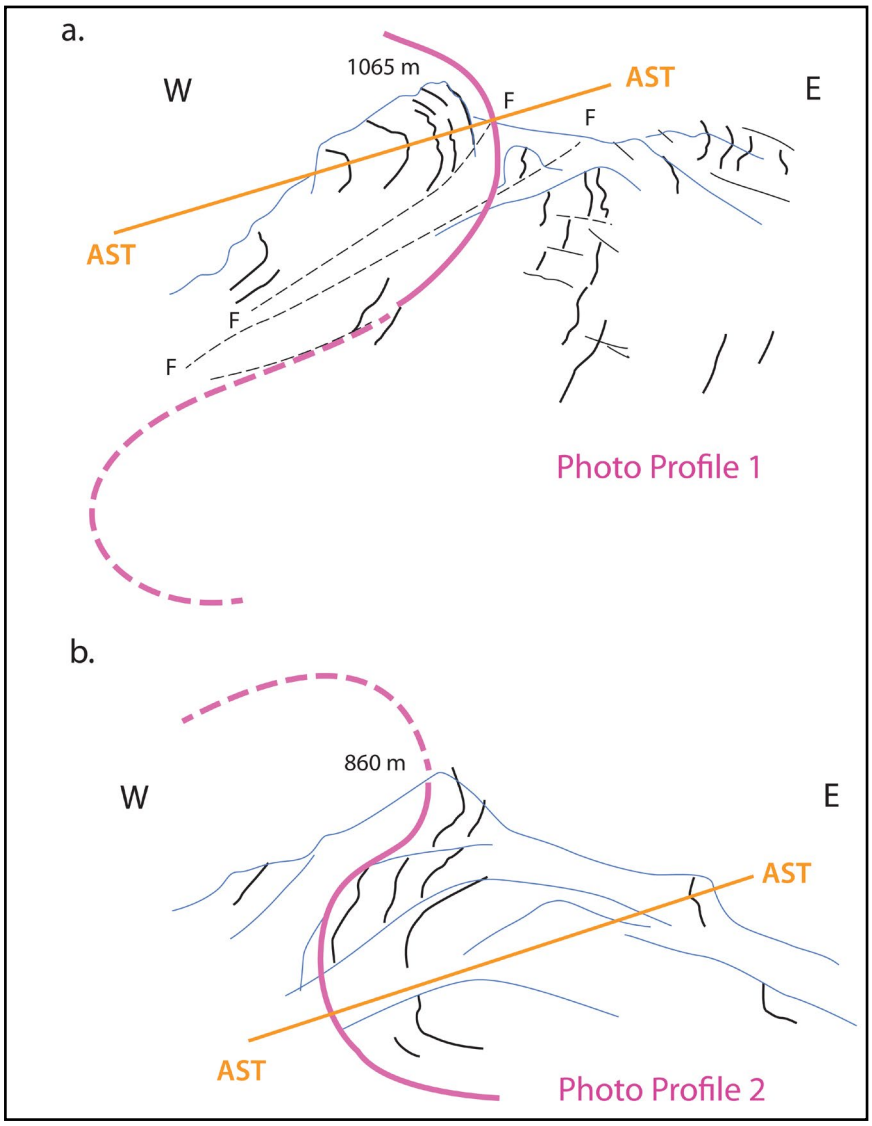

Figure 60 (Left). Photo profiles across the Mt Curly ridgeline showing the relicts of the partially preserved, asymmetric, Z-vergent (looking north) recumbent, isoclinal macro-fold pair. a) Photo profile 1: south end of the Mt Curly ridgeline showing the structurally higher, east-closing macro-fold in the highest part of the ridgeline. b) Photo profile 2: north end of the Mt Curly ridgeline showing the structurally lowest west-closing macro-fold, with the upper east-closing hinge eroded. Photo profile locations are shown in Figure 58a.

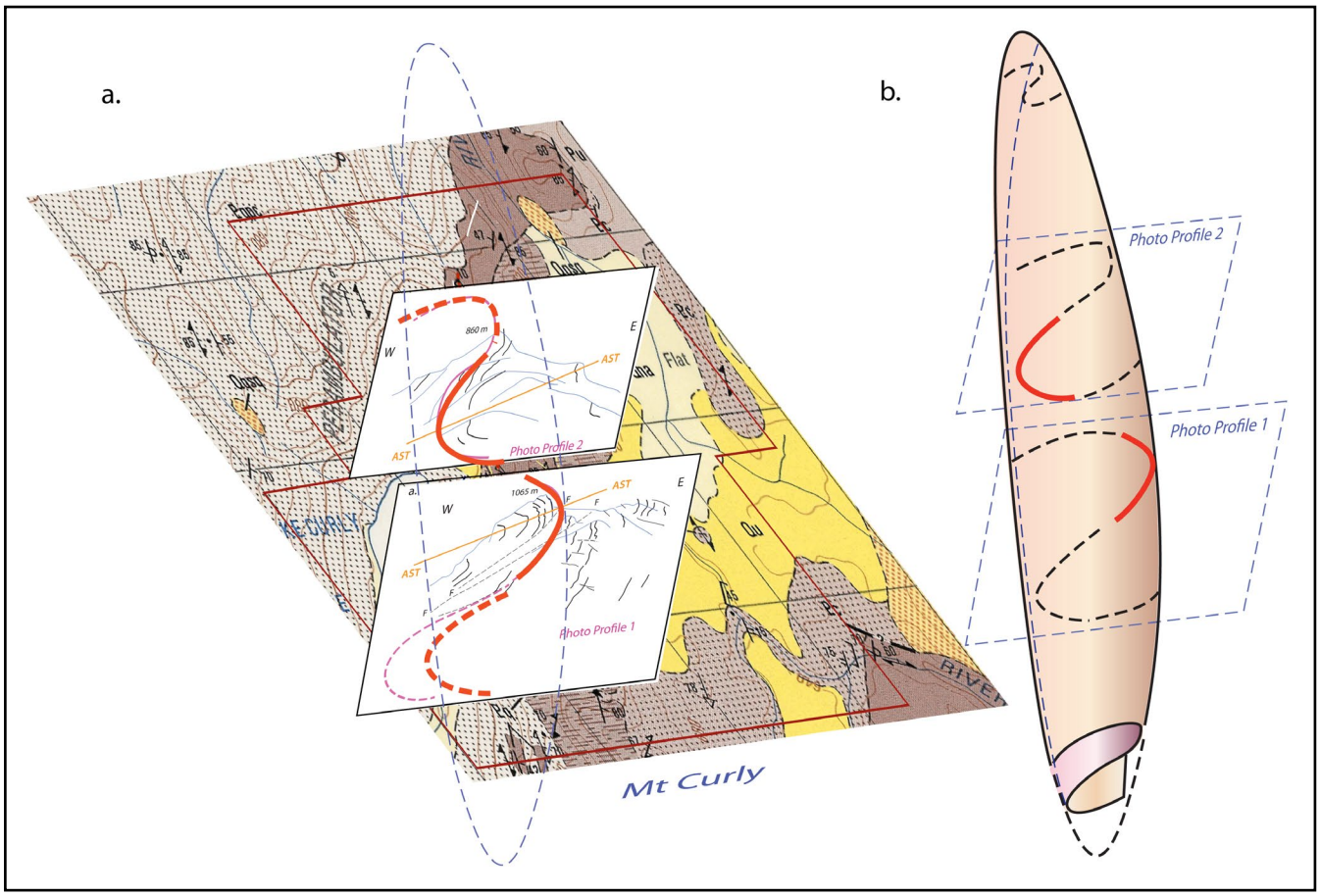

Figure 61. Oblique tilted view looking to the northeast of the structure of the Mt Curly area. a) Tilted map view with superimposed Photo Profile1 to Photo Profile 2 (compare with Figure 60). b) Reconstructed 3D form of the quartzite macro-fold structure along The Spires. Fold plunges are unknown but appear to be sub-horizontal though may differ at the terminations. The cigar-shaped form matches the outcrop pattern (see Figure 58).

5.3 The Nature of the Quartzite Basal Contact

The lower contact of the quartzites that hold up all of the ridgelines in the Eastern Tyennan subdomain is distinct and clearly: 1) truncates macro-fold structures internal to the quartzite; 2) is commonly associated with an intensely foliated zone; and 3) has been reactivated by brittle faulting.

The best-exposed contacts are along the northern flank of the southern part of the Frankland Range (Figure 62) and the western flank of the ridgeline below Mt Curly (Figure 63). Macro-fold hinges are truncated in quartzite above the contact and below the contact (Figure 63). At Mt Curly the quartzite shows distinct zonation with a macro-fold hinge in thicker bedded quartzite overlying a folded zone with strong axial surface foliation, both overlying a basal deformed zone of higher-strain flaggy quartzite (Figure 63). Below Secheron and Frankland Peak an intensely foliated zone is present and also discordant to the south-closing macro-fold hinge transected in both peaks (Figure 64). In places the contact is irregular with fault-like character, particularly at Shining Mountain (Figure 56).

The elements and character of the quartzite lower contact in the Eastern Tyennan subdomain are very similar to: 1) that of the quartzite - brown calcareous phyllite contact below Frenchmans Cap and Clytemnestra in the Central Tyennan subdomain (Gray and Vicary, 2021a, 2021b); and 2) the transition of the macro-folded quartzite in the Spero Range into a basal high strain zone (Gray and Vicary, 2023).

5.4 Starfish-Knob Basin Macro-fold system

The Starfish-Knob Basin macro-fold (Element 4, Figure 14) is a north-south elongated, ovoid element cored by high-grade garnet-bearing pelite that is enveloped by quartzite and low-grade pelite (Figure 65a). It extends from the Starfish in the south to the Knob Basin part of Lake Gordon in the north (Figure 65).

The structural interpretation of the Starfish-Knob Basin macro-fold system is based on structural and lithological mapping of Boulter (1978, Figures 4.16, 4.17 and 4.18), the Huntley and Pedder 1:50,000 map sheets and traverses by the authors across the macro-fold along the Gordon River Road, the Bell Basin-Bell Narrows and the shoreline of Starfish Hill along Wilmot Bay. Mapping by Boulter (1978, Figures 4.16 and 4.18) demonstrated a refolded outcrop pattern and overprinting structural relationships in The Starfish and Detached Peak areas.

Two geometrical forms of the overall macro-fold form are presented based on different interpretations of the northern termination or closure (Figures 65 and 66). These are: 1) a geometrically simple F3 synformal closure derived from the Huntley 1:50,000 map sheet (Figure 66a); and 2) a refolded hook-like nose (Figure 66b) based on formline interpretation of the ridgelines northwest of Knob Basin from Google satellite imagery (Figures 67and 68).

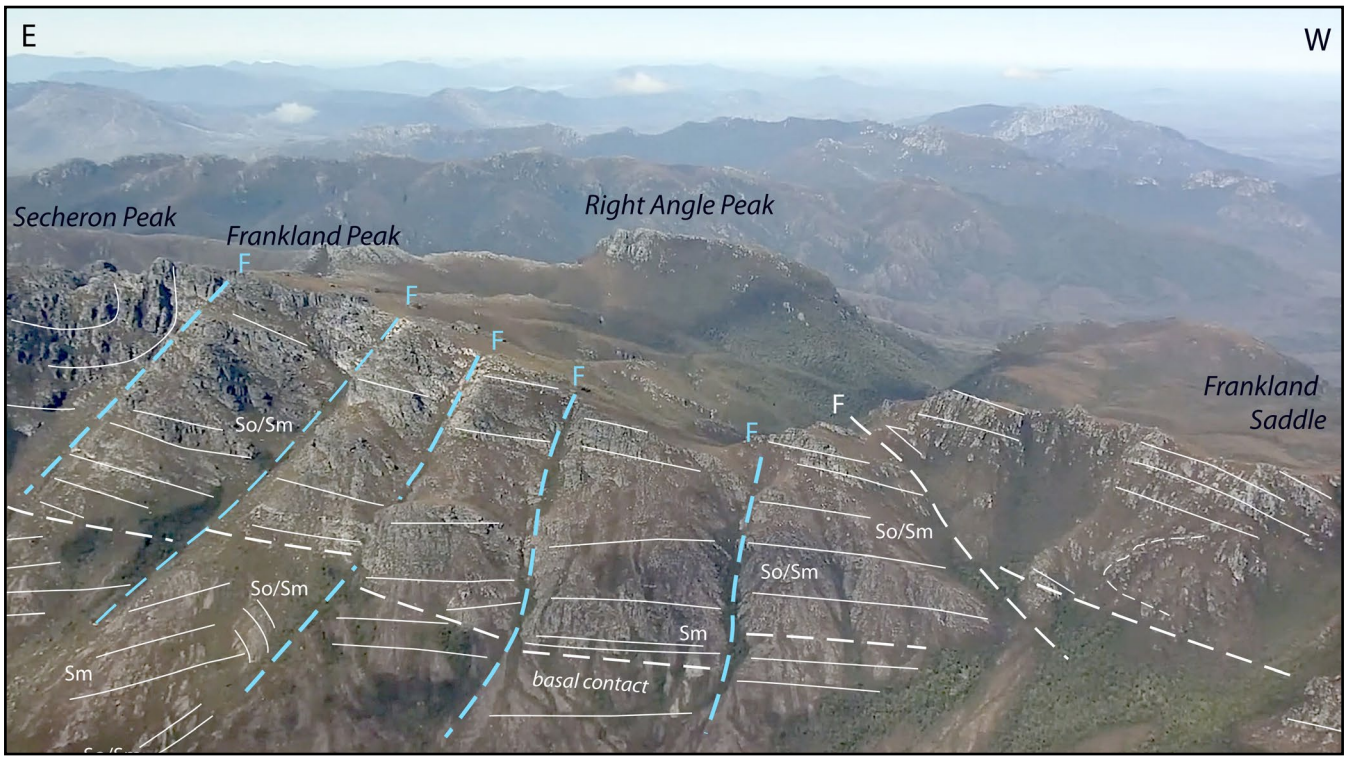

Figure 62 (Above). View of the basal quartzite contact along the southern part of the Frankland Range from Frankland saddle (photo right) to Secheron Peak (photo left). A series of normal faults (blue dashed line traces) offset layering So/Sm in the quartzite and the basal contact of the quartzite. (Photo credit: Wandering Foxbat)

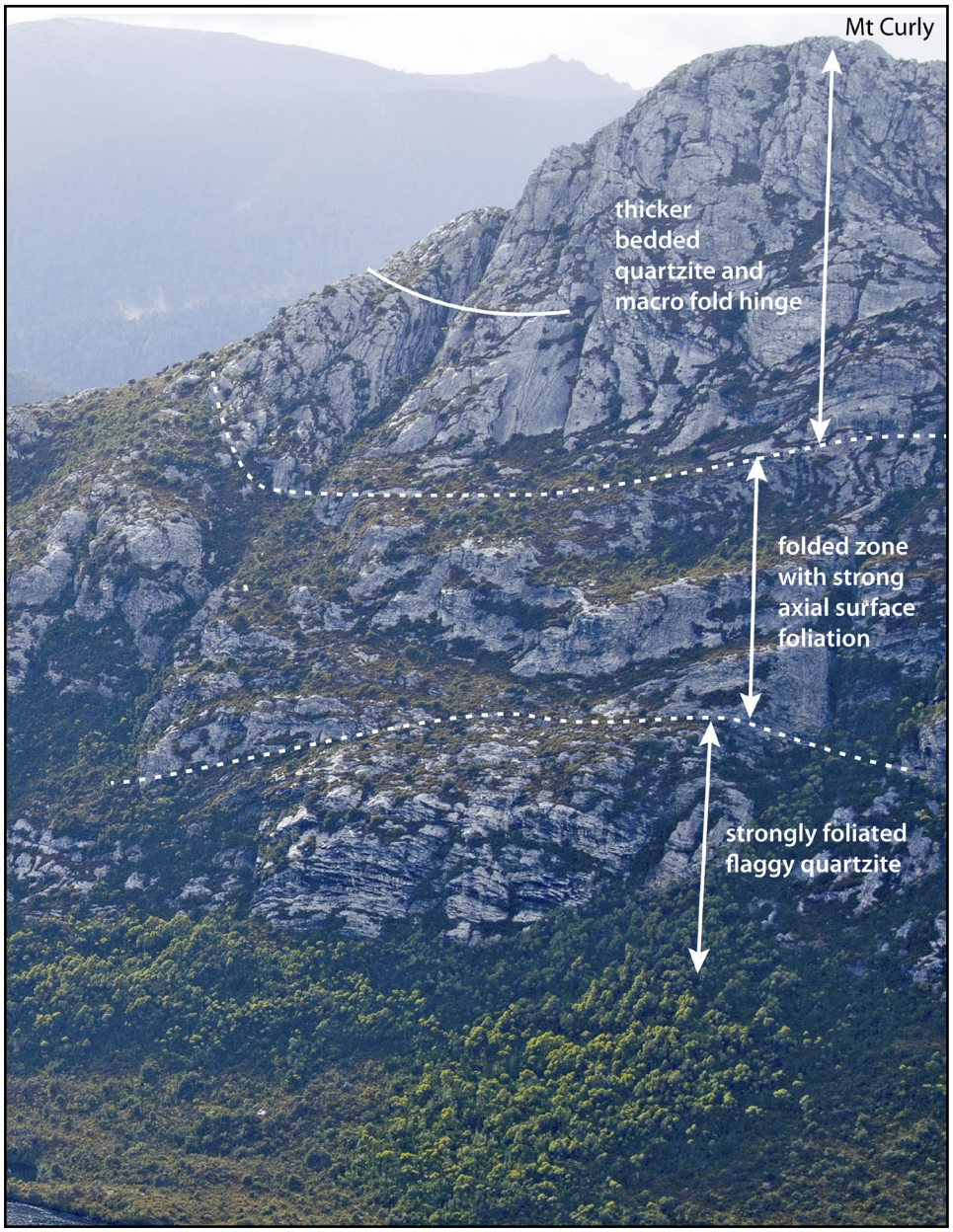

Figure 63 (Left). Vertical profile through part of the lower quartzite exposed on the western side of Mt Curly showing three distinct structural morphological zones. The view is approximately at right angles to the strike of the layering. The lowest part shows flaggy, strongly foliated quartzite. (Photo credit: Grant Dixon)

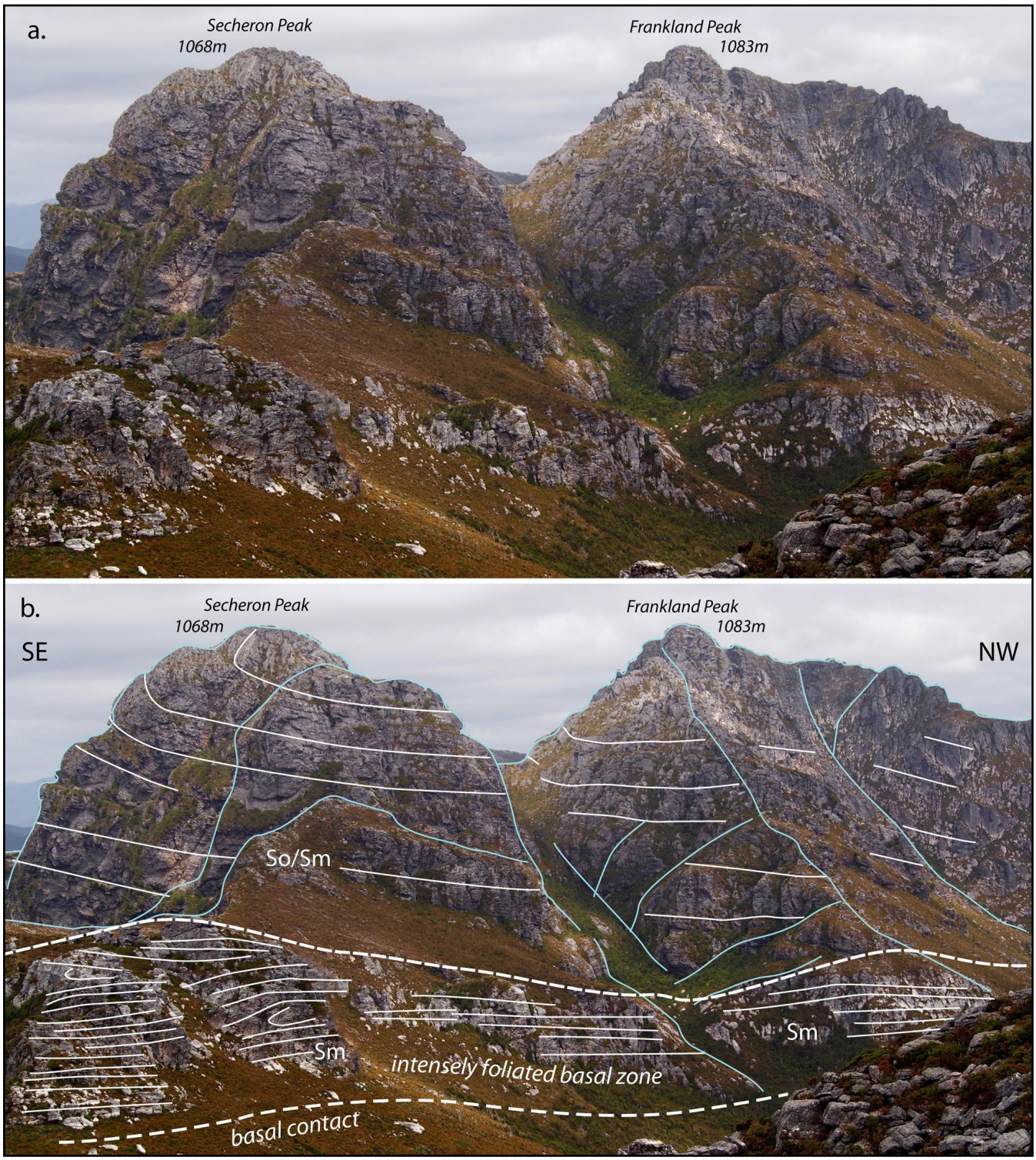

Figure 64. View of Secheron and Frankland Peaks looking towards the west from the ridgeline west of Mount Lloyd Jones. The photograph is oblique to the south-closing macro-fold that intersects both peaks. The lower, basal quartzite band that underlies both peaks appears discordant to the macro-fold limbs and has a strongly foliated character typical of a high-strain zone below the macro-fold pair and above the basal contact. The heavy white dashed line delineates the interface. (Photo credit: Becca Lunnon, rockmonkeyadvetures)

These different interpretations result in two geometrical versions of the macro-fold system. Both are synformal with a core of high-grade schist (orange domain, Figure 66).

Geometry 1 has a closed loop-like pattern of the early F1/F2 axial surface trace that is bisected by a north-south trending F3 axial surface trace (Figure 66a).

Geometry 2 has an ovoid form with "seahorse-like" pattern in the F1/F2 axial surface trace where oppositely closing F1/F2 hinges occur as refolded fold noses at the northern and southern terminations of the macro-fold (Figure 66b).

In both scenarios the early F1/F2 axial surface trace is refolded by en echelon F3 macro-folds (blue dashed-dot-dot line traces) with north-south trending axial surface traces (Figure 66).

The Starfish-Knob Basin macro-fold is geometrically similar to the Davey Gorge part of the De Witt-Propsting mega-sheath fold (Gray and Vicary, 2022a; Gray and Vicary, 2023, Figures 41 and 45) and the South West Cape mega-sheath fold (Gray and Vicary, 2022a; Gray and Vicary, 2023, Figures 46 and 47) in the Southern Tyennan

subdomain. Both areas have a sigmoidal form in So/Sm where the early F1/F2 isoclinal macro-folds are refolded by regional scale, upright F3 isoclinal folds. Both were interpreted as oppositely-closing mega sheath folds (Gray and Vicary, 2023, Figure 64). The lineation Lm is either northeast-trending or southeast-trending at a high angle to the north-south elongated, ovoid form of the macrofold system dominated by the north-trending F3 folds (Figure 69a).

The Starfish-Knob Basin macro-fold has an ovoid core with hook-shaped noses as tails coming off the central core (Figure 66). Lineation Lm data show the mineral stretching lineation is at high angles to this elongated ovoid map form (Figure 69a), with either northeast trend or southeast trend reflecting isoclinal refolding of the early lineation by the north-trending F3 folds. Fold axis data for the macro-fold shows varying relations around and across the fold structure (Figure 69b). At Detached Peak, in the central part of the ovoid closure, the fold axes are sub-parallel to So/Sm. At the southern end at the Starfish the isocline fold axes either wrap around the F3 hinge, or point towards the central part or synformal hinge. In the vicinity of Strathgordon, on the northern side the ovoid fold closure, the fold axes are northeast-trending and plunging, again trending in the direction of the synformal hinge. Fold axes should fan inwards towards the nose of a sheath fold where fold axes should parallel the formlines in So/Sm (Gray and Vicary, 2022a, Figures. 7a and 7b). In the Starfish-Knob Basin macro-fold (Figure 69b) there is a broad fit of the fold axis pattern to this model (see Alsop and Holdsworth, 2004, Figure 13b) suggesting a sheath-like overall geometry to the early F1/F2 macro-fold.

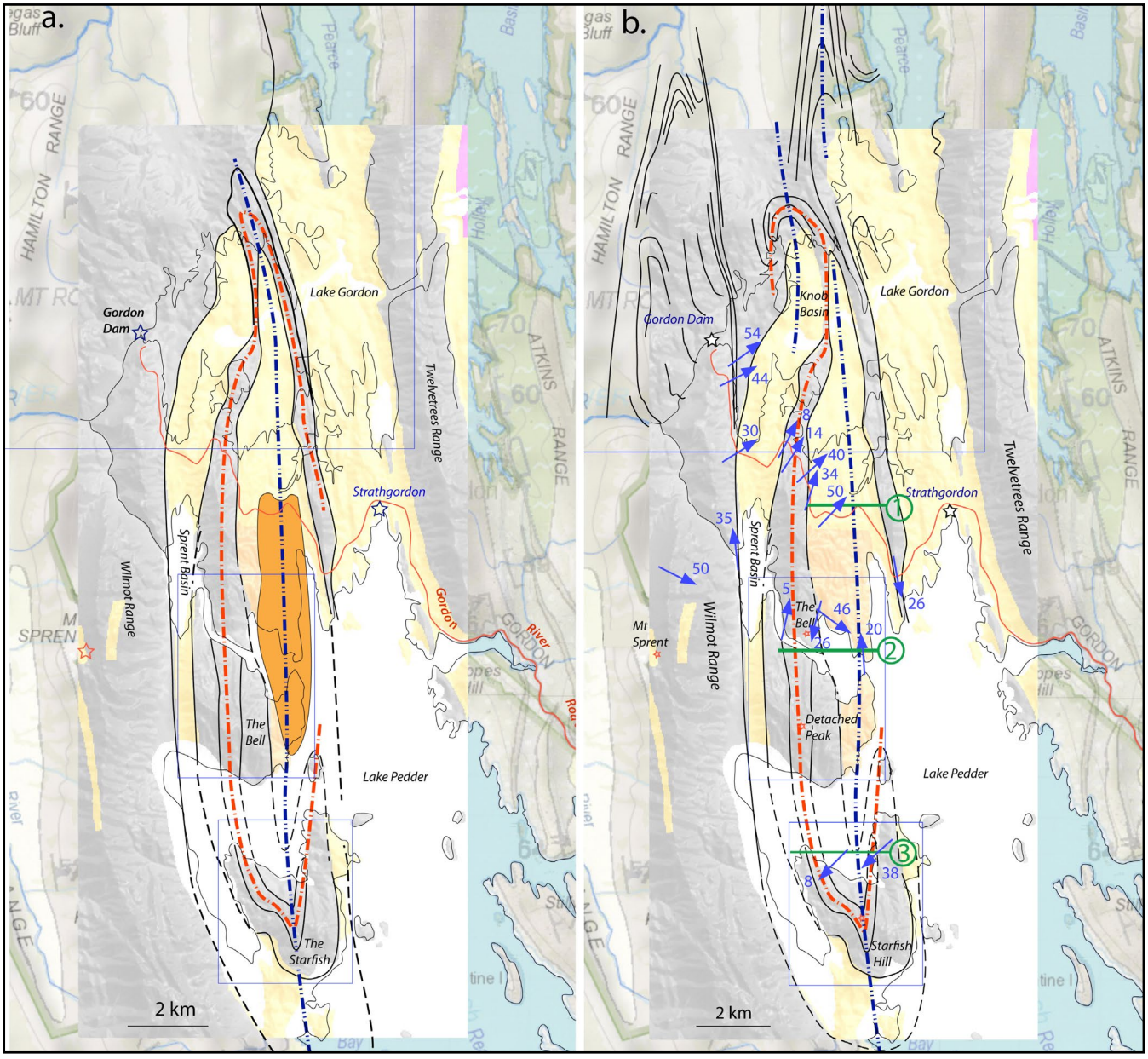

Figure 65. The Starfish-Knob Basin macro-fold (element 4, Figure 14). Geographic location and form of the macro-fold system superimposed on ListMap topographic base with a Mineral Resources Tasmania 1:250,000 digital atlas overlay. a) Geometry 1 showing a refolded hook closure at the southern termination and a synformal closure at the northern termination. The garnet bearing high-grade rocks (after Boulter, 1978, figure 5.1) occur in the core of the fold system (orange region). b) Geometry 2 showing a refolded hook closure at both the southern and northern terminations. The location of structural profiles 1 (Figure 70), 2 (Figure 71) and 3 (Figure 72) are shown by the green lines.
Blue arrows: mineral lineation Lm trends.
Red dot-dashed line: axial surface trace of the early F2 isoclinal fold
Blue dot-dashed line: axial surface trace of F3 tight to isoclinal folds

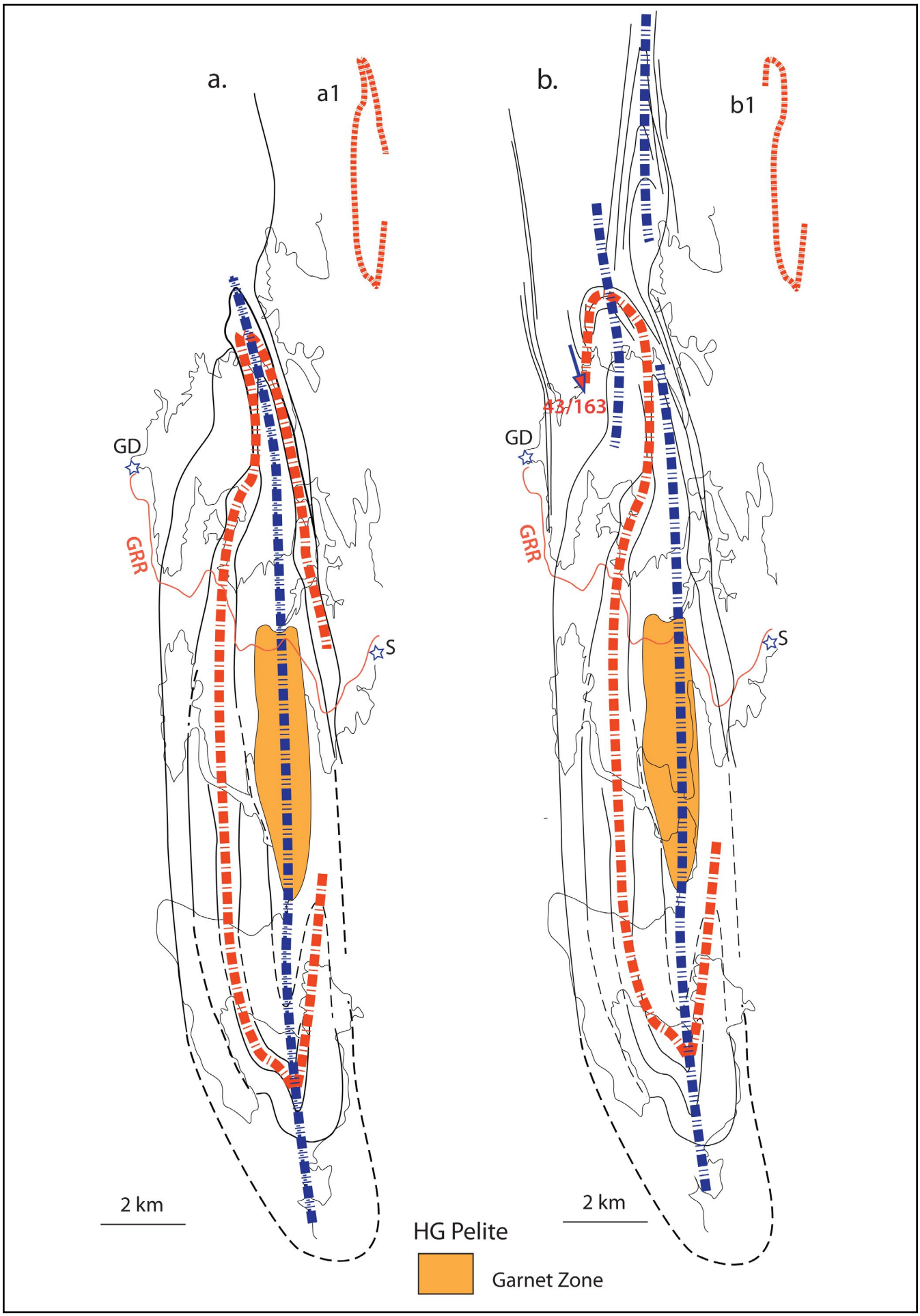

Figure 66. Simplified axial surface trace maps of the two geometrical interpretations of the Starfish - Knob Basin macro-fold system. Red dot-dashed line trace: F1/F2 axial surface trace. Blue dashed-dot line trace: F3 axial surface trace. The simplified hook variations for the two geometries are shown in a1 and b1. S: Strathgordon. GD: Gordon Dam. GRR: Gordon River Road (thin red line trace)

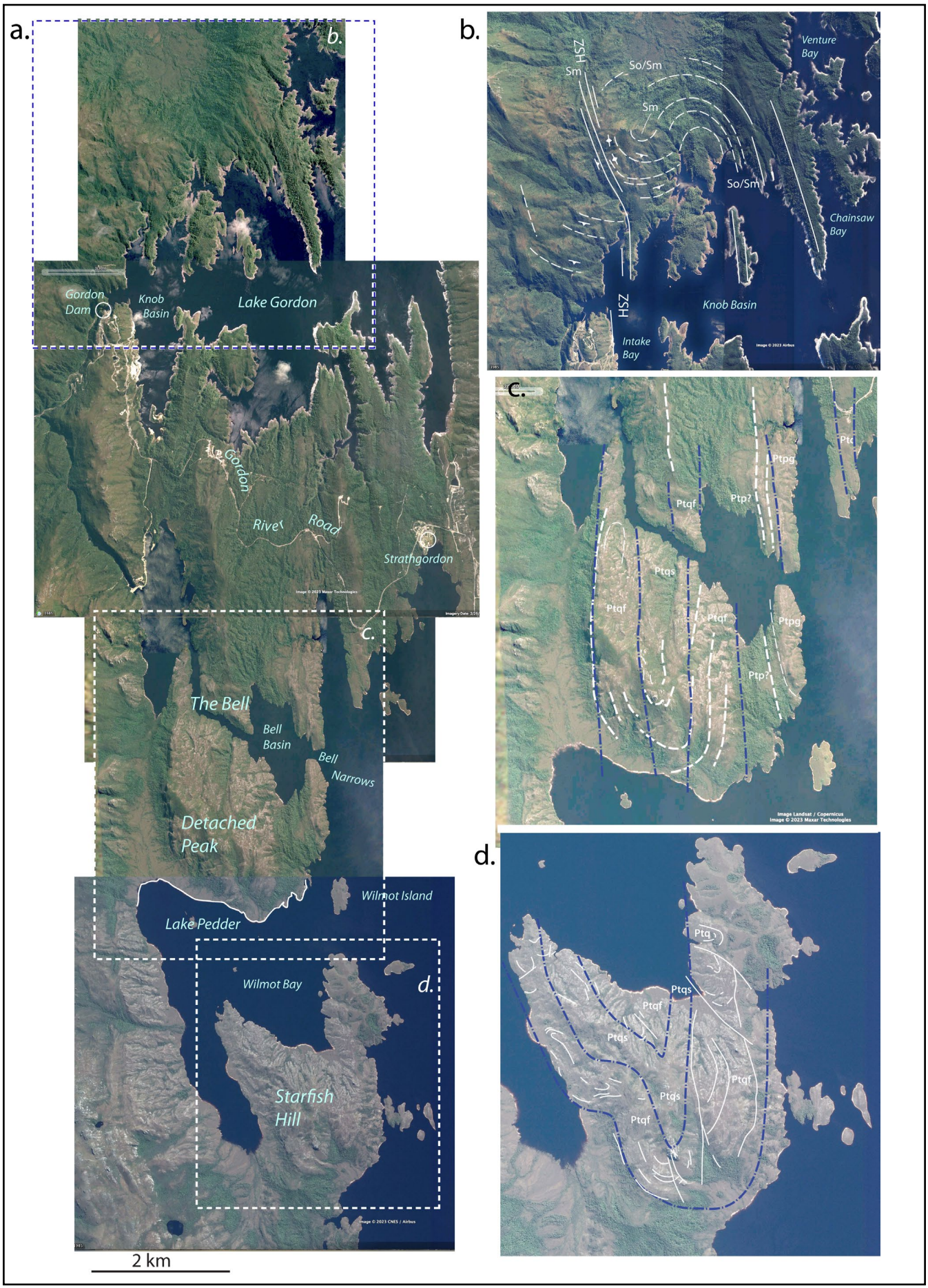

Figure 67. a) Stitched Google satellite images of the Starfish - Knob Basin macro-fold system. Positions of the enlarged images are shown. b) Enlarged image of the Knob Basin with formline interpretation (white line and dashed line traces). c) The Detached Peak enlarged image showing formline interpretation in So/Sm as blue dashed line traces. d) The Starfish Hill enlarged image showing formline interpretation in So/Sm as blue dashed line traces.

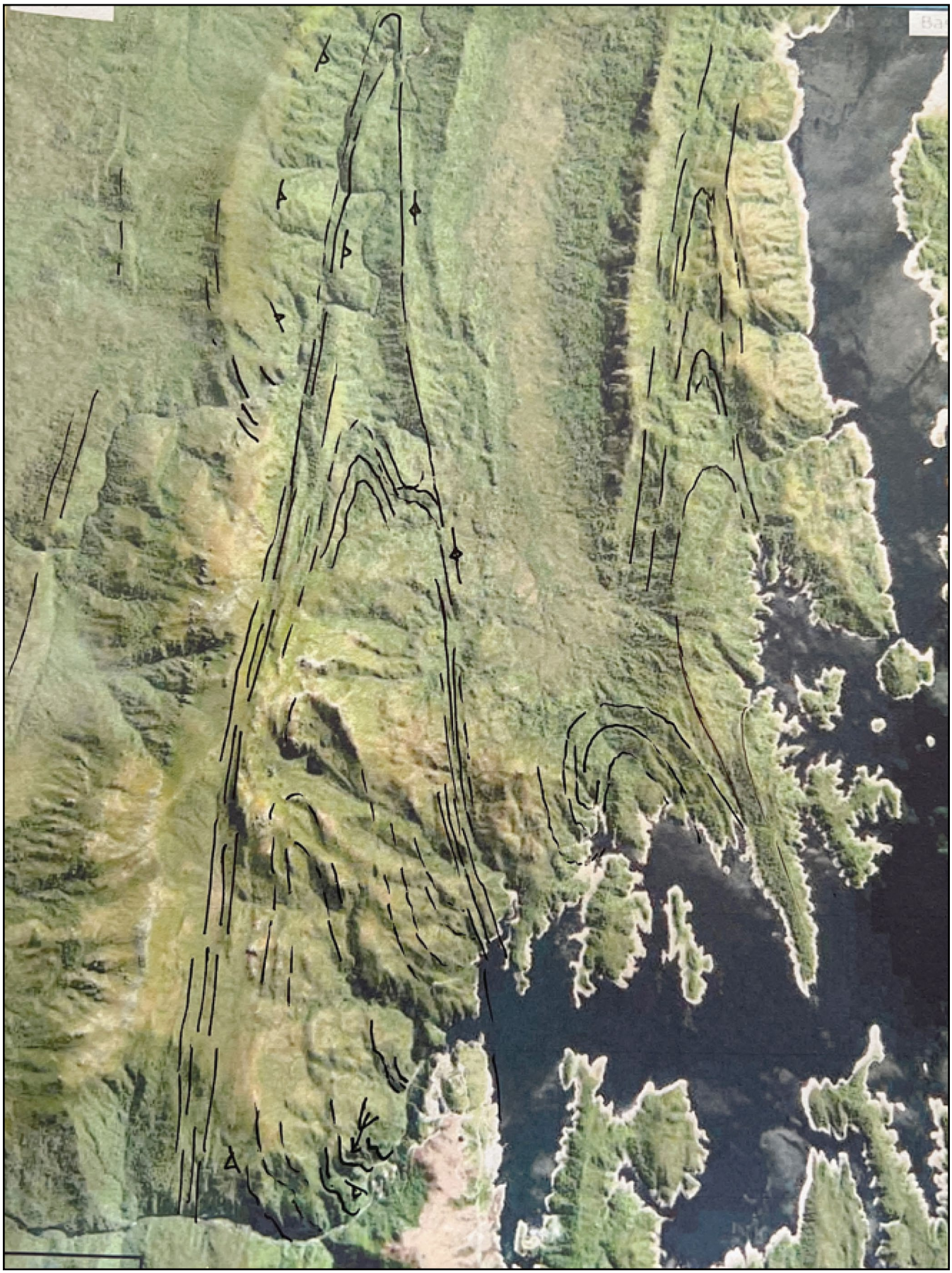

Figure 68. Google satellite image with So/Sm formline interpretation. Knob Basin is the dark lake area in the bottom right. The ridgeline topography suggests a rounded, south-plunging and closing isoclinal macro-fold closure at the northern termination of The Starfish - Knob Basin macro-fold.

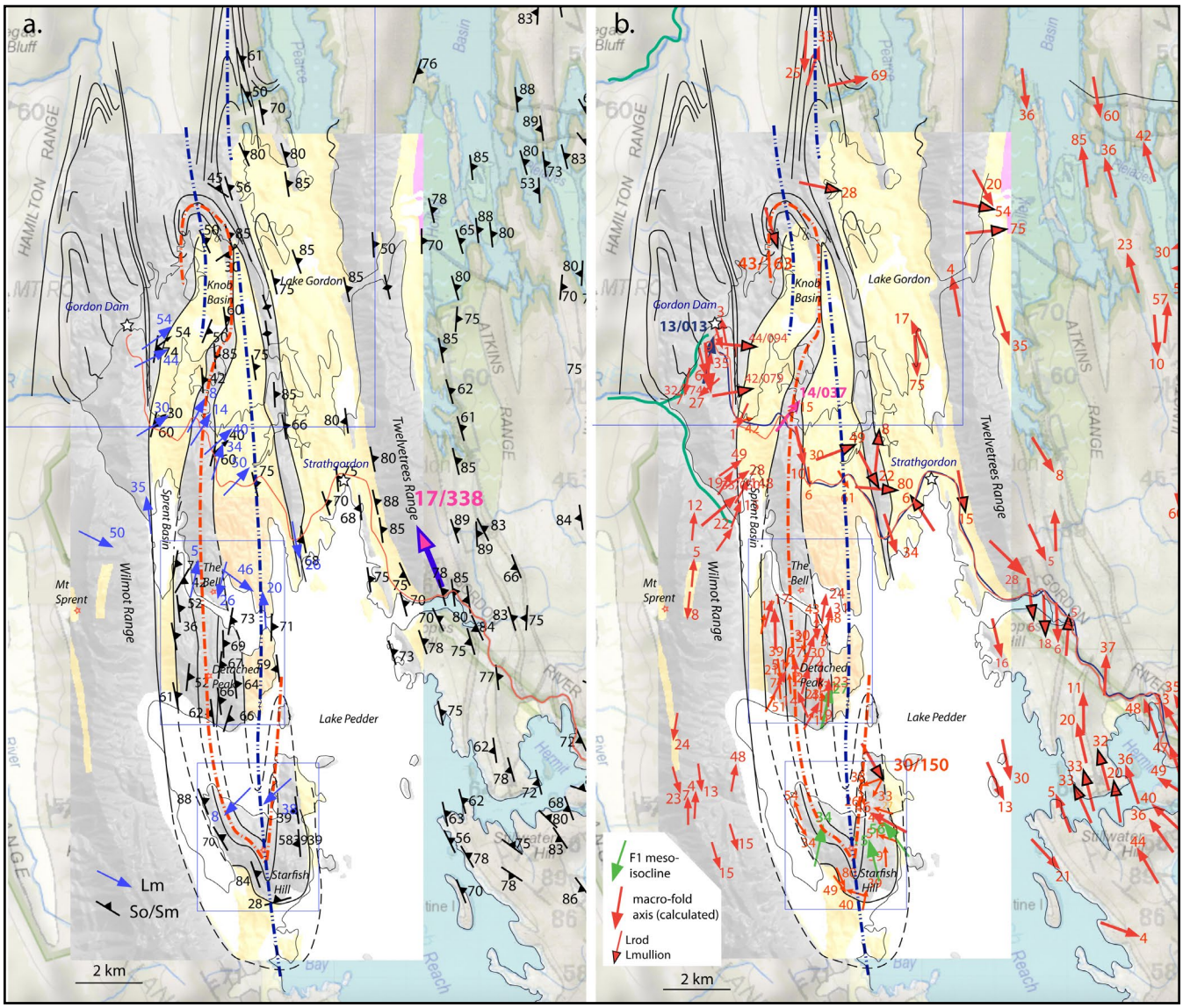

Figure 69. Structure maps of the Starfish-Knob Basin macro-fold system. a) Lineation Lm and foliation Sm attitude and distribution map. b) Mesoscopic fold axes and rodding lineations (Lrod) attitude and distribution map.

Three regional profiles across the Starfish - Knob Basin macro-fold (Figures 70, 71 and 72) provide "one-dimensional" views of the macrofold geometry. These are as narrow slices in the Gordon River Road cuttings (Profile 1), or as shoreline outcrops (<2 m height) along the Bell Basin - Bell Narrows (Profile 2) and the Starfish Hill shoreline through Wilmot Bay (Profile 3). Regionally, the F3 synform that dominates the macrofold has upright, tight cuspate or pinched form (Profile 4, Figure 22). However, each of the three profiles presents a unique and different geometry at different levels and positions along the Starfish - Knob Basin macro-fold. They also show that the Starfish - Knob Basin macro-fold is geometrically complex and faulted at the local scale.

Profile 1 (Figure 70) has a general elevation of ~400 m and mid-north position along the macro-fold. The profile (Figure 70b) shows a steeply east-dipping sequence with a faulted out synformal F3 closure (compare with Figure 73a). The schist "core" involves repetition of an inverted medium grade (MG) sequence consisting of carbonaceous phyllite (LgsP) overlain by biotite schist (MgsS) overlain by garnet schist (MgsG). This was recognised and interpreted by Port (2023, Figure 6.7) as a stacked series of east-vergent metamorphic sheets. These stacked MG sheets are structurally overlain by broadly warped carbonaceous schist/phyllite overlain by a strongly deformed, east-dipping bedded quartzite (Figures 70b, c).

Profile 2 (Figure 71) has a general elevation of ~315 m (current lake level) and mid-south position along the macro-fold. It shows belts of poly-deformed micaceous quartzite (Ptqs), bedded, flaggy quartzite (Ptqf) and MG schist (Pts) (Figures 71 and 73b). The schist occupies the east side of profile segment A-A'. The poly-deformed micaceous quartzite defines the hinge of an inferred cuspate synformal or apparent east-closing F2 macro-fold (segment C-C'). It appears to structurally overlie the flaggy quartzite exposed on the lake shoreline below The Bell (profile segment B-B' and Figure 73b). Profile 2, through the larger scale macro-fold must also be faulted, as there is no repetition of the high-grade (H-G) schists across an inferred synformal closure (middle of structural profile A-A'). Upright F3 folds refold the strongly foliated high-grade (H-G) pelitic schists and show a gently west-dipping enveloping surface towards an inferred synformal F3 hinge (Figure 73b).

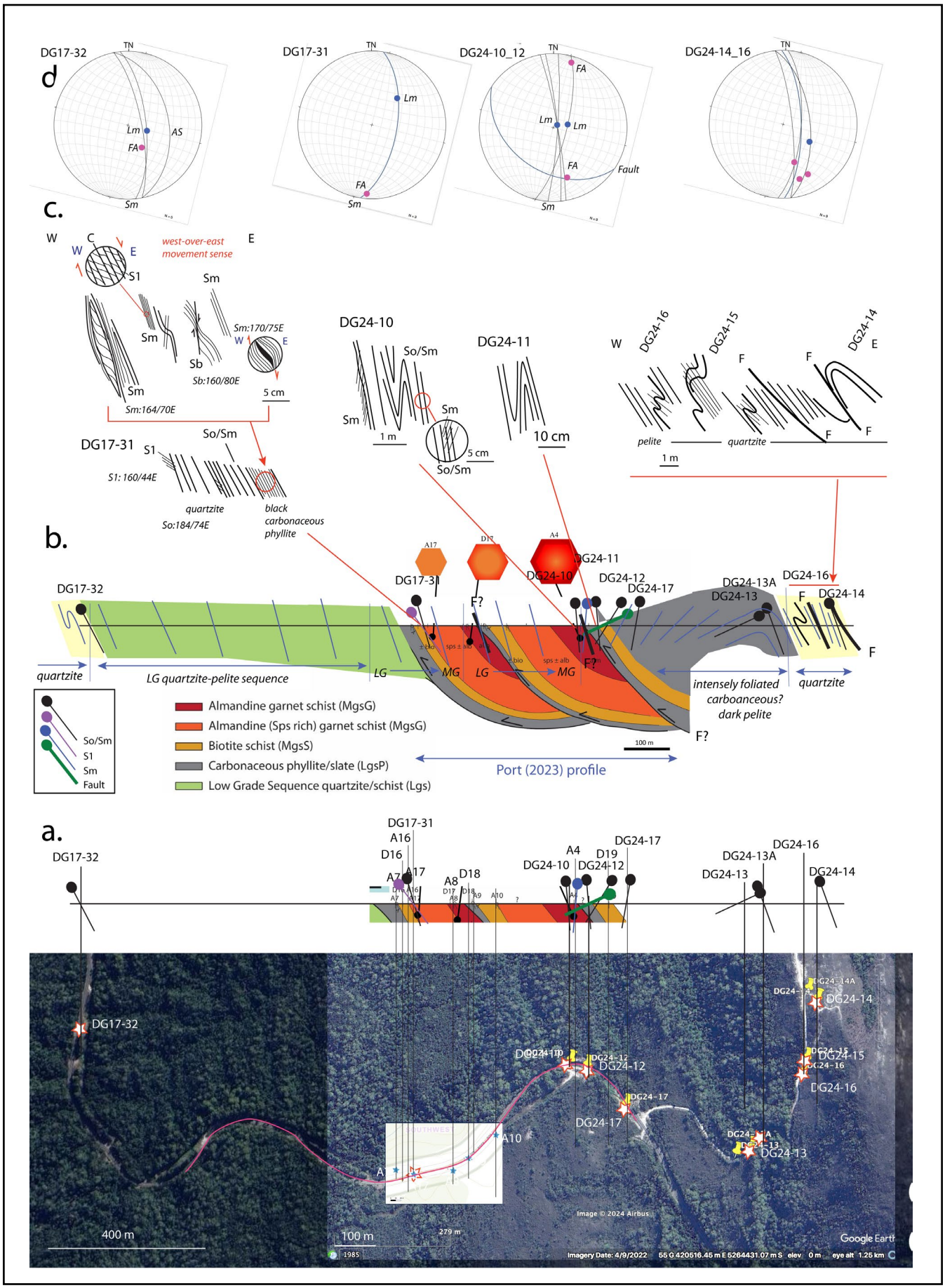

Figure 70. The Gordon River Road sketch profile (Profile 1, Figure 65b). a) Google satellite image showing DG17 and DG24 locations and locations from Port (2023) along the Gordon River Road. Individual stations are projected onto an east-west profile. b) Interpreted structural profile incorporating the interpretative profile of Post (2023, Figure 6.7). c) Sketch structural relationships from outcrops along the profile that were used along with projected dip lines to construct the profile (see b). d) Stereonets of structural data from locations along the profile. Great circles show the attitudes of Sm. Blue dots: lineation Lm attitudes. Pink dots: fold axis attitudes. Note the mineral lineation Lm is steeply northeast plunging along the east-dipping foliation Sm across the synform.

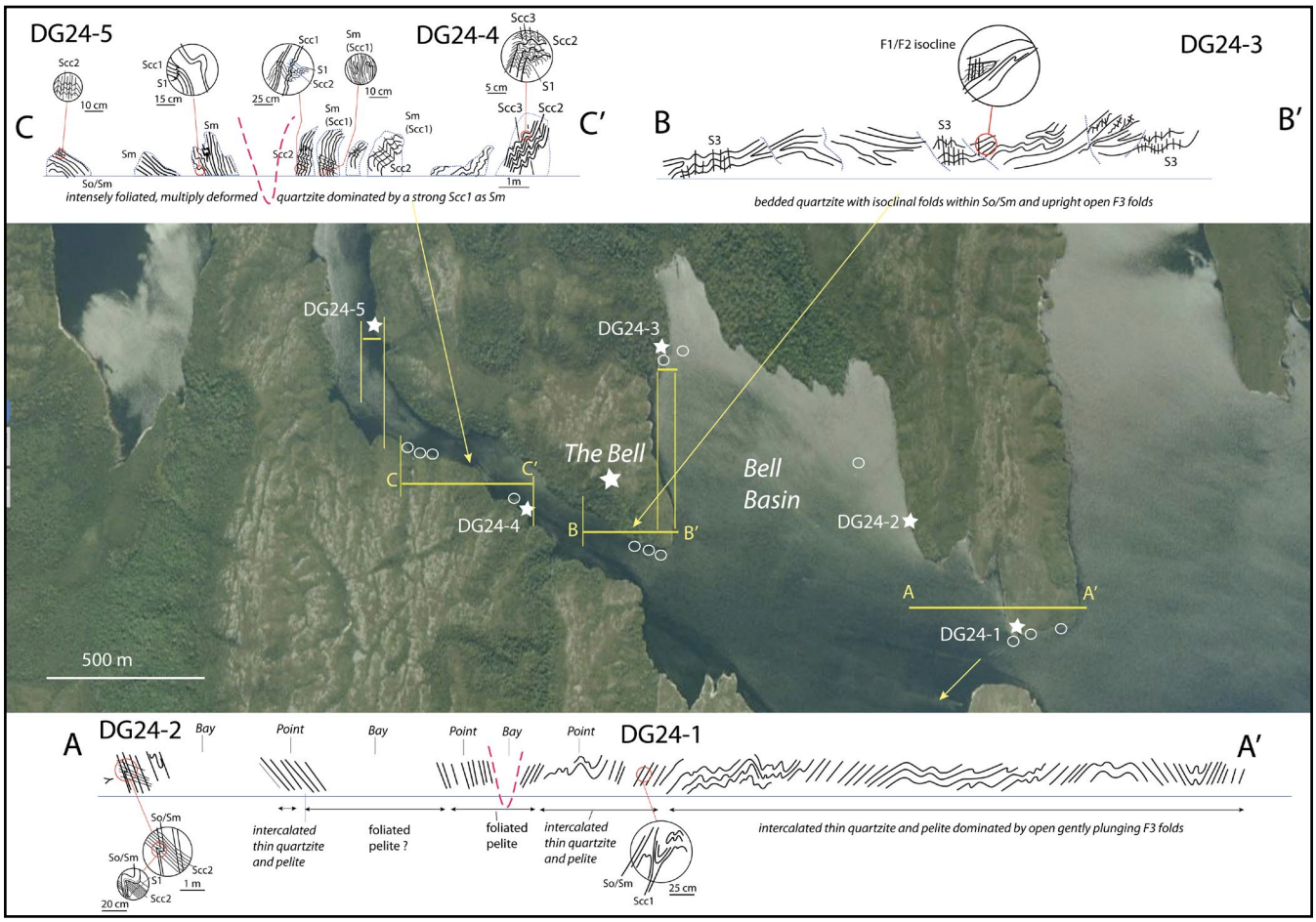

Figure 71. The Bell Basin - Bell Narrows sketch structural profiles (Profile 2, Figure 65b) based on a Zodiac boat traverse along the lake shoreline through the Bell Basin and the Bell Narrows. The Google satellite image (centre) shows the positions of the profiles.

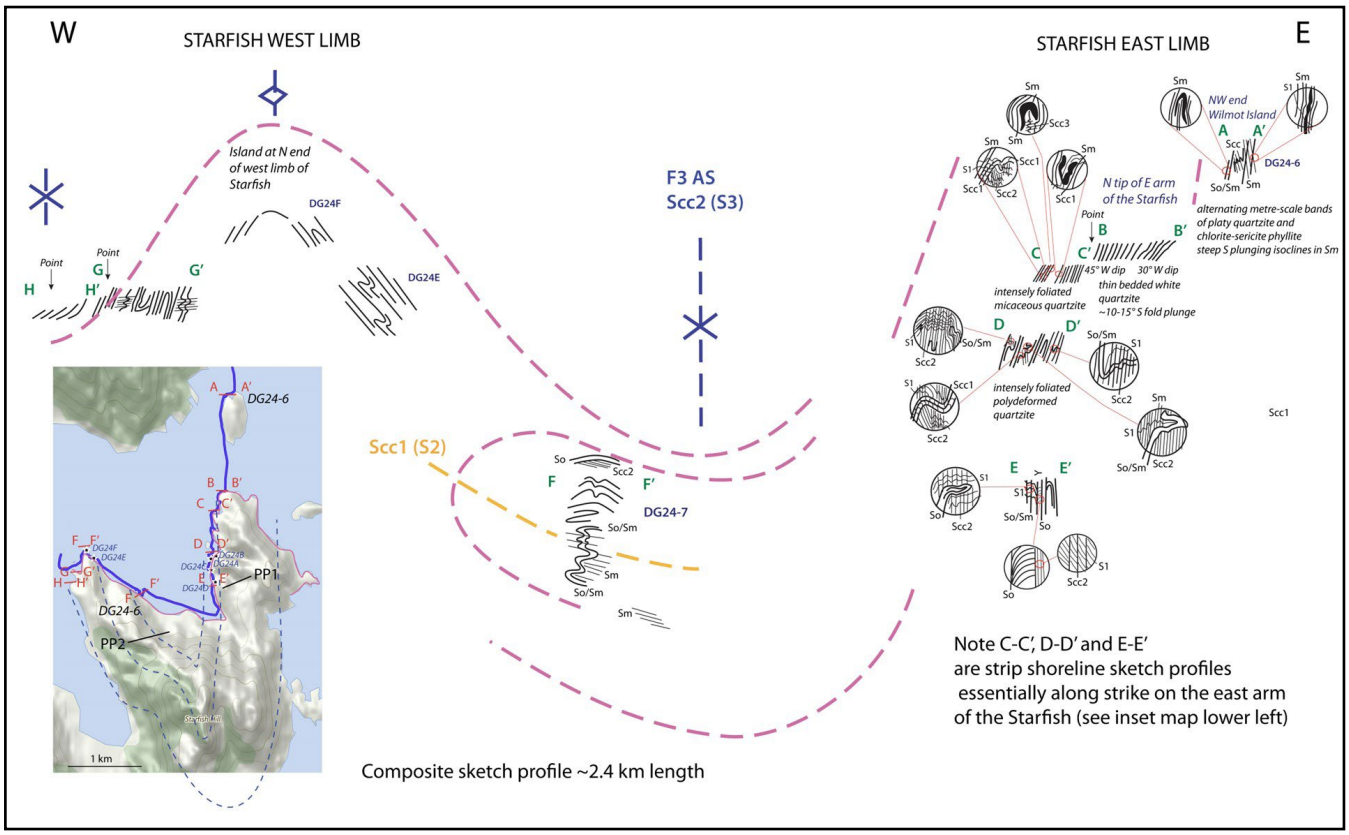

Figure 72. Starfish structural profile (Profile 3, Figure 65b) based on sketches from photographs taken in a Zodiac boat traverse along the shoreline. The inset map (lower left) shows the position of the boat traverse (blue line trace) , the positions of the sketches and the individual sketch profiles A-A' to H-H' (red lettering). Magenta dashed line: an interpreted formline for So/Sm. Orange dashed line: F2 macro-isocline axial surface trace. Blue dashed line: F3 axial surface trace.

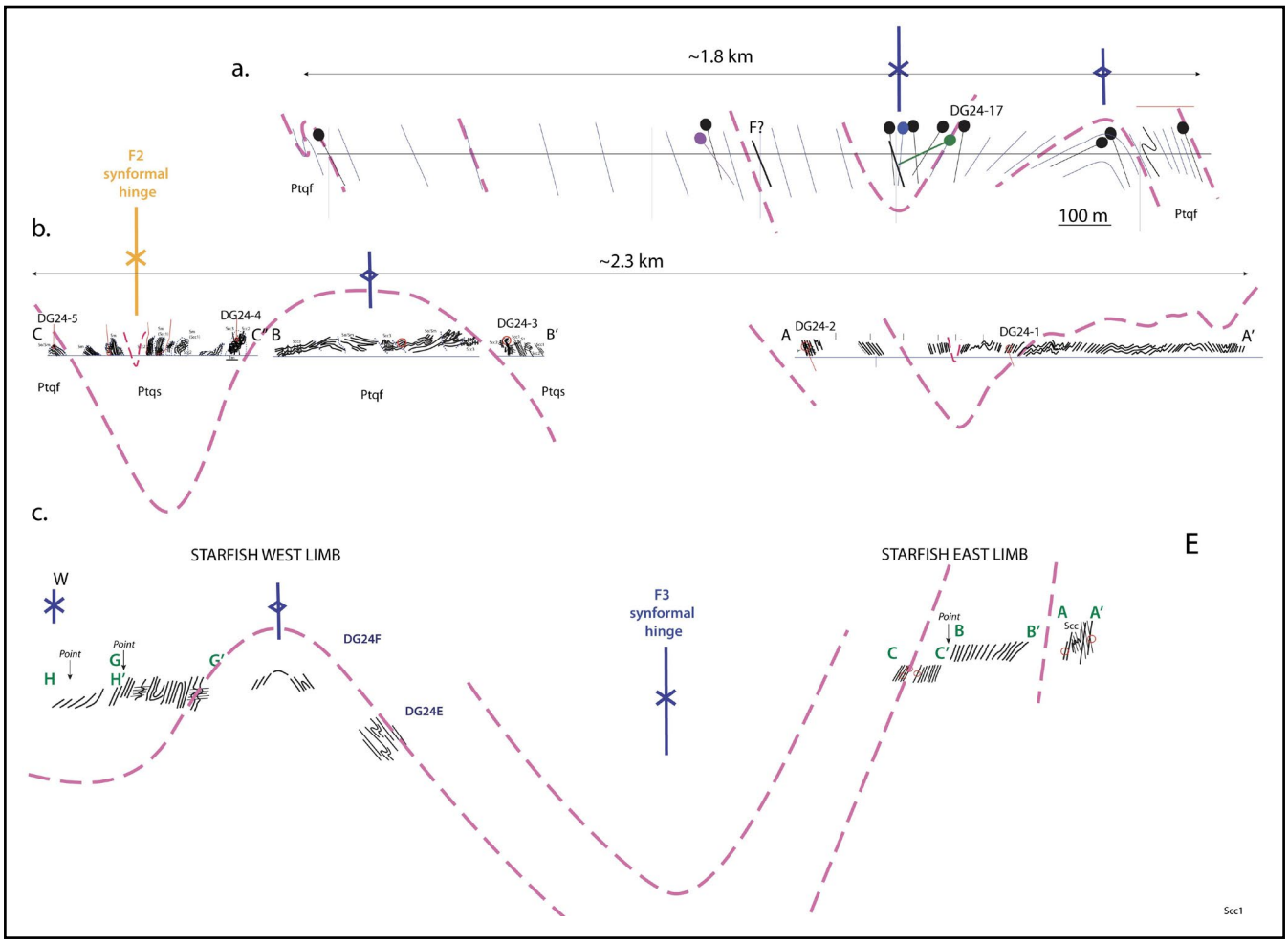

Figure 73. Summary structural sketch profiles across the Starfish - Knob Basin macro-fold. See Figure 65b for profile locations. a) Profile 1 along the Gordon River Road. b) Profile 2 along the Bell Narrows. c) Schematic Profile 3 across Wilmot Bay encompassing the east and west arms of the Starfish. Magenta dashed line: an interpreted formline for So/Sm. Orange dashed line: F2 macro-isocline axial surface trace. Blue dashed line: F3 axial surface trace. The thick magenta dashed lines are formlines in So/Sm that depict the simplified structure.

Profile 3 (Figure 72) has a general elevation of ~315 m (current lake level) positioned at the south end of the macro-fold. It shows a broad F3 synformal closure that bisects the arms of the Starfish. This F3 synform refolds early formed F2 recumbent isoclinal folds exposed in the hillsides above the lake (Figure 74) and along the shoreline (DG24-7, Figure 72). The core of the synform is occupied by strongly and poly-deformed micaceous quartzite. This is underlain by a structurally lower flaggy quartzite towards the synform flanks (Figure 72).

5.5 The Atkins Range Macro-element

The Atkins Range macro-element is an elongated, north-south trending, lenticular pod of amphibolite with tapered terminations (Element 2, Figure 13 and Element 7, Figure 14) between the Twelvetrees and Atkins Ranges (Figure 75). The amphibolite is made up of chlorite-actinolite-epidote-albite schist where porphyroblasts of epidote and chlorite overgrow the dominant S2 foliation (Brown et al., 1989, p.14). Haematitic banded ironstones containing high-P sodic, blue amphiboles (Brown et al., 1989) are also structurally intercalated in an envelope around the amphibolite pod (Figure 75). The amphibolite body is bound by sub-vertical to steeply east-dipping, strongly to intensely foliated shear zones (orange lines Figure 75). This is supported by a distinct geophysical "worm" signature suggesting a steep, east-dipping magnetic body (Figure 75b). The northern termination is however geometrically complex with a slice of quartzite entrained within the amphibolite by bounding shear zones (Figure 75a). The southern termination appears within an F3 isoclinal fold that has been overridden and offset by the main amphibolite pod along the bounding shear zones (Figure 75a). This F3 fold has a north plunge of 18°/018°. The inferred northern closure in quartzite is sub-vertical to steep easterly-dipping with a 35°/175° fold plunge (Figure 76). The macro-fold pod is therefore doubly plunging requiring a synformal form.

The Atkins Range macro-element has apparent complex character, potentially initiated as a shear zone-bound pod that is subsequently entrained by the underlying quartzite-pelite sequence during the regional isoclinal F3 folding. The pod/F3 synformal fold sits between the refolded Twelvetrees Range macro-fold and the complexly refolded Junction Range - Pleaides - North Star macro-fold, with the upright, isoclinal F3 folding dominating this part of the Eastern Tyennan subdomain (blue dashed-dot axial surface traces, Figure 76).

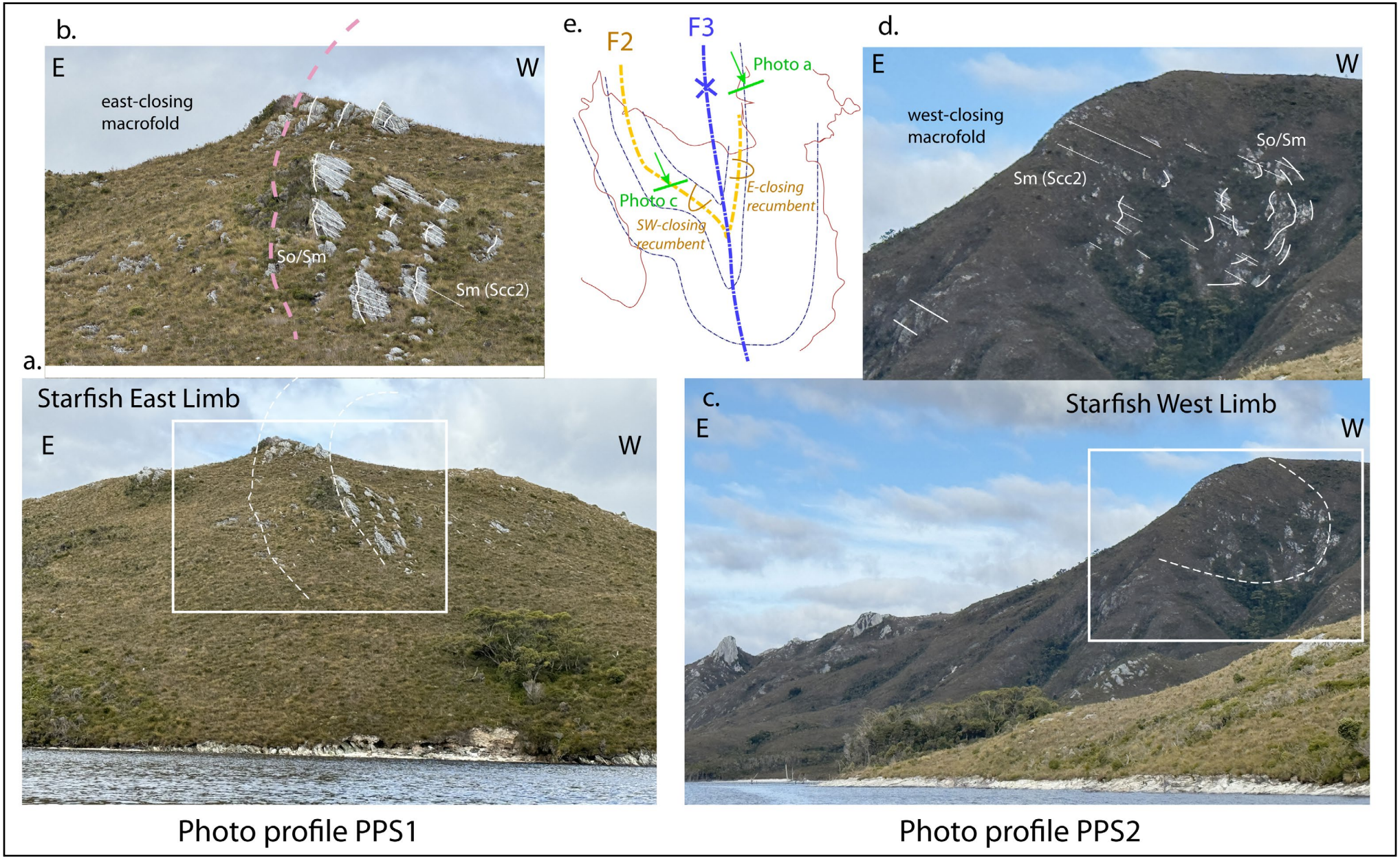

Figure 74. Photo profiles looking south of the ridgelines along the east arm of the Starfish (a, b) and the west arm of the Starfish (c, d). Enlargements b and d show formlines in So/Sm (white lines and white dashed lines) and Sm (thin white lines). e) Starfish Hill simplified structure map showing the F2 fold axial surface traces (orange dashed line trace) and the major F3 synformal axial surface trace (blue dashed line trace). Positions of the photo profiles are shown by the short green lines.

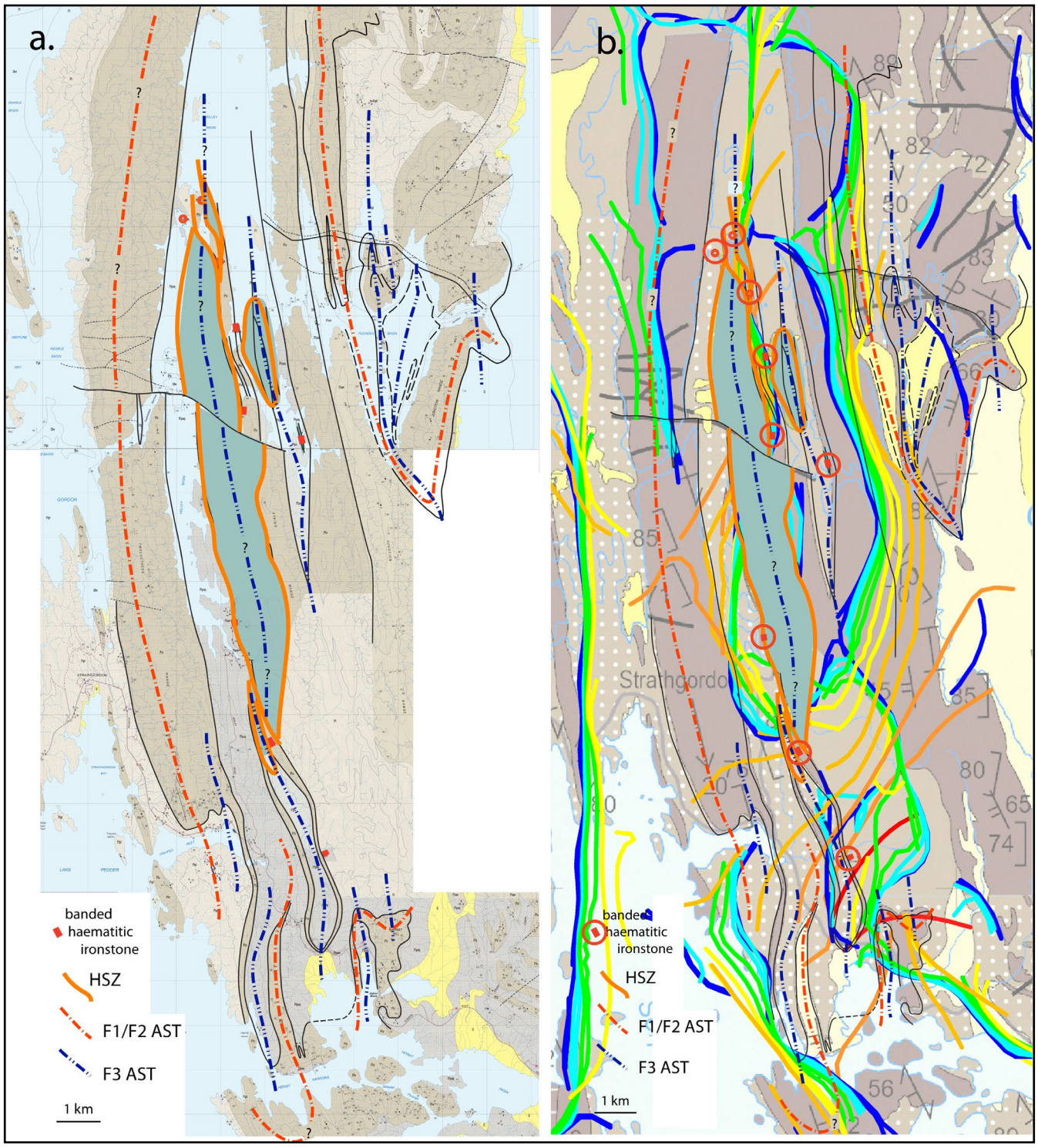

Figure 75. The Atkins Range amphibolite pod (Element 7, Figure 14). a) Revised lithological map of the macro-fold system based on the Mineral Resources Tasmania 1:25,000 digital atlas. b) Aeromagnetic "worm" image based on the contoured gradients in magnetic intensity overlain on the 1:250,000 MRT digital geological atlas.

5.6 The Pleaides - Junction Range - North Star Macro-fold

The northeastern margin of the Eastern Tyennan subdomain is dominated structurally by a large regional, ovoid shaped macro-fold with a distinct V-shaped closure (Element 3, Figure 13) in the south as part of the Junction Range (Figure 77). The quartzites of the Junction Range, the eastern Pleiades Range and the North Star region represent the eastern limb of this F3 macro-fold.

The macro-fold occurs within a lithotectonic stack of pelite (Pl), overlying quartzite (Pq), overlying interlayered quartzite and quartz-mica phyllite (Pqp), overlying a discontinuous layer of black carbonaceous phyllite (Pg) (Figure 77; Turner, 1989b). This package is interpreted to overlie the structurally lowest "sheet" of interlayered carbonate and mica-quartz phyllite (Pqpc) and dolomite (Pc). The lowest sheet has lithological and structural affinities with the Scotchfire metamorphic sheet of the Central Tyennan subdomain (Gray and Vicary, 2021b).

The Pleiades - Junction Range - North Star macro-fold is a compound fold system made up 3 orders of folds (Figure 78), each at different scales and formed at different times in a rotational shear-related deformation. The macro-fold has a pseudo-ovoid, sheath-like form with plunges away from the northern and southern close outs, or plunging terminations (Figures 79 and 80). The main fold form is controlled by the Macro 1 folds having approximately north-south-trending axial surface traces (blue dashed-dot lines, Figure 79) and trace lengths up to 20-30 km. These are the youngest folds (considered F3) that refold the early F2 Macro 1 fold (red dashed-dot trace, Figure 79) and the northeast-trending F2 Macro 2 folds in quartzite along the eastern limb (orange line traces, Figure 79) with lengths of ~1-2 km.

The map pattern shows the southern part of the macro-fold is defined by a distinctive fold-nose with closeout in the quartzite of the Junction Range (grey unit, Figure 79). This fold nose has reclined geometry (Figure 80) and is cored by pelite (orange unit, Figure 79). The flanking eastern and western fold limbs appear to thin and taper northwards, with another fold nose closeout of the eastern limb quartzite, also cored by pelite (Figure 79). Quartzite of the western limb also tapers northwards beyond North Star, but has a greater apparent thickness due to the presence of the isoclinal F2 Macro 2 asymmetric fold pairs (Figure 79). The Pleiades core of the macro-fold contains several smaller in-folds with alternating belts of pelite and quartzite (Figure 79).

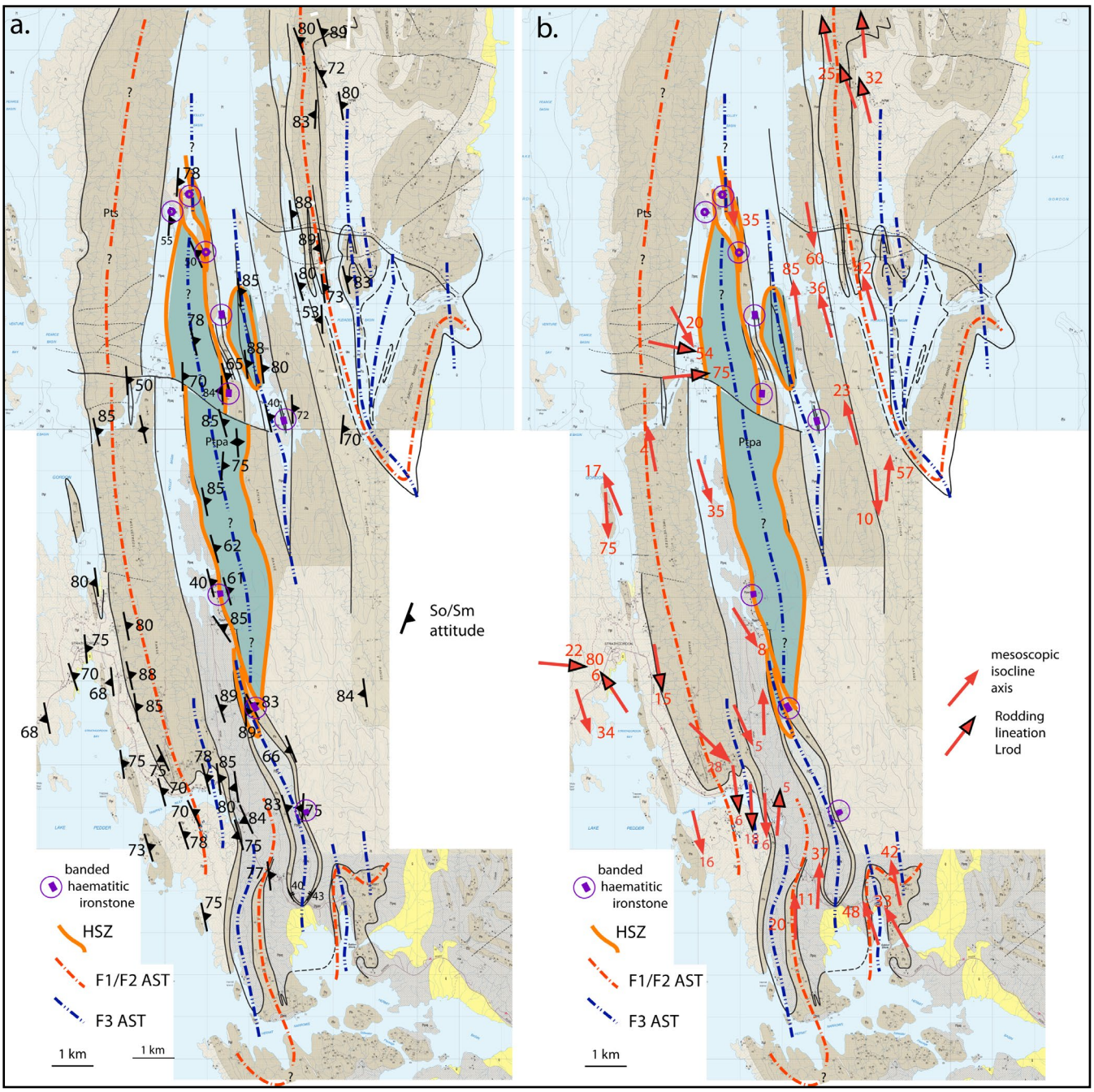

Figure 76. Structure map of the Atkins Range macro-fold pod. a) Foliation Sm attitude and distribution map (shown by the black strike and dip symbols). b) Mesoscopic fold axes (red arrows) and rodding lineations Lrod (red arrows with blue outlined arrowheads) attitudes.

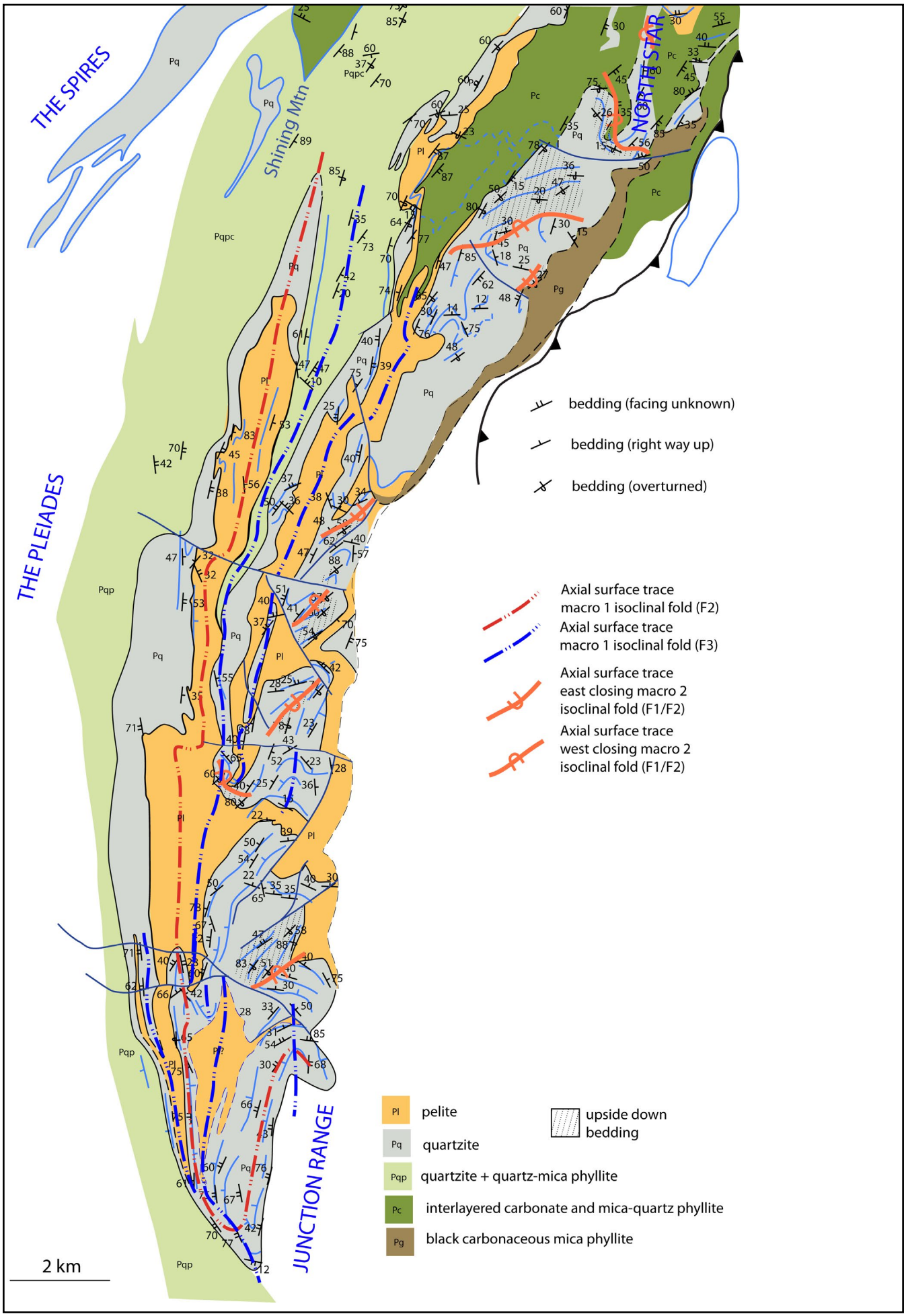

Figure 77. Geological map of the Pleiades-Junction Range-North Star fold system based on the Huntley 1:50,000 Series map sheet (Brown et al., 1982). The map shows lithological distribution, attitudes of bedding (So) as dip/strike symbols and formlines in the bedding as blue line traces.

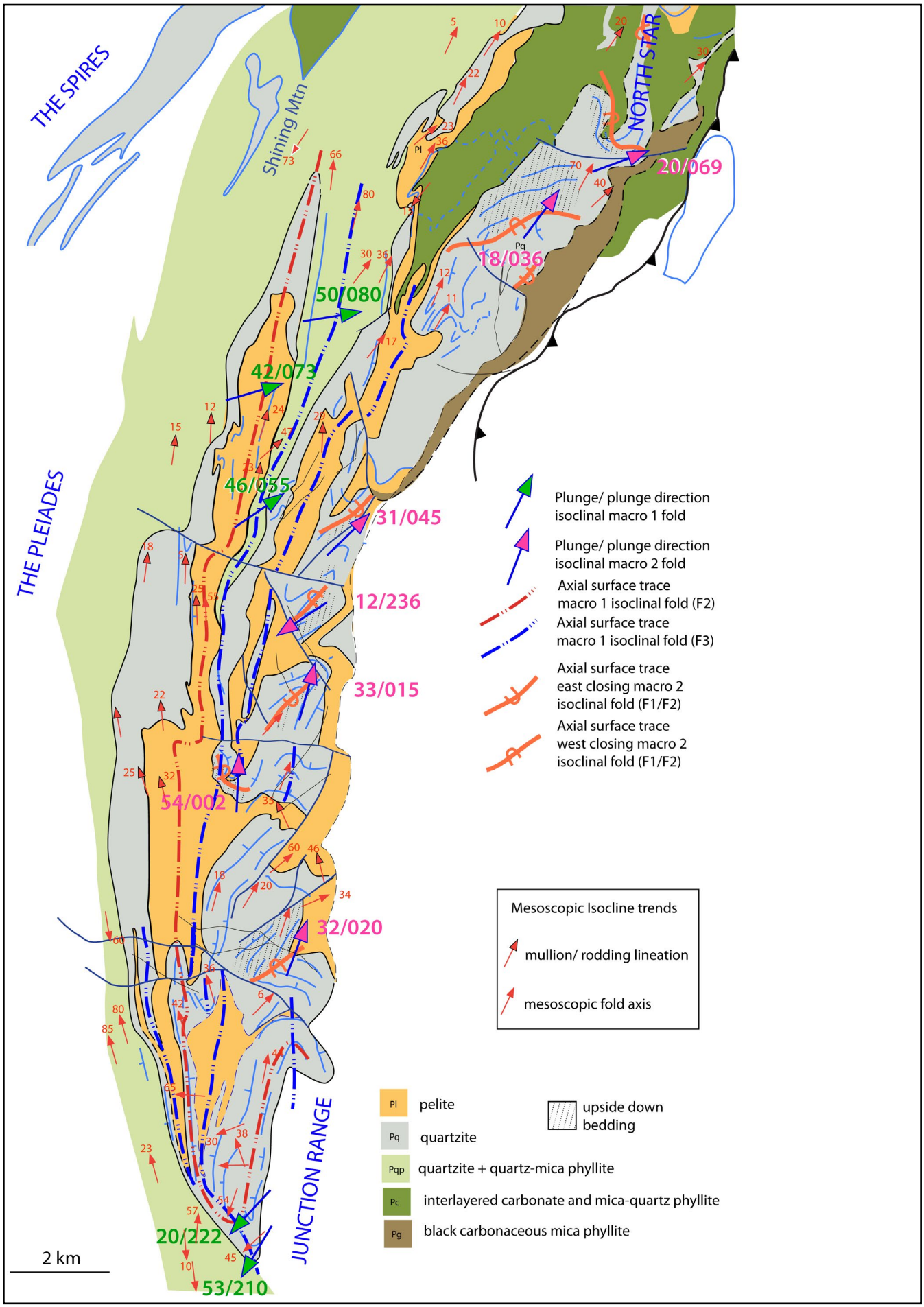

Figure 78. Axial trace map showing the two major fold sets that define the compound Pleiades-Junction Range-North Star fold system. The largest folds are designated as Macro 1 folds with axial surface traces shown by the red dashed-dot lines (F2) and the blue dashed-dot lines (F3). The youngest folds (F3) refold the earlier-formed Macro 1 (F2) and Macro 2 folds (considered largely F2) shown by the orange line traces. Fold axis plunges for macro 1 fold hinges (calculated; Figure 79) are shown by the green-filled arrows. The Macro 2 fold hinge attitudes (calculated; Figure 79) are shown by the red-filled arrows. Mesoscopic fold hinges (measured; Huntley map sheet) are shown by the smaller red arrows.

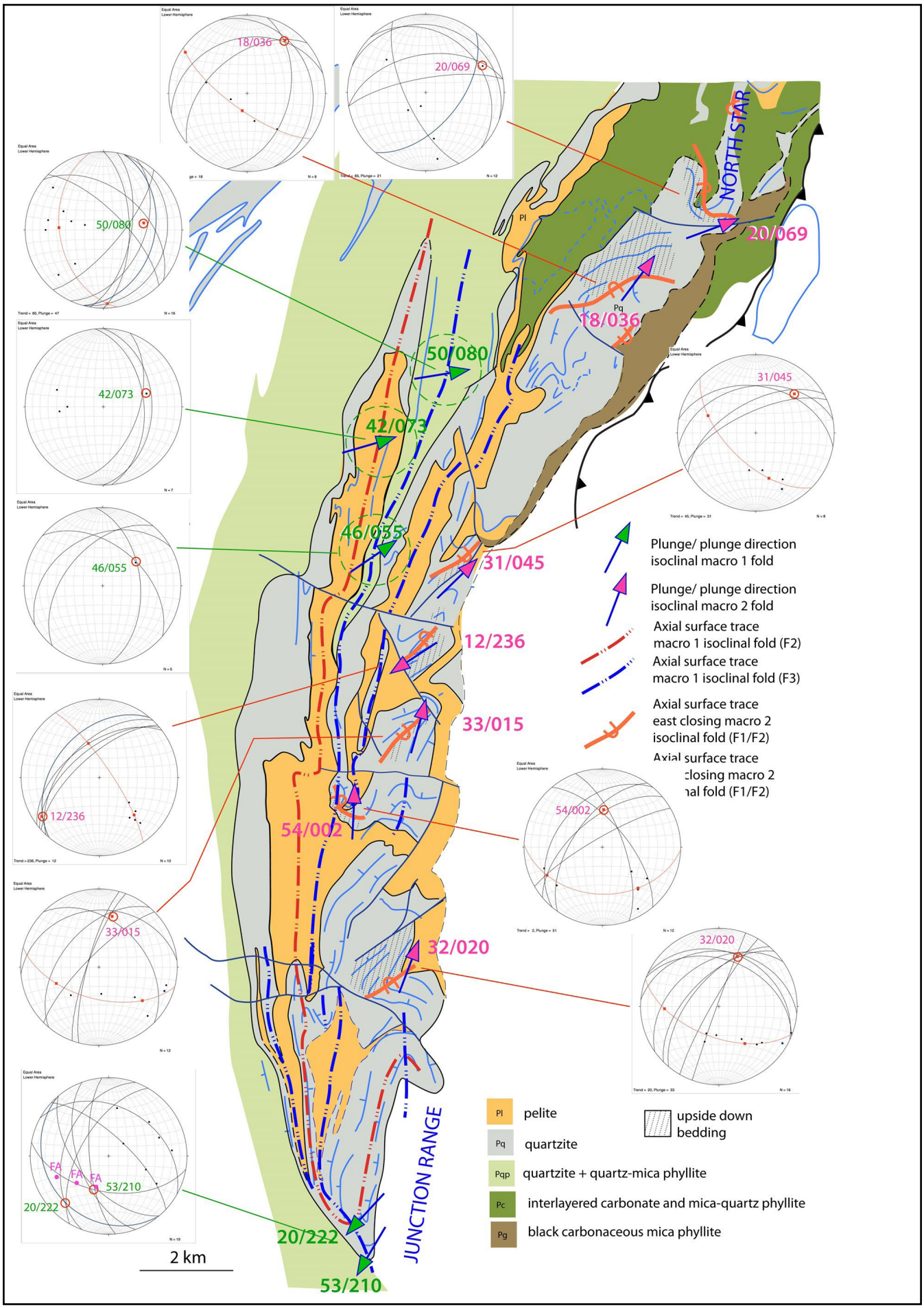

Figure 79. Stereographic projection plots of So and So/Sm data from the Huntley map plotted as poles and great circle traces. The data are from different parts of the Pleiades-Junction Range-North Star fold system. The stereonets show the bedding great circles as curved line traces as well as their respective poles-to-planes (black dots), Great circle intersections define β points and pole great circle fits π points giving calculated fold plunges at different segments of the macro-fold.

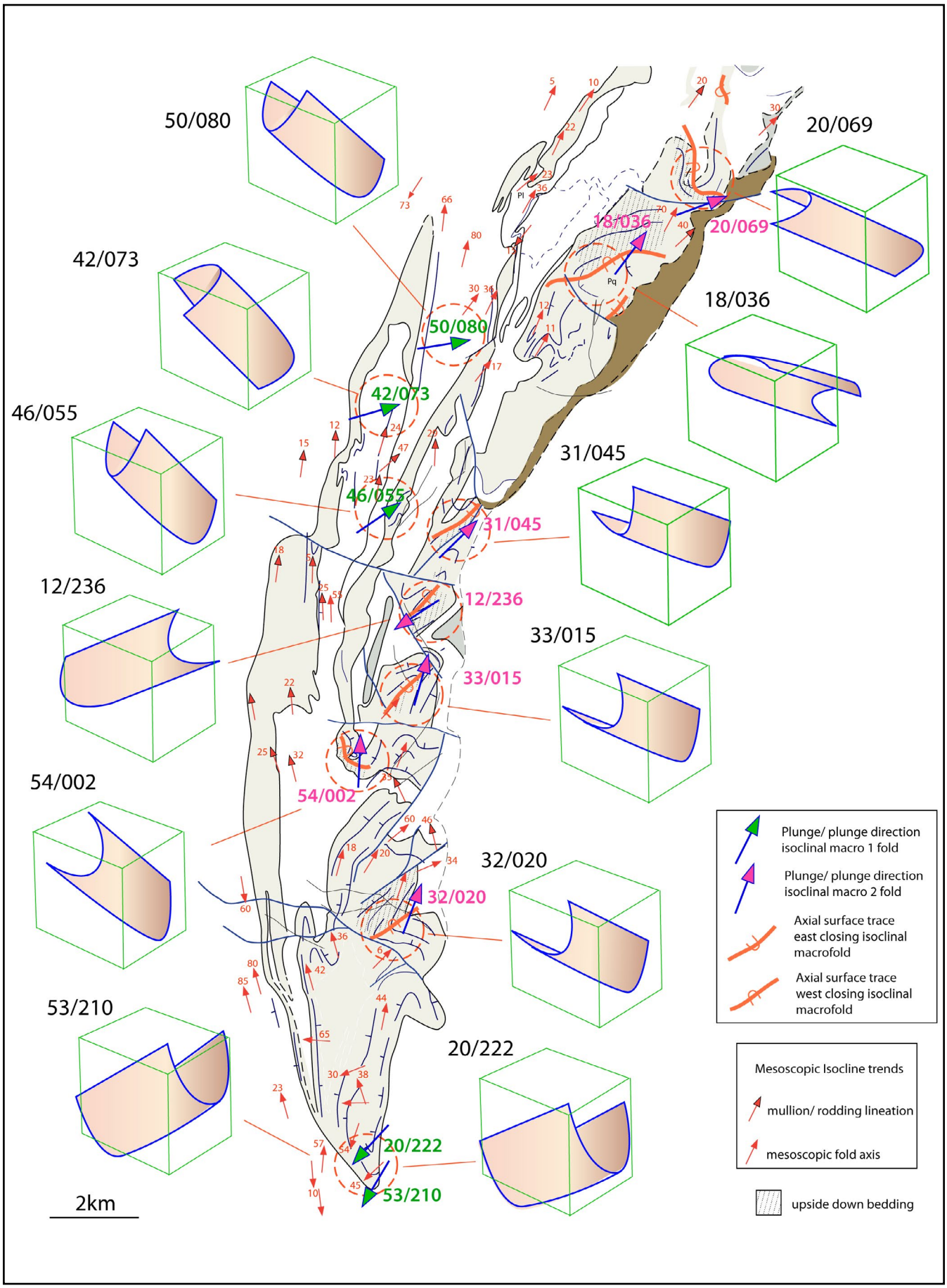

Figure 80. Geometry of component fold elements of the Pleiades-Junction Range-North Star macro-fold system. The geometry of each fold element is defined by it's fold plunge, direction of closure and the position of the overturned (upside down) bedding. Determined, or calculated, Macro 1 and Macro 2 fold plunges are shown by the respective green and red filled arrows (see Figure 79). Measured, mesoscopic fold plunges are shown by the smaller red arrows. Bedding-foliation attitude data were selected from the Huntley map sheet across the suspected fold hinge lines to obtain the stereonet π points.

The mesoscopic isoclinal folds (predominantly F1 and F2) show strike-parallel trends within the quartzite of the central part of the western macro-fold limb, but clearly deviate away from this pattern at the fold terminations (Figures 79 and 80).

1. The macro-fold plunges were determined for different fold segments across the macro-fold system. Hinge-limb areas were selected and stereograph plots of So/Sm were constructed to define So/Sm great circle intersection points (β) and great circle fit to So/Sm poles to give π points (Figure 79).
2. The map and determined fold axis data were then used to construct the geometry of the different macro-fold segments (Figure 80).
3. These geometrical fold elements were then combined to produce the overall Junction Range - Pleiades macro-fold 3D geometry (Figure 81).

The constructed 3D form shows oppositely closing and plunging terminations to the macro-fold system with a pseudo closed loop or ovoid form. The southern termination is a distinct, single west-closing nose in the Junction Range, whereas the northern termination is defined by a series of alternating and interdigitating, east- and west-closing macro-fold hinges (Figures 78 and 79). The geometry necessitates the western limb is steeply west-dipping, structurally higher and overturned, but there is limited younging (facing unknown) along this western belt of quartzite. The mesoscopic fold trends along this western limb are generally sub-parallel to the strike of the limb (Figure 78).

5.7 Algonkian Mountain Klippe

High-grade garnet schist has been reported from Algonkian Mountain (Turner, 1989a, 1990). The domal geomorphic form of Algonkian Mountain is associated with:

1. A domed flat lying foliation (Figures 82 and 83); and
2. A curved outcrop trace of a band of quartzite along the northwestern slope. Hall et al. (1969) suggests high-grade schist at the summit overlies the quartzite of the lower sheet.

This sequence is interpreted to overlie calcareous phyllite and quartzite of the Scotchfire metamorphic sheet (parautochthon) (Figure 13 and Figure 22, Profile 1).

6.0 APPARENT ROTATION AXES

The southern part of the Eastern Tyennan subdomain has a marked curvature in the quartzite forming ridgelines of the Frankland and Folded Ranges, as well as in the ridgelines with Mt Cawthorn and Buckies Bonnet through to The Coronets and The Sentinels (Figure 3). Differences in curvature between the area south of Lake Pedder and the area around the Helder Inlet require two rotation axes or pivot points (Figures 84 and 85). The bulk regional rotation is counterclockwise facilitated by: 1) predominantly "bending" rotation in the area of the Helder Inlet (red dot, inner rotation axis: 69°/254°, n=5); and 2) combined bending and fault-facilitated rotation in the Cleft Peak - Grey Cap area (blue dot, outer arc rotation axis: 62°/237°, n=8) on the re-activated Prince of Wales Fault imbricate-horsetail-fan-fault system (Figure 85). The Sentinel Range also shows an opposite curvature towards the southeast reflecting a smaller, subsidiary clockwise rotation about an apparent rotation point (green dot, rotation axis: 41°/277°, Figure 85).

The regional fault network is interpreted as an oblique slip system with both reverse and dextral strike slip components. This motion facilitates the major, bulk-regional, counter-clockwise rotation of the southern part of the Eastern Tyennan subdomain. The fault traces are based on ridge offsets, truncations and valley trends. The rotation axis points (pivot points) are shown by the dot positions and the curved arrows (Figures 84 and 85). The fault imbricate splay system offsets the macro-isoclinal fold pair along the combined length of the Wilmot - Frankland Ranges.

7.0 STRUCTURE OF THE PARAUTOCHTHON

7.1 The Maxwell River Valley macro-fold

The region of the Maxwell River macro-fold is triangular shaped, occupying the Maxwell River Valley between the between the Princess Range and Prince of Wales Range south of Algonkian Mountain ((Element 1, Figures 14 and Figure 86). It has an apparent synformal character, but limited So/Sm data from the Mineral Resources Tasmania 1:250,000 Geological Atlas indicates the fold is south-closing, has steeply east-dipping limbs and an overall inclined plunging geometry (Figure 16).

The Maxwell River macro-fold occurs within dolomitic phyllite and dolomite of the lowermost, para-autochthonous Scotchfire Metamorphic sheet exposed within the Maxwell River valley (Figure 86). The region is thickly vegetated with difficult access, apart from river transects accessible by the Denison River (central part) and Gordon River (southern part) and the Maxwell River (central northern part) (Figures 87and 88).

The interpretation presented is based on pack-rafting photographs taken along the Denison and Gordon Rivers (Figures 89, 90, 92 and 93), combined with structural data and field photographs (Figure 91) from Electrolytic Zinc Company Exploration Reports (Wade, 1956; Scott, 1960) and the Mineral Resources Tasmania 1:250,000 digital atlas. These sources enabled construction of a preliminary structure map of the Maxwell River macro-fold and help establish the geometry of this macro-fold (Figure 94). The northern part shows refolding by a series of younger open, northeast-trending Devonian folds (see Figures 16 and 86).

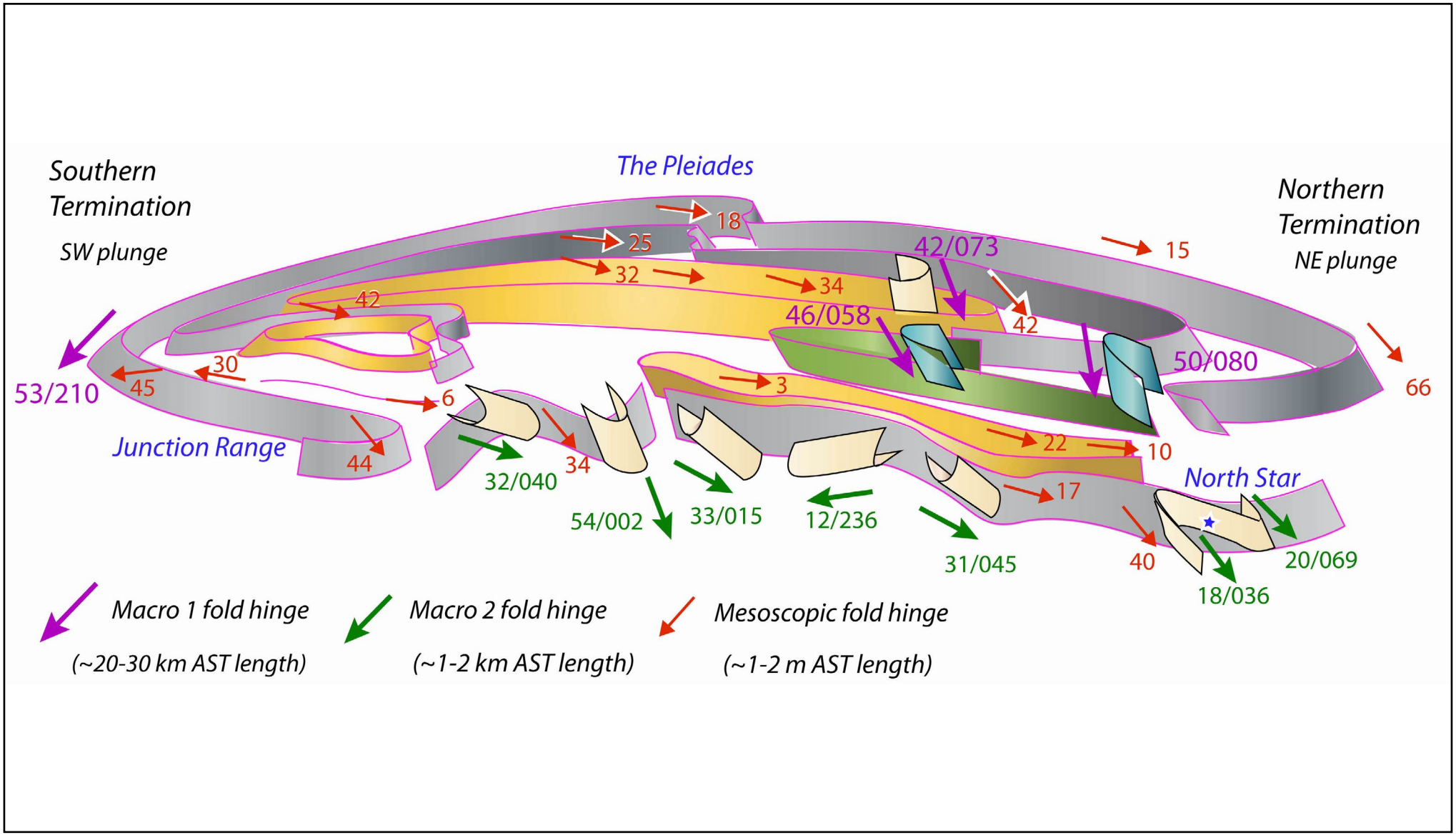

Figure 81. 3D schematic structural diagram of the Pleiades-Junction Range-North Star macro-fold structural geometry viewed looking west. The macro-fold form is depicted by a series of form line-derived shells in bedding, with lithology highlighted by colour (grey: quartzite; orange: pelite; green: calcareous phyllite). Three orders of folds are shown with the largest macro 1 hinge lines as purple arrows, the macro 2 hinge lines as green arrows and mesoscopic fold hinge lines by smaller red arrows. The gross form is sheath-like with an ovoid-shaped, sectional map view showing oppositely plunging fold culminations at the northern and southern terminations.

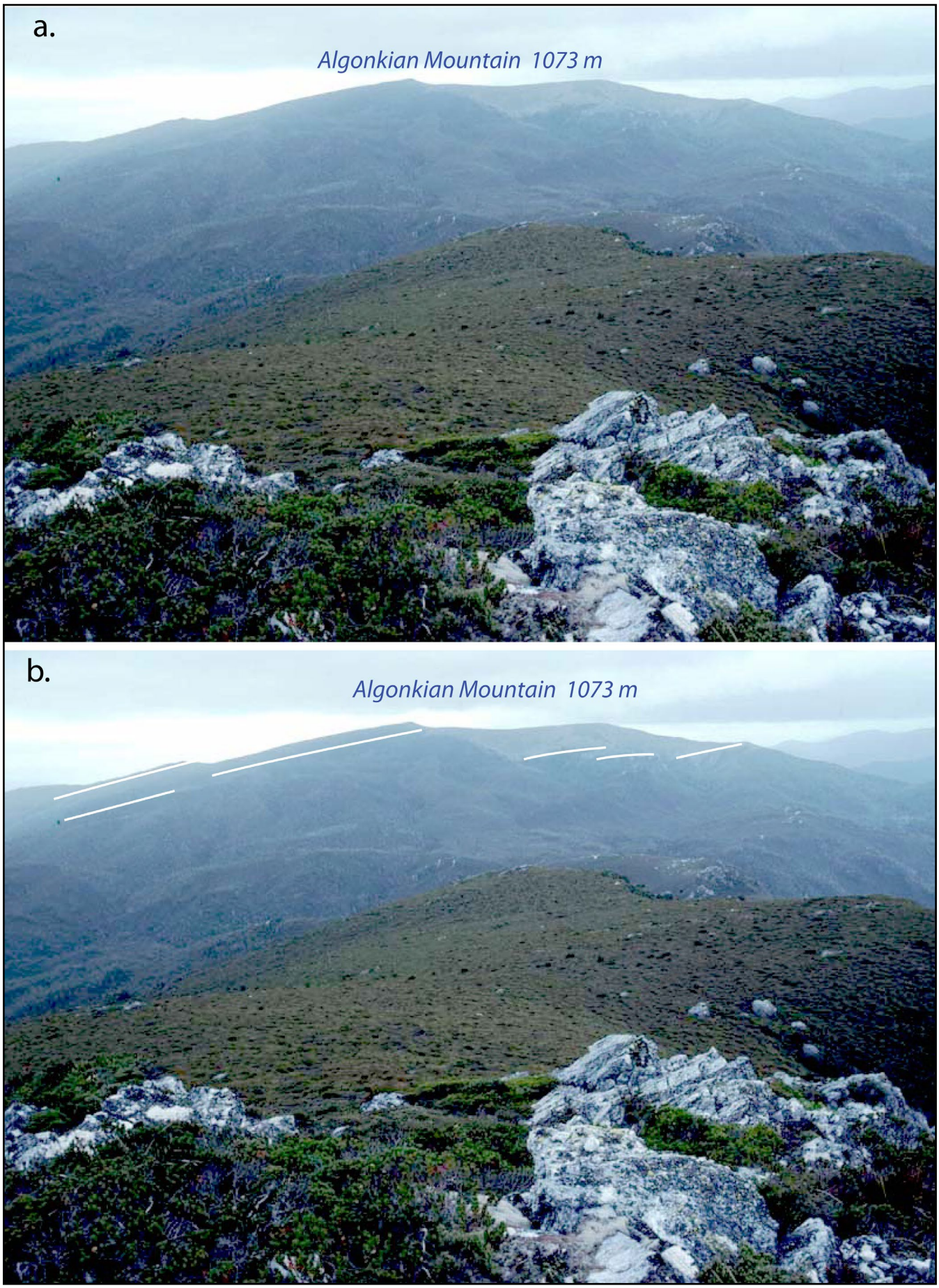

Figure 82. View of Algonkian Mountain from the quartzite ridgeline to the northwest of Observation Point. The ridge view suggests apparent doming within a flat-lying foliation Sm. Foliation at the summit of Algonkian Mountain (Figure 83) supports this interpretation (Photo credit: David Noble)

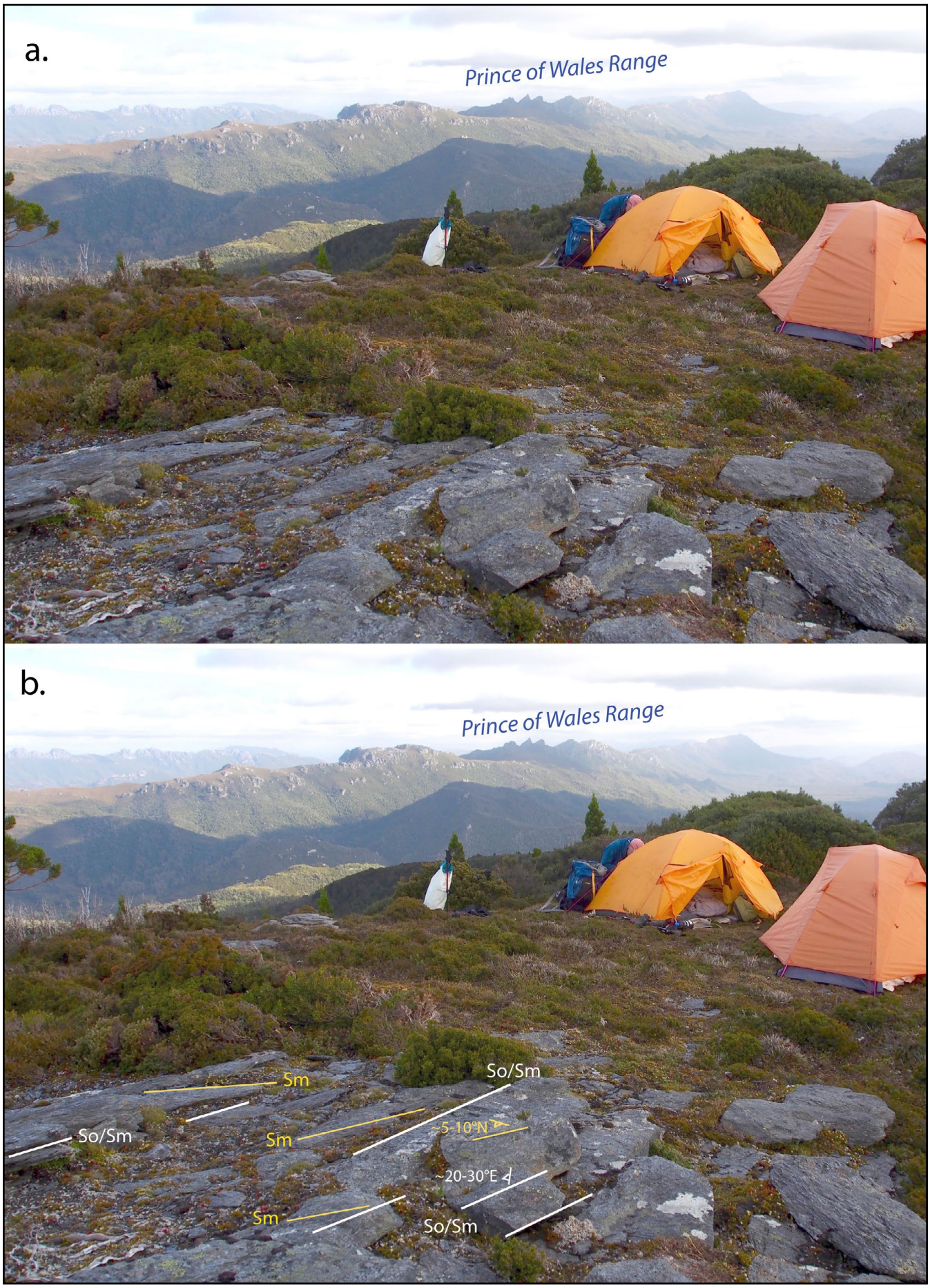

Figure 83. Algonkian Mountain summit view towards the Prince of Wales Range. The foreground rocks show a an almost flat lying foliation (Sm) intersecting compositional banding (So/Sm) at low angles. (Photo credit: Becca Lunnon: rockmonkeyadvetures)

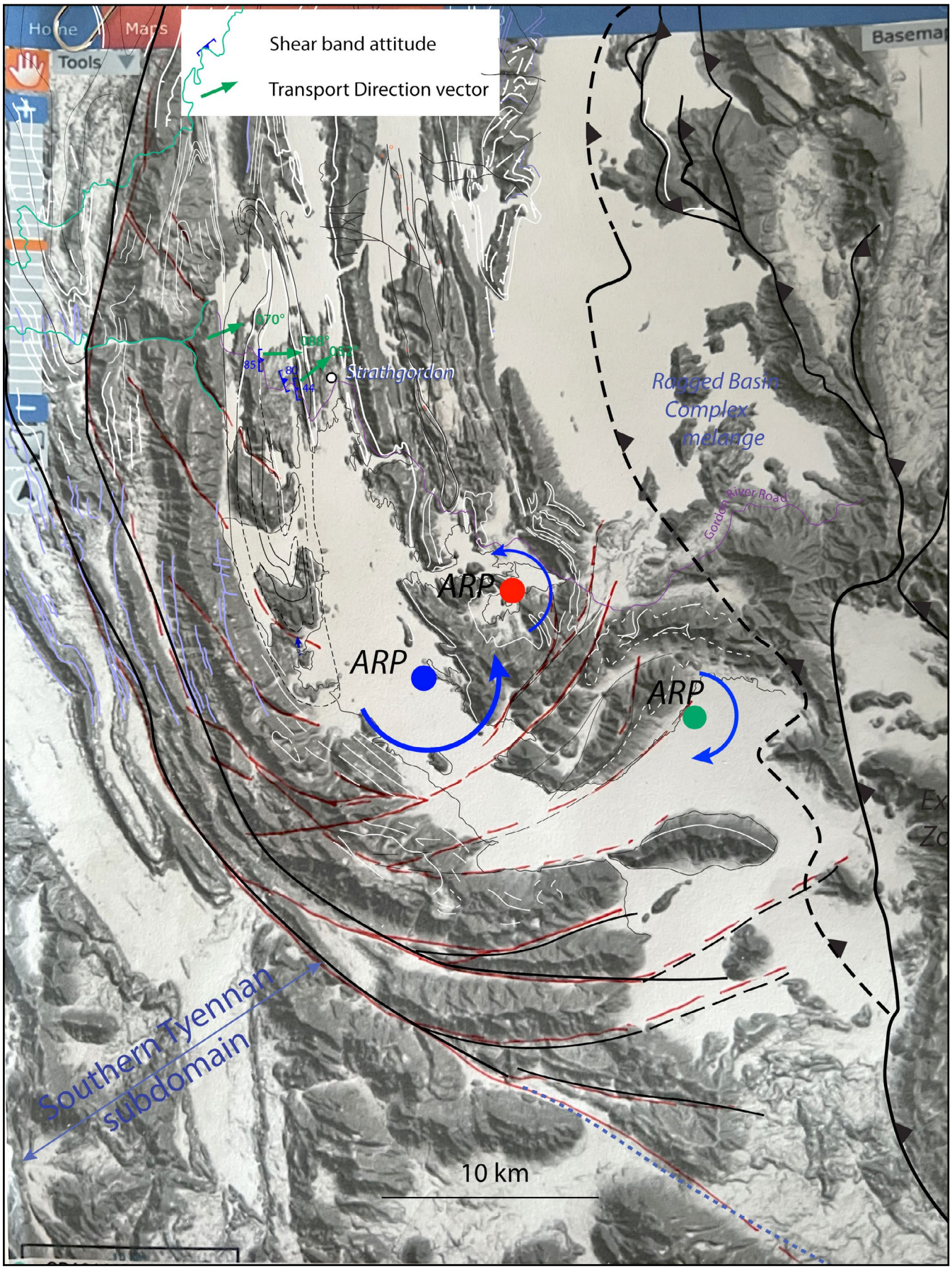

Figure 84. ListMap digital elevation model (DEM) of the southern part of the Eastern Tyennan subdomain showing the Prince of Wales Fault system with an imbricated horse-tail fan at the southern termination. The fan has facilitated, and is accompanied by, a bending-style rotation in the quartzite-pelite sequence. An inner arc rotation axis (red dot) and an outer arc rotation axis (blue dot) have been identified.

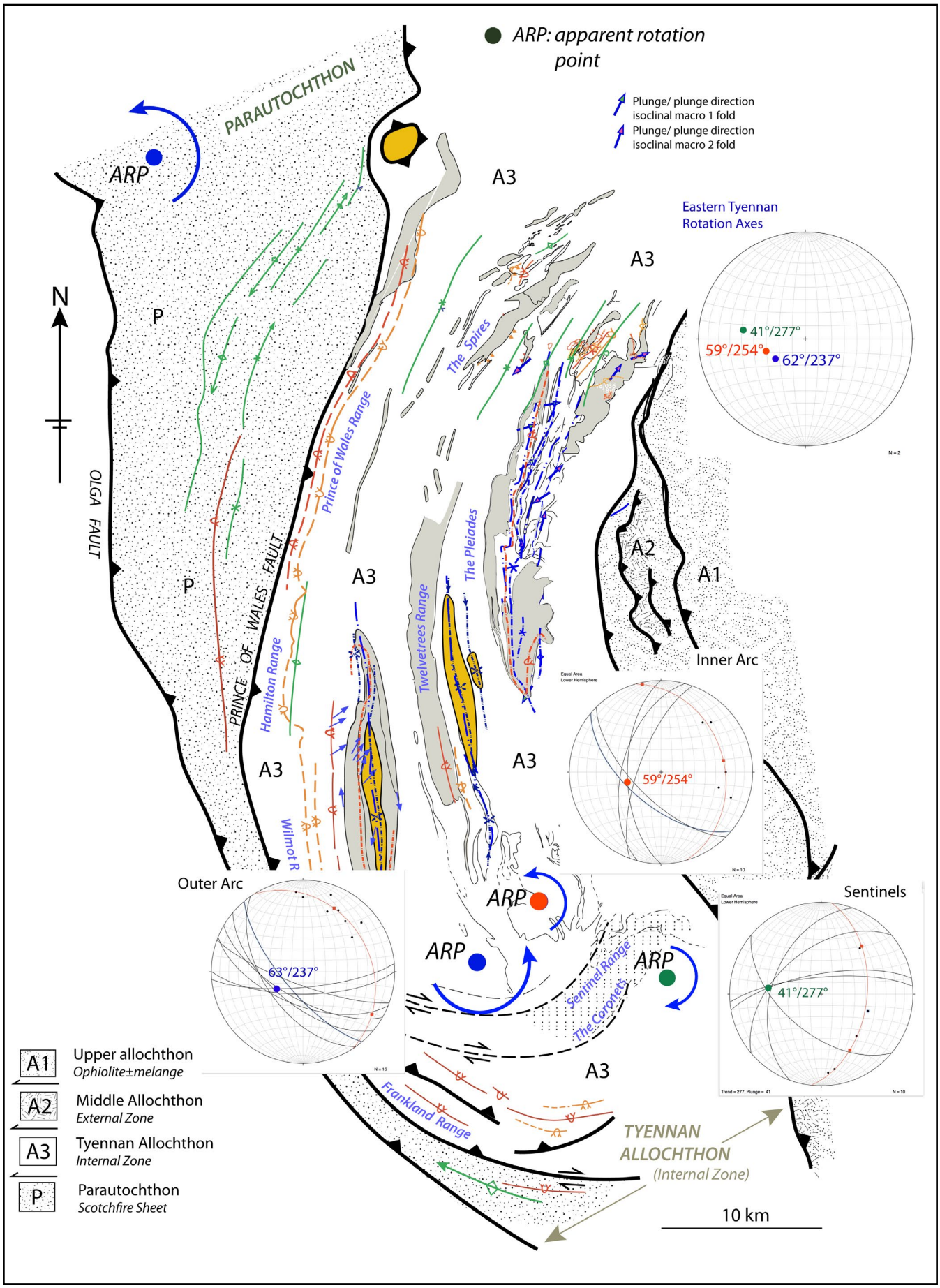

Figure 85. Rotation axis determinations for the southern end of the Eastern Tyennan subdomain. The rotation axes are determined from β points as great circle intersections of bedding (So) and/or compositional layering (S0/Sm) attitudes at different points along the curved segments along the Frankland Range and the Helder Inlet. Note strike values were selected from the different segments that comprise the "bend" but planar segments were used with the same dip sense to the west, southwest and south to give the best β point. Upper right stereonet shows the similarity in rotation axes between the inner and outer arcs of the bend.

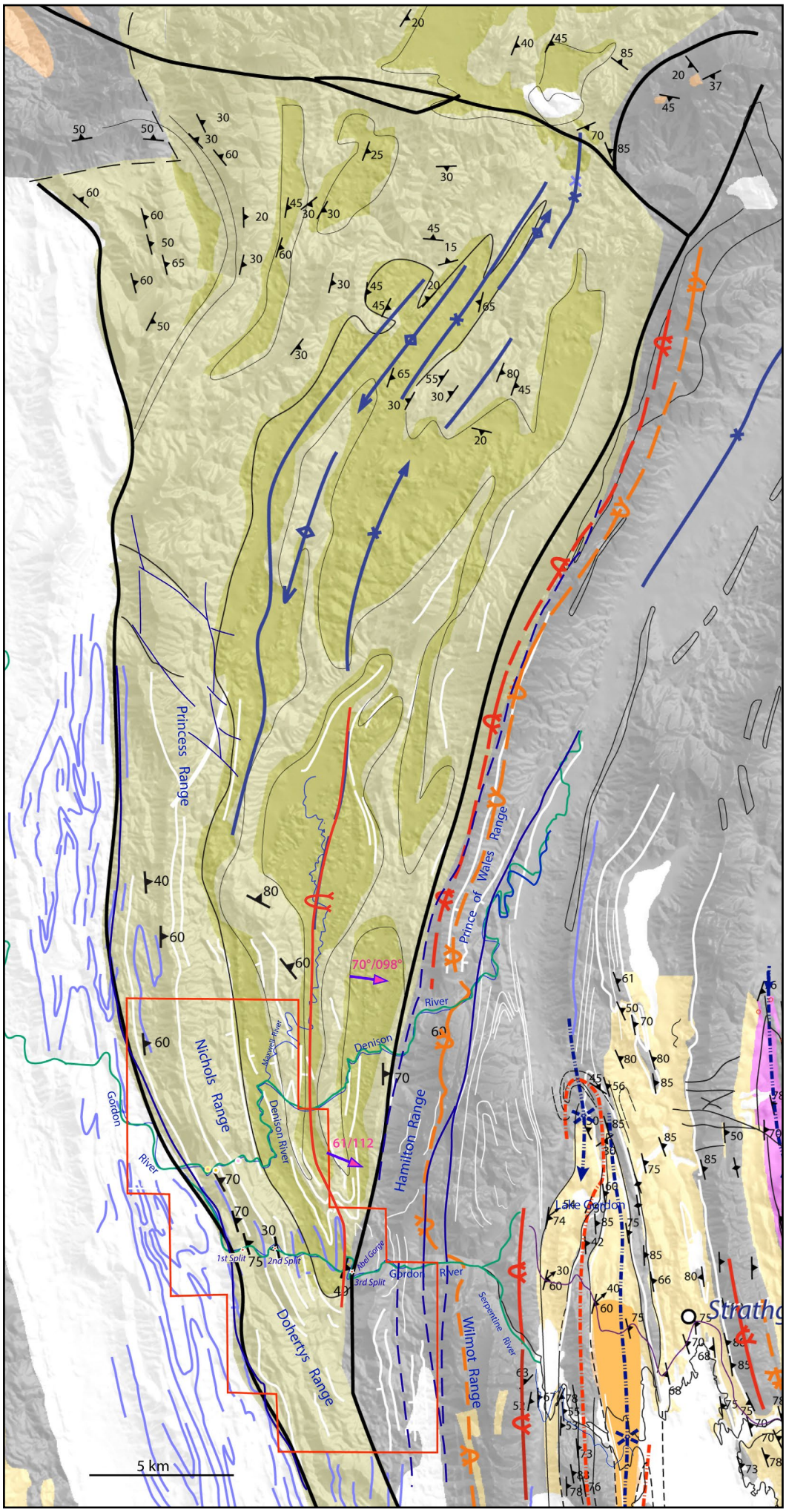

Figure 86. The Maxwell River Valley macro-fold So/Sm formline map white line traces on a revised 1:250,000 Mineral Resources Tasmania digital atlas map base. The red-boxed area delineates the position of the satellite mosaic image in Figure 88.

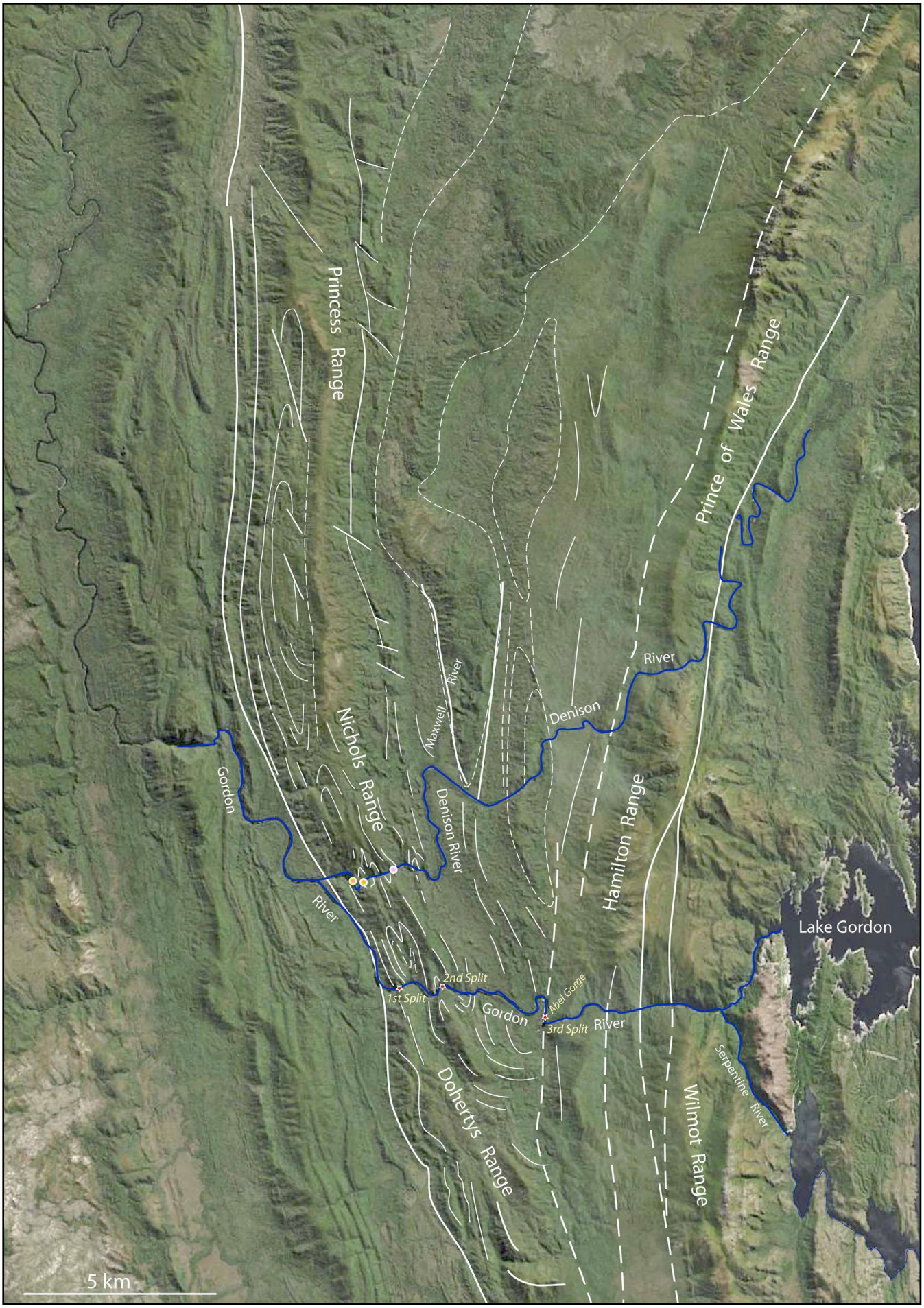

Figure 87. Google Earth image of the region occupied by the Maxwell River Valley macro-fold. The region is heavily vegetated and is transected by the major Denison and Gordon River systems. The flanks or limbs of the interpreted macro-fold coincide with the combined Princess-Nicholls-Dohertys Range on the west and the Prince of Wales-Hamilton Range on the east. Convergence of these ranges to the south defines the hinge of the macro-fold showing a closure in formlines south of the Gordon River east of the Dohertys Range.

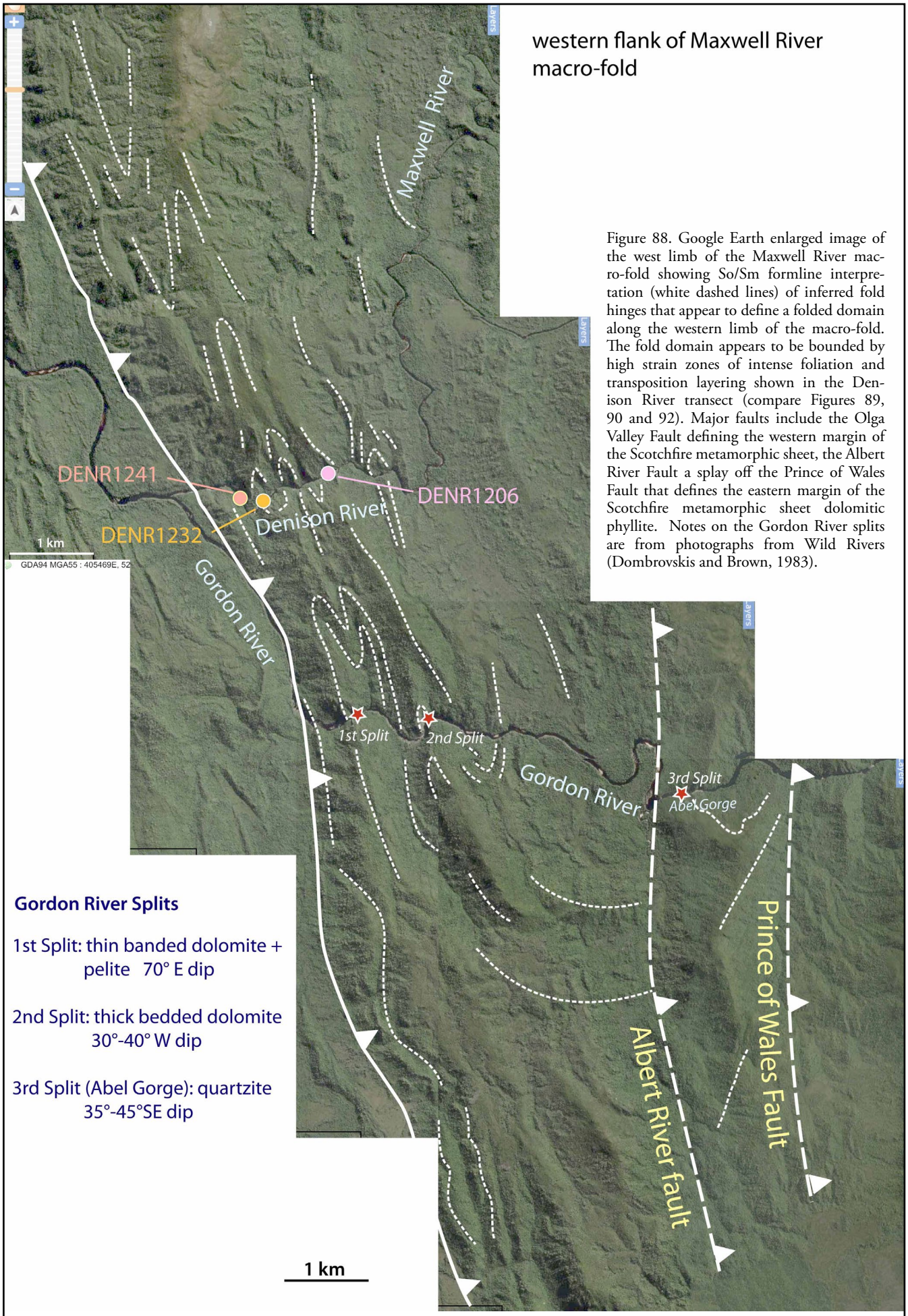

Figure 88. Google Earth enlarged image of the west limb of the Maxwell River macro-fold showing So/Sm formline interpretation (white dashed lines) of inferred fold hinges that appear to define a folded domain along the western limb of the macro-fold. The fold domain appears to be bounded by high strain zones of intense foliation and transposition layering shown in the Denison River transect (compare Figures 89, 90 and 92). Major faults include the Olga Valley Fault defining the western margin of the Scotchfire metamorphic sheet, the Albert River Fault a splay off the Prince of Wales Fault that defines the eastern margin of the Scotchfire metamorphic sheet dolomitic phyllite. Notes on the Gordon River splits are from photographs from Wild Rivers (Dombrovskis and Brown, 1983).

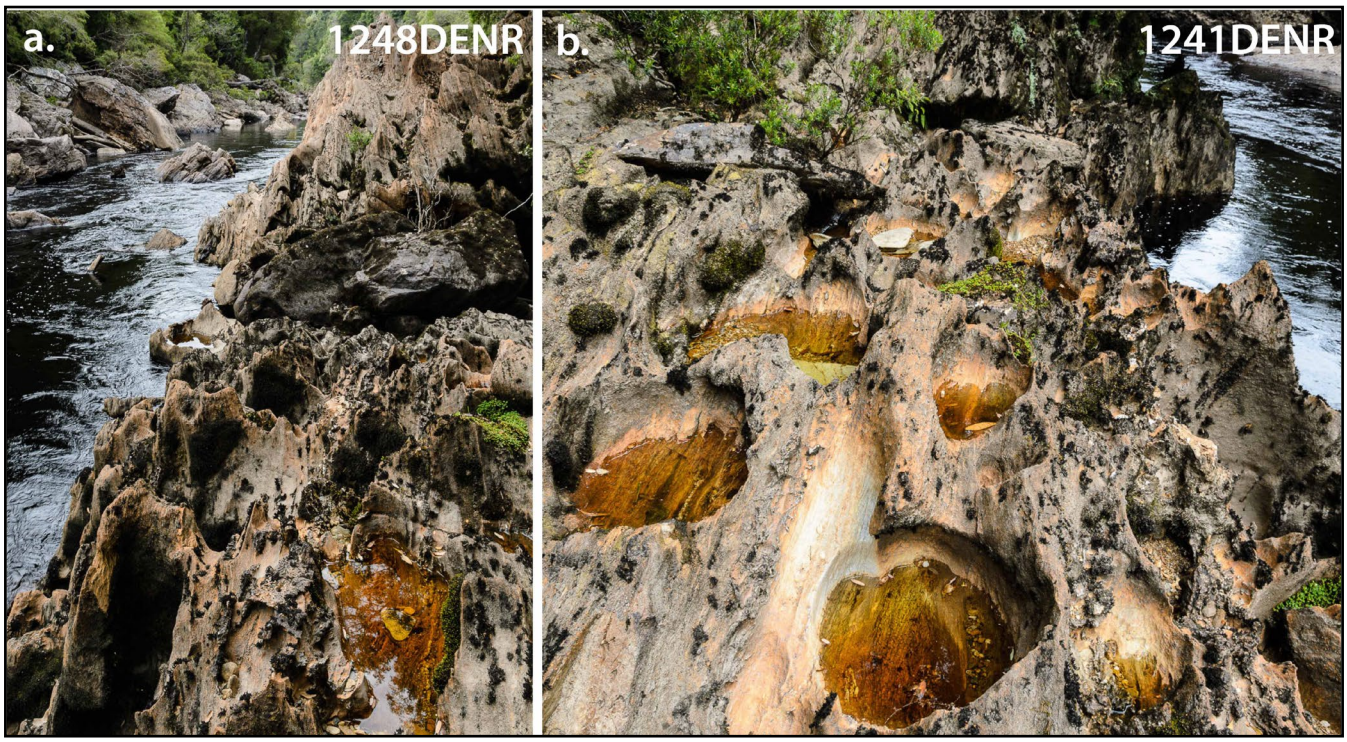

Figure 89. Intensely foliated dolomitic phyllite in Denison River outcrops DENR1248 (a) and DENR1241 (b). For locations see Figure 88. Both exposures are metres apart and show the steep 80°-85° east dip on the western flank of the Maxwell River macro-fold. (Photo credits: Grant Dixon)

Figure 90. Intensely foliated, east-dipping dolomitic phyllite showing transposition layering/foliation Sm enveloping rootless isoclinal fold hinges (white outlines in foliation So/Sm). Station DENR1206 (for location see Figure 88). Asymmetric boudinage in thicker (~15cm thick) dolomitic? layer (above hand) suggests a west-over-east (east-side-down) movement sense. (Photo credit: Grant Dixon)

Figure 91 (Left). Asymmetric S-vergence folds in bedded quartzite along the Nicholls Range ridgeline. The photo is looking south with the quartzites dipping to the east. Note the curved form of the lower fold hinge line with a swing of almost 60° from a gentle (<20°) east-northeast plunge to a gentle north plunge. The photo is from an unpublished EZ Exploration Report (Wade, 1956).

Figure 92 (Below). Stitched photographs of the western end of Denison River gorge (photo credits: Grant Dixon). View is to the southeast with downstream to the right on the photographs. Station DENR1232 (for location see Figure 88). a) Non-annotated photographs. b) Structural interpretation showing So/Sm formlines (thick white line traces), axial surface foliation (fine white lines), overprinting cleavage Scl and faults (heavy yellow line traces).

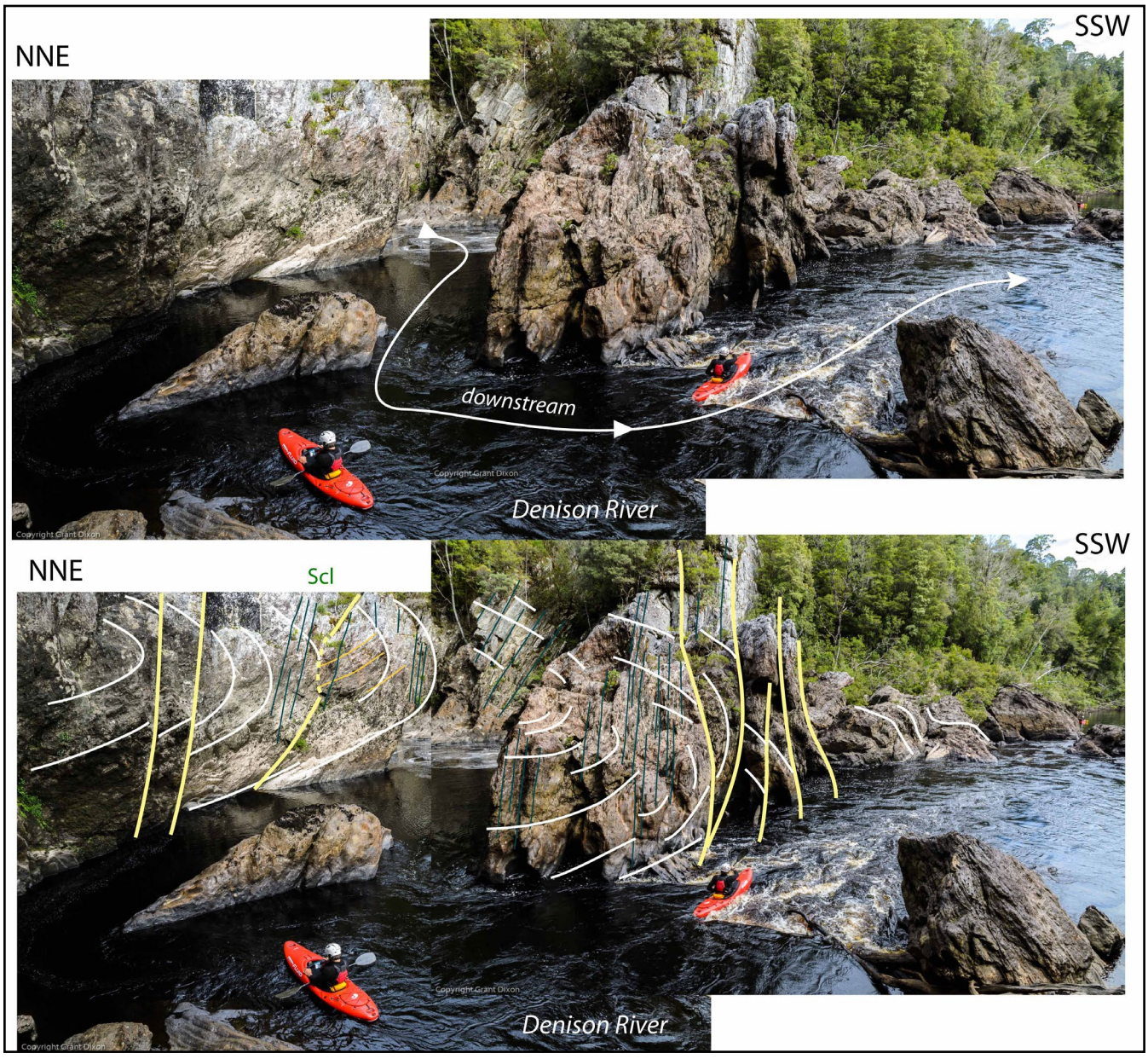

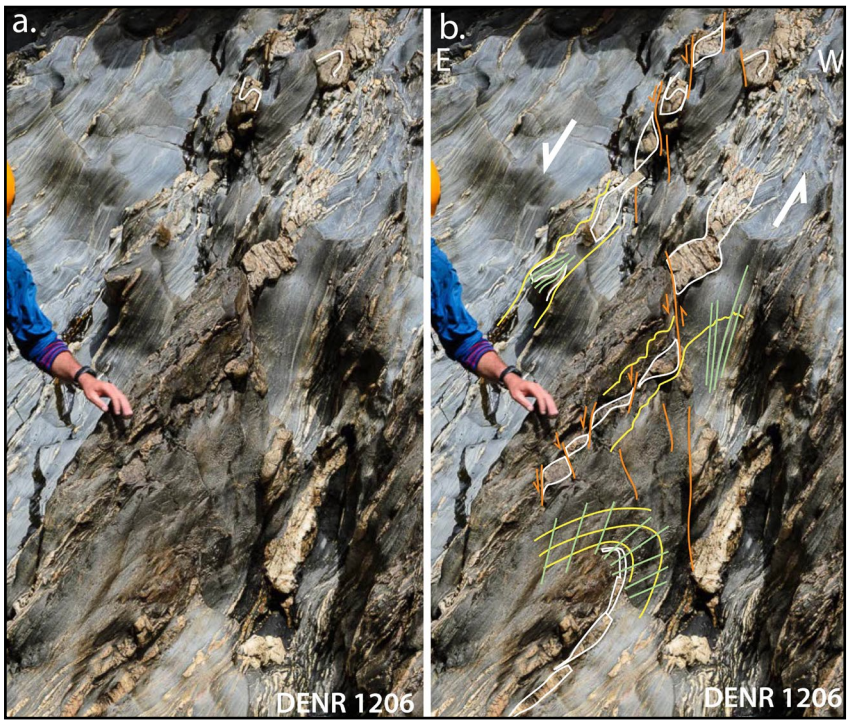

Figure 93 (Left). Shear band boudinage within thin dolomitic layers in intensely deformed dolomitic phyllite. Outcrop location DENR1206. Thin (<2cm) dolomitic layers show small-scale asymmetric 'S'-shaped vergence folds throughout the outcrop (DENR1206; for location see Figure 88). Relict, larger wavelength, metre-scale folds occur within zones enveloped by the intense dominant Sm (centre bottom of photo). These folds show axial surface to fanning cleavage.

Figure 94 (Below). Structure map of the Maxwell River valley region (a) incorporating sketch insets of structural relationships based on photograph interpretation of pack rafting photographs taken by Grant Dixon along the Denison River. b) 3D geometry of the Maxwell River macro-fold showing the inclined plunging to reclined form. The macro-fold plunge is shown by the red and green arrows. c) Stereonet of the foliation Sm attitude data from the MRT 1:250,000 digital geological atlas showing Sm great circles traces, a great circle fit to Sm poles and the calculated fold axis shown by the red arrow.

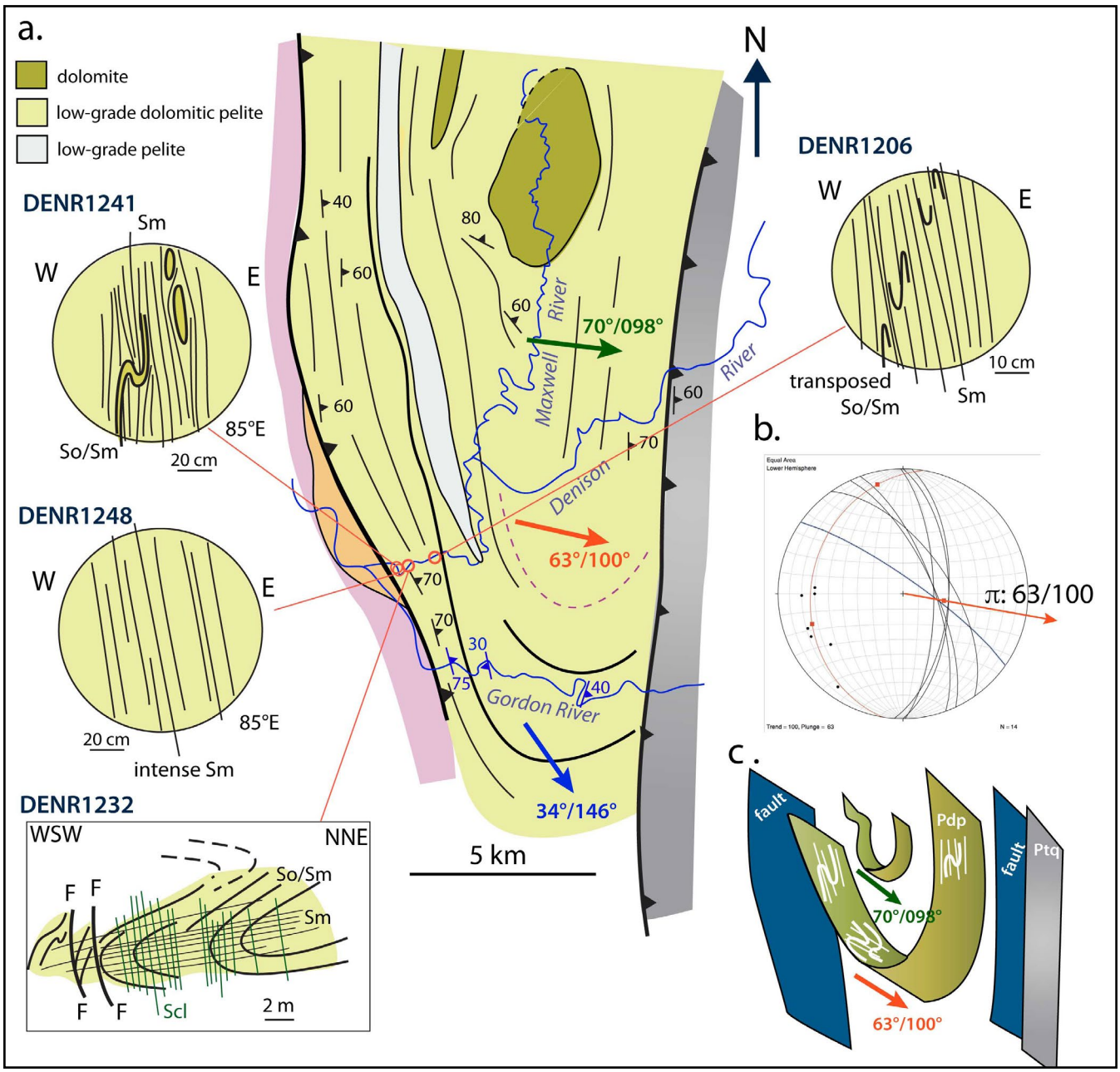

Convergence of ridgelines at both the regional (Figure 87) and local scales suggest the presence of fold closures, particularly along the western flank of the interpreted macro-fold (Figures 88 and 94). The formline interpretation of ridges converging as fold hinges is supported by the recognition of recumbent isoclines along the Denison River at DENR1232 (Figure 92). The ridgelines north of the Denison River show a pod or augen-like form coincident with the interpreted fold domain (Figure 87). This folded domain appears bounded by high strain zones with intense foliation and transposition layering shown by outcrops DENR1248 (Figure 89a) and DENR1241 (Figure 89b) on the west side and DENR1206 (Figure 90) on the east side.

7.1.1 Structure

Zones of intense foliation transitional into transposition layering (Figures 89 and 90) bound a folded domain along the west flank of the Maxwell River macro-fold (Figures 88 and 94). The interpretation is based on outcrop photographs taken along the Denison River by Grant Dixon, as well as regional So/Sm form line interpretation of Google Earth imagery (Figures 87 and 88).

7.1.2 Shear Sense

Shear sense data comes from only one outcrop (DENR 1206) on the Denison River (Figure 90). Asymmetric isoclinal vergence folds and shear band boudins within dolomitic bands within intensely foliated dolomitic phyllite (Figure 93) show west-over-east movement sense.

8.0 IMPLICATIONS OF THE EASTERN TYENNAN SUBDOMAIN STRUCTURE

The Eastern Tyennan subdomain has distinct structural character that provides information about the structural evolution and emplacement of sheets relative to the other Tyennan subdomains (cf. Gray et al., 2024).

8.1 Polydeformation

Polydeformation was first recognised by the early workers Powell (1969), Boulter (1974, 1978) but was assumed part of regional deformational orogenic pulses. In contrast, the concept of progressive shear related deformation (Figure 95a) to explain the overprinting deformations has been considered by McNeill (1985), Turner (1989a) and Meffre et al. (2001). The apparent clockwise rotation of all the developed fabrics So, S1, S2 and S3 at Strathgordon, as originally noted by Boulter (1978), can be related to an overall west-over-east sense of shear (Figures 95b, c).

Re-crenulation leading to overprinting crenulation cleavages occurs by rotation of the earlier formed fabrics towards the shear plane (Figure 95a). These foliations eventually enter the shortening field of the strain ellipse (cf. Ramsay, 1967, Figure 3-64) and undergo shortening by crenulation to eventually produce a new, overprinting crenulation cleavage. At very high shear strains (γ>10) multiple overprinting foliations can form in a cyclical manner by repeated cycles of foliation development, foliation rotation and then re-crenulation to produce a new crenulation cleavage (Figure 95a). In left-directed shear, or west-over-east shear sense as at Strathgordon, these successive fabrics and foliations show a clockwise rotation of the respective foliation surfaces (Figure 95b). This progressive, rotational shear-related deformation dominates in the core of the Eastern Tyennan subdomain (magenta dashed polygon area, Figure 13). This is evidenced at the regional scale by isoclinal F3 macro-folds that localise the preservation of the high-grade schist and amphibolite in synformal "keels" (blue dashed-dot F3 axial surface traces, Figure 13).

This increased shear strain and the resultant polydeformation reflects incipient macro-sheath fold formation, or the early stages of large-scale sheath fold development (cf. Gray and Vicary, 2022b, 2023) for the Southern Tyennan subdomain. Increased shear strain rate and shear strain magnitude have been localised within the "kernel" of the subdomain. The lateral decrease in shear strain both to the north and to the south, as evidenced by the lack of overprinting cleavages and the lack of F3 refolding (Figure 13), may be responsible for the strong counter-clockwise rotational component (Figures 84 and 85). In summary, the mapped layering pattern does not accord geometrically with a classic sheath fold form (see Figures 10 and 11).

8.2 Stacking order

A generalised stacking sequence of H-G schist/pelite/quartzite/dolomitic phyllite has been deduced from the map patterns and an understanding of the regional structures (Figure 4). This is consistent with the stacking of "sheets" in the apparently contiguous Central and Northern Tyennan subdomains. Limited preservation of parts of these sheets in the Eastern Tyennan subdomain suggests that the overall sequence is thinner in what is now the easternmost part of the exposed subducted margin.

8.3 Strain gradients

Changes in strain throughout the Eastern Tyennan subdomain (Appendix 3) are recorded by:

1. Grain-scale fabrics (Boulter, 1978), preservation of bedding and sedimentary features to intensely deformed layering as isoclinally folded transposition layering. This was mapped in the Wilmot - Frankland Range transition from higher strain (north) from Mt Sprent to lower strain (southeast) to Terminal Peak (Boulter, 1978).
2. To complement this, the southernmost quartzites through The Coronets and The Sentinels are relatively undeformed.
3. A transition from long, continuous quartzite layers as ridges (tens of kilometre length scales) to dismembered, discrete, elongated augen-like "fragments" (km length scales) as seen in the Twelvetrees Range northwards to The Spires (Figure 13).

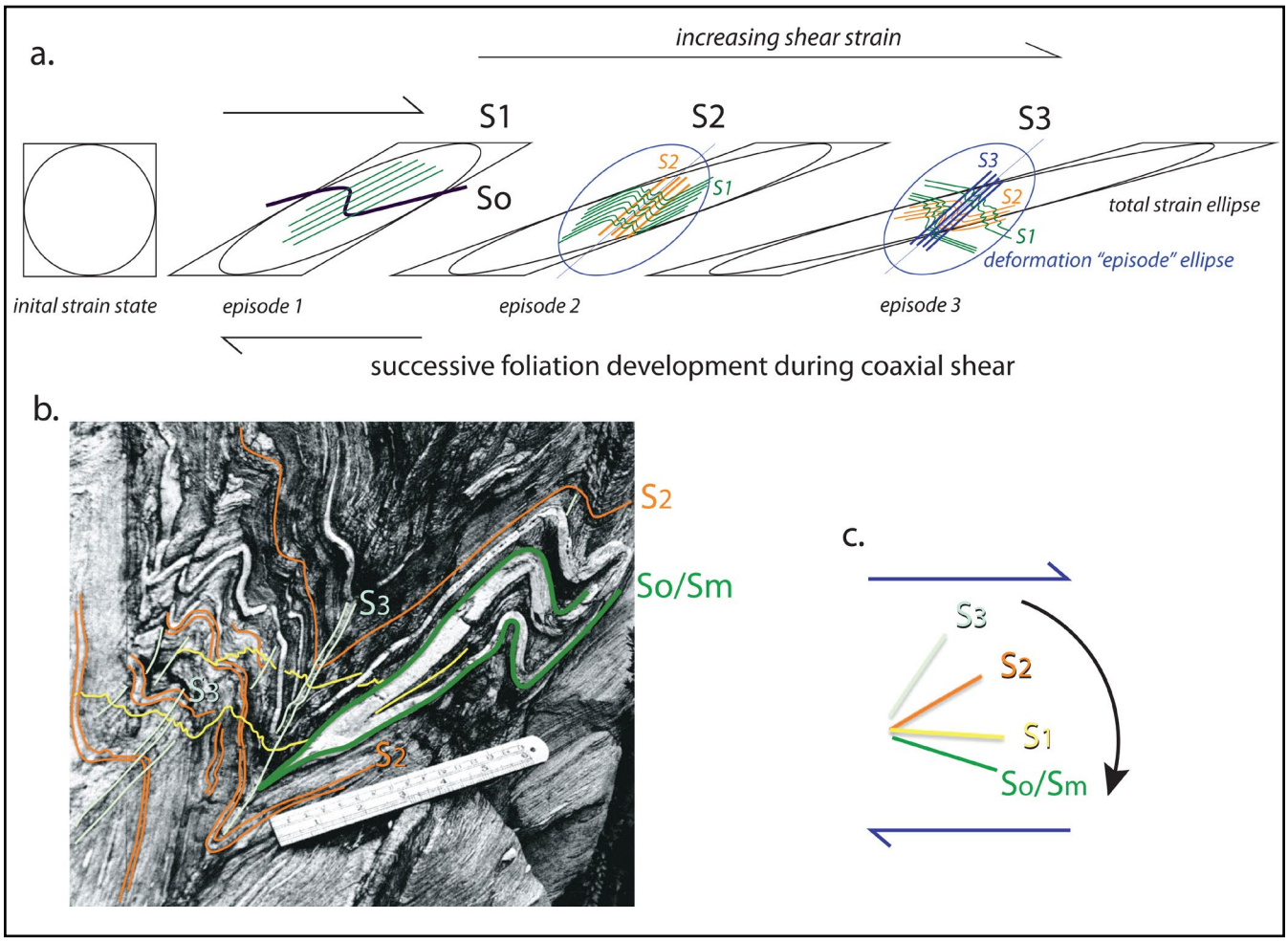

Figure 95. Successive foliation development in progressive, non-coaxial shear related deformation. a) Schematic sequence of overprinting foliation development in general or simple shear. b) Photograph of complex refolding, overprinting crenulations and foliations in Strathgordon damsite quarry outcrop (Photo credit: Clive Boulter, 1979, p.70). Successive foliations are colour-coded and annotated on the photograph. c) Cyclical development and counter-clockwise rotation sequence of the foliations determined from the outcrop relationships shown in (b).

8.4 Curvature of structural elements within the subdomain

The marked curvature of the Frankland Range is a striking element of the Eastern Tyennan subdomain (Figure 3). Assuming an original north-south strike, the bulk regional rotation is counterclockwise facilated by "bending" rotation and combined bending and fault-facilitated rotation (Figures 84 and 85). The bending rotation facilitated both the parautochthon and the Tyennan allochthon behaving as a single "unit" overlying the basement of the Rocky Cape autochthon during this process (Figure 85).

The Eastern Tyennan subdomain is part of a series of apparent rotation points that are required to explain the changes in strike orientation along the length of the belt. These rotations may be related to block movements associated with mid- to late-Cambrian rifting of the Dundas - Fossey graben system (Gray et al., 2024).

9.0 CONCLUSIONS

The Eastern Tyennan subdomain is dominated by a core, or kernel, of refolded macro-isoclinal folds that contain remnants of an interpreted H-G sheet. The high-grade units include garnet schist, amphibolite and haematitic banded ironstones (± Na amphibole). They are preserved within synformal keels in large-scale F3 folds. The structurally lower, and enclosing low-grade quartzite-pelite sequence is structurally unconformable on the calcareous phyllites and dolomite of the Scotchfire sheet (parautochthon). Over most of the Eastern Tyennan subdomain quartzites cap the ridges as klippe containing an east-vergent, isoclinal macro-isoclinal fold pair. The repeated isoclinal fold pair through the various ridgelines is part of a fold "wave train" in the lowest part of the Tyennan allochthon.

The quartzite-pelite sequence of the Eastern Tyennan subdomain appears to be structurally and lithologically contiguous with the Central Tyennan subdomain. The quartzite-pelite sequences in both subdomains are structurally unconformable with, and discordant to, the underlying Scotchfire metamorphic sheet (parautochthon). The sequences also show a marked increase in strain and foliation intensity towards the basal part of the sheet (Tyennan allochthon). The contact with the underlying Scotchfire metamorphic sheet is also commonly reactivated by younger, brittle faulting (cf. Gray and Vicary, 2021a, b). In contrast, the major part of the Southern Tyennan subdomain south of the Olga Fault has an inverted stacking sequence with the high-grade sheet at the base and a west-vergent, isoclinal macro-fold pair in the quartzite-pelite sequence (Gray and Vicary, 2023).

10.0 ACKNOWLEDGEMENTS

- Mineral Resources Tasmania (Andrew McNeill) for providing financial support and critically editing and reviewing the document.
- David Green for assistance during mapping in the Strathgordon area.
- Bushwalker photographs by Grant Dixon, David Noble, Becca Lunnon and Zane Robnik.
- Chris Large for editing and formatting this Tasmanian Geological Survey publication.
- Jason Bradbury NRE (Department of Natural Resources and Environment) for assistance with WHA and PWS permits for scientific research.
- Rick Allmendinger and Nestor Cardozzo for use of OSX Stereonet.

11.0 REFERENCES

Alsop, G. and Holdsworth, R. E. 2004. The geometry and topology of natural sheath folds: a new tool for structural analysis. *Journal of Structural Geology*, 26, 1561-1589.

Berry, R. F. 2014. Chapter 4.2 Cambrian Tectonics –The Tyennan Orogeny. In Corbett, K. D., Quilty, P.G & Calver, C. R. (Editors), Geological Evolution of Tasmania pp 95-110. *Geological Society of Tasmania Special Publication*, 24, Geological Society of Australia (Tasmania Division). 270p.

Berry, R. F. and Crawford, A. J. 1988. The tectonic significance of Cambrian allochthonous mafic-ultramafic complexes in Tasmania. *Australian Journal of Earth Sciences*, 35, 523-533.

Boulter, C. A. 1974. Structural sequence in the metamorphosed Precambrian rocks of the Frankland and Wilmot Ranges, southwestern Tasmania. *Papers and Proceedings of the Royal Society of Tasmania*, 107, 105-115.

Boulter, C. A. 1978. *The structure and metamorphic history of the Wilmot and Frankland Ranges, south-west Tasmania*. Honours Thesis, The University of Tasmania.

Boulter, C. A. 1979. Geology, In Gee, H. & Fenton, J. (Editors), *The Southwest Book— A Tasmanian Wilderness*, pp.70-75. Australian Conservation Foundation.

Boulter, C. A. 1990. Frankland Range. In: Calver et al., Pedder. *Explanatory Report Geological Survey of Tasmania*, p.14-15.

Boulter, C. A. and Råheim, A. 1974. Variation in the Si4+ content of phengites through a three stage deformation sequence. *Contributions to Mineralogy and Petrology*, 48, 57-71.

Brown, A. V., McClenaghan, M. P., Turner, N. J., Baillie, P. W., McClenaghan, J., Lennox, P. and Williams, P. R. 1982. Geological Atlas 1:50 000 series. Sheet 73 (8112N). *Huntley*. Department of Mines, Tasmania.

Brown, A. V., McClenaghan, M. P., Turner, N. J., Baillie, P. W., McClenaghan, J, and Calver, C. R., 1989. Geological Atlas 1:50,000 Series. Sheet 73 (8112N), Huntley. *Explanatory Report Geological Survey of Tasmania*, 109p.

Brown, E. H. 1977. The crossite content of Ca-amphibole as a guide to pressure of metamorphism. *Journal of Petrology*, 18, 53-72.

Calver, C. R., Turner, N. J., McClenaghan, M. P., and McClenaghan, J. 1990. Geological Atlas 1:50,000 Series. Sheet 80 (8112S), Pedder. *Explanatory Report Geological Survey of Tasmania*. 105p.

Chmielowski, R. M. 2009. The Cambrian metamorphic history of Tasmania. PhD Thesis, University of Tasmania.

Crawford, A. J., Everard, J. L., and Bottrill, R. S. 2014. Chapter 4.4 Mafic-ultramafic complexes and associated mineral deposits. In Corbett, K. D., Quilty, P.G & Calver, C. R. (Editors), Geological Evolution of Tasmania pp 95-145. *Geological Society of Tasmania Special Publication*, 24, Geological Society of Australia (Tasmania Division). 270p.

Dixon, G. 1992. Notes on the geology, geomorphology and soils of the Algonkian Rivulet - upper Maxwell River area, Tasmanian Wilderness World Heritage Area, *Papers and Proceedings of the Royal Society of Tasmania*, 126, 13-18.

Dombrovkis, P., Brown, R., Jackson, P. and Kirkpatrick, J. 1983. *Wild Rivers*. Peter Dombrovskis Pty Ltd. Tasmania.

Everard, J. L. and Calver, C. R. 2014. Chapter 4.3 Early Cambrian allochthonous and Parautochthonous Sequences. In Corbett, K. D., Quilty, P.G & Calver, C. R. (Editors), Geological Evolution of Tasmania pp 110-145. *Geological Society of Tasmania Special Publication*, 24, Geological Society of Australia (Tasmania Division). 270p.

Gray, D. R. and Vicary, M. J. 2021a. Structural Geology of Frenchmans Cap, Central Tyennan Region, Tasmania. Mineral Resources Tasmania, *Geological Survey Paper,* 6, 44.

Gray, D. R. and Vicary, M. J. 2021b. Structural Geology of the Central Tyennan Region, Tasmania. Mineral Resources Tasmania, *Geological Survey Paper*, 7, 69p.

Gray, D. R. and Vicary, M. J. 2022a. Mega-sheath fold core of the Southern Tyennan domain, Tasmania. The De Witt-Propsting and South West Cape mega-sheath folds. *Geological Survey Paper*, 10, 80p.

Gray, D. R. and Vicary, M. J. 2022b. Structural Geology of the eastern Southern Tyennan Domain, Tasmania. Mineral Resources Tasmania, *Geological Survey Paper*, 11, 43p.

Gray, D. R. and Vicary, M. J. 2023. Structural Geology of the Southern Tyennan Domain, Tasmania—An Overview, Synthesis and Structural Implications. Mineral Resources Tasmania, *Geological Survey Paper*, 13, 82p.

Gray, D. R., Vicary, M. J. and McNeill, A. W. 2022. Structure of the High-grade Coastal Belt, Southern Tyennan Domain, Tasmania. Mineral Resources Tasmania, *Geological Survey Paper*, 9, 87p

Gray, D. R., Vicary, M. J. and McNeill, A. W. 2024. The Tasmanian Tyennan Domain—a structural synthesis and review with tectonic and dynamic implications for continental margin subduction and exhumation. *Australian Journal of Earth Sciences*, 71(2), 153-210. https://doi.org/10.1080/08120099.2023.2280604.

Hall, W. D. M., McIntyre, M. I., Corbett, E. B., McGregor, P. W., Fenton, G. R, Arndt, C. D. and Bumstead, E. D. 1969. Report on Field Work in Exploration Licence 13/65, South-West Tasmania During 1967- 68 Field Season. *Tasmanian Company Report*, 69_0555.

Kiernan, K. 1995. *An Atlas of Tasmanian Karst*. Tasmanian Forest Research Council, Inc. Research Report No. 10. ISBN 0 7246 3550 5.

McClenaghan, M. P. and McClenaghan, J., Structural Geology, p. 66-79. In: Brown, A.V., McClenaghan, M.P., Turner, N.J., Baillie, P.W., McClenaghan, J, and Calver, C.R., 1989. Geological Atlas 1:50,000 Series. Sheet 73 (8112N). Huntley. *Explanatory Report Geological Survey of Tasmania*, 109p.

McNeill, A. W., 1985. *The structure and petrology of the Nye Bay area, south west Tasmania*. Honours Thesis, The University of Tasmania.

Massonne, H. J. and Schreyer, W. 1987. Phengite geobarometry based on the limiting assemblage with K-feldspar, phlogopite and quartz. *Contributions to Mineralogy and Petrology*, 96, 212-224.

Meffre, S., Berry, R. F. and Hall, M., 2000. Cambrian metamorphic complexes in Tasmania: tectonic implications. *Australian Journal of Earth Sciences*, 47, 971 – 985.

Meffre, S., Berry, R.F., Hall, M. and McNeill, A., 2001. The Structural Style of Cambrian Metamorphic Complexes in Tasmania: SW Tasmanian examples. *Geological Society of Australia Abstracts*, 64, 118-120.

Meffre, S., Green, D. and Roach, M. 2021. Unpublished field observations in the Cleft Peak – Murphys Bluff and Hermit Channel areas.

Mulder, J. A. 2013. *The Structure and Metamorphism of the Cox Bight-Red Point Area*, South West Tasmania. Honours Thesis, The University of Tasmania, 76p.

Port, I. A. 2023. *The Structural and Metamorphic History of the Eastern Tyennan Region, Lake Pedder, Tasmania*. Honours Thesis, The University of Tasmania.

Powell, C. McA. 1969. Polyphase folding in Precambrian, low-grade metamorphic rocks, Middle Gordon River, southwestern Tasmania. *Papers and Proceedings of the Royal Society of Tasmania*, 103, 47-51.

Råheim, A. 1977. Petrology of the Strathgordon area, western Tasmania: Si4+ content of phengite mica as monitor of metamorphic grade. *Journal of the Geological Society Australia*, 24, 329-338.

Ramsay, J.G. 1967. *Folding and Fracturing of Rocks*. McGraw Hill, New York, 568p.

Sampey, D. 1957. Report on Examination of Hamilton Range Area. Unpublished report for Electrolytic Zinc Company and Mt Lyell Mining and Railway Company Ltd. *Tasmania Company Report*, TCR 57_0144.

Scott, B. 1959. Precambrian of S.W. Tasmania. Unpublished report for Electrolytic Zinc Company and Mt Lyell Mining and Railway Company Ltd. *Tasmania Company Report*, TCR 59_0294.

Scott, D. 1960. Structure of South West Tasmania. Unpublished report for Electrolytic Zinc Company and Mt Lyell Mining and Railway Company Ltd. *Tasmania Company Report*, TCR 60_0319.

Spry, A.H. 1963. Precambrian rocks of Tasmania, Part V: Petrology and structure of the Frenchman's Cap area. *Papers and Proceedings of the Royal Society of Tasmania*, 97, 105-128.

Turner, N. 1989a. Precambrian. In: Burrett, C. F. and Martin, E. L. (Editors), Geology and Mineral Resources of Tasmania. *Geological Society of Australia Special Publication*, 15, 5-46.

Turner, N. 1989b. North Star Area, p. 80-87. In: Brown, A.V., McClenaghan, M.P., Turner, N.J., Baillie, P.W., McClenaghan, J, and Calver, C.R., 1989. Geological Atlas 1:50,000 Series. Sheet 73 (8112N), Huntley. *Explanatory Report Geological Survey of Tasmania*, 109p.

Turner, N. J. 1990. Jane River goldfield - rock analyses and preliminary account of investigation. Tasmania Department of Resources and Energy. Division of Mines and Mineral Resources, Unpublished Report 1990_16.

Turner, N. J., Calver, C. R., McClenaghan, M. P., McClenaghan, J., Brown, A. V., Lennox, P. G. 1985. Geological Atlas 1:50 000 series. Sheet 80 (8112S). *Pedder*. Department of Mines, Tasmania.

Velde, B. 1967. The Si+4 content of natural phengites. *Contributions to Mineralogy and Petrology*, 14, 250-258.

Wade, M. L. 1956. The Nicholls Range. Unpublished report for Electrolytic Zinc Company and Mt Lyell Mining and Railway Company Ltd. *Tasmania Company Report*, TCR 56_0126.

Williams, S. J. 1973. *Structure and metamorphism of the McPartlan Pass-Sentinels area*. Honours Thesis, The University of Tasmania.

Williams, S. J. 1976. Structure and metamorphism of the McPartlan Pass-Sentinels area. *Papers and Proceedings of the Royal Society of Tasmania*, 110, 25-34.

APPENDIX 1

The structure of the ranges of the eastern Tyennan subdomain in photographs

APPENDIX 1

The structure of the ranges of the eastern Tyennan subdomain in photographs

The ranges of the Eastern Tyennan subdomain (Figure 1) form the "backbone" of the subdomain and through their peaks provide glimpses of the regional structure. Inaccessibility and lack of mapping, limited to reconnaissance mapping, largely by mineral exploration companies has made structural interpretation difficult. The ridgelines provide the only information on the structure of these vegetated largely inaccessible parts. This Appendix presents the interpreted structural geology of the ranges of the Eastern Tyennan subdomain largely from bushwalker photographs.

Photographs taken by bushwalkers sourced from social media (Frontispiece) have enabled structural reconstructions along individual ranges and across the ranges. The annotated photos enabled construction of the regional structural relationships in areas where structural data and observations are limited or non-existent. The interpreted photographs form the basis for the maps and profiles presented in the Geological Survey Publication14.

Frontispiece: White Pyramid (1071m) along the Spires showing partial preservation of an east-closing recumbent macro-fold in thick-bedded quartzite. View is looking to the south. Taken in 1977 during traverses of the King William Range, The Spires and the Prince of Wales Range by David Noble (Photo Credit: David Noble)

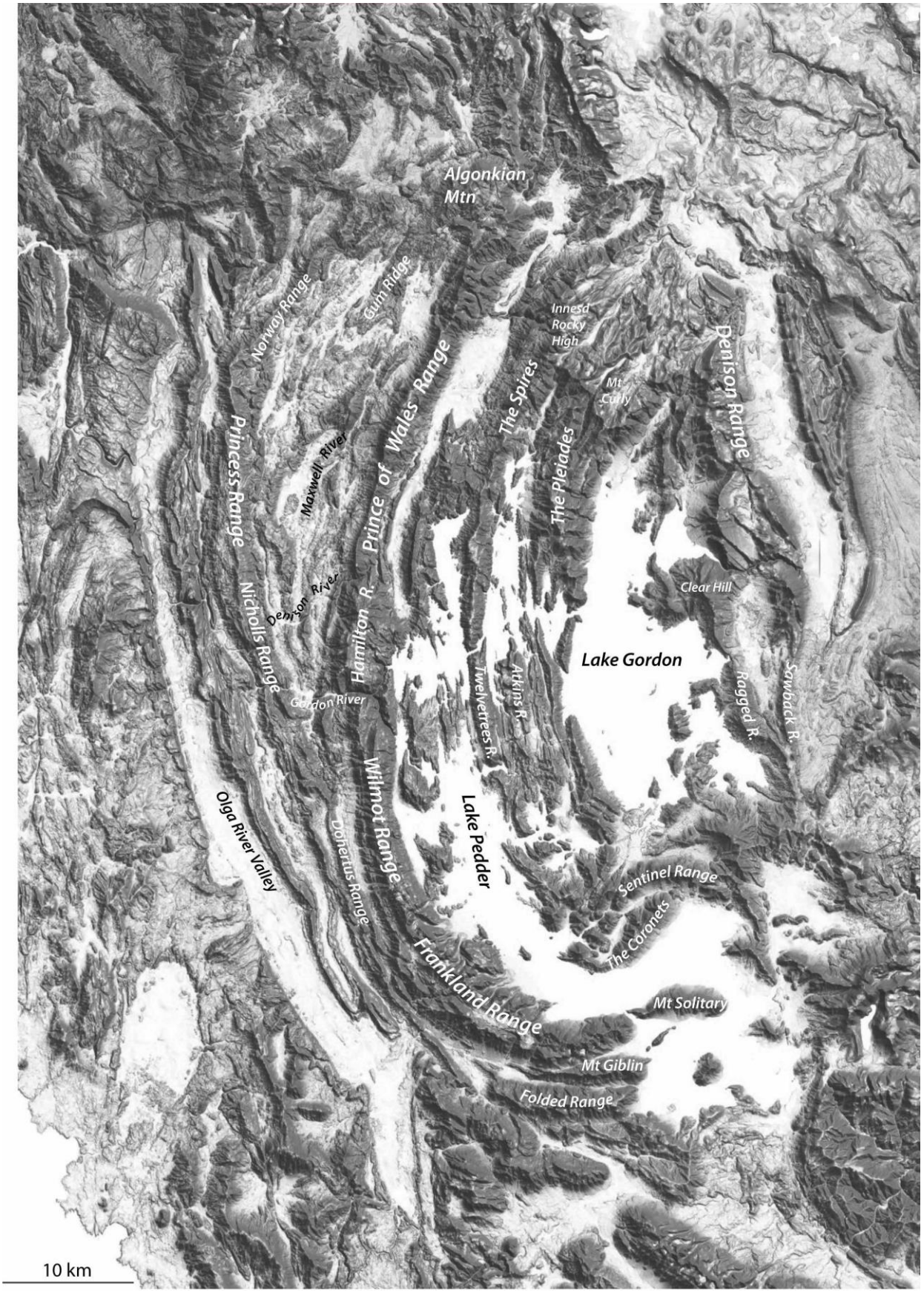

Figure 1: The ranges of the Eastern Tyennan subdomain shown on a ListMap digital elevation model.

1. The Prince of Wales Range

The Prince of Wales Range (Figures 1 and 2) is dominated by Diamond Peak (Figures 3 and 4), an un-named peak north of Humboldt (Figure 5), Mt Humboldt (Figure 6) and Olegas Bluff (Figure 7).

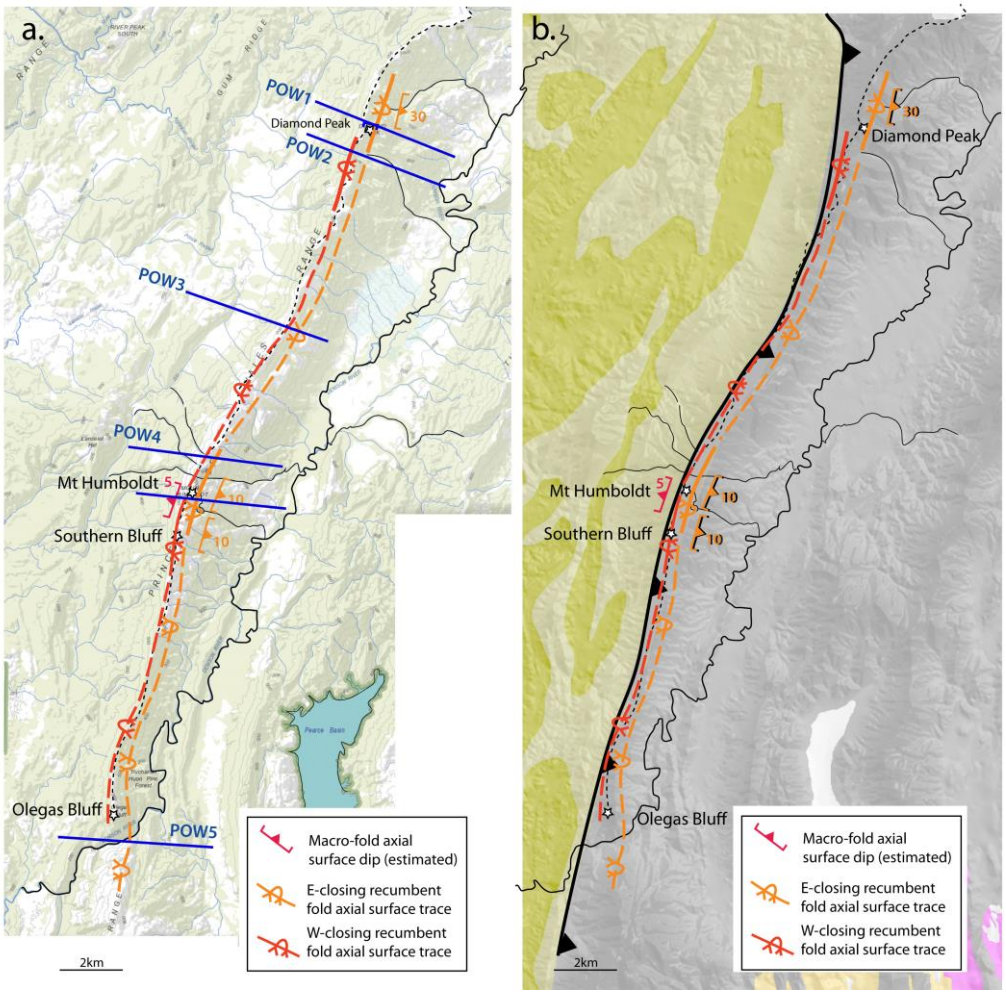

Figure 2: Positions of the photo profiles along the Prince of Wales Range. The blue lines are the positions of the photo profiles POW1 to POW5. a) ListMap topographic base. b) Lithological map base modified from the Mineral Resources Tasmania1:250,000 digital atlas.

Figure 3: Photographs of Diamond Peak (1066 m) in the northern Prince of Wales Range (POW1 profile). a) and b) distant views of Diamond Peak showing pronounced dip slopes in foliation Sm that is axial surface to the east-closing macro-fold hinge at Diamond Peak. Views are to the south. c) Close up view looking south of Diamond Peak with dashed rectangle showing the location of shear bands in (d). d) A series of down-to-the-east or west-over-east shear bands within intensely foliated transposition layering within the east-closing macro-fold hinge at Diamond Peak. (Photo credits: David Noble)

Figure 4: West-closing macro-isoclinal fold along the west side of the Prince of Wales Range sitting below the east-closing macro-fold at Diamond Peak (see Figure 6). The asymmetric folds in the foreground occur along the lower limb of the west-closing fold. View is to the north. (POW2 profile)
(Photo credit: Becca Lunnon, rockmonkeyadventures)

Figure 5: Structural interpretation of ridgeline photography approximately 1km north of Mt Humboldt. a) Oblique view of ridgeline showing an east-closing macro-fold hinge. View is looking south along the Prince of Wales Range. (POW3 profile) (Photo credit: David Noble)

Figure 6: Structural interpretation of Mt Humboldt showing the east-closing macro-fold hinge. View is looking south along the Prince of Wales Range. (POW4 profile) (Photo credit: David Noble)

Figure 7: Olegas Bluff from the northern end of the Hamilton Range with the Denison River in the valley between them. Dips in Olegas Bluff are approximately 80° east with a west-closing macro-fold hinge exposed in Southern Bluff and a partially hidden east-closing hinge in Mt Humboldt. (POW 5 profile)
(Photo credit: Grant Dixon)

The resulting profiles for the Prince of Wales Range are shown in Figure 8. They show the Range preserves a structurally highest east-closing macro-fold hinge (Profiles POW1, POW2, POW3 and POW4, Figure 8). The structurally lower west-closing hinge is seen in the ridgeline west of Diamond Peak (profile POW2, Figure 8b) and west of Mt Humboldt (profile POW5, Figure 8g).

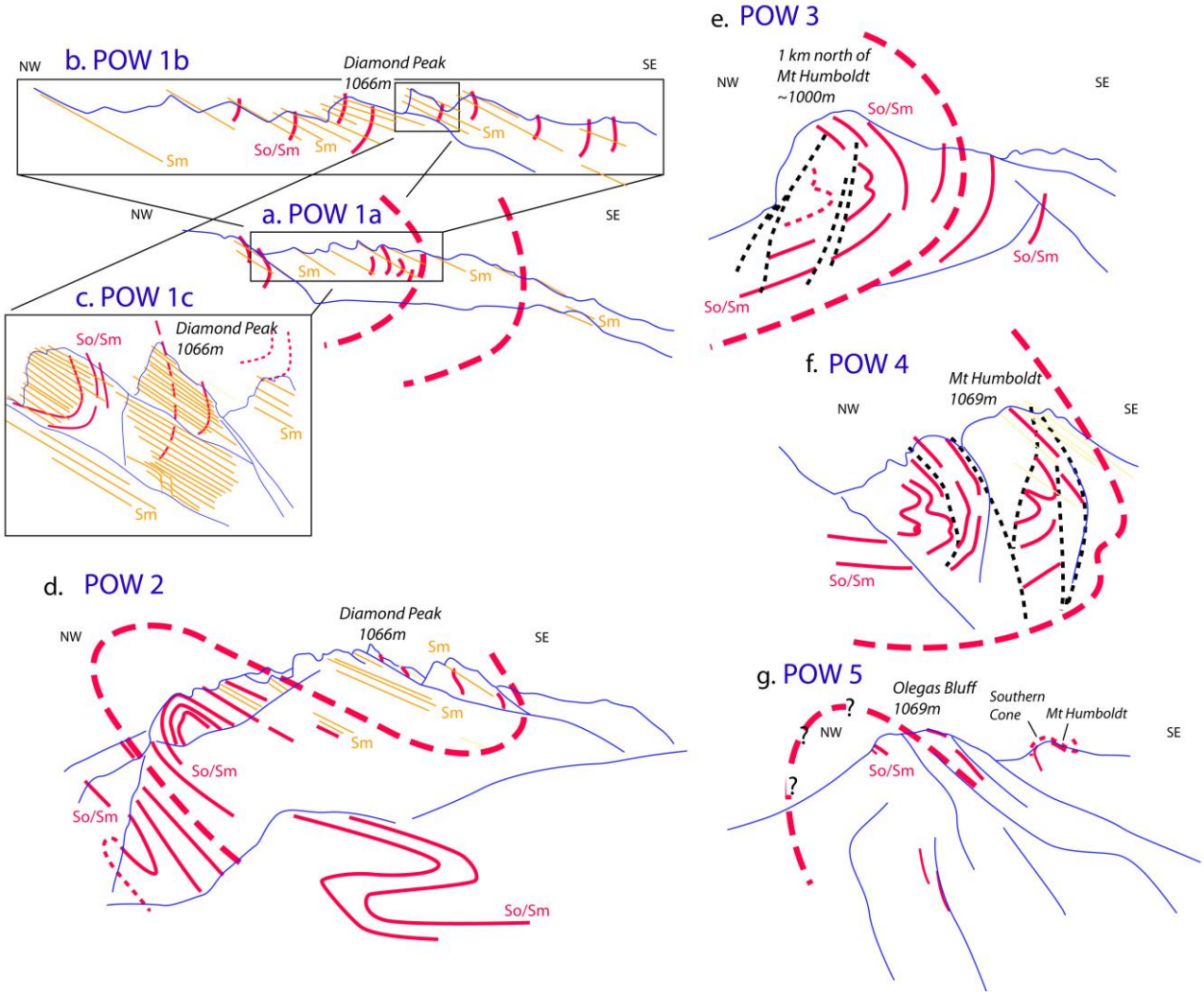

Figure 8: The photo profiles constructed along the Prince of Wales Range. Pink line traces showing the macro-fold geometry. Profiles a), b), c) and d) are at the north end of the range near Diamond Peak showing prominent east-dipping dip slopes in the foliation Sm (orange line traces). e) and f) are photo profiles near Mt. Humboldt. g) Photo profile through Olegas Bluff with Mt. Humboldt in the distance.

2. Hamilton Range

The Hamilton Range is the southern continuation of the Prince of Wales Range beyond the Denison River extending to the Gordon River (Figure 1). The positions of the Hamilton Range photo profiles are shown in Figure 9 with interpretive photo profiles in Figures 10 to 13.

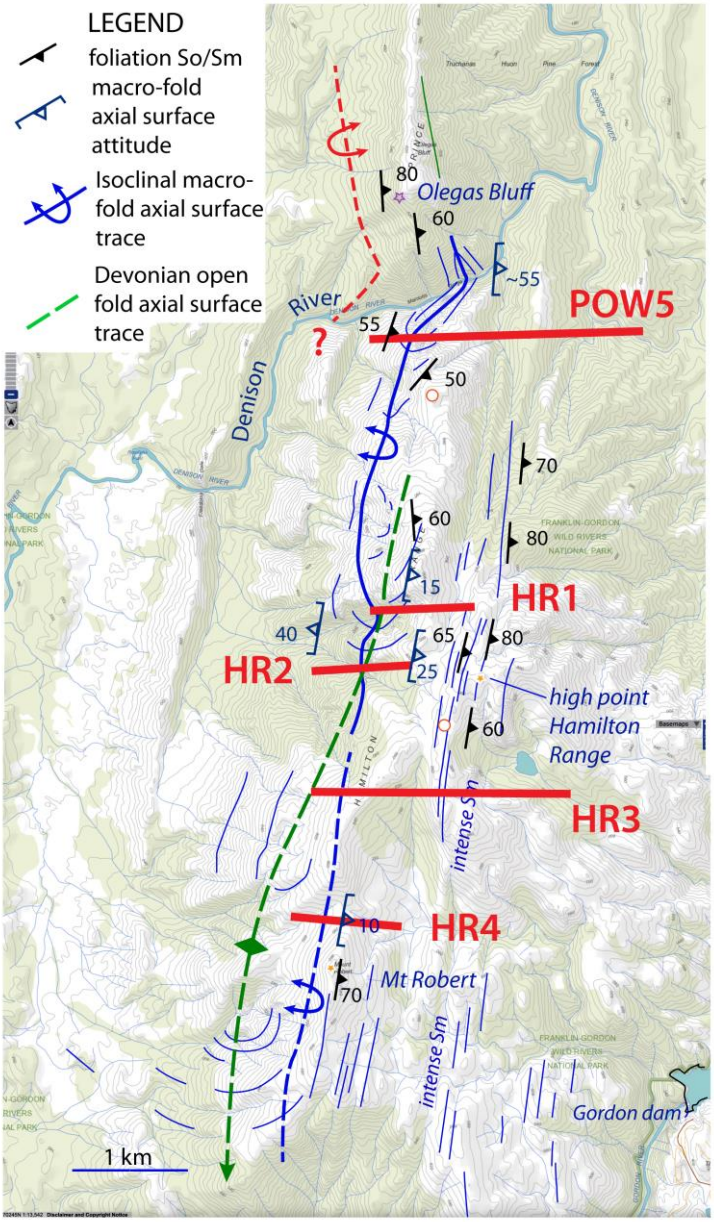

Figure 9: Photo profiles along the Hamilton Range structure map on a ListMap topographic base. The red lines are the locations of the photo profiles.

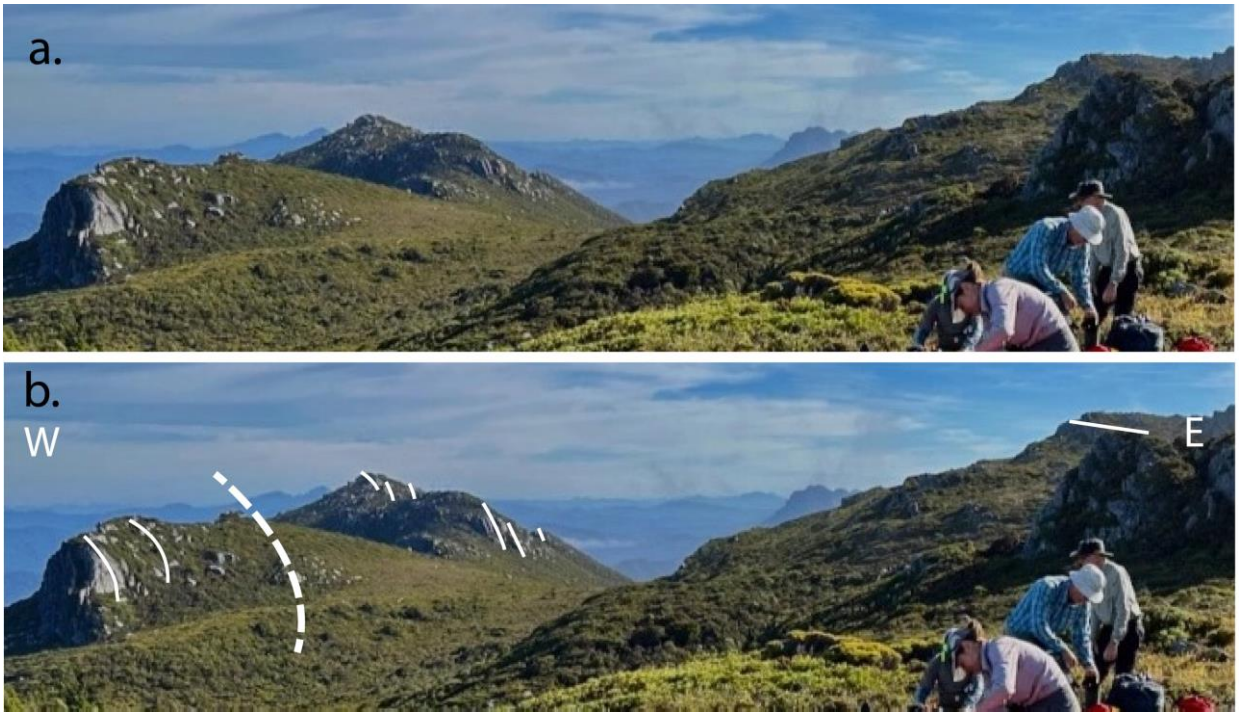

Figure 10: View to the northwest off the main Hamilton Range ridgeline showing an oblique view of an east-closing macro-isoclinal fold (profile HR1 in Figure 9). The fold hinge occupies the west flank of the Hamilton Range. (Photo credit: Becca Lunnon, rockmonkeyadventures)

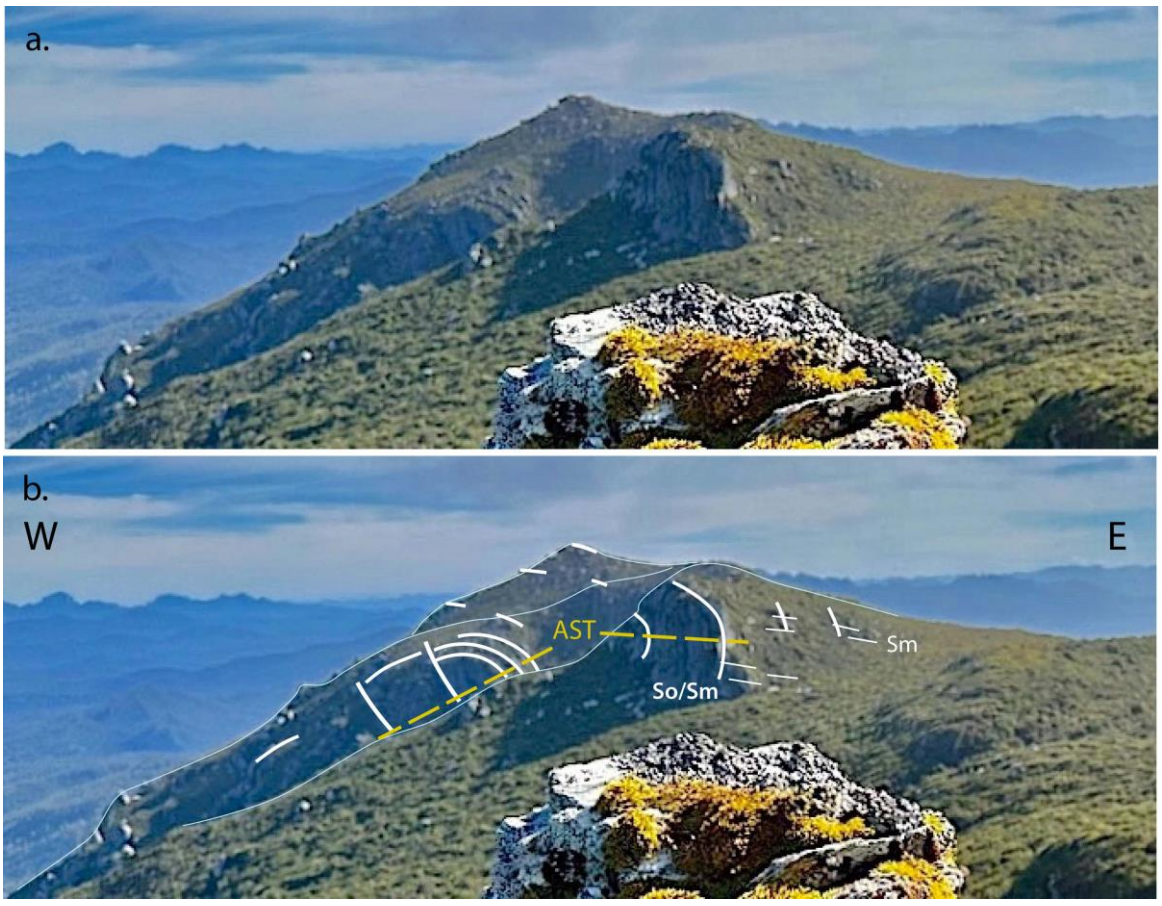

Figure 11: View to the north from the northern slope of Mt Robert showing an east-closing macro-isoclinal fold cut by steeply east-dipping reverse faults (Profile HR2 in Figure 9). The view is of the west flank of the Hamilton Range. AST: axial surface trace. (Photo credit: Becca Lunnon, rockmonkeyadventures)

Figure 12: View north along the Hamilton Range from Mt Robert. Mt Humboldt is on the distant ridgeline (photo left). The photo is an east-west profiles across the Hamilton Range (Profile HR3 in Figure 9). (Photo credit: Becca Lunnon, rockmonkeyadventures)

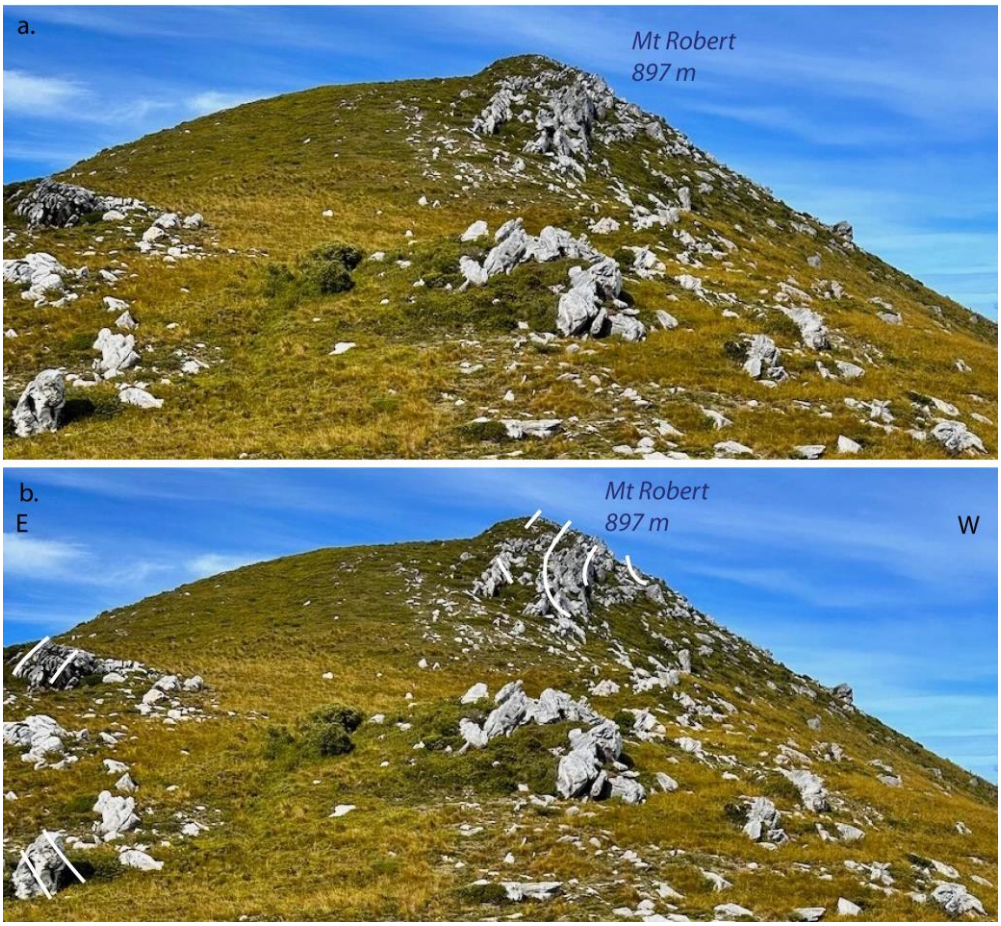

Figure 13: Photo profile of Mt Robert showing an apparent east-closing, macro-fold hinge exposed on the western flank (Profile HR4 in Figure 9). The macro-fold axial surface is dipping at ~10° east (Photo credit: Becca Lunnon, rockmonkeyadventures)

The nature of the layering folded across the east-closing, Hamilton Range macro-fold is a transposition layering dominated by Sm (yellow lines in Figure 14). It folds an early So/S1 transposition layering (white lines in Figures 14).

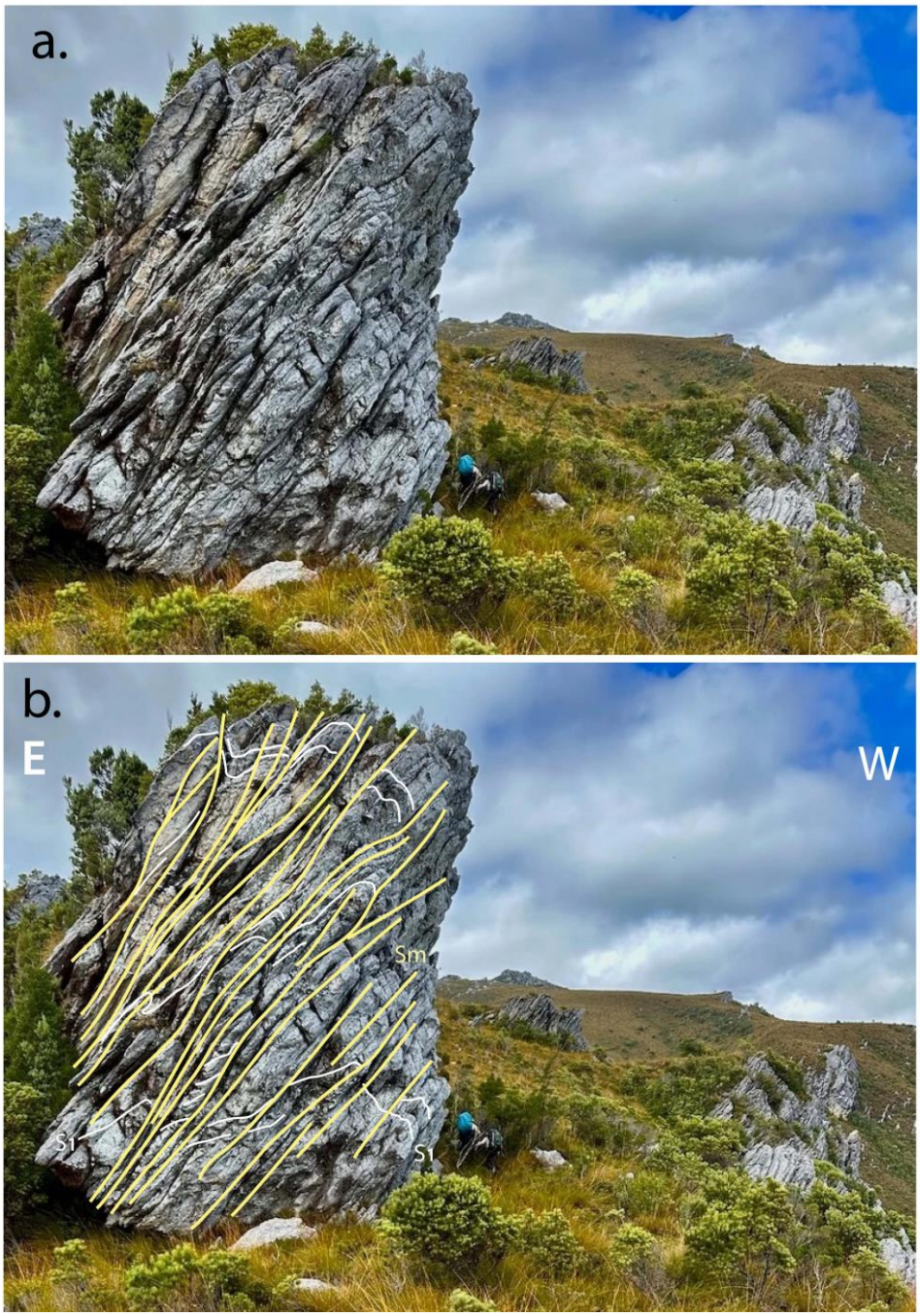

Figure 14: Large quartzite tor showing transposed layering So/S1 cut by steeply east-dipping foliation Sm (yellow traces). The view is looking south on the northern end of the Hamilton Range ridgeline above the Denison River. Bushwalkers for scale at bottom right of outcrop tor.
(Photo credit: Becca Lunnon, rockmonkeyadventures)

The zone of intense Sm that bounds the eastern side of the Hamilton Range (Figure 9) is also dominated by an east-dipping transposition foliation (Figure 15). This transposition foliation folds an earlier So/S1 fabric (Figure 15a) where incipient sheath-like, curved hinge-lines lie within the foliation Sm (see surfaces of loose blocks in Figure 15a). Both foliations are crenulated by a sub-vertical crenulation cleavage (blue line traces in Figure 15a). In places there is also a pronounced rodding fabric (Lrod/Lm) within the transposition foliation (Figure15b).

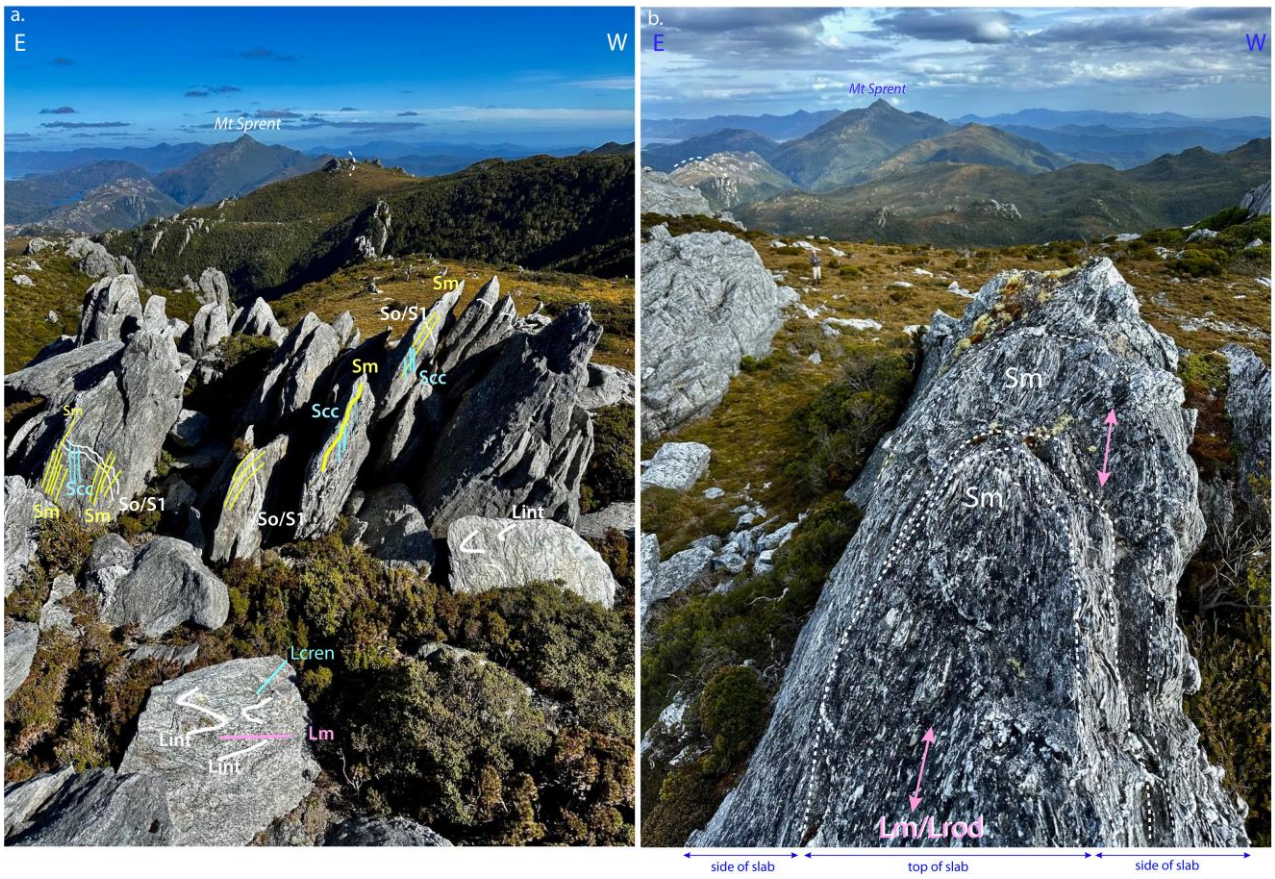

Figure 15: Views south from the highpoint on the Hamilton Range with the pointed peak of Mt Sprent on the horizon. a) Classic "shark fin" outcrop with east-dipping slabs of foliated quartzite with an intense foliation/transposition layering. The loose blocks in the foreground show flattened isoclinal folds within the Sm surface. b) Outcrop with intense rodding fabric within a flat-lying transposition layering (top of slab). The right side of the slab shows a cm scale layering that is folded within this zone of intense foliation Sm. The white dashed lines delineate the top and sides of the slab as well as foliation "steps" within the slab. (Photo credits: Becca Lunnon, rockmonkeyadventures)

The final compiled photo profiles are shown in Figure 16 with profile locations shown on Figure 9.

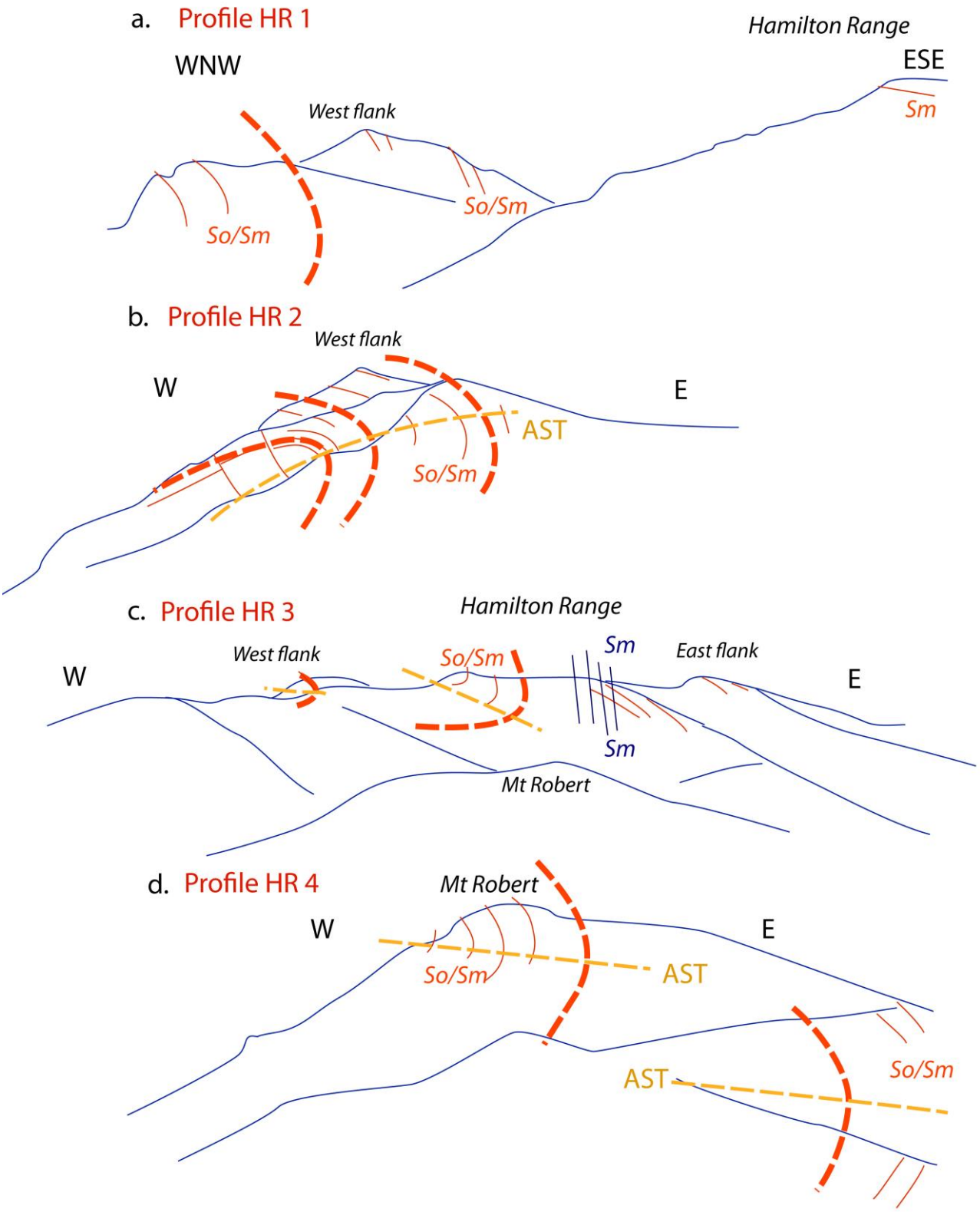

Figure 16: Photo profiles across ridgeline segments of the Hamilton Range. Arranged from north to south the photo profiles are at different scales with (c) across the entire Hamilton Range with (a), (b) and (c) more local profiles.

3. The Wilmot-Frankland Ranges

The contiguous Wilmot and Frankland Ranges (Figure 17) extend some 50 km and flank the western side of the Lake Pedder hydro-storage (Figure 1). The Frankland Range shows a marked curvature with a strike swing from north-south to east-west at the termination near Terminal Peak and Mt Solitary.

Figure 17: Aerial view to the northwest of the glacially dissected Frankland Range (photo centre) and Companion Range (photo left). Lake Pedder storage is on the upper right. Both range ridgelines are occupied by west-closing, isoclinal macro-fold hinges within quartzite, with a possible reverse fault and/or syncline occupying the intervening valley between them. The white unit along the eastern side of the Frankland Range is micaceous quartzite. (Photo credit: Wandering Foxbat)

3.1 *Background*

In the early 1970's Boulter (1974, 1978) undertook structural mapping through the Gordon and Serpentine dam sites, the Wilmot and Frankland Ranges (Figures 18 and 19). This work involved detailed structural analysis at the outcrop scale, microstructural fabric investigation and strain analysis in the quartzite utilising quartz grain shape analysis after Elliott (1970) and deformation of clastic dykes. Boulter (1978, p.34) established five deformation phases that were heterogeneous in development "not just from lithology to another but within the same rock type". Boulter (1974, 1978) argued that the largest structures were D1 isoclinal macro-folds and more open D4 folds that refolded the early isoclines (Figure 19). Plunges of the major folds are low and generally <20° (Figure 20). This has important implications for profile construction.

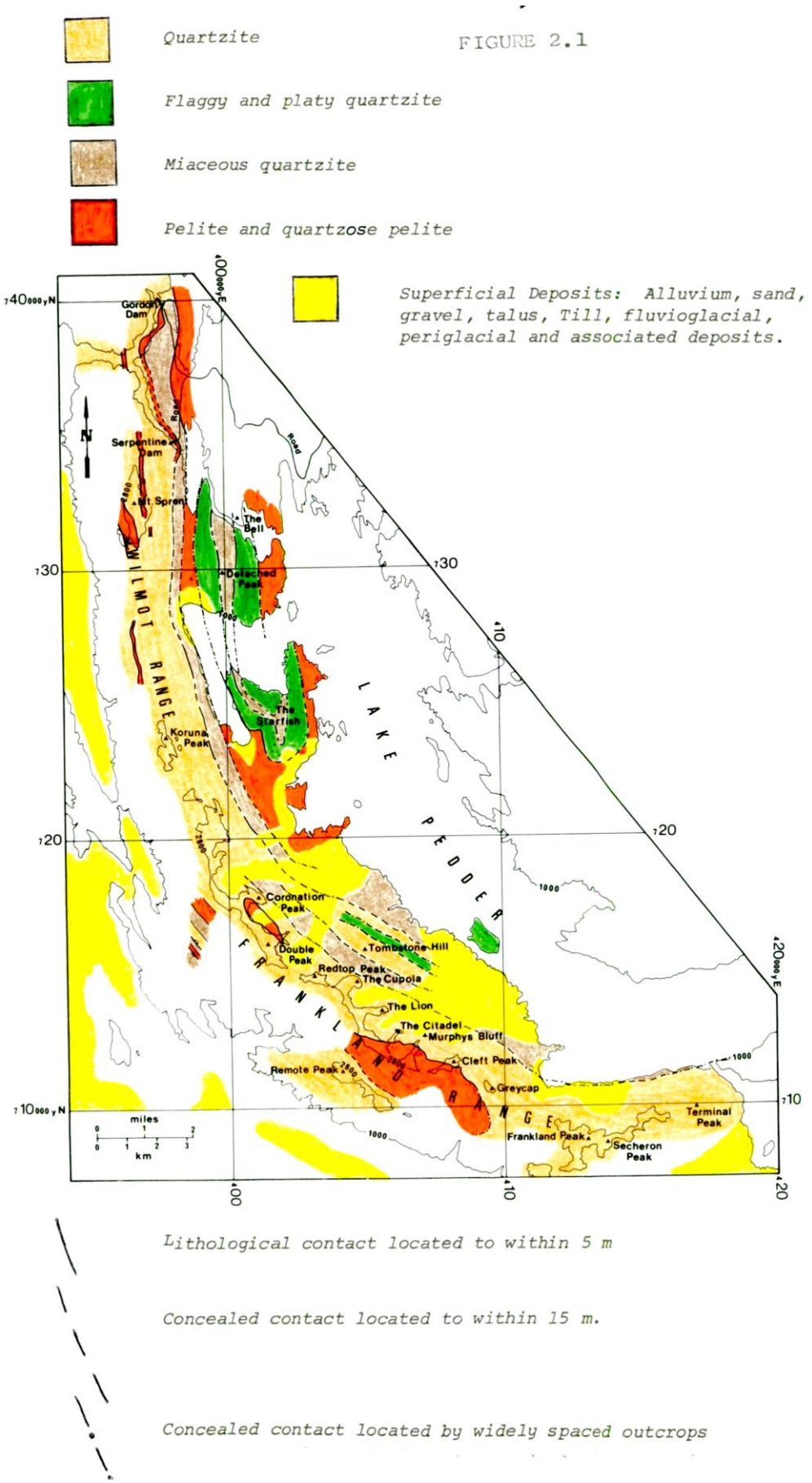

Figure 18: Lithological map of the Wilmot-Frankland Range (Boulter, 1978, fig. 2.1).

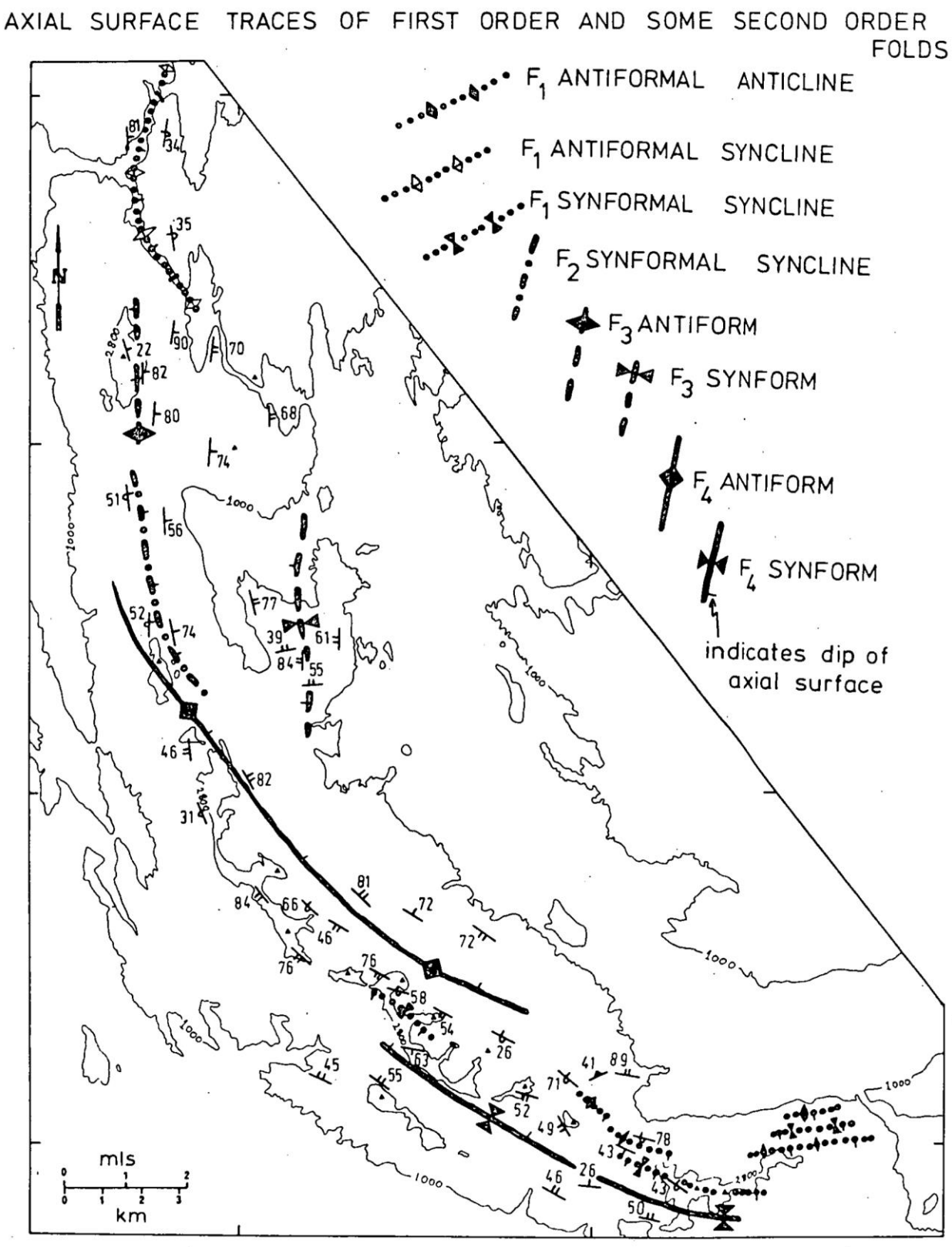

Figure 19: Axial surface trace map of regional scale folds along the Wilmot-Frankland Range (Boulter, 1978, fig. 4.48).

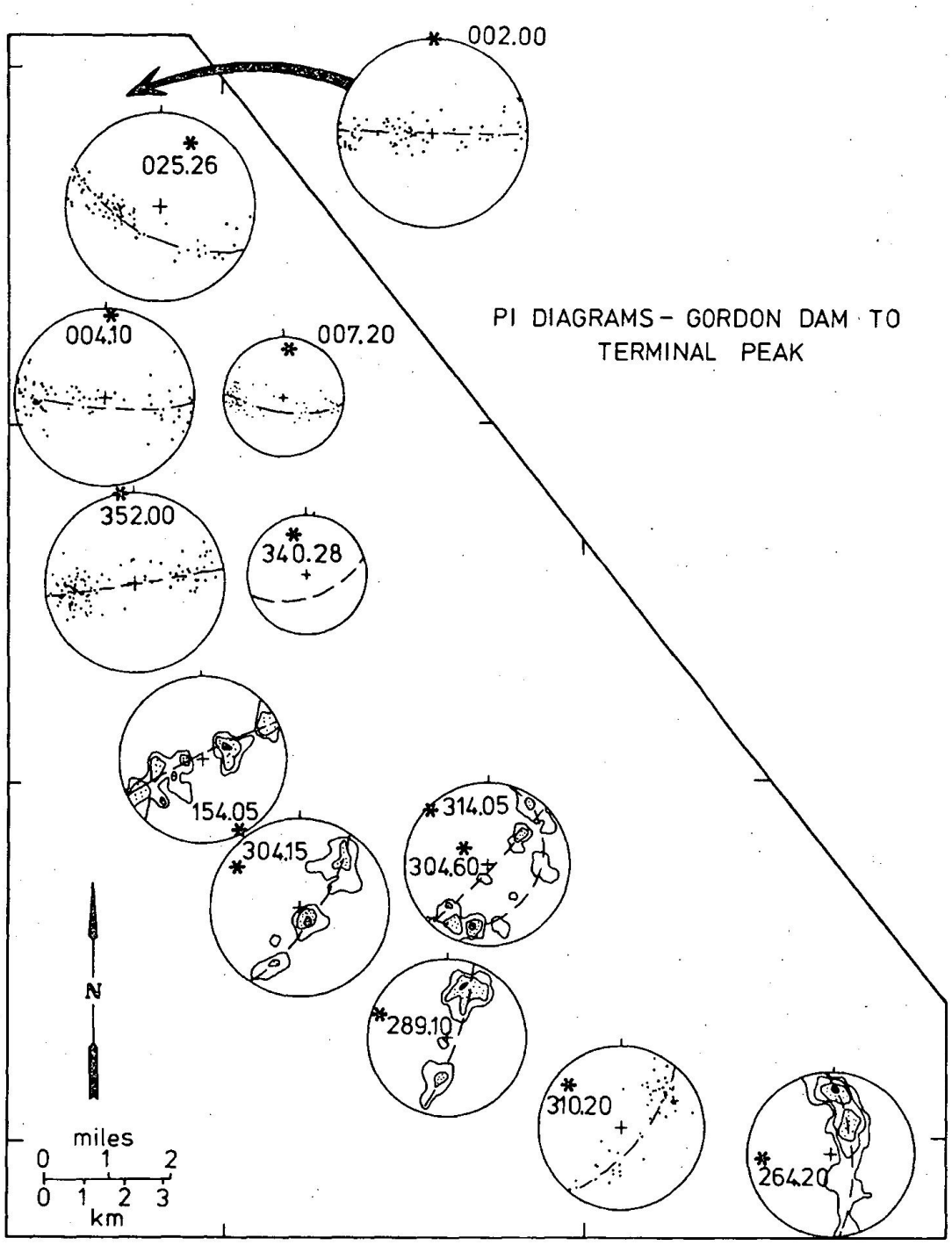

Figure 20: Stereonet π diagrams for great circle fits to poles to compositional banding So/Sm at different segments of the Wilmot-Frankland Range (Boulter, 1978, fig. 4.47). The stars denote the fold axis plunge with plunge direction/plunge shown.

3.2 *Macroscopic Regional Folds and Geometry*

Geometrically complex at the outcrop scale (Boulter, 1974, 1978) a relatively simple macrostructure defines the structure of the ranges. As in other parts of the Eastern Tyennan subdomain the macrostructure consists of an asymmetric, east-vergent fold pair in quartzite that is variably exposed along the range (Figures 21 and 22). Outcrops in the northern part of the range, from Mt Sprent to Greycap, are dominated by the west-closing macro-fold with the upper, east-closing macro-fold eroded and no longer preserved along the western side of the range (Figure 21). The fold pair is only preserved in the southeastern part of the Frankland

Range from Frankland Saddle to Terminal Peak (Figure 21). Belts or domains of overturned and right-way-up bedding have helped to define the macro-fold limb versus hinge positions. Limitations in exposure however, provide a patchy data distribution that has made macro-fold recognition as well as macro-fold axial surface trace definition problematical. The macro-fold recognition, their positions and axial surface trace delineation (Figure 21) have largely been done by formline analysis of outcrops in bushwalker photographs taken at various positions through the range ridgelines (Figures 22 and 23). This was enabled by construction of a series of photo profiles (Figures 24, 25, 27, 28, 29, 31, 32, 33, 34, 35 and 36) where the axial trace position was joined from photo profile to adjacent profiles to create the axial surface trace map (Figure 21).

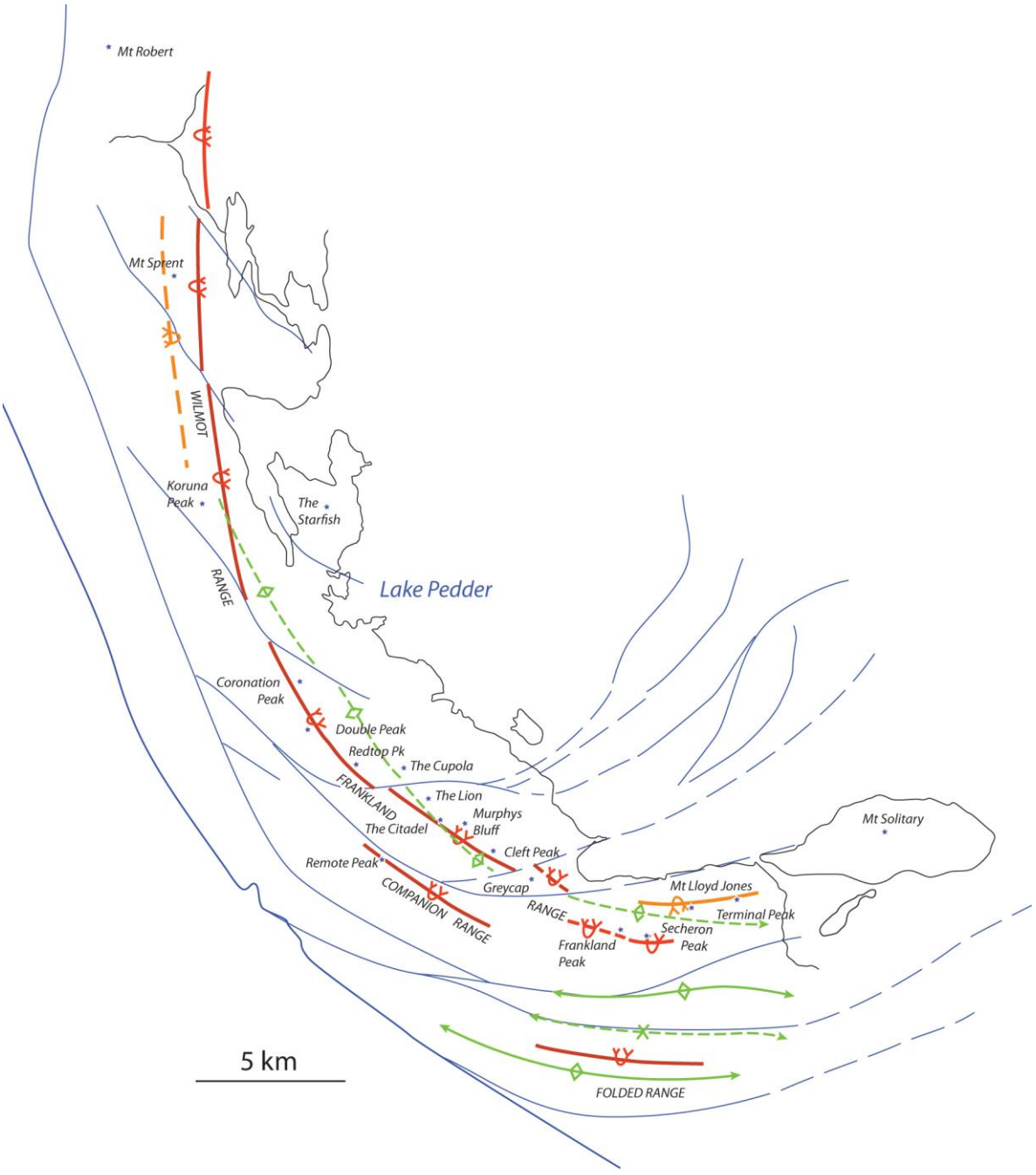

Figure 21: Axial surface trace map of the Wilmot-Frankland Ranges based on photo profiles (see Figures 23 to 36). Red line traces: west-closing recumbent isoclinal macro-fold axial surface trace. Orange line traces: west-closing recumbent isoclinal macro-fold axial surface trace. Green line traces: younger syncline and anticline axial surface traces. Blue line traces: fault outcrop traces.

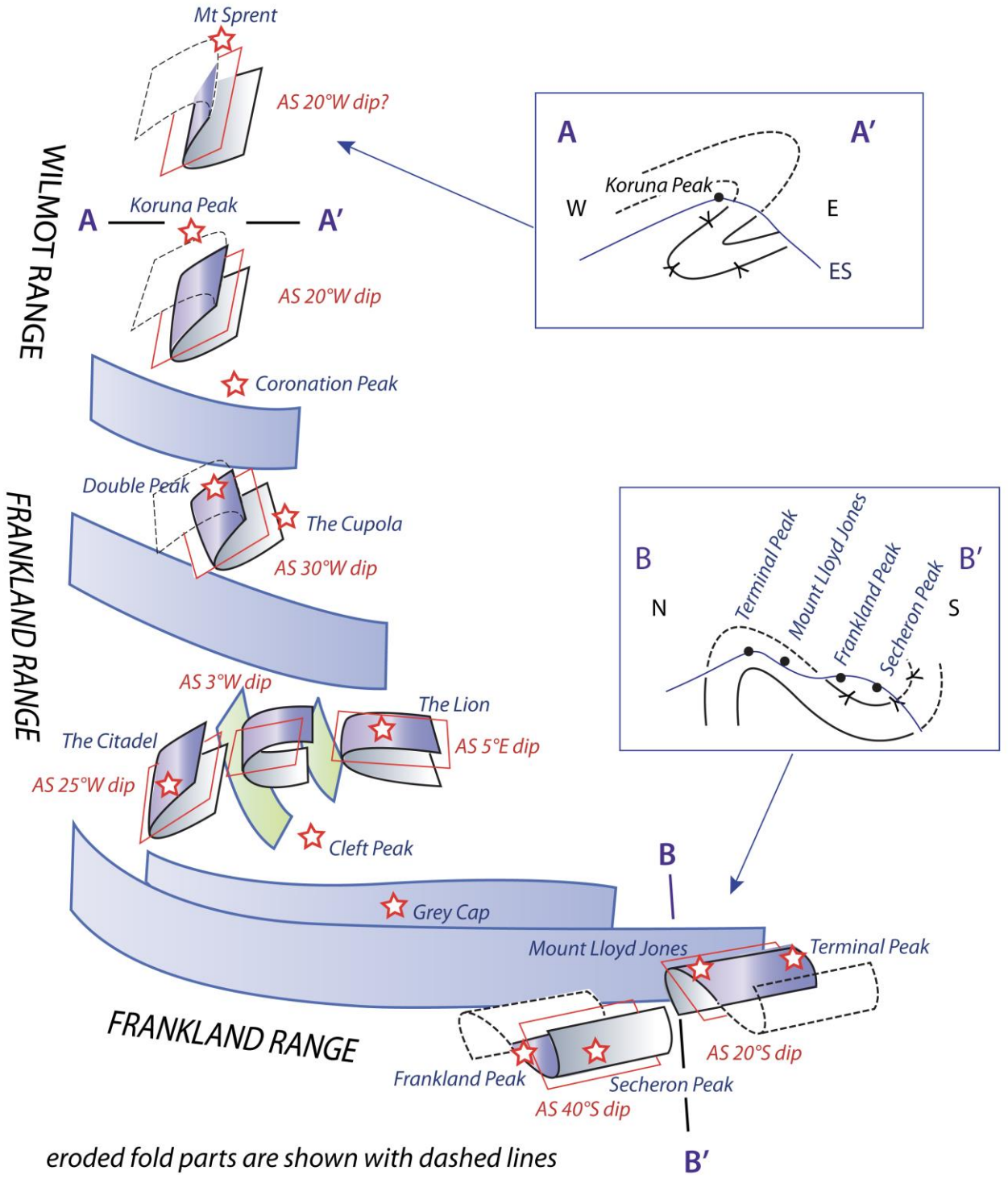

Figure 22: 3D macro-fold geometry diagram of the Wilmot- Frankland Ranges. The diagram shows the varying fold attitude changes of the asymmetric, isoclinal macro fold pair along the length of the range ridgeline. This is highlighted by the changes in axial surface dip and the swing in orientation from north-south trending to east-west trending along the range. The grey surfaces represent the curved sub-vertical faults that offset the macro-fold pair particularly in the southern part of the range.
Section A-A' across the Wilmot Range near Mt Sprent shows the dominant, west-closing, recumbent macro-fold with a inferred eroded complementary east-closing macro-fold.
Section B-B' is a composite profile with outcrop relations at Mount Lloyd Jones and Terminal Peak projected onto a plane through Frankland Peak and Secheron Peak. The profile shows the asymmetric fold pair with axial surfaces dipping to the south.

3.3 *Wilmot-Frankland Range Photo Profiles*

Nine photo profiles are shown for the Wilmot-Frankland Ranges (Figure 23). These include photo profiles for the Wilmot and northern Frankland Ranges (Figures 24, 25 and 27) and photo profiles for the southern Frankland Range (Figures 28, 29, 31, 32, 33, 34, 35 and 36). The profiles show the Wilmot-northern Frankland ridgeline is dominated by a west-closing, isoclinal, recumbent, macro-fold hinge (Figure 39). This hinge is cut by several high angle reverse faults (Figures 28, 29 and 39). A younger Devonian cleavage overprints the folded layering (green line traces in Figures 24b and 39a,c). The macro-fold hinge, as shown by the orange axial surface trace, is folded by a younger anticline with the dip of the axial surface changing along the range (Figure 39).

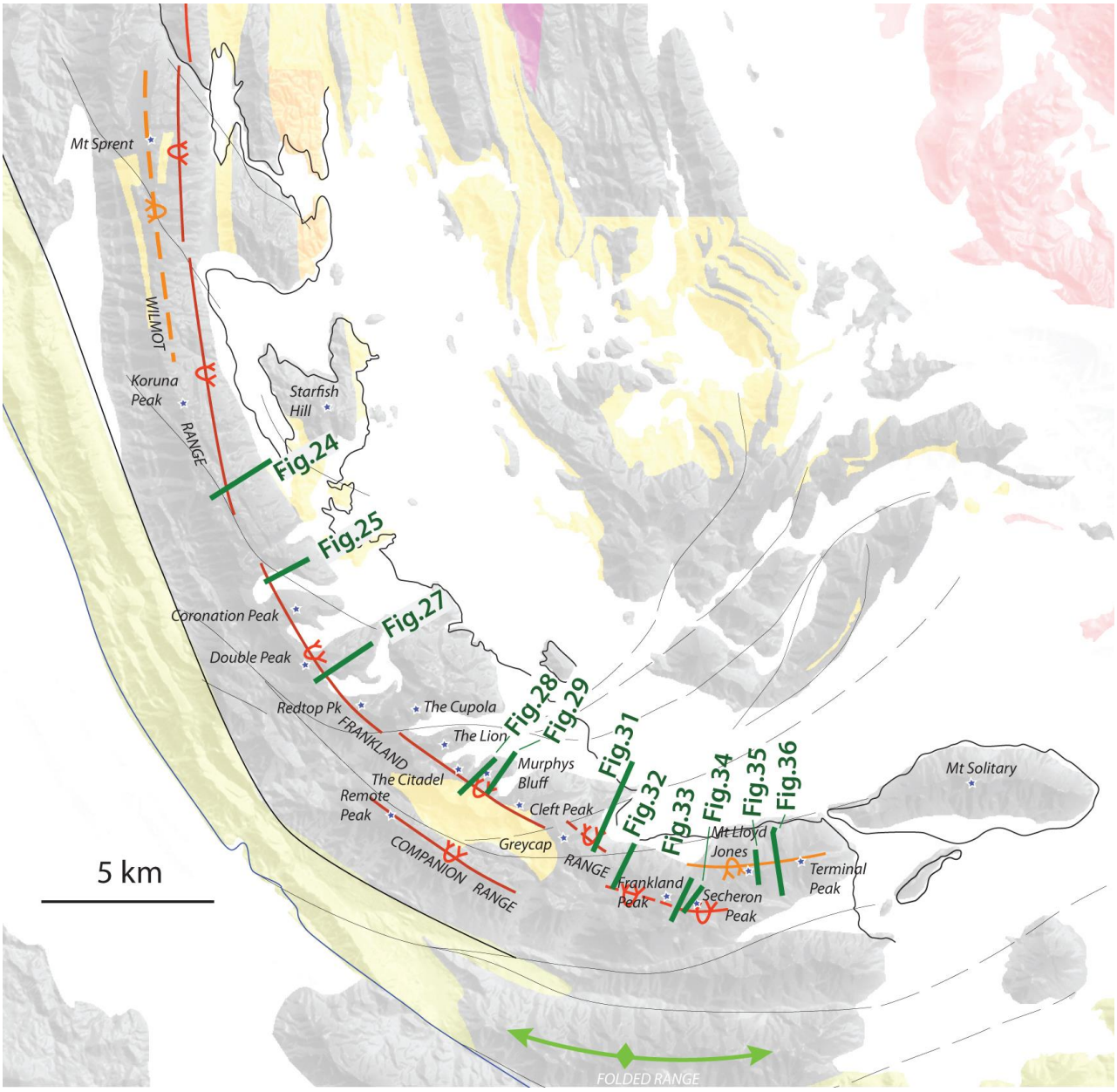

Figure 23: Axial surface trace map of macro isoclinal folds along the Wilmot and Frankland Ranges showing the photo profiles (PP) used in their construction. Photo profile locations are shown by the thick green line traces. The positions of the axial surface traces are based on formline interpretation from the individual photo profiles. The orange line shows the axial surface trace of the structurally higher, east-closing macro-fold. The red line trace is the axial surface trace of the west-closing macro-fold that dominates the range.

Figures 24 through 36 provide the basis for the interpretation presented in Figures 39 and 40. They consist of both annotated and non-annotated versions of a series of bushwalker photographs taken along the range (Figure 23 for locations). Between Koruna Peak and north of Coronation Peak the macro-fold is discernable along the east side of the southern Wilmot Range with eroded gullies defining the positions of high angle reverse faults (Figure 24). The structurally higher, east-closing hinge is eroded through this part of the range (see interpretation in Figure 22). The photograph north of Coronation Peak (Figure 25) shows the hinge within Coronation peak and highlights the complexity of the So/Sm layering that is folded around the macro-fold hinge (Figures 25b and 26).

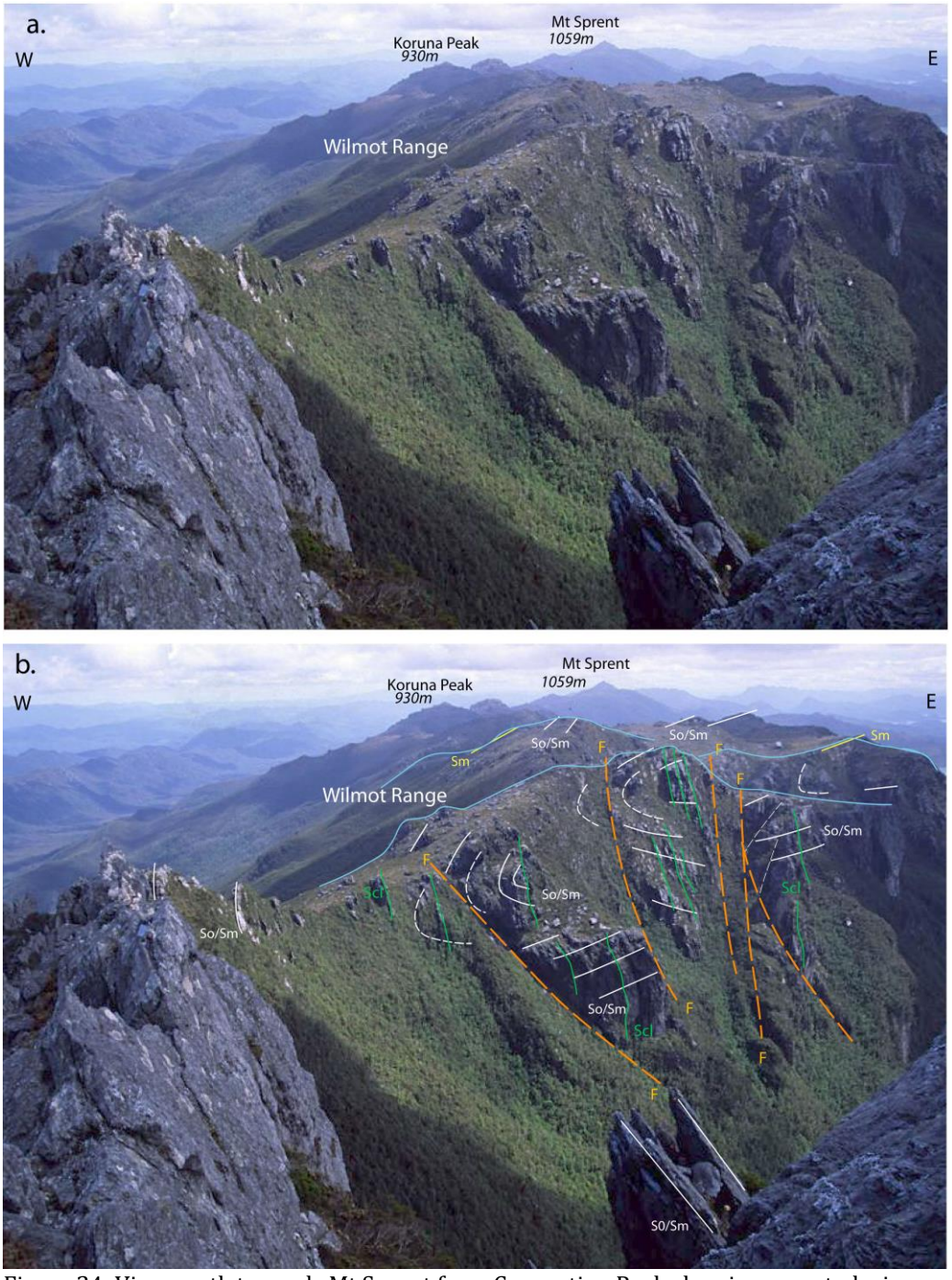

Figure 24: View north towards Mt Sprent from Coronation Peak showing a west-closing macro-isocline cut by east-dipping reverse faults within the ridgeline east of Koruna Peak. Photo profile PP1. White lines: bedding So/Sm traces. Orange dashed lines: high angle reverse faults. Green line traces: sub-vertical, younger overprinting cleavage. (Photo Credit: David Noble)

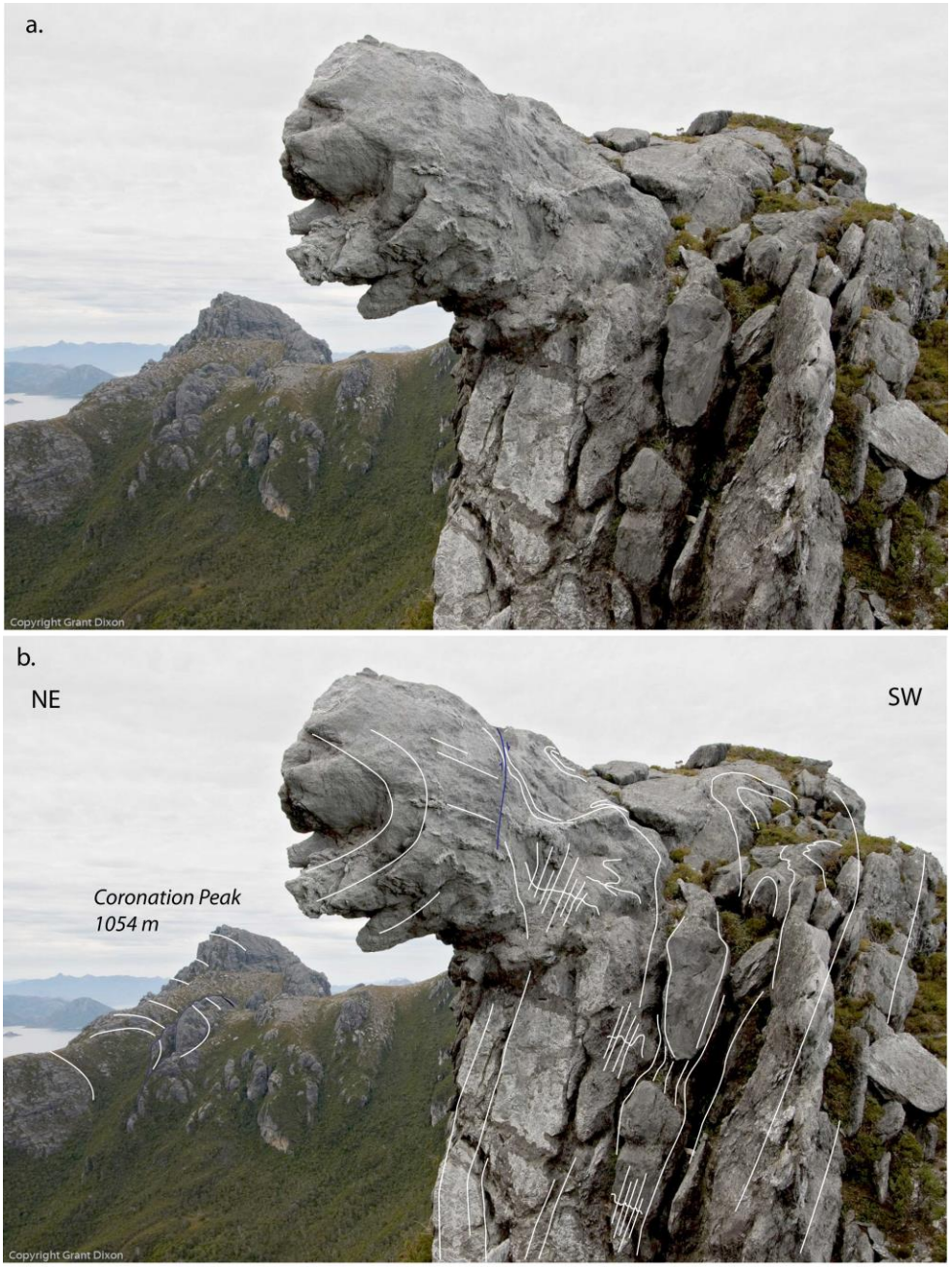

Figure 25: Coronation Peak macro-fold in the background (photo left) showing a west-closing form within So/Sm (Photo profile PP2). The sculptured-outcrop in the foreground shows the partial macro-fold hinge along strike, as well as an early isocline (F1) within the compositional layering So/Sm, and an overprinting, steeply east-dipping crenulation cleavage. The photo is looking south. (Photo credit: Grant Dixon)

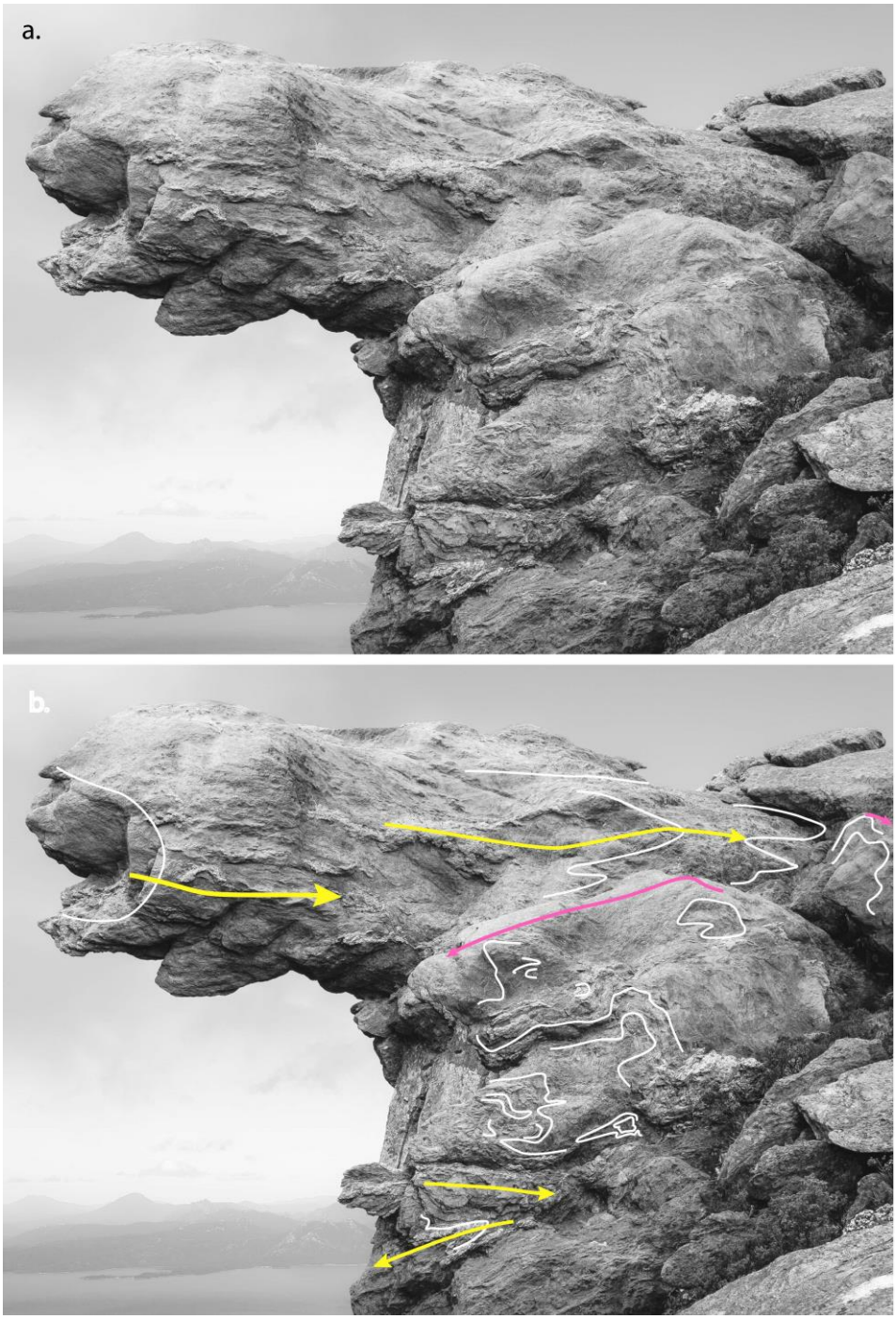

Figure 26: Small recumbent macro-isoclinal fold hinge (photo top) north of Coronation Peak coaxially refolded by tight, upright folds (purple hinge lines)(Photo Credit: Patrick Toohey). The So/Sm formlines (white line traces) on the northern flank of the small open antiformal fold (photo right centre) shows fold interference patterns in Sm between the early mesoscopic isoclines and the upright fold set.

An aerial view of the glacially eroded northern Frankland Range ridgeline from Coronation Peak to Double Peak (Figure 27) provides serial sections through the macro-fold hinge. The axial surface foliation Sm (yellow line traces, Figure 27b) are all west dipping through this part of the range.

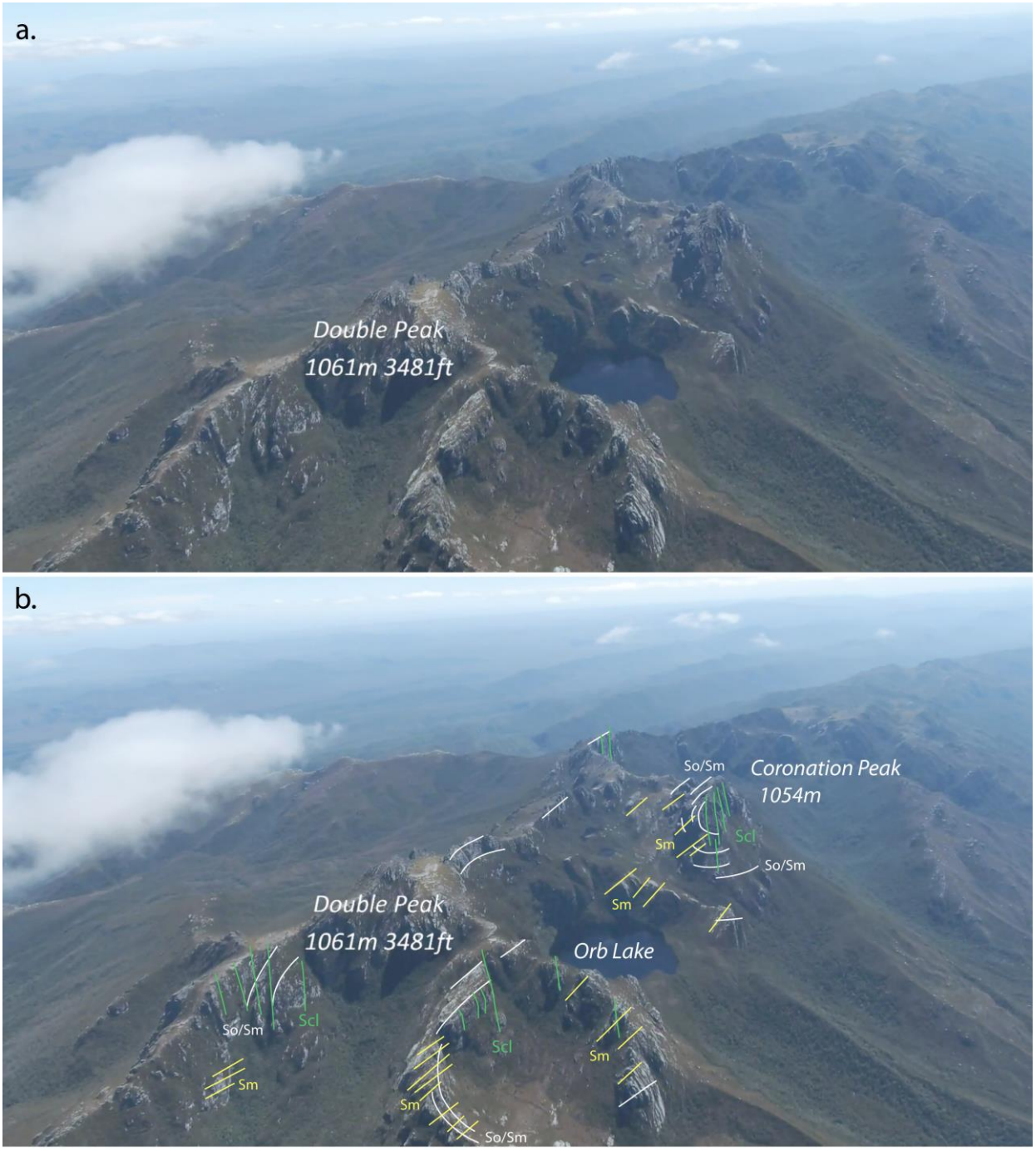

Figure 27: Aerial view looking northwards along the Frankland Range showing serial ridge sections between Coronation Peak and Double Peak at the junction between the Wilmot Range and the Frankland Range. a) Non-annotated photograph (Photo Credit: Wandering Foxbat Video). b) Structural interpretation showing the ridgeline dominated by a west-closing and westerly inclined, synformal macro-isoclinal fold. The fold axial surface trace sits on the east side of each peak and passes through Orb Lake. So/Sm: white line traces. Sm: yellow line traces. Devonian cleavage: green line traces. Photo profile PP3. (Photo credit: Wandering Foxbat)

The Frankland Range centred around The Citadel, The Lion, Murphys Bluff and Cleft Peak show sections of the southwest-closing hinge cut by steeply east-dipping reverse faults (Figures 28 and 29). The Citadel exposure (Figure 28) and the central part of Murphys Bluff exposure (Figure 29) are at the hinge of the open anticline. Both exposures show a sub-horizontal axial surface in the core of younger anticline.

The Boulter (1978, fig. 4.32) profile (Figure 30) supports the west-closing macro-fold interpretation. It is based on detailed structural mapping from Coronation Peak to Cleft Peak

and utilises a plunge projection for each of the different ridgeline segments based on the structural data collected (Figure 20). β and/or π stereographic net determinations were 15°/304° for Coronation Peak to Double Peak, and 10°/289° for The Lion, The Citadel and Murphys Bluff segment (Figure 20). It shows the southwest closing, recumbent macro-fold closure with southwest dipping axial surface, but each ridgeline segment is stacked despite the consistent gentle plunge (<20°) of the fold structures along the range. The photo profiles provide individual serial sections across the recumbent macro-fold whereas the plunge profile of Boulter shows "stacking" of these ridgeline profile segments.

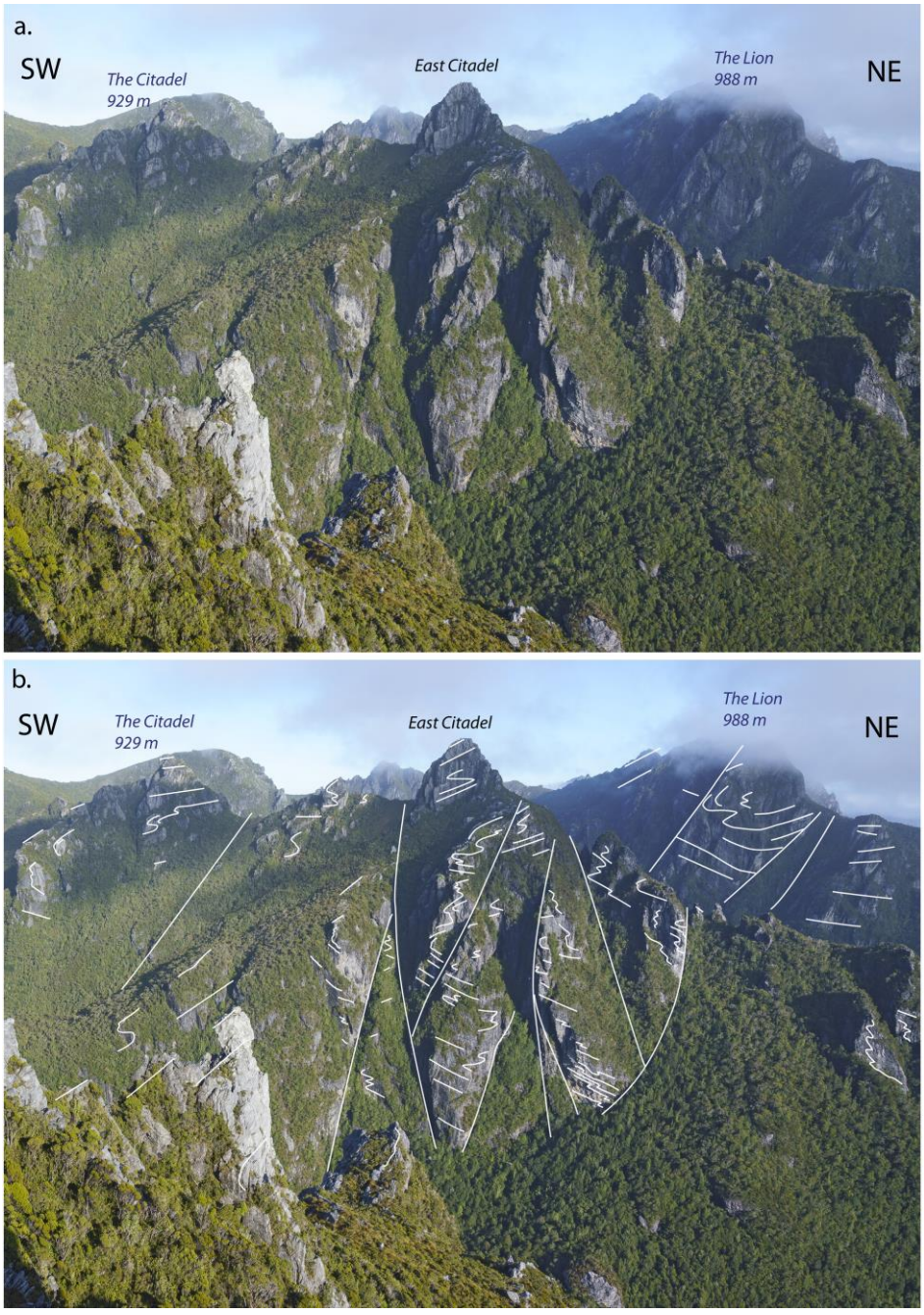

Figure 28: Photograph of the southern face of The Citadel ridgeline with The Lion shrouded in cloud as part of the next ridge (photo right). Formlines in So/Sm (thicker white lines) depict a profile through a southwest-closing recumbent macro-fold, cut and offset by a series of steeply dipping reverse faults (fine white line traces). Photo profile PP4. (Photo credit: Grant Dixon)

Figure 29: Murphys Bluff view looking northwest from Cleft Peak showing the southwest-closing, recumbent macro-isoclinal fold hinge cut by a series of reverse faults. Photo profile PP5. (Photo Credit: David Green).

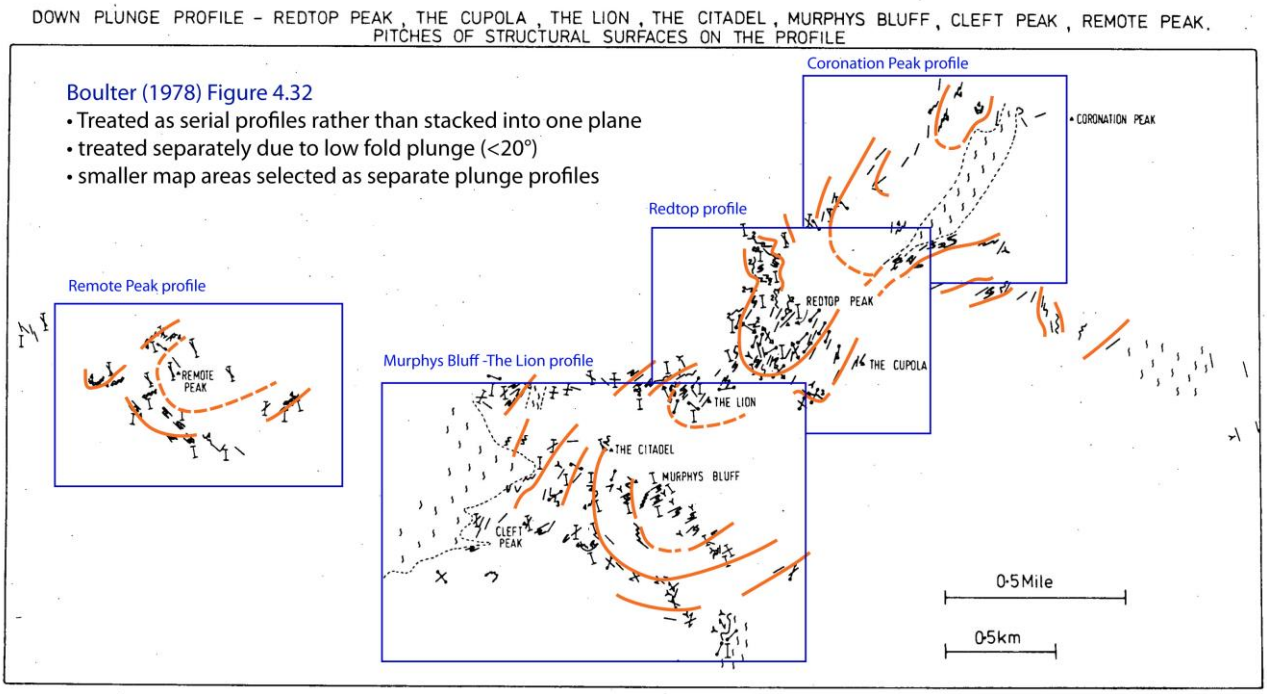

Figure 30: Boulter (1978, fig.4.32) down plunge profile from map projection from Coronation Peak to Cleft Peak including Remote Peak. The red formlines are an interpretation based on Boulter's figure utilising So traces on the projection plane.

The southern part of the Frankland Range shows a dramatic strike swing from north-south to east-west trending, as well as offsets from the curved oblique-slip fault system (Figures 18, 19 and 21). The hingelines of the recumbent macro-fold pair and the younger anticline are offset with combined apparent sinistral and hanging-wall-up, east-over-west movement sense (Figure 21). Maximum throw along the fault through Greycap trending along the southern shoreline of Lake Pedder is suggested by 1) an apparent dextral offset of the macro-fold pair at Cleft Peak/Greycap and 2) the presence of the east-closing recumbent fold along the north side of the ridgeline from Frankland saddle to Terminal Peak. This produces a complex geometry along the range (see Figure 22).

Due to the strike swing of the southern Frankland Range the west-over-east, Z-vergent asymmetric macro-fold pair now show a south-over north shear sense (Figure 22). The structurally east-closing macro-fold is now north-closing and is preserved through Mount Lloyd Jones and Terminal Peak (Figures 31, 35 and 36). The complementary original west-closing fold hinge that dominates the Wilmot Range and northern Frankland Range is now south closing and preserved in Frankland saddle, Frankland and Secheron Peaks (Figures 32, 33 and 34).

The Boulter (1978, fig. 4.34) "plunge" profile from Greycap to Terminal Peak including Frankland Peak defines the macro-fold pair, but his "stacked" profile shows the major south-closing macro-fold through Frankland Peak structurally higher than the major north-closing macro-fold through Terminal Peak (Figure 37). This is in contrast to the isoclinal, asymmetric macro-fold pair relationships throughout the eastern Tyennan subdomain, where the east-closing fold-hinge sits above the west-closing hinge (see Gray & Vicary, 2024). The profiles should not be stacked, based on previous arguments above (Figure 30), but presented as serial profiles (Figure 38). The relationships between these two serial profiles is complicated by 1) folding of the isoclinal pair by the younger anticline (see Figures 21 and 22) and 2) down-dropping to the west by a series of normal faults through Frankland Saddle (Gray & Vicary, 2024, fig. 38). The southern end of the Frankland Range is also offset laterally and displaced vertically by the oblique slip reverse faults of the curved, horsetail fault system (Figure 21). The relationships between the fold pair is best seen in a view along the southern Frankland Range from Cleft Peak (Figure 31), where the north closing hinge (i.e. the rotated east-closing hinge) sits above the south-closing hinge (i.e. the rotated west-closing hinge) along a structurally overturned common limb (foreground, Figure 31).

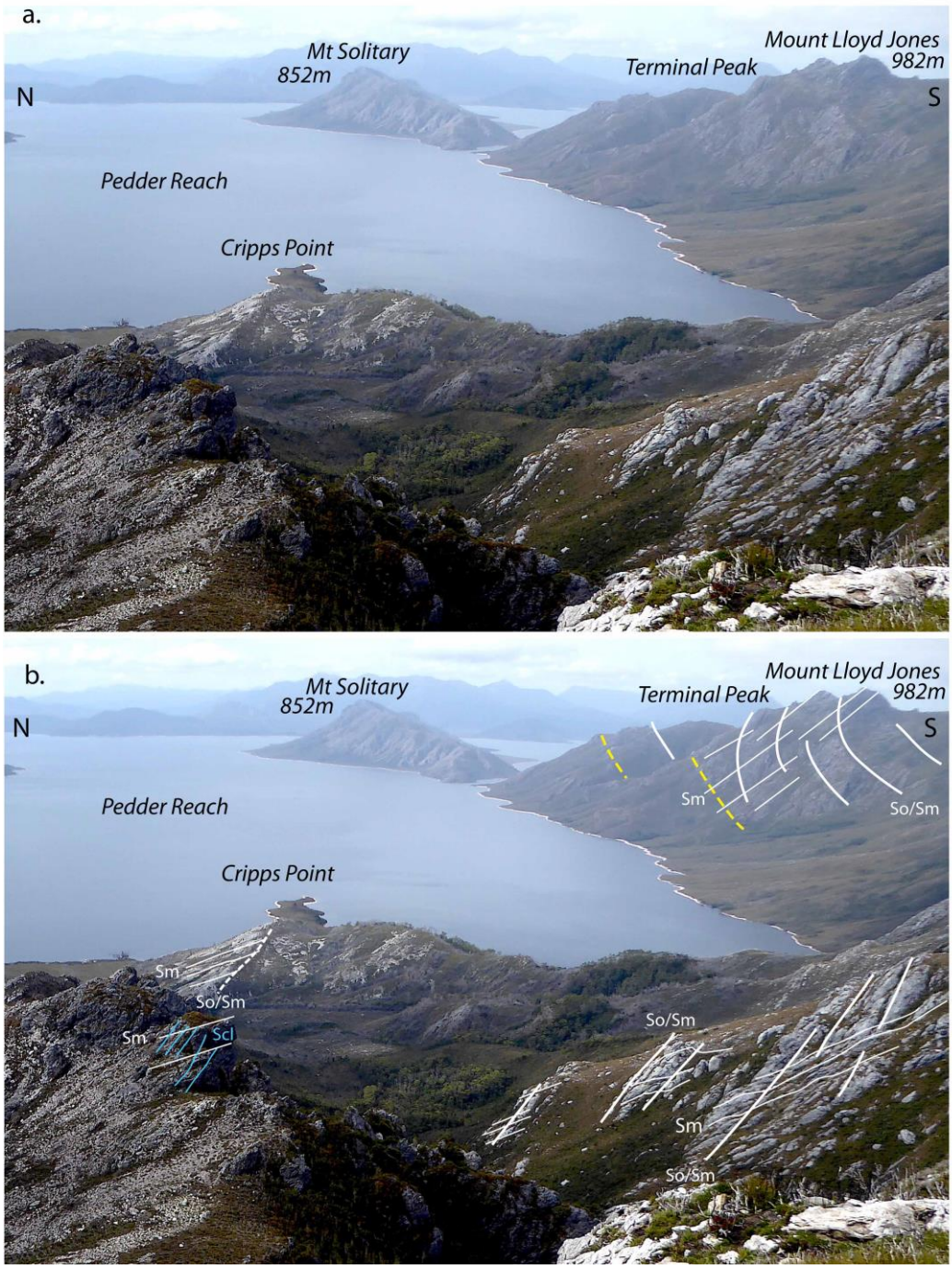

Figure 31: View from Cleft Peak ridgeline above Cripps Point looking eastwards towards Mt Solitary. Terminal Peak and Mount Lloyd Jones (photo upper right) depict a northerly inclined, north-closing macro-fold. The foreground shows the upper, structurally overturned limb of the underlying south-closing macro-fold (see Figures 32, 33 and 34). (Photo credit: David Green)

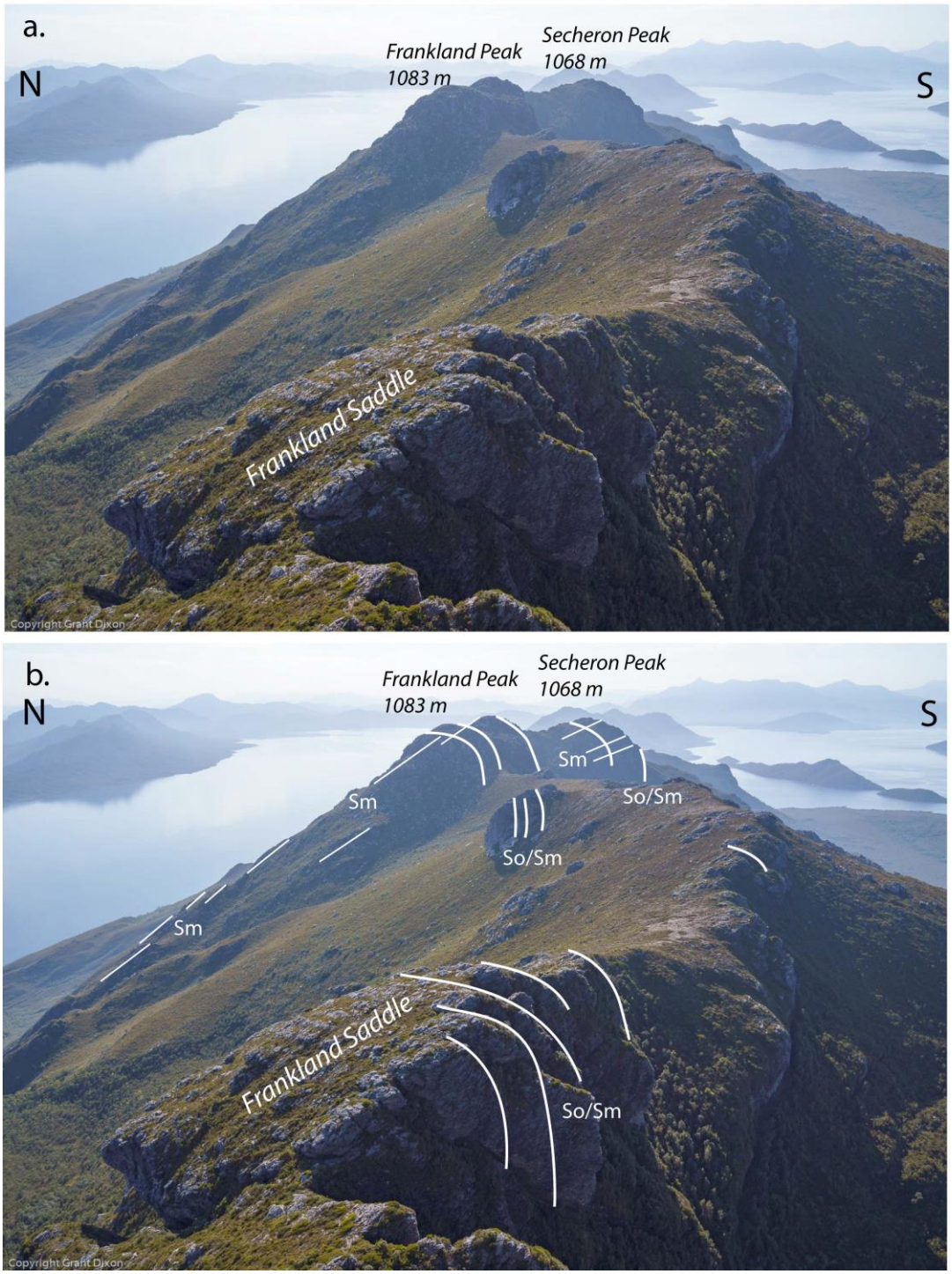

Figure 32: View of Frankland and Secheron Peaks from Frankland saddle. Formlines in So/Sm depict a south-closing, northerly inclined macro-fold (Photo credit: Grant Dixon).

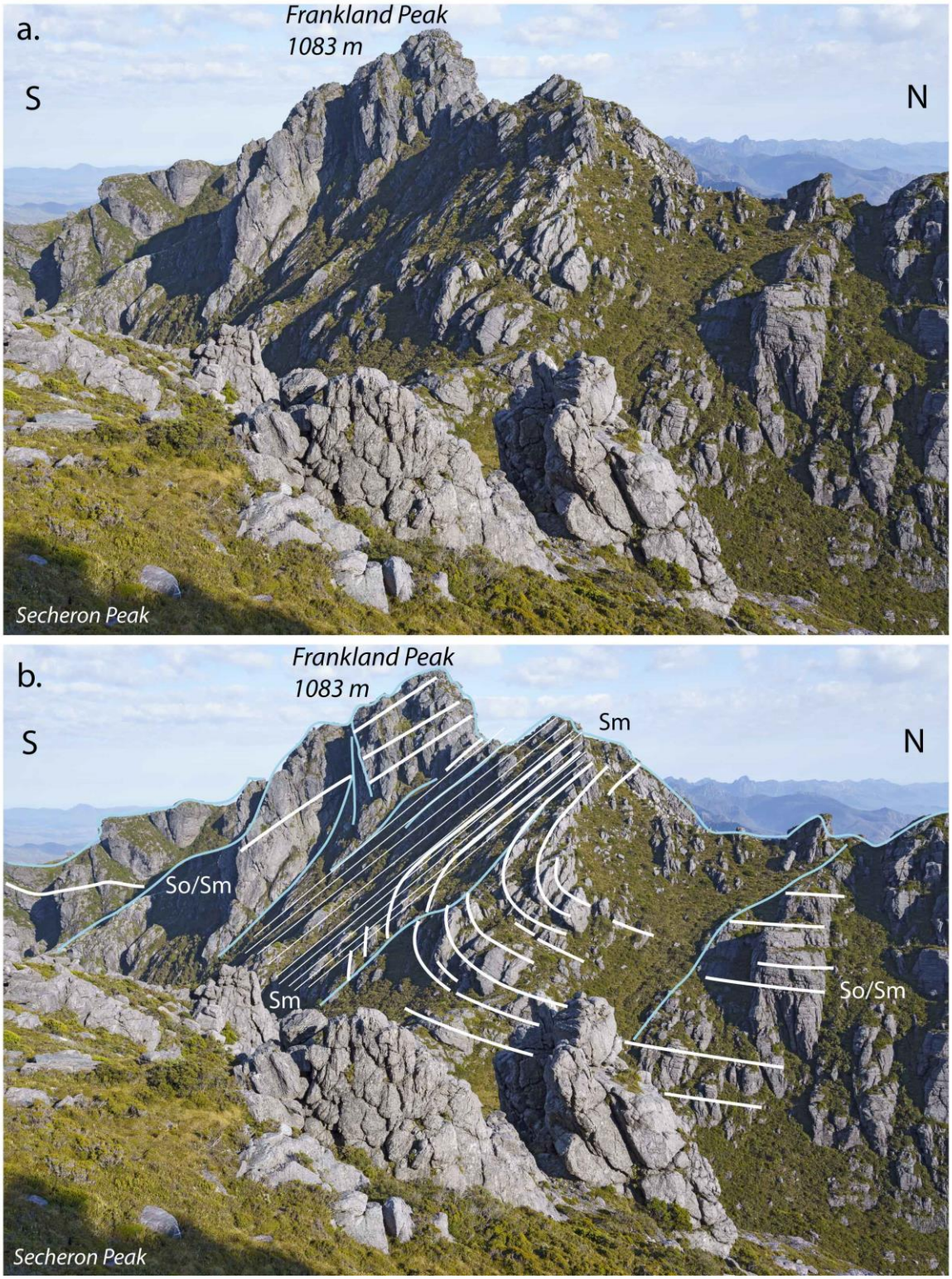

Figure 33: View of Frankland Peak from the north flank of Secheron Peak. The formlines in So/Sm depict a southerly inclined, south-closing macrofiold hinge with an intense zone of cleavage developed along the upper structurally overturned, south-dipping limb. Photo profile PP6. (Photo credit: Grant Dixon)

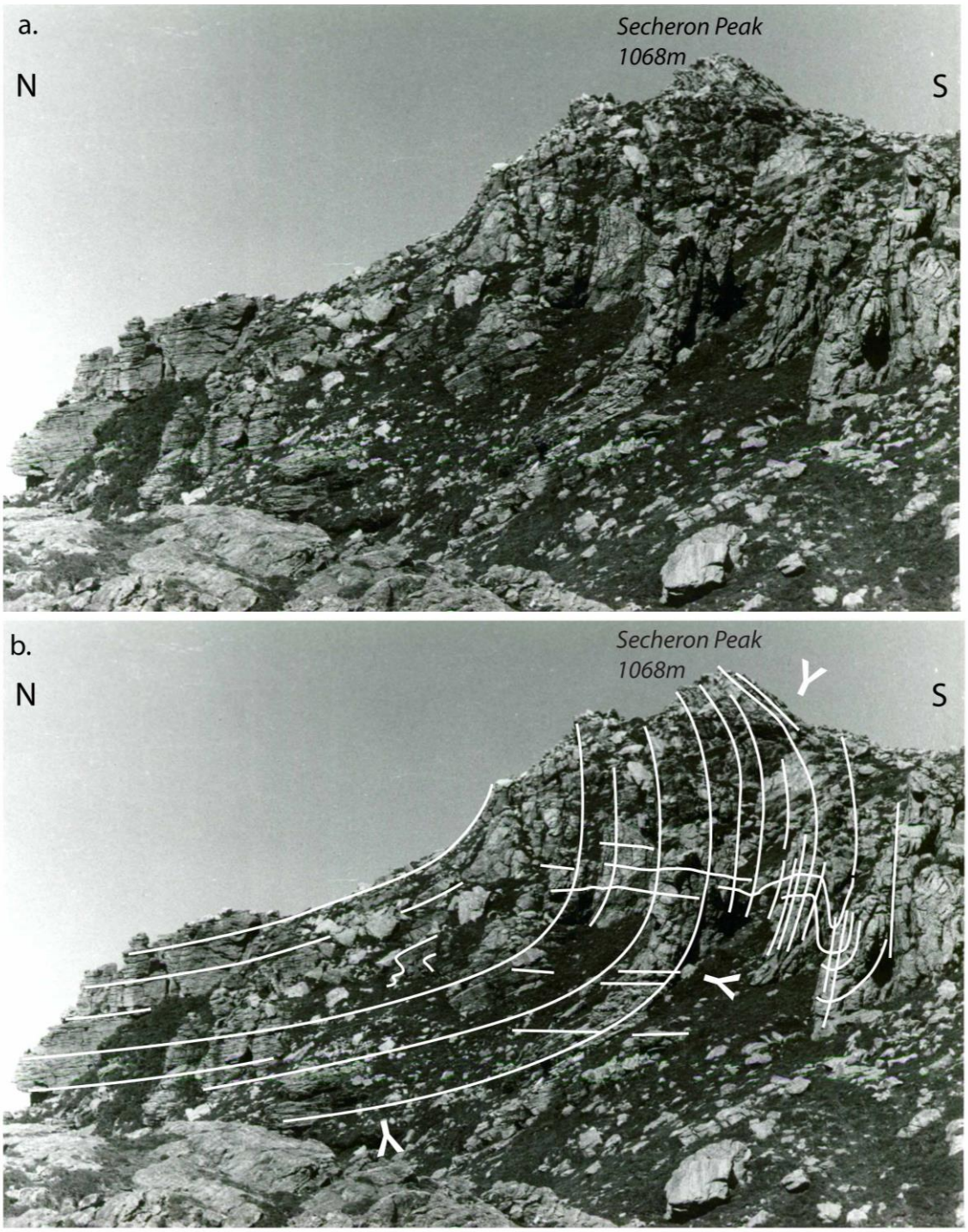

Figure 34: Photograph of Secheron Peak showing the eroded hinge of a south-closing recumbent macro-fold (Boulter, 1978, fig. 4.42). Thick white line traces: So/Sm. Thin white line traces: foliation Sm. Younging (Y) shows the upper limb is overturned. Photo profile PP7. (Photo credit: Clive Boulter).

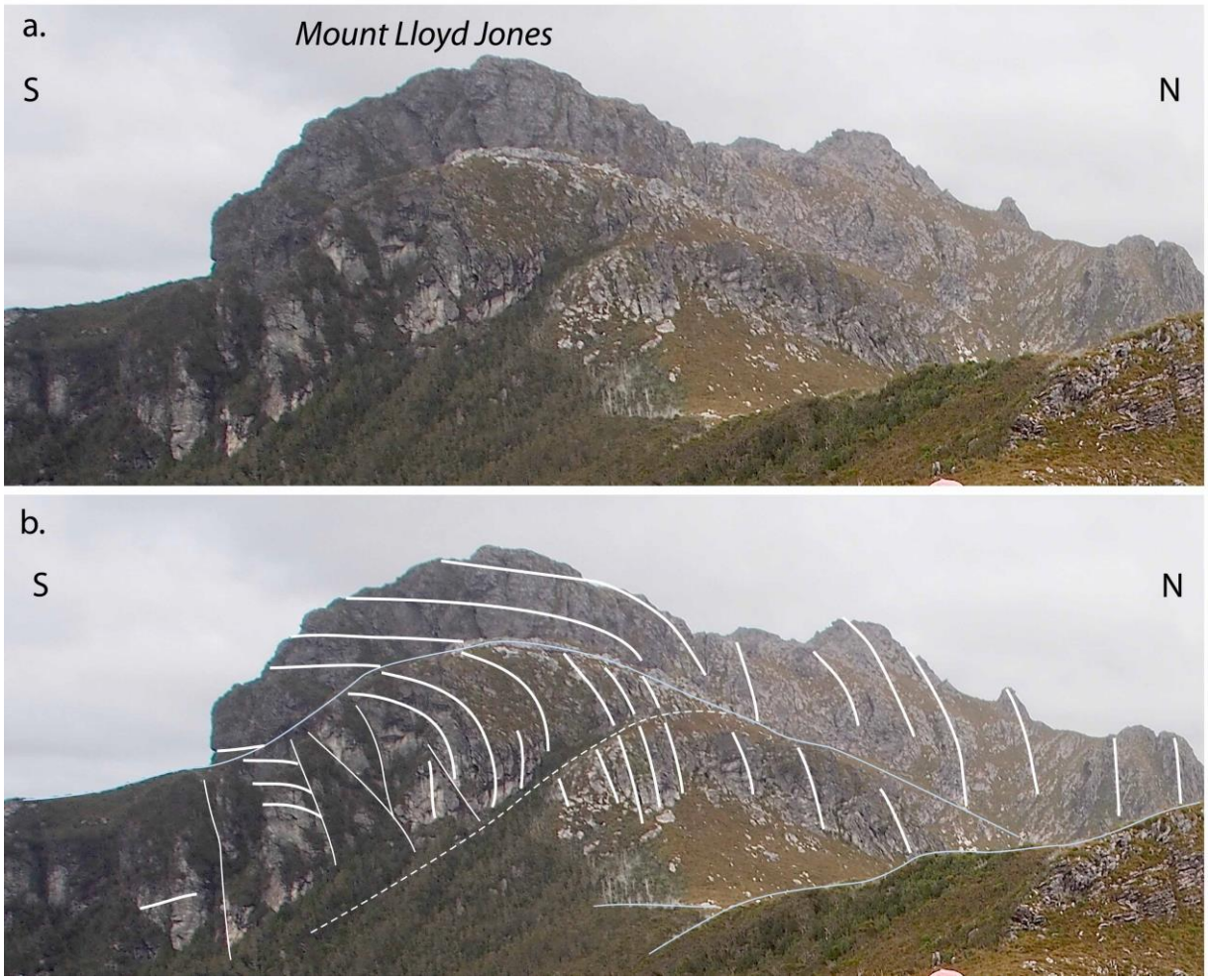

Figure 35: View of Mount Lloyd Jones from the ridgeline west of Terminal Peak. The view is to the west. Outcrop relationships in So/Sm depict a north-closing macro-fold hinge (white lines). Photo profile PP8. (Becca Lunnon, rockmonkeyadventures)

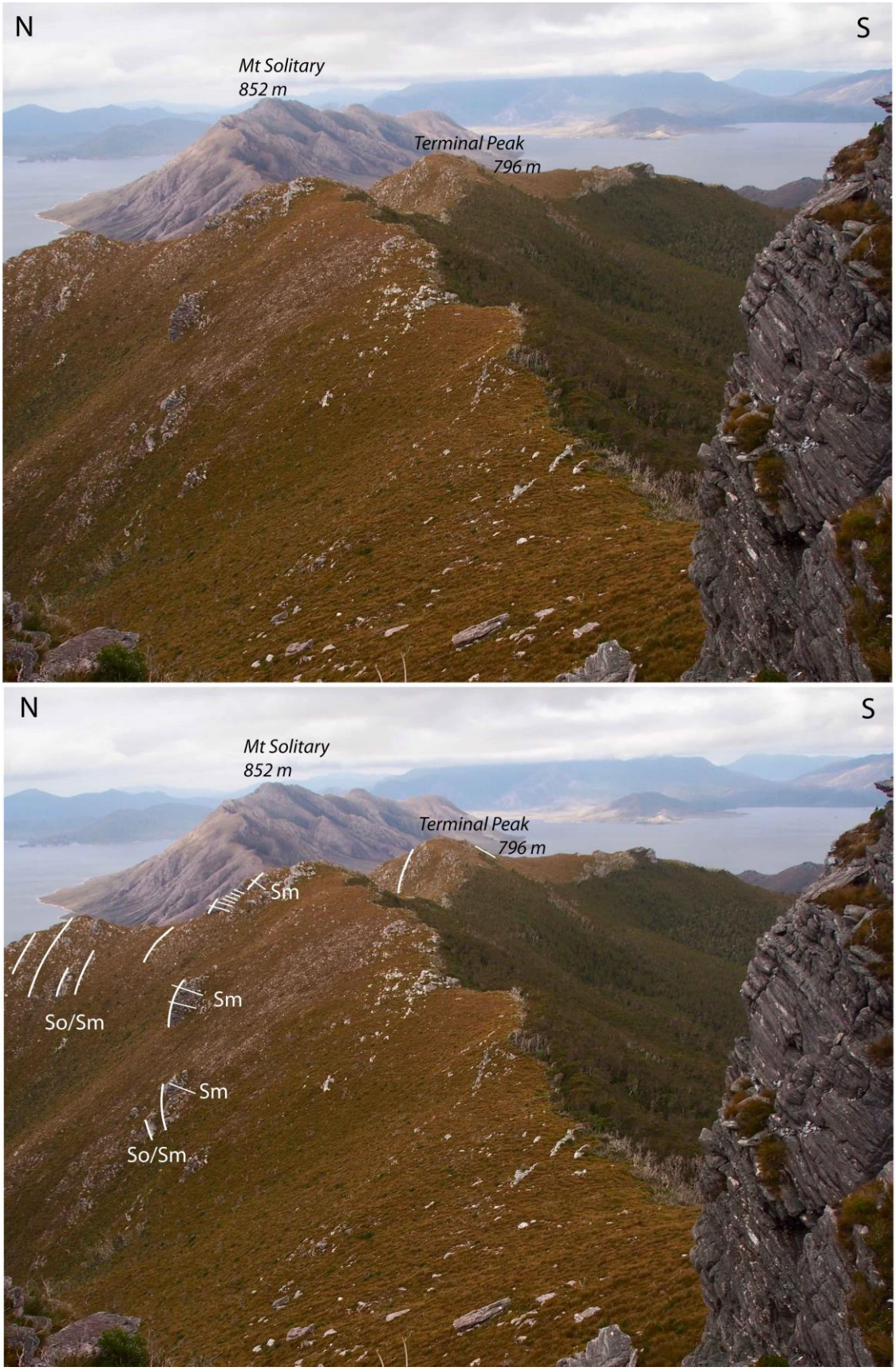

Figure 36: Ridgeline view of Terminal Peak from Mount Lloyd Jones showing outcrop relicts of a north-closing macro-fold hinge with a southerly inclined axial surface. Photo profile PP9. (Photo credit: Becca Lunnon, rockmonkeyadventures)

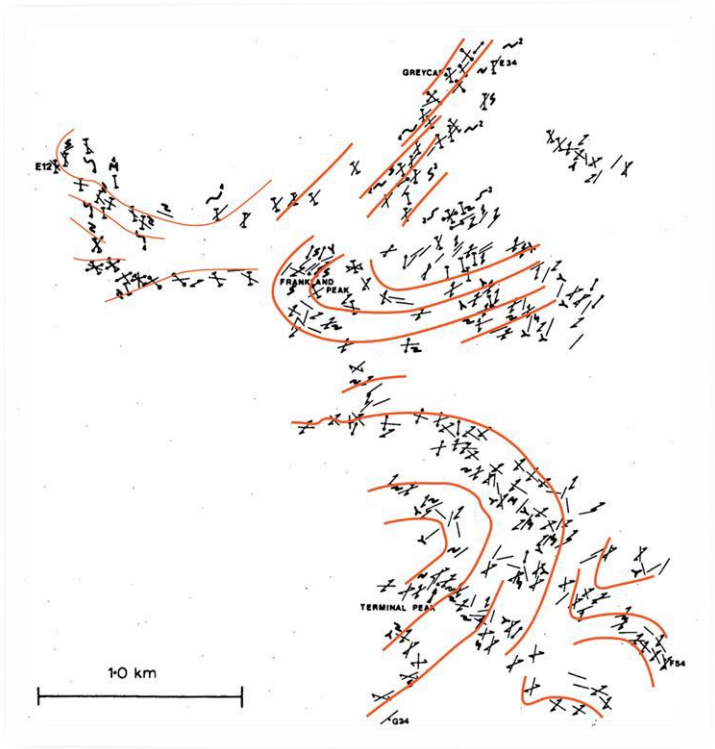

Figure 37: Boulter (1978, fig. 4.34) plunge profile from Greycap to Terminal Peak including Frankland Peak. The red line traces are formlines drawn in So/Sm pitches on the respective plunge profiles. Compare with Boulter (1978, fig.4.35). Plunges of 15°/274° (Frankland saddle), 30°/250° (Secheron Peak) and 30/260° (Terminal Peak) were used in the conbstruction (see Boulter, 1978, fig. 4.38). These trend changes are shown in Boulter (1978, fig.4.39).

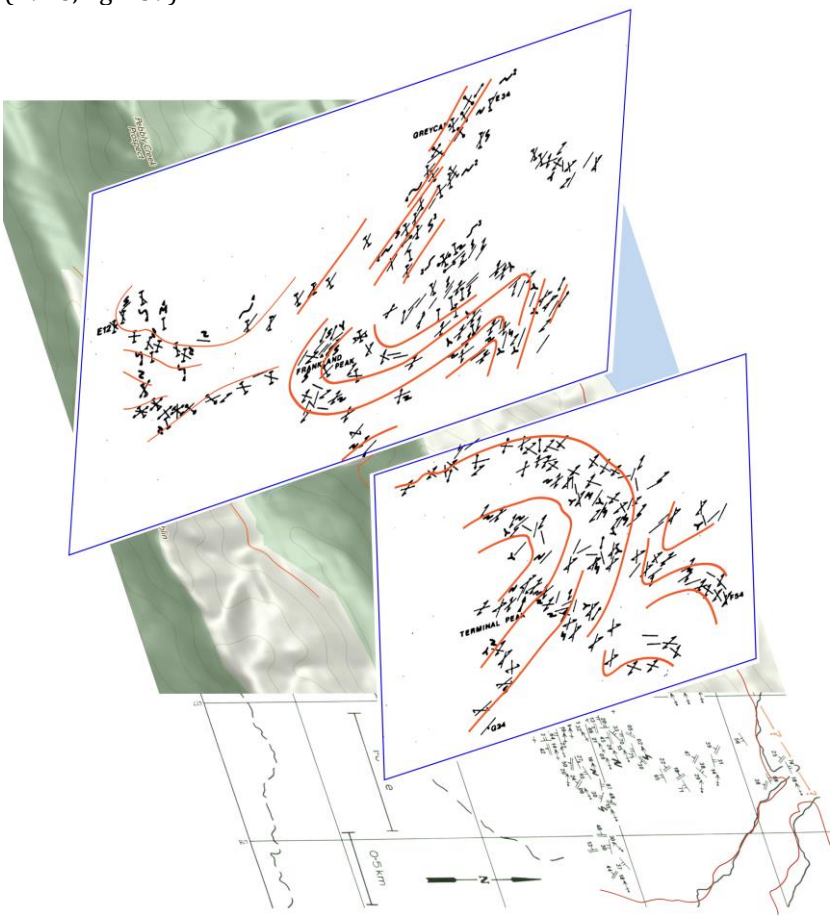

Figure 38; Boulter (1978) profile depicted as serial profile map projections of Frankland Peak and Termninal Peak structural data in contrast to the stacked profile of Figure 37.

The final compiled photo profiles are shown in Figures 39 and 40 with profile locations shown in Figure 23.

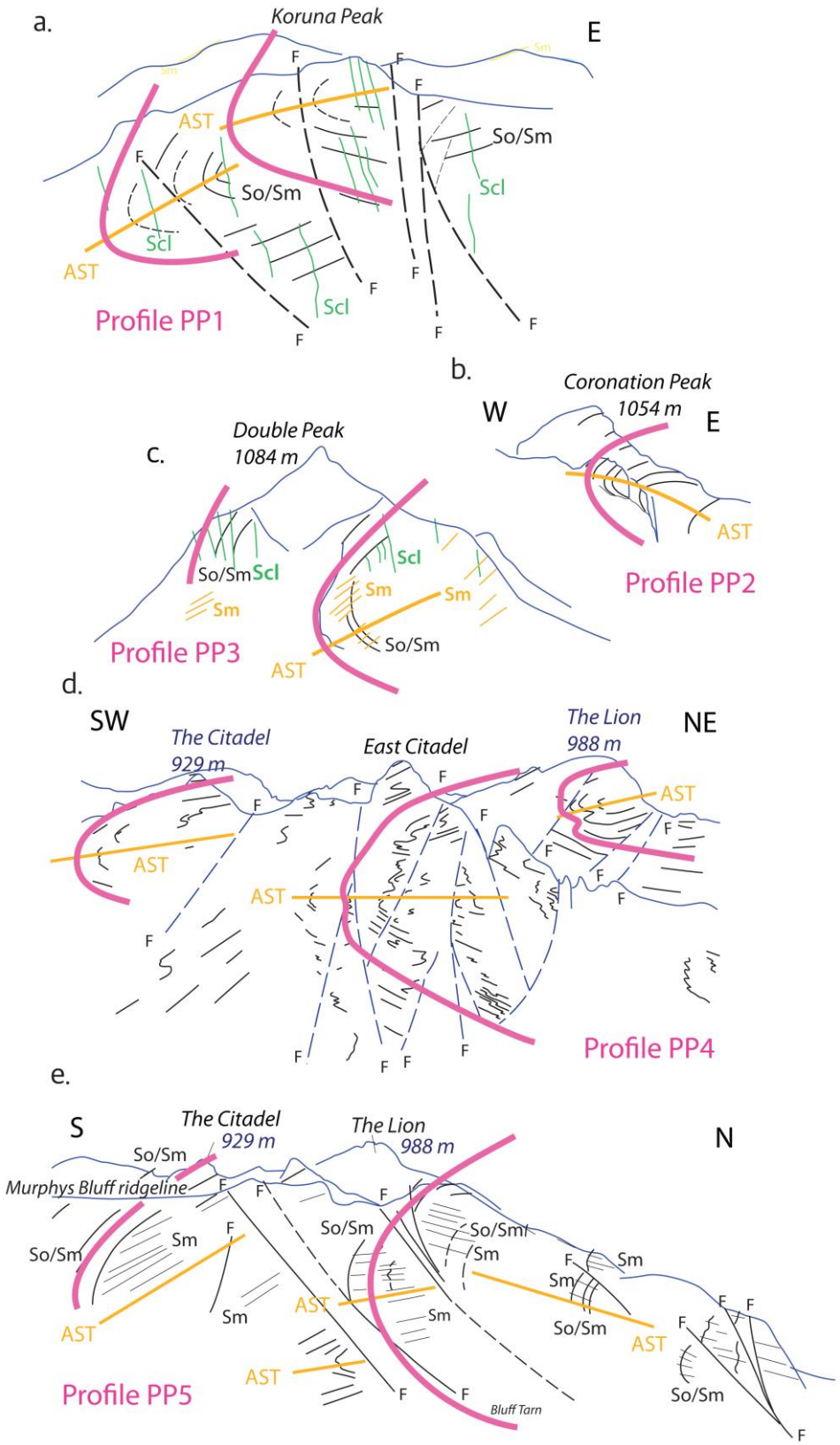

Figure 39: Summary photo profiles for the Wilmot and northern Frankland Ranges. The ridgeline is dominated by a south-closing, recumbent, isoclinal macro-fold. Pink lines define the geometrical form of the fold closure in the individual profiles. Orange lines depict the axial surface traces. So/Sm are the heavier black lines traces and Sm are the fine black line traces.

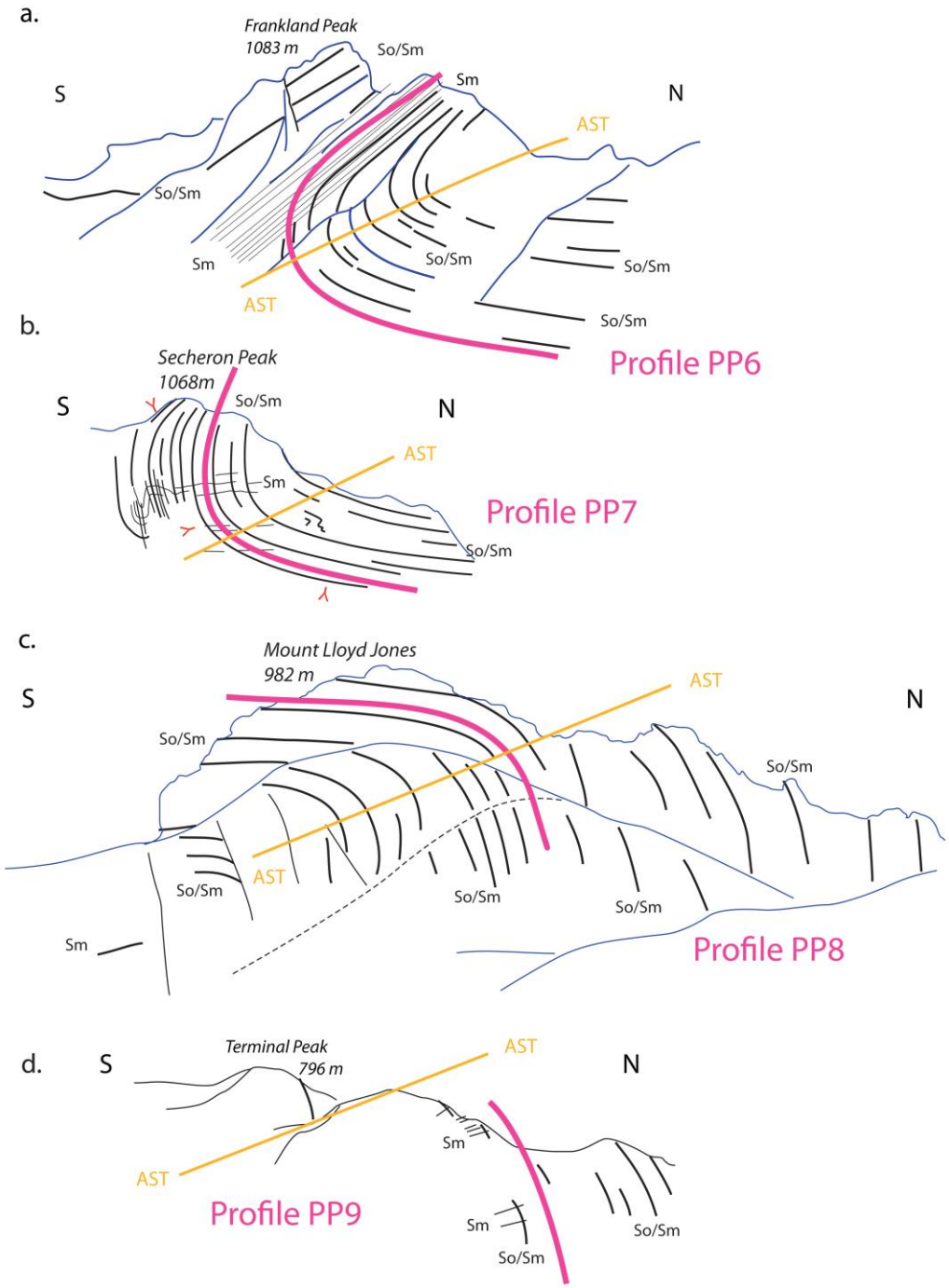

Figure 40: Summary photo profiles for the southern Frankland Range from Frankland Peak to Terminal Peak. The ridgeline is dominated by both south-closing (profiles a, b) and north closing (profiles c, d), recumbent, isoclinal macro-fold hinges. Pink lines define the geometrical form of the fold closures in the individual profiles. a) Profile PP6 through Frankland Peak. b) Profile PP7 through Secheron Peak. c) Profile PP8 through Mt Lloyd Jones. d) Profile PP9 through the Terminal Peak. Orange lines depict the axial surface traces. So/Sm are the heavier black lines traces and Sm are the fine black line traces.

3.4 *Structure of The Companion Range*

The Companion Range is a northwest-southeast trending, ~5 km long outlying range southwest of the main Frankland Range (Figures 1 and 21). The ridgeline shows west-dipping quartzite bands with 1) an apparent eroded southwest-closing macro-fold hinge through Remote Peak at the northern end, and 2) with layer convergence suggesting a more complete profile through the same macro-fold at the southern end (Figure 41). Younger, open refolding of the macro-fold hinge is suggested by the dip reversals in the macro-fold axial

surfaces across the intervening valley between Murphys Bluff and the Companion Range. At Murphys Bluff the western part of the Bluff ridge has a southwest dipping axial surface (Figure 39e) whereas along the Companion Range it is northeast dipping (Figure 41). This requires an open syncline along the intervening valley west of the Frankland Range. A syncline is also shown in Boulter's profiles (Boulter, 1978, figs. 4.34 and 4.35) (Figure 37).

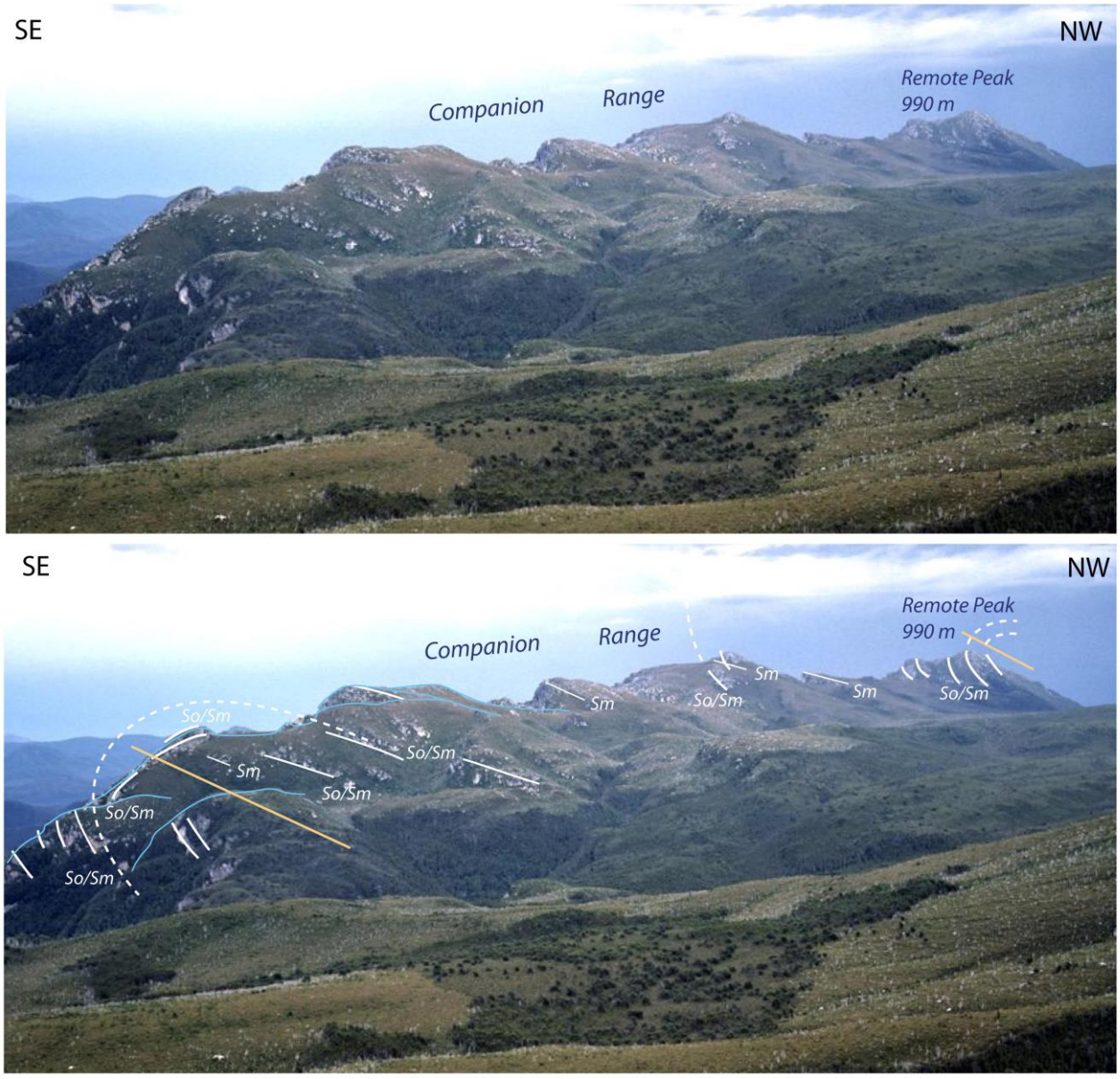

Figure 41: Photograph of the Companion Range showing partial outcrop of a northeasterly inclined, southwest closing macro-fold, The southern part of the ridge shows a closure with an apparent northeast dipping axial surface (orange line trace on photo left). (Photo credit: David Noble)

3.5 *Mesoscopic F1 Isoclinal Folds*

Early F1/F2 mesoscopic folds in quartzite display varying geometries (Figures 42 to 49). These photographs from Boulter (1978) display the complexity of the fold geometry at the local scale. The variations are related to the nature, composition and thickness of the layering. The folds either have 1) angular, chevron-like hinges in thicker bedded quartzite (20-40 cm bed thickness) (Figure 42), 2) rounded hinges in isolated thicker quartzite layers (20-30 cm thickness) within thin-bedded pelite (Figures 43 and 44), and 3) flattened and

extremely attenuated isoclinal form in zones of higher strain (Figure 45, 48 and 49). They can also occur as chevron fold stacks in thin-bedded quartzite multilayers (10-20 cm bed thickness) (Figure 46).

Some of the folds have curvilinear hinges typical of incipient sheath forms (Figure 47).

Boulter (1978) argued that
1) early mesoscopic isoclinal folds were predominantly first generation (F1),
2) second generation (F2) mesoscopic were folds were relatively rare, and that
3) asymmetric F1 folds were parasitic on larger regional scale F1 macro-folds.

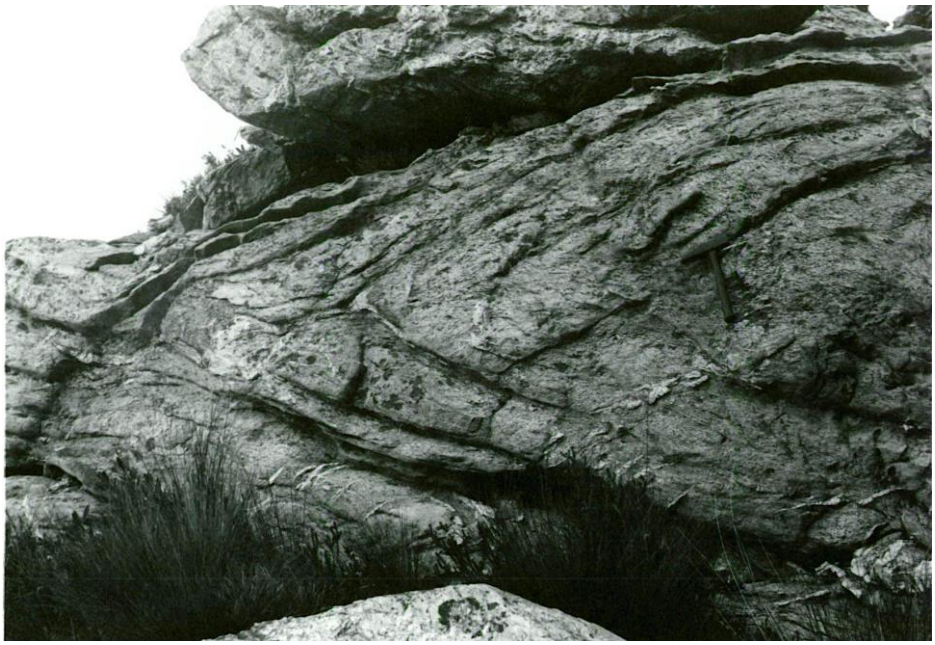

Figure 42: Flattened, recumbent isoclinal fold with chevron-like form and a flat-lying axial surface foliation. 1 km southwest of Frankland Saddle. View is looking west northwest. (from Boulter, 1978, fig. 4.44a)

Figure 43: Isoclinal asymmetric fold-pair in quartzite between The Lion and The Cupola on the main ridge. The fold pair may have nucleated on a small scour fill "channel". The hammer is 40 cm long. (from Boulter, 1978, fig. 3.5b)

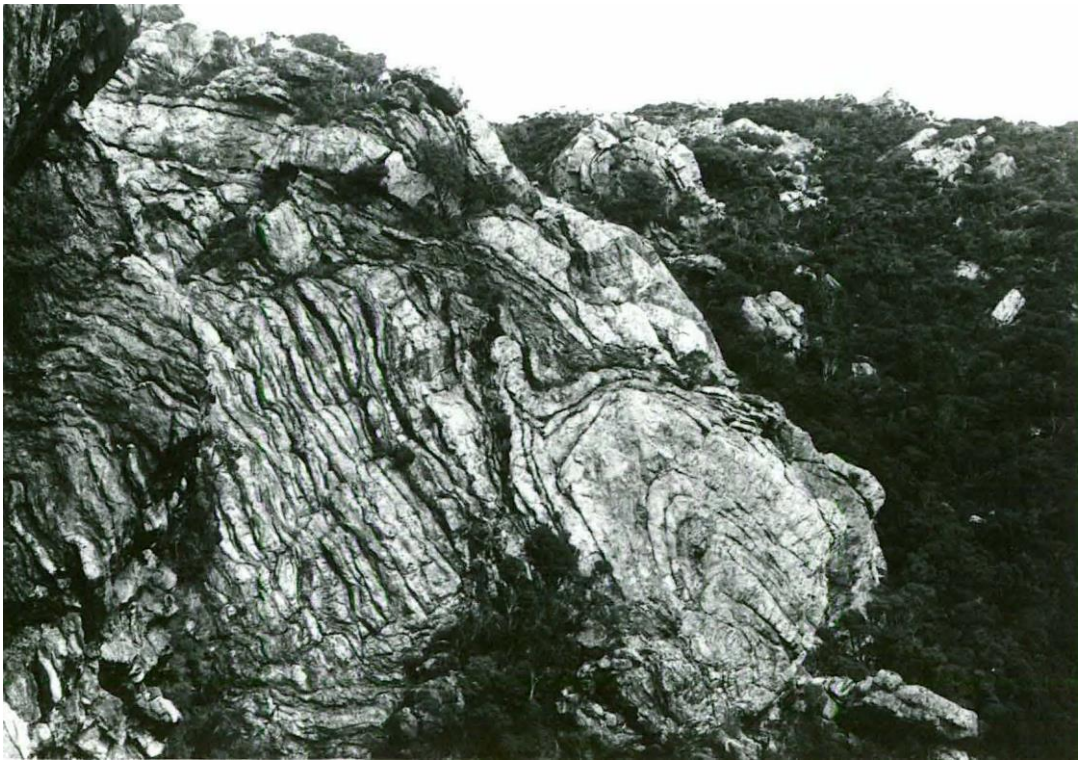

Figure 44: Contrasting F1 fold forms in ~30 m high quartzite cliff face, 500 m southeast of Double Peak. The cliff face shows a flattened and extremely attenuate isocline (photo middle) above a bulbous, rounded upward-closing hinge in a thicker quartzite layer. The hillside (upper right) also shows rounded hinges within thicker quartzite layers. (from Boulter, 1978, fig. 3.3b)

Figure 45: Intensely flattened and attenuated isoclinal F1 folds with boudinaged limbs within thicker bedded quartzite (20-30 cm bed thickness), 500 m southeast of Double Peak. The plane of separation of the boudins (125/70) indicates the principal stretching direction is at high angles top the fold hingelines. The folds are suggested by apparent, oppositely closing pinch-outs that taper to a point where the layer "disappears". The hammer is 40 cm in length (from Boulter, 1978, fig. 3.3a)

Figure 46: Asymmetric, tight to isoclinal, recumbent chevron folds in ~20 m high cliff face on the slopes north of Murphys Bluff (from Boulter, 1978, fig. 3.6)

Figure 47: Sheath-like nose of folded quartzite layer showing a curved F1 hinge line emerging from the hillside on one side and re-entering it on the other. The location is 300 m southeast of Double Peak (from Boulter, 1978, fig. 4.28)

3.6 *Mesoscopic Outcrop Scale Structural Relationships of the Wilmot-Frankland Ranges*

Polydeformation is another element that adds to the complexity of the structural interpretation for the Wilmot-Frankland Range with a zone of refolding along the spine of the range. This refolding is typified by upright folds (Figures 48 and 49) that 1) refold the early formed isoclinal folds (Figures 25, 26 and 49) and 2) have an axial surface spaced cleavage and/or crenulation cleavage Scc (see blue line traces in Figure 49b).

This polydeformation is part of an interpreted refolded and polydeformed core to the Eastern Tyennan subdomain that has been further modified by younger, coplanar Devonian folding (see Section 8.1, Gray & Vicary, 2024).

Figure 48: Structural relationships on Mt Sprent showing upright, north trending folds with an axial surface crenulation cleavage Scc. These folds are approximately coaxial with the recumbent macro-fold pair (Photo Credit: Andrew Wakefield).

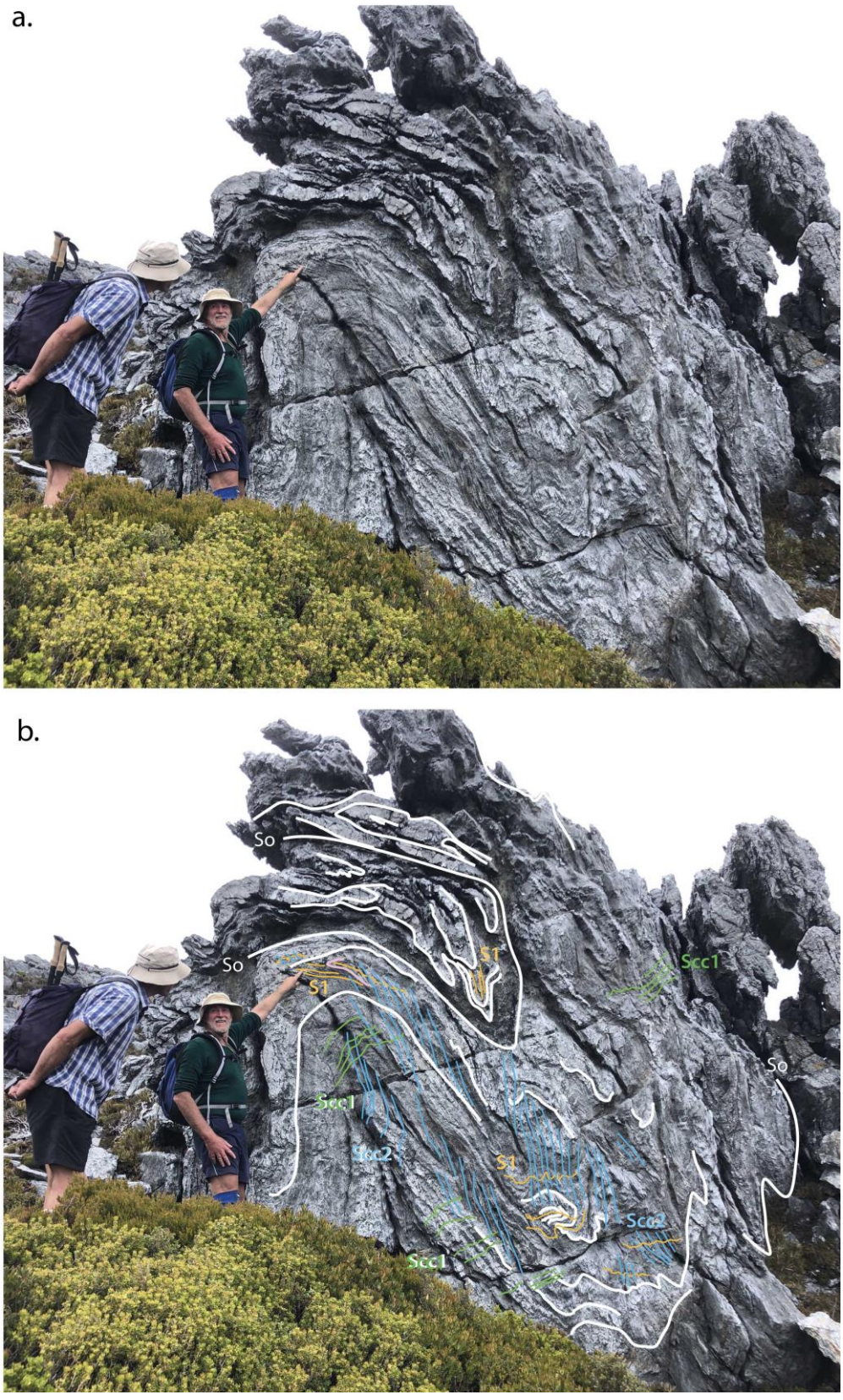

Figure 49: Complex structural and refolding relationships on Murphys Bluff ridgeline. View is looking north. Early isoclinal folds within So/Sm (white line traces) are highlighted by the lithological layering and a darker pelitic band (photo upper middle). The isoclinal folds have an axial surface "S1" foliation (orange line traces) that is refolded about upright folds with an axial surface crenulation cleavage Scc2 (blue line traces). An earlier crenulation cleavage Scc1 (green line traces) is locally refolded by Scc2 (see hinge of anticline pointed out by Michael Roche. David Green also for scale. (Photo credit: Sebastien Meffre)

3.7 *Structure of the Folded Range*

The Folded Range, south of Terminal Peak and Mt Giblin, is dominated by a broad anticline (Figure 50) that refolds a north-closing early macro-fold (Figure 51). The younger anticline is tight and northerly-inclined with a fanning cleavage (Figure 50b). The interpreted axial surface traces for the early recumbent fold (orange line trace) and the younger more open folds (green line traces) are shown in Figure 52.

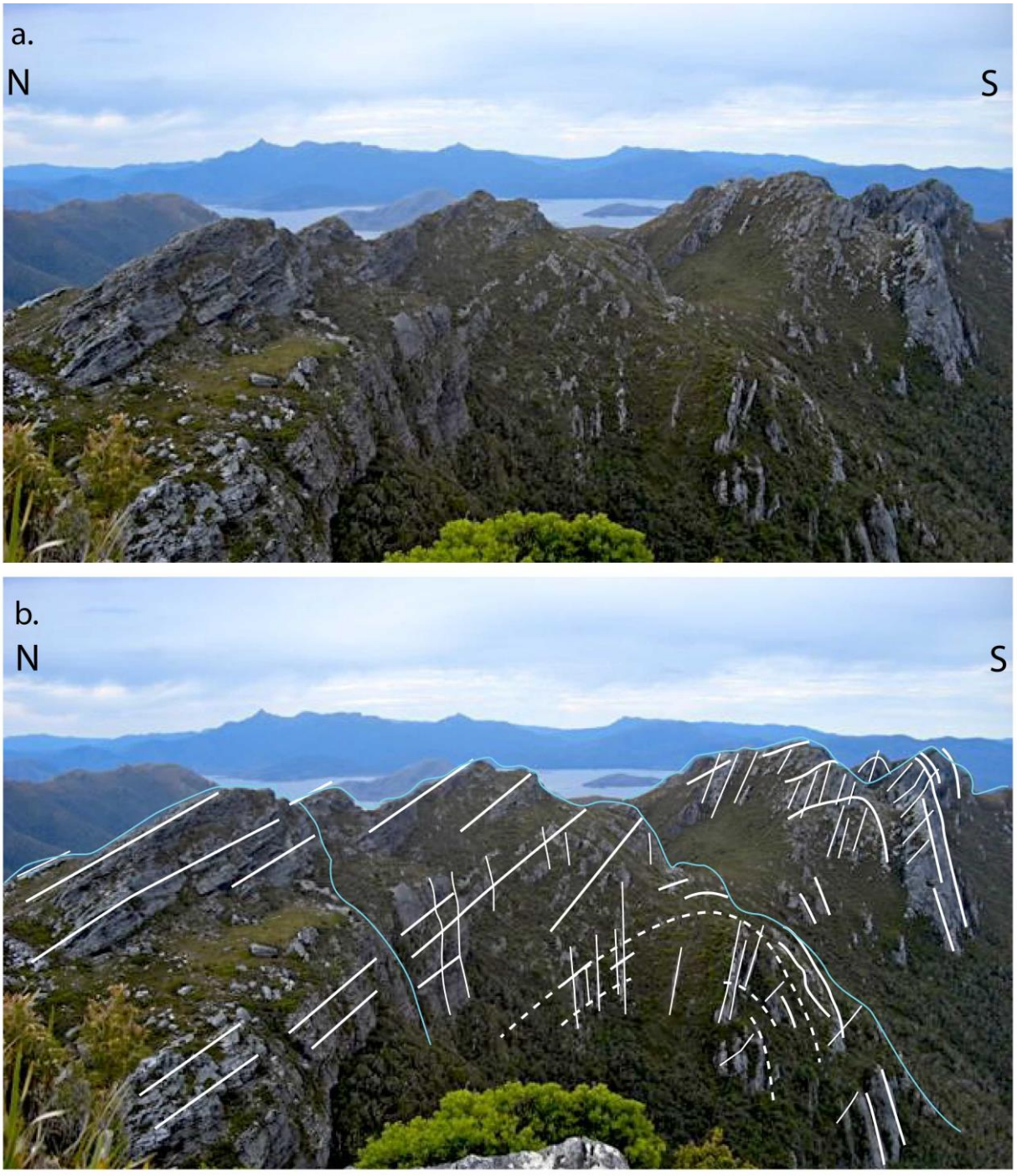

Figure 50: View along the Folded Range looking to the east showing a broad, tight, northerly-inclined anticline with a fanning cleavage. (Photo credit: Becca Lunnon, rockmonkeyadventures)

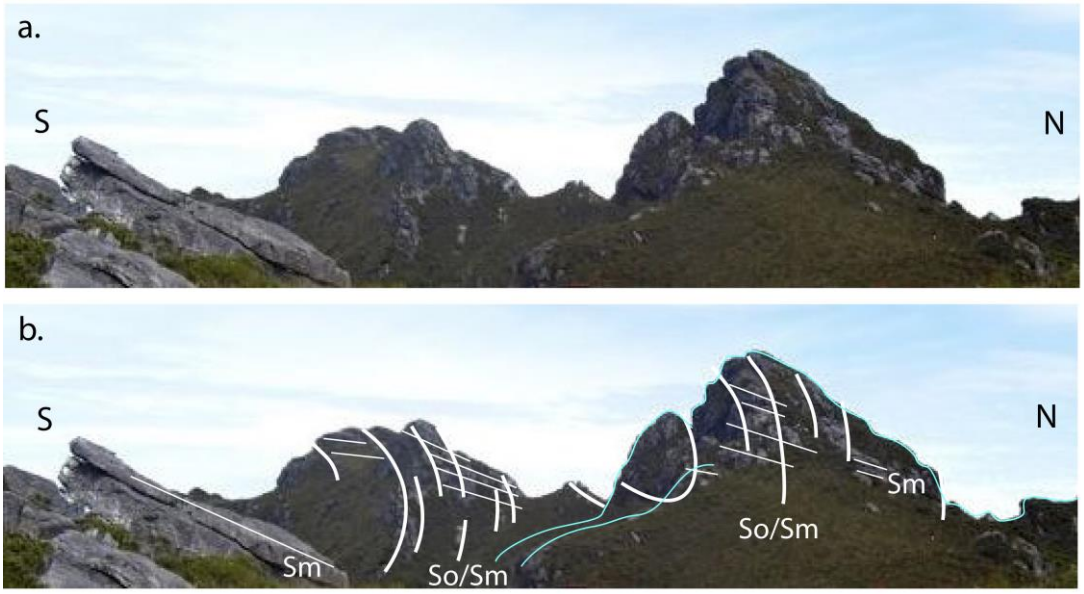

Figure 51: Early macro-fold along the ridge crest of the Folded Range. The photo shows the eroded hinge of this north-closing recumbent macro-fold with the axial surface foliation Sm dipping to the north. (Photo credit: Becca Lunnon, rockmonkeyadventures)

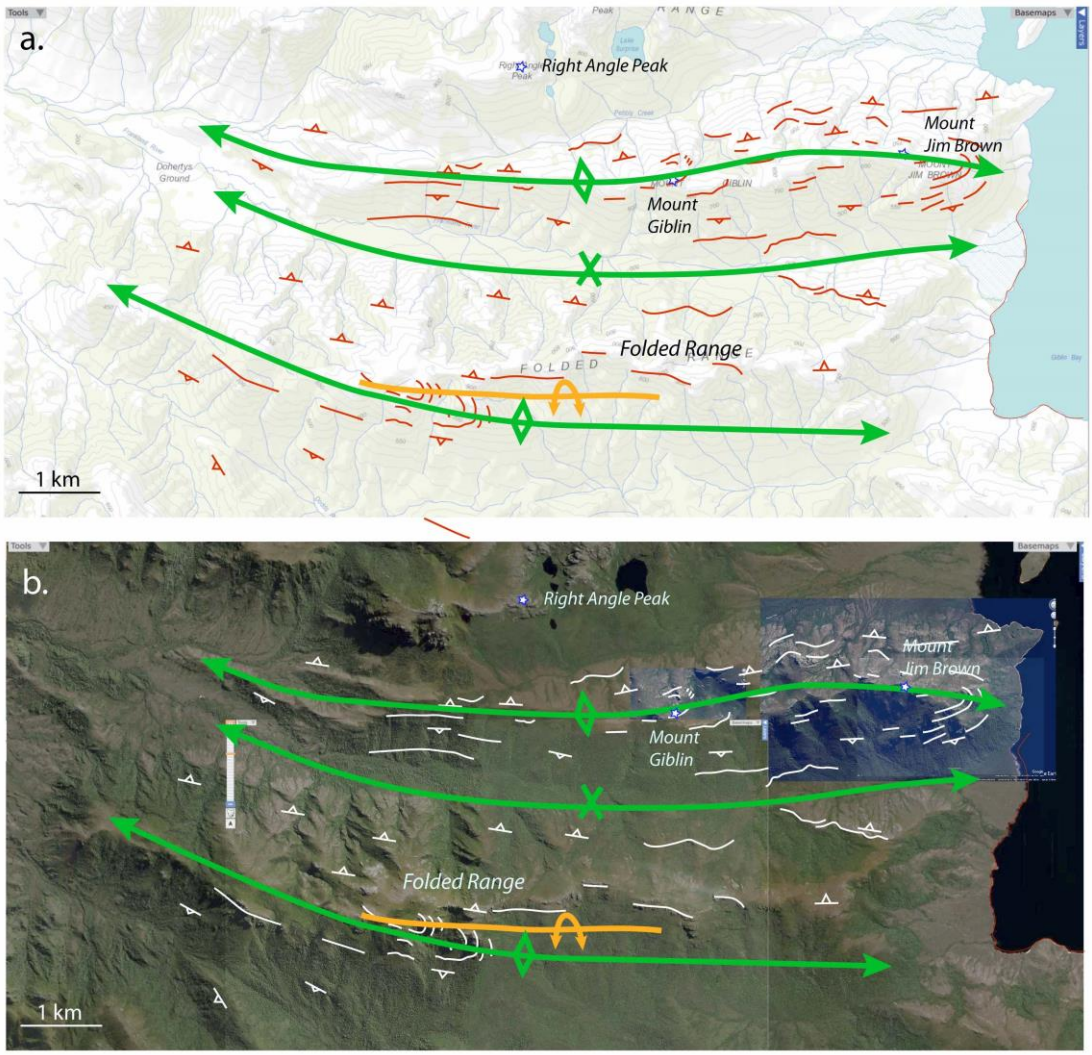

Figure 52: Structure of the Folded Range. a) ListMap topographic map with superimposed formlines in So/Sm (red line traces), early F1/F2 axial surface trace (orange) and the younger open folds axial surface traces (green). b) Google earth satellite image base with structural relationships shown as in (a).

4. The Spires

The Spires is an elongated, northeast-trending, pod-shaped, tapered quartzite ridgeline with the northern and southern terminations with opposing fold plunges. The ridgeline exposes varying intersections through the asymmetric Z-vergent (looking north), recumbent fold pair (Figures 53, 54 and 56). The fold pair consists of a structurally higher east-closing synformal macro-fold connected to a structurally lower west-vergent macro-fold (Figure 55).

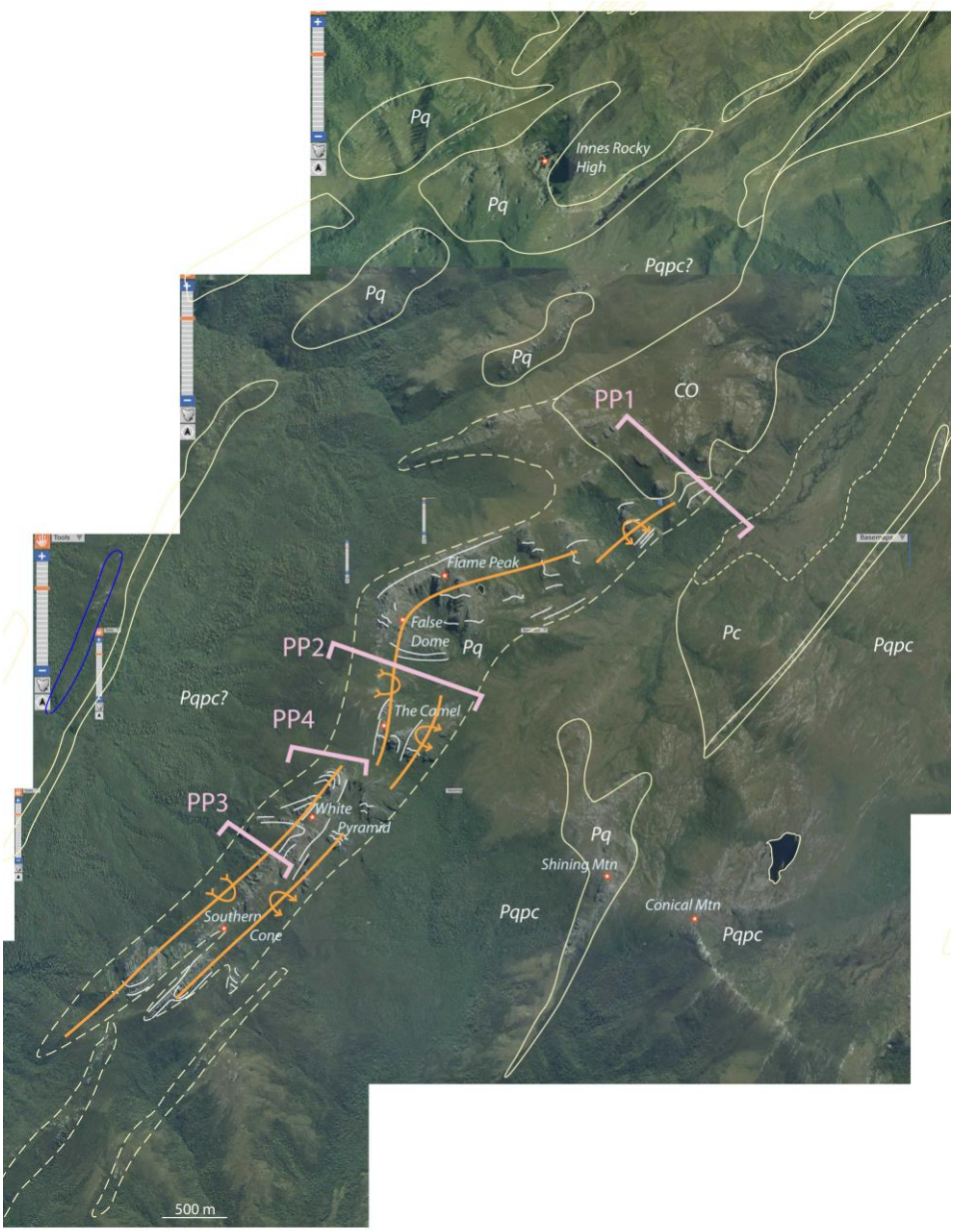

Figure 53: Structural interpretation map of The Spires range showing formlines in So/Sm (white line traces), interpreted geological contacts (dashed pale yellow line traces), mapped geological contacts (pale yellow line traces) and the axial surface traces of the regional, isoclinal macro-fold pair (orange line traces). Listmap airphoto base. The positions and directions of the photo profiles are shown by the heavy pink lines labelled PP1 to PP4.

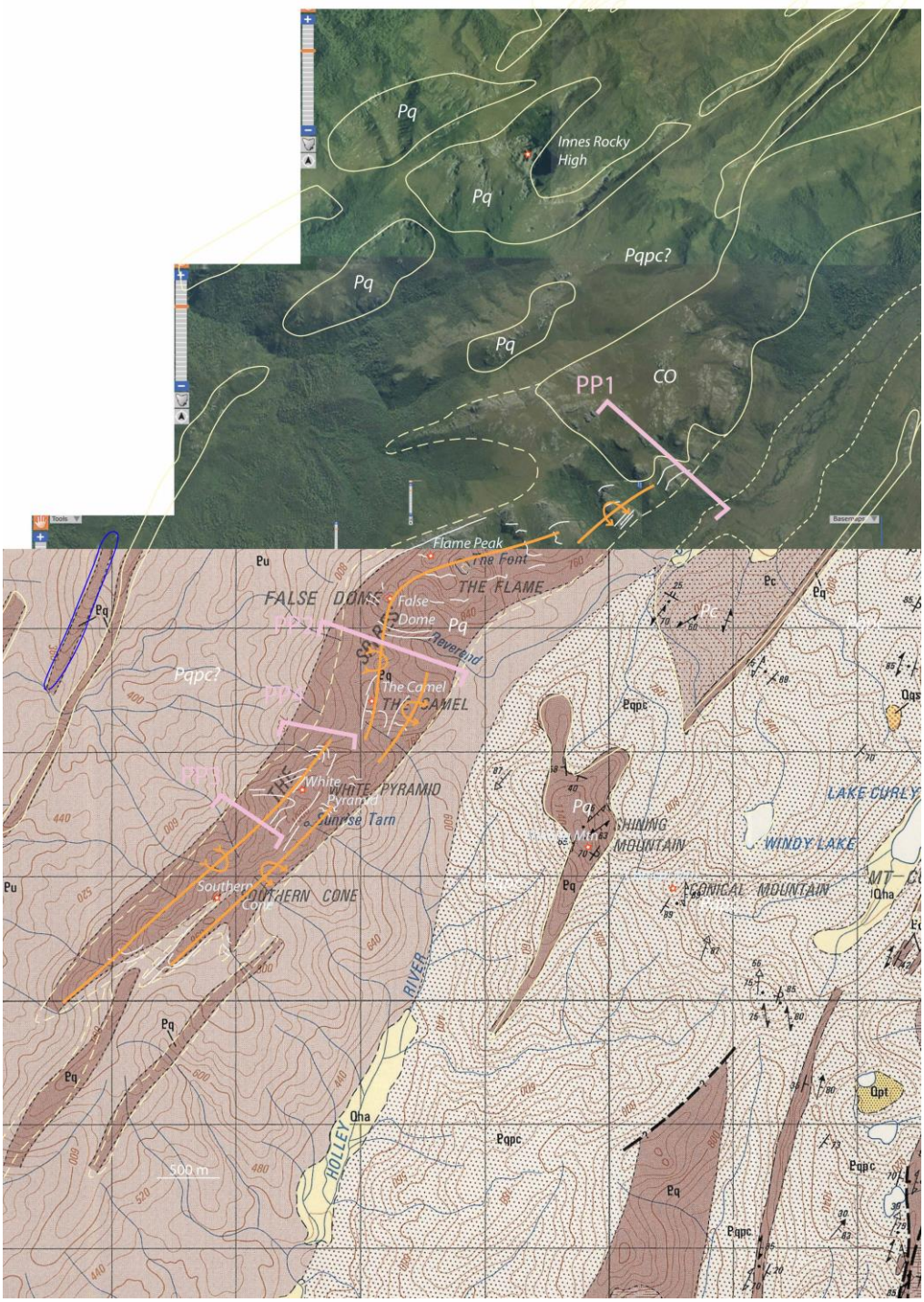

Figure 54: Huntley 1:50,000 map sheet (Brown et al., 1982) superimposed on the ListMap airphoto base of Figure 53.

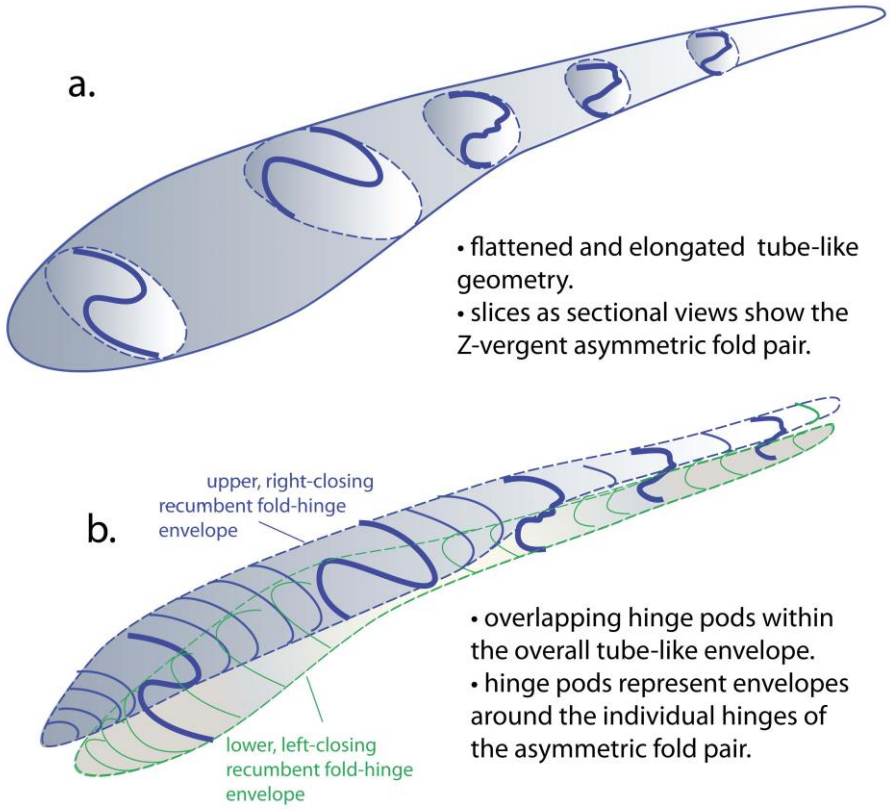

Figure 55: Schematic diagrams of the interpreted 3D structure of The Spires as a flattened and elongated, pod-shaped augen. a) The quartzite envelope (grey) enclosing the Z-vergent, recumbent, asymmetric fold pair of the range. Sectional views are superimposed. b) Envelopes about the upper and lower oppositely closing hinges of the fold pair. Note the hinge separation at the left closeout matches the forked nature of the southern termination of The Spires (Figure 58).

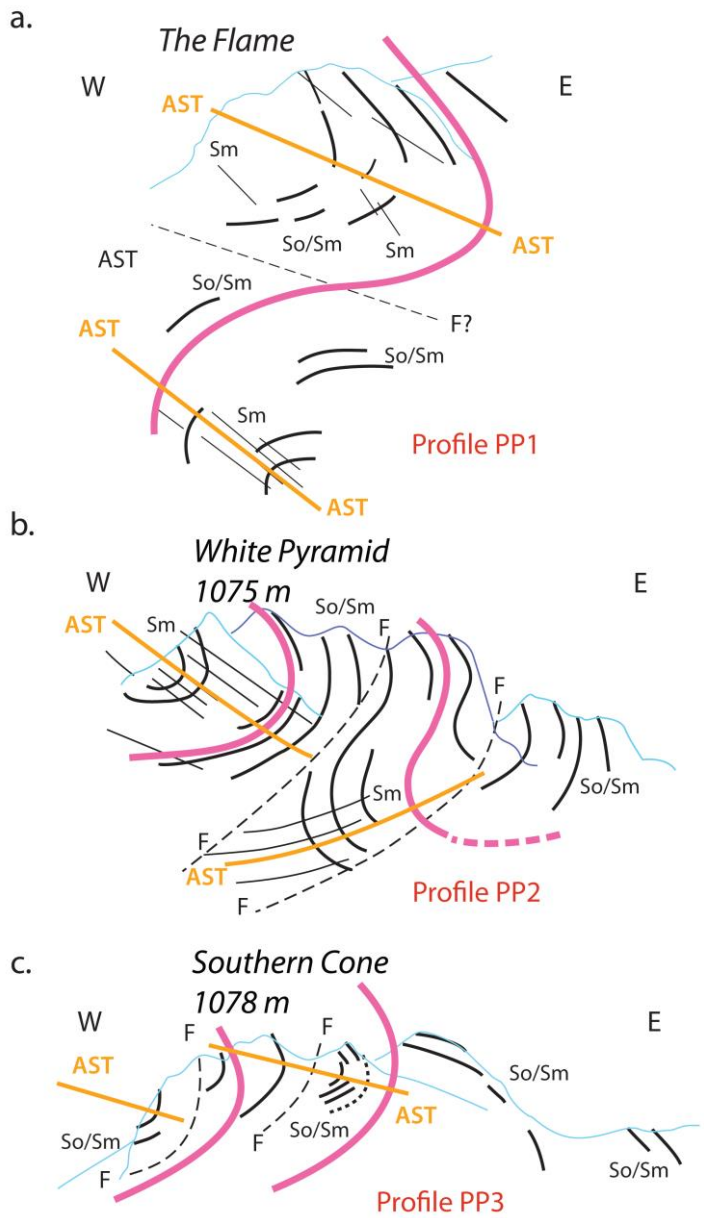

Figure 56: Photo profiles across The Spires. The positions of the photo profiles are shown in Figure 53 and 54.

The photo profiles and other photographs along the Spires are shown in Figures 57 through 60 showing the asymmetric, west-over-east or S-vergent (looking south as in Figures 57 and 59) fold pair.

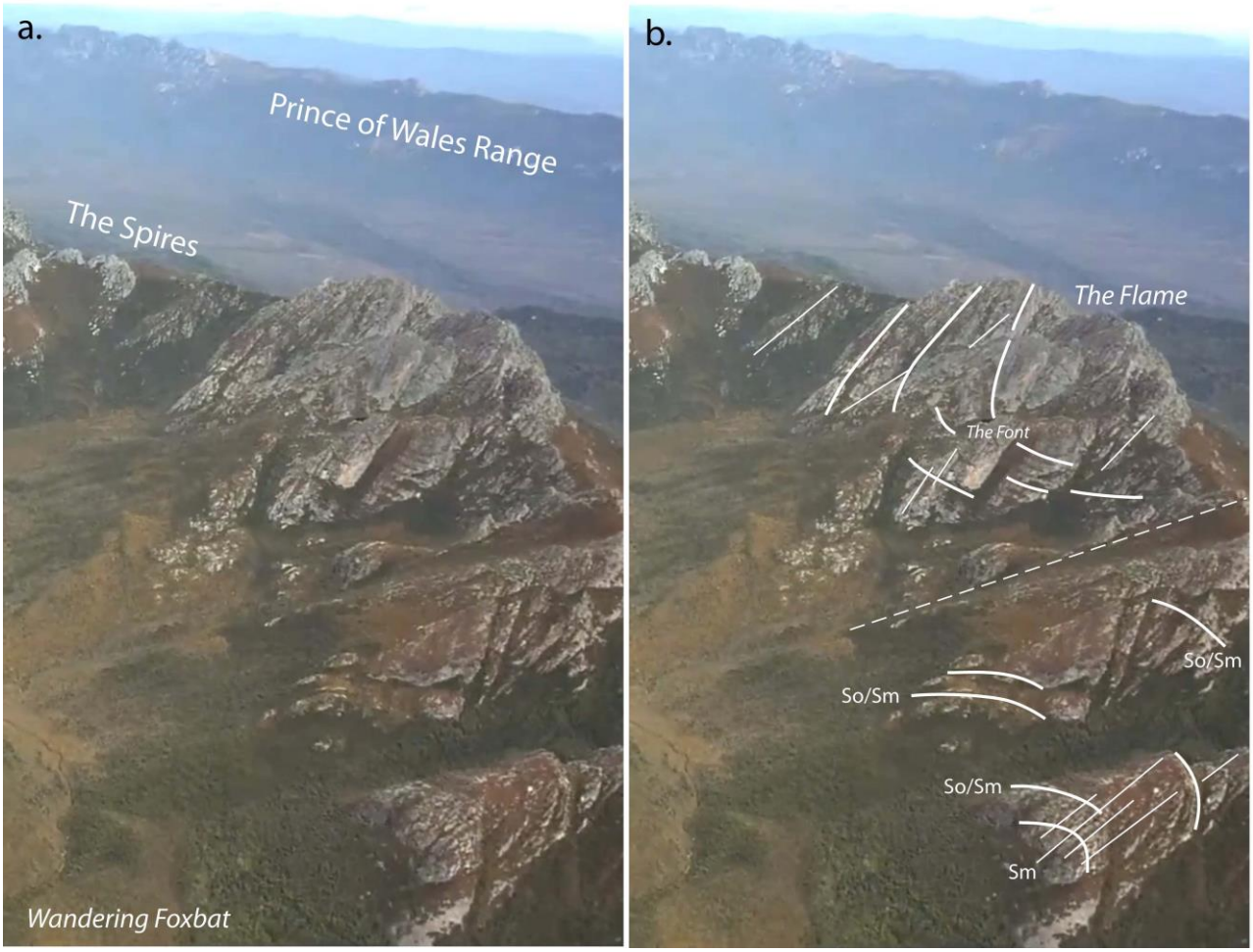

Figure 57: Aerial view of the north end of the Spires Range with the Prince of Wales Range in the distant background (photo credit: Wandering Foxbat). The photo shows an oblique view of the S-vergent, asymmetric recumbent fold pair in that dominates the quartzite ridgeline. This is Photo profile PP1. For location see Figure 53.

Figure 58: The Spires range from False Dome looking south towards White Pyramid and Southern Cone with The Pleiades background (photo upper left). b) View showing the peaks along the Spires. b) Annotated version of (a) with So/Sm formline interpretation shown by the white lines. This is Photo profile PP2. For location see Figure 53. (Photo credit: Becca Lunnon, rockmonkeyadventures)

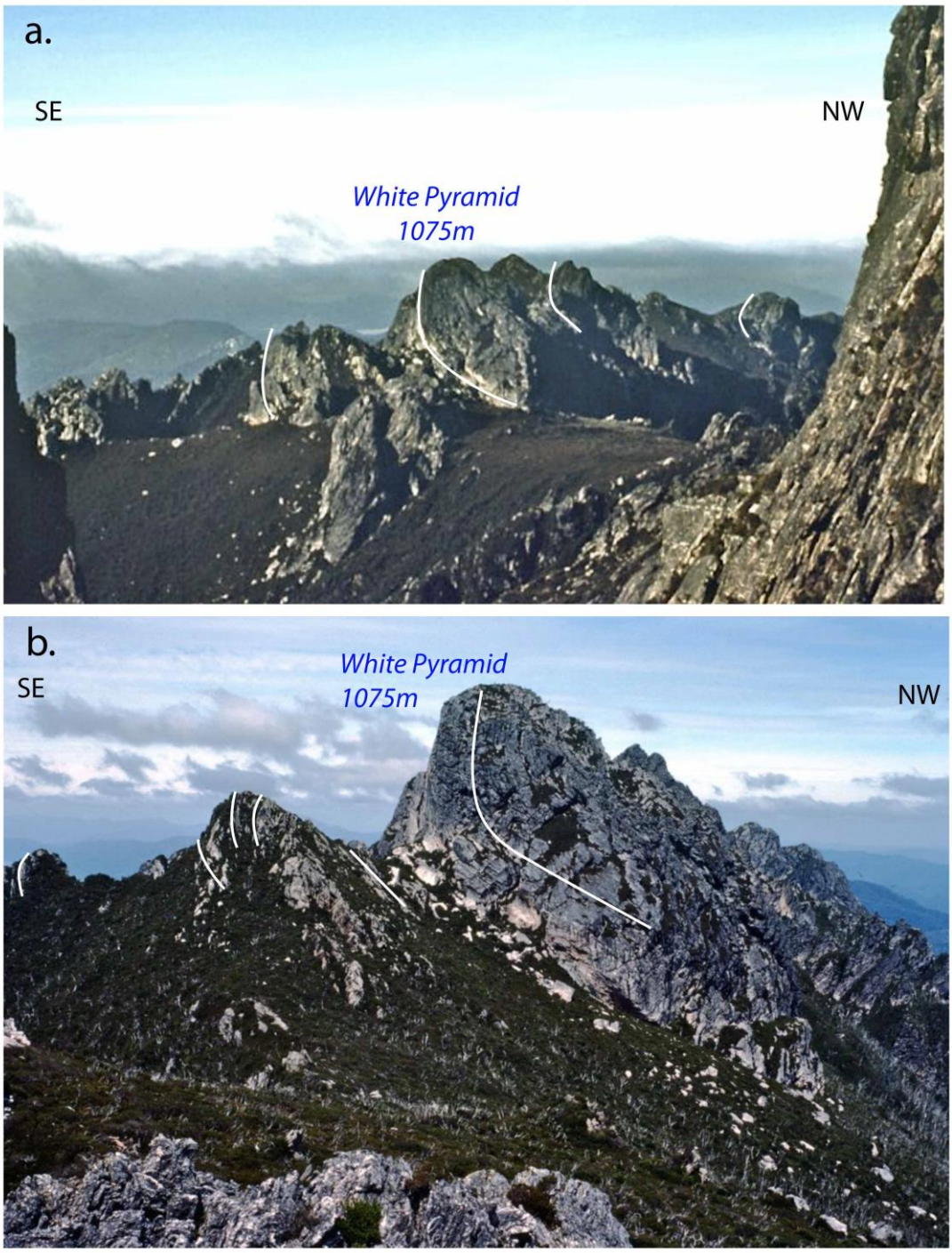

Figure 59: Views of White Pyramid showing east-closing recumbent macro-isoclinal fold hinge. a) View of White Pyramid from the Flame. b) View of White Pyramid looking south along the Spires ridgeline. This is Photo profile 2. For location see Figure 53. (Photo Credits: David Noble)

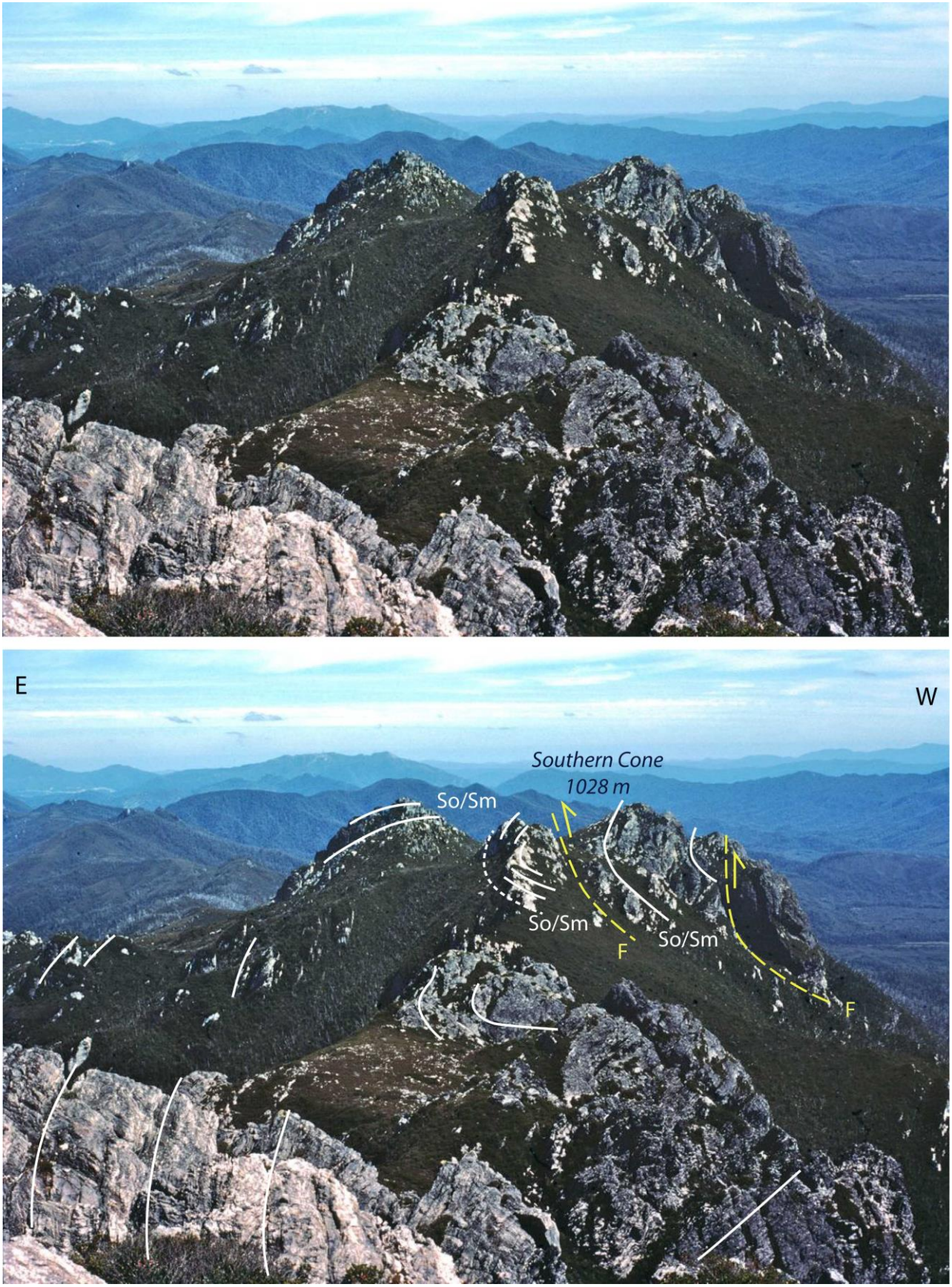

Figure 60: Views of Southern Cone from White Pyramid showing east-closing recumbent macro-isoclinal fold hinge. a) and b) Non-annotated and annotated photographs of Southern Cone showing the faulted, partial hinge major east-closing recumbent macro-fold. The interpreted faults are reverse faults with west-over-east movement sense. This is Photo profile PP3. For location see Figure 53. (Photo Credits: David Noble)

The fold pair is also partially preserved across strike through the east-west trending ridgeline that encompasses Shining Mountain, Conical Mountain and Mount Curly (Figures 54 and 67). In this section the upper east-closing fold is cut and offset by a set of west-dipping thrust-reverse faults.

5. Shining Mountain-Conical Mountain Ridgeline

Shining Mountain consists of an elongated, northeast-trending, tadpole-like outcrop of quartzite (Figures 54 and 61). The southern tail of the quartzite "tadpole" contains a prominent southwest plunging hinge of the early fold that shows the bedding So/Sm formline traces truncated or discontinuous against the enveloping mixed layer quartzite-phyllite (Pqpc) sequence (inset, Figure 61). The structure of the Shining Mountain area is presented in the body of Geological Survey Publication 14 (see Section 5.2.2).

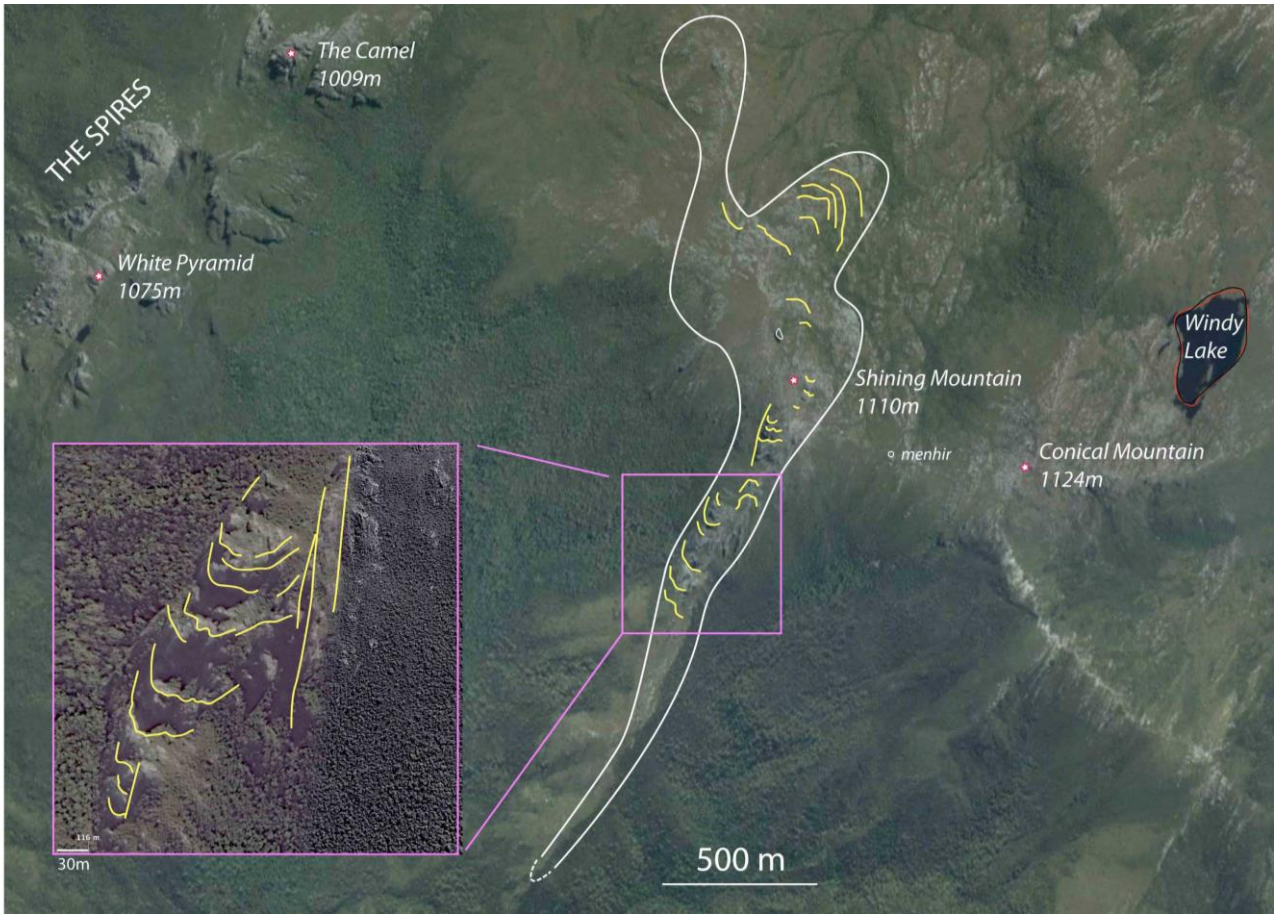

Figure 61: Structure of Shining Mountain-Conical Mountain ridgeline showing a structural formline interpretation of ridgeline. The enlargement (bottom left) shows the plunging fold nose within the attenuated tail of the folded quartzite. Formlines in So/Sm are shown by the yellow line traces. The white line is the quartzite outcrop trace taken from the Huntley 1:50,000 map sheet. The location of the menhir (Figure 62) is shown by the white circle on the ridgeline between Shining and Conical Mountains.

Figure 62. Quartzite menhir on the ridgeline between Conical Mountain and Shining Mountain. The pillar is the nose of a steeply plunging fold. The darker ridgeline on the photo right (middleground) is the plunging fold nose within the tadpole-like tail of the quartzite that makes up Shining Mountain (see Figure 61). (Photo credit: Pat Toohey)

6. Mt Curly Ridge

The Mt Curly region shows two, elongated, northeast-trending, spaced, en echelon bodies of quartzite that define two ridgelines separated by a valley low in pelite (Pl) (Figures 63 and 64). The overall structural geometry of the Mt Curly region was determined from bushwalker photographs (Figures 65, 66, 67, 68 and 69). Photo profiles were constructed (Figure 70) and the axial surface traces fitted to the Google imagery and the Huntley sheet geological map base (Figure 63).

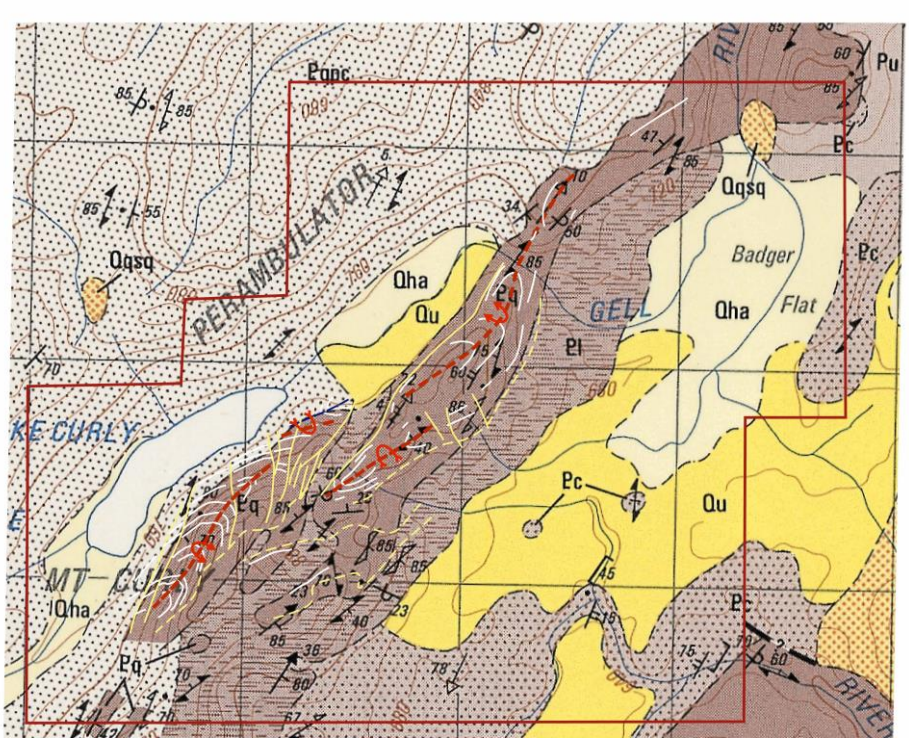

Figure 63: Structural interpretation superimposed on the Huntley 1:50,00 map sheet base. The axial surface traces of the major recumbent isoclinal folds are shown by the red dashed line traces. Formlines in So/Sm are shown by the white line traces and faults shown by the yellow line traces. Grid squares are 1km. The red rectangular outline is the position of the satellite photo collage shown in Figure 64.

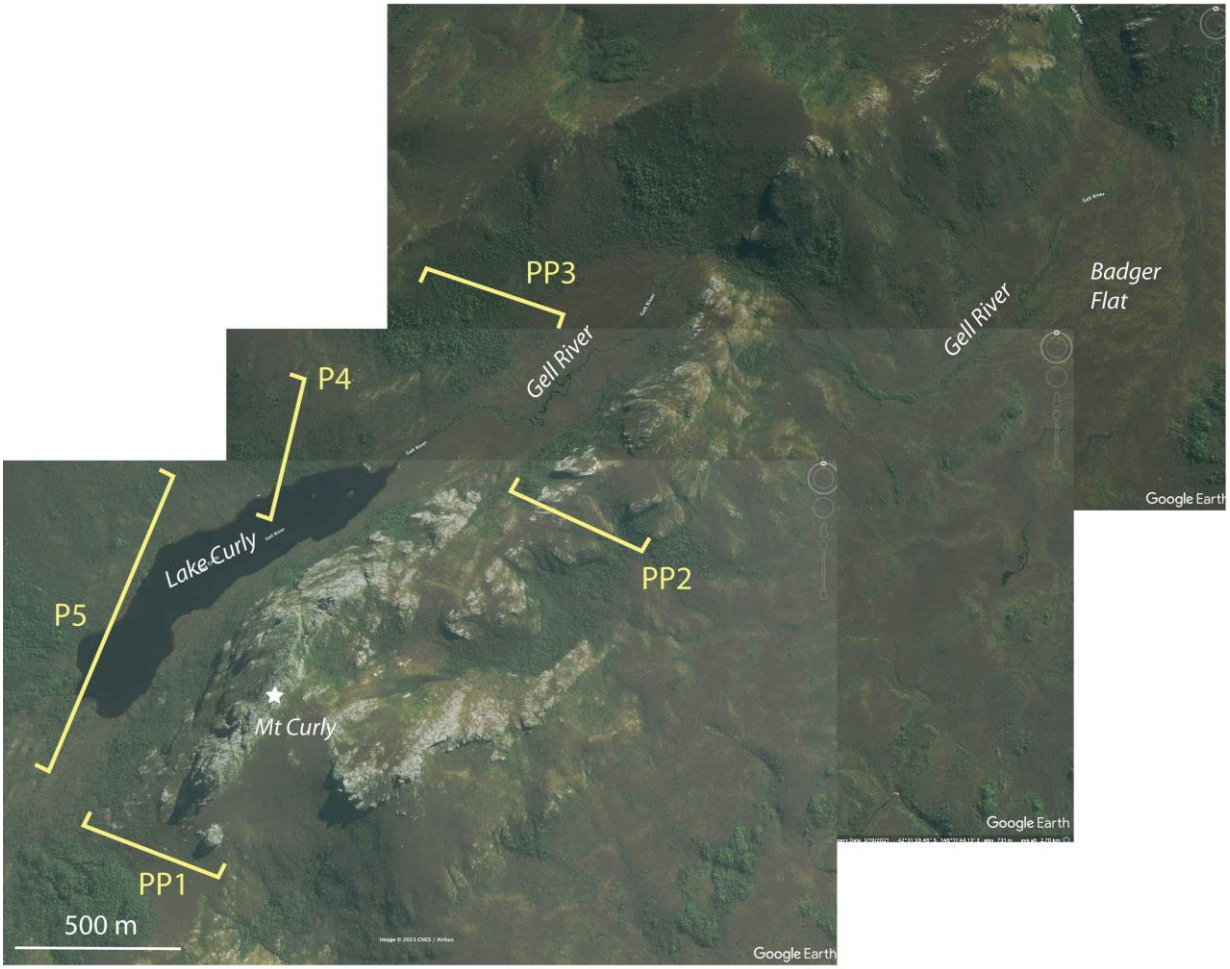

Figure 64: Google satellite image showing geographic elements and the positions of photo profiles designated PP1 (Figure 65), PP2 (Figure 66) and PP3 (Figure 67). P4 (Figure 68) and P5 (Figure 69) are oblique photographs of the Mt Curly ridgeline used in the map scale structural interpretation.

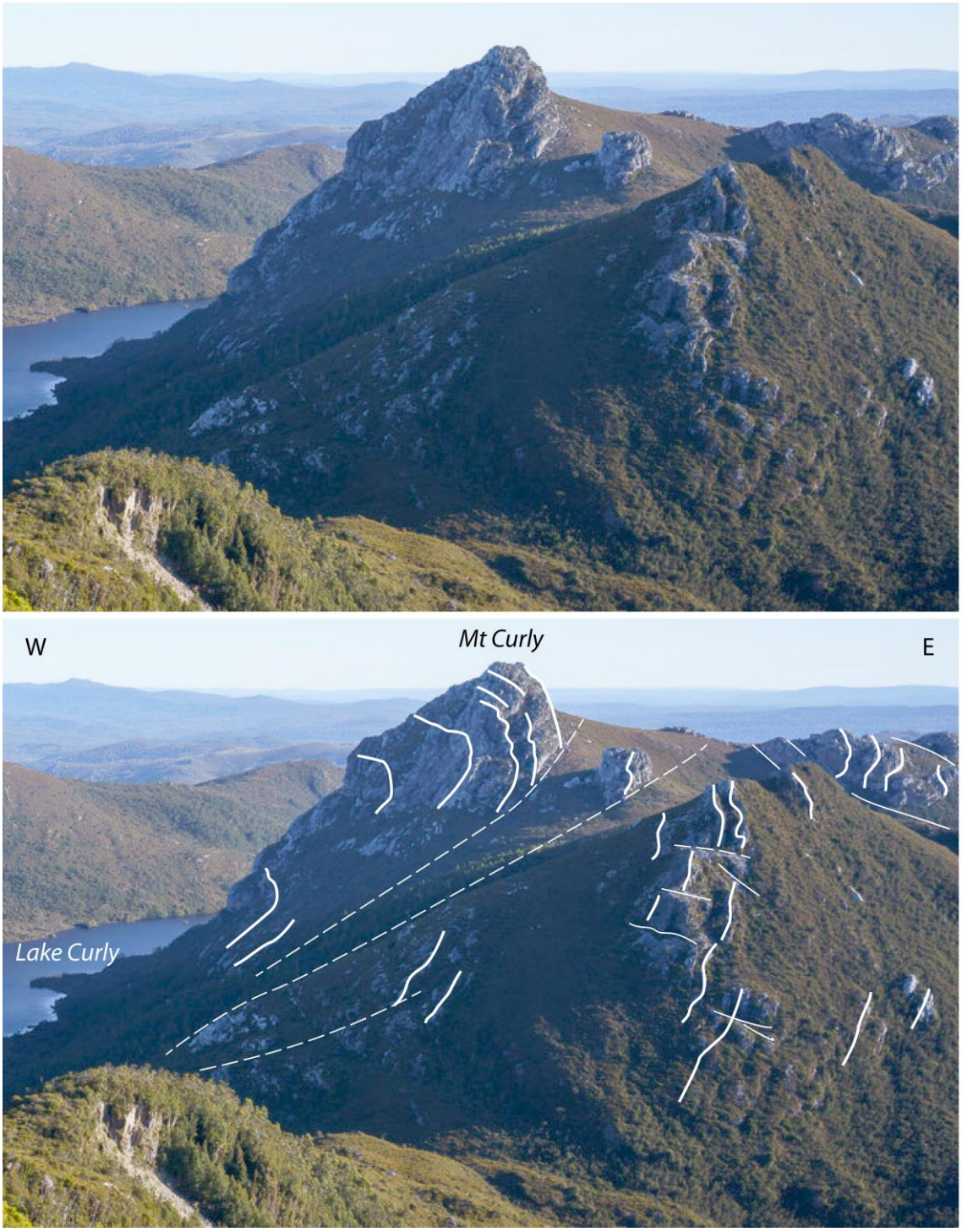

Figure 65: South end of Mt Curly ridgeline showing an east-closing macro-isoclinal fold cut by west-dipping oblique-slip faults. Photo profile PP1 with location shown in Figure 64. (Photo Credit: Grant Dixon)

Figure 66: View to the northeast along the northern continuation the Mt Curly ridgeline with Gell Valley on the right. a) and b) are non-annotated and annotated photographs with structural interpretation respectively. The north end shows a west-closing macro-isoclinal fold. The highest point of the ridge shows part preservation of the complementary east-closing hinge. This photo profile PP2 with location shown in Figure 64. (Photo Credit: Grant Dixon).

Figure 67: View of the north end of Mt Curly ridgeline looking northwest along Lake Curly taken from Perambulator Ridge. Photo profile PP3 (see Figure 64 for location). The upper part of the ridgeline shows an east-closing macro-isoclinal fold, with a west-closing macro-fold in the lower part. (Photo Credit: David Noble).

Figure 68: View of northwest face of the Mt Curly ridgeline taken from Conical Mountain showing recumbent isoclinal folds in So/Sm (white line traces). Photo Profile P4 (see Figure 64 for location). (Photo Credit: David Noble).

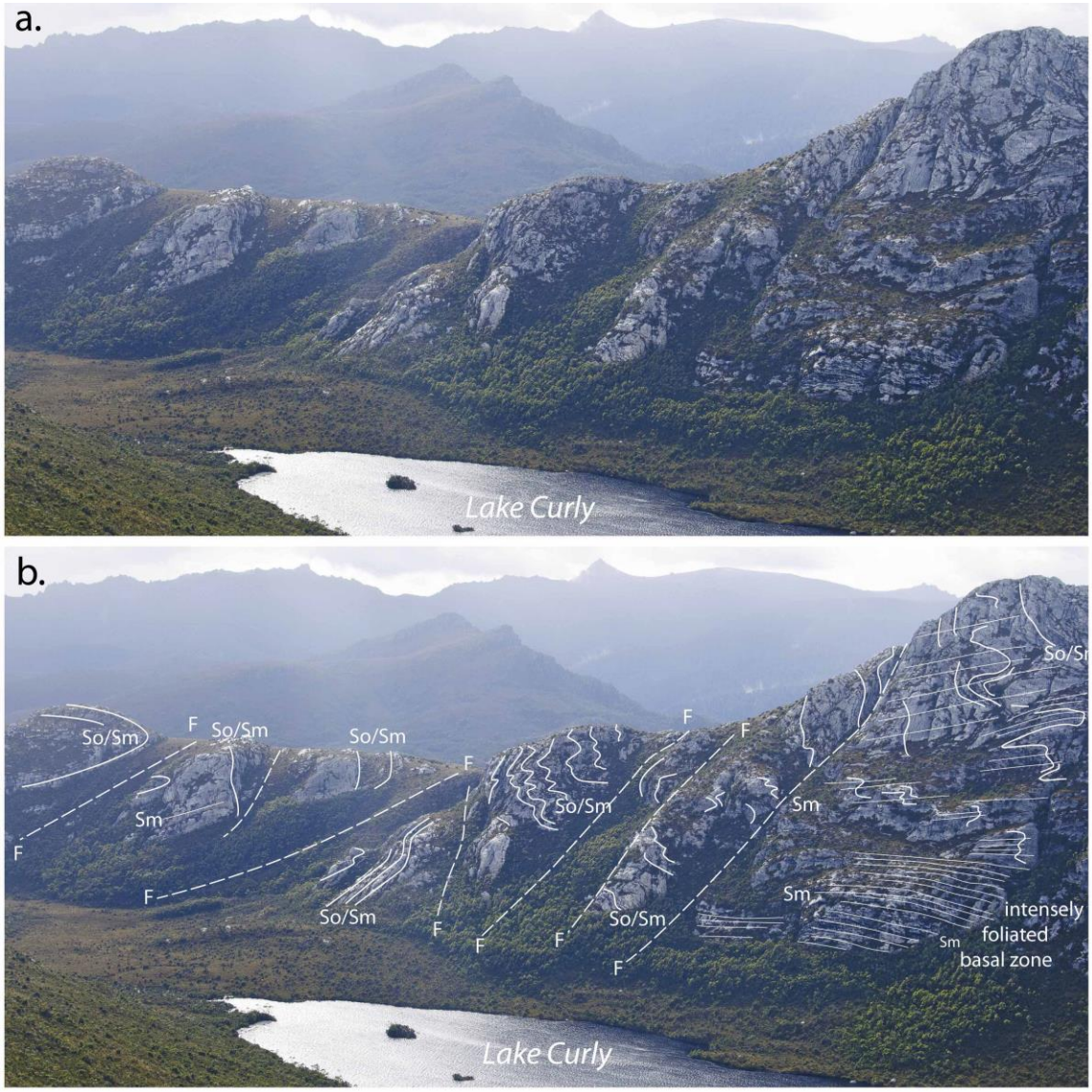

Figure 69: View of the Mt Curly ridgeline looking to the east with Lake Curly in the foreground. a) and b)are non-annotated and annotated photos respectively. The photo shows an oblique view of the macro-folds in the quartzite that defines the ridgeline. On the photo right a west-closing recumbent macro-fold intersects the main ridgeline showing symmetrical, second and third order folds with W-symmetry in the fold hinge. On the fault-offset, trailing part of the ridgeline (photo left) an oblique intersection of the complementary east-closing, recumbent, isoclinal macro-fold can be seen. The basal part of the quartzite (photo bottom right) exposes an intensely foliated zone. This is Photo Profile 5 with location shown in Figure 64. (Photo credit: Grant Dixon)

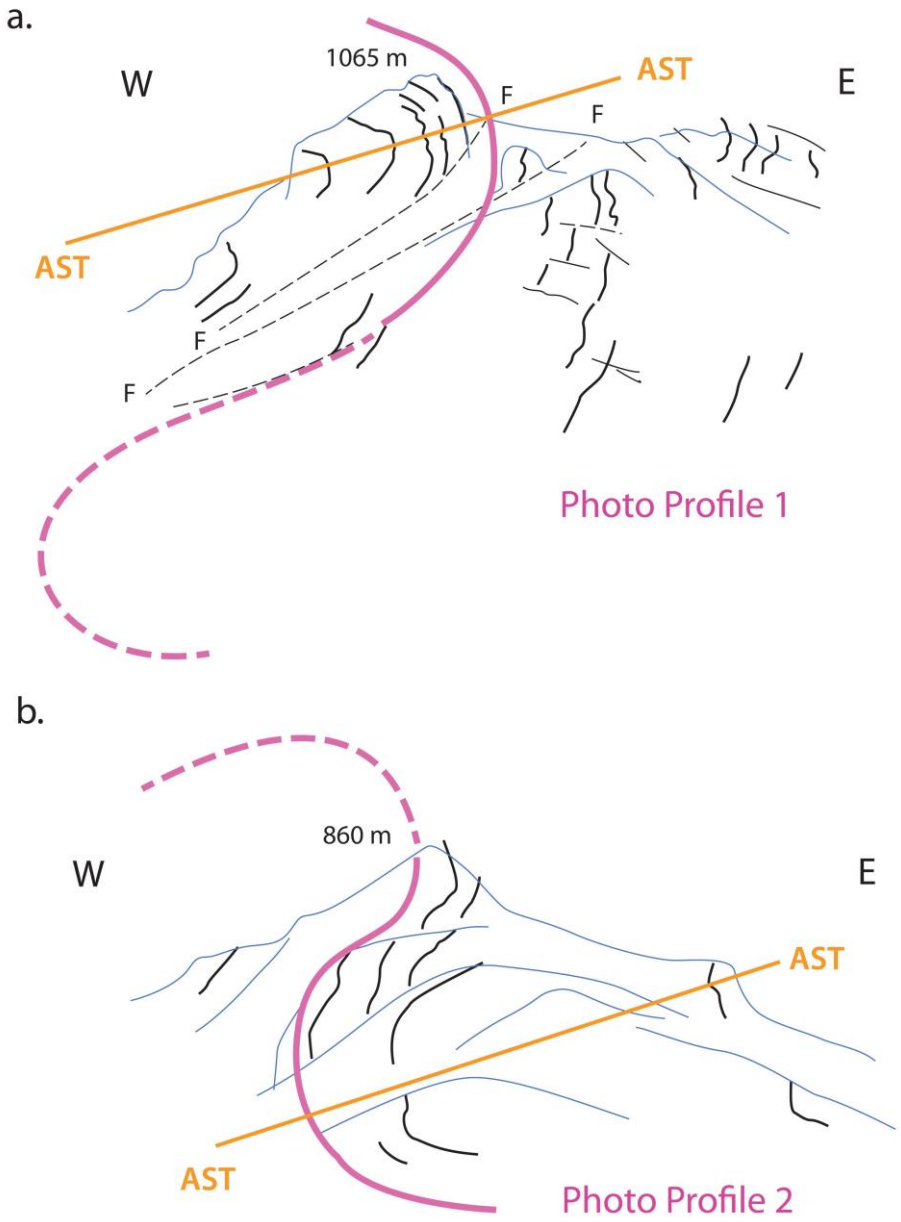

Figure 70: Photo profiles across the Mt Curly ridgeline showing the relicts of the partially preserved, asymmetric , Z-vergent (looking north) recumbent, isoclinal macro-fold pair. a) Photo profile 1: south end of the Mt Curly ridgeline showing the structurally higher, east-closing macro-fold in the highest part of the ridgeline. b) Photo profile 2: north end of the Mt Curly ridgeline showing the structurally lowest west-closing macro-fold, with the upper east-closing hinge eroded. For photo profile locations see Figure 64.

7. Innes High Rocky

Innes High Rocky is an elevated part of the intermediate ridgeline west of The Spires (Figure 71). The ridgeline is dominated by an apparent south-closing, recumbent macro-fold hinge (Figures 71 and 72). Outcrop traces shown as formlines in Figure 71 suggest there is a complementary west- or northwest-closing macro-fold hinge to the southwest (Figure 72). Mesoscopic recumbent folds (Figures 73b, c) on the summit of Innes High Rocky show gentle plunges east or west plunges (Figure 73a).

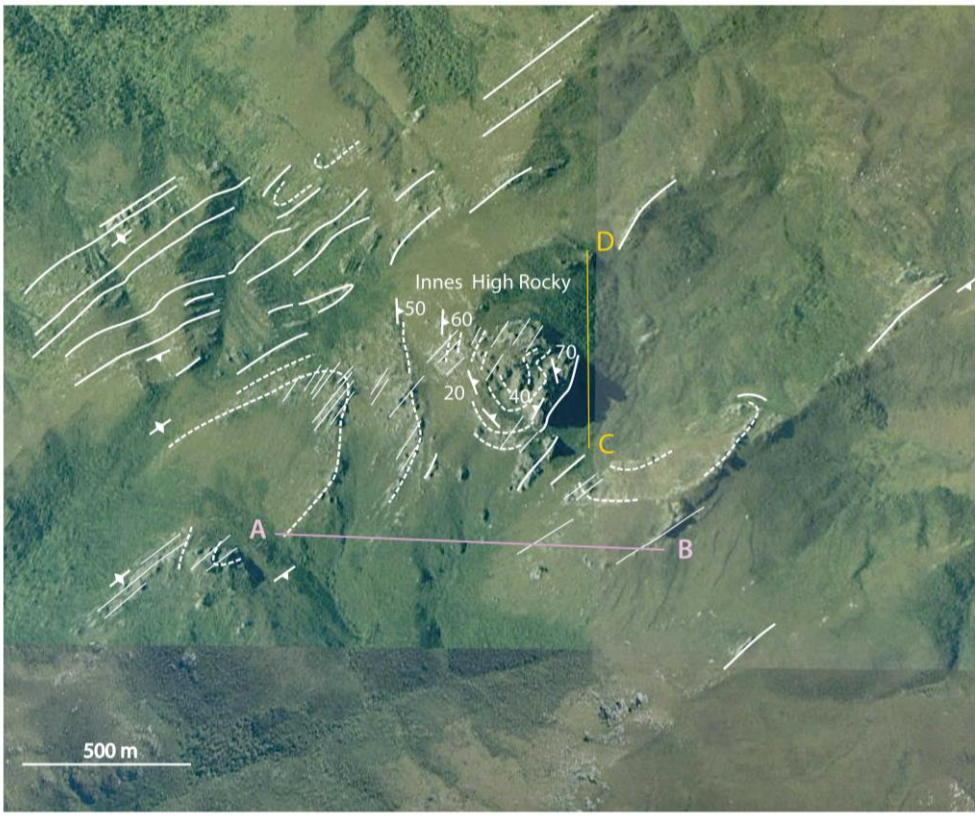

Figure 71: Formline interpretation of the Innes High Rocky region with So/Sm outcrop traces shown by the white lines. Profile A-B is photo profile shown in Figure 72a taken from Pokana Peak. Profile C-D is photo profile shown in Figure 72b of the eastern face of Innes High Rocky.

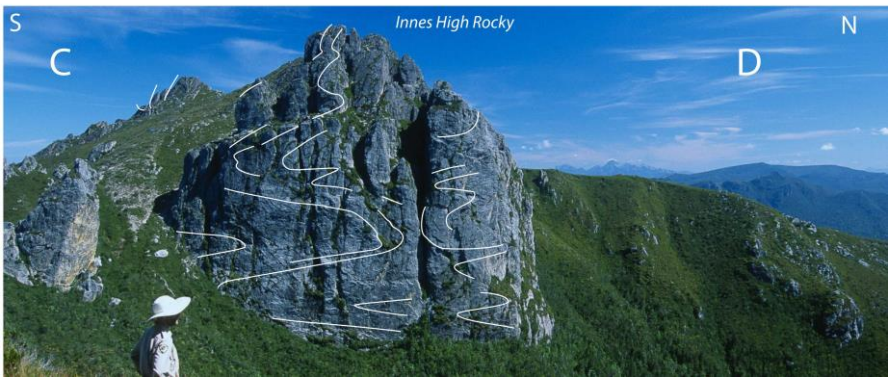

Figure 72: Views of Innes High Rocky. a) Photo Proflie A-B taken from Pokana Peak suggests an east- or south-closing macro-fold hinge (Photo Credit: Mowser.com).
b) Photo Profile C-D of eastern face of Innes High Rocky with intersection of an apparent south-closing macro-fold hinge with more complex internal folding (Photo Credit: Grant Dixon). For location of the photo profiles see Figure 71.

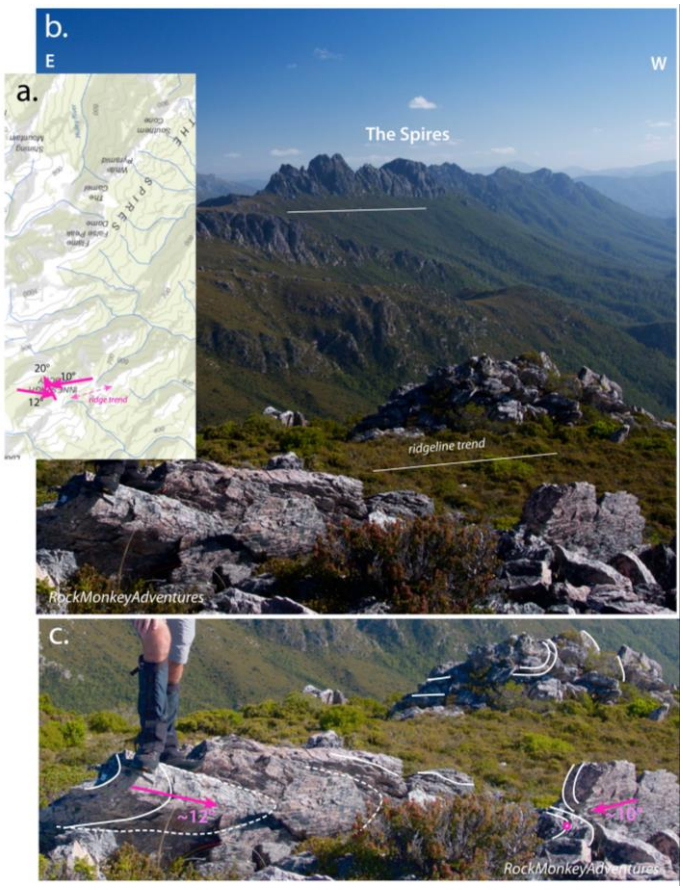

Figure 73: Mesoscopic folds on Innes High Rocky. a) ListMap topographic map inverted to show the photo direction in (b). View of the Spires from Innes High Rocky. c) Recumbent to inclined plunging mesoscopic isoclinal folds on Innes High Rocky. Fold plunges shown by the pink arrows. Formlines in So/Sm shown by the white line traces. (photo credits: Becca Lunnon, rockmonkeyadventures)

8. The Twelvetrees Range

All structural data and interpretations of the Twelvetrees Range are presented in the body of Geological Survey Publication 14. These data were collected by the authors on the track traverse to the telecommunication tower on the southern end of the Twelvetrees Range.

9. The Pleiades- Junction Range

All structural data and interpretations of the The Pleiades-Junction Range-North Star macrofold are presented in the body of Geological Survey Publication 14. The interpretation is based on the mapping, structural data and interpretations by Marcus McClenaghan, Jean McClenaghan and Nic Turner in the Huntley Explanatory Report (Brown et al., 1989). A summary of their work is presented below. It provides a synthesis of the structures and structural relationships established during the Tasmanian Geological Survey mapping of the Huntley and Pedder sheets (Brown et al., 1989; Calver et al., 1990)

9.1 The Pleiades

The structural character of the Pleiades (McClenaghan in Brown et al., 1989, p.75-79) consists of:

1) Uniformly coarse-grained massive, current bedded quartzites that have a single axial planar foliation to minor folds with hinges trending and plunging north-east and axial planes dipping northwest.

2) A series of major folds of similar attitude along the eastern side of the range.

3) The dominant foliation in the quartzites is a crenulation cleavage S2, whereas in the phyllites it is a crenulation cleavage S3, such that the S1 foliation is almost entirely obliterated.

McClenaghan in Brown et al. (1989, p.75-79) constructed 1) a structural domain map with stereonets of the included structural elements for each domain (Figure 74), and 2) a series of down plunge profiles that show upper and lower quartzites and phyllite members that represent the limbs of the isoclinal macrofolds (Figure 75).

The combined stereonets (Figure 74) show:
1) Domains P1, P2, P3, P10 and P11 (Figure 74, e, f, g, c and d) in the southwest part of the macrofold (western limb) have north-south foliation trends and overall north plunge for mesoscopic folds.
2) The remaining domains on the eastern macrofold limb have more northeast S2 foliation trends associated with an overall north-northeast to northeast fold plunge (Figures 74, h, i, j, k, l, m, n, o, p, q, a and b). This matches the overall swing in map pattern from north-south trending in the south to northeast-trending towards North Star.
3) The quartzite band along the western macrofold limb in Domain 1 shows approximately coplanar S2 and S3 foliations, but F2 fold axes have marked, sheath-like plunge variations within the dominant S2 foliation. The F3 fold axes are north-plunging (Figure 74e).
4) Mesoscopic F3 folds fold the S2 foliation (Domains P2, P5, P6, P8, P9, P12, P13, P15, P16, P17 and P18, Figures 74, f, h, i, k, b, l, m, n, p, q and a) and show trends that match the overall macro-folds.
5) Domain 2 in the core of the macrofold shows distinct coaxial F2 and F3 mesoscopic folding (Figure 74f), whereas on the eastern limb in Domains 4 and 5 the F2 macrofolds plunge northeast and the F3 folds have north plunge (Figures 74, i and j).
6) The macrofolds on the eastern limb involving tracts of overturned bedding are F2 folds (Domains 6 and 8, Figures 74h and k).

These outcrop relationships indicate that the major, north-south trending folds that control the geometry of the Junction Range-Pleiades sheath-like macrofold (Figure 74) are F3 folds. These F3 also refold the larger overturned F2 folds that dominate the quartzite of the eastern, structurally lower fold limb.

The grouped constructed profiles from North Star to the south end of the Pleiades (Figure 75) show 1) a quartzite layer bounded by an apparent upper and lower phyllite layer along the eastern side of the range (Figures 75 e, f and g), and 2) a Z-vergent, asymmetric, recumbent isoclinal macro-fold pair in the northern North Star down plunge profile (Figure 75b). The fold pair becomes progressively faulted and refolded along the Pleiades range (Figures 75c-g). The Pleiades profiles suggest that these folds are F2 folds with an axial surface S2 crenulation cleavage.

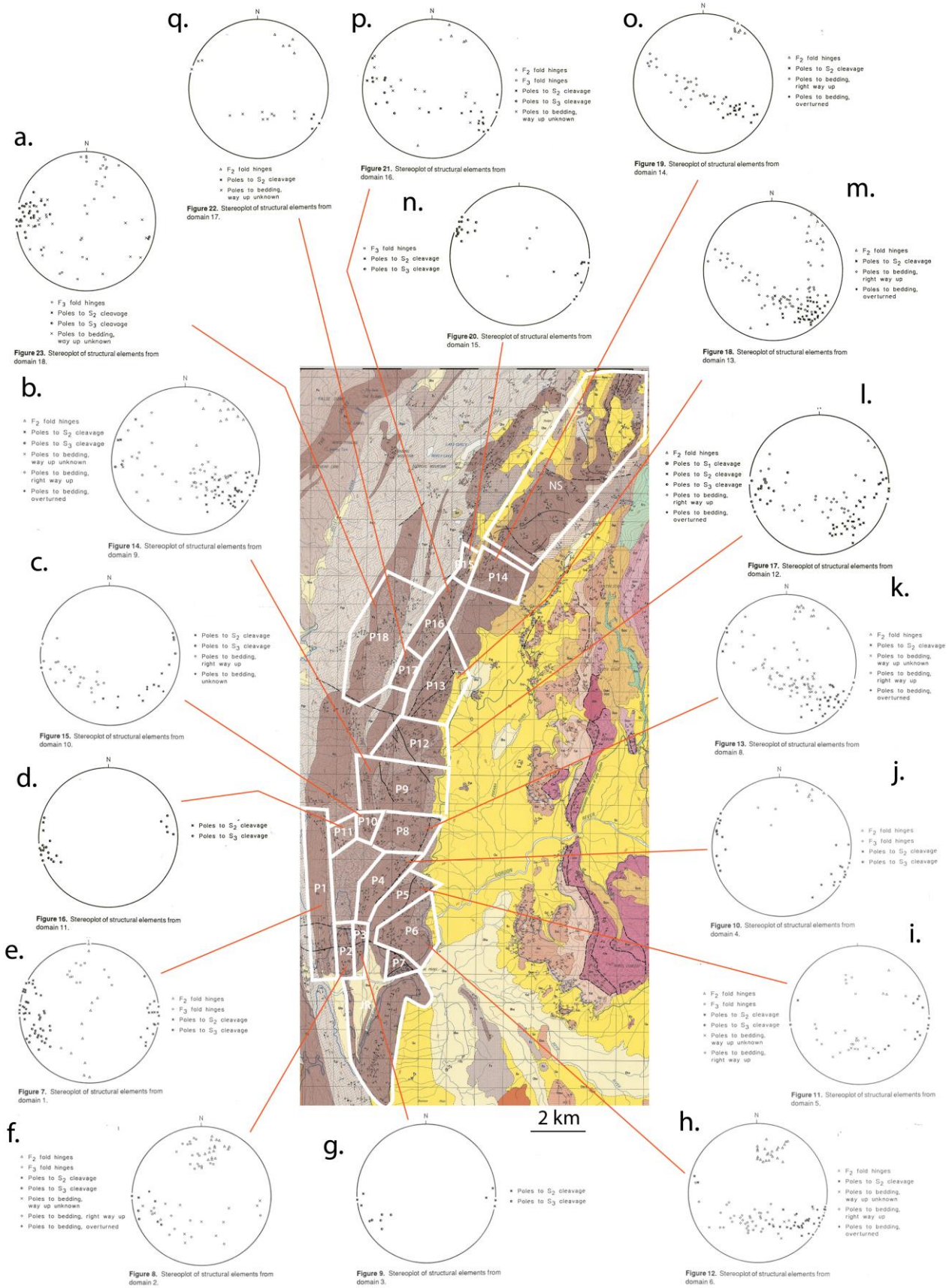

Figure 74: The Junction Range-Pleiades macrofold domain and stereonet map based on McClegnahan (1989, figs. 6 to 23 in Brown et al., 1989). Base for outlined domains (white boxed areas) is the Huntley 1:50,000 map sheet (Brown et al., 1982).

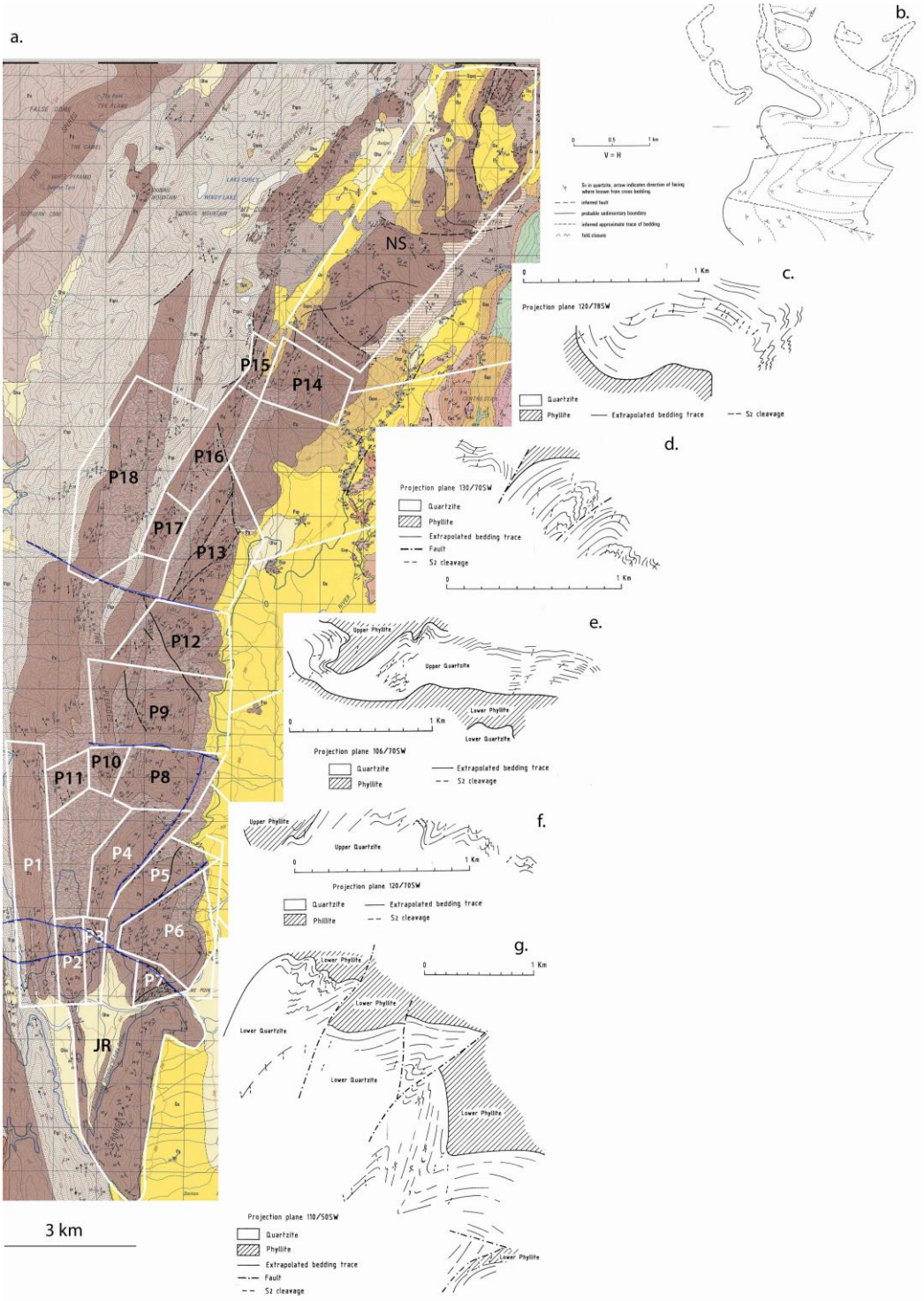

Figure 75: Previously published down plunge structural profiles for the Pleiades range and North Star (Brown et al., 1989). a) Pleiades part of Huntley 1:50,000 map sheet (Brown, et al., 1982) with domains and domain boundaries. JR: Junction Range. P1-P18: Pleiades domains. NS: North Star. b) North Star profile (fig.34, Turner 1989a). c) Profile P14 (Pleiades Domain 14) structural profile (fig.28, McClegnahan in Brown et al., 1989). d) Profile P13 (Pleiades Domain 13) structural profile (fig.27, McClegnahan in Brown et al., 1989). e) Profile P9 (Pleiades Domain 9) structural profile (fig.26, McClegnahan in Brown et al., 1989). f) Profile P8 (Pleiades Domain 8) structural profile (fig.25, McClegnahan in Brown et al., 1989). g) Profile P4-7 (Pleiades Domains 4-7) structural profile (fig.24, McClegnahan in Brown et al., 1989).

9.2 The Junction Range (western ridge)

Quartzite of the Junction Range occupies the V-shaped, west-closing Junction-Range Pleiades macrofold hinge (Figure 76). The Junction Range hinge area has coplanar S1 and S2 structural elements related to similarly oriented 1) mesoscopic folds F1 folds (axial surface

S1 cleavage) with thickened apices, variable steep plunges (fig.29, Turner 1989a) and fold dihedral angles of 20 to 30°, and 2) flattened F2 folds (S2 crenulation cleavage as axial surface) with larger dihedral angles (~80°) and predominant north to northwest plunges (fig. 30, Turner, 1989a). Turner also discussed the possibility of two coaxial and coplanar fold phases (Turner, 1989b, p.80). Shape ratios of elongate quartz grains within S1 are 3:1. These occur in mica-rich quartzites due largely to dissolution on grain margins sub-parallel to cleavage and mica beard growth at the ends of grains.

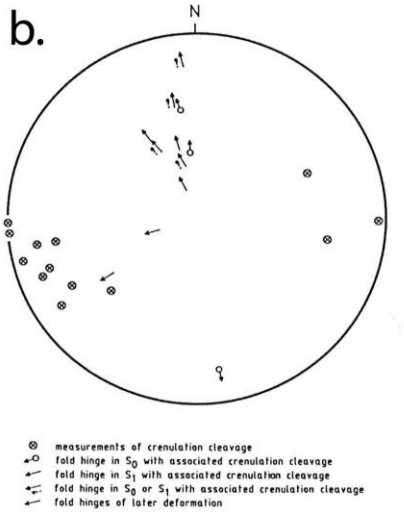

Figure 30. Lambert projection of measurements of orientation of crenulation cleavage in Pqp on Junction Range (west). Folds associated with crenulation cleavage and two minor cross-folds are also shown.

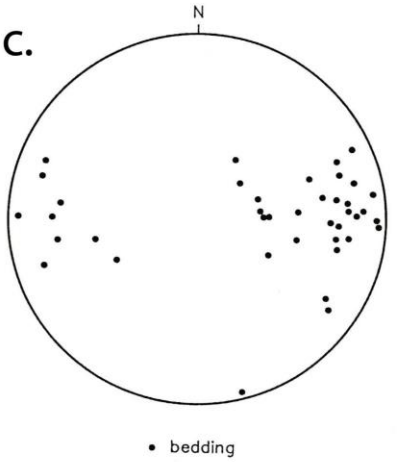

Figure 31. Lambert projection of measurement of bedding orientation in Pqp on Junction Range (west).

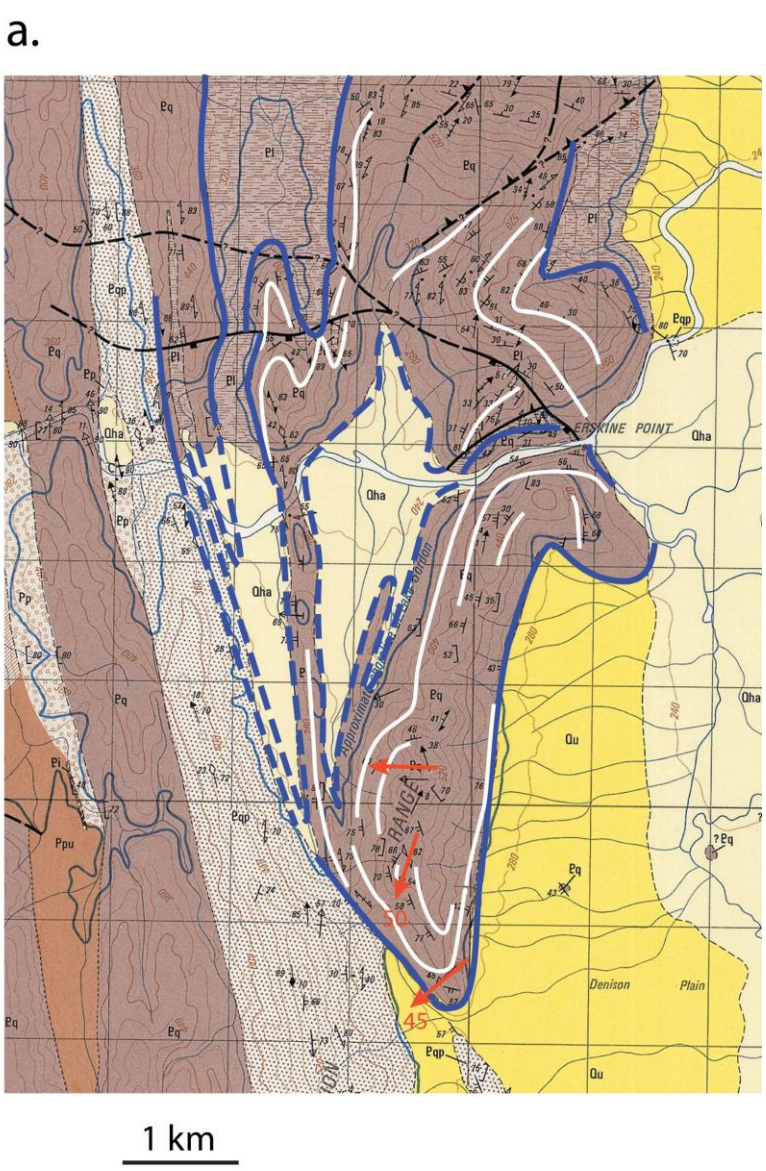

Figure 76: Structure of the Junction Range macrofold closure. a) Enlargement of the Huntley 1:50,000 map sheet (Brown et al., 1982). Geological contacts: blue line traces. So/Sm Formlines: white line traces. Red arrows: early F1 isocline fold plunges. b) Stereographic projection of crenulation cleavage (poles) and associated folds in So and S1 along the western quartzite. c) Stereographic projection of poles to bedding So along the western quartzite. Note the stereonets are from Turner (1989a, figs. 30 and 31).

9.3 The North Star Region

The North Star region is at the northern end of the Pleiades Range. Structural mapping by

Turner (1989b, p.75-79) delineated a faulted, recumbent, asymmetric, S-vergent isoclinal macro-fold pair (Figures 77 and 78). The hinge of the upper, east-closing recumbent fold crops out at North Star (Figure 79).

Analysis of the North Star region structure is presented as a series of stereonets (Figure 77) based on Turner (1989b, p. 80-88). These data collected by Turner show
1) Folding of both S1 and S2 cleavages about a northeast-plunging fold axis within the main quartzite band (subareas 1-4). The determined π axes are 28°/037° for S1 (Figure 77b) and 25°/043° for S2. (Figure 77d)
2) F1 and F2 axes are sub-parallel (i.e. coaxial refolding of F1 and F2 folding events) (Figure 77b, d).
3) Folding of the S2 cleavage in the underlying dolomite is also about a northeast plunging fold axis (35°/051°) (Figure 77f).
4) Quartzite outliers (subareas 7, 8), immediately west of the main quartzite band through North Star, appear as isolated pods at varying scales. These also show folding of bedding So, cleavages S1 and S2 about northeast-trending folds with a northeast plunge in subarea 8 (Figure 77e) and southwest plunge in subarea 7 (Figure 77c).
5) Folds in the Mt Curly area (subarea 6) have an axial surface S2 fabric that is not folded and is associated with a determined fold axis π of 23°/035° (Figure 77a).

This implies that the dominant folding event is F3 as both S1 and S2 fabrics are folded. The F3 folding is about a generalised, northeast plunging fold axis.

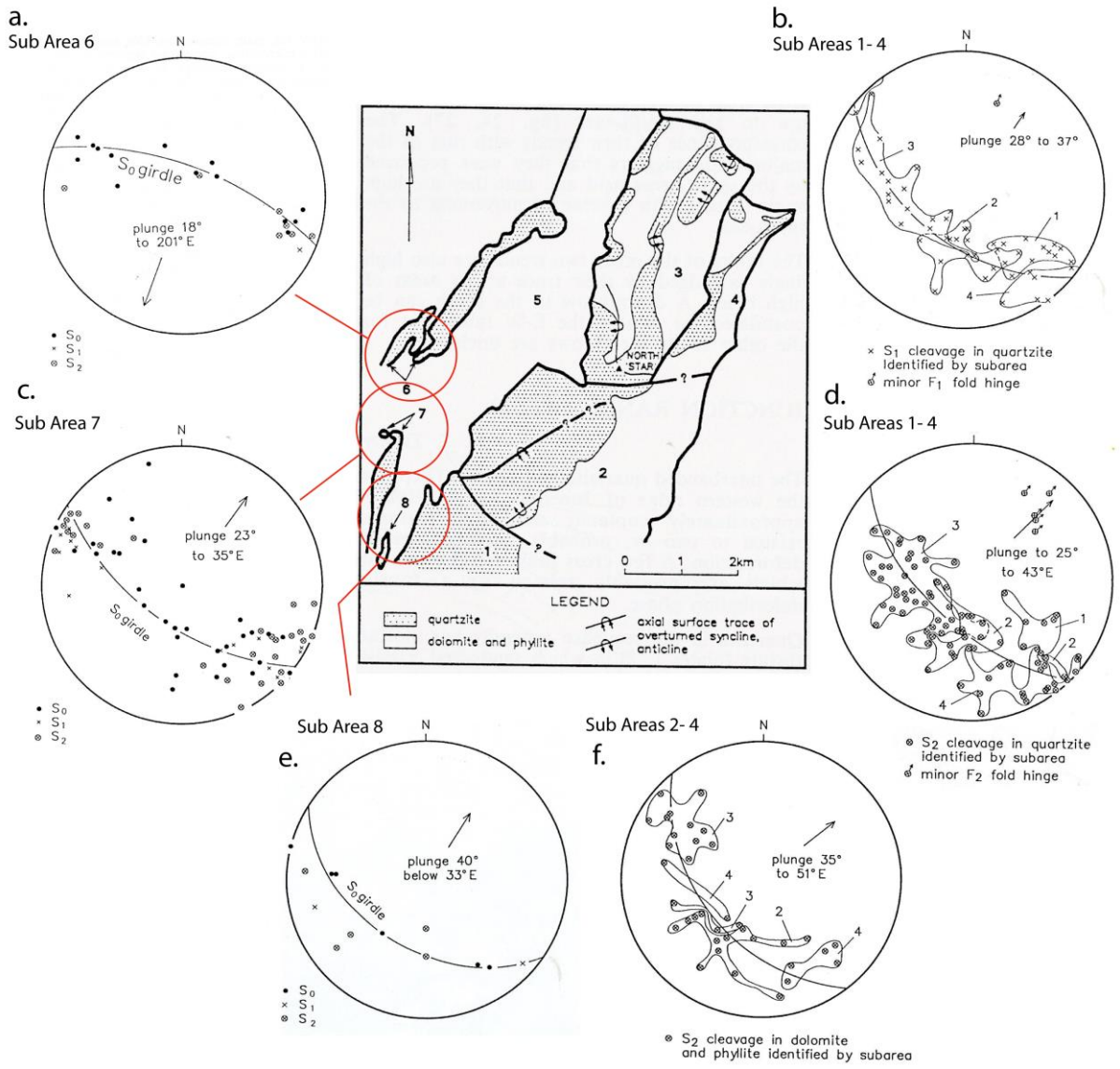

Figure 77: North Star summary map showing stereonets of structural elements within 8 domains. The diagram represents a combination of figures from Turner (1989b, figs 32, 33, 36, 37, 38, 41, 42 and 43).

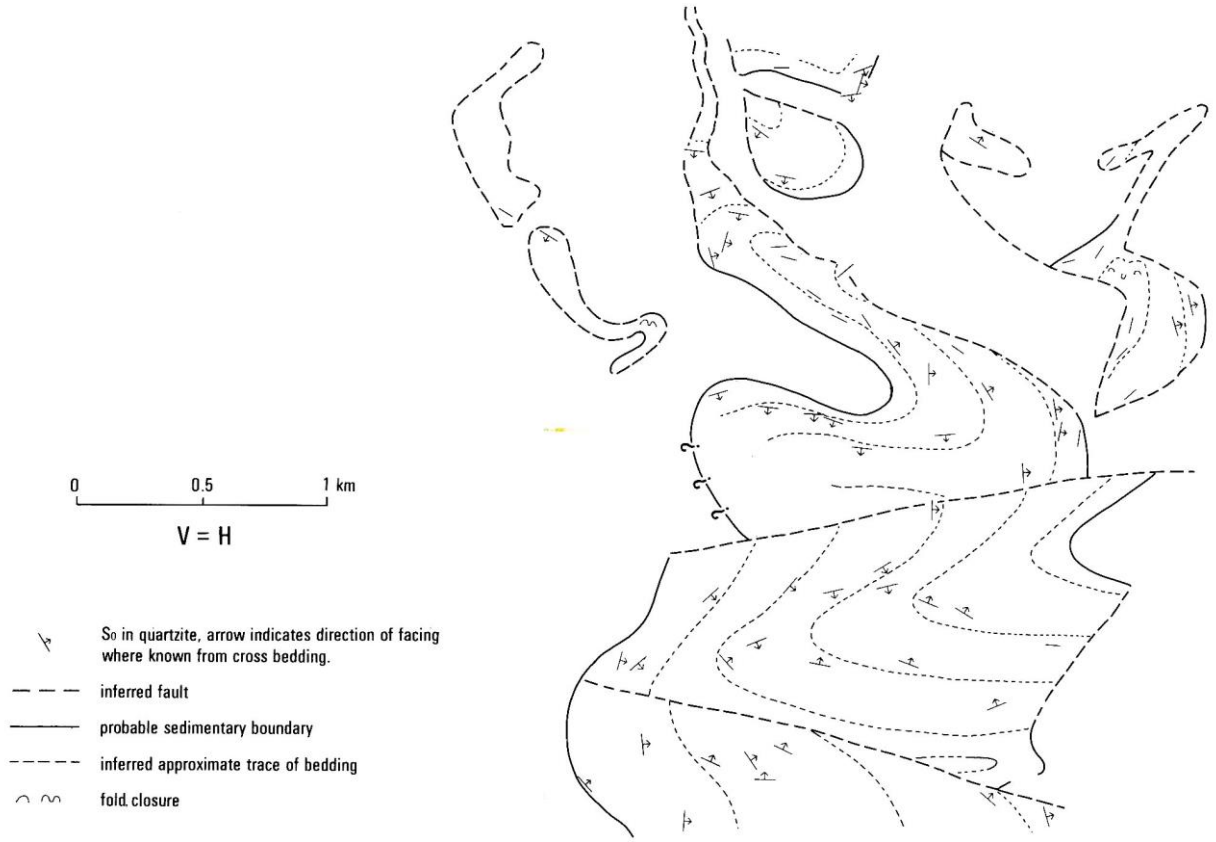

Figure 78: Down plunge axial projection of bedding and bedding traces (dotted line traces) in in quartzite of sub-areas 1-4 (see Figure 77) of the North Star region of the northern Pleiades range (fig.34, Turner, 1989b). Two cross cutting faults are shown by the dashed lines with apparent flat traces in the projection plane. The plane of projection strikes 125° and dips 70°SW.

Figure 79: Hinge of a recumbent east-closing macro-fold at North Star (plate 16, Turner, 1989b).

10. Trappes Hill-Hermit Narrows-Stillwater Hill-Mt Helder-Mt Cawthorn Area
Detailed description and structural interpretations of this region including the Barrier Islands and Mt Solitary are provided by M. P. McClenaghan in Calver et al. (1990, p. 62-78). The following Figures 80 and 81 show the lateral eastern terminations of the Frankland Range horsetail fault system and the marked refolding of the early macro-isoclinal folds.

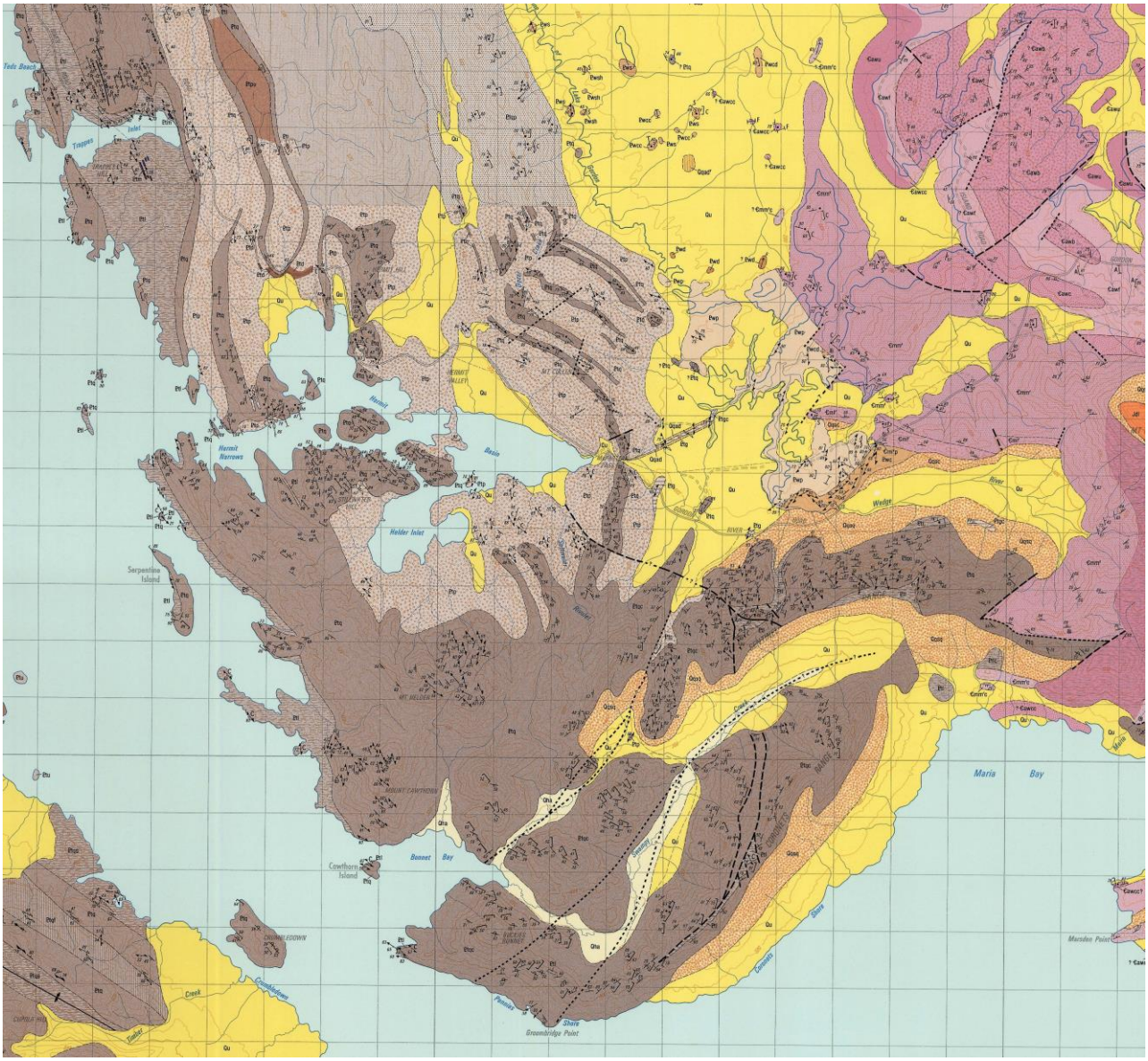

Figure 80: Segment of the Pedder 1:50,000 geological map sheet (Turner et al., 1985) showing the southern Twelvetrees Range and extending through Hermit Narrows to Mt Cawthorn, Buckies Bonnet, The Coronets and the Sentinel Range.

Features of the map area are: 1) The eastern shoreline of Lake Pedder consists largely of homoclinally west dipping quartzite passing into 2) an isoclinal syncline south of Bonnet Bay (Figures 80 and 81) (see fig. 53 in Calver et al., 1990), and 3) The pelite-quartzite contact south of Hermit Basin and Helder Inlet shows marked interdigitation due to refolding of the early isoclinal folds by north-trending F3 folds. This interdgitation and the associatioin early isoclinal folds can be observed in the Mount Cullen area (see Section 10.1).

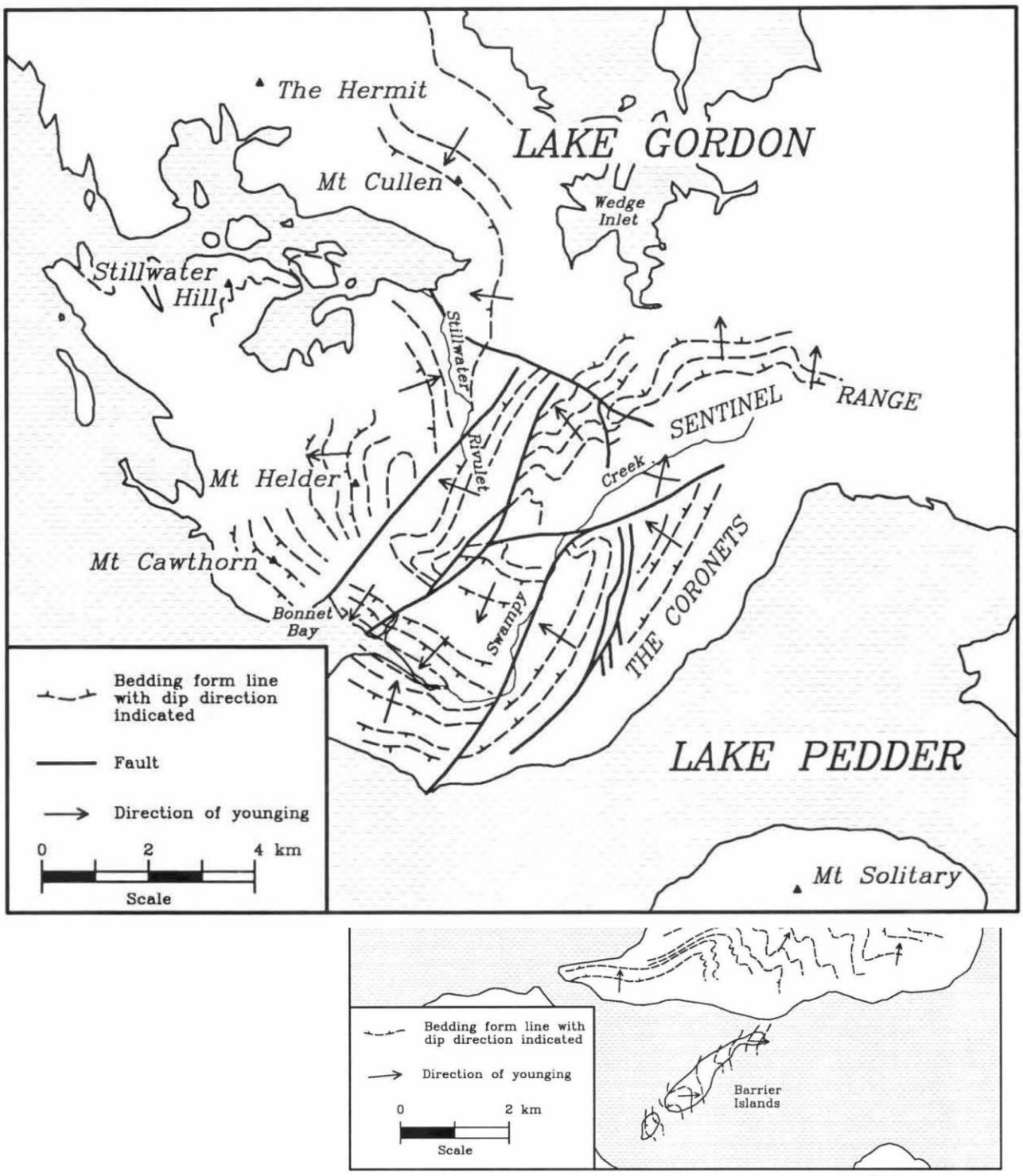

Figure 81: Formline map of the Sentinel Range-The Coronets including Mt Cawthorn, Mt Helder and Mt Solitary. (figs. 22 and 74 in Calver et al., 1990). The formline map shows fold interference between early F1/F2 isoclinal, formerly recumbent, macro-folds now approximately east-west trending refolded about approximately north-trending F3 folds.

The nature of the quartzite on this section of Lake Pedder shoreline is shown in Figure 82. It is characterised by alternating zones of flaggy quartzite and intensely foliated quartzite that are folded by upright tight to open F3 folds (see Port, 2023). The ridgelines around Mt Helder and Mt Cawthorn show homoclinally west dipping bedded, flaggy quartzite (Figures 83 and 84).

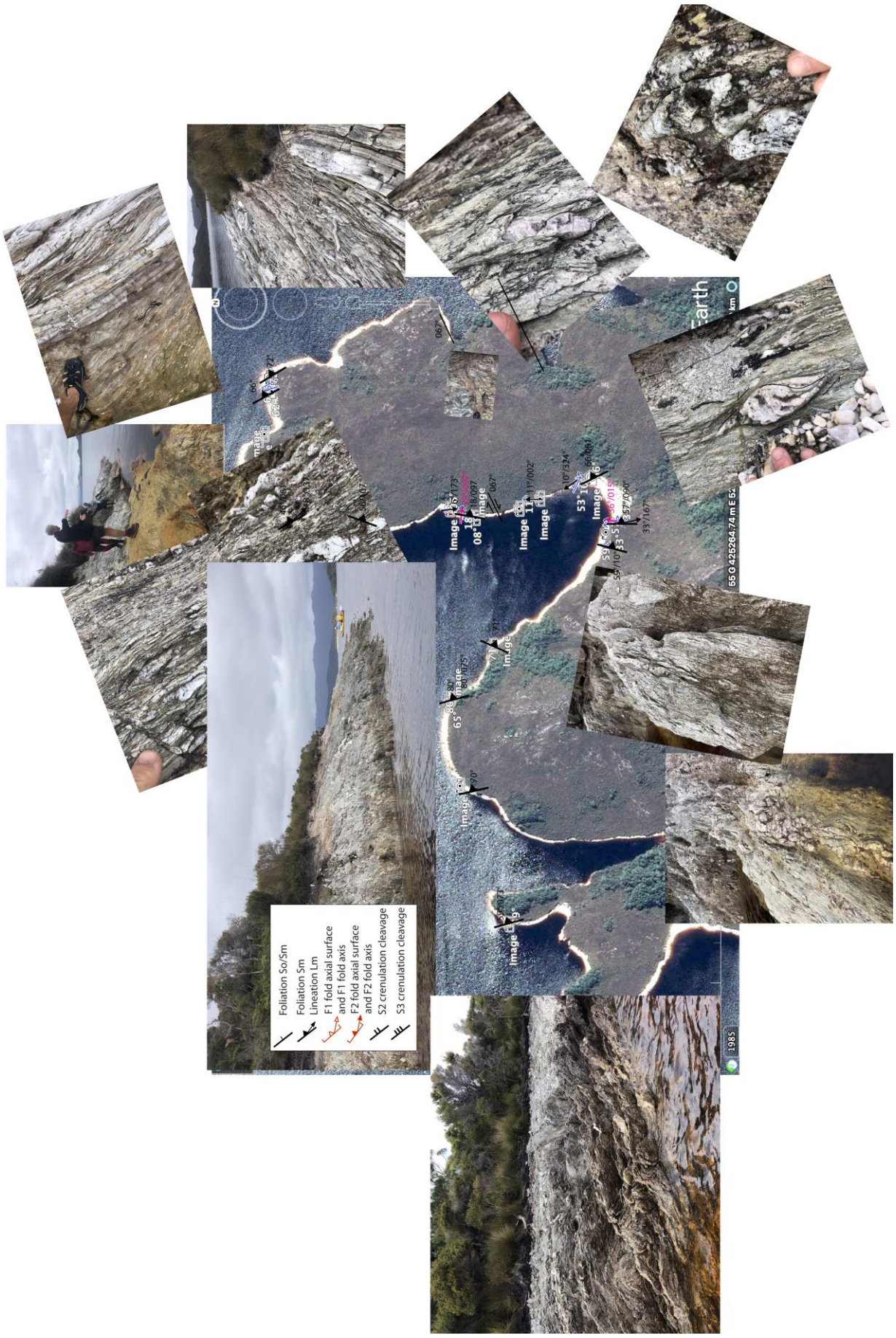

Figure 82: Photo compilation map of the Trappe Inlet area south of the Hermit Narrows. Structural data and photographs from Meffre unpublished (see Appendix 4).

Figure 83: View of Mt Helder (photo left) and Mt Cawthorn (photo right middle ground) showing homoclinally west-dipping quartzite. (Photo credit: Becca Lunnon, rockmonkeyadventures)

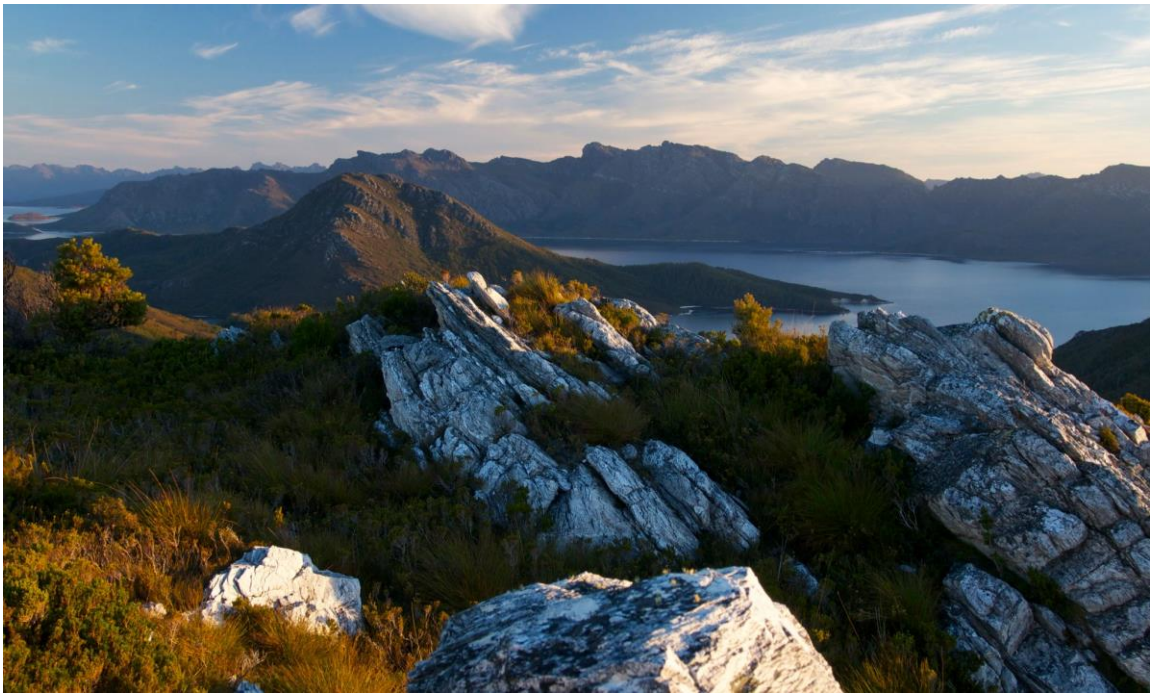

Figure 84: View of Mt Cawthorn with the southern Frankland Range on the horizon and thin-bedded quartzite in the foreground. (Photo credit: Becca Lunnon, rockmonkeyadventures)

10.1 The Hermit Hill-Mt Cullen-McPartlan Pass Area

The region shows a series of discontinuous quartzite bands with some as fold closures (map top centre, Figure 85). Unusual tapered forms, apparent fold closures and fold inter-

digitations characterise the Hermit Hill area (Figure 85). The quartzites show inflections changing from north-trending to northwest-trending through Mount Cullen to north-northwest trending through McPartlans Pass (Figures 86a and 86b). Internally the quartzites are folded (Figures 87b and 88b) with terminations as fold noses (Figures 87b and 87d).

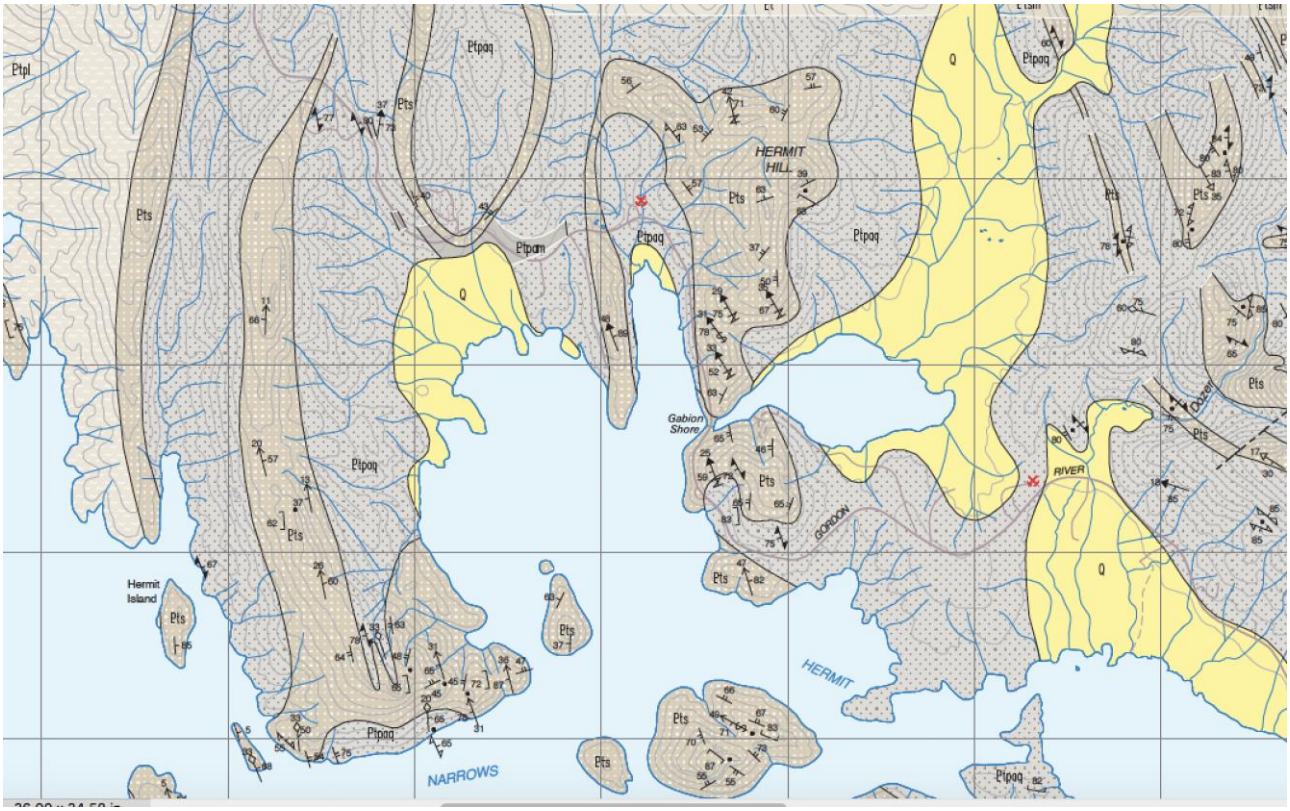

Figure 85: Hermit Hill region geological map (MacPartlan 25 map sheet, Mineral Resources Tasmania 1:25,000 digital atlas).

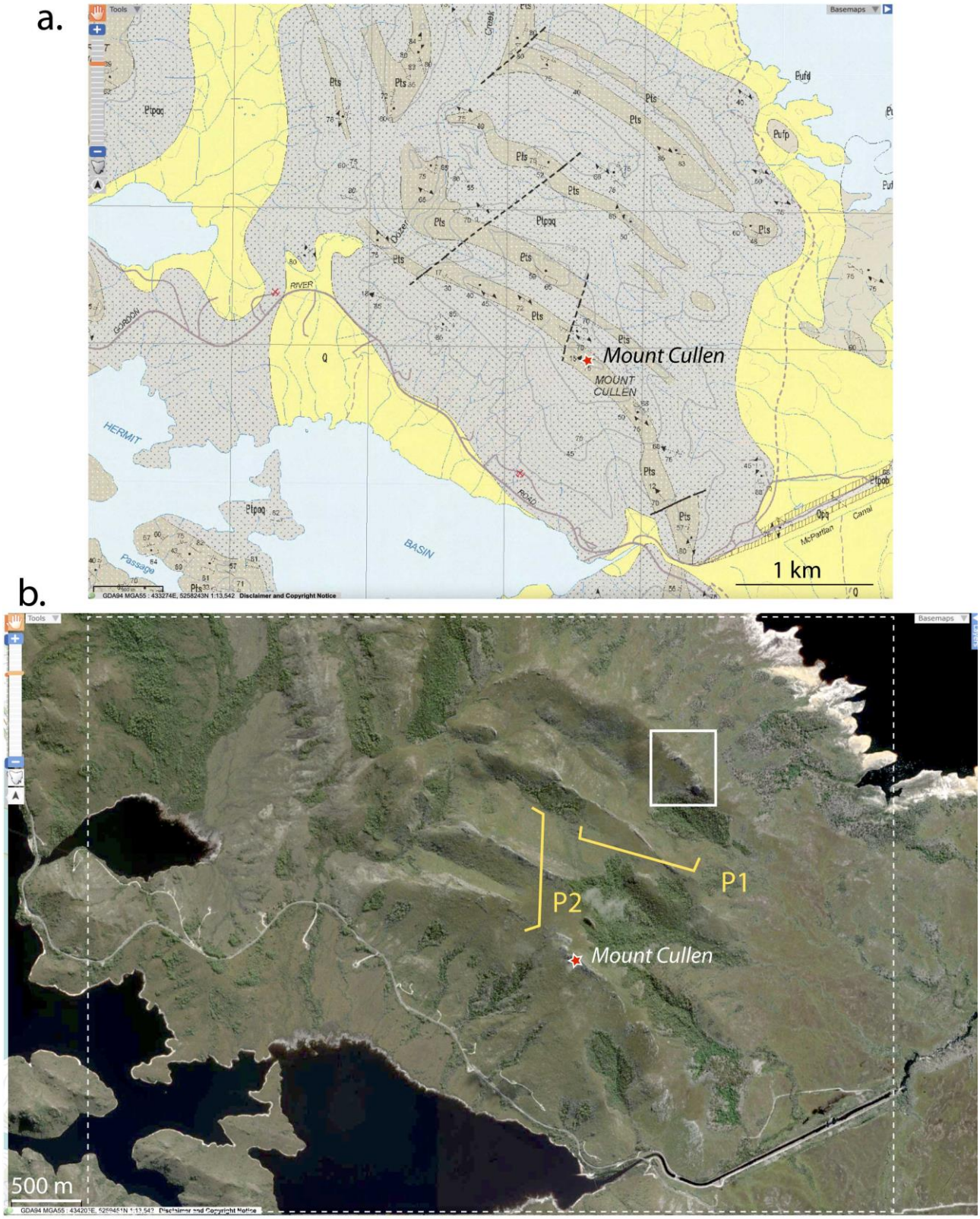

Figure 86: Geology of the Mount Cullen area. a) Geological map of the Mount Cullen area based on the Mineral Resources Tasmania 1:25,000 digital geological atlas. b) Matching Google satellite image showing the quartzite ridgelines. The yellow lines indicate the location and directions of the photographs in Figure 87 (P1) and Figure 88 (P2). The Gordon River road to Strathgordon is shown in the bottom left and the McPartlan canal on the bottom right.

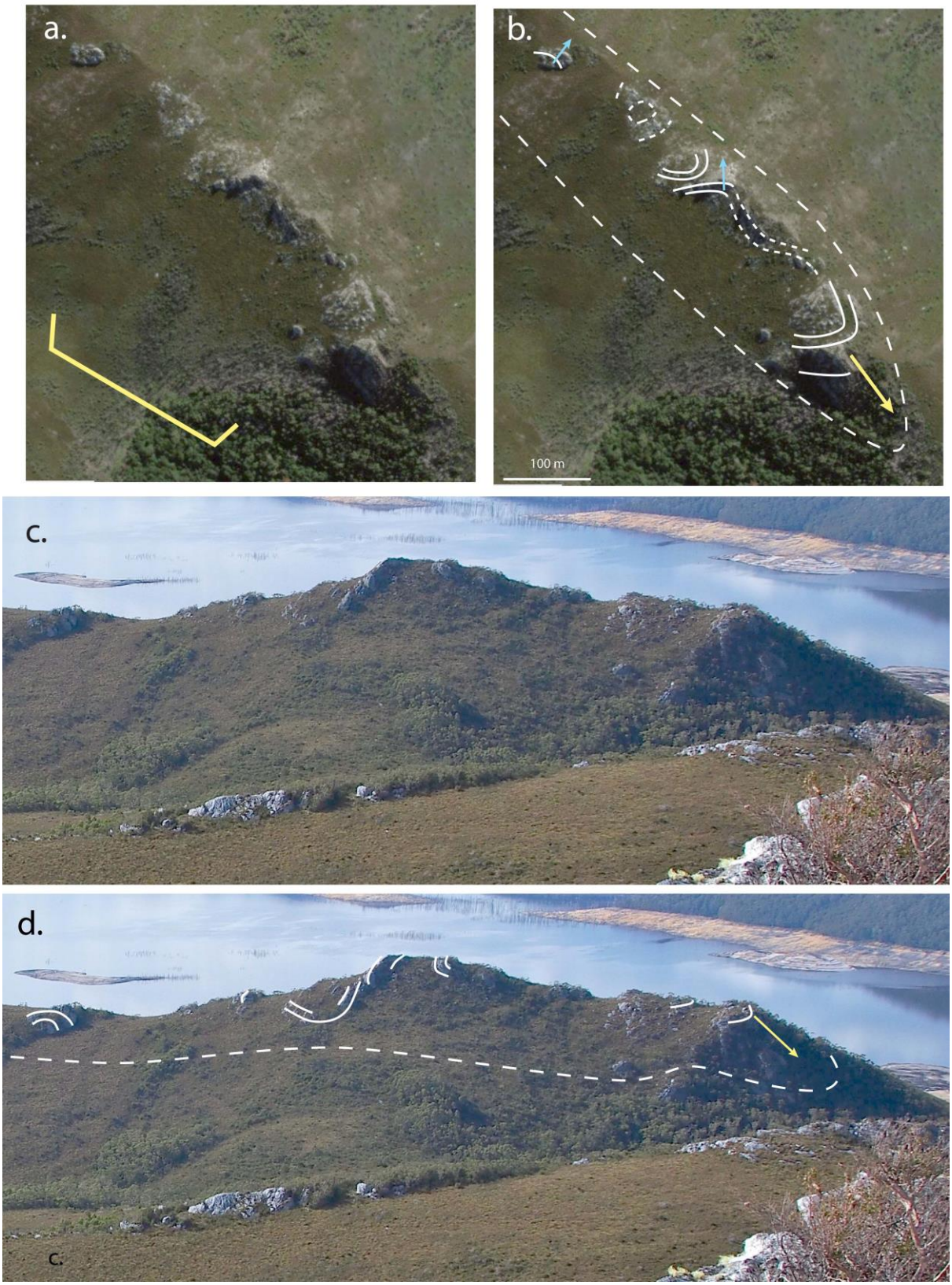

Figure 87: Northernmost quartzite ridgeline beside Lake Gordon and north of Mt Cullen. a) Google image of quartzite ridgeline. b) Formline interpretation of the ridgeline suggesting plunging fold nose at the quartzite termination and refolding by more open, northeast-trending folds .
c) and d) Oblique view of the ridgeline with formlines depicting plunging fold nose at the quartzite termination and refolding by more open, northeast-trending folds. Photo P1 (see Figure 86 for location)(Photo credit: Becca Lunnon, rockmonkeyadventures)

Figure 88: View to the east from Mount Cullen with Lake Pedder and the Frankland Range in the background and the Gordon River road in the middle ground. b) The quartzite ridge is east-trending showing an oblique intersection with an asymmetric fold pair. Photo P2 (see Figure 86 for location). (Photo credit: Becca Lunnon, rockmonkeyadventures)

11. Structure of the Coronets and Sentinel Range

Quartzite of the Coronets and the Sentinels Range (Figures 89, 90 and 91) appears relatively undeformed at the grain scale (Figure 92), shows well preserved cross bedding (Figure 93) and is broadly folded about two apparent rotation points (ARP, Figure 94). The quartzite is however, isoclinally folded by a north-closing macrofold in the eastern part of the Sentinel Range and the Buckies Bonnet area (pink dashed line traces, Figure 94).

Figure 89: View of the quartzite dominated Sentinel Range from Mt Cullen. The photo is looking southeast. (Photo credit: Becca Lunnon, rockmonkeyadventures)

Figure 90: Panoramic view of steeply, north-dipping bedding in quartzite of the middle section ridgeline of the Sentinel Range with The Coronets on the photo right (middle ground). Lake Pedder and Mt Solitary are in the centre background. (Photo credit: David Gray)

Figure 91: The Coronet Range from the Sentinel Range looking south. The axial surface trace of the north-closing isoclinal macrofold runs along the base of the range in the valley to the west (photo right) (see map, Figure 94). (Photo credit: David Gray)

Figure 92: Quartzite bedding surface from the Sentinel Range showing undeformed, well-rounded, equigranular quartz grains, Photo width is ~5 cm. (Photo credit: David Gray)

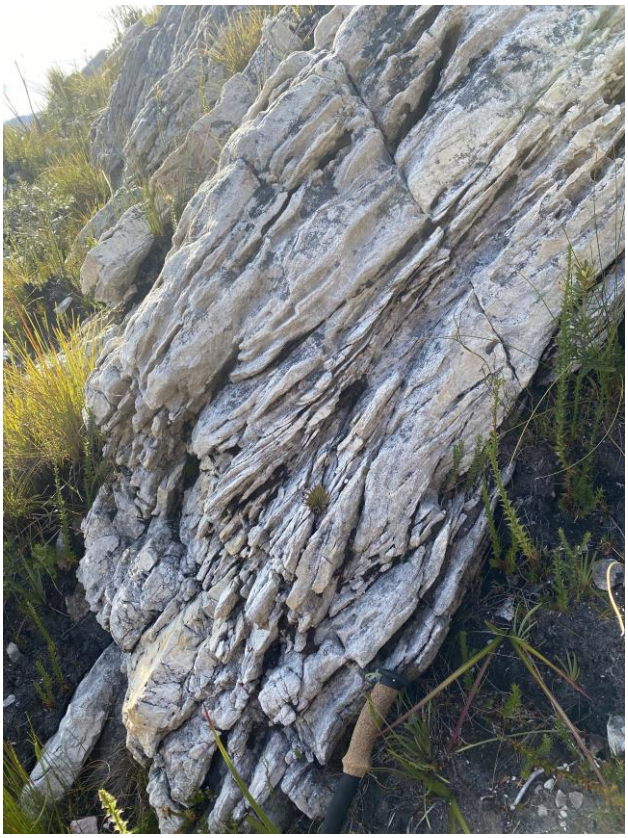

Figure 93: Truncated top sets in cross-bedded quartzite of the Sentinel Range. View is looking east such that younging is to the north. (Photo credit: David Gray)

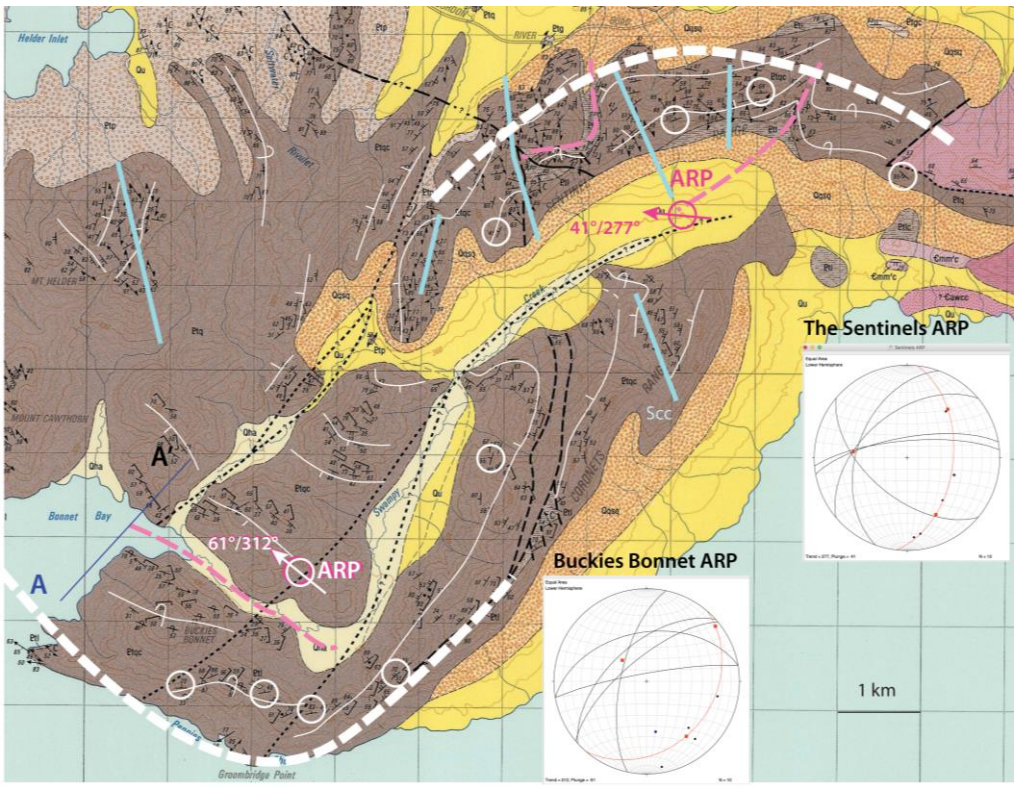

Figure 94: Map of The Sentinels and The Coronets from the Pedder 1:50,000 map sheet showing two apparent rotation points (ARP). The Sentinels ARP is 41°/277° and the Buckies Bonnet ARP is 61°/312°. The heavy white dashed lines approximate the broad arcs in S0/Sm. Formlines in S0 are shown by the fine white lines. The pink dashed lines represent the axial surface traces of early F1/F2 macrofolds in So/Sm. Section line A-A' is the Buckies Bonnet profile (Calver et al., 1990, fig.53). White circles are the locations of bedding attitudes used to produce the π axis (fold axis) stereonet diagrams. Blue line traces are the Scc (S3) axial surface cleavage to the macro-folds shoiwn by the white dashed lines.

12. REFERENCES

Boulter, C.A., 1974. Structural sequence in the metamorphosed Precambrian rocks of the Frankland and Wilmot Ranges, southwestern Tasmania. *Papers and Proceedings of the Royal Society of Tasmania*, 107, 105-115.

Boulter, C. A., 1978. The structure and metamorphic history of the Wilmot and Frankland Ranges, south-west Tasmania. Unpublished PhD Thesis, The University of Tasmania.

Brown, A. V.; McClenaghan, M. P.; Turner, N. J.; Baillie, P. W.; McClenaghan, J.; Lennox, P.; Williams, P. R. 1982. Geological Atlas 1:50 000 series. Sheet 73 (8112N). *Huntley*. Department of Mines, Tasmania.

Brown, A.V., McClenaghan, M.P., Turner, N.J., Baillie, P.W., McClenaghan, J, and Calver, C.R., 1989. Geological Atlas 1:50,000 Series. Sheet 73 (8112N), Huntley. *Explanatory Report Geological Survey of Tasmania.* 109p.

Calver, C.R., Turner, N.J., McClenaghan, M.P., and McClenaghan, J, 1990. Geological Atlas 1:50,000 Series. Sheet 80 (8112S), Pedder. *Explanatory Report Geological Survey of Tasmania.* 105p.

Elliott, D. 1970. Determination of finite strain and initial shape from deformed elliptical objects. *Bulletin of the Geological Society of America*, 81, 2221-2236.

Gray, D.R. and Vicary, M. J., 2024. Structural Geology of the Eastern Tyennan Domain, Tasmania—An Overview and Structural Synthesis and Implications. Mineral Resources Tasmania, *Geological Survey Paper,* 14.

Port, I.A. 2023. The Structural and Metamorphic History of the Eastern Tyennan Region, Lake Pedder, Tasmania. BSc (Hons), Thesis University of Tasmania (unpublished).

Turner, N. J.; Calver, C. R.; McClenaghan, M. P.; McClenaghan, J.; Brown, A. V.; Lennox, P. G. 1985. Geological Atlas 1:50 000 series. Sheet 80 (8112S). Pedder. Department of Mines, Tasmania.

Turner, N. 1989a. Junction Range (West), p. 79-80. In: Brown, A.V., McClenaghan, M.P., Turner, N.J., Baillie, P.W., McClenaghan, J, and Calver, C.R., 1989. Geological Atlas 1:50,000 Series. Sheet 73 (8112N), Huntley. *Explanatory Report Geological Survey of Tasmania.* 109p.

Turner, N. 1989b. North Star Area, p. 80-87. In: Brown, A.V., McClenaghan, M.P., Turner, N.J., Baillie, P.W., McClenaghan, J, and Calver, C.R., 1989. Geological Atlas 1:50,000 Series. Sheet 73 (8112N), Huntley. *Explanatory Report Geological Survey of Tasmania.* 109p.

APPENDIX 2

Structural Geology of the Gordon River Road — Construction of a structural profile from Gordon Dam to Hermit Hill

APPENDIX 2

Structural Geology of the Gordon River Road — Construction of a structural profile from Gordon Dam to Hermit Hill

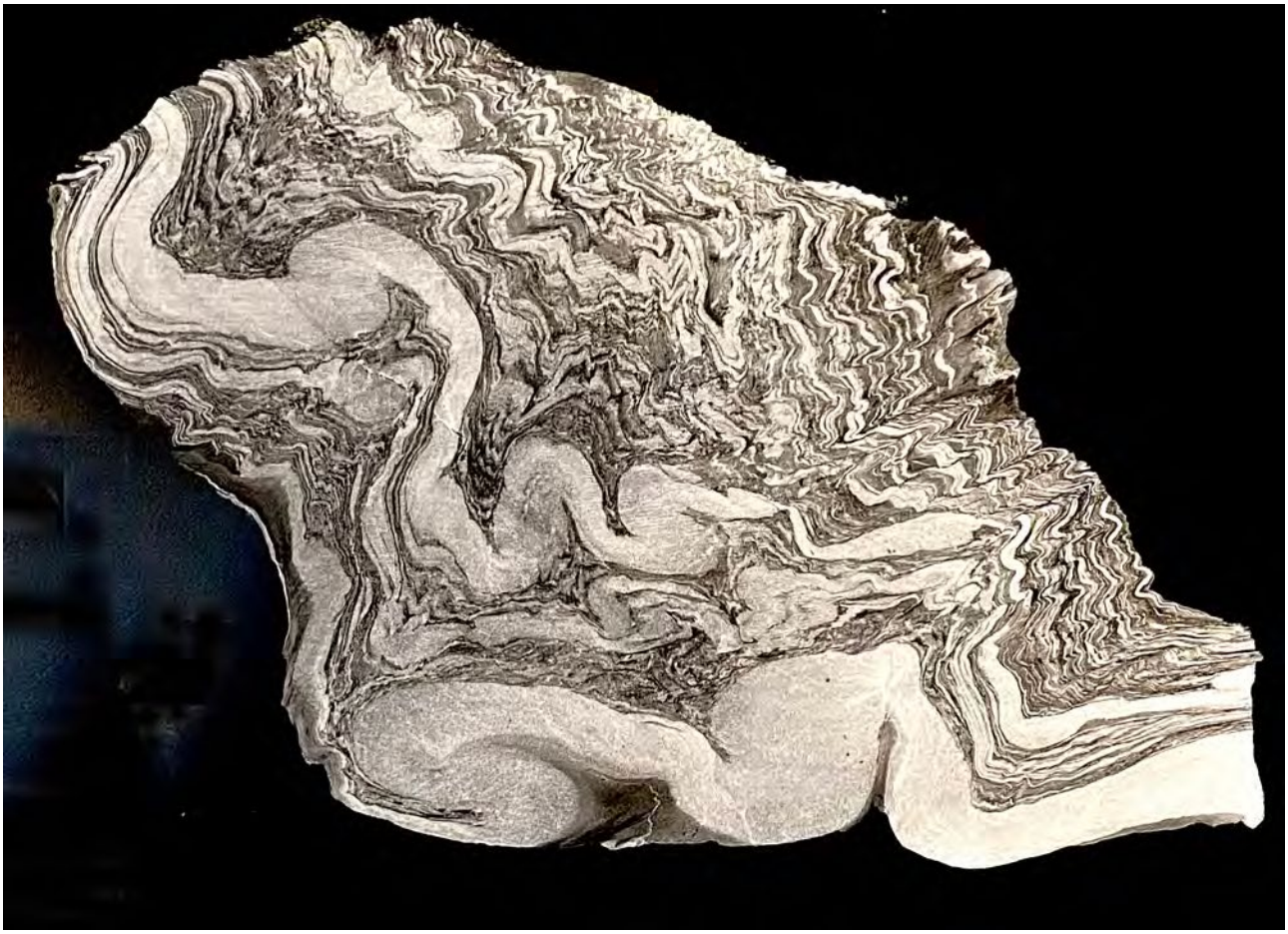

Frontispiece: The complexly, poly-deformed nature of the Eastern Tyennan subdomain. Example of a coaxially refolded, small scale, recumbent isoclinal asymmetric fold pairs in thin quartzite layers, Gordon Damsite. The quartzite bands occur within interlayered micaceous quartzite and quartz-mica schist. Two sets of folds refold the early fold pairs. The dominant set (F2) has axial surfaces dipping to the photo left with pronounced axial surface crenulation cleavage. A localised upright fold set with vertical axial surfrace crenulation cleavage is visible in darker micaceous layers (photo centre). Photo Source: slab on display at the Tasmanian Museum and Art Gallery.

Appendix 2 presented provides an example of "sketch" structural profile construction in a terrain lacking significant relief and with complex polydeformation (Frontispiece). The technique is a modification of the classic Alpine "sketch" profiles drawn from the actual mountainsides enabled by the mountainous relief and superb exposure of the European Alps (Figure 1). This modified Alpine technique of structural profile construction utilises detailed structural sketches at different scales from variously spaced outcrops to construct regional structural profiles that define the regional macrostructure.

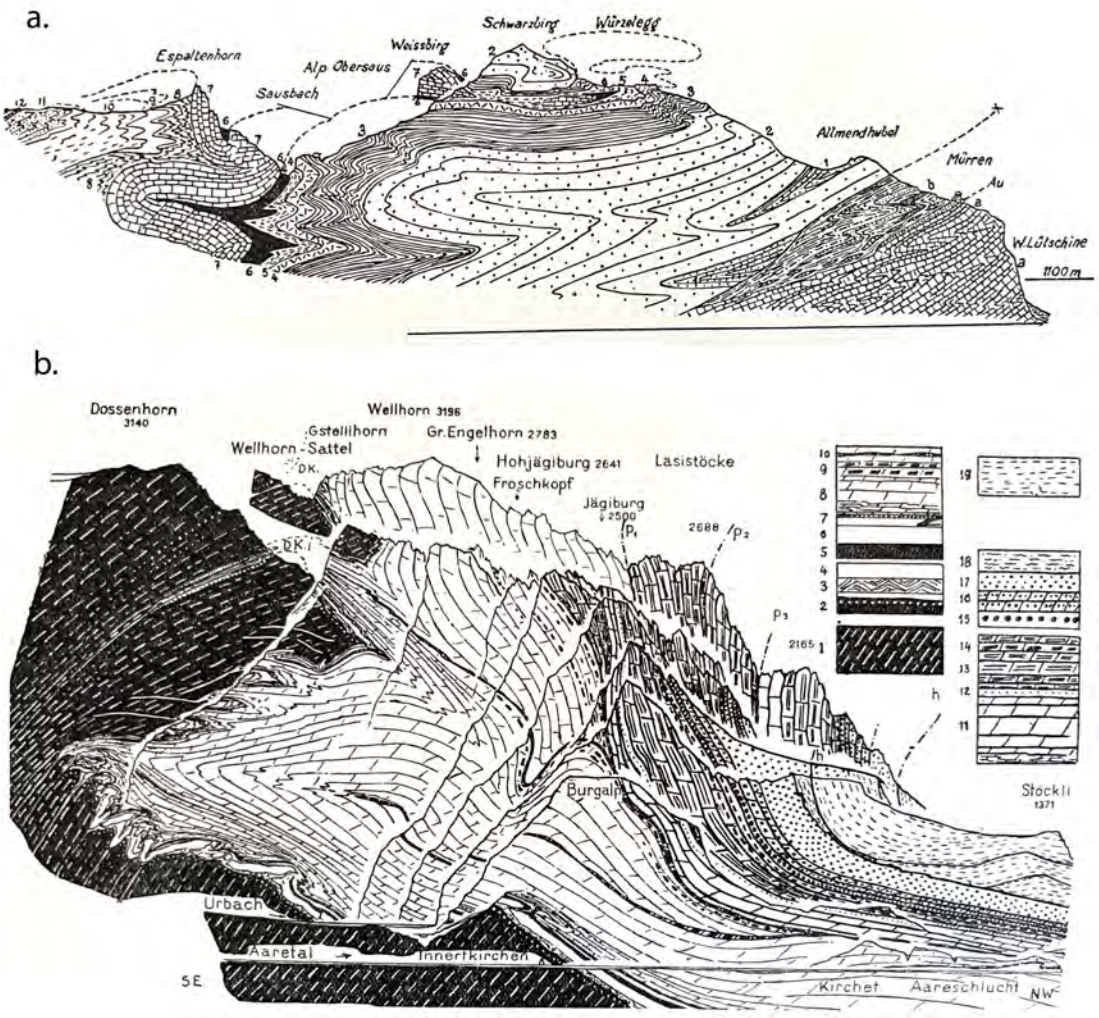

Figure 1: Examples of structural profiles from the European Alps. They typify the classic Alpine structural profiles that represent sketch profiles of the mountainous terrain (Collet, 1927). a) Section across the Mürren region (Collet, 1927, fig. 20). b) Section across the Engelhörner (Collet, 1927, fig. 26).

The Gordon River Road provides easy access to the central eastern part of the Eastern Tyennan subdomain (Figure 2) with road outcrops enabling construction of a structural profile centred on Strathgordon township (Figures 3 and 4).

This Appendix presents all the photographs, measurements and field notebook sketches and description that were used in the development and construction of the Strathgordon structural profile. There is no extensive text and the photo groups per each major structural element need to be considered individually and then as a group to define the particular element. The figure captions are more detailed in an attempt to describe the structure and structural relationships shown in each photograph/diagram.

1. Background

The Strathgordon structural profile (Figure 4) is based on structural mapping by the authors in 2017 (Figure 5) as well as mapping by Boulter (1978). The first structural investigation of the region was by Powell (1969) at the newly developing Gordon Damsite in July and August 1967. This work was part of contract work for the Hydro-Electric Commission of Tasmania. It documented the polydeformed nature of the quartzite-pelite sequence at Strathgordon. Boulter (1974, 1978) undertook structural mapping of the Wilmot-Frankland Ranges and the area around the Gordon Damsite from April 1971 over a 2-3 year period culminating in a PhD (Boulter, 1978). Other work includes 1) Williams (1973, 1976) that involved structural mapping in the McPartlans Pass area as part of a University of Tasmania BSc Hons thesis, and Port (2023) in the Strathgordon area also as part of a University of Tasmania BSc Hons thesis.

The early work established strong north-south structural trends and gentle plunges through the Gordon Dam-Strathgordon-Twelvetrees Range area. This knowledge was important in construction of a sub-vertical, east-west oriented, structural profile (Figures 3 and 4).

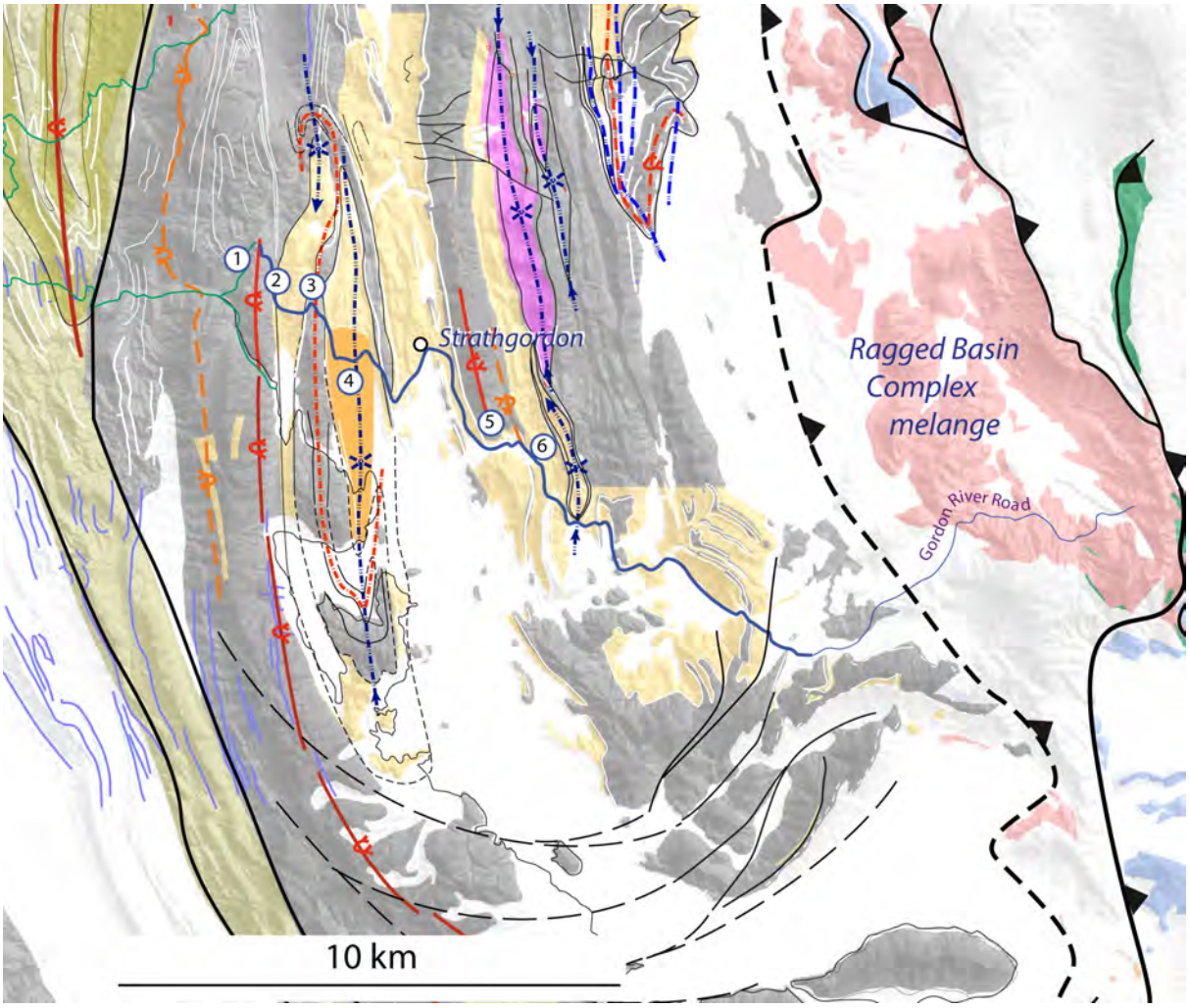

Figure 2: Central part of the Eastern Tyennan subdomain showing the Gordon River Road (heavy dark blue line) between Gordon dam, Hermit Hill and MacPartlan Pass. Major structural elements of the Strathgordon structural profile are shown by the circled numbers. These elements include:

1: The Knob F1/F2 macro-fold
2: Boat Ramp High strain zone (HSZ)
3: The Bend F1/F2 macro-fold
4: High-grade synformal F3 keel
5: Twelvetrees refolded macro-fold
6: Atkins Range HSZ

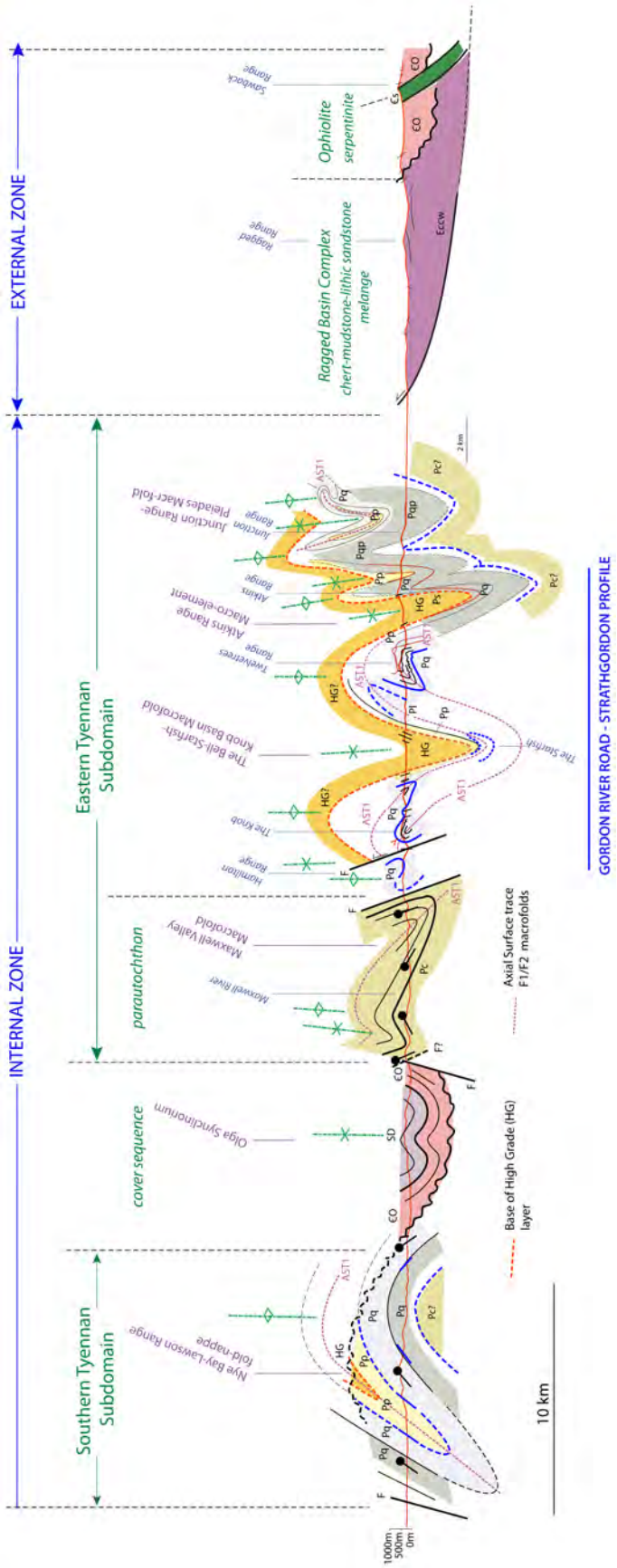

Figure 3: Regional structural profile across the central part of the Eastern Tyennan subdomain. The Gordon River Road-Strathgordon segment is highlighted (cf. Figure 4).

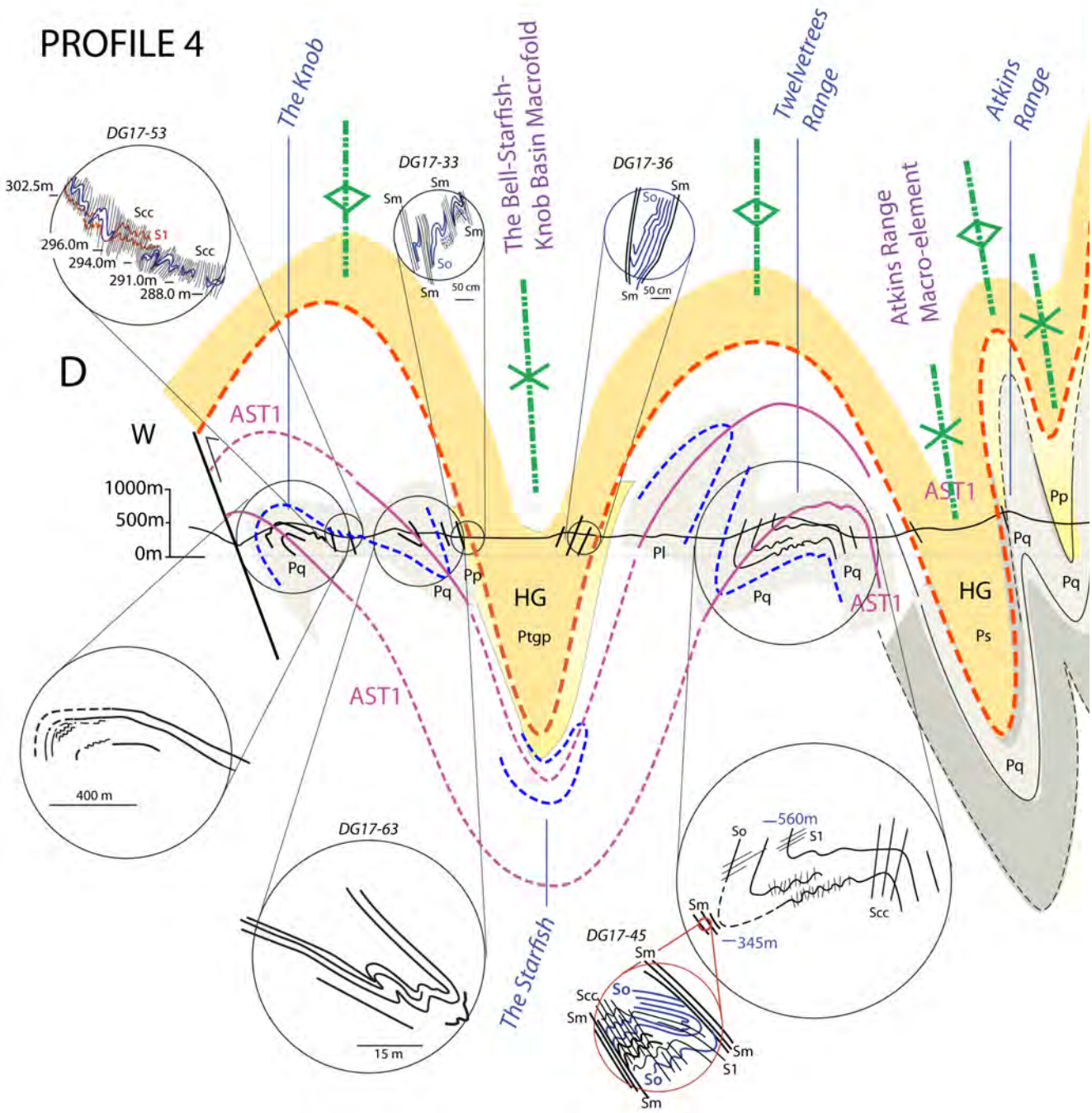

Figure 4: The Gordon River Road-Strathgordon structural profile based on structural data and sketches made from outcrops along the Gordon River Road from Gordon Dam to Hermit Hill.

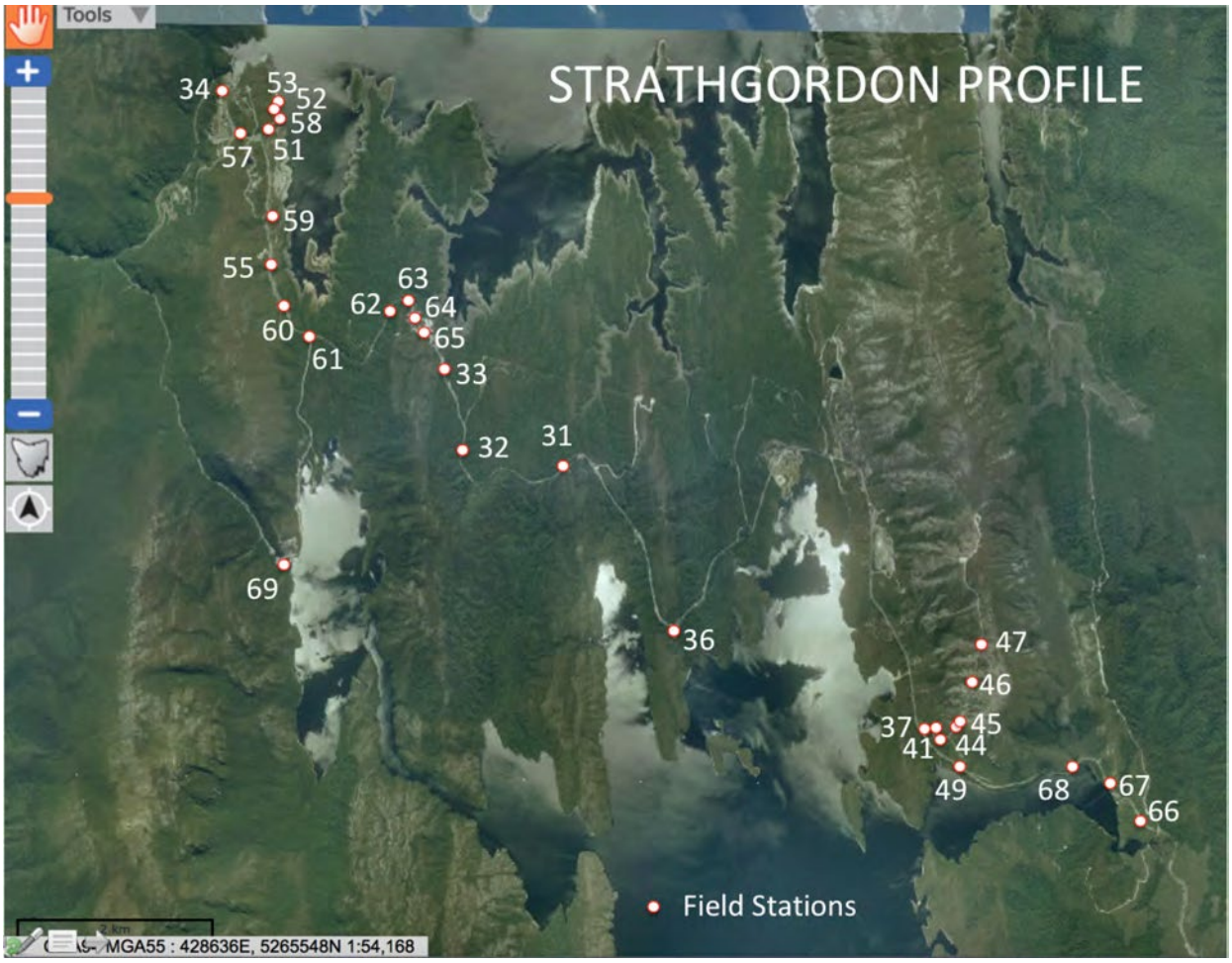

Figure 5: The 2017 Strathgordon field stations plotted on a ListMap Google satellite image base. The stations are prefixed by DG17.

2. Approach/Technique for Profile Construction

• ***At each outcrop the following was undertaken:***

1) Examination of the outcrop to establish the presence of bedding and/or compositional banding (So/Sm), foliation Sm, crenulation cleavages (Scc,), fold plunge, intersection lineations and mineral lineation.

2) Determine/measure the attitudes of the respective elements observed in the outcrop. This includes the attitudes of layering So, So/Sm, Sm and Scc as strike and dip or dip and dip direction, and the plunge and plunge directions of folds and lineations.

3) Make simple sketch stereonets in your field notebook of the attitude measurements. This helps establish the geometry and geometrical relationships and fixes them in your brain.

4) Establish the profile direction based on the attitudes of the major elements in the outcrop.

5) Sketch the structure of the outcrop in the profile plane that you have determined. Make sketches at different scales to show enlargements of the detailed elements if the structure is complex (see Figures 6, 7 and 8).

6) Obtain a GPS position and elevation of the outcrop.

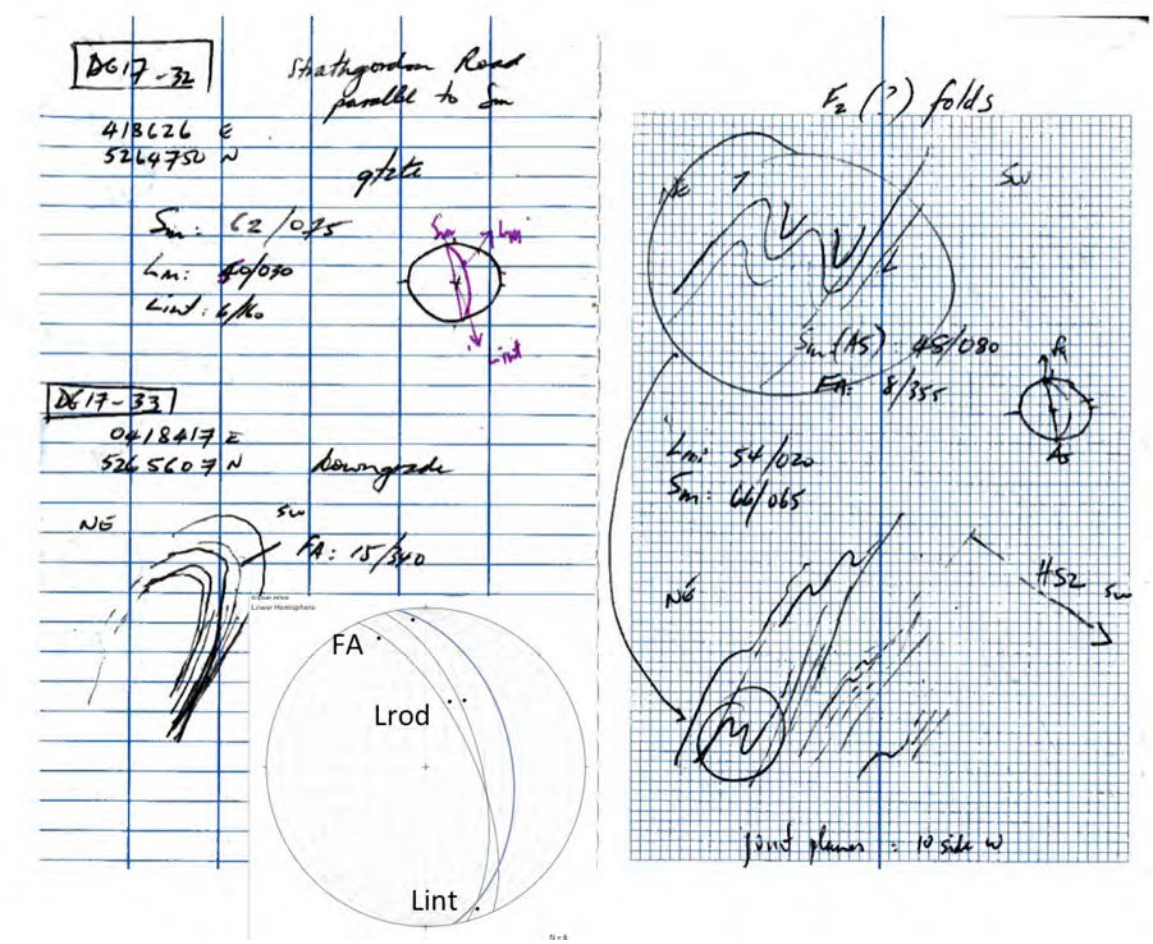

Figure 6; Example of Notebook entries for DG17-32 and DG17-33 from the Gordon River Road traverse.

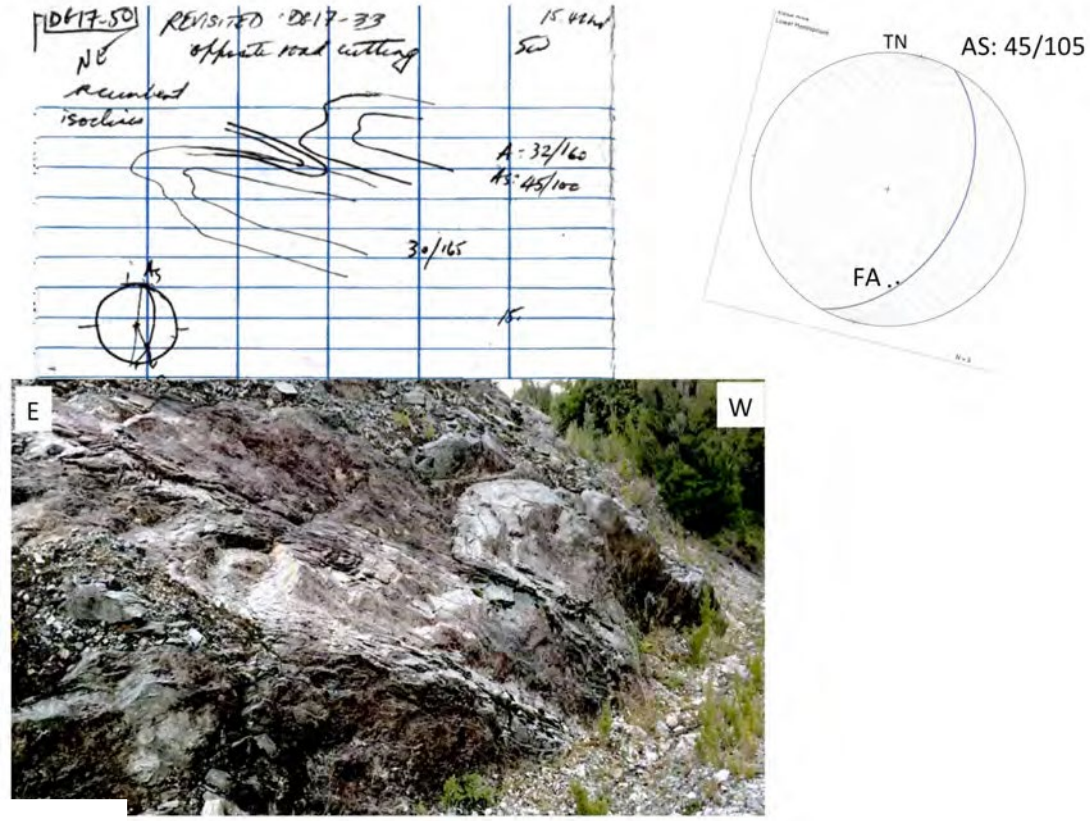

Figure 7; Example of Notebook entry for DG17-50 opposite side of road to outcrop DG17-33.

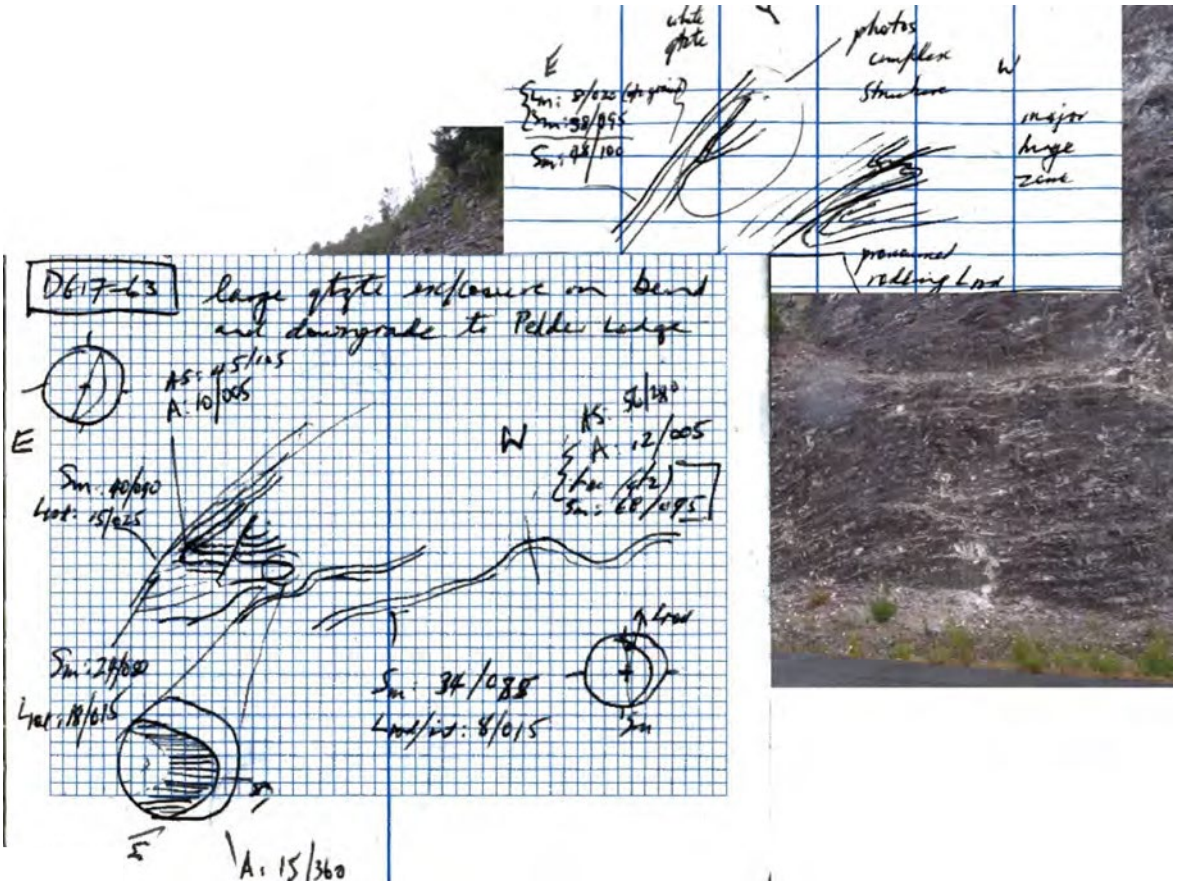

Figure 8: Example of Notebook entries for DG17-63 from the Gordon River Road traverse.

Profile Construction:

• *Position a regional profile plane on the map base to minimise the distances of individual outcrop profile sketches away from the main profile as they will be projected into this profile plane (Figure 9).*

• *A stepped profile of individual component sections can also be used to create a composite stitched profile (Figure 10).*

• *Add the sketch outcrop profiles to the main profile using position and elevation (see Twelvetrees Range profile, Figure 78).*

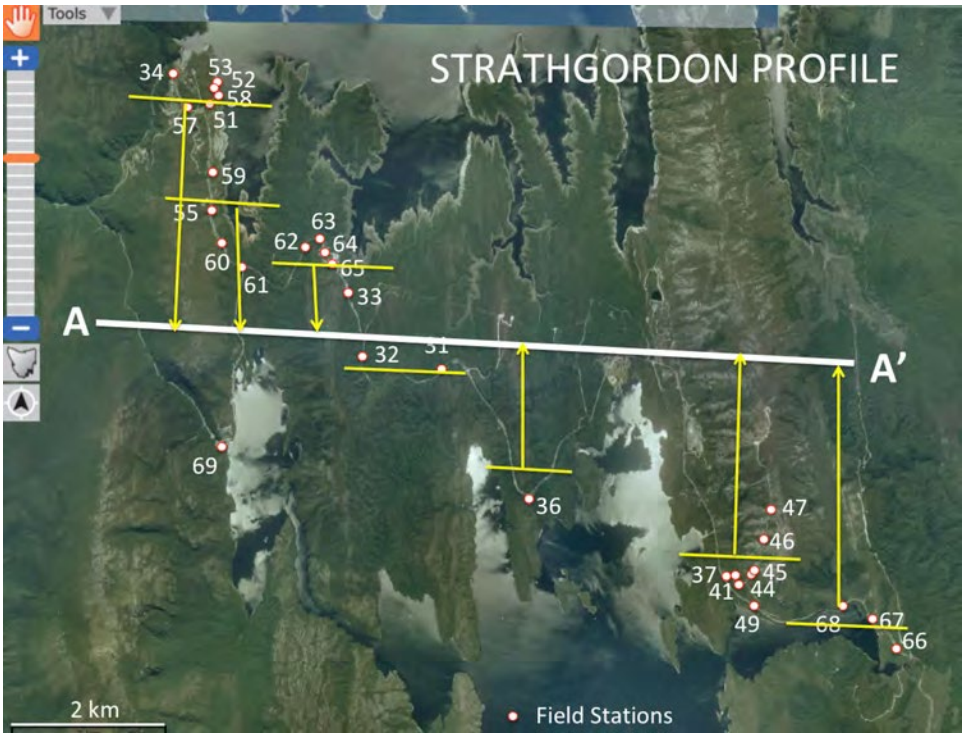

Figure 9: Stepped, composite profile construction utilising the 2017 Strathgordon field stations on a ListMap Google satellite image base. Small segment profiles away from the section line are projected onto the main profile. This works in areas with gentle to low plunges.

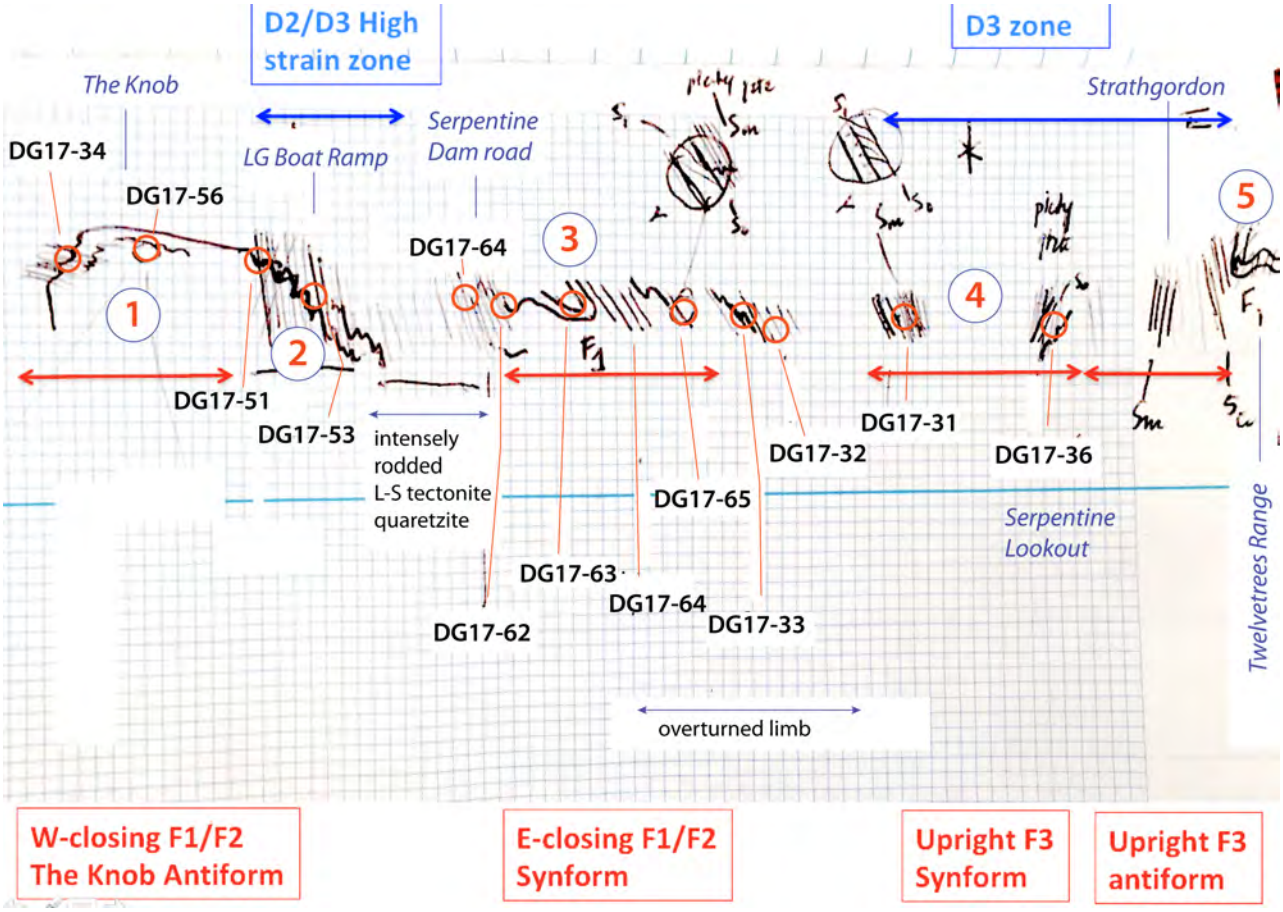

Figure 10: The initial field notebook Strathgordon "sketch" structural profile. The "sketch" profile is based on structural data and sketches made from outcrops along the Gordon River Road from Gordon Dam to Hermit Hill. The sketch profile was undertaken in the field after the road section had been completed.

3. Structural Elements of the Strathgordon Profile

The major structural elements identified in the Gordon Road traverse (Figure 2) from west to east include:

1) The Knob west-closing antiformal macro-fold
2) The Gordon Boat Ramp high strain zone (HSZ)
3) The east-closing synformal fold hinge
4) High grade (HG) synformal F3 keel
5) The Twelvetrees west closing fold
6) Atkins Range HSZ

These elements will now be defined and described based on the structural observations and measurements made in the 2017 field traverse as well as incorporating data and observations from Powell (1969) and Boulter (1974, 1978). The observations and measurements provide the basis for the geometrical interpretation that results in the regional composite profile (Figures 3 and 4) through development stages Figures 5 to 10.

3.1 The Knob west-closing antiformal macro-fold (Element 1, Figure 2)

3.1.1 *Gordon Damsite region*

The Knob-Gordon Damsite region with the Knob ridgeline bounded by the Gordon River on the western side contains the Knob macro-fold (Boulter 1978) (Figure 11). The fold is gently north-plunging with a strong to intense axial surface crenulation cleavage (Scc) (Figures 11 and 12, DG17-34, DG17-56 and DG17-57 stereonets) associated with variably plunging sheath-like mesoscopic folds within psammitic bands in carbonaceous phyllite (Figures 16 and 17). In the southeast the fold is strongly overprinted by an intense zone of north-northeast-trending S3 crenulation cleavage (Figures 11 and 12) that is part of the Boat Ramp high strain zone (HSZ).

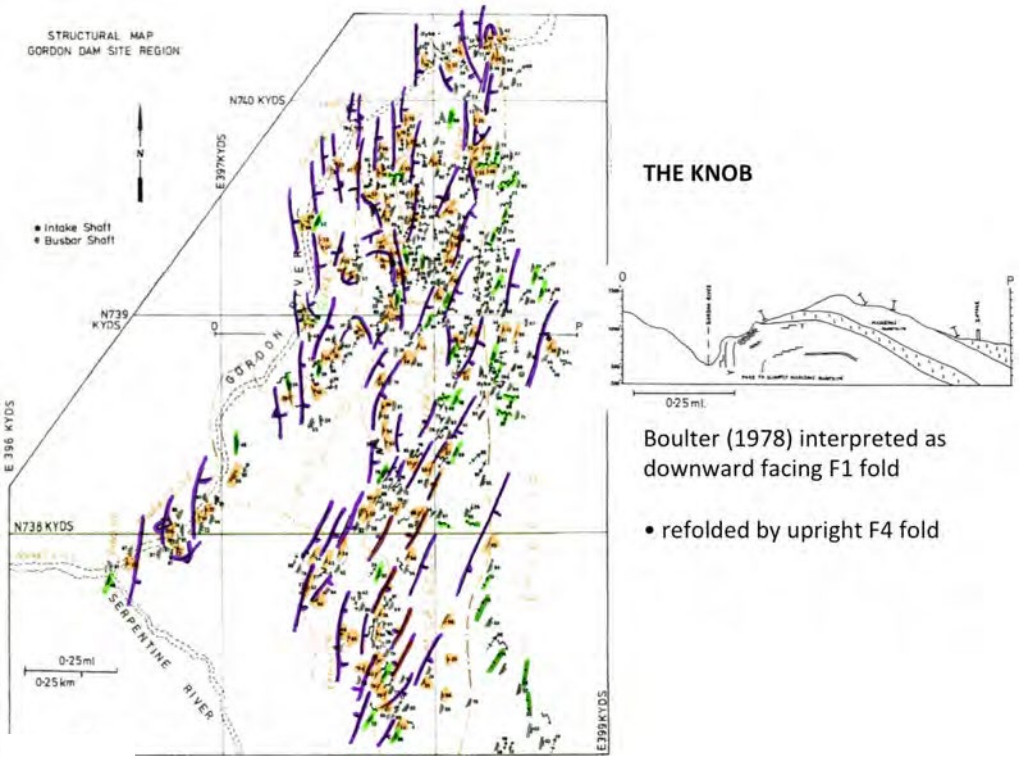

Figure 11: The Knob macro-fold bounded by the Gordon River on the west and Lake Gordon on the east. a) Structural formline map based on map from Boulter (1978, fig. 4.3) showing the macro-fold cut by a north-northeast-trending S3 intense foliation (high strain) zone. This is part of the Boat Ramp high strain zone (HSZ) (Element 2).

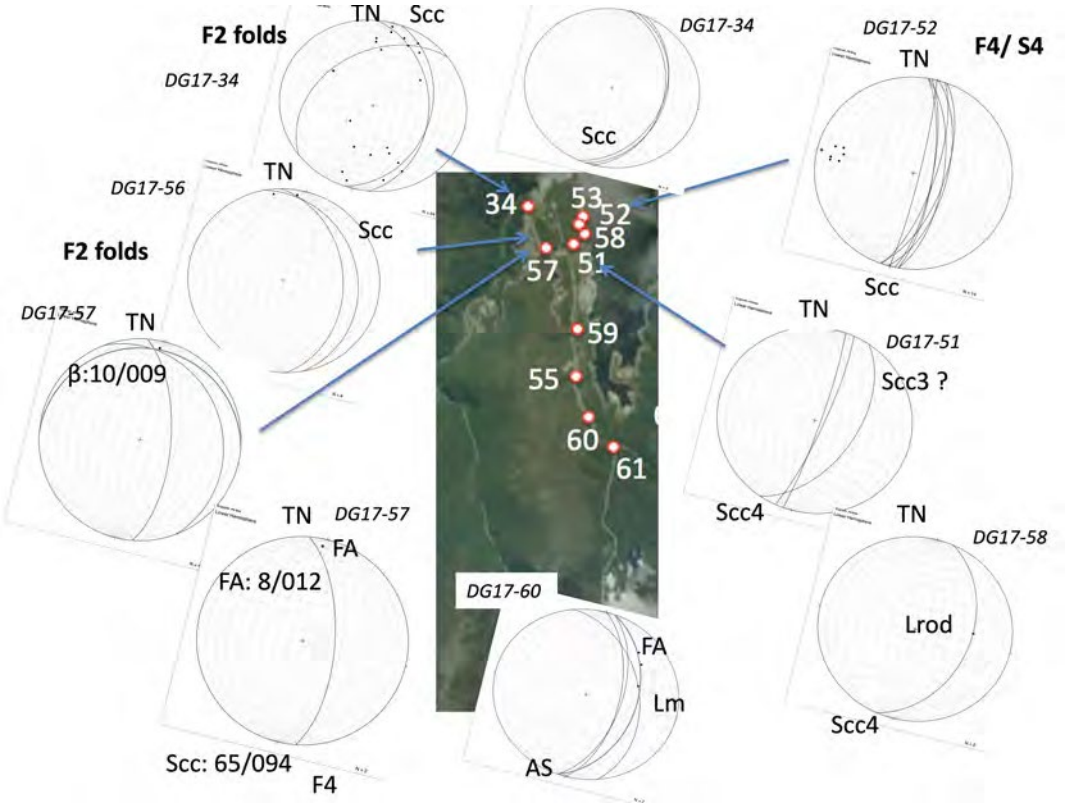

Figure 12: Stereonet projections of foliations and mesoscopic fold axial surfaces from Gordon River Road cuttings in the Gordon Dam area. Locations are numbered in the Google image (centre). Quartzite defines the hump shaped form of the fold structure visible in the Google Earth image.
a) F2 fold axis (black dots) and axial surface measurements (great circle traces) in thin psammitic layers within carbonaceous phyllite near the Gordon Damsite picnic shelter (DG17-34). b) Axial surface Scc measurements in the carbonaceous phyllite (DG17-34). c) , d) and e) are F2 fold axis and axial surface data from outcrops DG17-56 and DG17-56 respectively.

The Knob macro-fold geometry is shown and defined in a formline map (Figures 11), structural atiitude data (stereonets in Figure 12) and a schematic profile constructed by Boulter in 1978 (Figure 13). Figure 14 shows a series of photographs that enabled reconstruction of the 1978 profile. The photos are approximately positioned in geographic space to define the component parts that make up the upper limb to hinge transition of the west-closing Knob macro-fold.

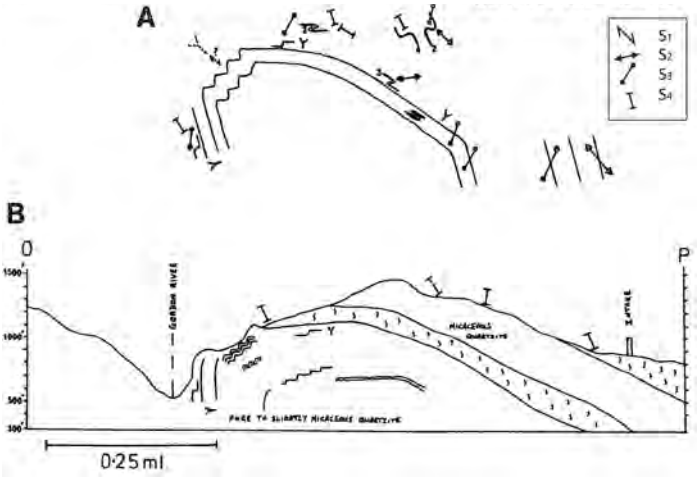

Figure 13: Boulter 1978 profile sketch of the Knob macro-fold, Gordon Dam (fig.4.7, Boulter, 1978).
a) Schematic profile showing relationships between the foliations S1, S2, S3 and S4. b) Structural profile showing the geometry of the Knob macro-fold in the region of the Gordon and Serpentine Dams. Compare with constructed profile in Figure 14 utilising photographs from the Gordon Damsite area.

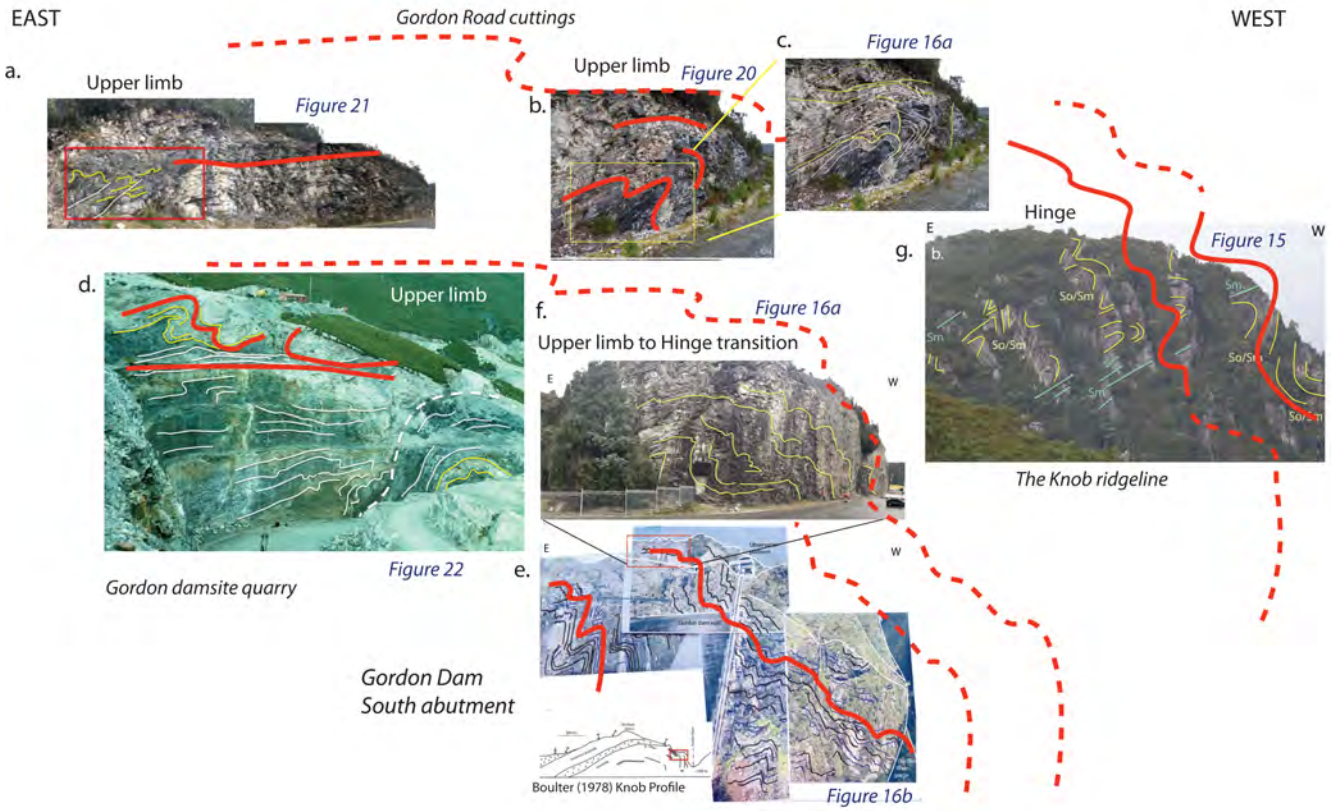

Figure 14: Stacked photo profile to create a composite structural profile across the west-closing Knob macro-fold. The photographs are from different positions and levels across the Knob region but have been compressed into one viewing plane. The view is to the south. Photos (a), (b) and (c) have been inverted to give a south view. a) and b) are photographs of cuttings along the Gordon River Road above the Gordon Dam quarry (Figures 20 and 21). c) Enlargement of part of (b). d) Gordon Dam quarry (photo taken in 1976) (Figure 22). e) Stitched photographs of the Gordon Dam south abutment (Figure 16b). f) Enlargement of part of (e). The cutting is behind the Dam Observation Deck (Figure 16a). g) View of the southern extension of the Knob ridgeline taken from above the Gordon Damsite quarry looking south (Figure 15).

The Knob macro-fold upper limb to hinge transition

The upper limb is gently to moderately east-dipping with a series of z-vergence asymmetric folds (looking south) as seen in Gordon River Road cuttings above the quarry (Figures 14a, b and c) and in the quarry (Figure 14d). Transitions into the macro-fold hinge can be seen in the cutting at the Gordon Damsite car park (Figures 14f and 16a), in the southern abutment viewed from the dam (Figures 14e and 16b) and in the distant hillside above the quarry looking to the south (Figures 14g and 15). The positions are matched by the asymmetry of the folds and the proximity to the hinge where the folds have more M-shaped form (Figures 14g and 15).

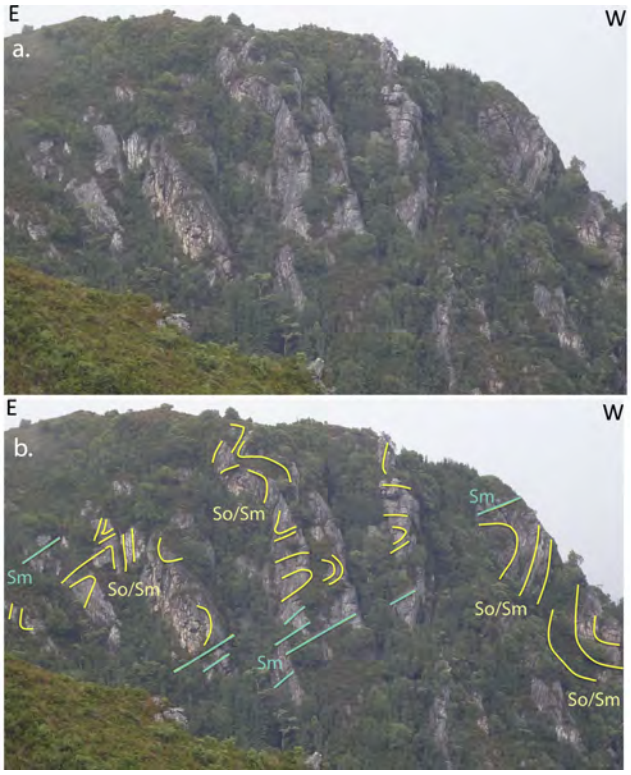

Figure 15: Views of the Knob ridgeline above the Gordon River showing an oblique view of symmetrical, M-vergent folds within So/Sm in the hinge of the Knob macro-fold. The axial surface foliation (Sm) appears east-dipping (Blue line traces).

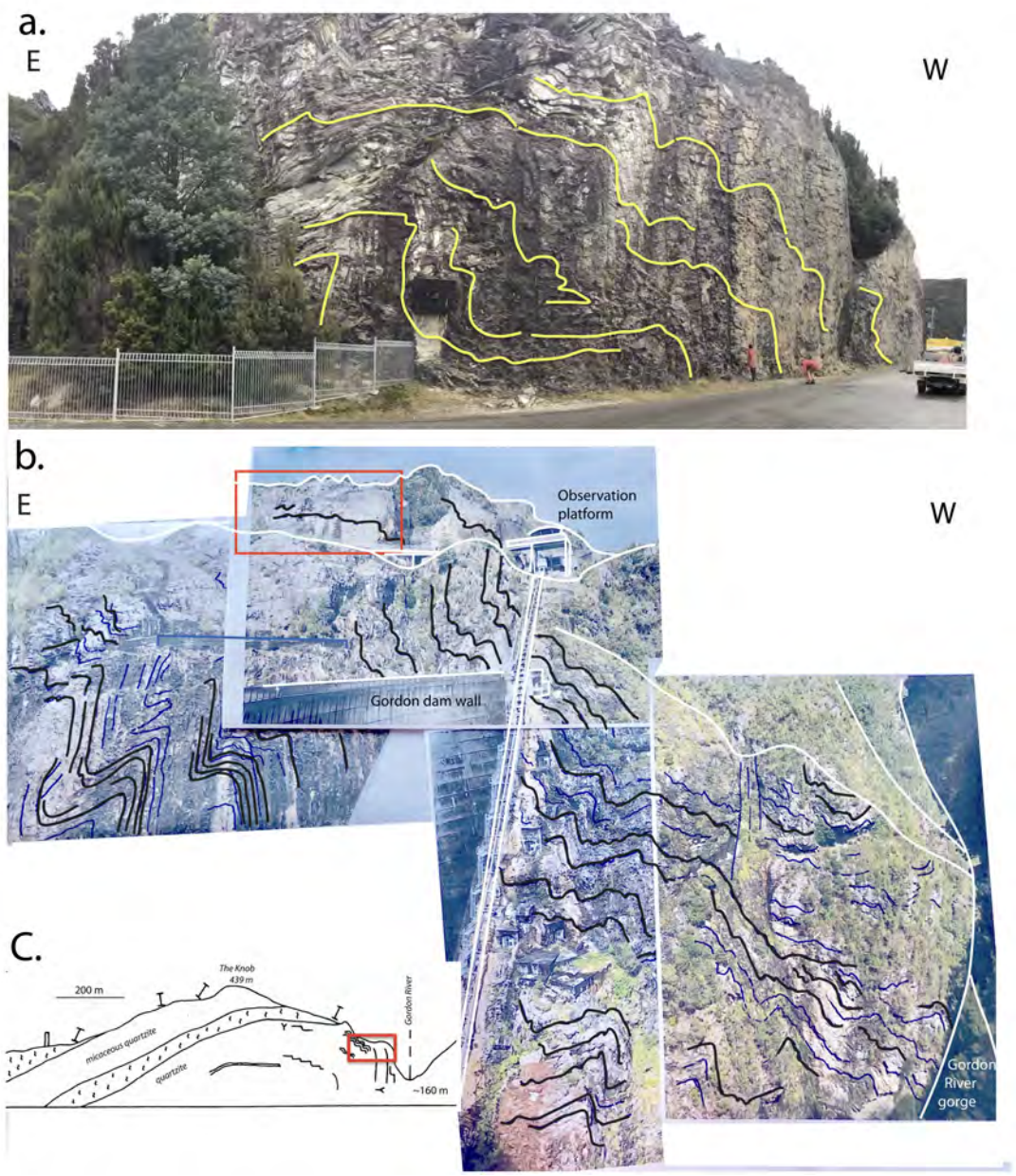

Figure 16: Chevron folded quartzite at Gordon Dam. a) Road outcrop near the Observation Platform showing chevron folds and a rollover in bedding (So/Sm) as part of the Knob macro-fold hinge. b) Stitched photo profile of the Gordon Dam southern abutment. The photos are taken from the northern end of the dam wall looking back along the dam to the south. The cliff shows a rollover into the Knob macro-fold hingeline. The uppermost part of The Knob hill above the observation platform has flat-lying bedding foliation (So/Sm). c) Sketch profile through the Knob showing the west-closing, knuckle-fold geometry of the Knob macro-fold (Boulter, 1978).

Within the cuttings adjacent to the Gordon Damsite shelter/picnic area dark carbonaceous phyllite with thin interlayered psammitic bands show sheath-like mesoscopic folds. They have markedly curved hingelines (Figures 17a, b) and show varying fold plunges and plunge directions Figure 17c). The fold axis scatter lies within the modal north-trending and east-dipping fold axial surface (Figure 18). The axial surfaces fan slightly about a β point 20°/152° (MN). The plane orthogonal to this rotation point defines a northeast-trending movement plane (Figure 18).

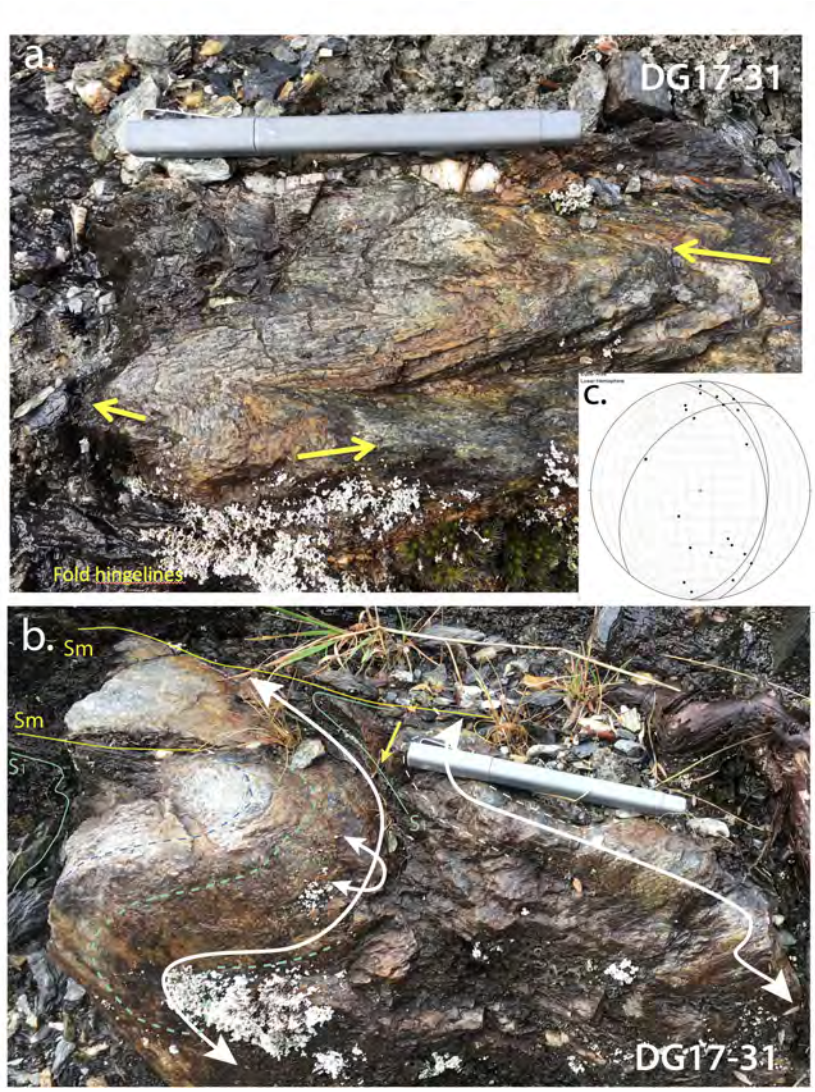

Figure 17: Sheath-like mesoscopic folds in thin psammitic bands within intensely foliated, micaceous, black phyllite within the hinge zone of the Knob fold. The outcrop is opposite the Gordon Damsite picnic shelter. The folds show varying fold plunges and plunge directions, many with curved hingelines showing a marked hingeline scatter (black dots in the inset stereonet).

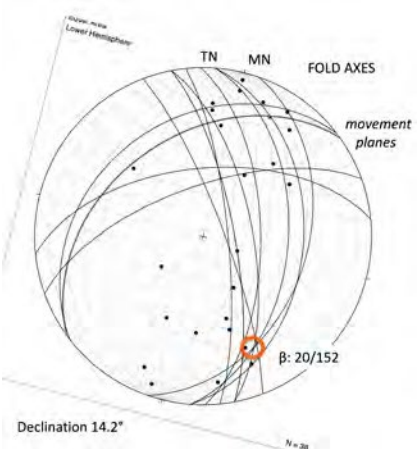

Figure 18: Movement plane calculations from outcrop DG17-31 in the hinge zone of the Knob macro-fold. All movement planes are northeast-trending. Fold axis measurements are shown by the dots. Axial surface attitudes are shown by the north-striking great circle traces.

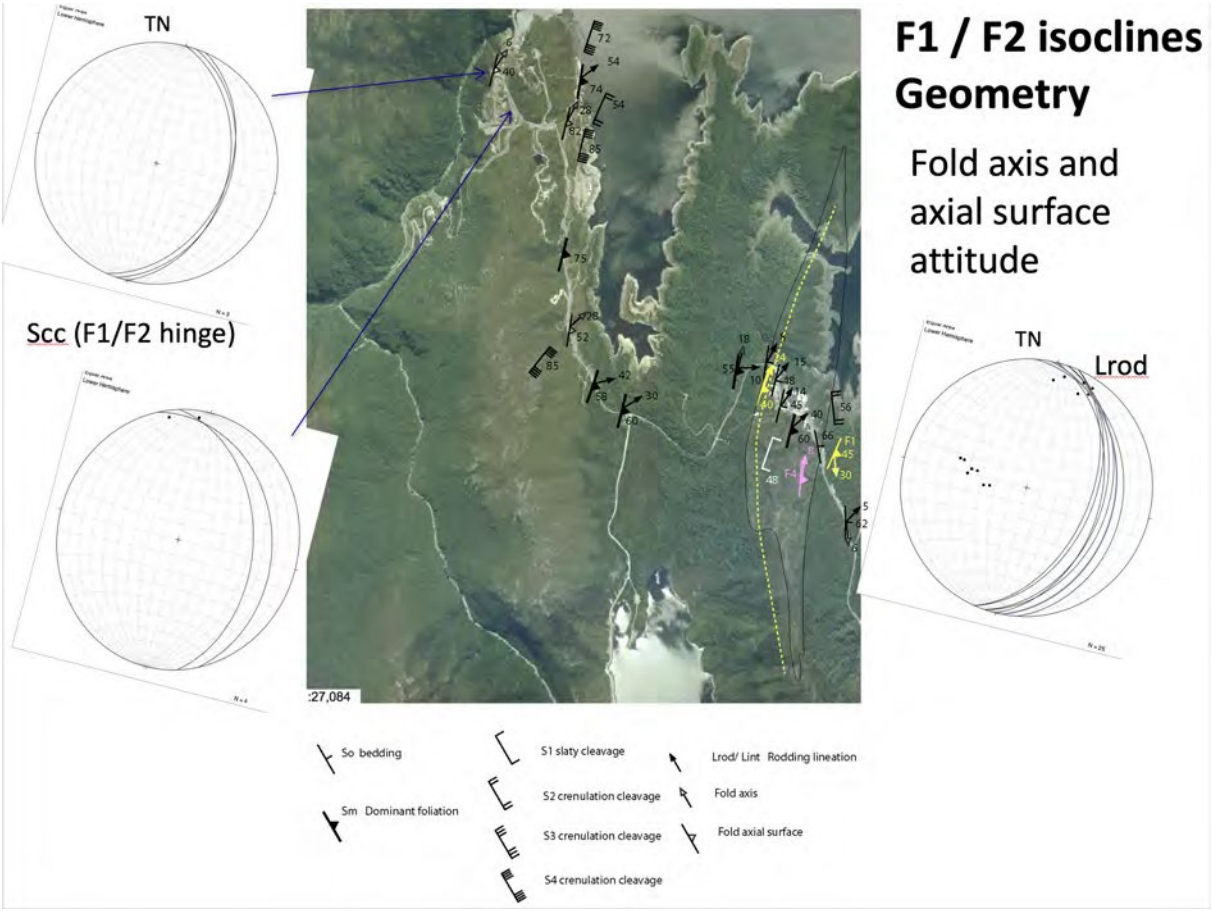

Figure 19: Geometrical elements of the Knob macro-fold. The macro-fold hingeline coincides with the arcuate, hump-shaped ridgeline that is bounded by the Gordon River (northwestern part), the Serpentine River (southwestern part), the Gordon River Road (northeastern part) and the Serpentine Dam road (southeastern part). a) Stereonet of the axial surface S2 foliation (Scc) showing an approximate north-south strike and a ~40° dip to the east. b) Mesoscopic F2 fold data with S2 axial surfaces (great circle traces) and fold axes (black dots). c) Stereonet of foliation Sm (great circle traces) and the associated rodding lineation Lrod.

Upper limb of Knob antiform

The following outcrop stations (DG17-56 and DG17-57) show the mesoscopic fold geometry and faulted nature of the gently east-dipping upper limb of the macrofold. Both folds and thrust faults show west-directed sense along this upper limb of the west-closing antiformal macro-fold (Figures 20 and 21).

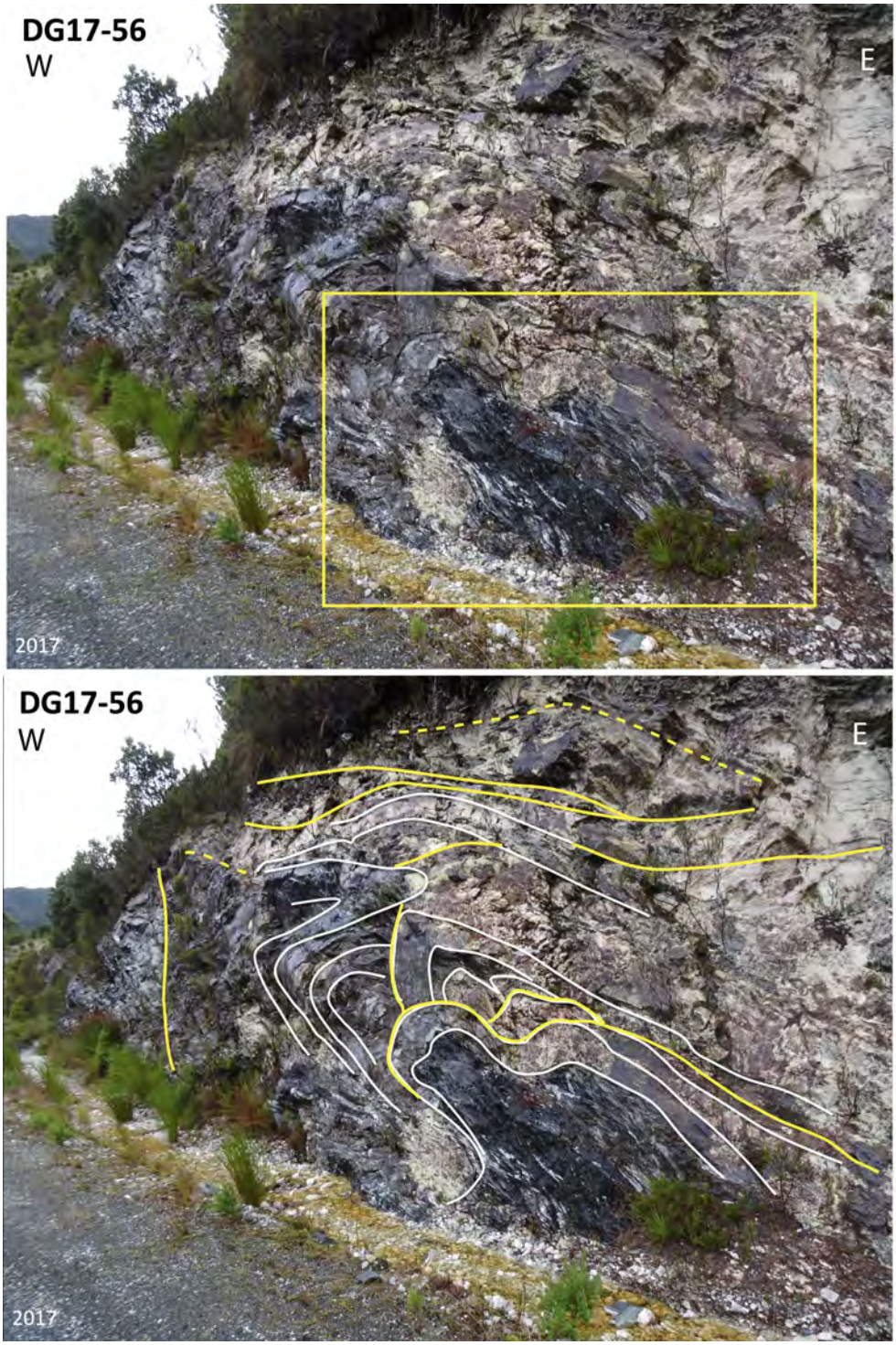

Figure 20: Structural relationships in the upper, gently east-dipping limb of the Knob macro-fold. Gordon River Road cutting above the Gordon Damsite quarry (location DG17-56). An F2 Z-vergent (viewed down plunge to the south) asymmetric fold pair dominates the outcrop. Earlier formed F1 fold hinges are folded by the F2 antiformal fold of the fold pair. There is also clear truncation of one hinge along the So/Sm foliation. Layer parallel faults dominate the upper part of the outcrop (yellow line traces).

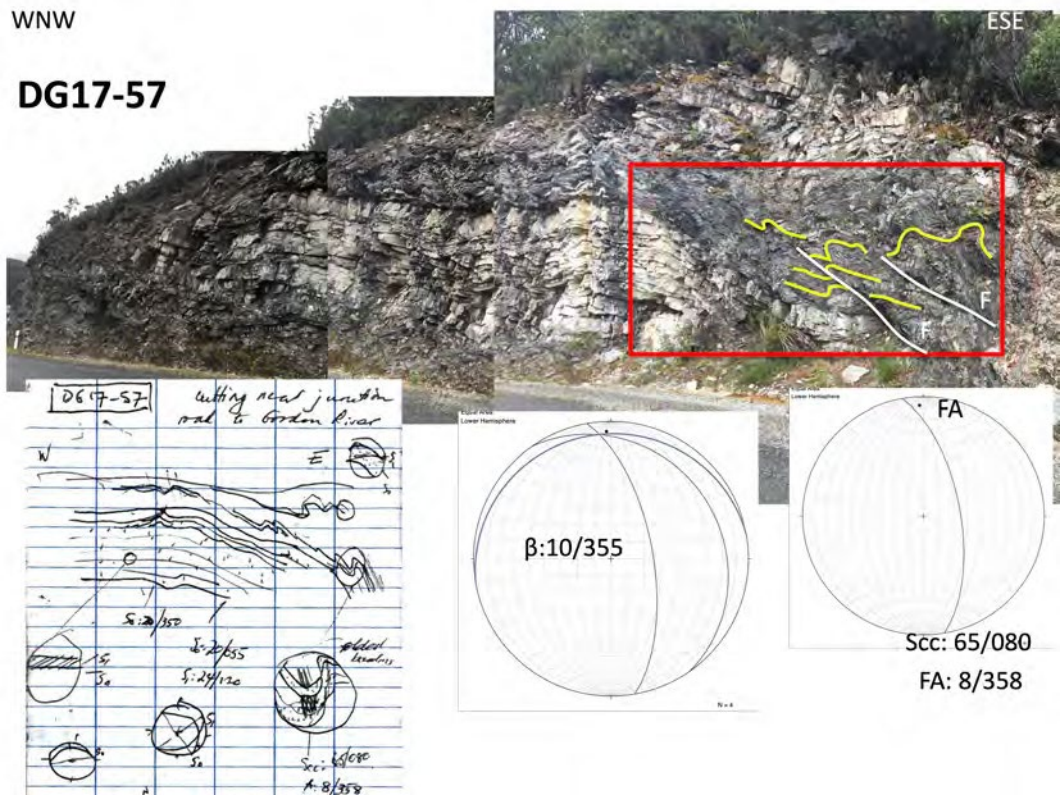

Figure 21: Shallow (~20° dip), north and northeast-dipping upper limb of the Knob macro-fold. Gordon River Road outcrop near road junction with Gordon River power station.

The Gordon Damsite quarry accessed in 1976 shows a series of high strain more intensely foliated to brittle cataclastic zones that separate panels of interlayered quartzite containing asymmetric west-verging fold pairs on the macro-fold upper limb (Figure 22). The quarry also shows the more complex, overprinting deformation at the local scale within these deformation zones through the sequence (Figures 23 and 24).

Figure 22: Gordon Damsite quarry viewed to the south showing an isoclinal asymmetric fold pair (photo upper left), a folded high strain zone (heavy dashed white line trace), a younger open antiform (photo lower right). Photo taken in 1976.

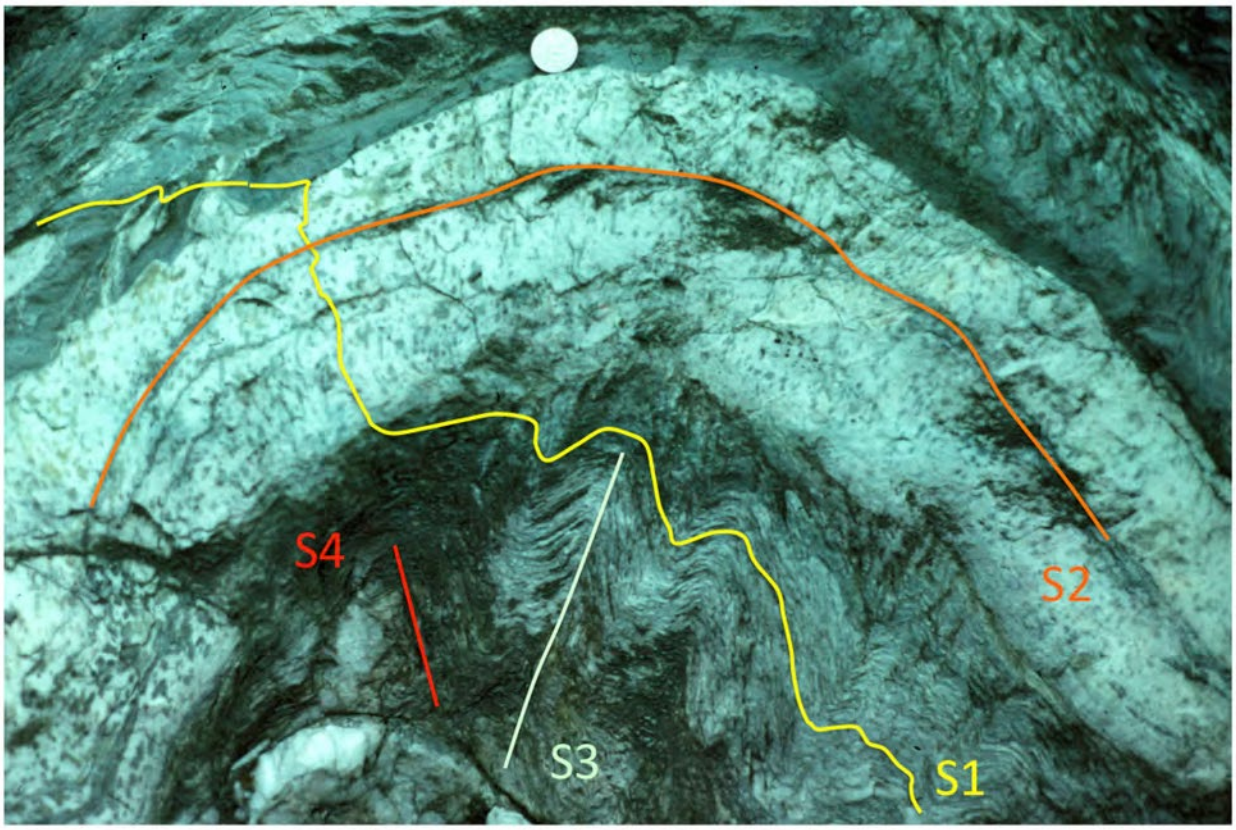

Figure 23: Overprinting relationships in Gordon Damsite quarry.

W E

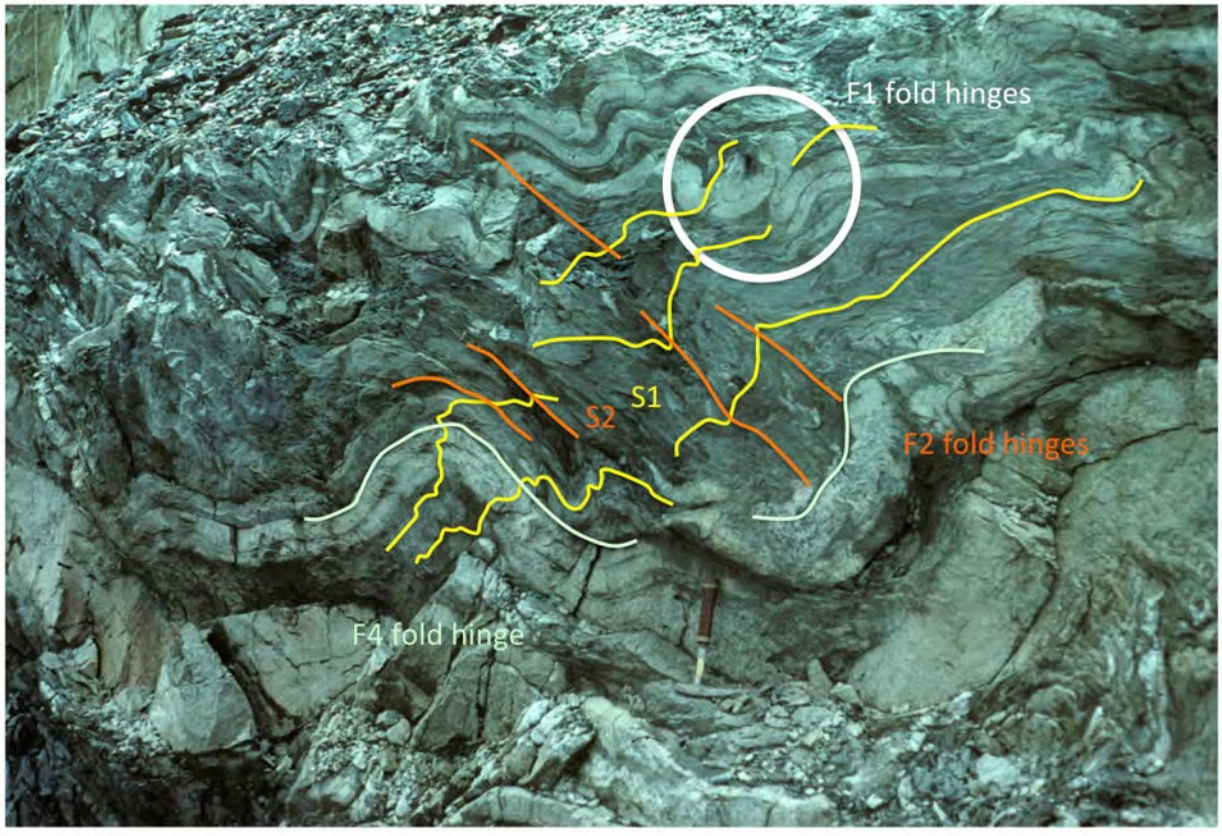

Figure 24: Overprinting relationships in Gordon Damsite quarry.

3.1.2 *The Serpentine Damsite*

Structural relationships at the south end of the Knob antiformal macro-fold are shown at the Serpentine damsite (Figures 25, 26, 27 and 28). These outcrops represent the steeply dipping western limb of the macrofold. The dominant So/Sm compositional layering shows intrafolial metre-scale isoclinal folds (Figures 26 and 27) and complex tectonic "slide"zones that show west-over east shear sense.

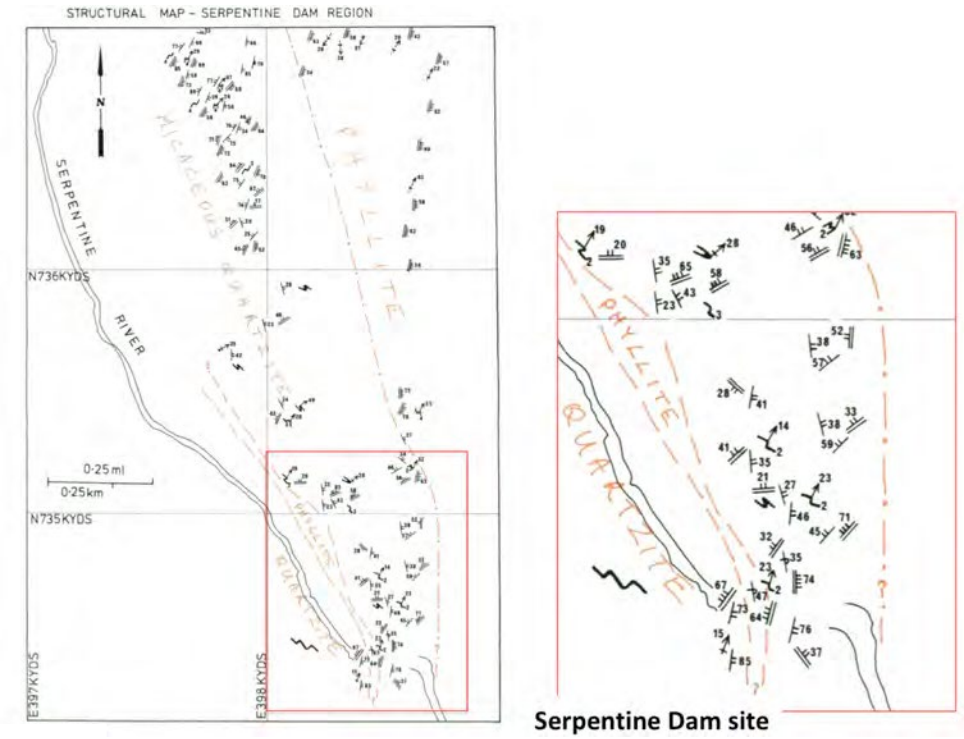

Figure 25: Boulter (1978, fig.4.4) structural map of the Serpentine damsite location (enlargement lower right).

Figure 26: Mesoscopic isoclinal F1/F2 fold bounded on the photo left by an intensely foliated phyllite (high strain zone) containing relict isoclinal fold hinges and strung out quartz veins. The fold occurs within isoclinally folded quartzite in the bed of the Serpentine River at the then newly constructed Serpentine Dam. The photo was taken in 1976 with Clive Boulter for scale.

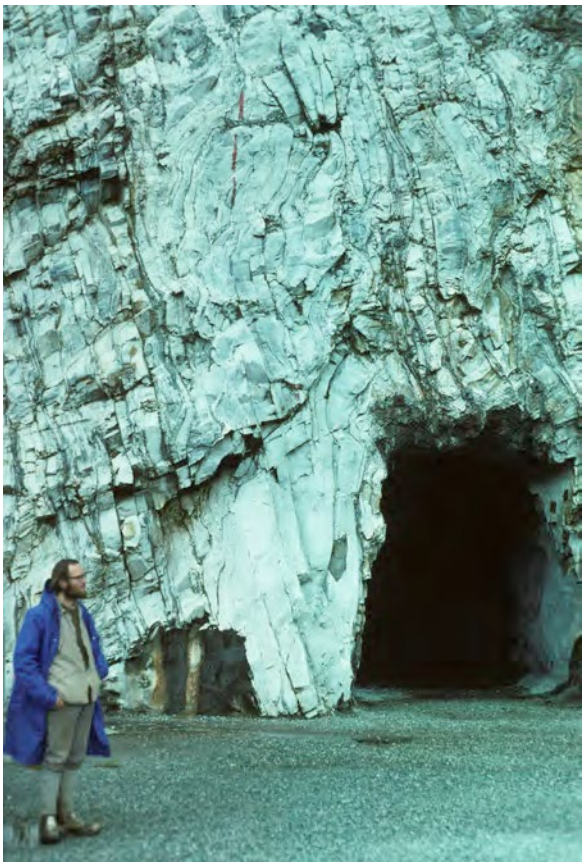

Figure 27: Thicker bedded homoclinally dipping quartzite at the southern Serpentine dam wall abutment. Clive Boulter for scale. Taken in 1976.

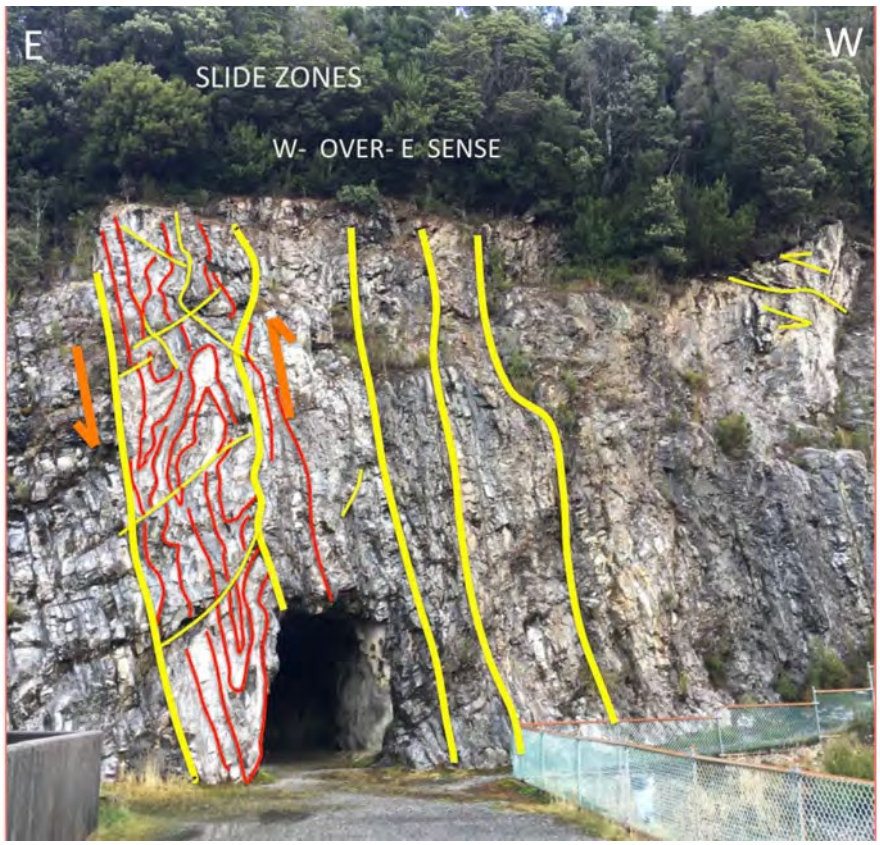

Figure 28: Interpretation of Serpentine Dam south abutment showing disturbed zone ("tectonic slide" after the Scottish Highlands) with west-over-east shear sense.

3.2 The Lake Gordon Boat Ramp high strain zone (HSZ) (Element 2, Figure 2)
The Lake Gordon boat ramp road provides a spectacular, but very oblique section through an intensely foliated high-strain zone (Figures 29 and 30). The zone shows multiple, overprinting crenulation cleavages (Figure 29, 30, 31 and 32) and small to large (up to 10m) dismembered asymmetric fold-augen in quartzite (Figures 34, 35, 36, 37 and 38). The augen are quartzite shear lozenges enveloped by the intense compound Sm foliation (Figures 32, 33 and 38). The Boat Ramp High-strain zone is defined and characterised by:
1) steeply east-dipping crenulation cleavages (S3 and S4, enlargement Figure 29) that together form the compound Scc/Sm (Figures 32, 33, 45 and 46),
2) early isoclinal folds in So/Sm compositional banding with a gently east-dipping enveloping surface (Figures 32, 38, 39), and
3) upright F3 folds that refold and isolate many of the coaxially refolded early folds (Figures 38, 39, 42, 43 and 44).

The flattened and attenuated early isoclinal fold hinges (Figure 37) display marked changes in fold plunge and plunge direction along their respective hingelines (Figures 34, 35, 36, 40, 41 and 42). Such relationships are typical of sheath-like folds that form at significant shear strain (γ>5) with potentially large shear displacements.

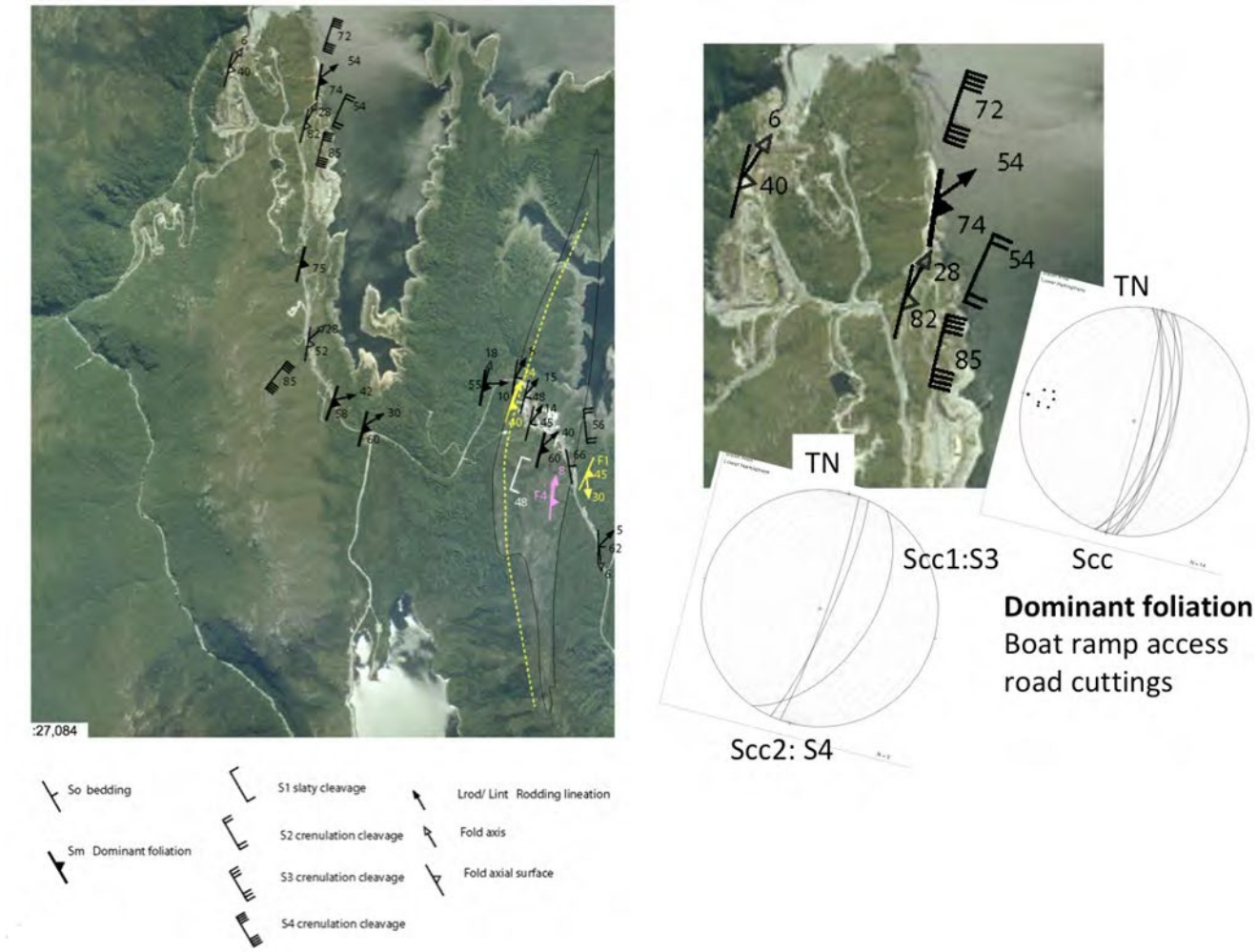

Figure 29: Foliation attitudes for the dominant foliation So/Sm and crenulation cleavages S2, S3 and S4 along the eastern side of the Knob antiformal macro-fold (see also Figure 11). a) Google image of the Knob ridgeline. b) Google image enlargement of the Boat Ramp access road. Stereonet insets show the attitude of the

overprinting dominant S4 foliation in the road cuttings (right) and relationships between the S3 and S4 foliations.

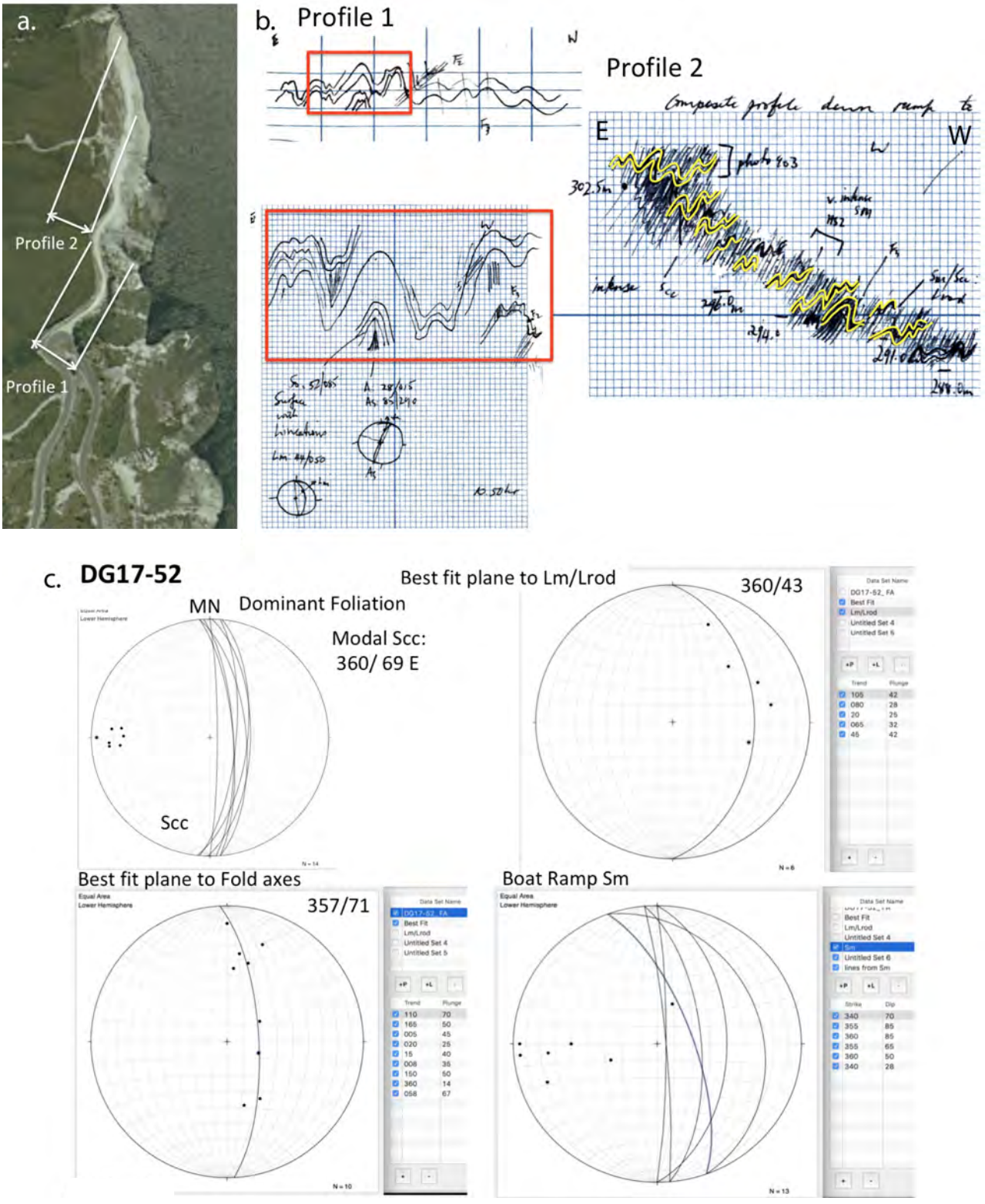

Figure 30: Boat Ramp high strain zone sketch profiles and structural data. a) Profile 1 and 2 locations on Google satellite image. b) Sketch profiles 1 and 2. c) Stereonets (Magnetic) of structural data on the road into the Boat Ramp.

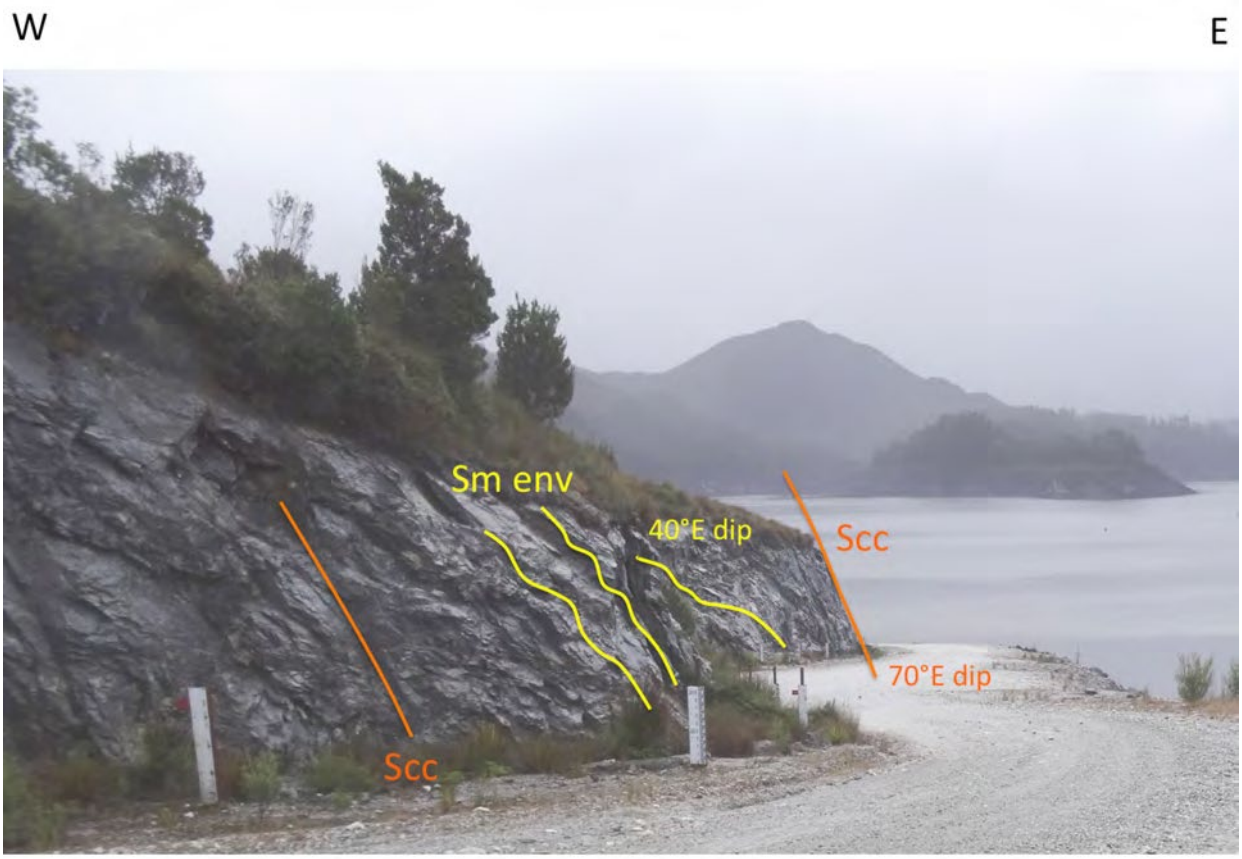

Figure 31: View to the north of road cuttings on road into the Lake Gordon boat ramp.

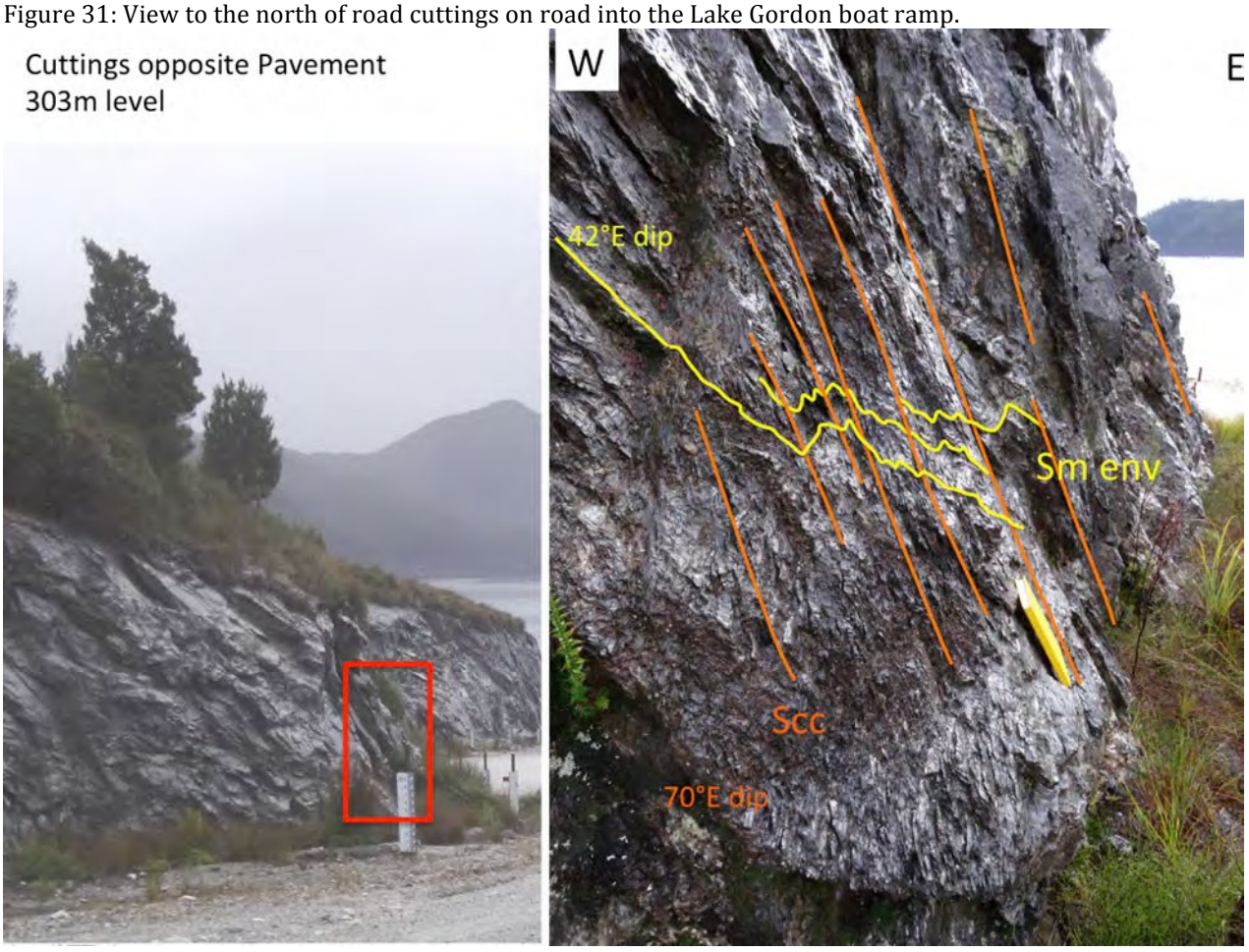

Figure 32: Structural overprinting relationships in the road cutting above.

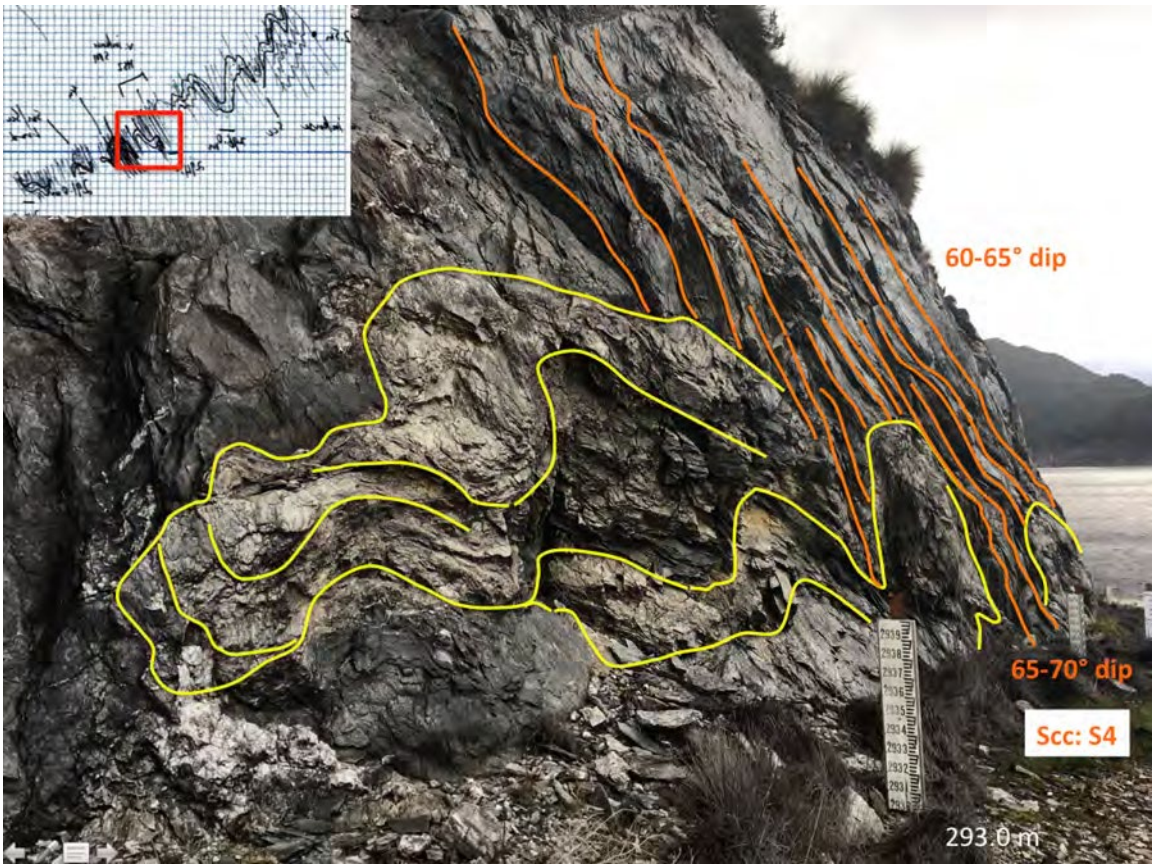

Figure 33: Oblique view of quartzite shear lozenge enveloped by a steeply dipping crenulation cleavage (S4) within the enclosing grey-black, micaceous phyllite.

Figure 34: Longitudinal profile of lower quartzite shear lozenge enclosed by grey-black, micaceous phyllite.

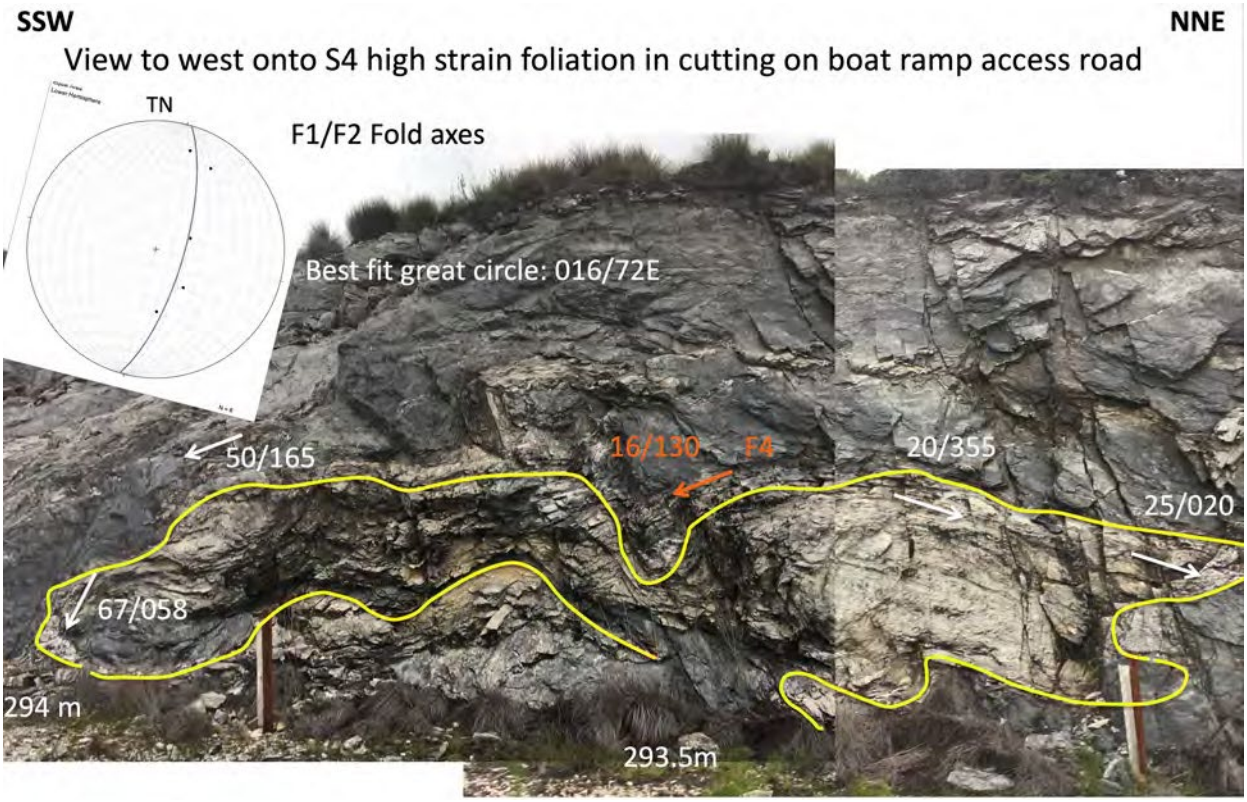

Figure 35: Longitudinal profile of upper quartzite shear lozenge enclosed by grey-black, micaceous phyllite. Intersection traces of segmented and boudinaged sheath-like folded quartzite layer within a D1/D2 high strain zone now refolded in a D4 high strain zone. Relict isoclinal F1/F2 fold hinges within the quartzite show markedly varying fold plunge (shown by the white arrows). The fold axis spread is ~120° within a best-fit great circle 016°/72°E (stereonet inset upper right).

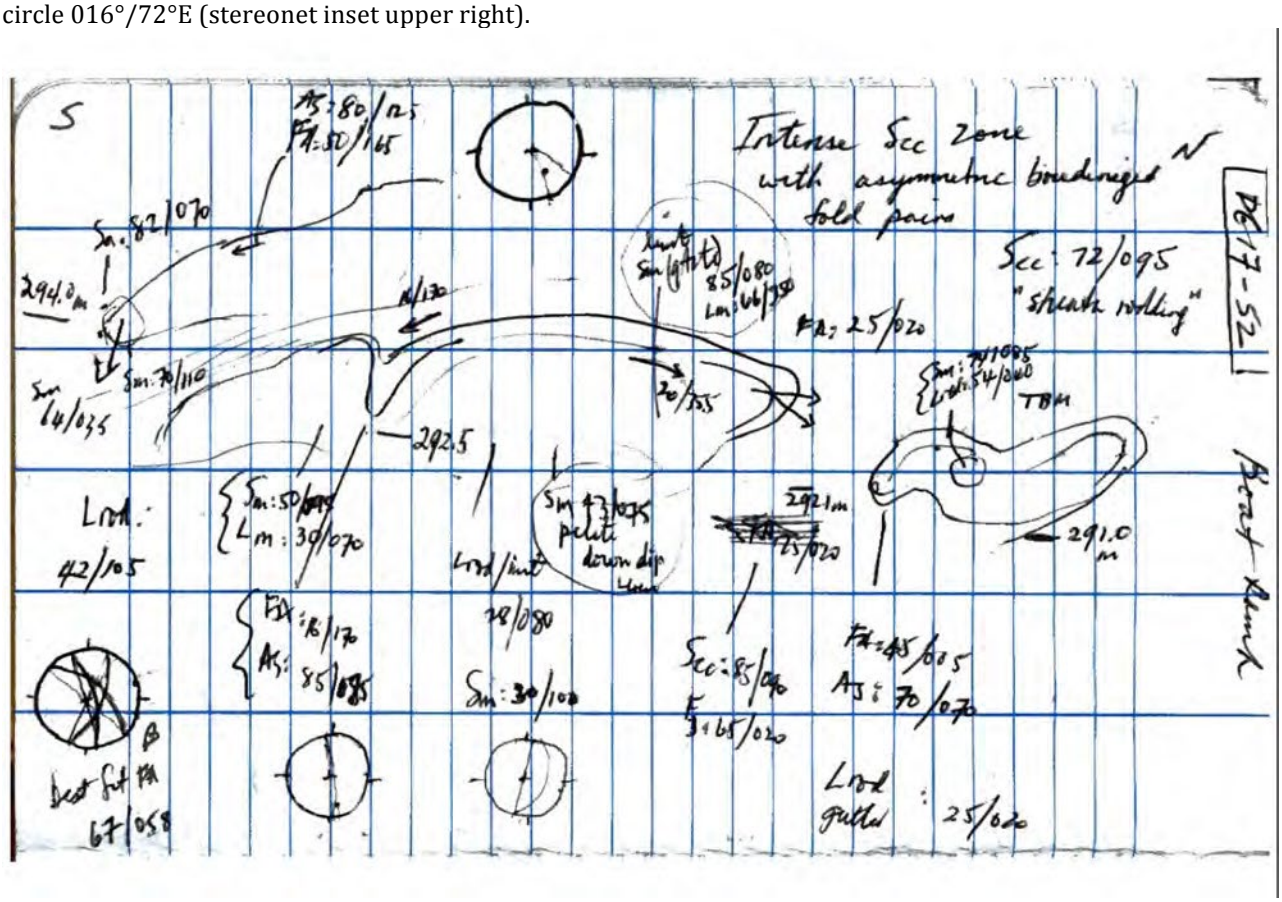

Figure 36: Notebook sketch of the outcrop in Figure 35 with structural measurements.

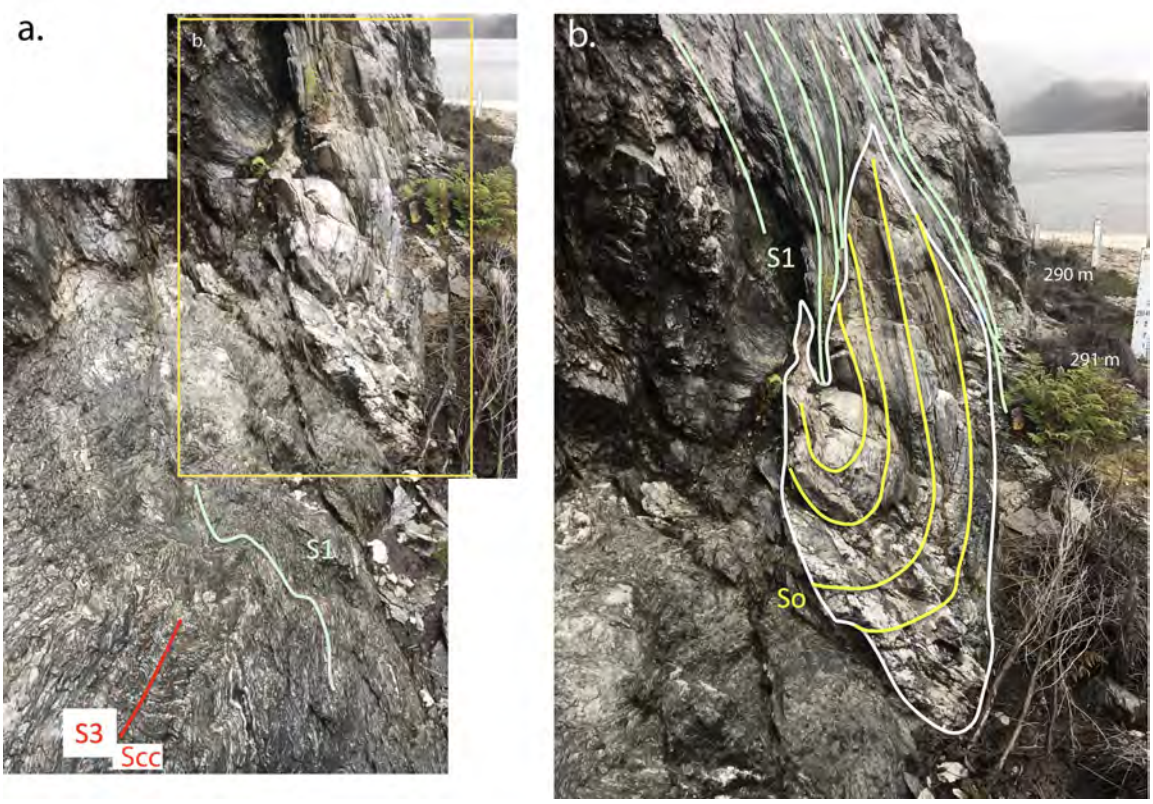

Figure 37: Structural profile through the south end of the quartzite macro-shear lozenge showing a lensoidal relict of a detached, isoclinal fold hinge within So/Sm (yellow line traces). The quartzite lozenge is enveloped by intense foliation Sm/S1 in a micaceous quartzite that is crenulated by a younger crenulation cleavage (Scc/S3) . Plane of photo is level with 292 m height level marker for dam water level.

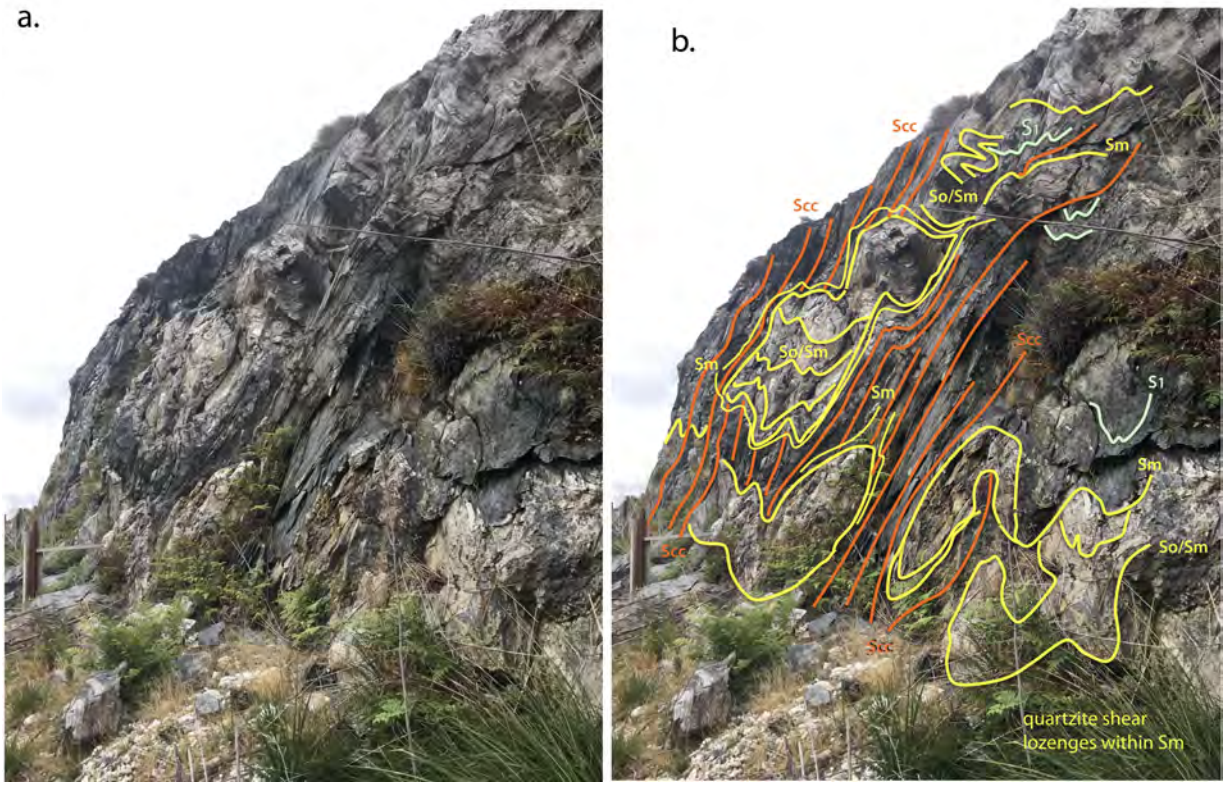

Figure 38: Structural profile through the high strain zone just north of the quartzite macro-shear lozenge showing lensoidal relicts of quartzite shear lozenges in So/Sm (yellow line traces) enveloped by intense foliation Sm/S1. Height level marker for dam water level is 294 m.

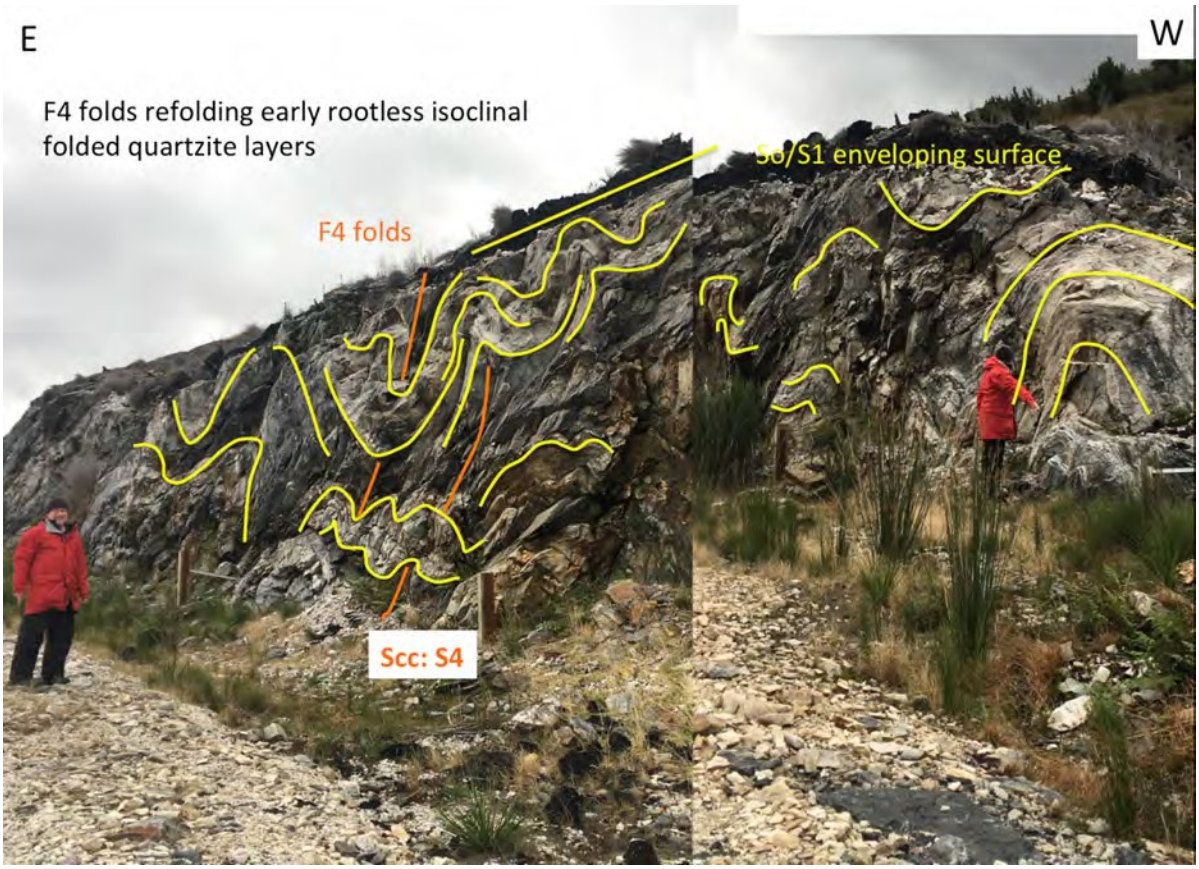

Figure 39: Road cutting (view looking south) showing folded and dismembered quartzite layers.

Figure 40: Road cutting (view looking west) showing marked variability in fold plunge and plunge direction. The folds occur in dismembered quartzite layers. Such variability is typical of sheath-like behaviour in generalised shear.

Figure 41: Road cutting (view looking south) showing a broad fold in a thicker quartzite layer. Michael Vicary is pointing in the direction of fold plunge for the sheath-like fold shown in Figures 41, 42 and 43.

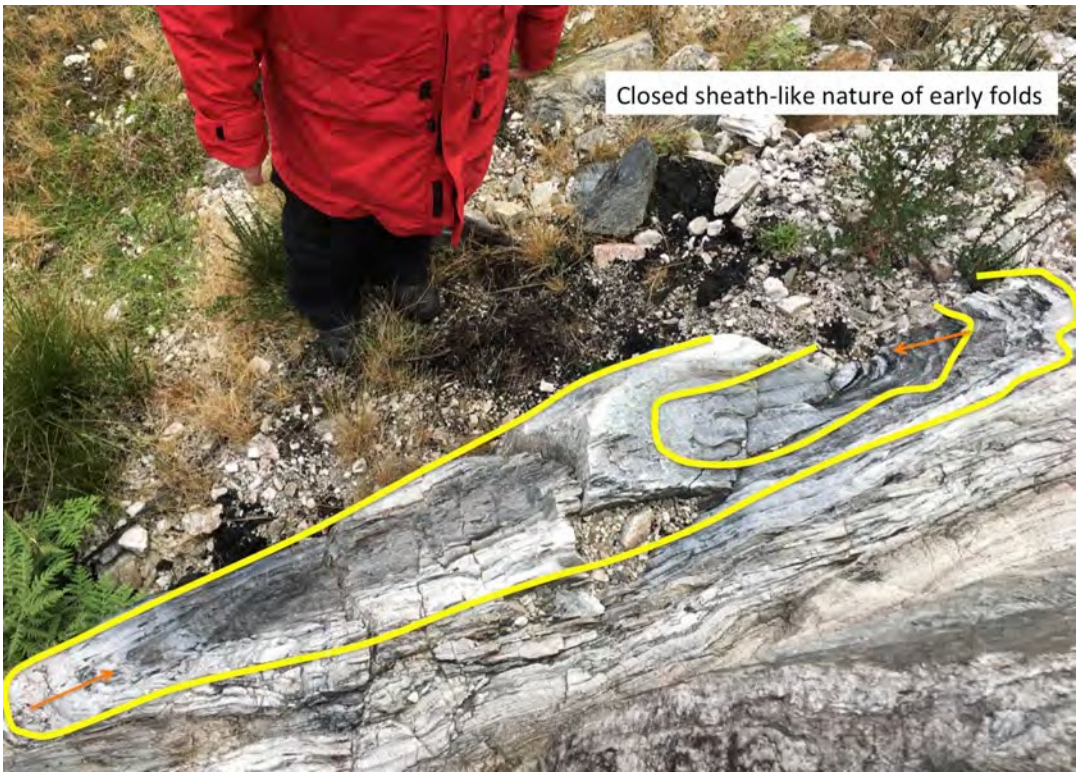

Figure 42: Plan view of plunging fold in Figure 39.

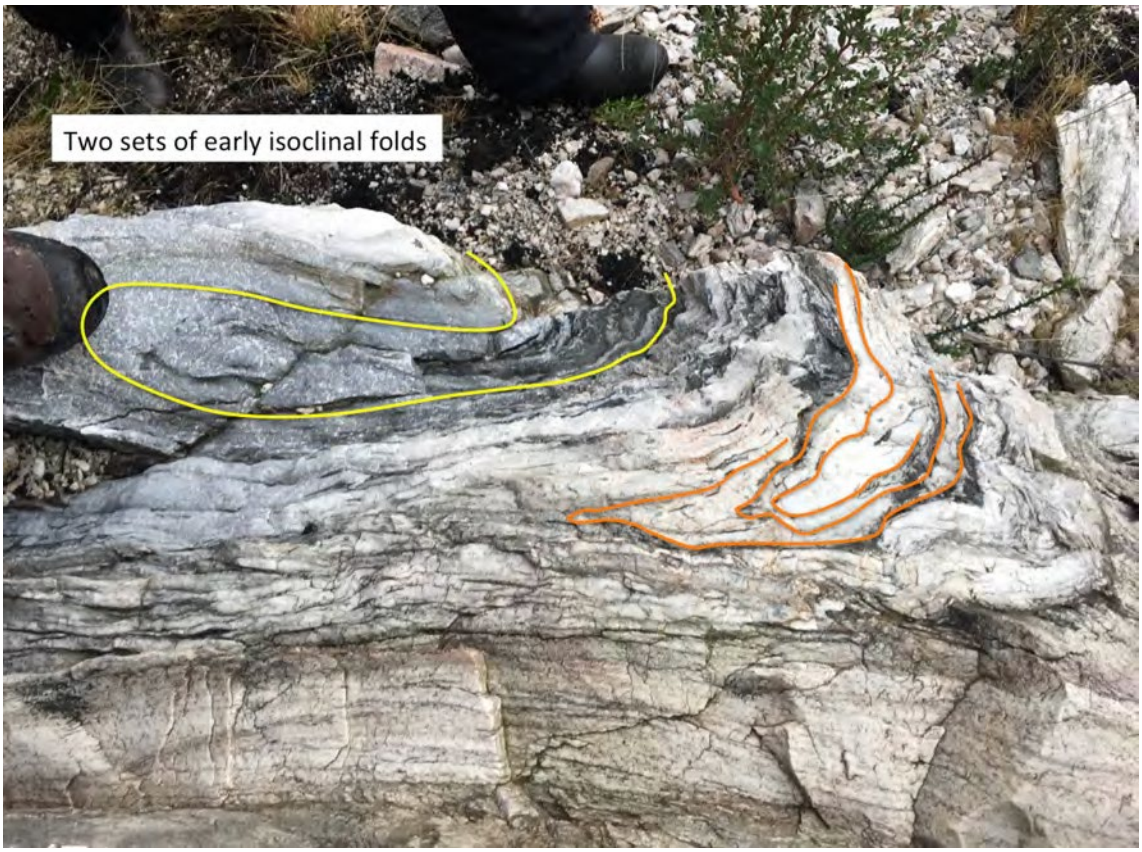

Figure 43: Refolded isoclinal folds within the sheath-like fold in Figure 42. See more detail in Figure 44.

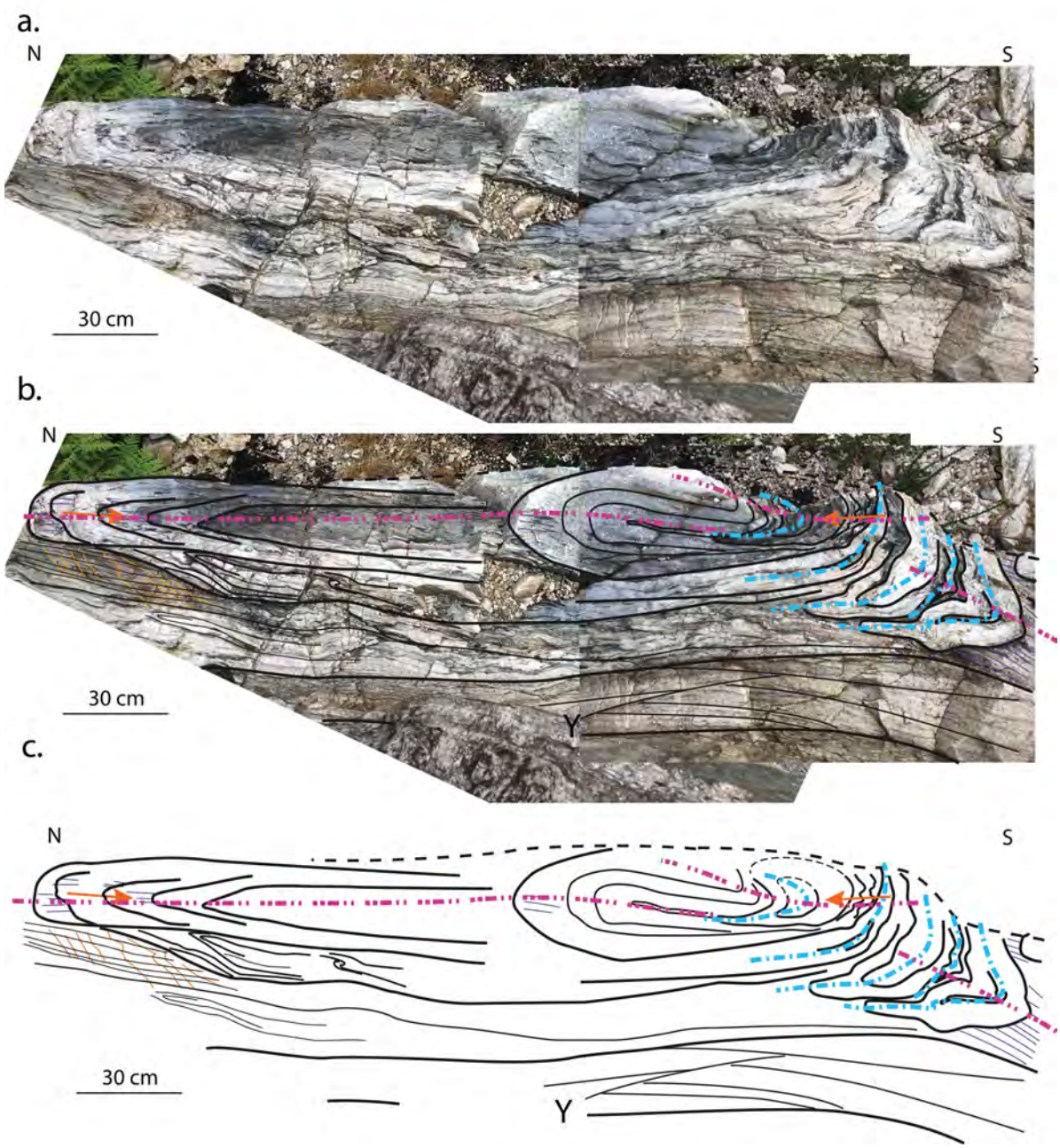

Figure 44: Horizontal section through moderately to steeply plunging sheath-like mesofold in quartzite at Lake Gordon Boat Ramp (water level height 200?m marker). The fold has an ovoid, augen form with closed, inward plunging terminations indicating that the sheath nose is closing into the ground. Heavy black lines: bedding foliation So/Sm. Thin black lines: bedding (So) traces. Thin blue lines: axial surface cleavage (S2) to sheath fold. Thin orange lines: cross cutting foliation (S3). Blue dashed-dot lines: First phase (F1) mesoscopic isoclinal folds. Purple dashed-dot: axial surface trace of second generation (F2) sheath forming folds. Truncated foresets (cross bedding) and scour channels indicate the western limb of the sheath fold youngs to the west.

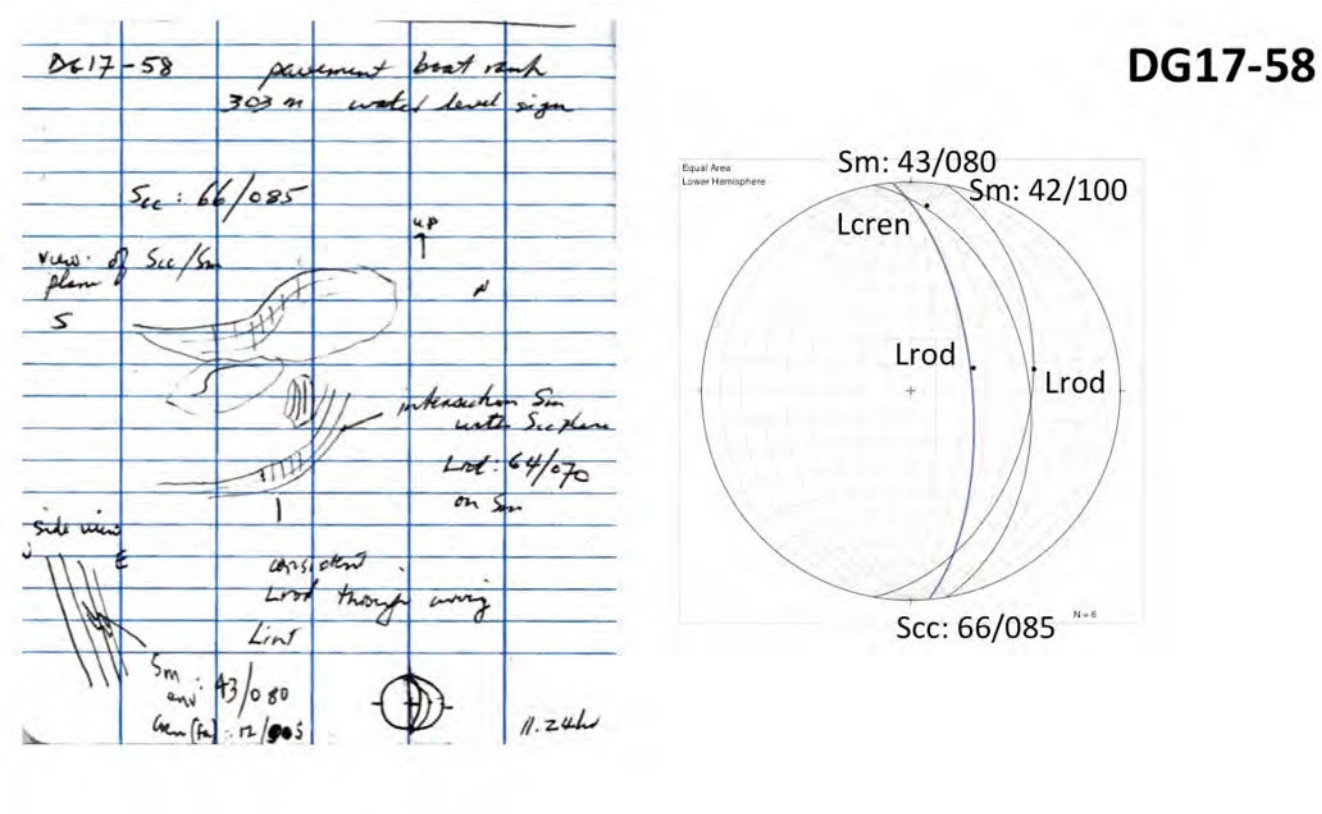

Figure 45: Notebook entry for the structure within a rock pavement on the lake-side of the Boat ramp road at 303 m lake level signage (Sketches are plan view). The stereonet shows the attitudes of structures in the outcrop (magnetic readings).

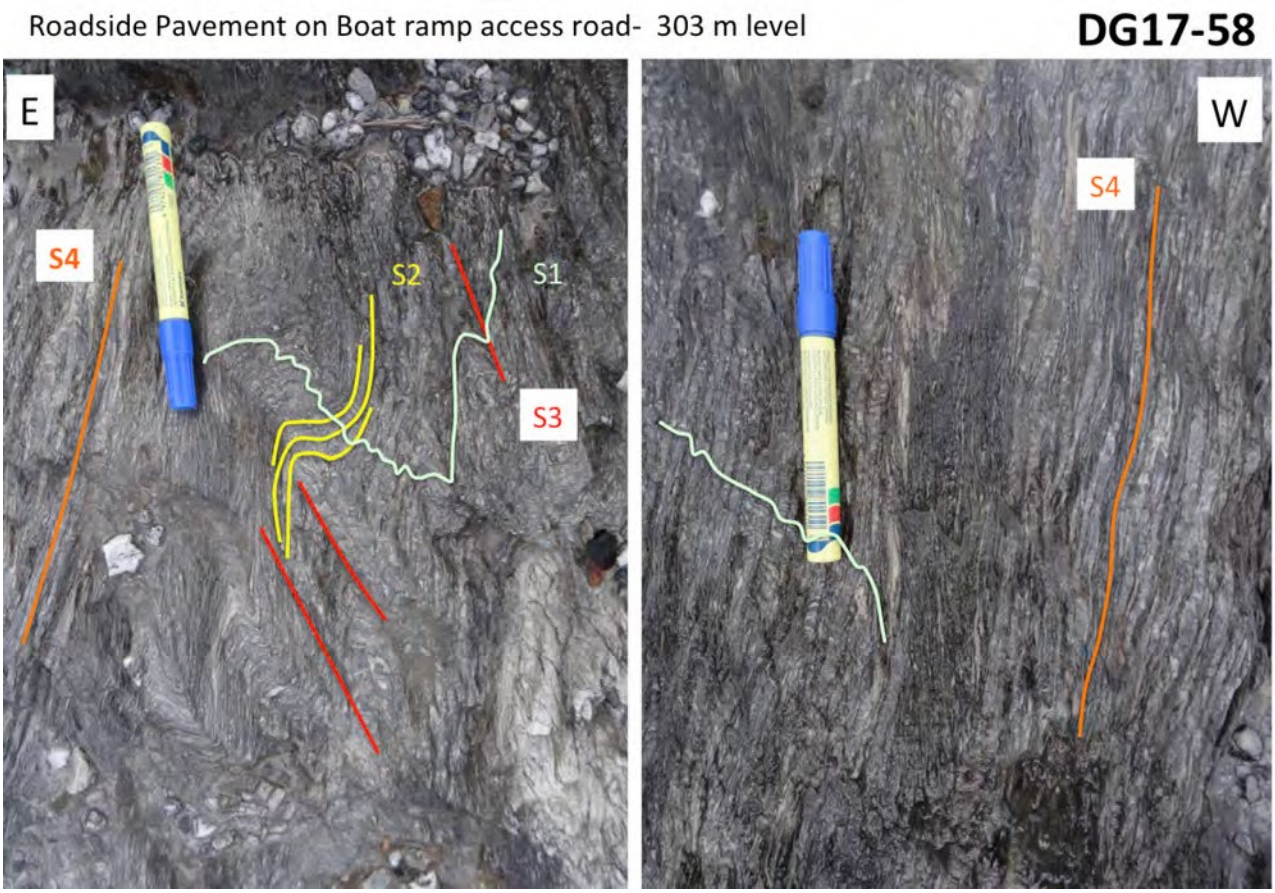

Figure 46: Pavement photographs (plan view) of structural relationships in the Boat Ramp HSZ.

3.3 The Gordon River Road: east-closing macro-fold in quartzite (Element 3, Figure 2)
At a major bend on the Gordon River Road (station DG17-63) the road intersects the hinge of an east-closing macro-fold in quartzite (Figures 47, 48, 49, 50 and 51). Quartzite thicknesses (Figure 48) and an intense Sm on the fold lower limb (Figures 50 and 51) suggest the lower limb is significantly attenuated relative to the upper structurally overturned limb (compare map limb apparent thicknesses, Figure 48). The hinge zone (Figure 51) is cut by foliated zones and/or brittle faults (Figures 51 and 52).

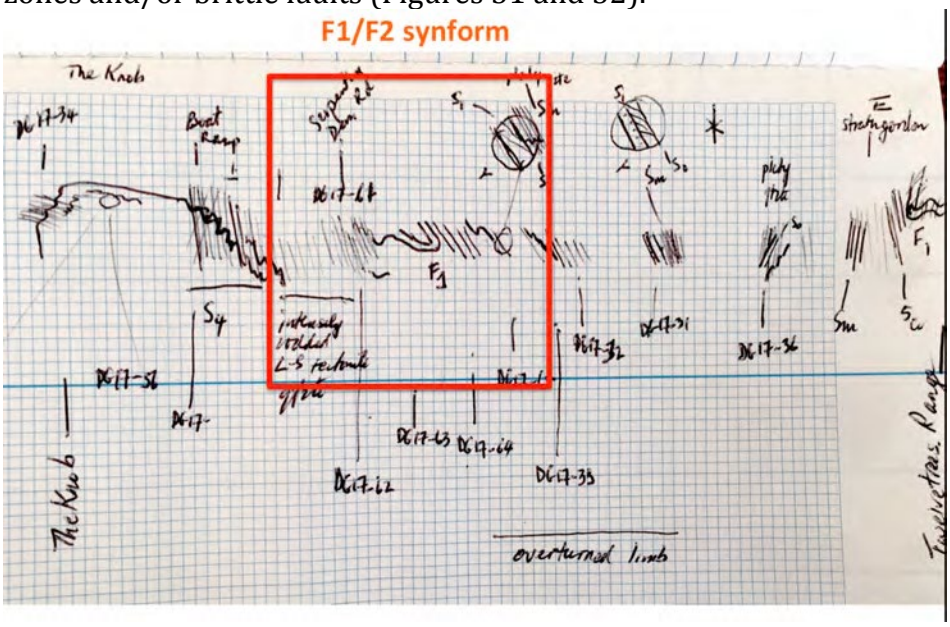

Figure 47: Element 3 major east-closing synform in quartzite.

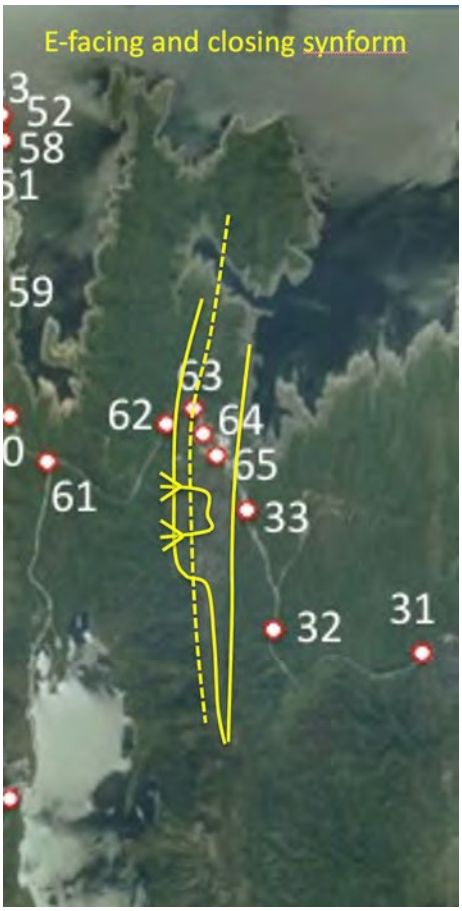

Figure 48: East-closing macro-fold hinge within quartzite showing stations on the Gordon River Road. Google satellite image map base.

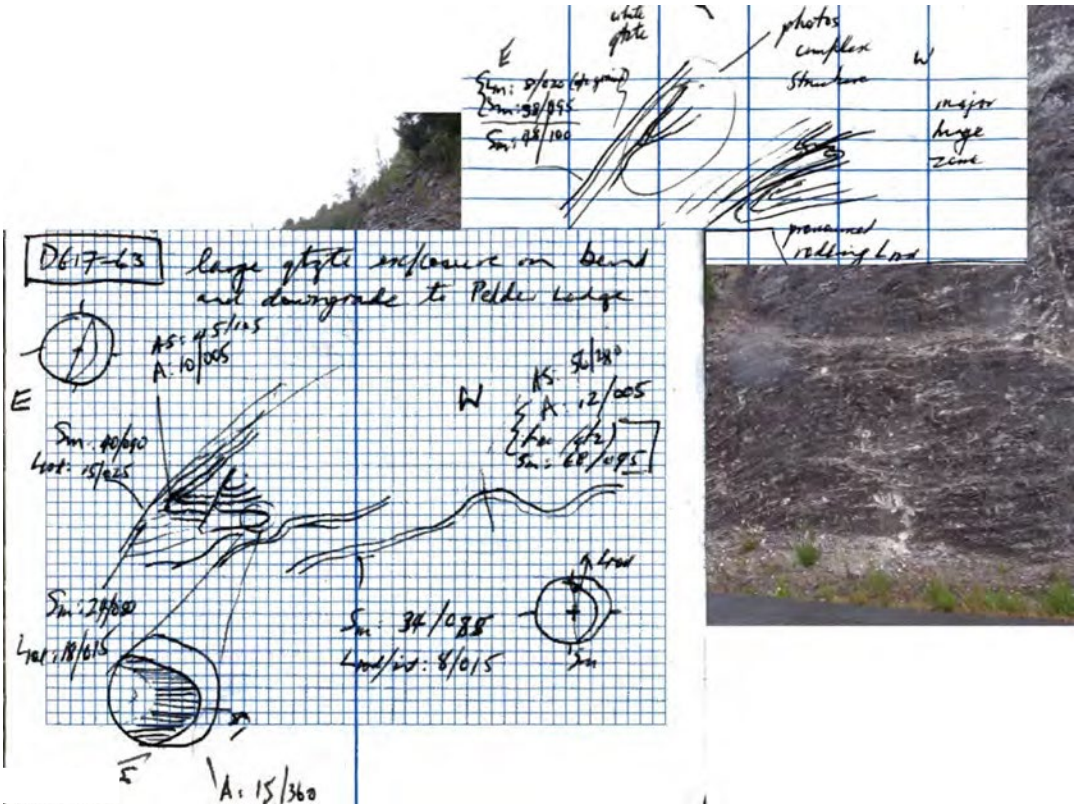

Figure 49: Fieldnote book sketch and measurements of the isoclinal macro-fold hinge on bend on the Gordon River Road (Station DG17-63).

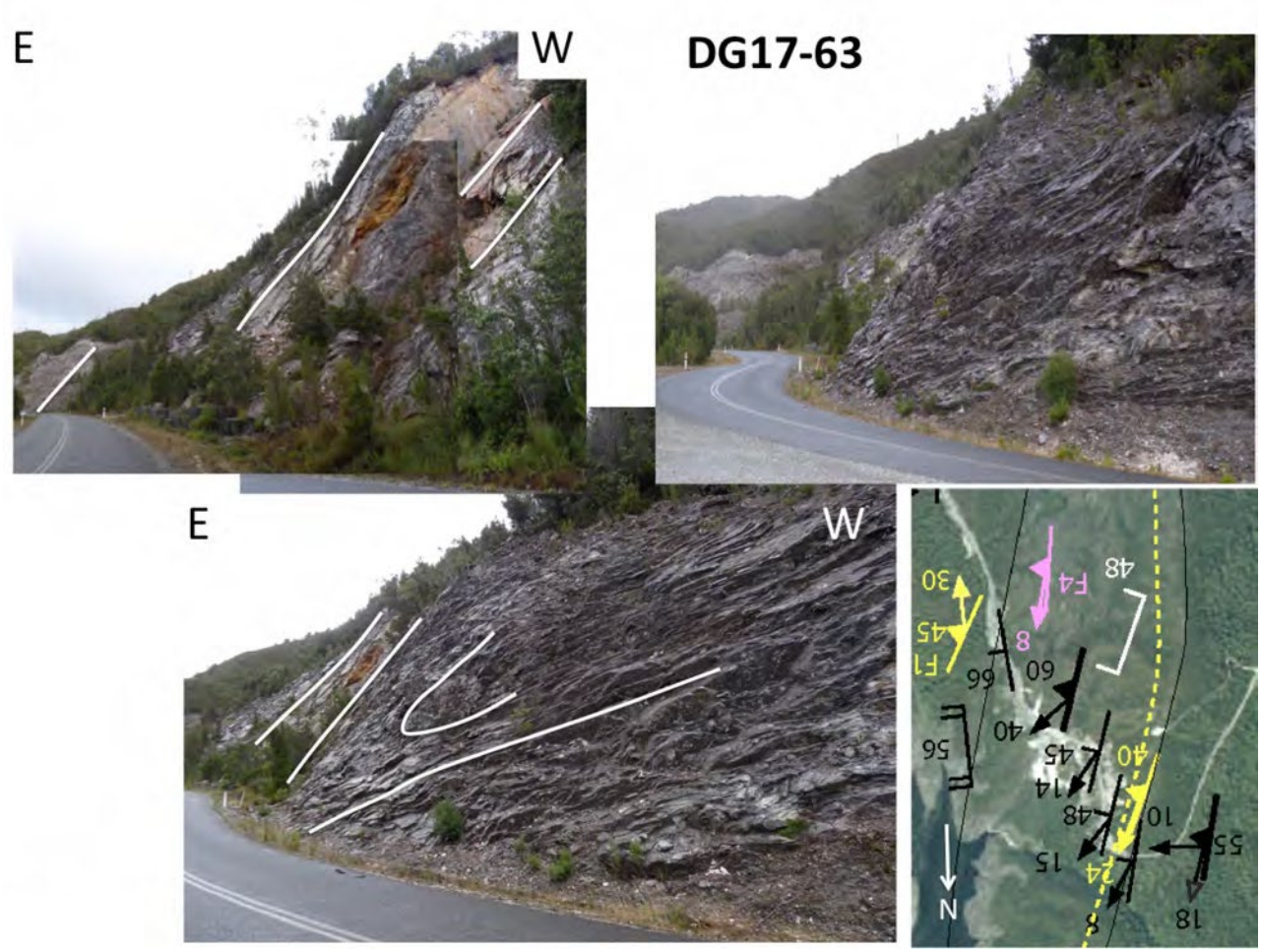

Figure 50: Road outcrop exposure on bend of major east-closing synform.

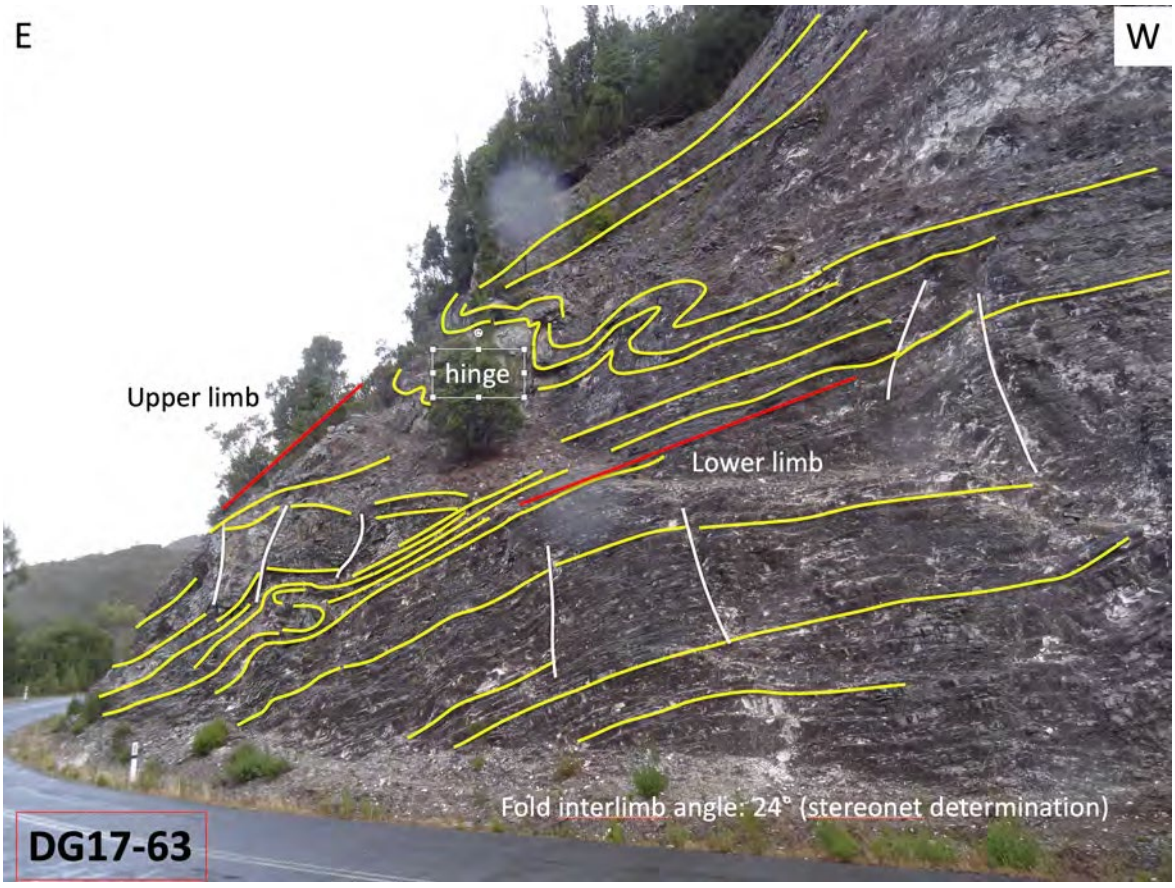

Figure 51: Detailed formline interpretation of the east-closing synform. The lower limb is dominated by intensely foliated Sm. The fold interlimb angle is 24° (stereonet determination from limb attitudes).

Figure 52: Enlargement of the lower part of hinge showing metre-scale, asymmetric isoclinal fold pair bounded by zones of intense foliation Sm and above by brittle faults. Yellow line traces: So/Sm. Heavy white trace: fault

3.4 Gordon River Road: High-Grade Core of upright F3 Synform (Element 4, Figure 2). Relationships between the east-closing macro-fold in quartzite (Element 3) and the interpreted upright, cuspate synform are shown in Figure 53. The structural form and character of the F3 synform are shown in Figures 54, 55, 56, 57, 58, 59, 60, 61, 62 and 63.

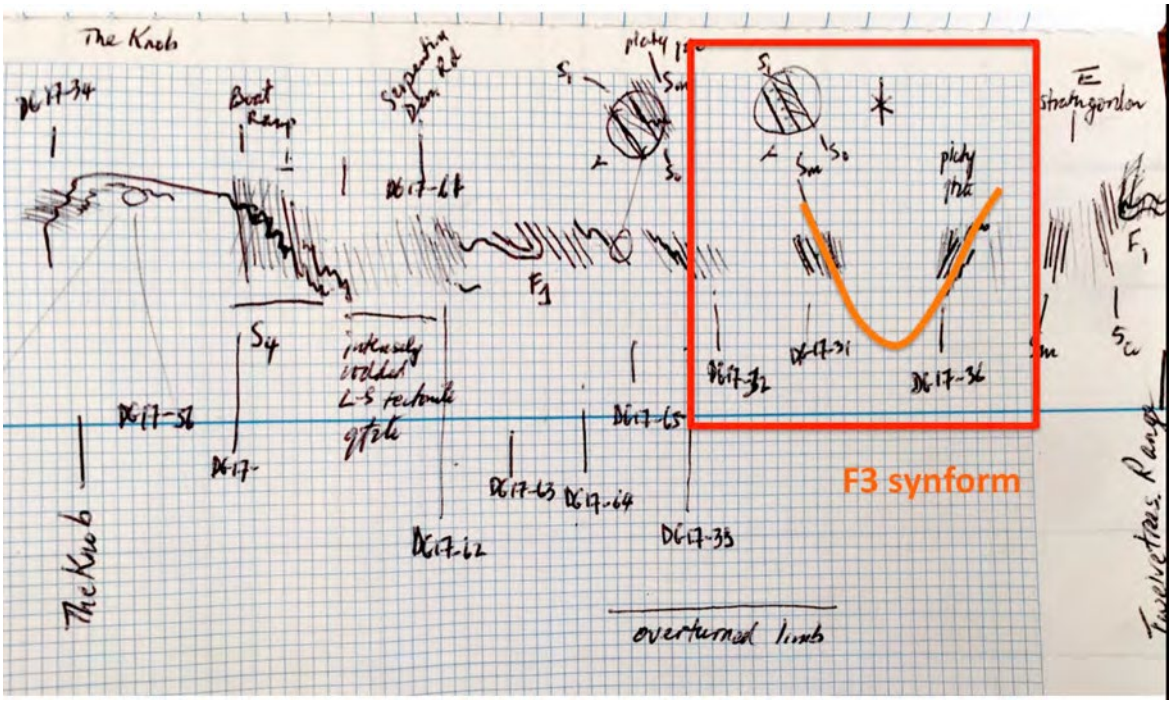

Figure 53: Sketch profile showing the position and form of the high-grade Core synform.

3.4.1 West Limb of F3 Synform (Element 4)

Station DG17-32 typifies quartzite of the western limb of the synform. It shows homoclinal east-dip containing a northeast plunging mineral stretching lineation Lm (Figure 54).

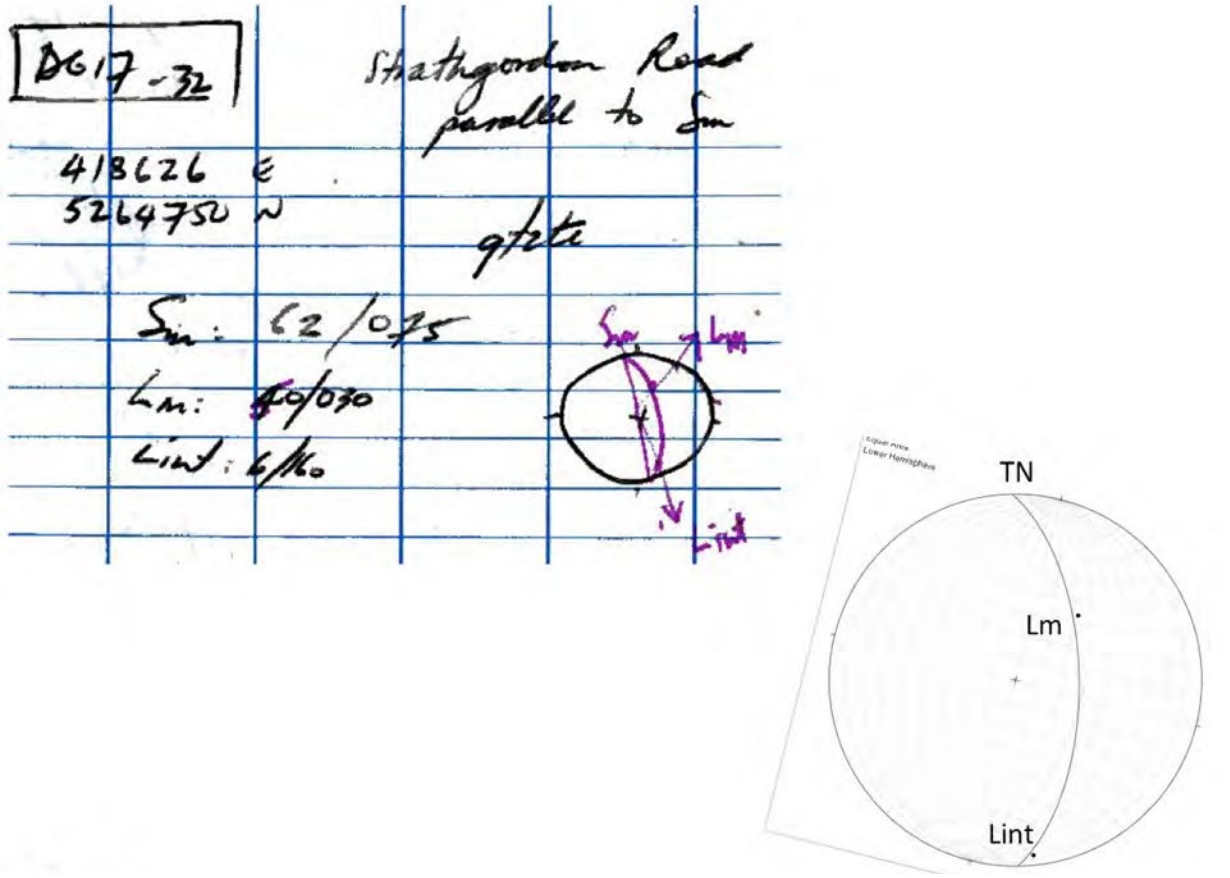

Figure 54: The outcrops DG17-31 and DG17-32 are situated on the eastern overturned limb of the east-closing isoclinal macro-fold (Element 3) or the western limb of the upright F3 synform with H-G core (Element 4).
Top: quartzite on the western limb of the HG synform showing northeast-plunging mineral lineation Lm on a steeply east-dipping foliation Sm
Bottom: Lineation and foliation Sm attitudes at station DG17-32 on the Gordon River Road.

3.4.2 Hinge of F3 synform (Element 4)

The interpreted hinge zone is dictated by a core of high-grade porphyroblastic schist situated between limbs in quartzite with opposing dips (Figures 53 and 55). The calculated F3 fold plunge is 10°/160° (stereonet inset, Figure 55). Variations in metamorphic grade (Port, 2023) suggest imbrication and/or sheet stacking within the high-grade synformal core (see Section 5.4, GSP14). The presence of lower grade, less deformed interlayered psammite-musdstone sequence (Figure 56), suggested by preservation of deformed mudcracks (Boulter, 1978, fig. 2.9) further supports imbrication of layers with varying metamorpohic grades at the 100 m scales.

A pelitic part of the road section (DG17-31) through the synformal closure shows multiple fabrics (Figures 57 and 58) and shear sense indicators including shear bands (Figure 59) sheared "clasts" (Figure 60). These show west-over-east movement sense in an east-northeast trending movement plane movement plane.

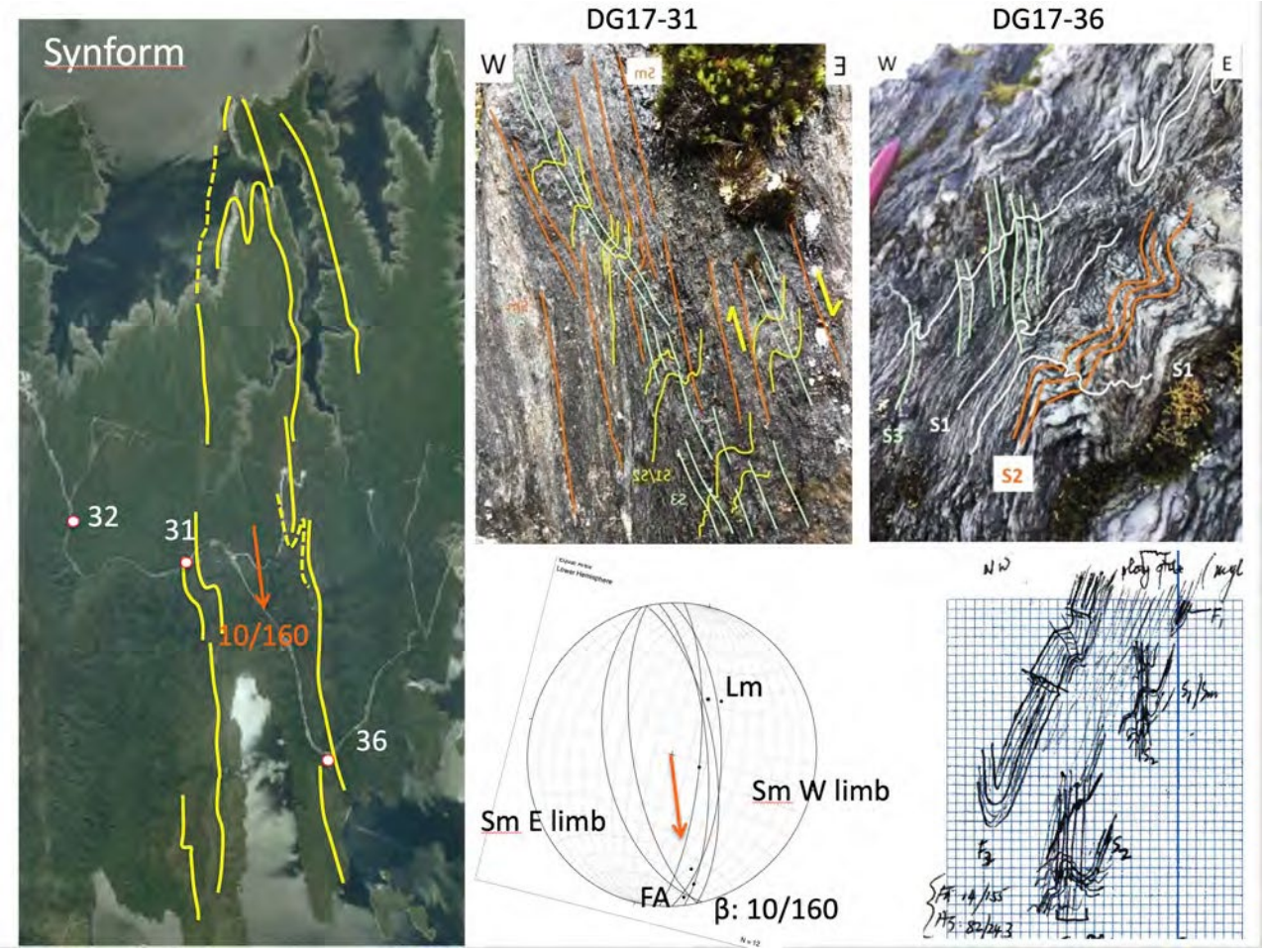

Figure 55: The central part of the Starfish-Knob Basin macro-fold showing the Gordon River Road and outcrop locations DG17-31, DG17-32 and DG17-36. The stereonet shows Sm attitudes from both limbs with a fold plunge of 10°/160° (TN).

Figure 56: Boulter (1978, fig. 2.9) deformed mudcrack locality with HG synformal keel.

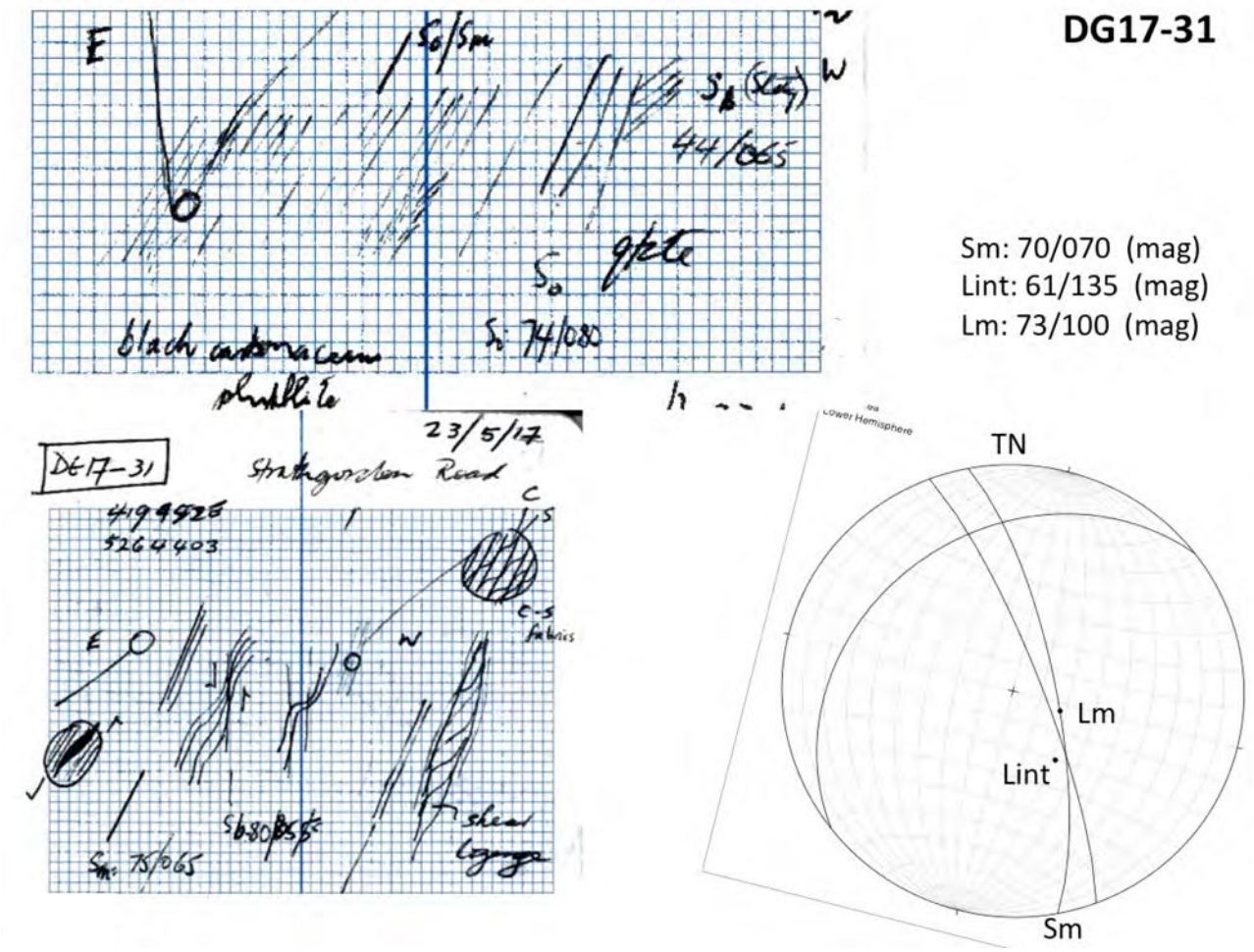

Figure 57: Outcrop sketch and structural relationships at station DG17-31 on the Gordon River Road. The stereonet shows the attitudes of Sm and the mineral lineation (Lm).

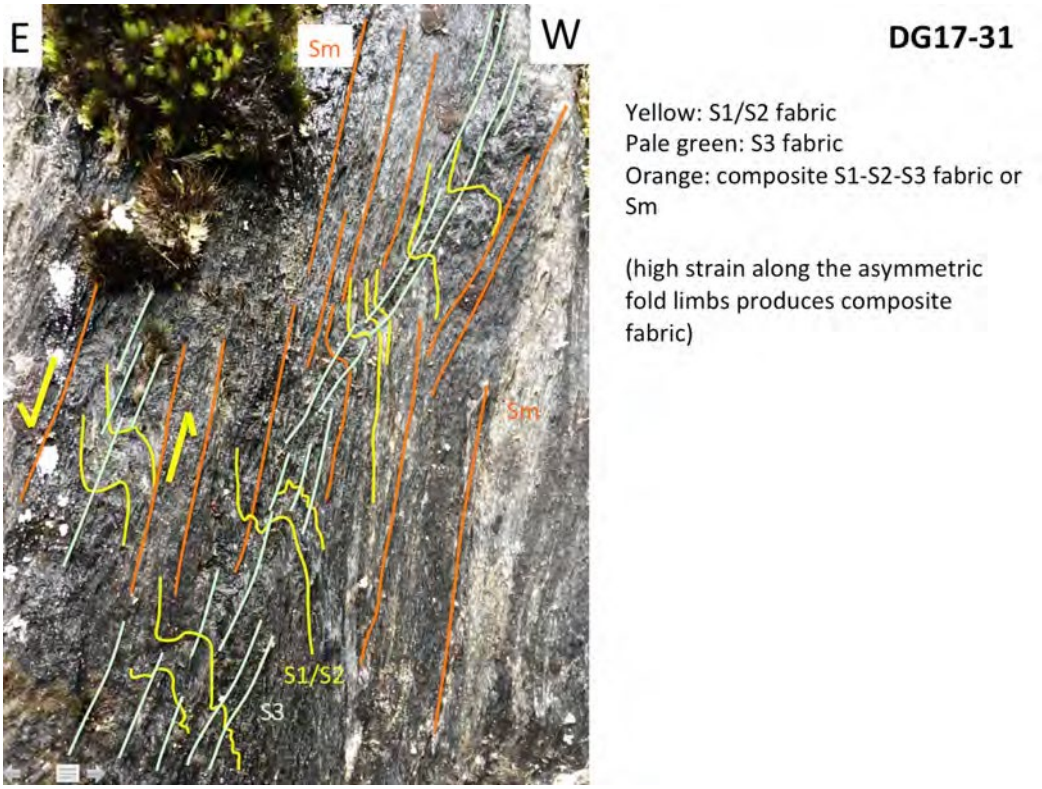

Figure 58: Mesoscopic asymmetric folds and crenulation cleavages in composite foliation Sm. Carbonaceous schist at DG17-31 on the Gordon River Road (see Figure 56 for location on Boulter 1978 map).

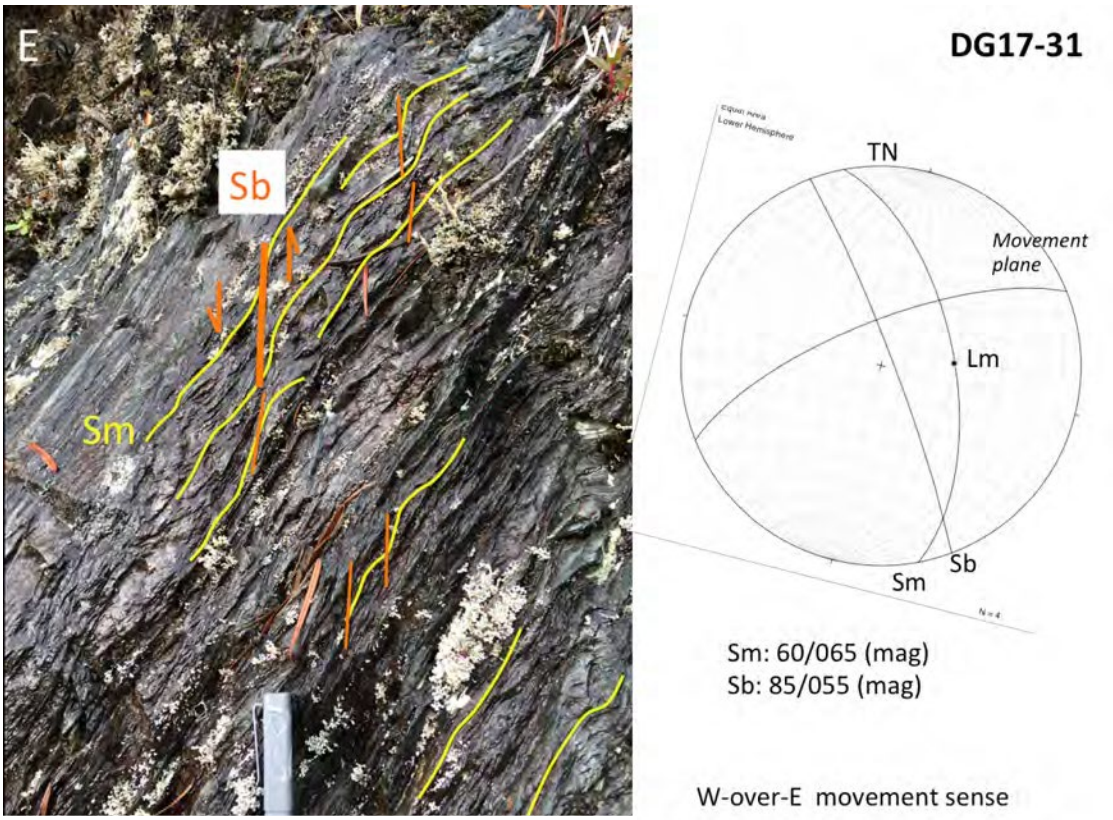

Figure 59: Steeply dipping shear band (S-C' structure) in foliated carbonaceous schist. These show west-over-east movement sense in an ENE movement plane.

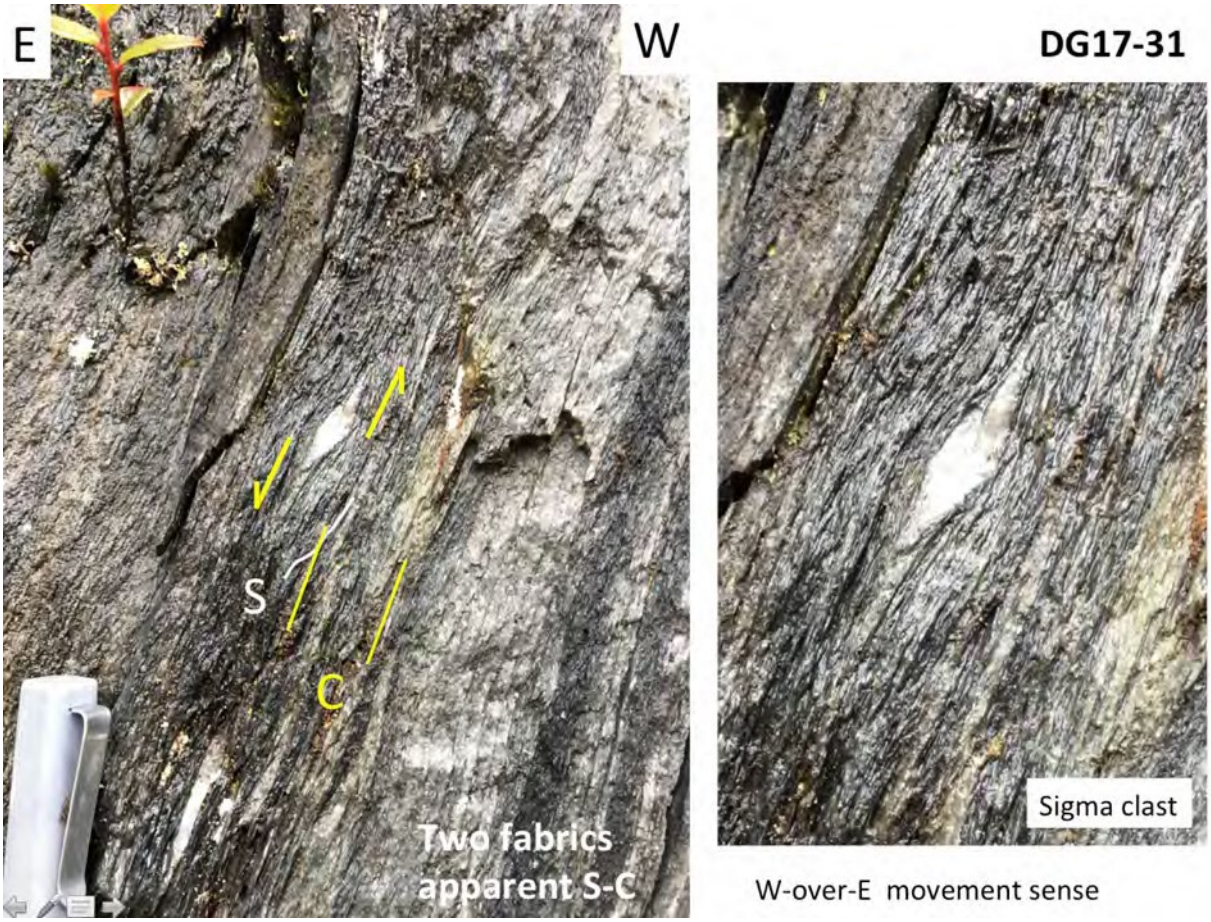

Figure 60: Sigma clast in relict quartz vein also showing west-over-east movement sense.

3.4.3 East Limb of Synform (Element 4)

At the Serpentine Lookout outcrop (DG17-36) a steeply west-dipping pod of quartzite is bounded by strongly foliated Sm shows multiple fabrics (Figures 61, 62 and 63).

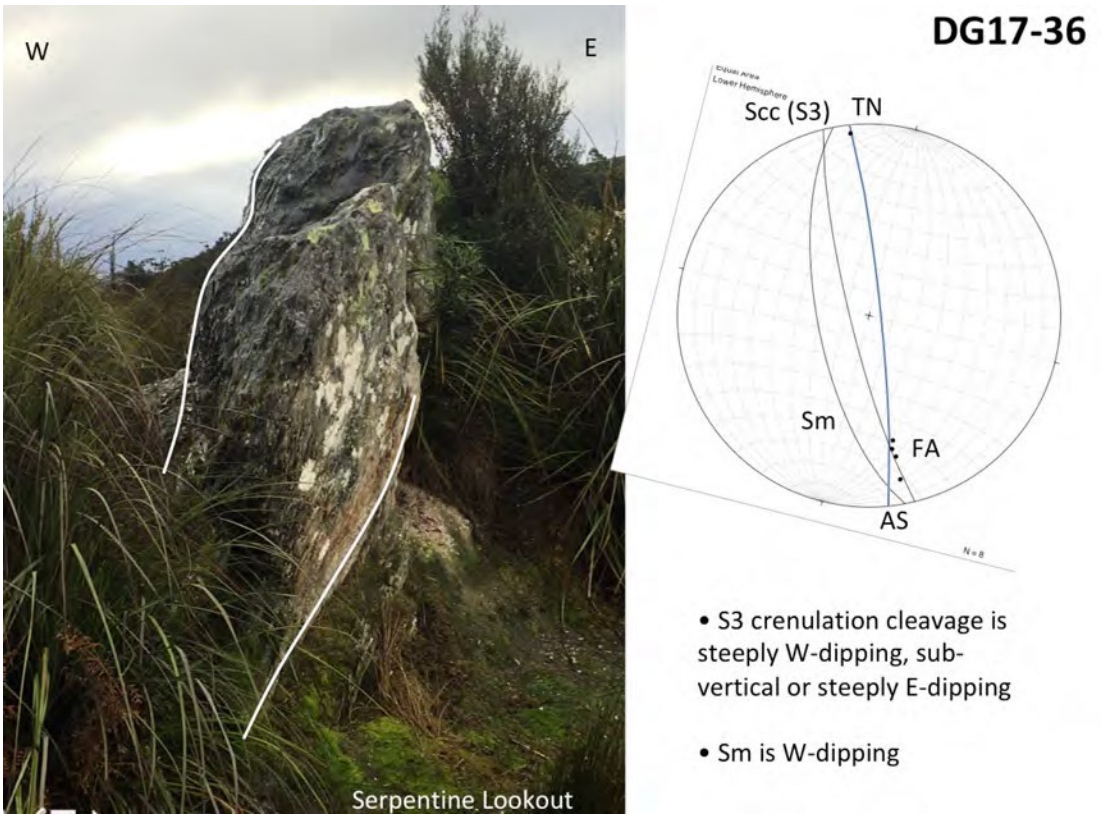

Figure 61: Serpentine Lookout outcrop- pod of quartzite bounded by Sm. Note the phacoidal shape of the quartzite. Station DG17-36.

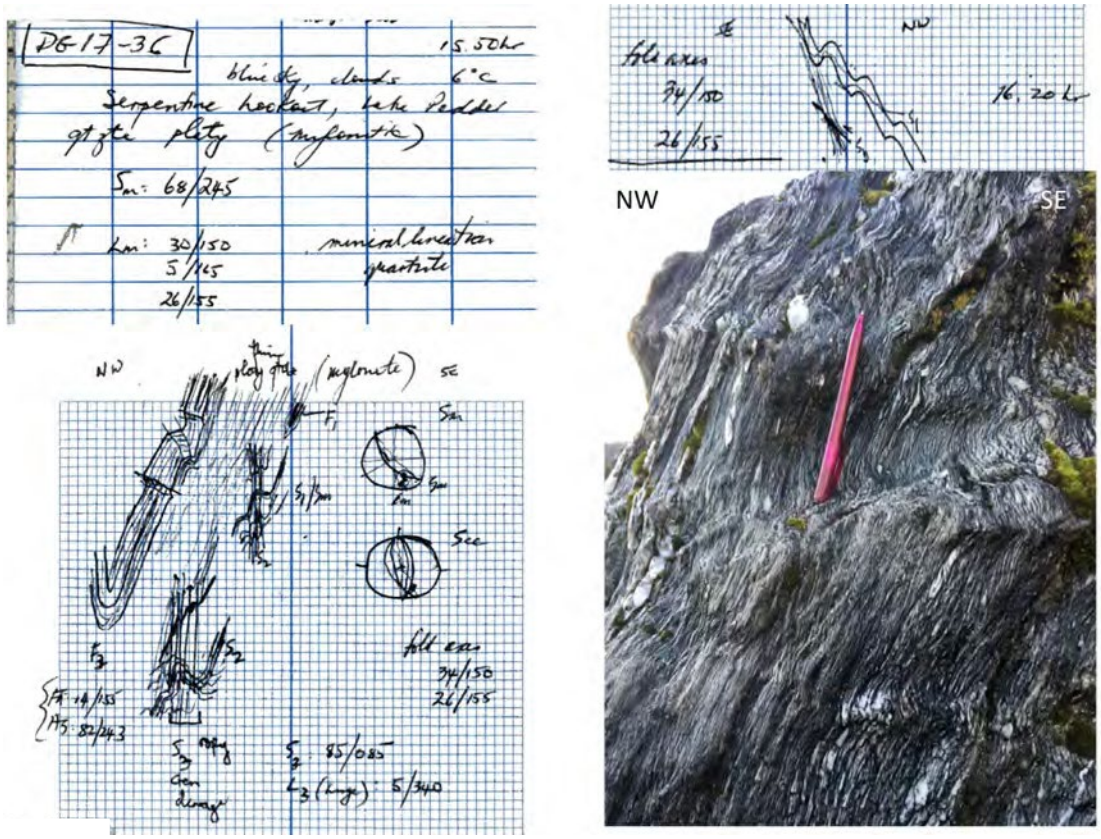

Figure 62: Outcrop relations within the quartzite phacoid or augen. Station DG17-36.

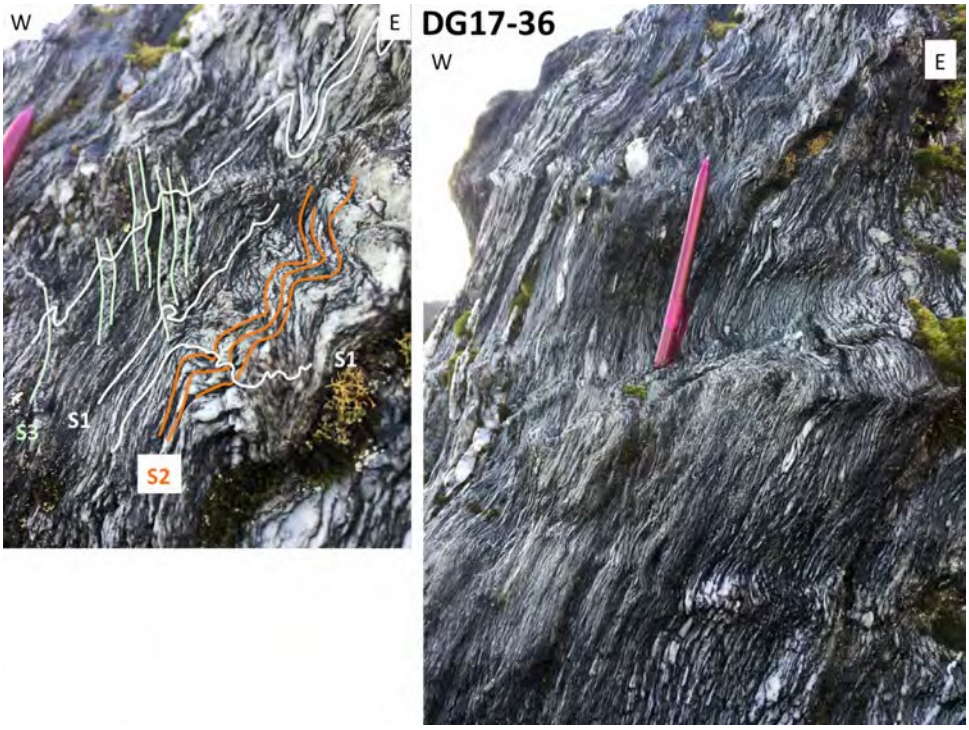

Figure 63: Intense foliation Sm within quartzite augen showing overprinting crenulation cleavages and kink bands.

3.5 Structure of the Twelvetrees Range (Element 5, Figure 2)
Previous investigation by Marcus McClenaghan reported the Twelvetrees Range shows 3 coaxial deformation phases (D1-D3) with F1 and F2 coplanar and similar fold plunges generally to the south at 20° to 40° (fig.3, Brown et al., 1989). The data is shown on the Digital Atlas 1:25,000 map sheet (Figure 64b). A traverse by the authors along the communications tower access road on the south end of the Twelvetrees Range (Figure 64a) enabled construction of a composite structural profile (Figures 65, 66, 67, 68 and 69). The interpreted structure is a west-closing, isoclinal macro-fold (Figure 65) with an upper overturned limb suggested by the foliation compositional layering relationships on the high western part of the range (Figure 70). The central part of the ridgeline is dominated by gently plunging, upright F3 folds (Figures 65, 66, 67 and 71).

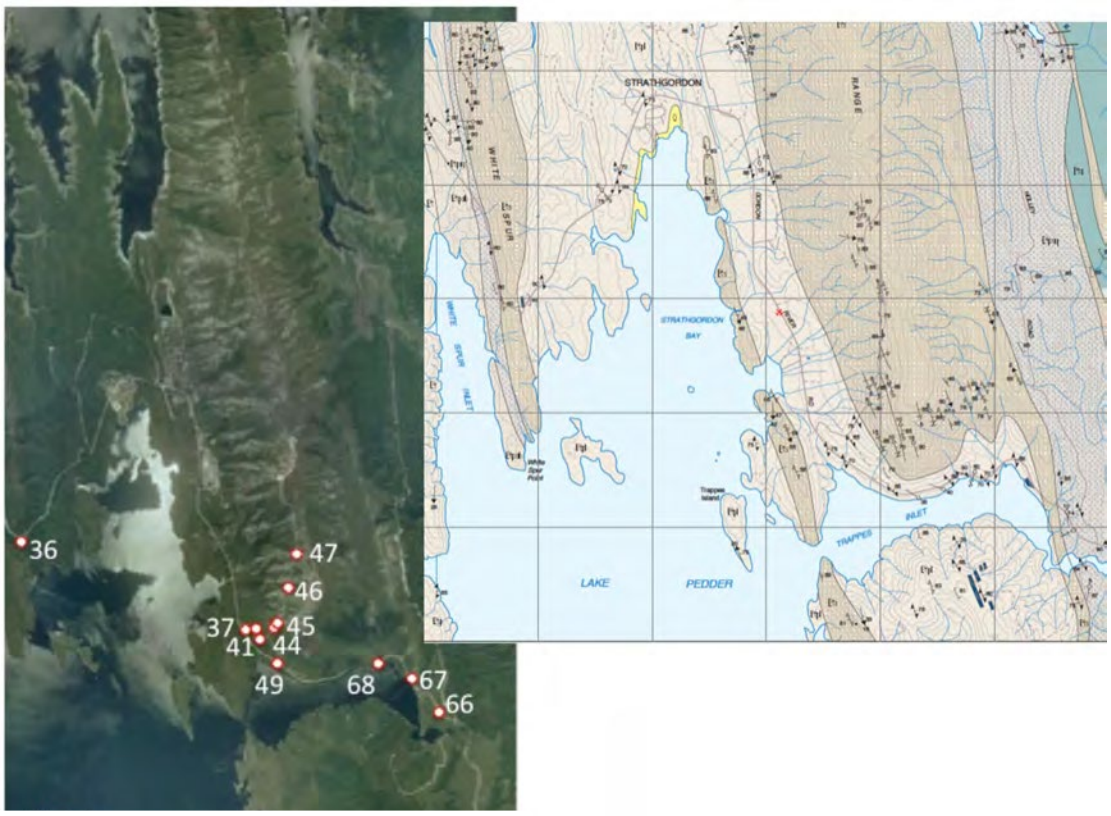

Figure 64: Twelvetrees Range station map on Google satellite image base and Mineral Resources Tasmania 1:25,000 geological atlas map

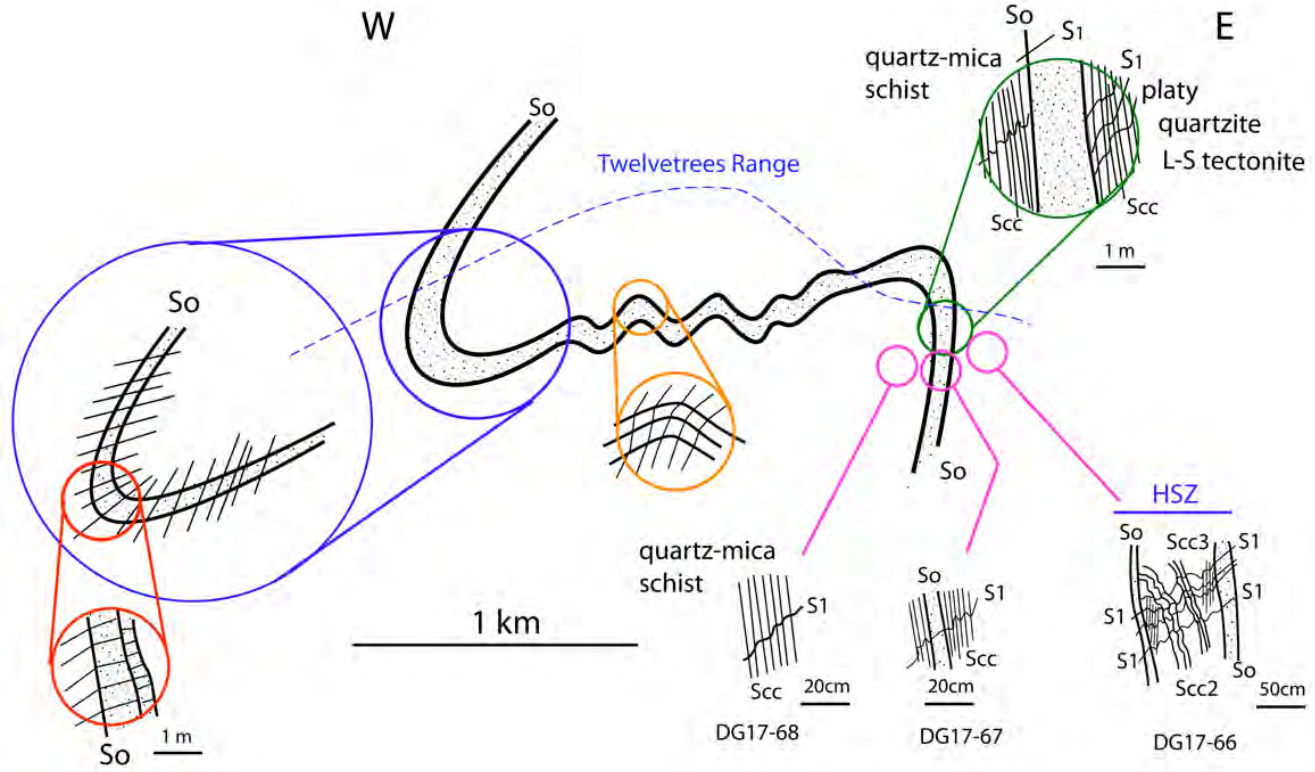

Figure 65: Geometry of the Twelvetrees Range macro-isoclinal fold pair shown as a structural profile across the south end of the Twelvetrees Range. The profile construction is based on road traverse up to the Twelvetrees Range communications tower (see Figure T2) and outcrops on the Strathgordon road along Trappes Inlet.

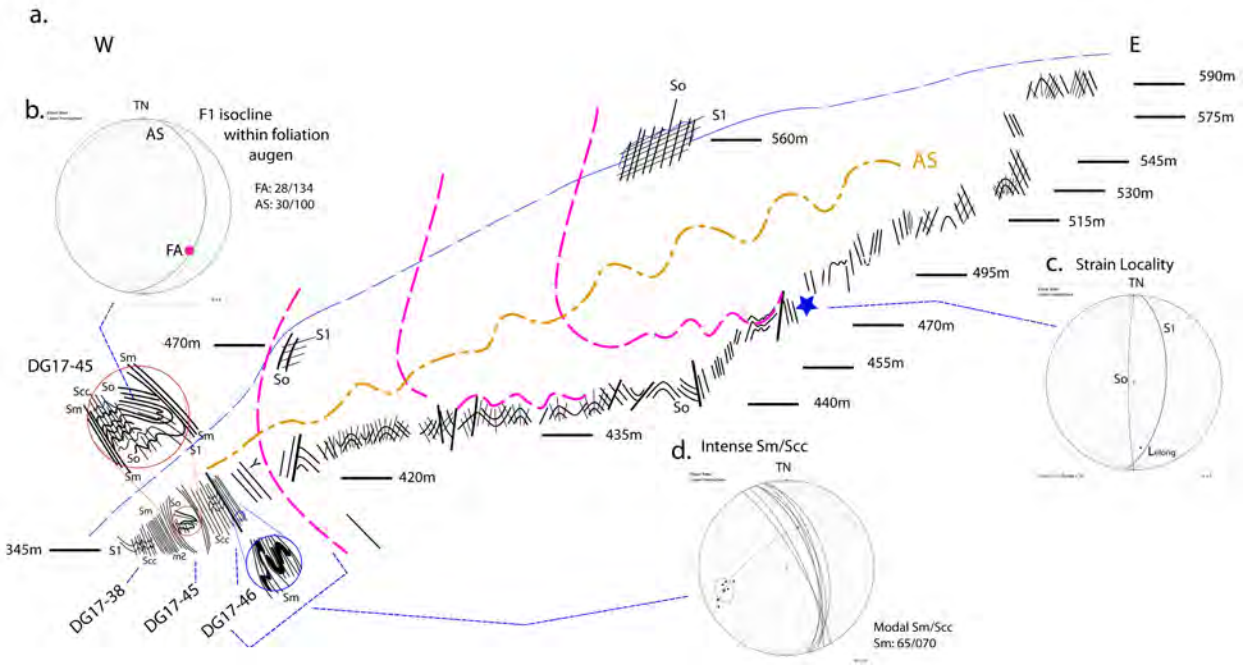

Figure 66: Composite, stacked sketch-profile based on the outcrop sketches along the road to the communications tower at the south end of Twelvetrees Range. The blue line is the approximate topographic range profile. Pink dashed lines are So/Sm trends that define the hinge of a west-closing Twelvetrees macro-isoclinal fold. a) Profile with enlargements of parts of the outcrop, particularly in the high strain zone that envelopes the fold closure. b) Stereonet of F1 isocline fold axis and axial surface. c) Stereonet with bedding and cleavage attitudes and the elongation direction (Lelong) at the strain locality (see Appendix 4). d) Stereonet of intense foliation Sm transitional with crenulation cleavage Scc within the high strain zone (HSZ) exposed in cuttings and outcrops along the lower part of the road.

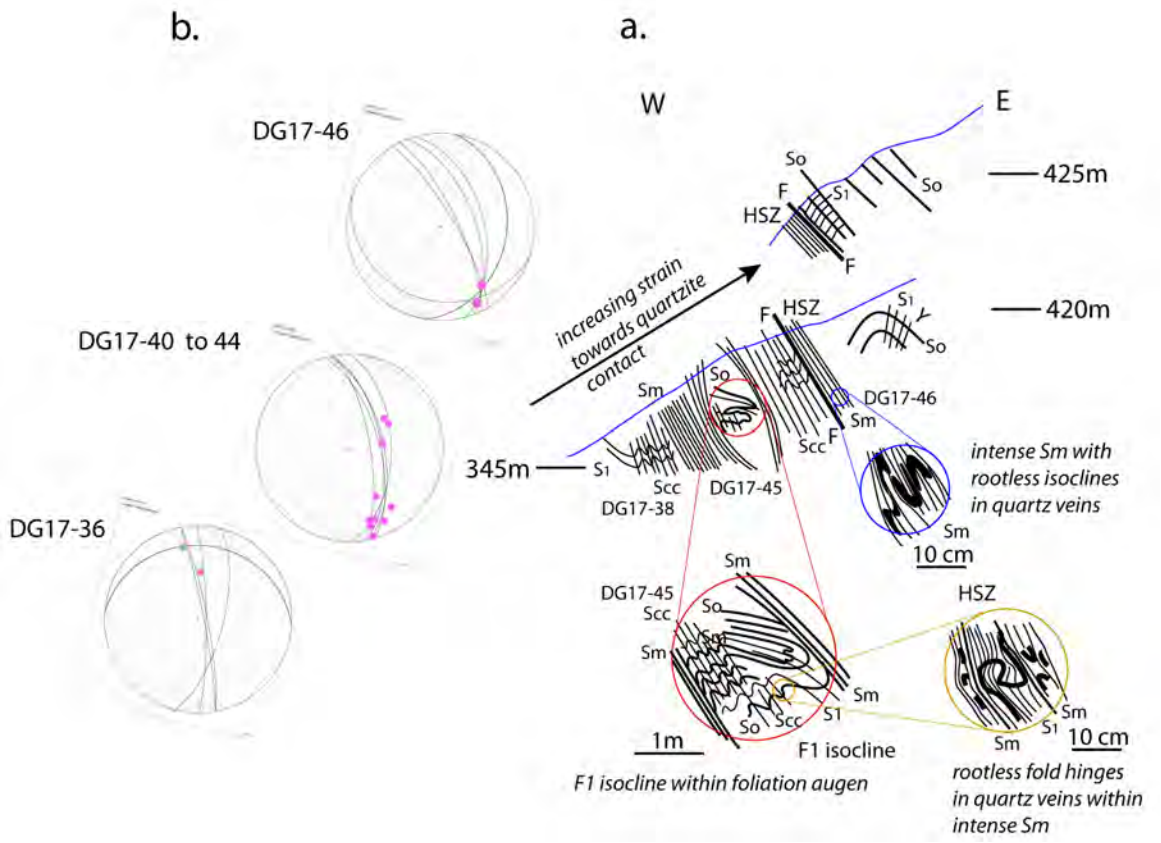

Figure 67: Twelvetrees Range strain gradient into the quartzite contact at the macro-isoclinal fold hinge. a) Superimposed sketch profiles on different road bends with enlargements of the observed fabric relationships. b) Stereonets of foliation Sm, fold axial surface (AS) and fold axis attitudes at different positions in the profile.

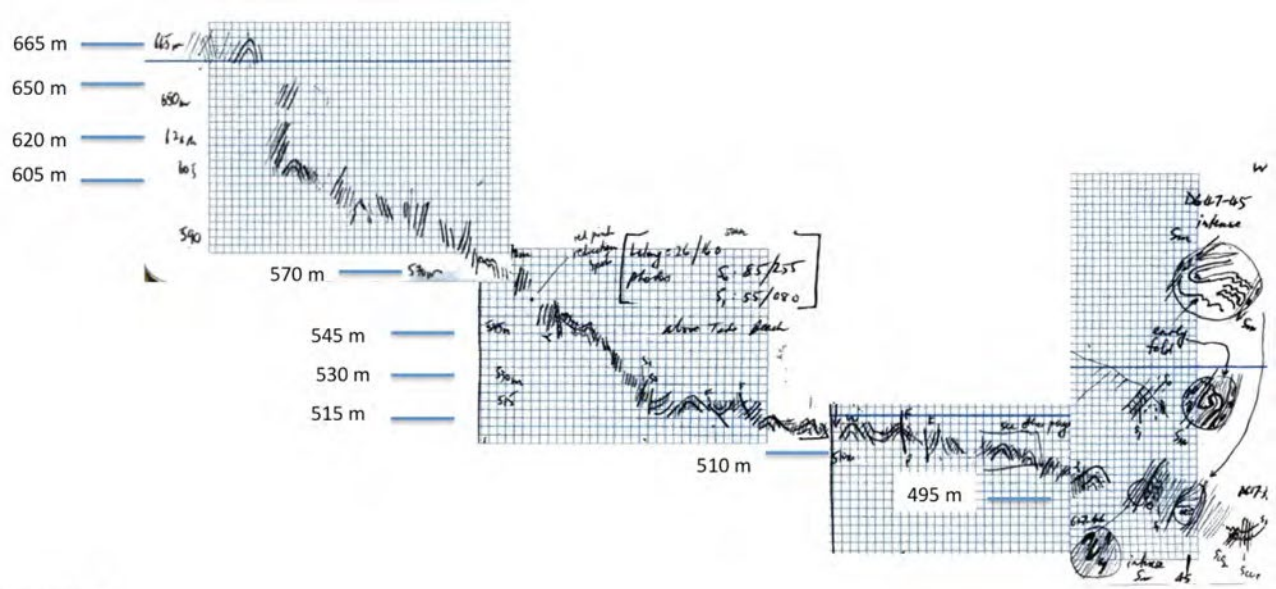

Figure 68: Initial sketch profile constructed whilst doing the traverse on the Twelvetrees Range along the Telecommunications Tower access road. Corrected elevations were added later.

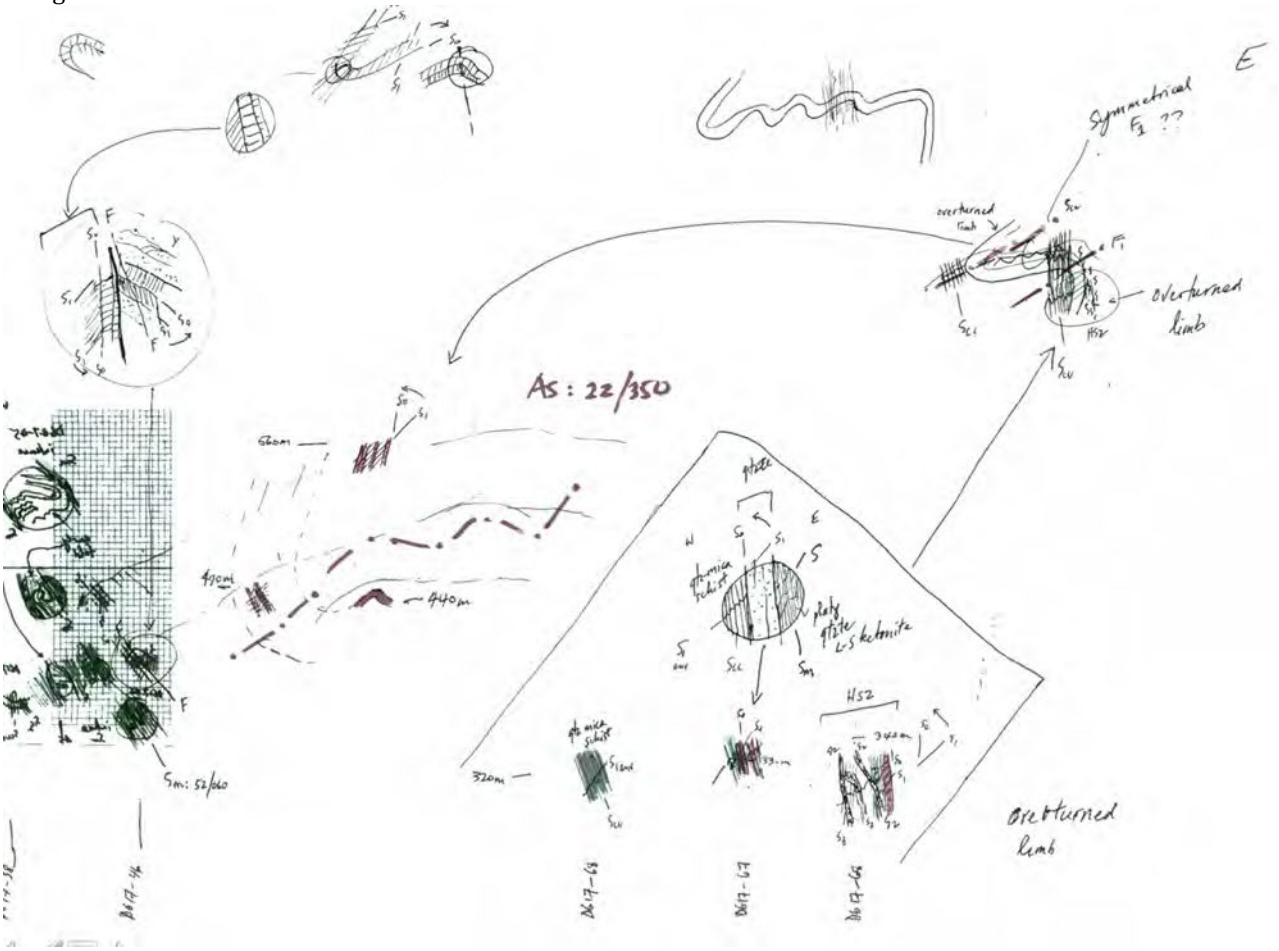

Figure 69: Initial sketches of the field structural relationships and the final interpreted geometry. Compare with

Figure 70: Western side of the Twelvetrees Range at ~560 m elevation. Steeply dipping So/Sm cut by a moderately dipping S1 foliation indicating overturned limb position on an inferred west-closing recumbent isoclinal macro-fold.

Figure 71: Upright to steeply inclined tight to open folds with sub-rounded hinges at ~665 m elevation

The western flank of the Twelvetrees Range is defined by an intensely foliated zone with intense foliation Sm , multiple cleavages and a strongly developed S3 crenulation cleavage (Figures 72, 73, 74, 75 and 76). Outcrops DG17-37, DG17-38, DG17-39 and DG17-40 represent parts of a bounding high strain zone to the quartzite that forms the Twelvetrees Range ridgeline (Figures 66 and 67).

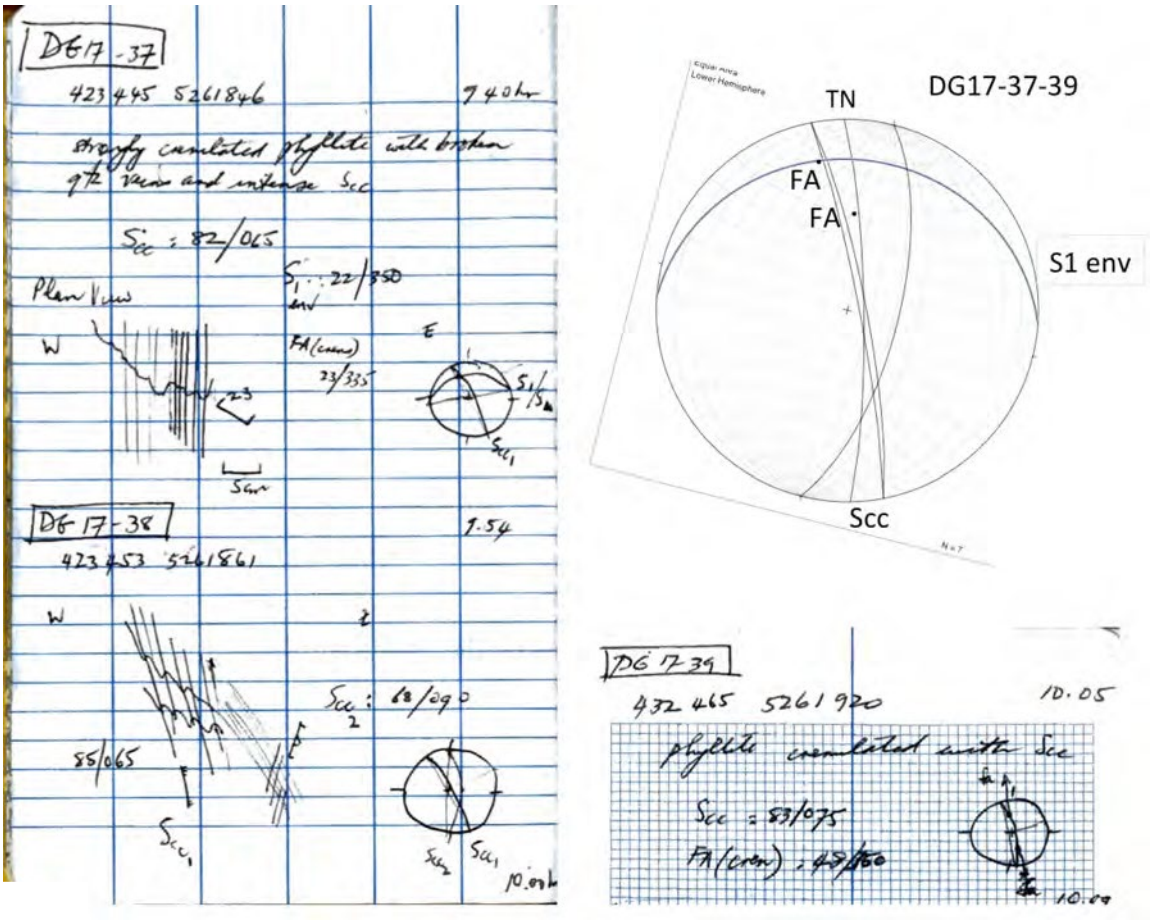

Figure 72: Field notebook entries for DG17-37, DG17-38 and DG17-39.

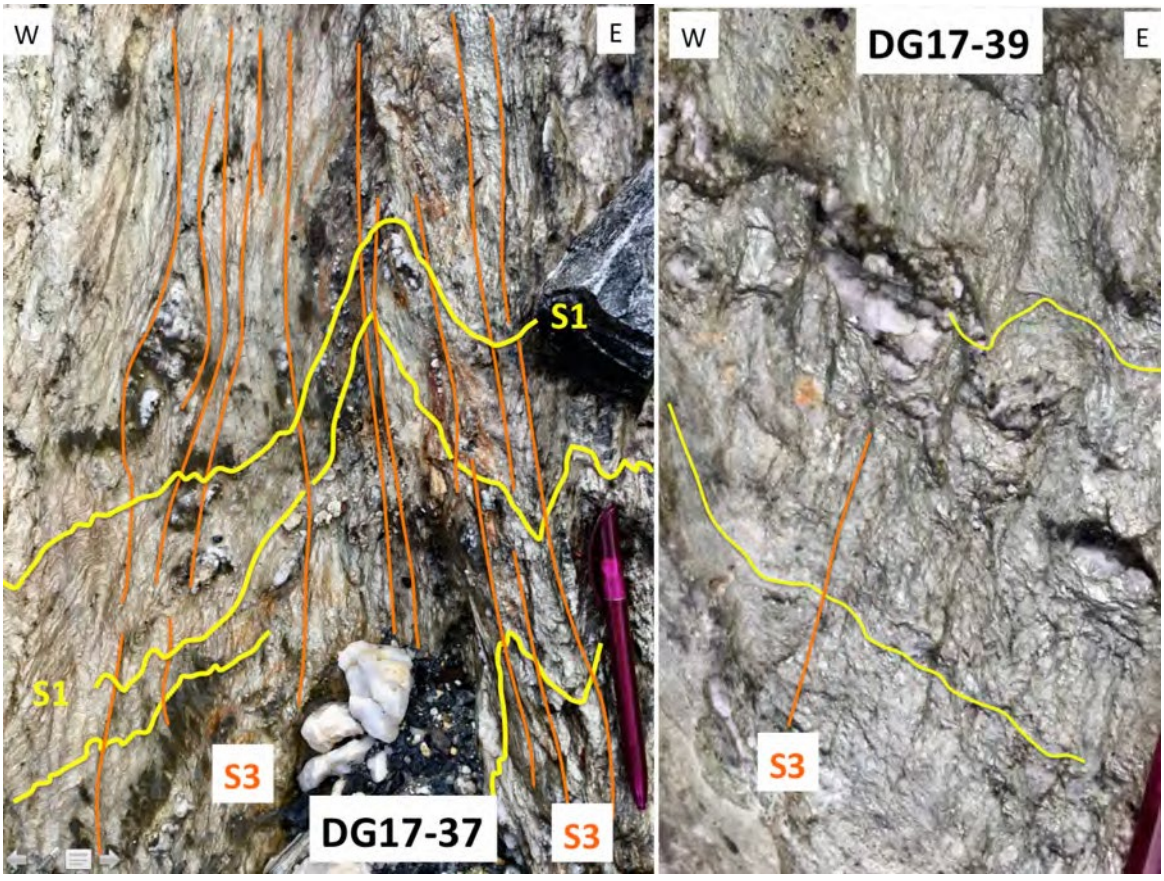

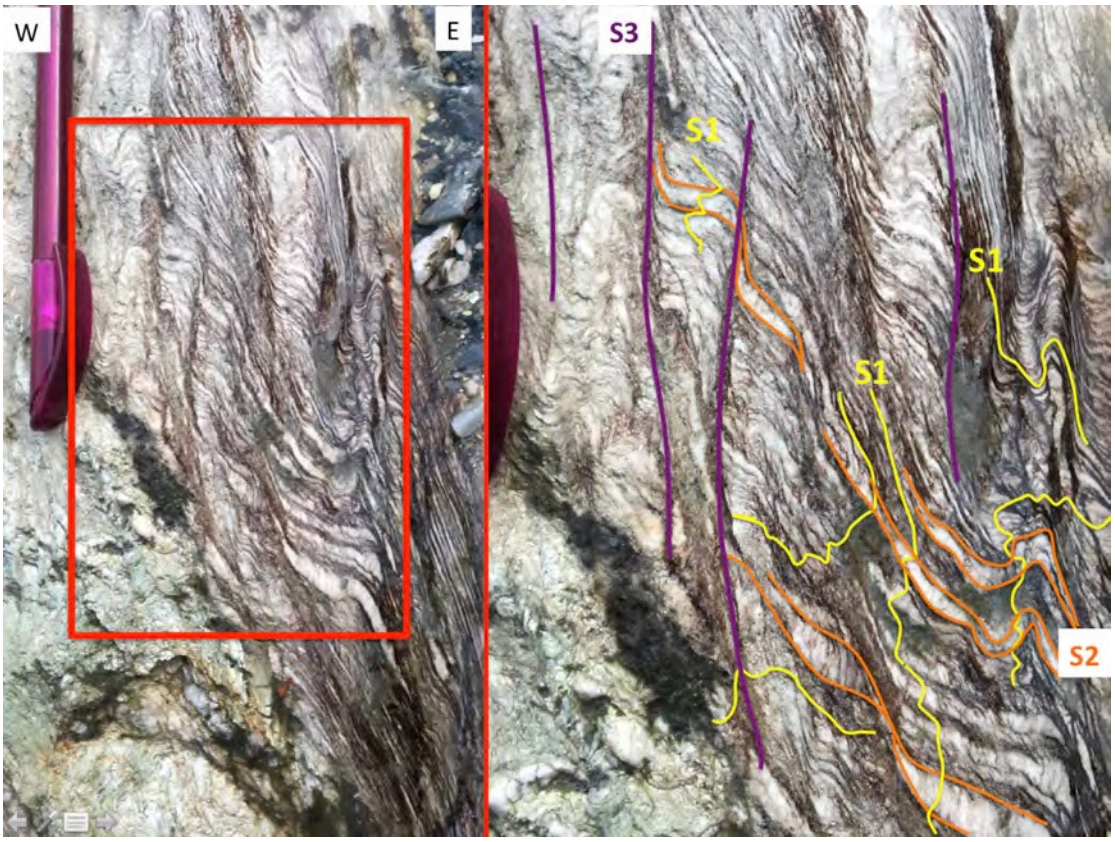

Figure 73: Outcrop relations in the bounding strain zone to the hinge zone of the Twelvetrees macro-fold. a) Outcrop station are DG17-37, and b) DG17-38.

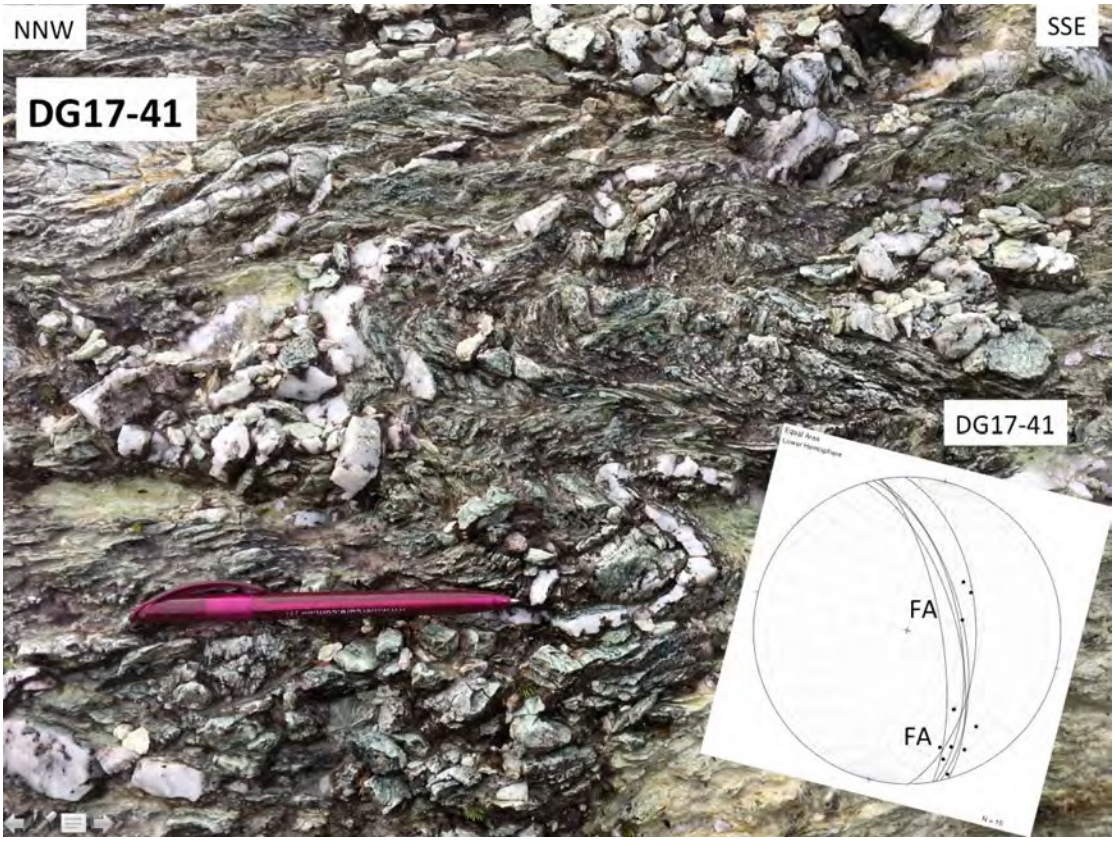

Figure 74: Outcrop relationships within intensely folded and foliated mica-quartz schist. The steronet shows the attitudes of the mesoscopic fold axial surfaces and the marked variation in fold axes.

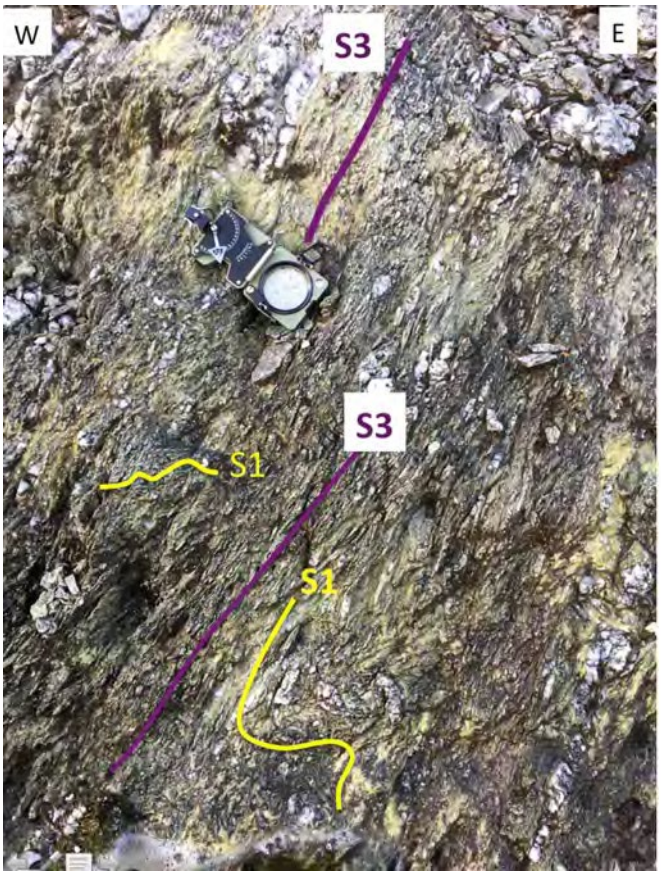

DG17-46

- high strain fabric with stretched disrupted quartz veins defining the earlier Sm (S1) fabric
- intense new fabric (S3) overprints the older fabric (S1)
- crenulation cleavage into a "schistosity"
- strain increases towards the contact with the quartzite (Twelvetrees Range)

Figure 75: Polydeformation within the intensely disrupted layering and quartz veins within the high strain zone adjacent to the nose of the Twelvetrees macro-fold hinge. Station DG17-46.

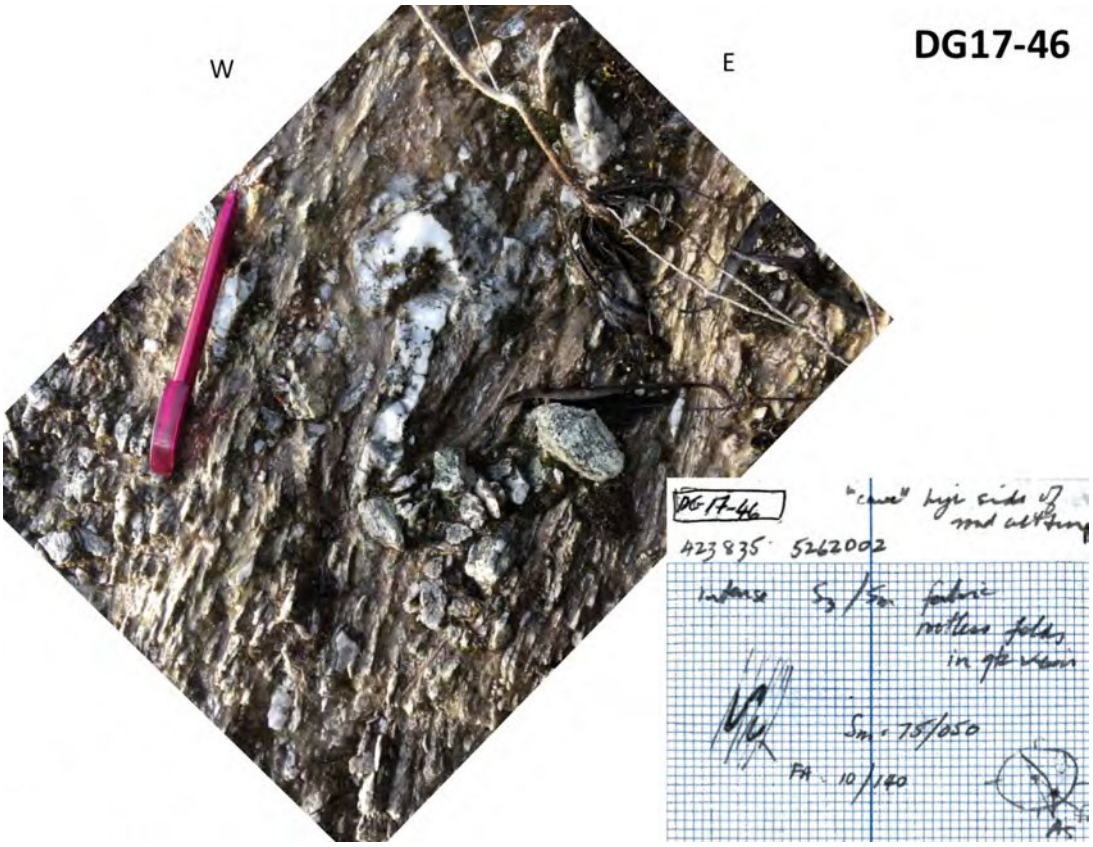

Figure 76: Close up view of the Intensely disrupted layering and quartz veins within the high strain zone adjacent to the nose of the Twelvetrees macro-fold hinge. Station DG17-46.

3.6 Atkins Range High Strain Zone (HSZ) (Element 6, Figure 2)
Outcrops DG17-66 and DG17-68 (Figures 77 to 85) show an intense crenulation cleavage (Scc) enveloping the trailing quartzite on the eastern limb of an F3 anticline that refolds the west-closing Twelvetrees macro-fold (Figure 78). The quartzite is part of the structurally lower right-way-up limb of the Twelvetrees macro-fold that is refolded with a trailing tail at the end of Trappes Inlet (Figure 77). These outcrops may be the equivalents of the bounding high strain zone that envelopes the quartzite of the Twelvetrees Range but is refolded by the strong, north-trending F3 fold set at the eastern end of the range.

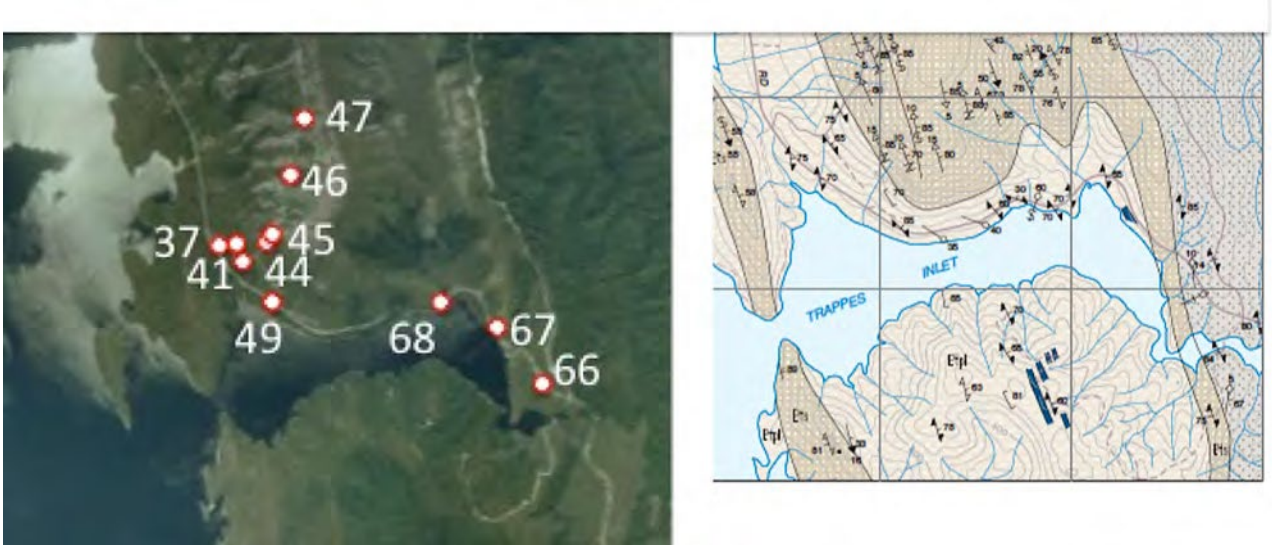

Figure 77: Outcrop location for the eastern side of the Twelvetrees Range north of Trappes Inlet (left) and the geological/structural relationships on the Mineral Resources Tasmania digital atlas 1:25,000 map sheet (right).

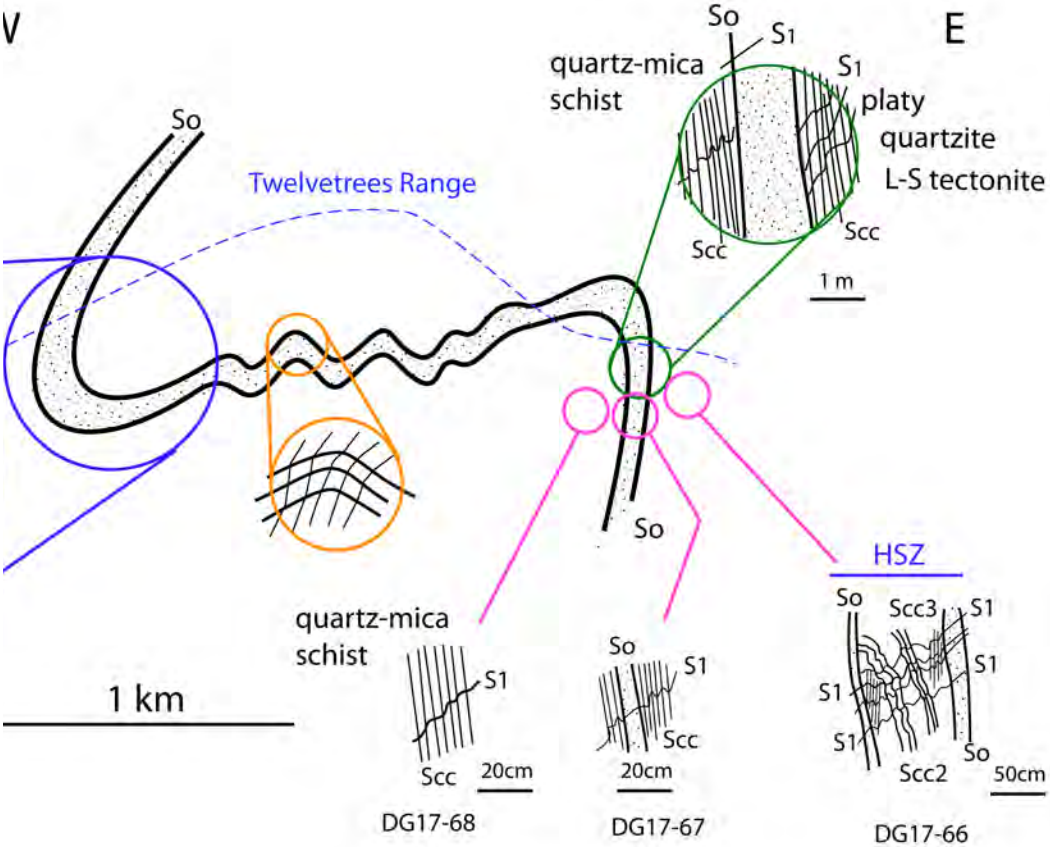

Figure 78: Sketch profile of the Twelvetrees Range west-closing macro-fold showing the structural relationships at road outcrops including stations DG17-66, DG17-67 and DG17-68 on the eastern flank of the Twelvetrees Range.

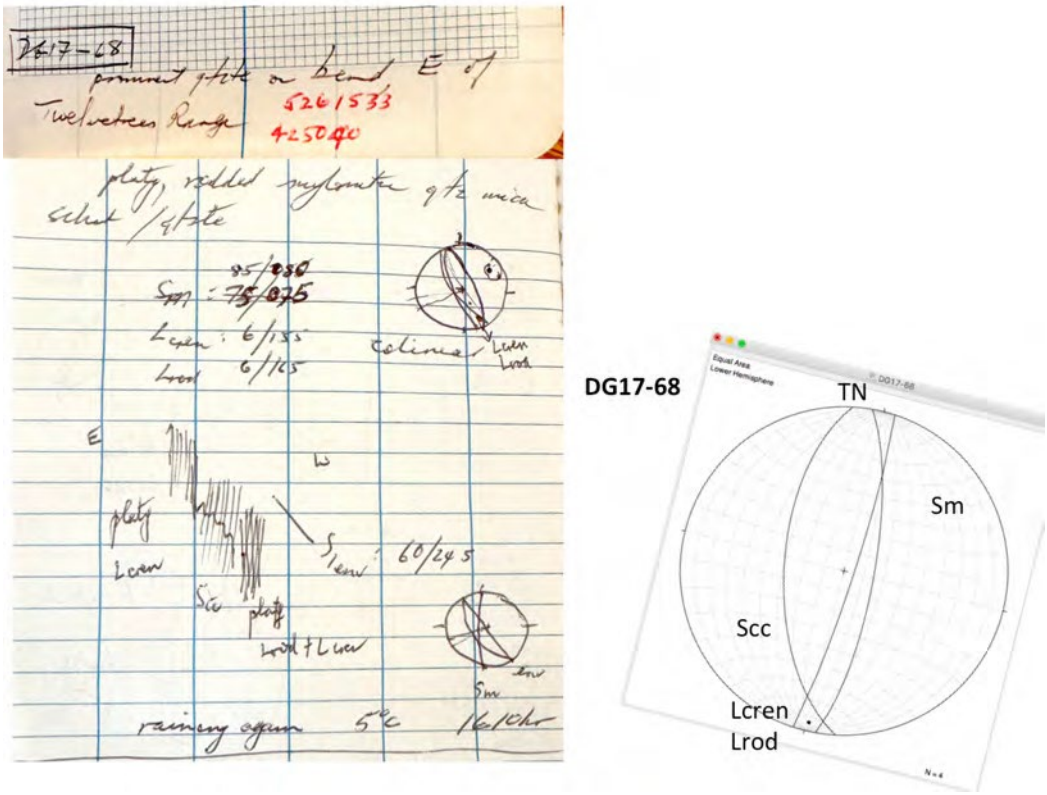

'Figure 79: Station DG17-66: prominent quartzite outcrop on bend showing an intense crenulation cleavage (Scc) overprint the dominant foliation north-trending Sm.

Figure 80: Outcrop relationships at DG17-66

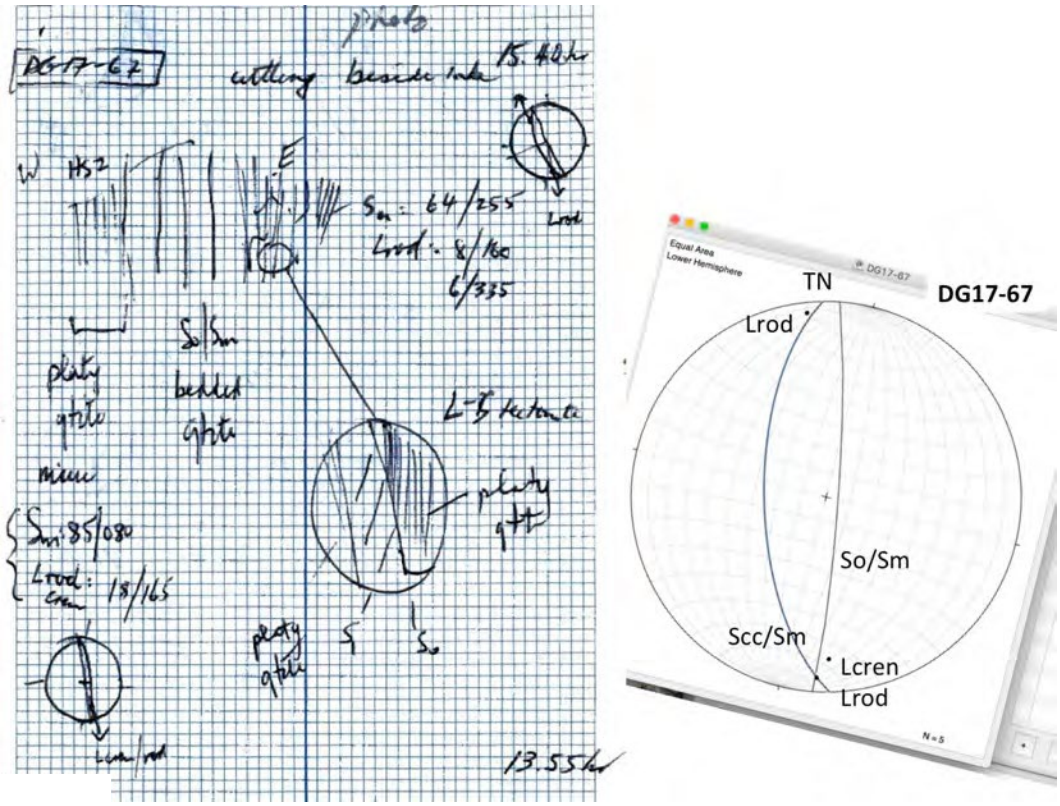

Figure 81: Station DG17-67: prominent quartzite outcrop on bend showing an intense crenulation cleavage (Scc) overprint the dominant foliation north-trending Sm.

Figure 82: Station DG17-67 showing the contact between schistose quartzite/quartz-mica schist and thicker bedded rodded
quartzite

Figure 83: Station DG17-67 showing the two dominant lithologies of schistose and rodded quartzite.

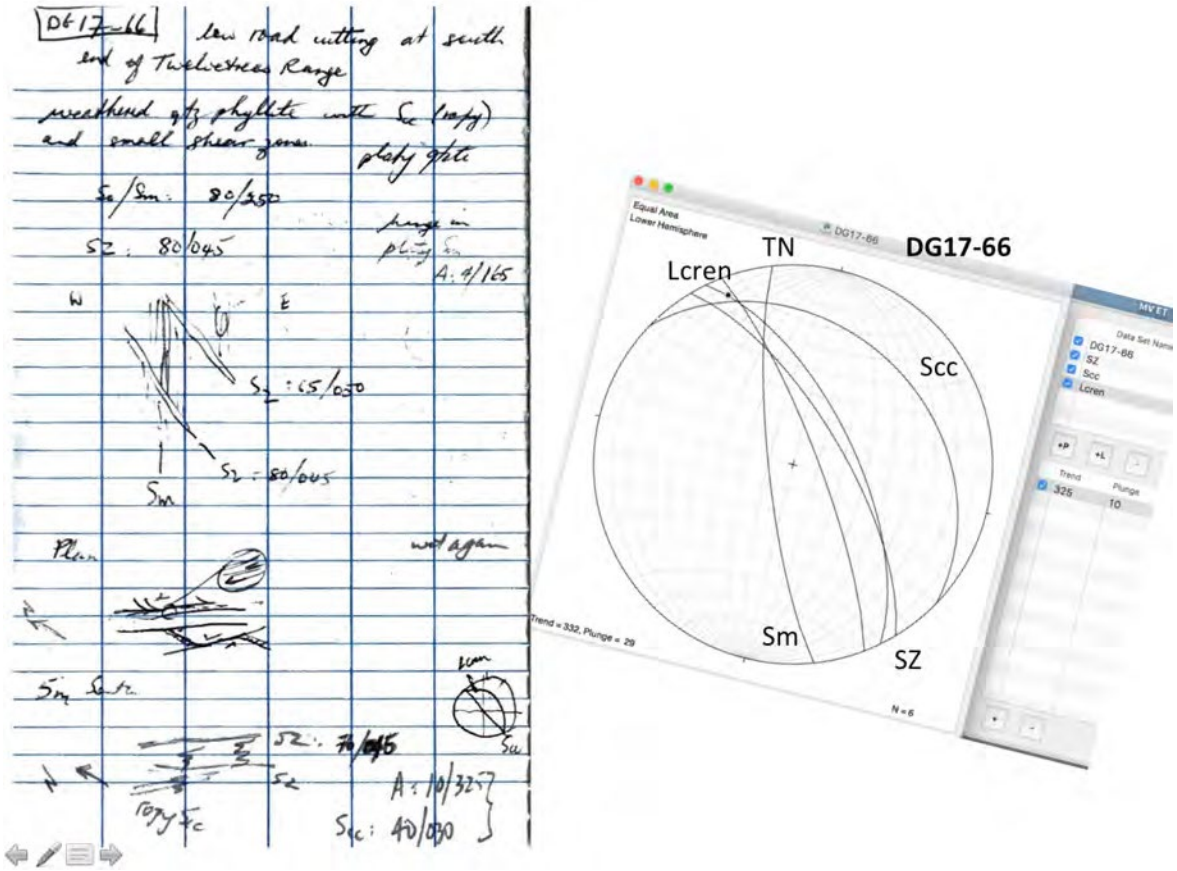

Figure 84: Station DG17-66 on the western margin of the Atkins Range HSZ (Element 6, Figure 2): outcrop of weathered schistose quartzite and quartz mica schist. Shear zones (zones of Scc) overprint the dominant foliation north-trending Sm.

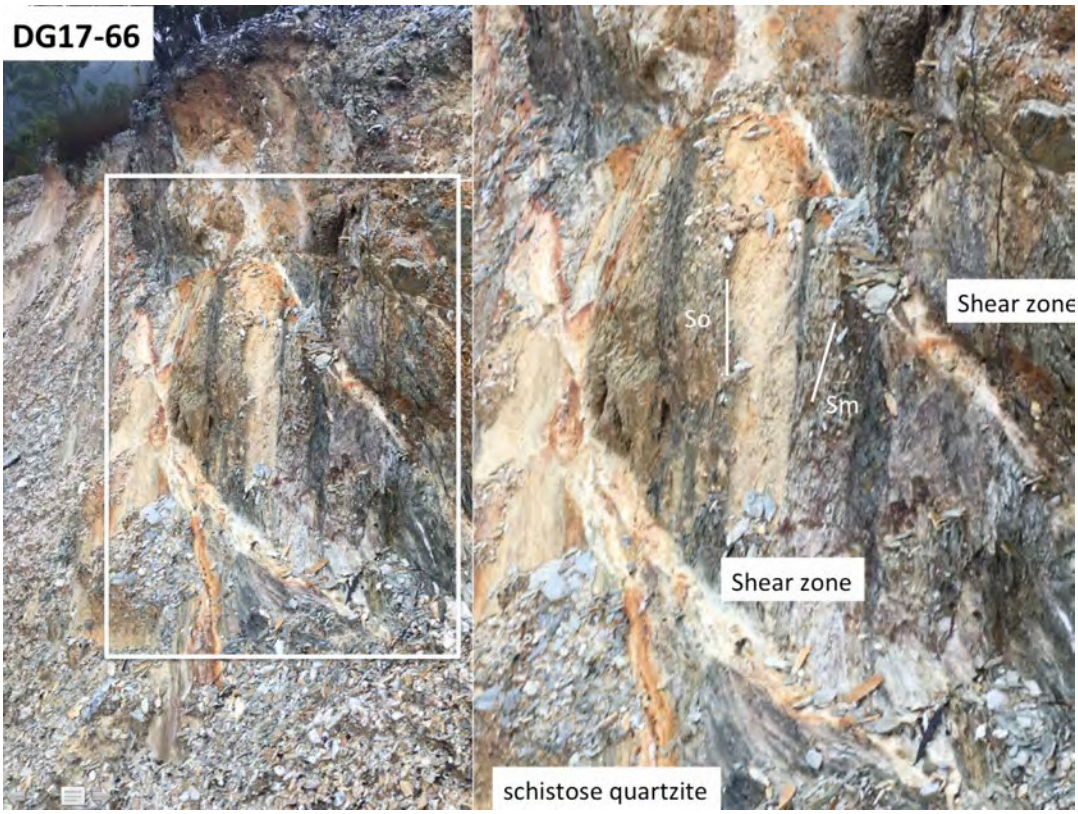

Figure 85: Outcrop relationships at station DSG17-66. Outcrop of weathered schistose quartzite and quartz mica schist with shear zone-like zones of intense Scc overprint the dominant foliation north-trending Sm.

4. References

Boulter, C.A., 1974. Structural sequence in the metamorphosed Precambrian rocks of the Frankland and Wilmot Ranges, southwestern Tasmania. *Paper and Proceedings of the Royal Society of Tasmania*, 107, 105-115.

Boulter, C. A., 1978. The structure and metamorphic history of the Wilmot and Frankland Ranges, south-west Tasmania. Unpublished PhD Thesis, The University of Tasmania.

Brown, A.V., McClenaghan, M.P., Turner, N.J., Baillie, P.W., McClenaghan, J, and Calver, C.R., 1989. Geological Atlas 1:50,000 Series. Sheet 73 (8112N), Huntley. *Explanatory Report Geological Survey of Tasmania.* 109p.

Collet, L.W. 1927. *The Structure of the Alps.* Edward Arnold & Co., London, 289pp.

Port, I.A. 2023. The Structural and Metamorphic History of the Eastern Tyennan Region, Lake Pedder, Tasmania. BSc (Hons), Thesis University of Tasmania (unpublished).

Powell, C.McA., 1969. Polyphase folding in Precambrian, low-grade metamorphic rocks, Middle Gordon River, southwestern Tasmania. *Paper and Proceedings of the Royal Society of Tasmania*, 103, 47-51.

Williams, S.J., 1973. Structure and metamorphism of the McPartlan Pass-Sentinels area. BSc (Hons), Thesis University of Tasmania (unpublished).

Williams, S.J., 1976. Structure and metamorphism of the McPartlan Pass-Sentinels area. *Paper and Proceedings of the Royal Society of Tasmania*, 110, 25-34.

APPENDIX 3

Strain determinations in the Eastern Tyennan
Subdomain Quartzites

APPENDIX 3
Strain Determinations in the Eastern Tyennan Subdomain Quartzites

Boulter (1978) undertook strain determinations using 1) quartz grain shape/orientation analysis in the quartzites of the Frankland Range and 2) shapes and angular relationships of mudcracks and clastic dykes in the along the Gordon River Road. Irregularly shaped, sub-spheroidal opaque meshworks provide another measure of strain variations through some of the early F1/F2 isoclinal folds and D1 boudins.

1. Quartz Grain shape/orientation

Strain analysis on selected quartzite samples from mesoscopic folds in the southern end of the Frankland Range (Figures 3.1, 3.2 and 3.3) used contoured polar graph plots of quartz grain aspect ratio versus orientation after Elliott (1970) to determine strain magnitudes and orientation of the principal stretches (see Boulter, 1978, fig. 7.1). The folds sampled and their sample numbers are shown in Figures 3.1 and 3.2. Their positions in the plunge profile of Boulter (1978, fig. 7.15) are shown in Figure 3.3a and their respective strain data are shown on a logarithmic strain plot (after Wood, 1973). The graph shows most of the samples analysed plotted within the flattening field with X elongation values between 10% and 40%, and shortening Z values between 15 and 40% shortening (Figure 3.3b).

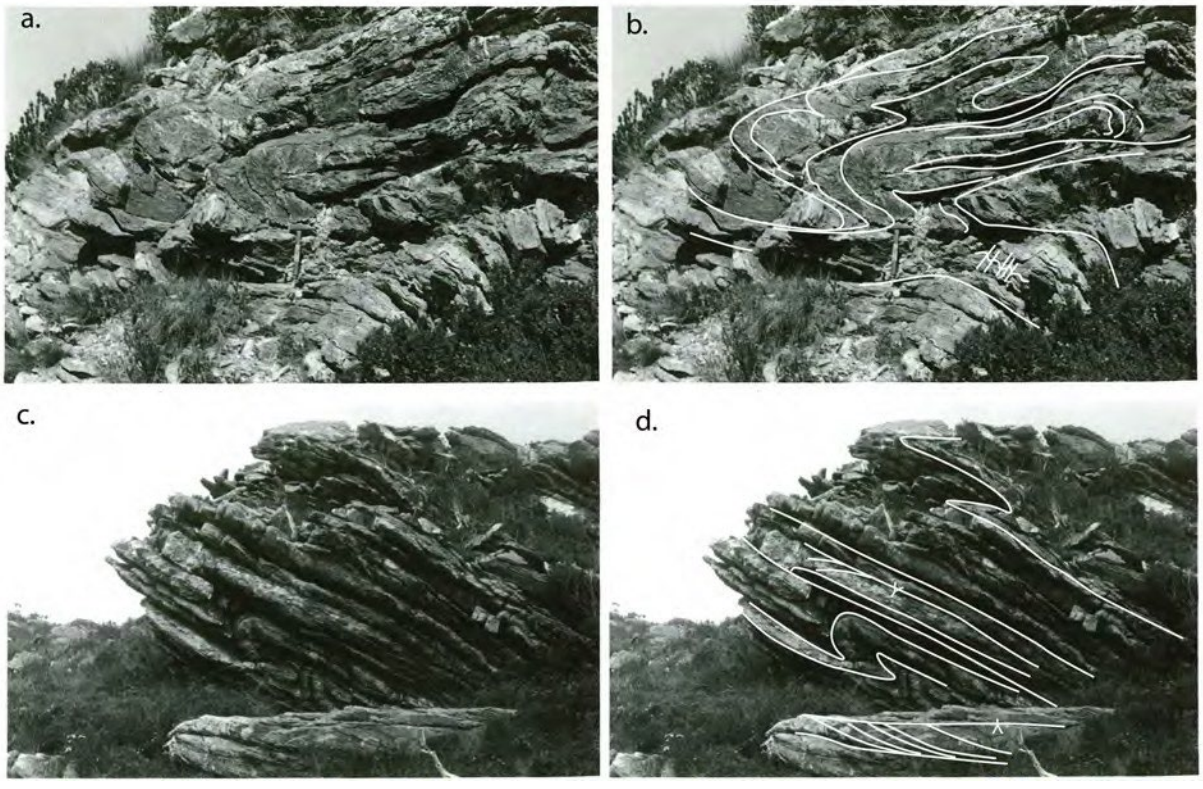

Figure 3.1: First generation tight to isoclinal folds in the eastern Frankland Range
a, b: Tight F1 fold from the lower slopes of Murphys Bluff showing complex, sheath-like close-outs within the isoclinal fold pile (from Boulter, 1978, fig. 7.22a). (Sample 44376 from hinge). Hammer is 40 cm.
c, d: Asymmetric coupled folds with parallel external limbs from the eastern Frankland Range (from Boulter, 1978, fig. 7.16a). View is to the east. (sample 44372 from hinge)

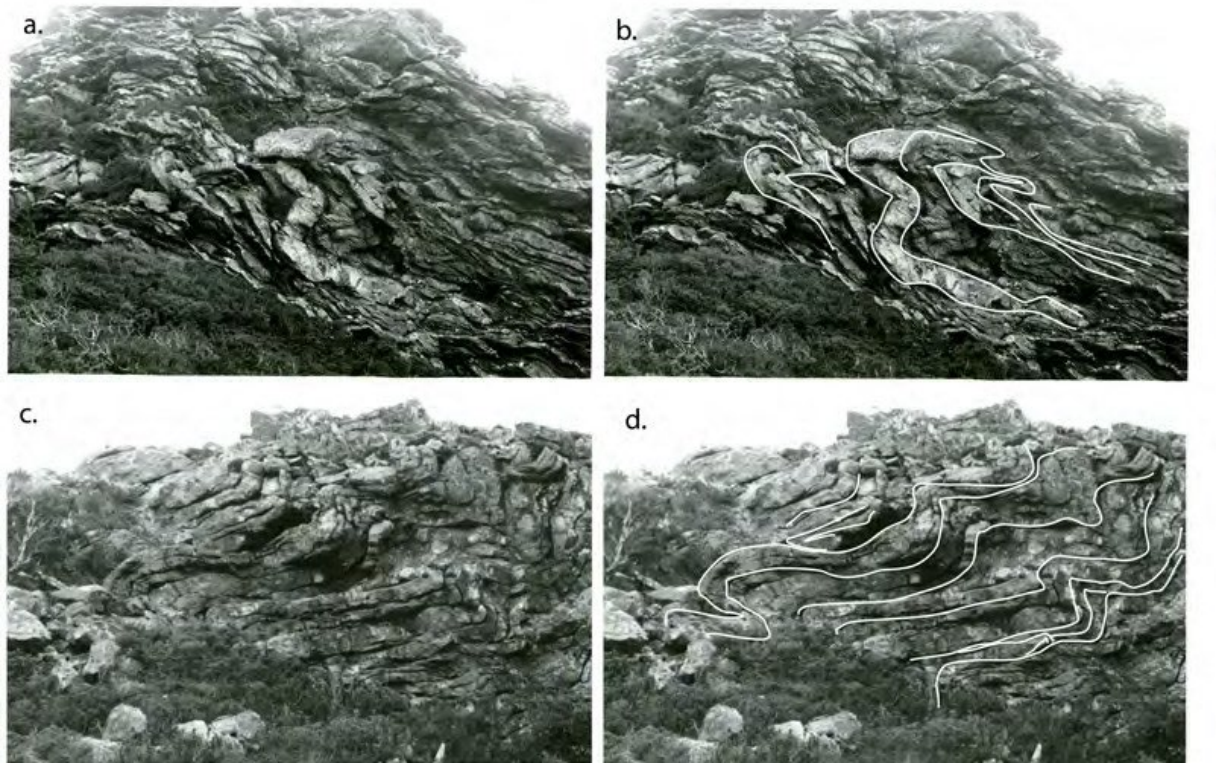

Figure 3.2: First generation tight to isoclinal folds in the eastern Frankland Range.
a, b: asymmetric, coupled first generation fold in the eastern Frankland Range viewed looking east. Samples 44372 (28% shortening) and 44375 (19% shortening) are from this fold.
c, d: Open to close asymmetric folds (from Boulter, 1978, fig. 7.16b). View is to the east. (samples 44368 and 44369).

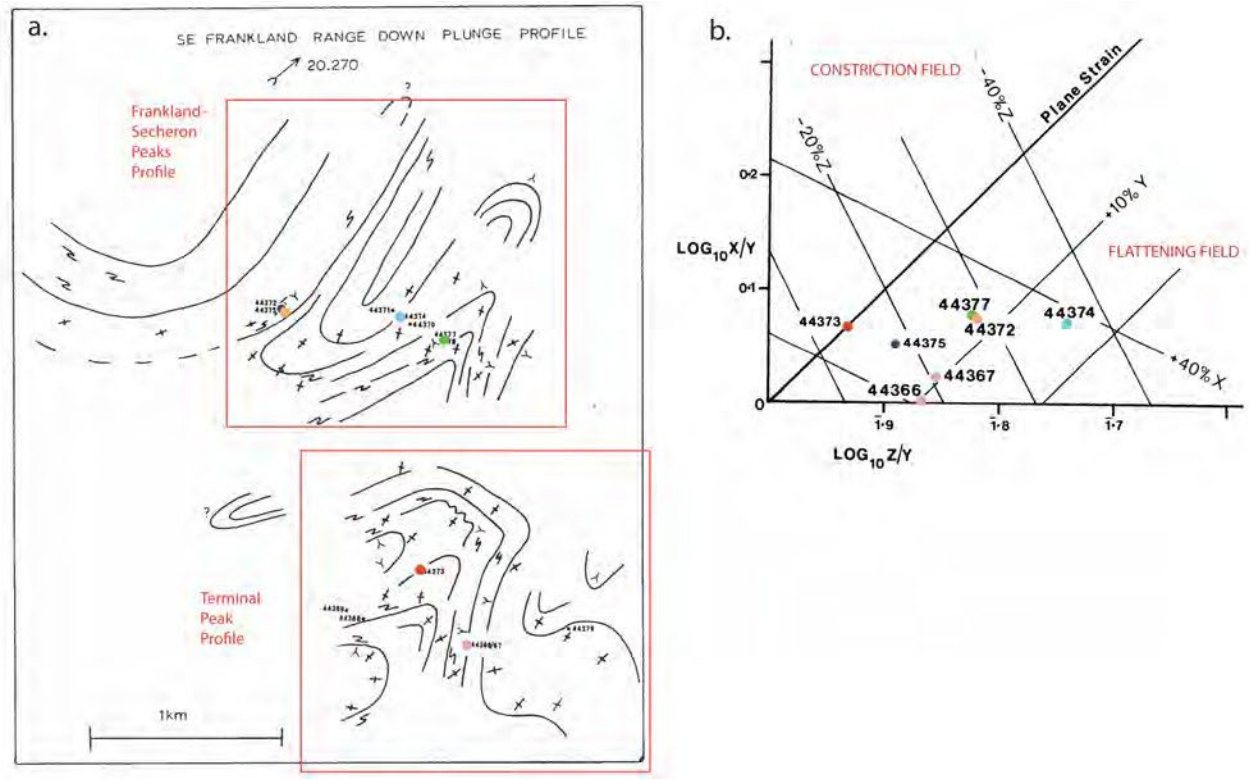

Figure 3.3: Strain analysis data from the Frankland Range. a) Sample locations within plunge profile (Boulter, 1978, fig. 7.15). b) Logarithmic strain plot (Boulter, 1978, fig. 7.30). The strain data are based on quartz grain dimensional analysis after Elliott (1970). The graph shows most of the samples analysed plotted within the flattening field with X elongation values between 10% and 40%, and shortening Z values between15% and 40%. Colour coded dots show the positions in the profile and their positions on the strain plot.

2.Opaque framboid? meshworks in Quartzite

2.1 Gordon Dam Quarry

Opaque markers in quartzite in the Gordon Dam quarry show marked variations around isoclinal folds (Figures 3.4, 3.5 and 3.8) and D1 boudins (Figures 3.6 and 3.7). They provide information on strain magnitude variations within Sm, in boudinaged layers and around isoclinal F2 folds.

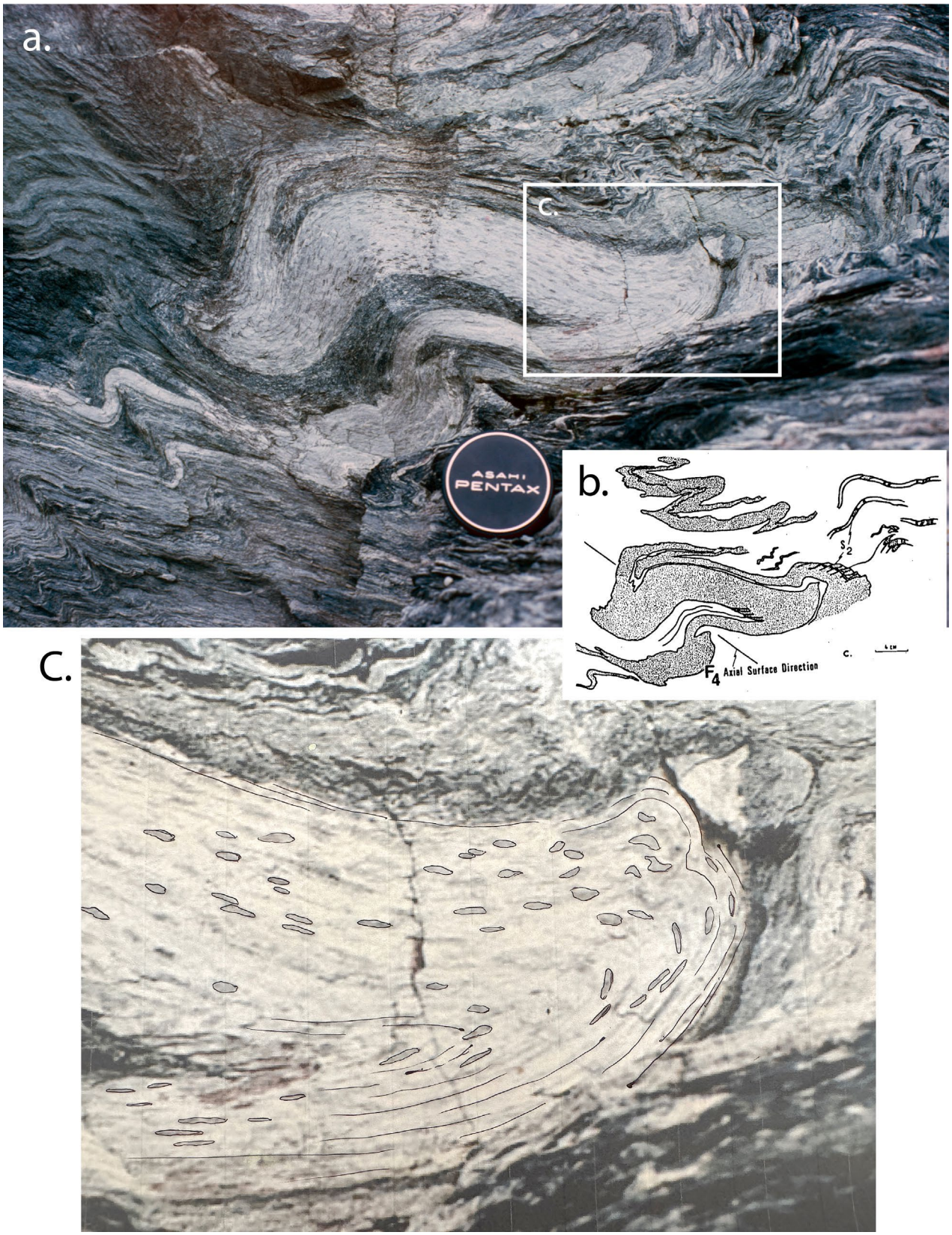

Figure 3.4: a) F2 isocline showing ellipsoidal strain markers (opaque meshworks) deformed in Sl, refolded and shape modified by the early Fl/F2 isocline. (Photo Credit: David Seymour, fig.2 in Seymour et al., 2007). b) Profile sketch of the F2 fold in Figure 3.4a (Boulter, 1978, fig. 3.8c) Gordon Dam site quarry. c) Enlargement of hinge area of isocline showing changes in shapes of markers re- deformed during the isoclinal folding.

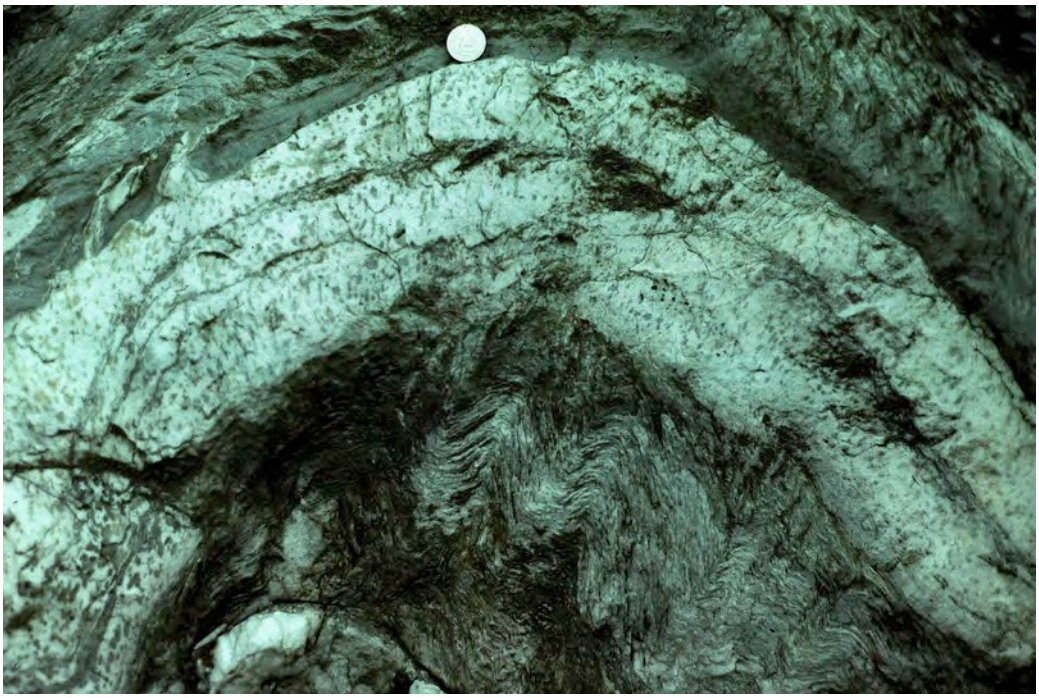

Figure 3.5: F3 fold hinge showing ellipsoidal strain markers (opaque meshworks) deformed in S1, refolded and shape modified during the younger folding. Gordon River Road outcrop above Gordon damsite? Photo taken in 1976 by D. Gray.

Figure 3.6: Complex deformation pattern with refolded boudinaged quartzite layer showing marked thinning through boudin necks. Gordon damsite quarry (Boulter, 1978, fig.3.17). See Figure 3.7 for enlargement of the folded boudin neck (photo lower centre). Photo taken in 1976 by D. Gray.

Figure 3.7: Strain pattern shown by bleb-like, irregularly shaped opaque markers (skeletal meshes) in the folded neck of a D1 boudin (Boulter, 1978, fig. 3.17). There is marked increase in strain into the necked region of the quartzite layer. The adjoining isoclines (photo upper left) show similar strain variations to the F2 isocline in Figure 3.4. Location quarry wall near Engineers office, Gordon Damsite.

Figure 3.8: Strain pattern shown by bleb-like, irregularly shaped opaque markers (skeletal meshes) in the hinge of an F3 fold. Gordon damsite quarry? Photo taken in 1976 by D. Gray.

2.2 Twelvetrees Range Quartzite

Quartzite on the Twelvetrees Range contained pink, ellipsoidal, oxide skeletal-meshes. Measurements of mesh aspect ratios were undertaken on the foliation surface (XY plane) and a plane normal to the foliation (XZ plane) (Figure 3.9). The average aspect ratios of the ellipses on both planes were calculated to give an X/Z=5.1 and X/Y:2.15 with a strain ratio X:Y:Z of 2.15:1:0.42

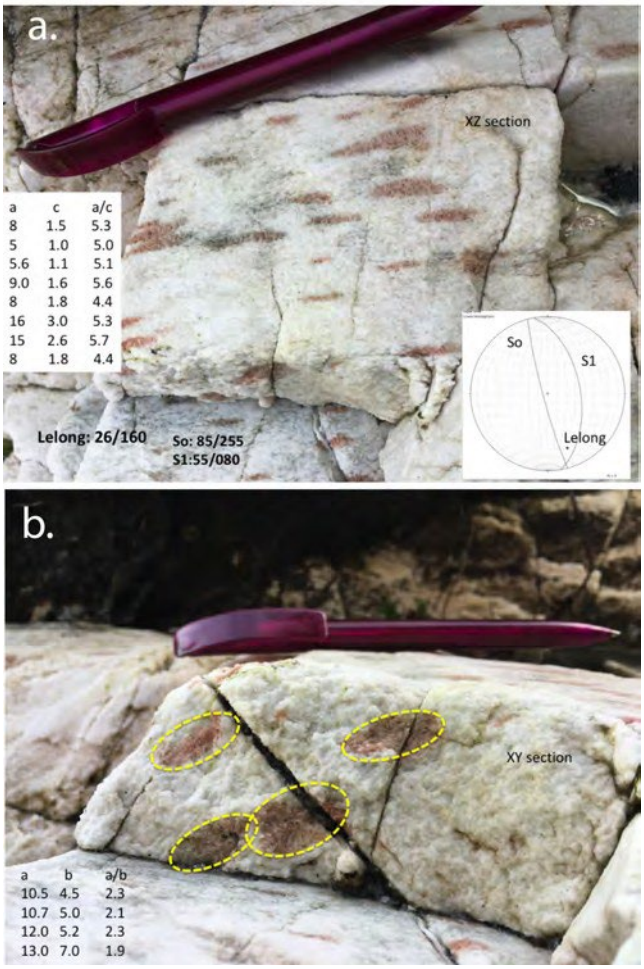

Figure 3.9: Twelvetrees quartzite layer strain determination utilising aspect ratios of pink oxide skeletal meshes on the foliation surface (XY plane) in (b) and a plane normal to the foliation (XZ plane) in (a). The strain calculation assumes the oxide meshes had an initial spheroidal shape. Average X/Z=5.1and average X/Y:2.15 with a strain ratio X:Y:Z of 2.15:1:0.42.

3. Summary

1) D1 strain is preserved as a flattening and elongation within the dominant foliation Sm.

2) D1 strain is further modified during D2 and D3 folding with differences in strain magnitude and orientation between the hinges and limbs of F2 folds (Figure 3.4c).

3) In most instances the recorded strain is a product of the D1 and D2 deformations.

4) The strain determinations of quartzite grain shapes undertaken by Boulter (1978) show that the bulk rock strain in the various F2 folds plots within the flattening field with X elongation values between 10% and 40%, and shortening Z values between 15 and 40% shortening.

4. References

Boulter, C. A., 1978. The structure and metamorphic history of the Wilmot and Frankland Ranges, south-west Tasmania. Unpublished PhD Thesis, The University of Tasmania.

Elliott, D. 1970. Determination of finite strain and initial shape from deformed elliptical objects. *Bulletin of the Geological Society of America*, 81, 2221-2236.

Seymour, D.B., Green, G.R. & Calver, C.R. 2007. The geology and mineral deposits of Tasmania: a summary (second edition). *Bulletin Geological Survey Tasmania* 72.

Wood, D.S. 1973. Patterns and magnitudes of natural strain in rocks. *Annual Reviews of Earth & Planetary Sciences*, 2, 369-401.

APPENDIX 4

Lithostratigraphic, chronostratigraphic and structural data

--Download only--

Download Appendix 4

Tasmanian Government

Mineral Resources Tasmania
PO Box 56 Rosny Park
Tasmania Australia 7018
Ph: +61 3 6165 4800

info@mrt.tas.gov.au www.mrt.tas.gov.au